Total Synthesis of 9-dechlorochrysophaentin Reveals a Novel Mechanism of Cell Wall Biosynthesis Inhibition

By

Christopher Ryan Fullenkamp

Dissertation

Submitted to the Faculty of the

Graduate School of Vanderbilt University

in partial fulfillment of the requirements

for the degree of

DOCTOR OF PHILOSOPHY

in

Chemistry

May 31, 2020

Nashville, Tennessee

Approved:

Gary A. Sulikowski, Ph.D.

Brian O. Bachmann, Ph.D.

Maria Hadjifrangiskou, Ph.D.

Steven D. Townsend, Ph.D.

To Kelcey

My parents

And Matt and Kelly

Acknowledgments

I must first acknowledge Dr. Gary Sulikowski for all his support and encouragement over the past five and a half years. Without his unwavering support and encouragement, I would not be the chemist I am today and would not have accomplished the work outlined in this thesis. Furthermore, I must also acknowledge my committee members for their support and discussions during committee meetings. Their valuable insight enabled my education and progress on my thesis project and aided in helping me get my post-doc position.

Secondly, I must thank the Sulikowski lab and VICB synthesis core members for helping keep my sanity and for always providing a laugh. I would not have been able to succeed in graduate school without advice, discussions, problem-solving, and constant laughter. Specifically, I need to thank my hood mate, Jason Hudlicky, for also knowing how to cheer me up and for the valuable discussions about chemistry. Your ridiculous work ethic and knowledge of chemistry constantly motivated and helped me become a better chemist. I also want to thank Quinn Bumpers, Zach Austin, and Alex Allweil for their support, discussions, and for making the lab a happier and brighter place. Thirdly, I want to thank the Synthesis Core for their help and support over the years, specifically, I want to thank Dr. Kwangho Kim, Dr. Somnath Jana, and Dr. Plamen Christov. Your initial work on chrysophaentin set me up for success and your constant support and help with instrumentation and purification made all my progress possible.

Finally, I want to thank my wife, Kelcey, without your constant support and love, I would not have been able to succeed in graduate school. You sacrificed a lot, to let me peruse this passion of mine and stuck by my side through all the ups and downs. You were my rock over these past six years and without you by my side this would not have been possible.

Table of Contents

Table of Tables

Table of Figures

List of Abbreviations

allyl-Bpin	Allyl pinacol boronate
allyl-Br	allyl bromide
AmiC	N-acetylmuramoyl-L-alanine amidase
B. *subtilis*	*Bacillus subtilis*
Bn	benzyl
BnBr	benzyl bromide
C. *taylori*	Chrysophaeum *taylori*
CDC	Centers of Disease control and Prevention
ClpX	ATP-dependent Clp proteases ATP-binding subunit
d	doublet
DCE	dichloroethane
DCM	dichloromethane
DEAD	diethyl azodicarboxylate
DIBAL	Diisobutylaluminium hydride
DMF	dimethylformamide
DMSO	dimethyl sulfoxide
E. *coli*	*Escherichia coli*
E. *faecalis*	*Enterococcus faecalis*
EcFtsZ	*Escherichia coli* filamenting temperature sensitive mutant Z
EnvC	Murein hydrolase activator EnvC
Et	ethyl
EzrA	Septation ring formation regulator EzrA
FDAAs	Fluorescently labeled D-amino acids
FtsA	Filamenting temperature sensitive mutant A
FtsB	Filamenting temperature sensitive mutant B
FtsE	Filamenting temperature sensitive mutant E
FtsI	Filamenting temperature sensitive mutant I
FtsK	Filamenting temperature sensitive mutant K

FtsL	Filamenting temperature sensitive mutant L
FtsN	Filamenting temperature sensitive mutant N
FtsQ	Filamenting temperature sensitive mutant Q
FtsW	Filamenting temperature sensitive mutant W
FtsX	Filamenting temperature sensitive mutant X
FtsZ	filamenting temperature sensitive mutant Z
GDP	Guanosine diphosphate
GFP	green fluorescent protein
GlcNAc	N-Acetylglucosamine
GpsB	cell cycle protein GpsB or Guiding PBP1-shuttling protein
GTP	Guanosine triphosphate
GTPase	Guanosine triphosphate hydrolase
GTPγS	5'-O-γ-thiotriphosphate
HADA	HCC-amino-D-alanine
HCC	7-hydroxycoumarin-3-carboxylic acid
HPLC	high performance liquid chromatography
IC50	half maximal inihbitory concentration
iPr	isopropyl
iPrBr	2-bromoproane
Ka	association constant
LAH	Lithium aluminum hydride
LC	liquid chromatography
LD50	median lethal dose
LytH	probable cell wall amidase LytH
m	mutiplet
mant-GTP	2'/3'-O-(N-Methyl-anthraniloyl)-guanosine-5'-triphosphate
MatP	Macrodomain Ter protein
MciZ	Cell division inhibitor MciZ or Mother cell inhibitor of FtsZ
m-CPBA	meta-chloroperoxybenzoic acid
MDRSA	multidrug-resistant Staphylococcus *aureus*

Me	Methyl
MePh	toluene
MIC	minimum inhibitory concentration
MMP	mitochondrial membrane potential
MMPP	magnesium monoperoxyphthalate
MreB	cell shape-determining protein MreB
MRSA	methicillin-resistant Staphylococcus aureus
NBS	N-bromosuccinimide
NCS	N-chlorosuccinimide
NHC	N-heterocyclic carbene
NIDDK	National Institute of Diabetes and Digestive and Kidney Diseases
NMR	nuclear magnetic resonance
NOE	nuclear Overhauser effect
PBP	penicillin-binding protein
PBP1	penicillin-binding protein 1
PBP2B	penicillin-binding protein 2B
PBP3	penicillin-binding protein 3
Ph	phenyl
PivCl	trimethylactetyl chloride
pTsOH	p-toluenesulfonic acid
RCM	ring-closing metathesis
RFP	red fluorescent protein
ROS	reactive oxygen species
S	singlet
S. aureus	Staphylococcus *aureus*
SaFtsZ	Staphylococcus *aureus* filamenting temperature sensitive mutant Z
SAR	Structure Activity Relationships
SepF	Cell division protein SepF
S_NAr	nucleophilic aromatic substitution reaction
STD NMR	Saturation transfer difference nuclear magnetic resonance

SulA	cell division inhibitor SulA
t	triplet
TBAF	tetrabutylammonium fluoride
TBAI	tetrabutylammonium iodide
TBS	tert-butyldimethylsilyl
TBSCl	tert-butyldimethylsilyl chloride
ter	DNA replication terminus
TFA	trifluoroacetic acid
THF	tetrahydrofuran
TMEDA	tetramethylethylenediamine
TMS	trimethylsilyl
TPP·Cl$_2$	triphenylphosphine dichloride
UDP	uridine diphosphate
UgtP	processive diacylglycerol beta-glucosyltransferase
VRE	vancomycin-resistant *Enterococci*
VREF	vancomycin-resistant Enterococcus *faecium*
XPhos	2-Dicyclohexylphosphino-2′,4′,6′-triisopropylbiphenyl
ZapA	cell division protein ZapA or Z ring-associated protein A
ZapB	cell division protein ZapB
ZipA	Cell division protein ZipA or FtsZ interacting protein A

Chapter 1

Chrysophaentin A: Isolation, Structural Assignment, and Antimicrobial Activity

1.1 Chrysophaentin A Isolation, Geographic Variability, and Structure

Chrysophaentin A (**1.1**) was isolated from the marine alga *Chrysophaeum taylori (C. taylori)* in 2007 off the coast of the U.S. Virgin Island St. John by Bewley and co-workers.[1] The alga was collected to discover new antimicrobial natural products by bioassay-guided fractionation of alga extracts. C. *taylori* is a benthic microalga that grows on coral reefs and rocky or sandy surfaces. The alga has been isolated in both tropical and temperate waters off the coasts of Australia, Puerto Rico, and the U.S. Virgin Islands.[2] However, the alga is relatively rare and the appearance of the alga can vary from year to year due to major weather events and other nutrient stressors, making the collection and isolation of secondary metabolites difficult. The original collection in 2007 yielded 200 grams of C. *taylori* and the methanol extract of the alga was found to inhibit the growth of Gram-positive bacteria including drug-resistant S. *aureus.*[1] The methanol extract was fractionated by reverse-phase HPLC leading to the identification of nine new antimicrobial secondary metabolites. The structures of the nine new secondary metabolites were assigned following extensive 2D-NMR and tandem mass spectrometry analysis. The common core structure of eight of the nine metabolites was a bis-biaryl ether macrocycle, composed of two biaryl ethers inter-linked by two *E*-chlorobutene fragments. The remaining secondary metabolite was assigned an open-chain linear structure (Figure 1.1). The nine new natural products were named chrysophaentin A-H and were isolated in the following quantities: chrysophaentin A (**1.1**) (3.5 mg), chrysophaentin B (**1.2**) (400 ng), chrysophaentin C (**1.3**) (800 ng), chrysophaentin D (**1.4**)

(1.8 mg), chrysophaentin E (**1.5**) (2.6 mg), chrysophaentin F (**1.8**) (1.5 mg), chrysophaentin G (**1.9**) (1.4 mg), and chrysophaentin H (**1.10**) (700 ng).

Bewley and co-workers returned to the isolation site (St. John) in 2009 to attempt a second isolation of the chrysophaentins. However, this time they collected *C. taylori* from both the Northern and Southern coasts of the island. Interestingly the Northern alga collection contained two new linear chrysophaentins, chrysophaentin E2 (**1.6**) and E3 (**1.7**), as well as the previously isolated symmetrically linked chrysophaentins F-H (**1.8-1.10**) (Figure 1.1).[3] However, the asymmetric, and more potent, chrysophaentins (A-D) were not isolated from these collection samples.[3] The isolated alga from the Southern side of the island contained the same distribution of symmetrical, asymmetrical, and linear chrysophaentins (A-H) as the original collection. To date, the chrysophaentins have only been isolated from *C. taylori* samples collected off the coast of U.S. Virgin Island St. John. Like other alga derived marine natural products, there appears to be a geographical and seasonal variability of production of these metabolites by *C. taylori*. Bewley and co-workers have made several unsuccessful attempts to locate *C. taylori* to isolate larger quantities of chrysophaentins A-H, indicating a need for an alternate supply source to advance the study of their antimicrobial properties.

1.1.1 Structural Analysis of Chrysophaentins A-H

The core structure of the macrocyclic chrysophaentins incorporates a cyclophane-like ring system.[1] The chrysophaentin structure can be further sub-divided into three structural classes consisting of four asymmetrical macrocycles [chrysophaentin A-D (**1.1-1.4)**], three symmetrical macrocycles [chrysophaentin F-H (**1.8-1.10**)], and three linear chrysophaentins [chrysophaentin E

(**1.5**), E2 (**1.6**), and E3 (**1.7**)] (Figure 1). The isolation of chrysophaentin E (**1.5**), E2 (**1.6**), and E3 (**1.7**) provide clues about their biosynthesis. Presumably, the three linear (open-chain) chrysophaentins, chrysophaentin E (**1.5**), E2 (**1.6**), and E3 (**1.7**) are shunt metabolites along the biosynthetic pathway leading to the macrocyclic chrysophaentins. Enzymatic oxidative cyclization of the linear (open-chain) metabolites at either C16 or C14 would result in the production of macrocyclic chrysophaentin A-D and F-H (Figure 1).

chrysophaentin A (**1.1**): X = Y = Cl
chrysophaentin B (**1.2**): X = Br, Y = Cl
chrysophaentin C (**1.3**): X = Cl, Y = Br
chrysophaentin D (**1.4**): X = Y = Br

chrysophaentin E (**1.5**): X = Y = Cl
chrysophaentin E2 (**1.6**): X = Cl; Y = Br
chrysophaentin E3 (**1.7**): X = Br; Y = Br

chrysophaentin F (**1.8**): X = Y = Cl; Z = H
chrysophaentin G (**1.9**): X = Br; Y = Cl; Z = H
chrysophaentin H (**1.10**): X = Y = Cl; Z =Br
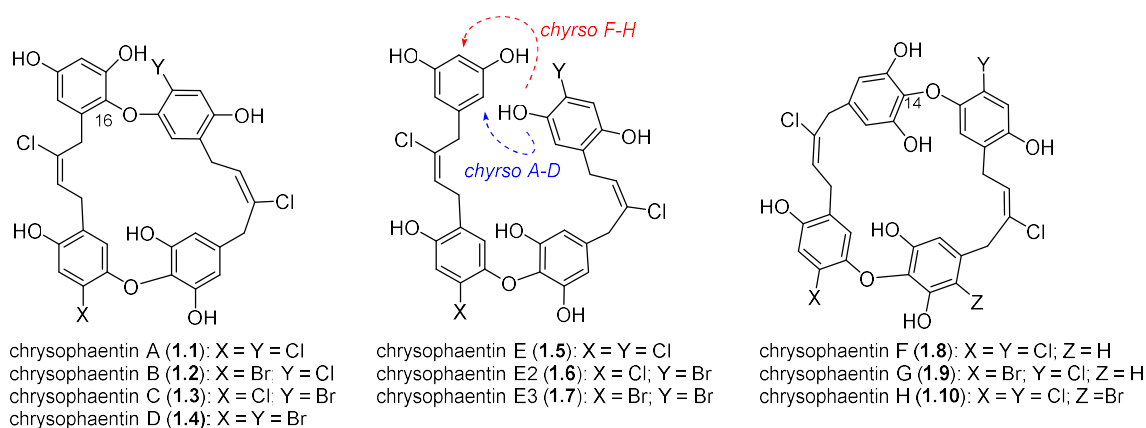
Figure 1.1. Structures of chrysophaentins A-H.

In this way, chrysophaentin E (**1.5**) could undergo an enzymatic cyclization at carbon 16 to afford chrysophaentin A (**1.1)**, while chrysophaentin E2 (**1.6**) would afford chrysophaentin C (**1.3**) and chrysophaentin E3 (**1.7**) would afford chrysophaentin D (**1.4**). Finally, chrysophaentin E (**1.5**) could undergo cyclization at C14 which would afford the symmetrically linked chrysophaentin F (**1.8**) (Figure 1). To address variable production of the chrysophaentins, Bewley and co-workers attempted laboratory culture of the producing alga.[2]

3

1.2   Laboratory Culture of *C. taylori*

Bewley and Davison[2] attempted the laboratory culture of *C. taylori* to access larger quantities of the chrysophaentins A-H. The *C. taylori* alga used for laboratory culture was acquired from the Japanese National Institute for Environmental Studies (NIES) microbial culture collection. The NIES *C. taylori* alga was originally isolated off the coast of Iriomote island in Okinawa, Japan. Genome comparison of the alga isolated from the U.S. Virgin Island St. John, to the alga from the NIES collection indicated a 99.7% sequence similarity. High conservation in the genomes of the two algae supported the likely presence of the biosynthetic machinery necessary for chrysophaentin production. However, the laboratory culture of C. *taylori* did not afford any of the known macrocyclic chrysophaentins A-D (**1.1-1.4**) or F-H (**1.8-1.10**). The major isolated metabolite from the alga extract was hormothamnione (**1.15**) (Figure 1.2), a known *C. taylori* secondary metabolite, which has been previously isolated from C. *taylori* off the coast of Puerto Rico.[4] The remaining chromatographic peaks from the extract of the lab culture were analyzed with electrospray ionization mass spectrometry (ESIMS) and were found to be polyhalogenated secondary metabolites based on their spectroscopic isotopic abundance patterns. The structures of the new polyhalogenated compounds were assigned based on extensive 2D-NMR and tandem mass spectrometry analysis. The new secondary metabolites were identified as four new linear chrysophaentin analogs, a chrysophaentin E analog, Chrysophaentin I (**1.11**), and three hemi-chrysophaentin analogs **1.12, 1.13** and **1.14,** which represent the Eastern and Western halves of chrysophaentins A-F (Figure 1.2).
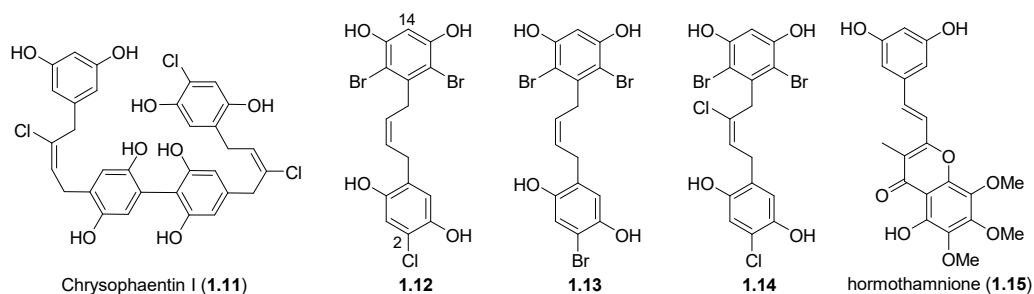
Figure 1.2. Structures of metabolites isolated from lab culture of *C. taylori*.

The newly isolated metabolites appear to be non-cyclized, halogenated shunt metabolites (**1.12, 1.13**, and **1.14**). The newly identified chrysophaentins were tested for growth inhibition of Gram-positive bacteria and were found to inhibit the growth of S. *aureus*, albeit with decreased potency with an MIC_{50} of ~10-40 μg/mL, compared to the chrysophaentins A-H's MIC_{50} range of ~1.8-25 μg/mL. Bewley and co-workers hypothesized that hemi-chrysophaentins **1.12**, **1.13**, and **1.14** are shunt metabolites diverging from the biosynthetic pathway, that are subjected to bromination at C12 and C16 thus preventing oxidative dimerization and cyclization, en route to chrysophaentins A-H. Hemi-chrysophaentins **1.12** and **1.13** did not contain the *E*-chloroalkene as is seen with the chrysophaentin A-H and the absence of the *E*-chloroalkene resulted in a further decrease in the antimicrobial activity against S. *aureus*, MIC_{50} of 10 μg/mL for *E*-chloroalkene containing, **1.14**, compared to ~40 μg/mL for **1.12** and **1.13**.[2] The decrease in potency indicates the importance of the *E*-chloroalkene moiety for the observed antimicrobial activity of the chrysophaentins. The most interesting metabolite isolated from the laboratory culture was the biaryl chrysophaentin I (**1.11**). Chrysophaentin I (**1.11**) is structurally similar to chrysophaentin E (**1.5**), and could theoretically be generated by a radical-mediated dechlorination-dimerization of two separate hemi-chrysophaentins **1.12** at C2 and C14. The isolation of the hemi-chrysophaentins **1.12, 1.13,** and **1.14** along with chrysophaentin I (**1.11**) provide insight into the biosynthetic

pathway of the chrysophaentins, indicating that hemi-chrysophaentins are generated first, followed by dimerization and cyclization to afford the macrocyclic chrysophaentins A-D (**1.1-1.4**) and F-H (**1.8-1.10**). However, no studies into the actual biosynthesis have been conducted at this time. Davison and Bewley[2] attempted to gather insights from the sequencing of the *C. taylori* genome, however, they were unsuccessful in determining which genes are responsible for the production of chrysophaentins A-H. Since the laboratory culture of *C. taylori* did not yield chrysophaentins A-H, a total synthesis would be required to access large enough quantities for biological study. A review of the synthetic approaches to chrysophaentin A (**1.1**) and F (**1.8**), along with our total synthesis of 9-dechlorochrysophaentin congeners will be discussed in Chapter 2. The following section will describe the antimicrobial activity and proposed target of chrysophaentin A (**1.1**).

1.3 Biological Activity and Proposed Target of Chrysophaentins A-H

Chrysophaentins A-H were found to inhibit the growth of Gram-positive bacteria, including clinically relevant drug-resistant bacterial strains such as methicillin-resistant staphylococcus *aureus* (MRSA) and vancomycin-resistant enterococcus *facecium* (VREF). The antimicrobial activity was determined with agar disk diffusion and microbroth dilution assays per the Clinical & Laboratory Standards Institute (CLSI) guidelines. The activity of the chrysophaentins is outlined in the table below (Table 1.1). Chrysophaentin A (**1.1**) was identified to be the most potent available chrysophaentin, showing a growth inhibition of Gram-positive bacteria with an MIC_{50} range of 1.8-3.8 µg/mL or 2.2-5.6 µM. Chrysophaentin F (**1.8**), a, symmetrically, linked chrysophaentin, was 2-5 fold less active compared to asymmetrically linked chrysophaentin A (**1.1**). Furthermore, chrysophaentin E (**1.5**), a linear (open-chain)

chrysophaentin, was 6-10 fold less active compared to chrysophaentin A (**1.1**). The loss of activity seen with the symmetrically linked and linear chrysophaentins provides circumstantial evidence that the overall macrocyclic structure and conformation of chrysophaentin A (**1.1**) could be important for its observed antimicrobial activity. Continuing their work, Bewley and co-workers evaluated the chrysophaentins against a panel of clinically relevant drug- and multi-drug resistant S. *aureus* isolates and found that chrysophaentin A, D, E, F, G, and H inhibited the growth of all of the strains tested, including multi-drug resistant S. *aureus* strains,[3] indicating that the chrysophaentins have a high therapeutic potential as new antimicrobials. Chrysophaentin A (**1.1**) was once again found to be the most active of the chrysophaentins with an MIC_{50} range of 1.8-5.1 µM and MIC_{90} range of 4.6-9.2 µM. The MIC_{50} and MIC_{90} are the concentrations at which there is an observed 50% or 90% decrease in bacterial cell growth, respectively. Chrysophaentin A (**1.1**) was determined to be bacteriostatic at its MIC_{90} and only became bactericidal at four to eight times the MIC_{90}.[3]

Table 1.1. Antimicrobial activity of chrysophaentin A-H.

Compound	Agar Disk (µg/disk)[a]				Microbroth MIC_{50} (µg/mL)			
	S. aureus	MRSA	E. faecium	VREF	S. aureus	MRSA	E. faecium	VREF
Chrysophaentin A (1.1)	2	2	2	2	1.8 ± 0.6	1.5 ± 0.7	3.8 ± 1.9	2.9 ± 0.8
Chrysophaentin D (1.4)	25	25	25	25	>25	20 ± 6.5	>50	>25
Chrysophaentin E (1.5)	25	10	10	10	11 ± 3.8	8.9 ± 2.8	>25	>25
Chrysophaentin F (1.8)	10	10	10	10	5.3 ± 2.0	4.2 ±1.3	>25	9.5 ± 3.0
Chrysophaentin G (1.9)	NA[b]	NA	NA	NA	17 ± 5.4	12 ± 3.1	>50	25 ± 7.3
Chrysophaentin H (1.10)	5	5	10	10	4.5 ±1.4	4.7 ± 1.4	>25	9.4 ± 2.8

[a]Lowest concentrations leading to 7-10 mm zones of inhibition. [b]NA, no zone of inhibition observed at 25 µg/disk. [c] Data adapted from Davison and Bewley[1].

Based on structural similarities to compounds reported in the literature, for example, Zantrin Z1 (**1.25**) (Figure 1.4),[5] chrysophaentins A-H were hypothesized to inhibit bacterial cytoskeletal protein, FtsZ.[1] FtsZ is a bacterial cytoskeletal protein essential for bacterial division cell division.[6] FtsZ undergoes a GTP-dependent polymerization to form a ring-like complex, called the Z-ring. The Z-ring forms at the midline of the cell and marks the site of cell division and acts as a scaffold for the recruitment and formation of the division complex or divisome. [7] A detailed discussion of FtsZ, its role, and function in bacterial cell division will be discussed in Chapter 3. The importance of FtsZ as an antimicrobial target will be discussed in section 1.4.

1.3.1 Preliminary Assessment of Chrysophaentin A as an FtsZ Inhibitor

Bewley and co-workers[1] demonstrated chrysophaentin A (**1.1**) binds to the GTP binding pocket of FtsZ through saturation transfer duration (STD) NMR. Competition STD NMR experiments were conducted in which increasing amounts of 5'-*O*-(3-thiotriphosphate) (GTPγS), a high-affinity GTP analog which cannot undergo hydrolysis, is titrated into a solution containing chrysophaentin A (**1.1**) and recombinant FtsZ. GTPγS was added to a solution containing a 100:1 complex of chrysophaentin A (**1.1**) and FtsZ. Proton NMR spectra were recorded at increasing concentrations of GTPγS and uniform decrease in chrysophaentin A (**1.1**) proton signals were observed, as well as, the formation of new proton signals corresponding to GTPγS. The STD NMR experiments demonstrated that chrysophaentin A (**1.1**) binds to the GTP binding site of FtsZ and that GTPγS competitively displaces chrysophaentin A (**1.1**), confirming chrysophaentin A (**1.1**) binds at the GTP-binding domain of FtsZ.

To determine whether chrysophaentin A's (**1.1**) binding to the GTP-binding site of FtsZ affects the GTPase activity, a malachite green-phosphomolybdate colorimetric assay was

conducted using chrysophaentin A (**1.1**) and recombinant E. *coli* FtsZ (EcFtsZ) and S. *aureus* FtsZ (SaFtsZ). The malachite green phosphomolybdate colorimetric assay is an end-point assay that measures the production of inorganic phosphate from the hydrolysis of GTP to GDP. Chrysophaentin A (**1.1**) was found to inhibit the GTPase activity of EcFtsZ with an IC_{50} of $9.9 \pm 2.5\ \mu M$ and SaFtsZ with an IC_{50} of $67 \pm 13\ \mu M$.[1,8] The GTPase inhibition coupled with STD NMR data, indicates that chrysophaentin A (**1.1**) is a competitive inhibitor of the GTPase activity of FtsZ by binding to the GTP-binding site. The ability of chrysophaentin A (**1.1**) to inhibit the activity of recombinant E. *coli* FtsZ, indicates that the chrysophaentins have the potential for broad-spectrum activity against both Gram-positive and Gram-negative bacteria and are most likely not getting through the outer membrane of Gram-negative bacteria.

To further test their hypothesis that the chrysophaentin A (**1.1**) has the potential of broad-spectrum activity, Bewley and co-workers treated the E. *coli* strain, *envA1* E. *coli*, which contains mutated UDP-3-O-acyl-GlcNAc deacetylase gene, with chrysophaentin A (**1.1**). The mutated UDP-3-O-acyl-GlcNAc is known to increase cell membrane permeability to antibiotics that traditionally cannot enter Gram-negative bacteria. Chrysophaentin A (**1.1**) inhibited the growth of *envA1* E. *coli* with an MIC_{50} of $27 \pm 9\ \mu M$, confirming that chrysophaentin A (**1.1**) has a conserved target in both Gram-positive and Gram-negative bacteria and is unable to pass through the outer membrane of Gram-negative bacteria, but with structural modification, could be developed as a broad-spectrum antibiotic.

To determine the effect of FtsZ GTPase inhibition caused by the binding of chrysophaentin A (**1.1**) to the GTP binding site of FtsZ on Z-ring formation, fluorescently labeled FtsZ protein fusions (pFtsZ-YFP) were expressed in *envA1* E. *coli.* Untreated *envA1* E. *coli,* when visualized under fluorescent microscopy, contained distinct bands at the midline of the cell, corresponding to

the formation of the Z-ring containing pFtsZ-YFP. However, when *envA1* E. *coli* was treated with chrysophaentin A (**1.1**) the Z-ring broke up and delocalized throughout the cell.[8] These initial studies on chrysophaentin A (**1.1**) binding to FtsZ and the observed delocalization of the Z-ring from the midline of the cell indicate that chrysophaentin A (**1.1**) is an inhibitor of the GTPase activity of FtsZ, and the binding of chrysophaentin A (**1.1**) to FtsZ inhibits the polymerization of FtsZ monomers into polymers, preventing the formation of the Z-ring complex. Bewley and co-workers also demonstrated that treatment of E. *coli* with chrysophaentin A (**1.1**) causes the destabilization of FtsZ protofilaments resulting in the delocalization of already formed Z-rings as well as preventing the formation of new Z-rings.[8] The inhibition of FtsZ is a novel mechanism of action that has not been targeted by a clinically approved antibiotic. However, due to the limited supply of chrysophaentin A (**1.1**) from isolation,[1] the variable of growth of the alga, and the inability of lab culture of *C. taylori* to produce chrysophaentin A (**1.1**),[2] a total synthesis would be required to continue the investigation into their promising antimicrobial activity. Synthetic efforts towards the total synthesis of chrysophaentin A (**1.1**) and F (**1.8**) will be discussed in Chapter 2. The next section will discuss the importance of FtsZ as an antimicrobial target.

1.4 FtsZ a Target for New Antibiotics?

Multidrug-resistant infections are a major health crisis that we are currently facing, with more than 2.8 million antibiotic-resistant infections a year, and over 35,000 deaths in the United States alone. The most recent report on antimicrobial resistance from the CDC has increased the antibiotic resistance threat list, to a total of 18 pathogens, with 5 urgent threats, 2 new threats, and 3 new-watch list threats.[9] The need for new antibiotics with new mechanisms of action are essential

for human health. Due to the key role FtsZ plays in bacterial cell division, it has been at the forefront of antibiotic research with numerous natural products and small molecules being identified as potential inhibitors of Z-ring formation and bacterial cell division.[10–13] Inhibition of FtsZ with small molecules results in the inhibition of FtsZ polymerization and Z-ring formation. The inhibition of Z-ring formation prevents cell division resulting in elongated or filamentous cells with delocalized FtsZ (Figure 1.3).[13]
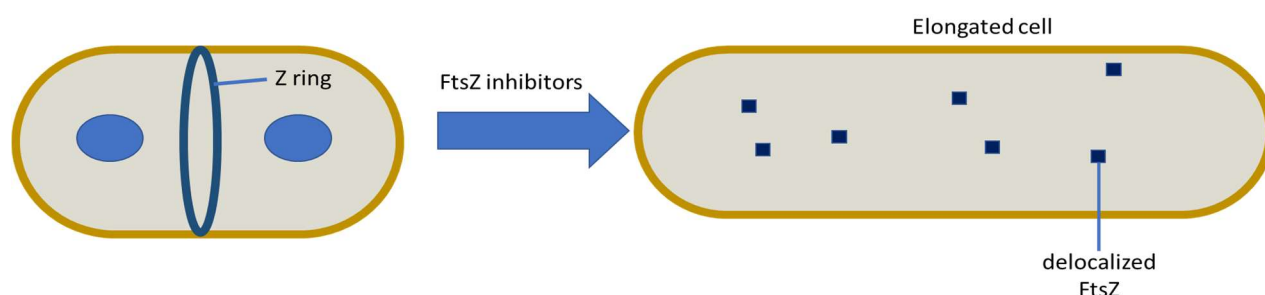
Figure 1.3. FtsZ inhibitors cause elongated phenotype.

Elongated and filamentous cells become susceptible to environmental stressors, such as osmotic pressure, leading to cell lysis and death. It has also been demonstrated that inhibition of FtsZ can lead to sensitization of drug-resistant bacteria to β-lactam antibiotics,[14] which could allow for the development of adjuvant therapeutics to help combat antimicrobial resistance through combination therapies. Outlined below, is a brief review of selected FtsZ inhibitors, their initial identification, reported activity, and key issues that have become apparent when studying FtsZ inhibiting antimicrobials. The inhibitors listed below can be divided into two classes of molecules, natural products, and small molecules. The small molecules were identified by high-throughput screening of small molecule libraries or medicinal chemistry campaigns based on small molecule ligand optimization. Historically, natural products have been a treasure trove for the discovery of new antibiotics.[15] However, due to the difficulty of isolation and resource and time-intensive total syntheses, they have been under studied and avoided by the pharmaceutical industry. The first well

studied natural product inhibitors of FtsZ polymerization were the berberines and sanguinarines (Figure 1.4, **1.16,** and **1.18**).

Berberine (**1.16**) is an alkaloid based natural product, isolated from the plant species *Berberis*, which has a rich history of use in Chinese and Native American medicine to fight various types of infections. Berberine (**1.16**) was found to target FtsZ in E. *coli*, and treatment of E. *coli* with berberine (**1.16**) resulted in the inhibition of Z-ring formation and cytokinesis. [16] Inhibition of FtsZ polymerization was detected utilizing a light-scattering assay, which demonstrated a dose-dependent decrease of FtsZ polymerization with an IC_{50} of 10 µM, and was further characterized by transmission electron microscopy of FtsZ protofilaments *in vitro.* Confirmation of berberine (**1.16**) binding to FtsZ was accomplished by fluorescence spectroscopy and STD NMR. The combination of binding and the *in vitro* inhibition of FtsZ polymerization indicted the mechanism of action of berberine (**1.16**) is through FtsZ inhibition. Furthermore, the treatment of GFP-labeled FtsZ (GFP-FtsZ) in E. *coli* resulted in disperse green fluorescence throughout the cell, and filamentous cell morphology was also observed, further confirming the mechanism of action of berberine (**1.16**).

berberine (**1.16**)

berberine 2 (**1.17**)

sanguinarine (**1.18**)

chrysophaentin A (**1.1**)

viridotoxin (**1.19**)

dichamanetin (**1.20**)

totarol (**1.21**)

colchicine (**1.22**)

SRI-3072 (**1.23**)

zantrin Z3 (**1.24**)

zantrin Z1 (**1.25**)

X = N, PC190723 (**1.26**)
X = CH, 8J (**1.27**)
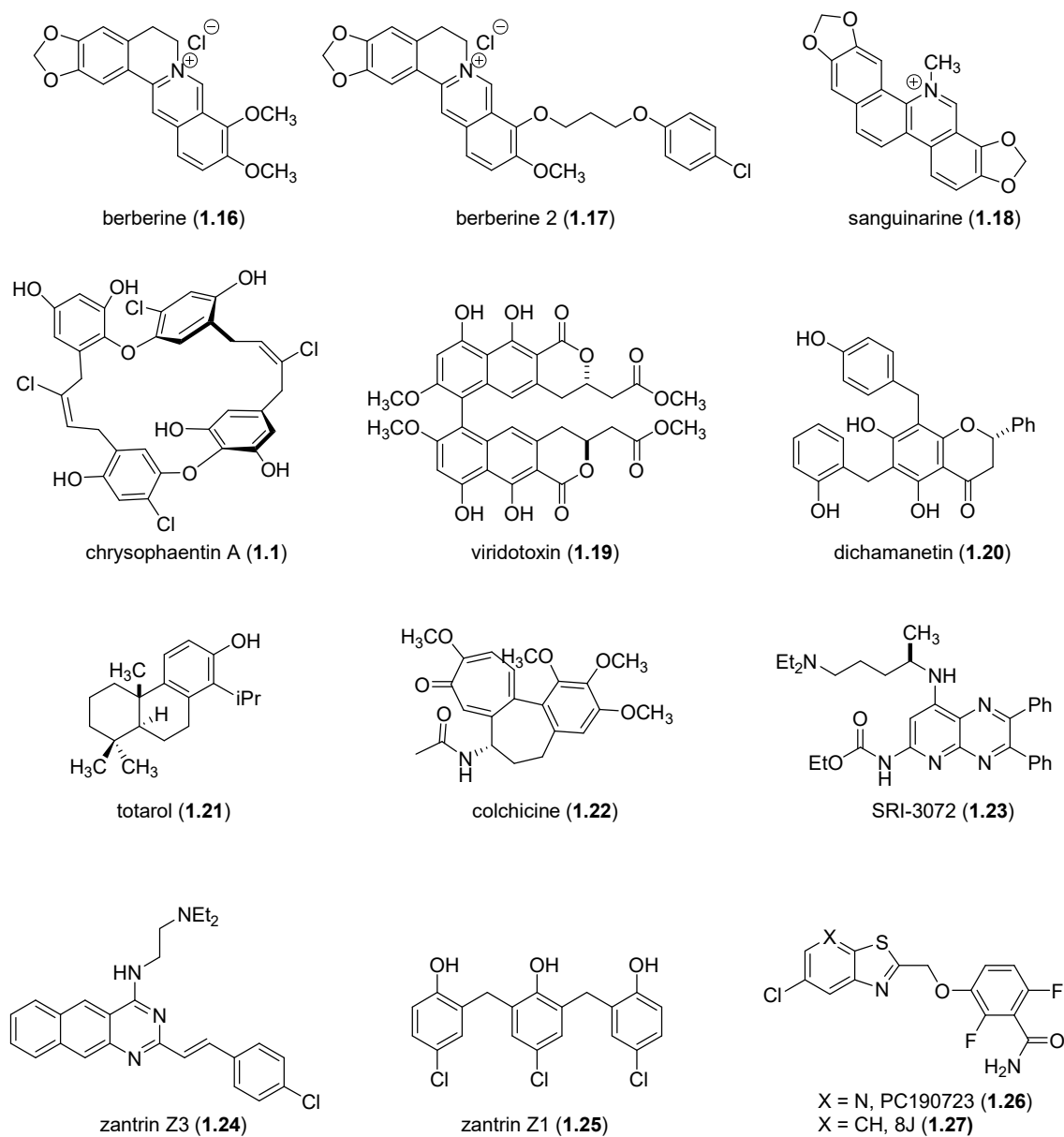
Figure 1.4. Examples of reported FtsZ interacting small molecules.

However, later work by Bewley and co-workers discovered that berberine (**1.16**) is itself autofluorescent and the diffuse fluorescence seen in previous studies was due to berberine's (**1.16**) autofluorescence and not due to the delocalization of GFP-labeled FtsZ.[8] This was further confirmed through the expression of a red fluorescent protein fusion of FtsZ (RFP-FtsZ), where treatment of berberine (**1.16**) did not lead to the dispersion of the Z-ring structure, indicating the

mechanism of berberine (**1.16**) is most likely not due to FtsZ inhibition but through another antimicrobial mechanism of action.[8]

Another reported natural product inhibitor of FtsZ is viriditoxin (**1.19**). Viriditoxin (**1.19**) was originally isolated and identified in 1971 and was found to be cytotoxic to mice with an LD_{50} of 2.8 mg/kg. [17] However, the original report incorrectly reported the structure and in 1990, a revised structure was reported.[18] The original report did not test whether viriditoxin (**1.19**) had any antimicrobial activity. However, in 2003, Merck pharmaceuticals developed a high-throughput FTsZT65C-fluorescein polymerization assay and screened the extracts from over 10,000 microbial fermentations and plant extracts to identify novel FtsZ inhibitors.[19] All active extracts were also tested for filamentous cell morphology and SOS induction to confirm FtsZ inhibition was the primary mechanism of action for the observed filamentous cell morphology. Viriditoxin (**1.19**) was isolated from the most promising extract and was found to inhibit the polymerization of FtsZ and GTPase activity with an IC_{50} of 8.2 μg/mL (~ 10 μM) and an IC_{50} of 7.0 μg/mL, respectively.[19] The mechanism of FtsZ inhibition was confirmed by observations of filamentous cell morphology, absence of SOS induction, and an increased inhibitory concentration of viriditoxin (**1.19**) was needed when FtsZ was overexpressed.

However, later attempts to reproduce and confirm the FtsZ inhibition of viriditoxin (**1.19**) in either B. *subtilis* or E. *coli* by Shaw group were unsuccessful. The Shaw group determined that only under very specific assay conditions does viriditoxin (**1.19**) inhibit FtsZ GTPase activity, but were unable to reproduce the results from the original report themselves.[10] Viriditoxin's toxicity and structural instability presented major hurdles for the development of viriditoxin (**1.19**) as an FtsZ targeting antimicrobial therapeutic.

Dichamanetin (**1.20**) is a flavone based natural product isolated from U. *chamae* and X. *africana* and exhibited antimicrobial activity against Gram-positive bacterial strains with similar MIC values to zantrin Z1 (**1.25**).[20] Based on the structural similarities of dichamanetin (**1.20**) to the zantrins, which will be discussed later, the Shaw group set out to complete the total synthesis of dichamanetin (**1.20**) and test its ability to inhibit FtsZ.[21] Following the total synthesis of dichamanetin (**1.20**), it was found to inhibit the GTPase activity of E. *coli* FtsZ *in vitro* with an IC$_{50}$ of 12.5 μM. This result provided evidence that the observed antimicrobial activity was likely caused by the inhibition of FtsZ. However, later studies by the Shaw group found that dichamanetin (**1.20**) forms aggregates in the GTPase assay, and when repeated in the presence of Triton X-100 buffer, a buffer known to reduce aggregation of small molecules, the observed FtsZ inhibition vanished.[10]

Dichamanetin (**1.20**) was later found to possess antiproliferative activity against cancer cell lines by affecting reactive oxygen species (ROS) signaling, causing DNA intercalation and causing a loss of mitochondrial membrane potential (MMP).[22] The ability of dichamanetin (**1.20**) to affect ROS and DNA intercalation could potentially result in the activation of the SOS response in bacteria, which results in the inhibition of FtsZ polymerization and a filamentous phenotype. The activation of the SOS response by dichamanetin (**1.20**) could explain the initial identification of FtsZ as the target and demonstrates the importance of a thorough investigation of the mechanism of action of reported FtsZ inhibitors.

As mentioned above, a promising class of small molecule FtsZ inhibitors is the zantrins. Zantrin Z3 (**1.24**) and zantrin Z1 (**1.25**) are two representative structures of the five zantrins identified in a high-throughput screen at Harvard Medical School.[5] The high-throughput screen was designed to look for small molecules that inhibit the GTPase activity of FtsZ through either

the destabilization or hyper-stabilization of FtsZ protofilaments.[5] The screen identified five new FtsZ modulating small molecules, however in the context of this document only zantrin Z3 (**1.24**) and zantrin Z1 (**1.25**) will be discussed. Zantrin Z1 (**1.25**) was found to destabilize FtsZ protofilaments, while zantrin Z3 (**1.24**) was found to stabilize the FtsZ protofilaments, indicating that FtsZ GTPase activity can be modulated in a similar two mechanism fashion as eukaryotic tubulin. The zantrins were found to inhibit the growth of both Gram-positive and Gram-negative strains and induced the disassembly of the Z-ring in E. *coli.* Interestingly, even though zantrin Z3 (**1.24**) was found to stabilize FtsZ protofilaments *in vitro*, the treatment of E. *coli* with zantrin Z3 (**1.24**) still resulted in a decrease in Z-ring formation. Later work by the Bewley and Shaw groups, independently reproduced and confirmed the observed FtsZ inhibitory activity of zantrin Z3 (**1.24**) in E. *coli.*[8,10] Zantrin Z3 (**1.24**) currently is one of the best FtsZ inhibitors that has been identified and had its activity reproduced independently by multiple groups. The reproducibility of zantrin Z3 (**1.24**) makes it a key positive control molecule for use in future studies of new FtsZ inhibitors.

Another promising natural product with broad-spectrum activity against bacteria is totarol (**1.21**). Totarol (**1.21**) is a diterpene secondary metabolite with antimicrobial activity against Mycobacterium *tuberculosis*, S. *aureus,* and *Streptococcus pneumoniae*, to name a few. Totarol (**1.21**) has also been identified as a key secondary metabolite in trees and helps protect trees from rot.[23] The total synthesis of totarol (**1.21**) has allowed for further investigation into the mechanism of action of its observed antimicrobial activity, and it was found to inhibit the GTPase activity of FtsZ in Mycobacterium *tuberculosis* and B. *subtilis.*[24] The Shaw group was able to complete the total synthesis of totarol (**1.21**) [25] and reproduced its observed FtsZ GTPase inhibition.[10] However, upon further inspection, they found that the GTPase activity of totarol (**1.21**) was abolished, in a similar manner seen with zantrin Z1 (**1.25**) and dichamanetin (**1.20**), when Triton X-100 buffer

was used in the GTPase activity. Based on the results of this study it has been determined that a number of reported FtsZ inhibitors derive their activity from aggregation and not direct small molecule-protein interaction.[10] This result indicates that the formation of aggregates should be a consideration when studying potential FtsZ inhibitors and that standard biochemical assay conditions need to be developed to accurately assess a small molecule or natural product's ability to inhibit FtsZ.

Over the past 20 years, benzamide containing small molecules have been extensively studied after 3-methoxybenzamide was found to have selective, but weak antimicrobial activity against B. *subtilis*. 3-methoxybenzamide was found to bind to FtsZ, through the use of genetic mutations resulting in the modulation of lethality. Prolysis, a start-up company out of Oxford University, undertook a medicinal chemistry campaign to design a more potent benzamide based inhibitor of FtsZ. Their efforts resulted in the design and synthesis of PC190723 (**1.26**), a potent benzamide based inhibitor of FtsZ in B. *subtilis* and *staphylococci* bacterial species, including drug and multi-drug resistant S. *arueus*.[26] PC190723 (**1.26**) was confirmed to inhibit the GTPase activity of recombinant S. *aureus* FtsZ and cause elongation or enlargement in B. *subtilis* and S. *aureus*, respectively. A cocrystal of PC190723 (**1.26**) and S. *aureus* FtsZ showed the binding pocket for PC190723 is located in a deep cleft formed by the H7 helix and T7 loop and that this region is unique from the GTP binding site.[14] Further investigation of PC190723 (**1.26**) indicated synergistic activity with β-lactam antibiotics, indicating its potential use as both a new antibiotic therapeutic or adjuvant therapeutic with β-lactam antibiotics.[14] PC190723 (**1.26**) is the most studied FtsZ inhibitor, however, contradictory reports about its mechanism of action and cross-species activity have become more common. The original report indicated inhibition of FtsZ GTPase activity in S. *aureus* and delocalization of FtsZ in B. *subtilis* to discrete foci in the bacterial

cell. However, Andreu and co-workers reported that PC190723 (**1.26**) stabilizes FtsZ protofilaments, contradicting the report of delocalization of the FtsZ to discrete foci.[27] Furthermore, two additional reports came out that indicated that PC190723 (**1.26**) does not inhibit the GTPase activity of FtsZ and actually induces a slight increase in the GTPase activity of S. *aureus* FtsZ.[10,28] The most recent contradictory report indicates that PC190723 (**1.26**), has an FtsZ independent mechanism of action in E. *coli*.[29] The combination of these reports demonstrates the difficulty of identifying FtsZ inhibitors with broad-spectrum activity.

PC190723 (**1.26**) has undergone further optimization by Taxis pharmaceuticals[30] and prodrug, TXA709[31], was developed to increase oral bioavailability and metabolic stability. Despite the contradictory evidence surrounding the mechanism of action of PC190723 (**1.26**), Taxis pharmaceuticals have taken prodrug, TXA709, into phase I clinical trials. The contradictory reports about PC190723 (**1.26**) can be contributed to two main factors, the complexity of bacterial cell division and the slight differences in cell division proteins and the divisome complex between different bacterial species. The cross-species activity and the mechanism of antimicrobial activity in different species of bacteria need to be confirmed independently of each other to ensure FtsZ is the target in the different bacterial species. As will be discussed in Chapter 3, E. *coli* and B. *subtilis* have different individual proteins that make up their respective divisomes, and the order in which the divisome is formed and the regulatory mechanisms vary from species to species. The development of standard biochemical assay conditions to measure the FtsZ GTPase activity which accounts for aggregation needs to be developed to allow for reproducible determination of FtsZ inhibitors and allow for comparison of FtsZ inhibitors to each other.

Even though the development of FtsZ inhibitors has been difficult, there is promise for the development of FtsZ inhibitors, as was seen with zantrin Z3 (**1.25**) and its confirmed mechanism

of action of targeting FtsZ. The development of FtsZ inhibitors is an important area of research to help our fight against antimicrobial resistance. Novel antimicrobial agents such as zantrin Z3 (**1.25**) and chrysophaentin A (**1.1**) could be key to fighting antimicrobial-resistant infections. The adaptation of standard biochemical assays, use of binding confirmation (STD NMR and X-ray crystallography), and resistant mutant generation can aid in the accurate identification of novel FtsZ inhibitors and reduce the number of false positives as was highlighted above.

Furthermore, the mechanism of antimicrobial activity needs to be determined independently in different bacterial species, due to differences in the divisome structure and formation in these different bacteria. The observation of filamentous cell morphology and delocalization of the Z-ring, as observed with fluorescently labeled FtsZ protein constructs, have become an important tool for the discovery of novel FtsZ inhibitors. However, filamentous cell morphology can result from activation of the SOS response and DNA damage and other cellular regulation processes should be accounted for in mechanism of action studies, like what was used for the determination of viriditoxin (**1.19**) mechanism of action.[17] The use of fluorescently labeled FtsZ protein fusions coupled with fluorescent microscopy has allowed for the observation of FtsZ localization and this data coupled with GTPase inhibition and cell elongation allows for higher confidence in FtsZ as a target. The future of the identification of novel FtsZ inhibitors is of utmost importance and the development and use of standard assay conditions, fluorescently-labeled FtsZ protein fusions and parallel assays to rule out SOS induction, aggregation or inhibition of other cell division proteins are a must, to accurately identify novel FtsZ inhibitors.

1.5 Conclusions

The chrysophaentins are a promising new class of natural products with antimicrobial activity against Gram-positive bacteria, including drug and multi-drug-resistant S. *aureus* and *VREF*. However, the producing alga C. *taylori* is quite rare and the production of the chrysophaentins varies based on geographic location and environmental stressors and weather.[3] Chrysophaentin A (**1.1**) was found to inhibit the GTPase activity of FtsZ and prevent the formation of the Z-ring, which results in the inhibition of bacterial cell division. To further investigate antimicrobial activity and mechanism of action of the chrysophaentins, a total synthesis is required. As discussed in the last section, numerous FtsZ inhibitors have been reported in the literature, however, reproducibility and reliability of biochemical assays have proven difficult, due to various factors such as aggregation and cross-species activity. The confirmation of the chrysophaentins mechanism of action will have to be based on the lessons learned from past experiments and with a fundamental knowledge of the regulation of FtsZ and the protein-protein interactions between FtsZ and the other divisome proteins.

In the remaining chapters of this thesis, I will outline the published synthetic approaches towards chrysophaentin A (**1.1**) and chrysophaentin F (**1.8**) and discuss my work on the total synthesis of four 9-dechlorochrysophaentin congeners. I will present preliminary biological data for the synthetic 9-dechlorochrysophaentins which elucidated a novel mechanism of cell wall synthesis inhibition, and finally, the remaining sections will discuss the role, formation and regulation of the Z-ring and hypothesize about potential protein targets that could explain the novel mechanism of cell wall synthesis inhibition caused by the chrysophaentins.

References:

(1)   Plaza, A.; Keffer, J. L.; Bifulco, G.; Lloyd, J. R.; Bewley, C. A. Chrysophaentins A−H, Antibacterial Bisdiarylbutene Macrocycles That Inhibit the Bacterial Cell Division Protein FtsZ. *Journal of the American Chemical Society* **2010**, *132* (26), 9069–9077. https://doi.org/10.1021/ja102100h.

(2)   Davison, J. R.; Bewley, C. A. Antimicrobial Chrysophaentin Analogs Identified from Laboratory Cultures of the Marine Microalga Chrysophaeum Taylorii. *Journal of Natural Products* **2019**, *82* (1), 148–153. https://doi.org/10.1021/acs.jnatprod.8b00858.

(3)   Keffer, J. L.; Hammill, J. T.; Lloyd, J. R.; Plaza, A.; Wipf, P.; Bewley, C. A. Geographic Variability and Anti-Staphylococcal Activity of the Chrysophaentins and Their Synthetic Fragments. *Marine Drugs*. 2012. https://doi.org/10.3390/md10051103.

(4)   Gerwick, W. H. *6-DESMETHOXYHORMOTHAMNIONE, A NEW CYTOTOXIC STYRYLCHROMONE FROM THE MARINE CRYPTOPHYTE CHRYSOPHAEUM TAYLORI*; Vol. 52.

(5)   Margalit, D. N.; Romberg, L.; Mets, R. B.; Hebert, A. M.; Mitchison, T. J.; Kirschner, M. W.; RayChaudhuri, D. Targeting Cell Division: Small-Molecule Inhibitors of FtsZ GTPase Perturb Cytokinetic Ring Assembly and Induce Bacterial Lethality. *Proceedings of the National Academy of Sciences of the United States of America* **2004**, *101* (32), 11821–11826. https://doi.org/10.1073/pnas.0404439101.

(6)   Lutkenhaus and, J.; Addinall, S. G. BACTERIAL CELL DIVISION AND THE Z RING. *Annual Review of Biochemistry* **1997**, *66* (1), 93–116. https://doi.org/10.1146/annurev.biochem.66.1.93.

(7)   Lutkenhaus, J.; Pichoff, S.; Du, S. Bacterial Cytokinesis: From Z Ring to Divisome. *Cytoskeleton* **2012**, *69* (10), 778–790. https://doi.org/10.1002/cm.21054.

(8)   Keffer, J. L.; Huecas, S.; Hammill, J. T.; Wipf, P.; Andreu, J. M.; Bewley, C. A. Chrysophaentins Are Competitive Inhibitors of FtsZ and Inhibit Z-Ring Formation in Live Bacteria. *Bioorganic & Medicinal Chemistry* **2013**, *21* (18), 5673–5678. https://doi.org/10.1016/j.bmc.2013.07.033.

(9)   Biggest Threats and Data | Antibiotic/Antimicrobial Resistance | CDC https://www.cdc.gov/drugresistance/biggest-threats.html (accessed Feb 26, 2020).

(10)   E. Anderson, D.; B. Kim, M.; T. Moore, J.; E. O'Brien, T.; A. Sorto, N.; I. Grove, C.; L. Lackner, L.; B. Ames, J.; T. Shaw, J. Comparison of Small Molecule Inhibitors of the Bacterial Cell Division Protein FtsZ and Identification of a Reliable Cross-Species Inhibitor. *ACS Chemical Biology* **2012**, *7* (11), 1918–1928. https://doi.org/10.1021/cb300340j.

(11)   Kusuma, K. D.; Payne, M.; Ung, A. T.; Bottomley, A. L.; Harry, E. J. FtsZ as an Antibacterial Target: Status and Guidelines for Progressing This Avenue. *ACS Infectious Diseases* **2019**, *5* (8), 1279–1294. https://doi.org/10.1021/acsinfecdis.9b00055.

(12)   Carro, L. Recent Progress in the Development of Small-Molecule FtsZ Inhibitors as Chemical Tools for the Development of Novel Antibiotics. *Antibiotics* **2019**, *8* (4), 217. https://doi.org/10.3390/antibiotics8040217.

(13)   Hurley, K. A.; Santos, T. M. A.; Nepomuceno, G. M.; Huynh, V.; Shaw, J. T.; Weibel, D. B. Targeting the Bacterial Division Protein FtsZ. *Journal of Medicinal Chemistry*. American Chemical Society August 11, 2016, pp 6975–6998. https://doi.org/10.1021/acs.jmedchem.5b01098.

(14)   Tan, C. M.; Therien, A. G.; Lu, J.; Lee, S. H.; Caron, A.; Gill, C. J.; Lebeau-Jacob, C.; Benton-Perdomo, L.; Monteiro, J. M.; Pereira, P. M.; et al. Restoring Methicillin-Resistant Staphylococcus Aureus Susceptibility to β-Lactam Antibiotics. *Science Translational Medicine* **2012**, *4* (126), 126ra35-126ra35. https://doi.org/10.1126/scitranslmed.3003592.

(15)   Newman, D. J.; Cragg, G. M. Natural Products as Sources of New Drugs from 1981 to 2014. *Journal of Natural Products*. American Chemical Society March 25, 2016, pp 629–661. https://doi.org/10.1021/acs.jnatprod.5b01055.

(16)   N. Domadia, P.; Bhunia, A.; Sivaraman, J.; Swarup, S.; Dasgupta, D. Berberine Targets Assembly of Escherichia Coli Cell Division Protein FtsZ. *Biochemistry* **2008**, *47* (10), 3225–3234. https://doi.org/10.1021/bi7018546.

(17)   Weisleder, D.; Lillehoj, E. B. Structure of Viriditoxin, a Toxic Metabolite of Aspergillus Viridi-Nutans. *Tetrahedron Letters* **1971**, *12* (48), 4705–4706. https://doi.org/10.1016/S0040-4039(01)97567-7.

(18)   SUZUKI, K.; NOZAWA, K.; NAKAJIMA, S.; KAWAI, K. Structure Revision of Mycotoxin, Viriditoxin, and Its Derivatives. *CHEMICAL & PHARMACEUTICAL BULLETIN* **1990**, *38* (11), 3180–3181. https://doi.org/10.1248/cpb.38.3180.

(19)   Wang, J.; Galgoci, A.; Kodali, S.; Herath, K. B.; Jayasuriya, H.; Dorso, K.; Vicente, F.; González, A.; Cully, D.; Bramhill, D.; et al. Discovery of a Small Molecule That Inhibits Cell Division by Blocking FtsZ, a Novel Therapeutic Target of Antibiotics. *Journal of Biological Chemistry* **2003**, *278* (45), 44424–44428. https://doi.org/10.1074/jbc.M307625200.

(20)   Hufford, C. D.; Lasswell, W. L. Antimicrobial Activities of Constituents of Uvaria Chamae. *Lloydia* **1978**, *41* (2), 156–160.

(21) Urgaonkar, S.; la Pierre, H. S.; Meir, I.; Lund, H.; RayChaudhuri, D.; Shaw, J. T. Synthesis of Antimicrobial Natural Products Targeting FtsZ: (±)-Dichamanetin and (±)-2‴-Hydroxy-5″- Benzylisouvarinol-B. *Organic Letters* **2005**, *7* (25), 5609–5612. https://doi.org/10.1021/ol052269z.

(22) Yong, Y.; Matthew, S.; Wittwer, J.; Pan, L.; Shen, Q.; Kinghorn, A. D.; Swanson, S. M.; Carcache De Blanco, E. J. Dichamanetin Inhibits Cancer Cell Growth by Affecting ROS-Related Signaling Components through Mitochondrial-Mediated Apoptosis. *Anticancer Research* **2013**, *33* (12), 5349–5355.

(23) Kubo, I.; Muroi, H.; Himejima, M. Antibacterial Activity of Totarol and Its Potentiation. *Journal of Natural Products* **1992**, *55* (10), 1436–1440. https://doi.org/10.1021/np50088a008.

(24) Jaiswal, R.; Beuria, T. K.; Mohan, R.; Mahajan, S. K.; Panda, D. Totarol Inhibits Bacterial Cytokinesis by Perturbing the Assembly Dynamics of FtsZ. *Biochemistry* **2007**, *46* (14), 4211–4220. https://doi.org/10.1021/bi602573e.

(25) Kim, M. B.; Shaw, J. T. Synthesis of Antimicrobial Natural Products Targeting FtsZ: (+)-Totarol and Related Totarane Diterpenes. *Organic Letters* **2010**, *12* (15), 3324–3327. https://doi.org/10.1021/ol100929z.

(26) Haydon, D. J.; Stokes, N. R.; Ure, R.; Galbraith, G.; Bennett, J. M.; Brown, D. R.; Baker, P. J.; Barynin, V. v.; Rice, D. W.; Sedelnikova, S. E.; et al. An Inhibitor of FtsZ with Potent and Selective Anti-Staphylococcal Activity. *Science* **2008**, *321* (5896), 1673–1675. https://doi.org/10.1126/science.1159961.

(27) Andreu, J. M.; Schaffner-Barbero, C.; Huecas, S.; Alonso, D.; Lopez-Rodriguez, M. L.; Ruiz-Avila, L. B.; Núñez-Ramírez, R.; Llorca, O.; Martín-Galiano, A. J. The Antibacterial

Cell Division Inhibitor PC190723 Is an FtsZ Polymer-Stabilizing Agent That Induces Filament Assembly and Condensation. *Journal of Biological Chemistry* **2010**, *285* (19), 14239–14246. https://doi.org/10.1074/jbc.M109.094722.

(28)   Elsen, N. L.; Lu, J.; Parthasarathy, G.; Reid, J. C.; Sharma, S.; Soisson, S. M.; Lumb, K. J. Mechanism of Action of the Cell-Division Inhibitor PC190723: Modulation of FtsZ Assembly Cooperativity. **2012**. https://doi.org/10.1021/ja303564a.

(29)   Khare, S.; Hsin, J.; Sorto, N. A.; Nepomuceno, G. M.; Shaw, J. T.; Shi, H.; Huang, K. C. FtsZ-Independent Mechanism of Division Inhibition by the Small Molecule PC190723 in Escherichia Coli. *Advanced Biosystems* **2019**, *3* (11), 1900021. https://doi.org/10.1002/adbi.201900021.

(30)   Kaul, M.; Mark, L.; Zhang, Y.; Parhi, A. K.; LaVoie, E. J.; Pilch, D. S. An FtsZ-Targeting Prodrug with Oral Antistaphylococcal Efficacy in Vivo. *Antimicrobial Agents and Chemotherapy* **2013**, *57* (12), 5860–5869. https://doi.org/10.1128/AAC.01016-13.

(31)   Kaul, M.; Mark, L.; Zhang, Y.; Parhi, A. K.; Lyu, Y. L.; Pawlak, J.; Saravolatz, S.; Saravolatz, L. D.; Weinstein, M. P.; LaVoie, E. J.; et al. TXA709, an FtsZ-Targeting Benzamide Prodrug with Improved Pharmacokinetics and Enhanced in Vivo Efficacy against Methicillin-Resistant Staphylococcus Aureus. *Antimicrobial Agents and Chemotherapy* **2015**, *59* (8), 4845–4855. https://doi.org/10.1128/AAC.00708-15.

Chapter 2

Chemical Synthesis of Four 9-dechlorochrysophaentin's

2.1 Introduction

As outlined in Chapter 1, chrysophaentin A (**2.1**) (Figure 2.1) is an antimicrobial natural product possessing a novel chemical structure and was proposed to express its antimicrobial activity through the inhibition of FtsZ, an essential bacterial cell division protein. However, isolation of chrysophaentin A (**2.1**) from *C. taylori* has proven unreliable[1] and efforts to produce chrysophaentins A-H by laboratory culture of *C. taylori,* have failed.[2] Chemical synthesis appears to be the only remaining option to access chrysophaentin A (**2.1**) in quantity as well as providing the added benefit of access to synthetic analogs.[3]

To date, three groups have reported efforts directed towards the total synthesis of chrysophaentins A (asymmetric macrocycle and most potent antimicrobial activity), E (an open-chain shunt metabolite), and F (symmetrical macrocycle).[1,4,5] In the following sections I will describe the previously reported synthetic approaches towards these three chrysophaentins. Following the discussion of this background literature, I will highlight the work completed in our group towards the chemical synthesis of chrysophaentin A (**2.1**), and describe our work culminating in the chemical synthesis of four 9-dechlorochrysophaentin congeners.

2.2 Wipf's Synthesis of Hemi-chrysophaentin

In 2012 Bewley and co-workers, in collaboration with the Wipf group (University of Pittsburg), initiated a program toward developing a total synthesis of chrysophaentin A (**2.1**)[1] and possible identification of the minimum pharmacophore.[6] With this goal in mind, the Pittsburgh group initiated synthetic studies aimed at developing a chemical synthesis and evaluation of produced synthetic fragments obtained en route for antimicrobial and FtsZ inhibition activity. From a synthetic perspective, inspection of the chrysophaentin A (**2.1**) structure does not present any immediately obvious disconnections. The Wipf group elected to divide chrysophaentin A (**2.1**) into fragments by disconnection at the biaryl ether bonds at C14' and C16 and chrysophaentin F (**2.2**) at C14 and C14' (Figure 2.1). This bond disconnection produces two identical fragments (hemi-chrysophaentin (**2.4**)) as primary synthetic targets (Figure 2.1). In the forward sense, oxidative coupling between C1-phenol and C14' would produce chrysophaentin E (**2.3**) and depending on the position of the second oxidative coupling chrysophaentin A (**2.1**) and F (**2.2**) (Figure 2.1) could be afforded.
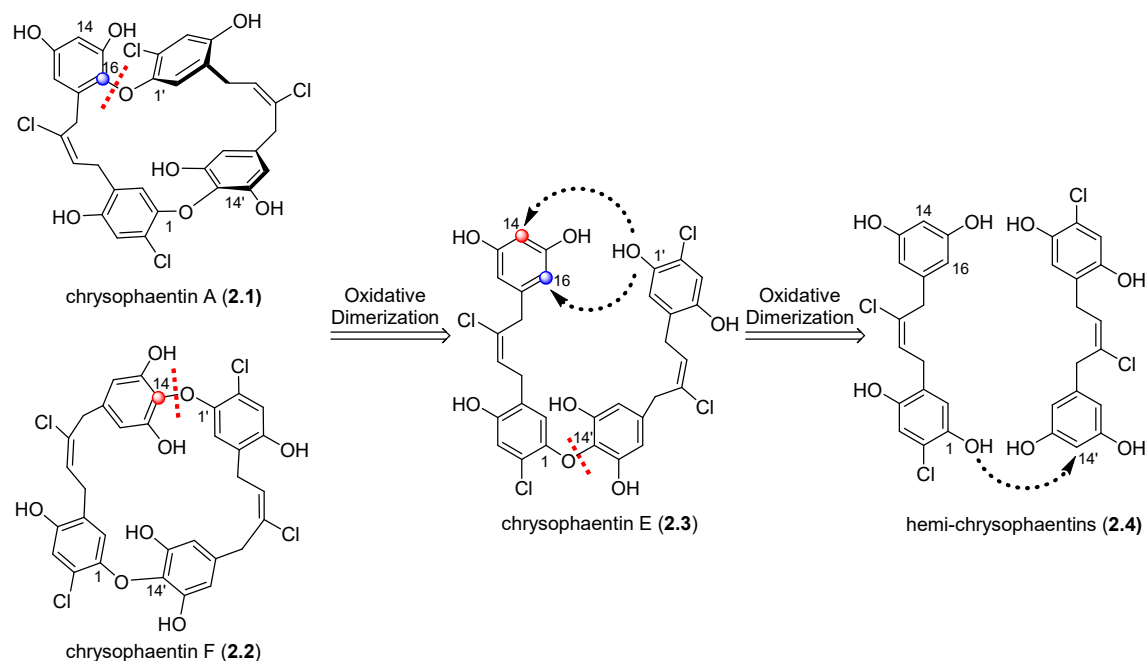
Figure 2.1. Retrosynthetic analysis reveals oxidative dimerization of hemi-chrysophaentins give rise to chrysophaentin A (**2.1**) or chrysophaentin F (**2.2**) via chrysophaentin E (**2.3**).

Wipf and co-worker's analysis of hemi-chrysophaentin (**2.4**) revealed bond disconnections between C8 and C7 leading to fragments **2.5** and **2.6** (Figure 2.2). In a forward sense, it was anticipated that hemi-chrysophaentin (**2.4**) could be derived from a Negishi coupling of benzyliczinc bromide **2.6** and vinyl iodide **2.5** (Figure 2.2). The latter would be derived from the addition of iodine monochloride to alkyne **2.7**, and benzyliczinc bromide **2.6** would be derived from 2,5-dimethoxychlorobenzene (**2.8**).
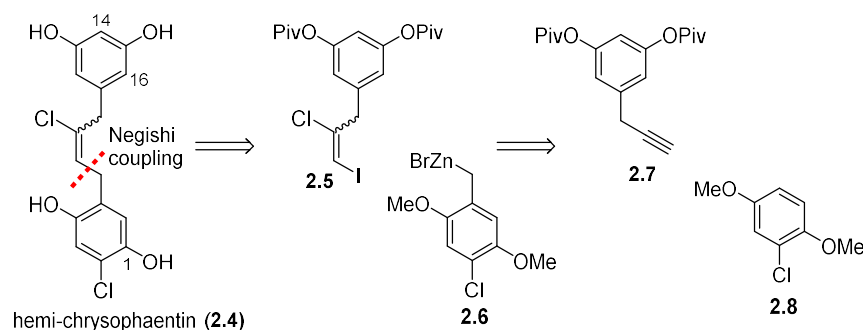
Figure 2.2. Retrosynthetic analysis of hem-chrysophaentin (**2.4**).

The synthesis of iodide **2.5** started with the reduction of 2,6-dimethoxybenozic acid (**2.9**), followed by the conversion of alcohol **2.10** to bromide **2.11** (Figure 2.3). Benzylic bromide **2.11** was then homologated to alkyne **2.12**, which on deprotection afforded alkyne **2.13.** Exchange of methyl ethers for pivaloyl esters was needed, to avoid undesired ring iodination, and was followed by iodo-chlorination of alkyne **2.7** afforded a 2:1 mixture of isomeric iodides **2.5** (Figure 2.3).[1] With the completion of iodide **2.5**, attention was turned toward the synthesis of benzyliczinc bromide **2.6**.
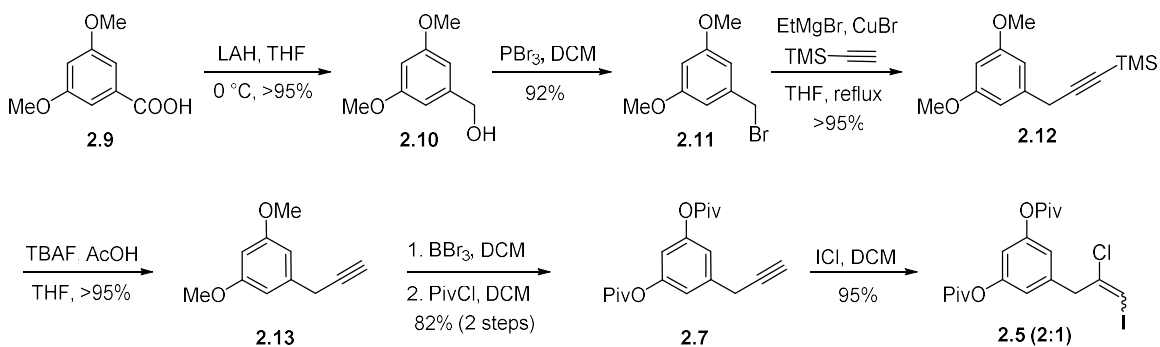
Figure 2.3. Wipf's Synthesis of iodidie **2.5.**

Benzylic zinc bromide **2.6** was synthesized in four steps from 2,5-dimethoxychlorobenzene (**2.8**) starting with formylation to afford aldehyde **2.14** (Figure 2.4)**.** Aldehyde **2.14** was converted to bromide **2.16** via alcohol **2.15**. The key Negishi cross-coupling was achieved starting with treatment of bromide **2.16** with Zn metal, followed by the addition of vinyl iodide **2.5** and Pd(OAc)$_2$ to afford product **2.17** as a 2:1 mixture of *E/Z* stereoisomers. Following deprotection, the *E/Z* stereoisomers were separated by supercritical fluid chromatography (SFC) to provide hemi-chrysophaentin (**2.4**). Wipf reported all attempts to effect an oxidative dimerization of **2.4** to access either chrysophaentin A (**2.1**) or chrysophaentin F (**2.2**) were unsuccessful.[7] However,

through collaboration with Bewley and co-workers, the antimicrobial activity and FtsZ GTPase inhibition of hemi-chrysophaentins **2.4** and **2.18** were determined.
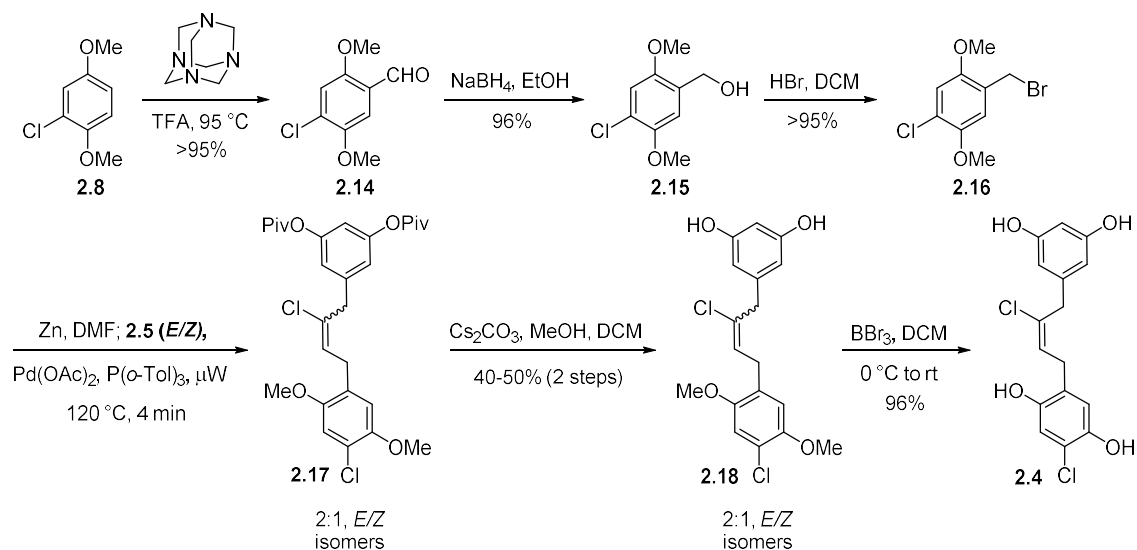
Figure 2.4. Wipf's synthesis of hemi-chrysophaentin **(2.4).**

Bewley and co-workers examined the antimicrobial activity of hemi-chrysophaentins **2.4** and **2.18** against drug- and multi-drug resistant strains of S. *aureus*. They determined hemi-chrysophaentins **2.4** and **2.18** inhibited the growth of all strains tested with an MIC_{50} range of 11-20 μM and MIC_{90} range of 34-73 μM (for comparison chrysophaentin A (**2.1**) has an MIC_{50} in the 2-4 μM range). Similar to chrysophaentin A (**2.1**), hemi-chrysophaentin **2.4** and **2.18** were bacteriostatic at their MIC_{90} and only become bactericidal at 2x MIC_{90} concentration. Hemi-chrysophaentins **2.4** and **2.18** were approximately 3-4x less potent compared to chrysophaentin A (**2.1**) (4.6-9.2 μM).[1] The loss of activity further supports the importance of the overall bis-biaryl ether core structure of the chrysophaentins to achieving maximal antimicrobial activity.

Attention was then turned toward comparing FtsZ inhibition activity of hemi-chrysophaentin (**2.18**), in the earlier described GTPase biochemical assay, to chrysophaentin A

(**2.2**). In their studies, Bewley and co-workers showed hemi-chrysophaentin (**2.18**) displaces GTP from the GTP-binding site on FtsZ in a competitive manner using fluorescently labeled GTP analog, *mant*-GTP, and with ^{3}H-GTP competition assay. Hemi-chrysophaentin (**2.18**) was found to bind to the GTP-binding region of FtsZ with a K_a of $1.5 \times 10^5 \, M^{-1}$ in the fluorescence anisotropy assay and the K_a of $0.87 \times 10^5 \, M^{-1}$ from the ^{3}H-GTP competition assay. Hemi-chrysophaentin (**2.18**) also inhibited the GTPase activity of EcFtsZ and SaFtsZ *in vitro*, as determined by malachite green phosphomolybdate assay.[8] Hemi-chrysophaentin (**2.18**) inhibits the GTPase activity of EcFtsZ with an IC_{50} of 37 µM and SaFtsZ with an IC_{50} of 38 µM *in vitro*. Hemi-chrysophaentin (**2.18**) was also found to disrupt Z-ring formation in E. *coli*.[8] Chrysophaentin A (**2.1**) inhibits the GTPase activity of EcFtsZ with an IC_{50} of 37 µM and SaFtsZ with an IC_{50} of 38 µM *in vitro*, with an approximately 3-4x lower MIC_{50} compared to hemi-chrysophaentin (**2.18**). The difference between growth inhibition and GTPase activity suggests the use of these GTPase assay may not be useful in a SAR study.

2.3 Shaw's Approach Towards Chrysophaentin A (2.1)

A few years following the synthesis of hemi-chrysophaentin (**2.4**), the Shaw group (UC Davis) published progress towards chrysophaentin A, E and F.[4] Unlike the Wipf group, the Shaw group disconnected chrysophaentin A (**2.1**) at the peripheral *E*-chloroalkenes leading to Northern and Southern fragments **2.19** and **2.20** as advanced intermediates. Shaw and co-workers planned on joining the fragments by way of two Wittig olefinations followed by the equivalent of a Hunsdiecker decarboxylative chlorination (Figure 2.5).
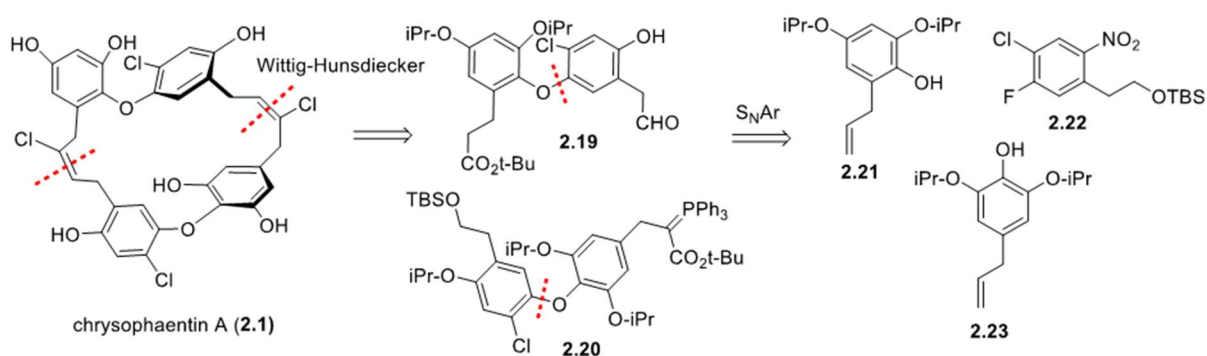
Figure 2.5. Shaw group's retrosynthetic analysis of chrysophaentin A **(2.1)**.

Shaw and co-workers proposed assembly of diaryl ethers **2.19** and **2.20** by way of either a Chan-Lam-Evans coupling[9–11] or nucleophilic aromatic substitution reaction (S_NAr). The Shaw group determined a Chan-Lam-Evans coupling would be difficult due to the sterically encumbering isopropyl ethers flanking the reactive phenol moiety on phenols **2.21** and **2.23**. Therefore, they elected to pursue S_NAr reactions to generate biaryl ethers **2.19** and **2.20**.

The synthesis of biaryl ethers **2.19** and **2.20** started from phenols **2.21** and **2.23**, both available in several steps from commercially available and inexpensive resorcinols **2.24** and **2.28**, respectively (Figure 2.6). The synthesis of **2.21** started with peralkylation of resorcinol **2.24** followed by oxidation with magnesium monoperoxyphthalate (MMPP) to afford phenol **2.25**. The later was O-alkylated with allyl bromide to afford allyl-ether **2.27**, which upon heating to 185 °C underwent Claisen rearrangement to afford phenol **2.21** in 54% over the four steps (Figure 2.6, first panel).
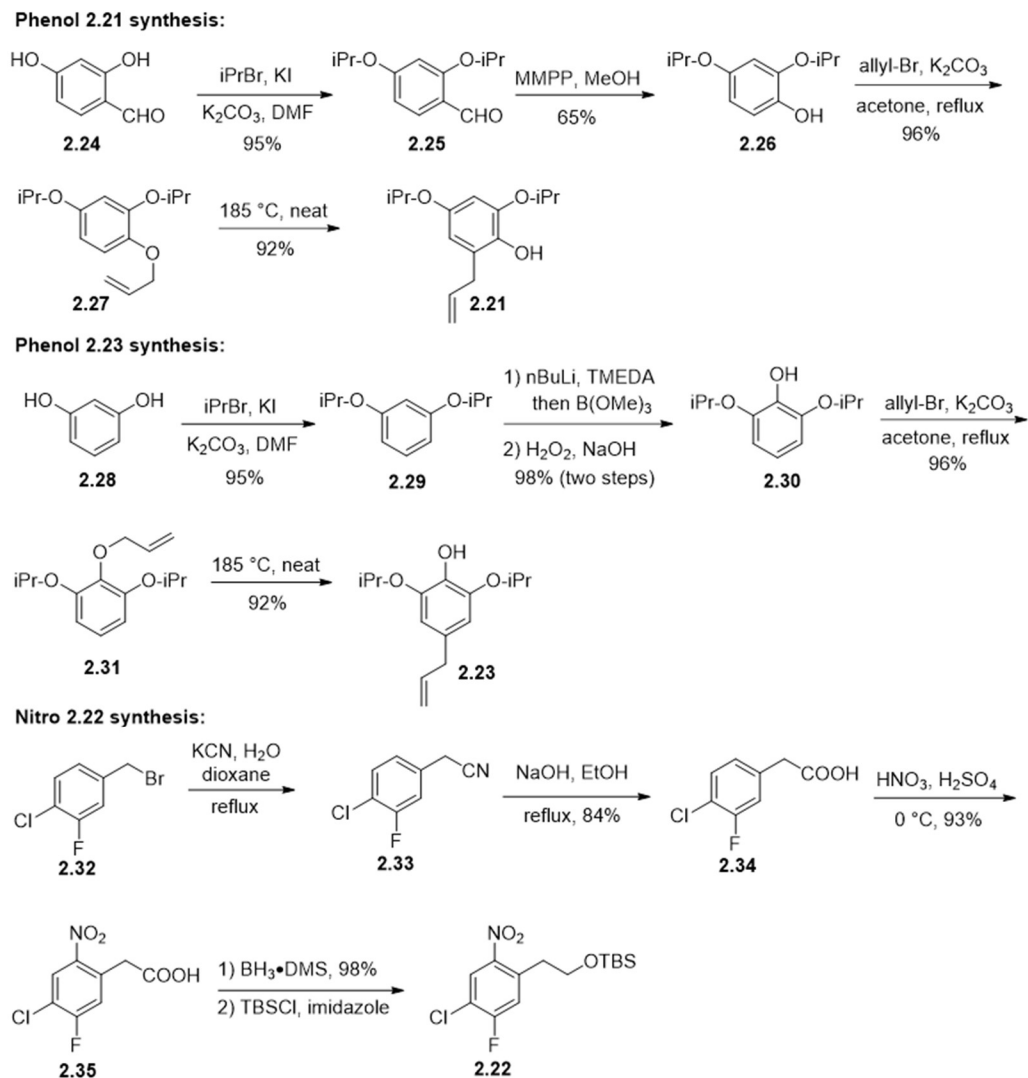
Figure 2.6. Shaw synthesis of S$_N$Ar coupling partners: **2.21, 2.22,** and **2.23.**

The synthesis of phenol **2.23** likewise commenced with the peralkylation of resorcinol (**2.28**) and in this case was followed by lithiation, borylation, and oxidation to give intermediate phenol **2.30**. A second Claisen rearrangement was initiated by alkylation of **2.30** with allyl bromide and the derived allyl ether upon heating underwent a tandem Claisen-Cope rearrangement reaction sequence to afford phenol **2.23** in 80% yield over the five steps (Figure 2.6, second panel).

33

Attention was then turned toward the synthesis of S$_N$Ar coupling partner **2.22** from commercially available bromide **2.31**. The reaction of the latter with potassium cyanide followed by basic hydrolysis afforded acid **2.33** in 78% yield. Nitration of **2.33** was followed by carboxylic acid reduction with borane dimethylsulfide and alcohol protection to complete S$_N$Ar coupling partner **2.22** (Figure 2.6, third panel).
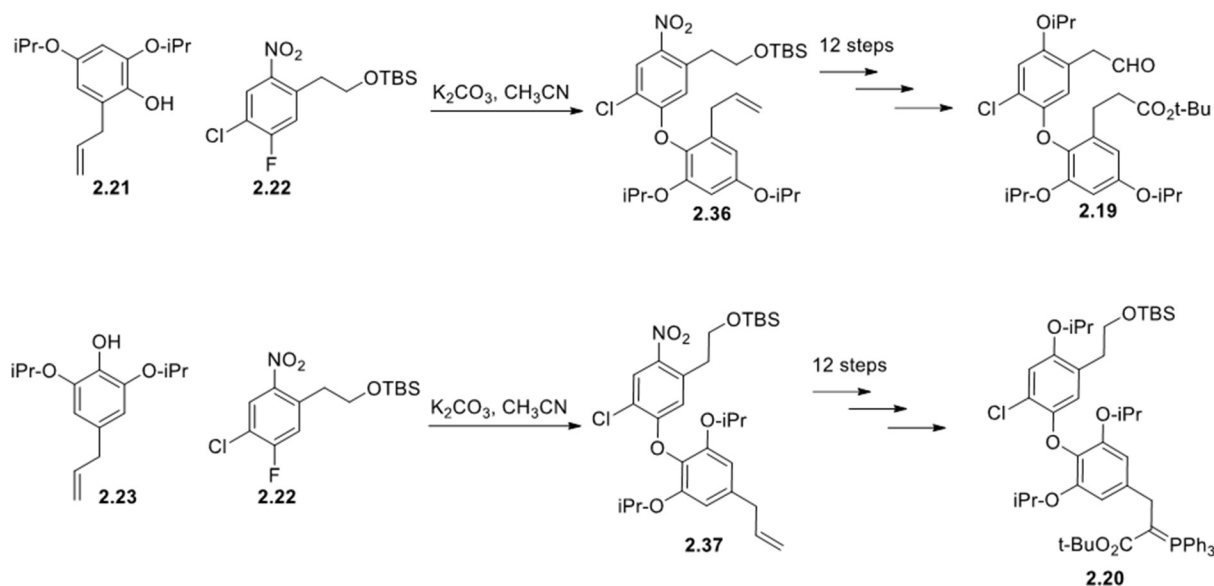
Figure 2.7. Shaw synthesis of diaryl ethers **2.19** and **2.20.**

Biaryl ether formation commenced with S$_N$Ar reaction of phenols **2.21** and **2.23** in parallel with aryl fluoride **2.22** under standard conditions to afford diaryl ethers **2.36** and **2.37** in 75% and 78% yields, respectively (Figure 2.7). Biaryl ethers **2.36** and **2.37** were then advanced to Northern fragment **2.19** and Southern fragment **2.20** as summarized in Figure 2.7.[4] Briefly, aldehyde **2.19** is accessed in twelve steps from **2.36** and phosphorus ylide **2.20** was accessed from **2.37** in twelve steps (Figure 2.7). While key fragments **2.19** and **2.20** proved accessible, their merger by way of Wittig olefination failed. A mixture of ylide **2.20** and aldehyde **2.17** did not afford any of the desired olefination product **2.38** but, instead, lead to decomposition of aldehyde **2.19** (Figure 2.8).

34

The screening of other reaction conditions was limited, as access to the advanced fragments proved difficult due to the length of the syntheses. The Shaw group also indicated the key Hunsdiecker-chlorination reaction (not shown) failed on simplified model substrates.
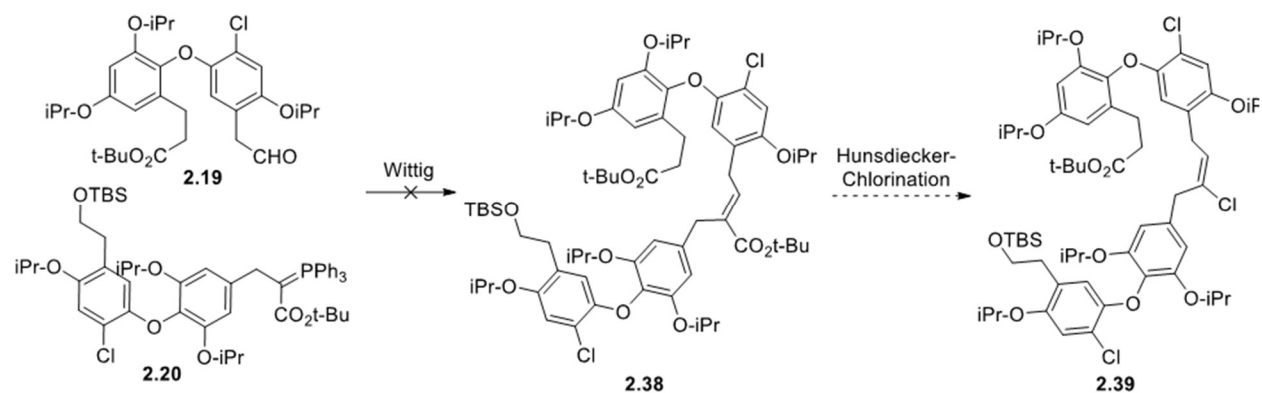
Figure 2.8. Shaw's Wittig and Hunsdiecker-chlorination.

2.4 Harrowven's Approach Toward Chrysophaentin F (1.8)

In 2019, the Harrowven group published on their progress towards symmetrical chrysophaentin F (**2.2**).[5] Key reactions in their studies are a Chan-Lam-Evans coupling (Figure 2.9, highlighted in red), ring-closing alkyne metathesis (Figure 2.9, highlighted in pink), palladium- (Figure 2.9, highlighted in blue) and nickel-catalyzed sp-sp^3 couplings (Figure 2.9, highlighted in green), and a hydrozirconation-halogenation (Figure 2.9, highlighted in orange).[5] Harrowven's study, similar to the Shaw's, disconnected the *E*-chloroalkenes in anticipation that sequential metal catalyzed reactions would afford **2.40**, which followed by a hydrozirconation-chlorination would afford chrysophaentin F (**2.8**) (Figure 2.9, highlighted in orange).
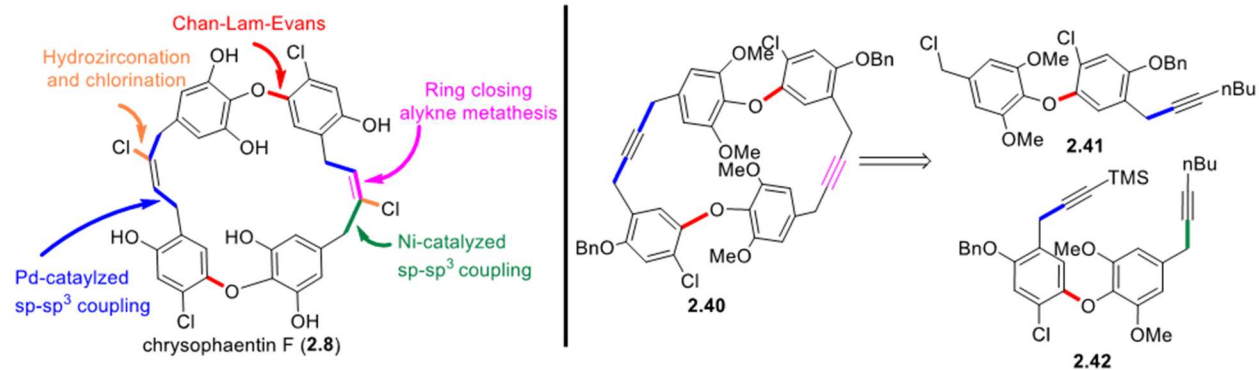
Figure 2.9. Harrowven's retrosynthetic analysis of chrysophaentin F **(2.2).**

The Harrowven group anticipated accessing bisalkyne **2.40** from advanced fragments **2.41** and **2.42,** which could be divergently derived from diaryl ether **2.45** (Figure 2.10)**.** The latter was derived from a Chan-Lam-Evans coupling between boronate **2.43** and phenol **2.44** and advanced to benzylic chloride **2.45** via an Appel chlorination. Chloride **2.46** underwent divergent palladium-catalyzed sp-sp^3 couplings to afford butyl-alkyne **2.47** and trimethylsilyl alkyne **2.48** (Figure 2.10, bonds highlighted in blue). Ester **2.47**, was reduced and converted benzyl chloride **2.41** in two steps**.** Alkyne **2.48** underwent a similar sequence to afford bromide **2.49**, which was subsequently homologated by nickel-catalyzed sp-sp^3 coupling (Figure 2.10, bond highlighted in green) to afford bisalkyne **2.42.**
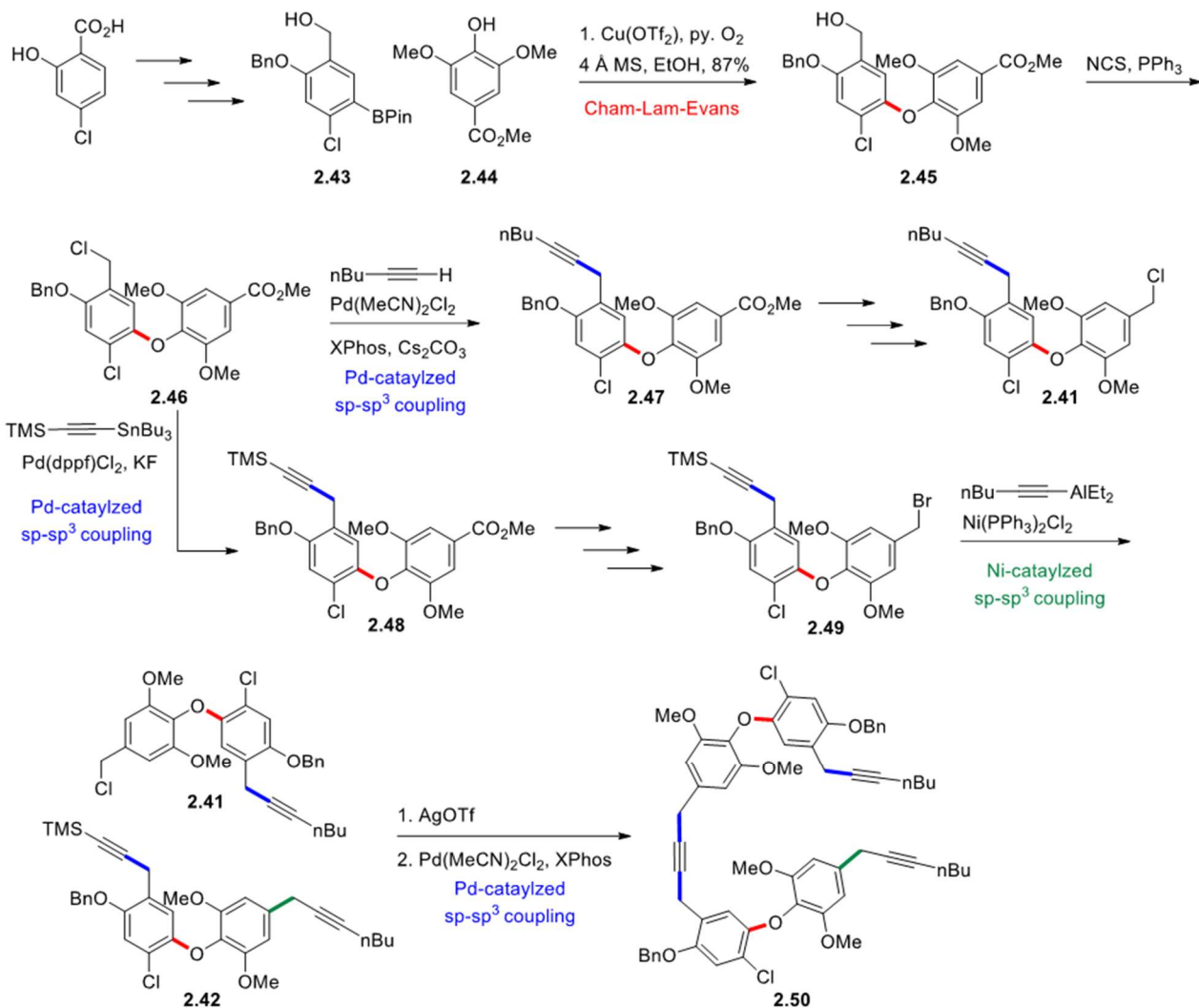
Figure 2.10. Harrowven's Synthesis of tris-alkyne **2.50.**

The Eastern alkyne of macrocycle **2.40** was constructed by a palladium-catalyzed sp-sp^3 coupling between chloride **2.41** and deprotected bisalkyne **2.42** to afford **2.50** (Figure 2.10, upper bond highlighted in blue). The completion of macrocycle **2.40** was accomplished through an alkyne ring-closing metathesis, utilizing Fürstner's molybdenum-phenanthroline pre-catalyst (Figure 2.11, bond highlighted in pink). Functionalization of bis-alkyne **2.40** afforded, after deprotection, a complex mixture of regioisomeric chlorination products, that were inseparable by HPLC preventing completion of the total synthesis of chrysophaentin F (**2.2**).
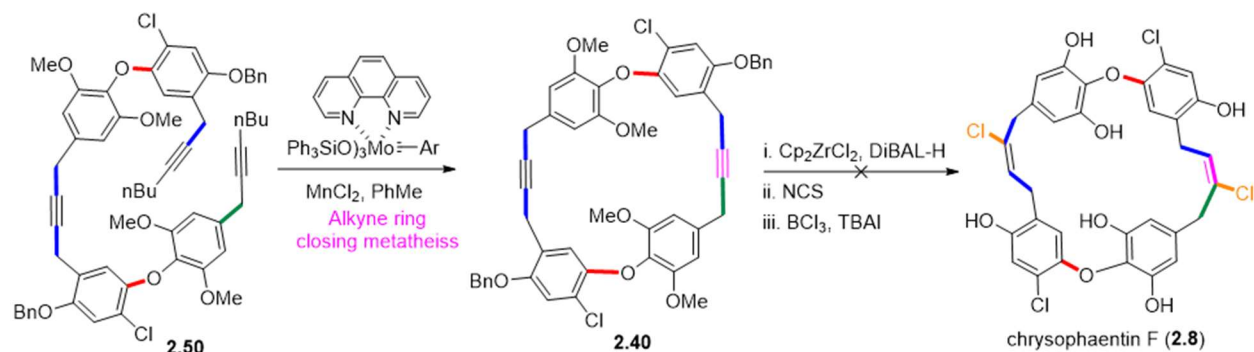
Figure 2.11. Harrowven's synthesis of macrocycle **2.40.**

In summary, three groups have reported different approaches towards chrysophaentin A (**2.1**) and chrysophaentin F (**2.2**), providing valuable lessons about the difficulty of accessing the bis-diaryl ether core structures. The Shaw and Harrowven group's work vetted key strategies for the synthesis of the diaryl ethers and the Wipf group demonstrated a nonselective method to install the *E*-chloroalkenes. To date the Eastern and Western halves of chrysophaentin A (**2.1**) and the Northern and Southern diaryl ethers have been synthesized however, only one group was able to access the macrocyclic core of the chrysophaentins, albeit without the incorporation of the *E*-chloroalkenes. Unfortunately, only the Wipf group tested their chrysophaentin analogs for antimicrobial activity limiting our knowledge of the structure-activity relationship of the chrysophaentins. During the same timeframe as the above studies, our lab was also working towards the total synthesis of chrysophaentin A (**2.1**). The following sections will outline our synthetic approach towards chrysophaentin A (**2.1**) and the key challenges that became apparent when attempting to form the *E*-chloroalkenes and the macrocyclic core of the chrysophaentins.

2.5 VICB Synthesis Core's Approach Towards Chrysophaentin A (2.1)

In 2013, Bewley and co-workers contracted the Vanderbilt Institute of Chemical Biology's Synthesis Core to design a scalable synthesis of chrysophaentin A (**2.1**) that would be amenable to the synthesis of chrysophaentin analogs for biological testing. From a strategic perspective, the Chemical Synthesis core anticipated the macrocyclic core of chrysophaentin A (**2.1**) could be formed through a ring-closing metathesis (RCM) reaction and the merger of two biaryl ethers by an O-alkylation followed by an O to C migration to establish the correct bond connectivity. However, due to the known incompatibility of vinyl halides in RCM reactions,[12,13] they initially set out to complete the synthesis of 9-dechlorochrysophaentin (**2.51**) which would allow for macrocyclic formation employing a more precedented, nonetheless challenging, *Z*-selective ring-closing metathesis.[14,15] The synthesis of 9-dechlorochrysophaentin (**2.51**) would require the development of methods for the installation of the *E*-chloroalkenes, optimization of conditions to invoke the O to C migration, a *Z*-selective RCM, and assembly of two diaryl ethers. The methods used to complete the total synthesis of 9-dechlorochrysophaentin (**2.51**) could then be applied to the total synthesis of chrysophaentin A (**2.1**).

Macrocycle **2.52** was thought to arise from Mitsunobu coupling of a Northern BC and Southern AD fragment followed by *cis*-selective RCM. The subsequent O to C migration could proceed either terminating at the C5' providing 9-dechlorochrysophaentin (**2.51**) or the C3' affording an iso-9-dechlorochrysophaentin analog, which could be a valuable synthetic derivative for biological testing. Alkyl ether **2.54** could be accessed from diaryl ethers **2.56** and **2.58,** which are generated by S$_N$Ar reaction between phenols **2.59** and **2.62** with commercially available

aldehyde **2.61**. Phenols **2.59** and **2.62** could be accessed in a few steps from low cost commercially available starting materials, such as vanillin (Figure 2.12).
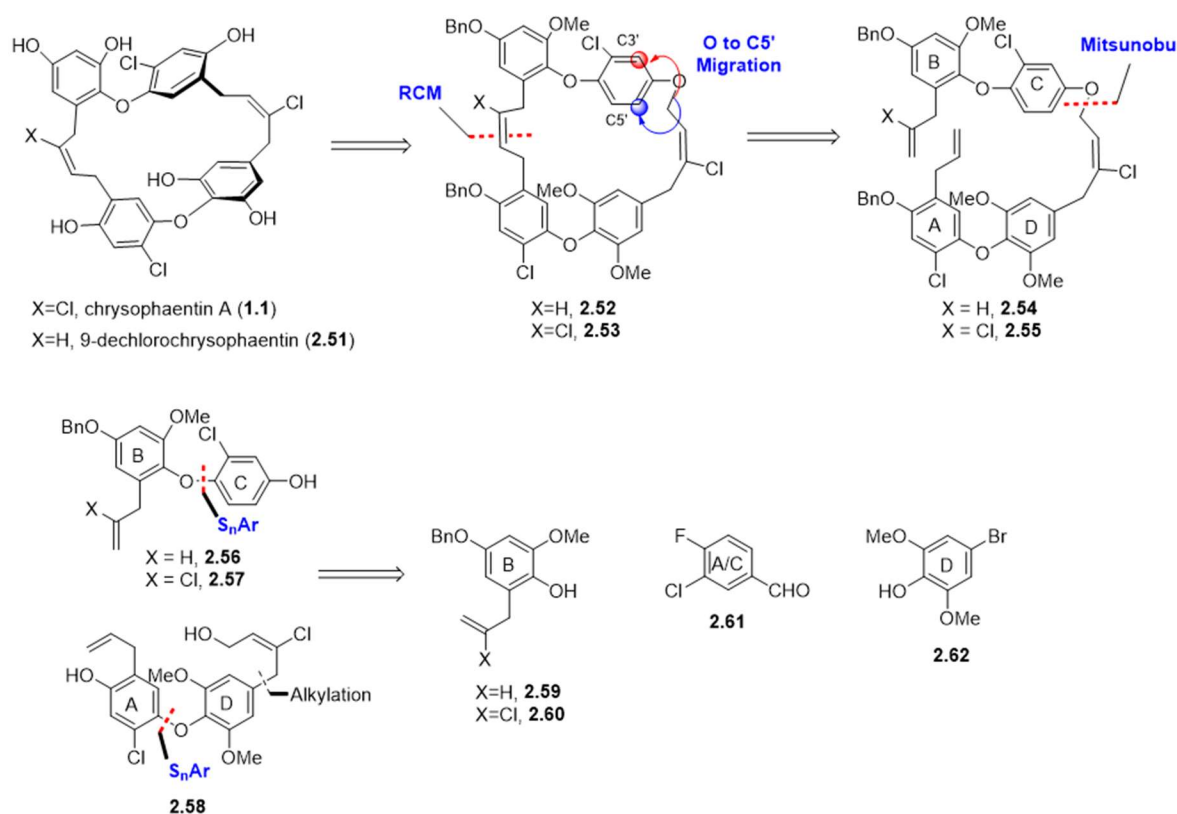
Figure 2.12. VICB CS core's approach towards chrysophaentin A **(2.1).**

The Synthesis Core synthesized the Northern BC fragment **2.56** in six steps starting from vanillin (**2.63**) (Figure 2.13), which was converted to allyl ether **2.64.** The later underwent Dakin oxidation followed by phenol benzylation to afford **2.65** in 42% over three steps. **2.65** was heated to 185 °C to induce a Claisen rearrangement to afford phenol **2.59** in 80% yield. Phenol **2.59** was coupled under standard S$_N$Ar reaction conditions to afford diaryl ether **2.67,** which underwent subsequent Baeyer-Villager oxidation conditions to complete the BC fragment **2.56** in 30-50% yield**.** (Figure 2.13).
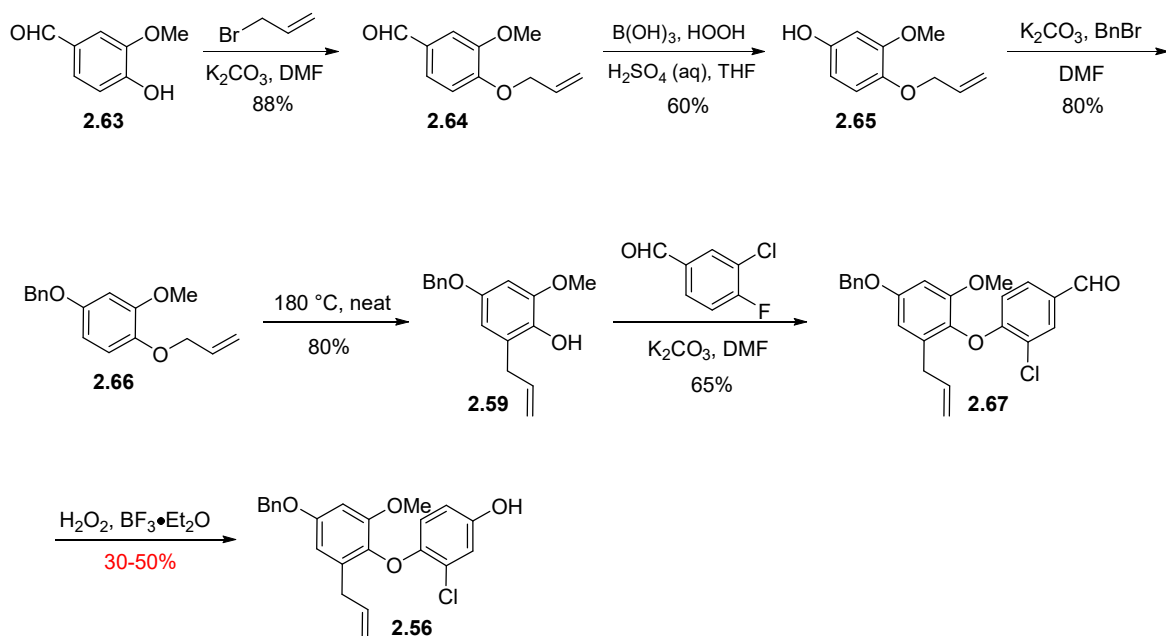
Figure 2.13. VICB CS core's synthesis of biaryl ether **2.56.**

Upon completion of the Northern BC fragment **2.56**, attention was then directed towards the Southern AD biaryl ether **2.58**. The latter presented the added challenge of the alkylation of the D-ring and *E*-chloroalkene installation (Figure 2.14). Starting with 2,6-dimethoxyphenol, it was converted to phenol **2.69** via three steps: bromination, S$_N$Ar, and Baeyer-Villiger oxidation. Phenol **2.69** was converted to an intermediate allyl ether, which upon heating, afforded Claisen rearrangement products **2.70** and **2.71**. The regioisomers were separated and treated with benzyl bromide to afford bromide **2.72.** The Chemical Synthesis core anticipated cuprate alkylation and alkyne functionalization would provide access to the *E*-chloroalkene. Cuprate generation of **2.72** followed by the addition of propargylic iodide **2.73** afforded alkyne **2.74** after deprotection in 45% yield over two steps. Installation of the *E*-chloroalkene was achieved by alcohol directed palladium-catalyzed hydrostannylation of **2.74** followed by a tin-chloride exchange with retention

of double bond geometry with N-chlorosuccinimide[16] to furnish the AD fragment **2.58** in 65%

yield (Figure 2.15).
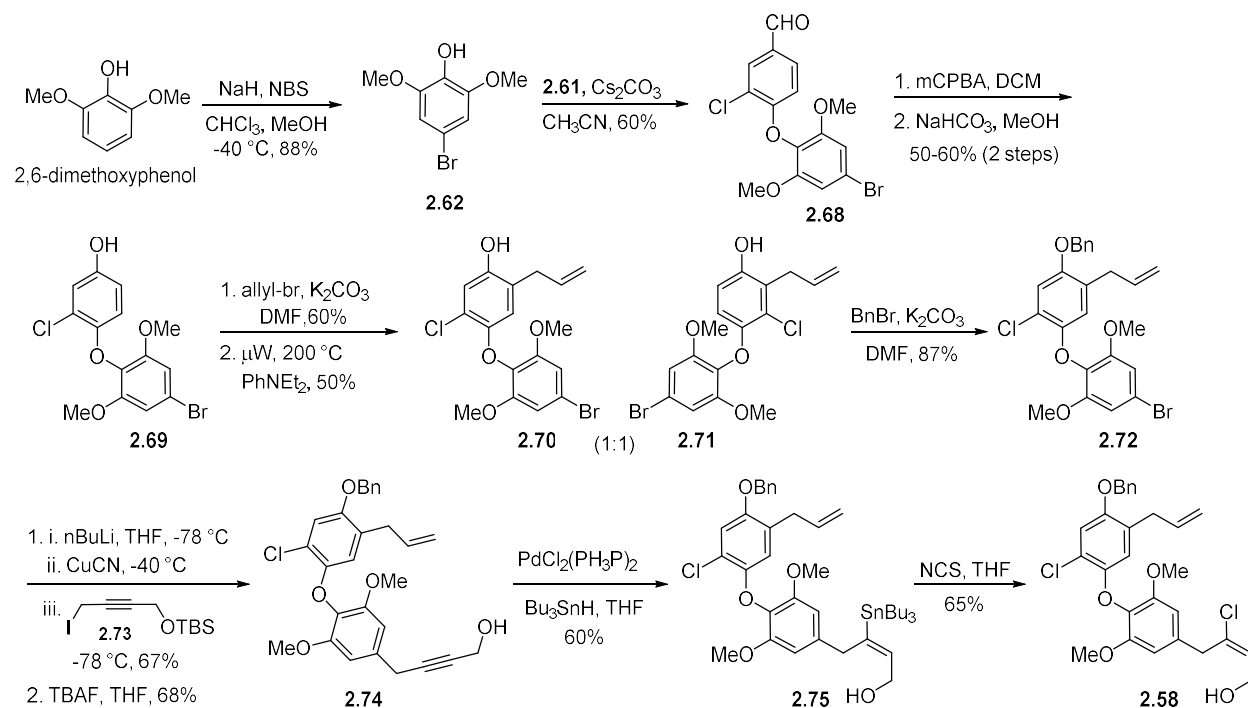
Figure 2.14. VICB CS core's synthesis of AD fragment **2.58.**

Merger of Northern and Southern fragments **2.56** and **2.58** under Mitsunobu coupling

conditions to afford alkyl ether **2.54** in 65% yield (Figure 2.15). The latter was treated with Grubbs

second-generation catalyst to invoke ring-closing metathesis reaction affording macrocycle **2.52**

as an inseparable 1:1 mixture of *E/Z* stereoisomers. Macrocycle **2.52** was treated with

montmorillonite K10 to catalyze an O to C migration. However, no migration products were

observed and due to the lack of material (<10 mg), further investigation of the O to C migration

was not possible. Deprotection of **2.53** afforded pseudo-chrysophaentin **2.76**. Attempts to remove

the methyl ethers and to separate the *E/Z* stereoisomers of **2.76** were unsuccessful. Furthermore,

42

the material throughput did not allow for a screen of ring-closing metathesis conditions or O to C

migration conditions.
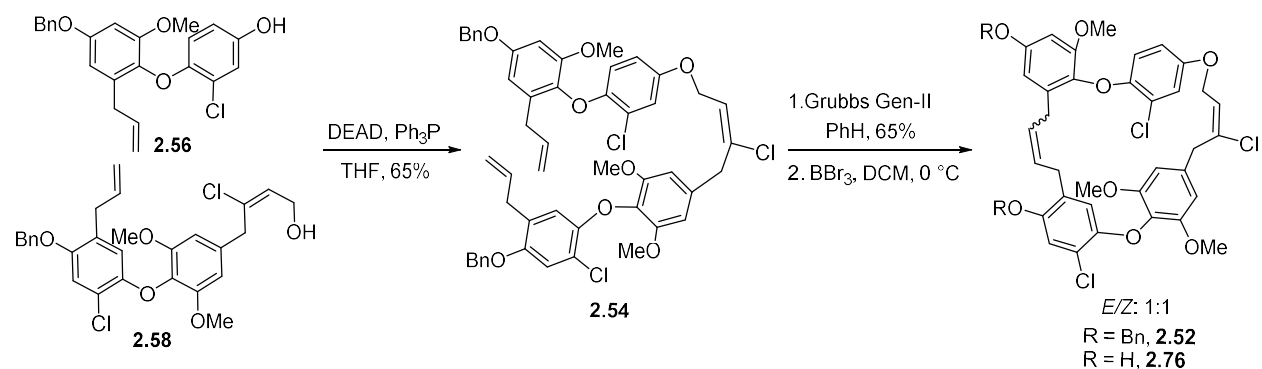
Figure 2.15. VICB CS core's synthesis of Chrysophaentin analog **2.76.**

Bewley and co-workers determined the antimicrobial activity and FtsZ GTPase inhibition

of **2.76, 2.72,** and **2.56** against Gram-positive bacteria: S. *aureus*, *MRSA,* multi-drug resistant S.

aureus (MDRSA) and E. *faecium* (Table 2.1). The synthetic analogs were found to be significantly

less active compared to chrysophaentin A (**2.1**) with MIC_{50} range of 8-38 μM compared to 1.8-5.6

μM and showed very little if any GTPase inhibition, with an IC_{50} range of 37-179 μM. The

decrease in activity compared to chrysophaentin A (**2.1**) further supports the importance of *E-*

chloroalkenes and the macrocyclic conformation of chrysophaentin A (**2.1**) for its maximal

antimicrobial activity.

Table 2.1. Antimicrobial activity for **2.76, 2.72,** and **2.56.**

Test Compound:	Microbroth MIC$_{50}$ (µg/mL)				Malachite green phosphomolybdate GTPase assay
	S. *aureus*	MRSA	MDRSA	E. faecium	EcFtsZ
Chrysophaentin A (**2.1**)	2.7	2.2	1.8	5.6	9.9 µM
Hemi-chrysophaentin (**2.4**)	20	23	27	NA	37 µM
2.76	18.2	NA	NA	18.2	NA
2.72	38	14	15	NA	86.5 µM
2.56	26	22	8	NA	179.7 µM

2.6 Total Synthesis of 9-dechlorochrysophaentins Congeners VU0848354 and VU0848355

In 2014 I joined the Sulikowski group where I was given the task to optimize the synthetic route developed by the Synthesis Core and work towards the completion of the total synthesis of 9-dechlorochrysophaentin (**2.51**) and chrysophaentin A (**2.1**). The initial work by the Synthesis Core, especially the work of Drs. Kwangho Kim and Somnath Jana laid the foundation for my work which lead to the completion of the total synthesis of 9-dechlorochrysophaentin (**2.51**), three other chrysophaentin A analogs and development of an improved synthesis of hemi-chrysophaentin (**2.4**). In the following sections, I will outline my work on the total synthesis of 9-dechlorochrysophaentins **VU0848354**, **VU0848355**, **VU0849838**, and **VU0849855** and how I overcame key obstacles such as the construction of the C-ring of the BC fragment in a reliable and scalable manner, stereoselective installation of the *E*-chloroalkene, O to C migration, protecting group manipulation to allow for facile deprotection sequence, and *cis*-selective ring-closing metathesis.

Initially, I started on the project where the Synthesis Core had ended and the main goal was to optimize and finish the total synthesis of 9-dechlorochrysophaentin (**2.51**). Using the strategy outlined above (Figure 2.13 and 2.14), synthesis of **2.54** was attempted on a multigram scale to afford >500 milligrams of material to enable a screen of conditions to invoke a *cis*-selective ring-closing metathesis and O to C migration (Figure 2.15). However, it became apparent early on in the synthesis of BC fragment **2.56** and AD fragment **2.58** that the Bayer-Villager oxidation used to convert aldehydes **2.66** and **2.68** into **2.56** and **2.69** was not selective for aryl migration resulting in a mixture of desired phenol and carboxylic acid products. A screen of different oxidation conditions was completed in an attempt to selectively afford the phenol product; however, the screen was unsuccessful (Table 2.2).

Table 2.2. Oxidation screen for the generation of phenols **2.54** and **2.69.**

Fragment	Oxidation conditions	Yield of phenol (**2.69**)	Fragment	Oxidation conditions	Yield of phenol (**2.56**)
AD aldehyde (**2.68**)	mCPBA	19%	BC aldehyde (**2.66**)	H_2O_2, $BF_3 \cdot Et_2O$	10-30%
AD Fragment (**2.68**)	H_2O_2, PhSeSePh	18%	BC aldehyde (**2.66**)	H_2O_2, H_2SO_4	18%
AD Fragment (**2.68**)	H_2O_2, SeO_2	acid	BC aldehyde (**2.66**)	MMPP	Acid (**2.78**)
AD Fragment (**2.68**)	MMPP	acid	BC aldehyde (**2.66**)	mCPBA	RSM
AD Fragment (**2.68**)	H_2O_2, TFAA KH_2PO_4	40%	BC Aldehyde (**2.66**)	UHP, TFAA	Decomp.
AD Fragment (**2.68**)	UHP, TFAA KH_2PO_4	40%	BC Aldehyde (**2.66**)	UHP, TFAA KH_2PO_4	Decomp.

Baeyer-Villager oxidation on benzaldehydes has two possible reaction pathways from the tetrahedral or Criegee intermediate (Figure 2.16, intermediate **2.77**). The Criegee intermediate can collapse with either migration the hydrogen of the aldehyde to afford carboxylic acid product **2.78** (Figure 2.16, red arrows) or the aryl ring migrates to afford a formate intermediate which upon methanolysis provides phenol **2.54** (Figure 2.16, blue arrows). Traditionally for alkyl ketones and aldehydes, it has been shown that the preferred migrating group is the more electron-rich group and the general order of migratory aptitude is as follows: 3° alkyl > cyclohexyl > 2° alkyl > benzyl > phenyl > 1° alkyl > cyclopropyl ≈ cyclopentyl > methyl.[17] The migratory aptitude is based on the migratory group's ability to stabilize positive charge that builds up during the migration as the Criegee intermediate (**2.77**) begins to break apart and the new carbon-oxygen or hydrogen-oxygen
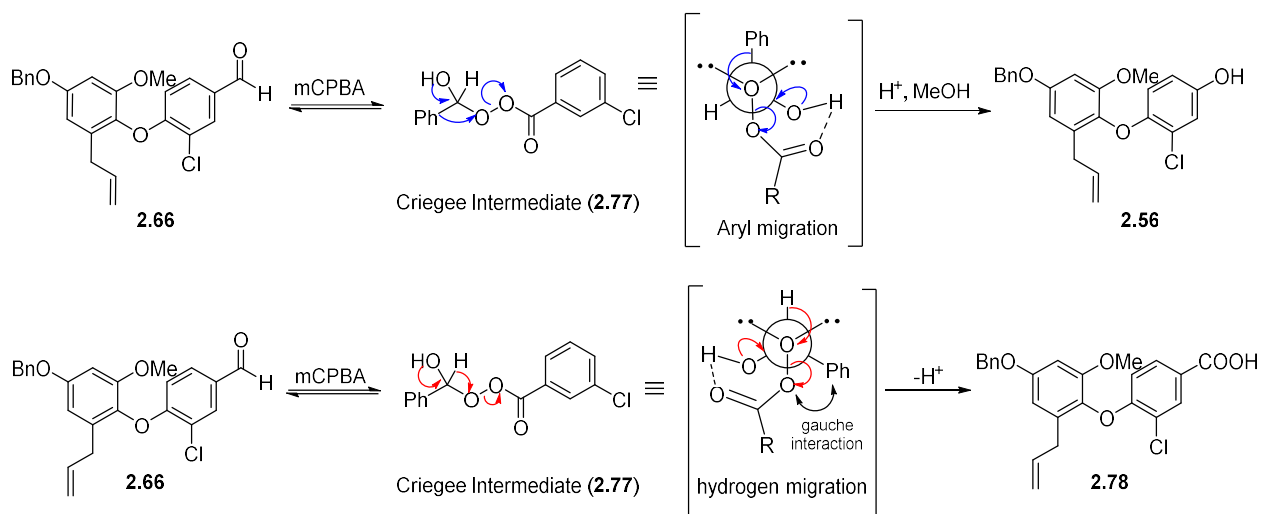
Figure 2.16. Rational or aryl versus hydrogen migration in Baeyer-Villiger oxidation of aldehyde **2.66.**

bond forms. Therefore, the more electron-rich groups provide more stabilization of the positive charge and thus have a higher migratory aptitude.

An additional factor that contributes to migratory aptitude is stereoelectronic in nature. For migration to occur, the migratory group has to be antiperiplanar to the peroxide oxygen, allowing for proper σ-σ* orbital overlap (stereoelectronic effect), which in the case for hydrogen migration creates a gauche interaction (sterics) between the aryl group and peracid (Figure 2.16). However, the electron density of the migrating group and its ability to stabilize the partial positive charge that builds up during migration has been found to have a greater contributing factor to the migratory aptitude than sterics.

Benzaldehydes are a unique case in which the migratory group is either the aryl ring or hydrogen of the aldehyde and the migratory aptitude of the aryl ring is greatly influenced by substituents attached the ring. Ogata and co-workers, studied the kinetics of the Baeyer-Villiger oxidation of substituted benzaldehydes and found that the migratory aptitude for substituted benzaldehydes in alkaline solutions follows the following trend: p-hydroxy and o-hydroxy >> o-OMe > p-OMe > H > o-Me > p-Me >> Ph, and in acidic conditions the order is the same, beside o-Me has higher migratory aptitude than H.[18] Ogata and co-workers, also demonstrated the weak contribution of sterics and the gauche interaction between the non-migratory groups and the peroxide oxygen on the migratory aptitude compared to the electron density of the migratory groups. Based on the results of this study, we hypothesize that the presence of the meta-chloride substituent on aldehyde **2.66** and **2.68** reduces the migratory aptitude of the aromatic ring enough that it becomes equivalent to hydrogen's migratory aptitude, resulting in a mixture of phenol and carboxylic acid products.

Based on the screen of conditions, the selective formation of phenols **2.56** and **2.69** in reproducible high yields was not possible. Thus, new synthetic routes would need to be investigated to facilitate the completion of the total synthesis of 9-dechlorochrysophaentin (**2.51**).

At this point, we set out to redesign the synthetic route for both the Northern BC fragment (**2.56**) and Southern AD fragment (**2.58**) that would facilitate the synthesis of 9-dechlorochrysophaentin (**2.51**).

2.6.1 Synthesis of the Northern BC Fragment of 9-dechlorochrysophaentin (2.51)

As we were unable to affect the clean conversion of aldehyde **2.66** to phenol **2.56**, we required an alternative aryl fluoride substrate in our key S_NAr reaction (see Figure 2.13, **2.59** plus **2.61** to **2.66**). Substitution of S_NAr coupling partner **2.61** to 3-chloro-4-fluoronitrobenzene (**2.79**) afforded diaryl ether **2.80** in 93% yield. Taking inspiration from the Shaw group's work,[4] we believed the nitro group could be reduced to the aniline followed by diatization-Sandmeyer[19,20] to afford aryl iodide **2.82**. We anticipated iodide **2.82** could be converted to an alkyl ether by way of an Ullmann reaction. Iodide **2.82** was treated under standard copper-mediated Ullmann conditions in isopropanol to afford the isopropyl ether. Unfortunately, in addition to the Ullmann reaction, the B-ring allyl group isomerized into conjugation affording ether **2.83** in 60% yield (Figure 2.17).
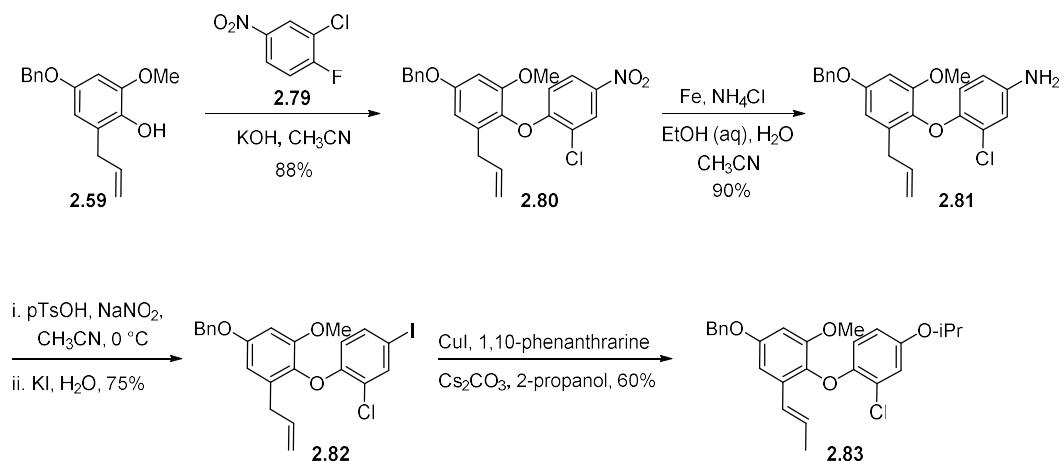
Figure 2.17. First generation BC fragment synthesis: Ullmann ether synthesis

Before additional attempts to convert iodide **2.82** into **2.54** were conducted, the methyl ether protecting groups need to be substituted for a different protecting group that would facilitate facile deprotection. Shaw found isopropyl ethers to be more easily removed than methyl ethers. [4] We, therefore, targeted isopropyl ether protected phenol **2.20** to overcome methyl ether deprotection issue. Using a slightly modified sequence of the Shaw group's work,[4] we were able to access phenol **2.20** in four steps and 50% overall yield. The only modification from the previously reported synthesis is the use of boric acid and hydrogen peroxide to invoke the Dakin oxidation,[21] instead of magnesium monoperoxyphthalate (MMPP). Phenol **2.20** and nitro **2.79** were coupled under standard S$_N$Ar reaction conditions to yield diaryl ether **2.84** in 93% yield. Following the same sequence as before, iodide **2.86** was generated in 60% yield. **2.86** was treated with nBuLi to form the lithiate, followed by borylation and oxidation to afford BC fragment **2.87** in 20-40% yield (Figure 2.18).
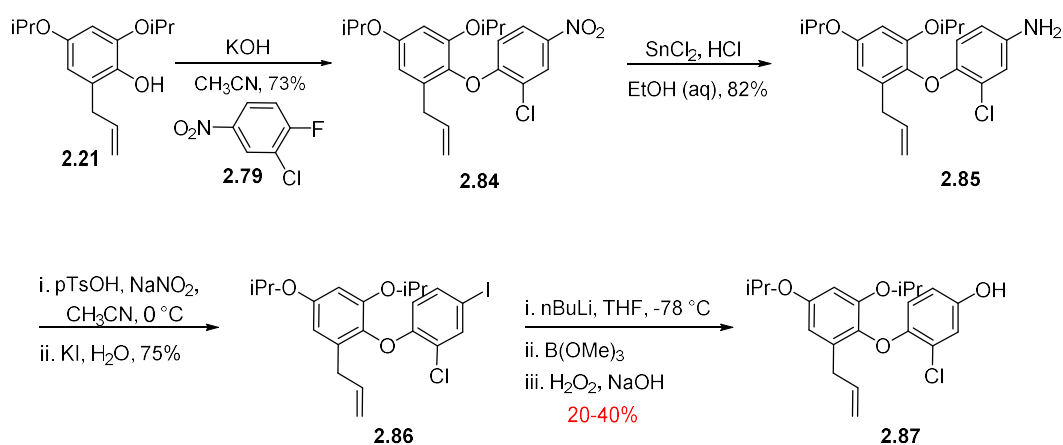
Figure 2.18. Second generation synthesis of BC fragment **2.87.**

Due to the low yield of the borylation-oxidation with nBuLi**,** magnesium-halogen exchange was attempted with Knochel's "turbo-Grignard" (iPrMgCl·LiCl),[22], however, metal-halogen

exchange did not occur resulting in complete recovery of iodide **2.86**. Subsequently, palladium-catalyzed Suzuki-Miyaura coupling[23] was attempted with bis(pinacolato)diboron which also resulted in recovery iodide **2.86**. The lack of reactivity of the iodide to metal-halogen exchange conditions and palladium oxidative addition indicated that the electronics of the ring were unfavorable towards our desired functionalization. Therefore, nitro **2.79** was substituted with bromide **2.94** as the S_NA_r coupling partner (Figure 2.19).

The withdrawing meta-nitro group of **2.94** was anticipated, based on work by Miyaura and co-workers,[23] to increase the speed of the oxidative addition of palladium(0) into the halogen-carbon bond facilitating Suzuki-Miyaura coupling to generate the intermediate boronate ester, which upon oxidation would afford phenol **2.87**. Phenol **2.20** and bromide **2.94** were treated under standard S_NAr conditions to afford diaryl ether **2.95** in 93% yield. Treatment of **2.95** under Suzuki-Miyaura conditions[23] afforded phenol **2.96,** after oxidation in 69% yield. The nitro moiety was then converted to the chloride via diatization-Sandmeyer [24] to afford BC fragment **2.87** (Figure 2.19). The yield of the diatization-Sandmeyer sequence was lower than anticipated, however, the reaction sequence was scalable and reproducible. To date, the reaction sequence has been completed on multi-gram scales and over 20 grams of BC fragment **2.87** have been synthesized.
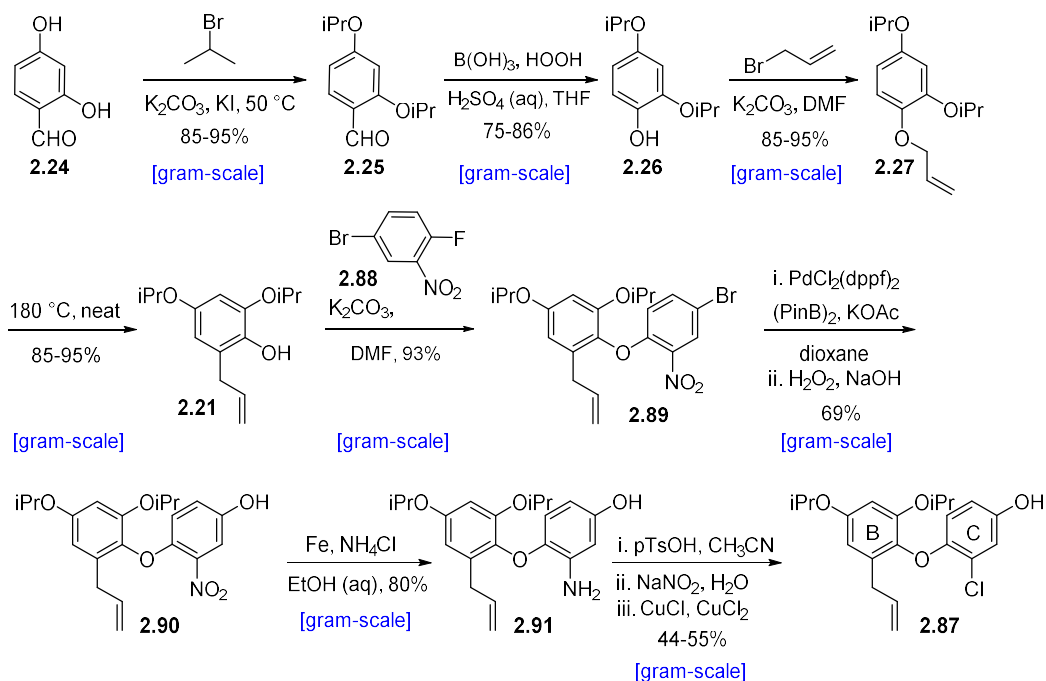
Figure 2.19. Third generation synthesis of BC biaryl ether **2.87**.

With the completion of the BC fragment, attention was directed to the synthesis of AD fragment **2.58.** As mentioned above Baeyer-Villager oxidation of aldehyde **2.68** afforded phenol **2.69** in 40% yield, however, the yield was not reproducible or conducive to provide enough material to complete the chemical synthesis of 9-dechlorochrysophaentin (**2.51**). Furthermore, since the Baeyer-Villager oxidation was unsuccessful, the synthetic strategy used previously by the Synthesis Core to install the *E*-chloroalkene through cuprate alkylation and alcohol-directed palladium-catalyzed hydrostannylation could no longer be used. Therefore, before designing a new synthetic route to AD fragment **2.58**, we wanted to develop a model system that allows for the development of a sequence for the installation of the *E*-chloroalkene in a stereoselective manner and determination of conditions to invoke the proposed O to C migration.

2.6.2 Model System: Synthesis of Hemi-chrysophaentins 2.92 and 2.18

We anticipated hemi-chrysophaentin **2.92** could serve as a model substrate for the development of a sequence to install the *E*-chloroalkene and screen conditions to invoke the O to C migration. Hemi-chrysophaentin **2.92** was divided into two fragments, known phenol **2.95**[25] and allylic alcohol **2.94**. Alcohol **2.94** and phenol **2.95** could be merged by Mitsunobu coupling followed by our proposed O to C migration to afford hemi-chrysophaentin **2.92**. Phenol **2.95** is available in one step from 3-chloro-4-methoxybenzaldehdye,[25] while allylic alcohol **2.94** was predicted to arise from alkynoate **2.96**. Alkynoate **2.96** could be treated under stannylcupration conditions to stereoselectively form an *E*-vinyl stannane, which upon tin-chloride exchange with retention of double bond geometry would generate the *E*-chloroalkene (Figure 2.20).[26]
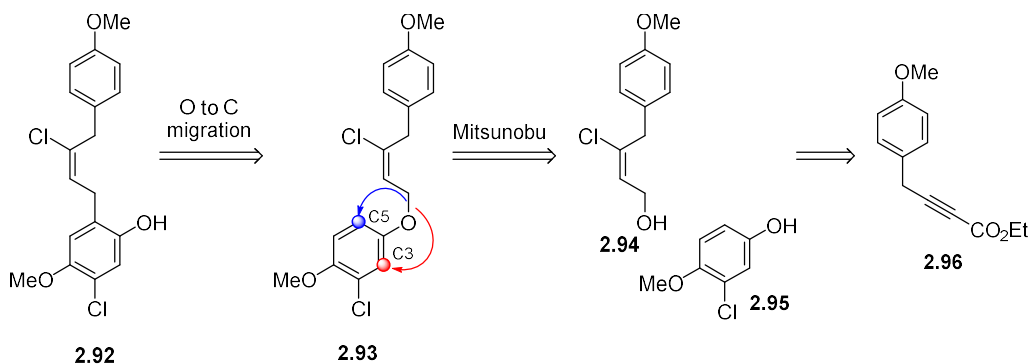
Figure 2.20. Approach towards hemi-chrysophaentin **2.92**.

The stereocontrolled installation of the *E*-chloroalkene utilizing the intermediate E-stannane was key to our success in the completion of hemi-chrysophaentin **2.92**. Stannylcupration reactions have been a widely studied and utilized method for the 1,4-conjugate addition of stannanes into propargylic alcohols, alkynones, and alkynoates.[27–29] The active cuprate species needed to form the proposed *E*-stannane was generated by the reaction of nBuLi and copper(I)cyanide followed by the addition of Bu$_3$SnH (Figure 2.21). The active cuprate species

generated under these conditions was investigated by Lipshutz and co-workers and found to be

2.98.[30] Lipshutz and co-workers, characterized the formation of two byproducts that arose during

the formation of the active cuprate species **2.98** as Bu_4Sn by GC/MS and hydrogen gas.[30] The

formation of Bu_4Sn and hydrogen gas indicates that the initial $(Bu_3Sn)_2BuCnCuLi_2$ complex

undergoes disintegration releasing hydrogen gas and Bu_4Sn resulting in the active species **2.98**

(Figure 2.21).
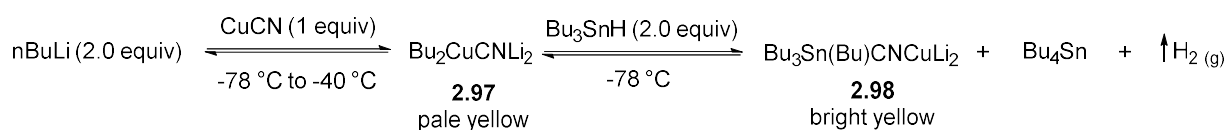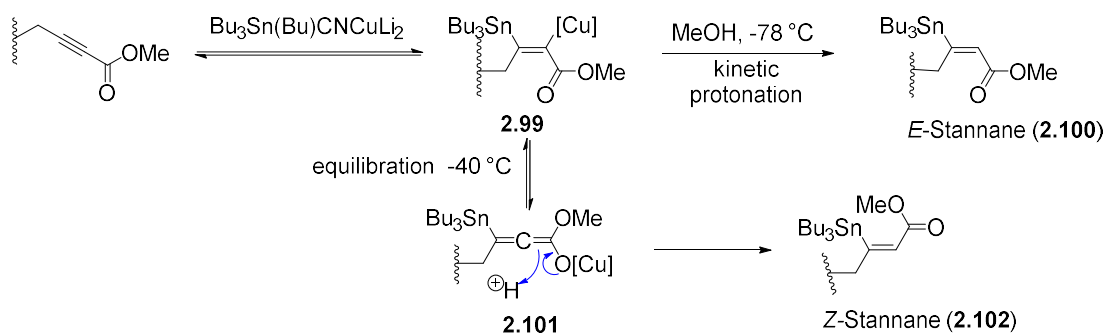
Figure 2.21. Mechanism of stannylcupration on alkynoates.

The conjugate addition of **2.98** into alkynoates can produce two different products, based

on the reaction conditions and temperature, the *E*-stannane, or the *Z*-stannane (Figure 2.21).

Selectivity for the *E*-stannane can be achieved with the presence of excess methanol (2-5 equiv.)

at low temperatures (-100 °C to -78 °C).[31] The low temperatures prevent isomerization of adduct

2.99 to allene intermediate **2.101** and the excess methanol results in kinetic protonation of **2.99**

affording *E*-stannane **2.100,** exclusively (Figure 2.21). However, the *Z*-stannane **2.102** can be selectively formed when the reaction is allowed to proceed at -40 °C and in the absence of methanol.[31] The warmer reaction temperature and absence of a proton source allow for the isomerization of the initial adduct **2.99** to allene intermediate **2.101**. **2.101** then will undergo protonation upon quenching to afford the thermodynamic Z-stannane **2.102** (Figure 2.21, blue arrows). The stereocontrolled formation of the stannane provided a robust method to access the *E*-chloroalkene **2.94** selectively after reduction and tin-chloride exchange.
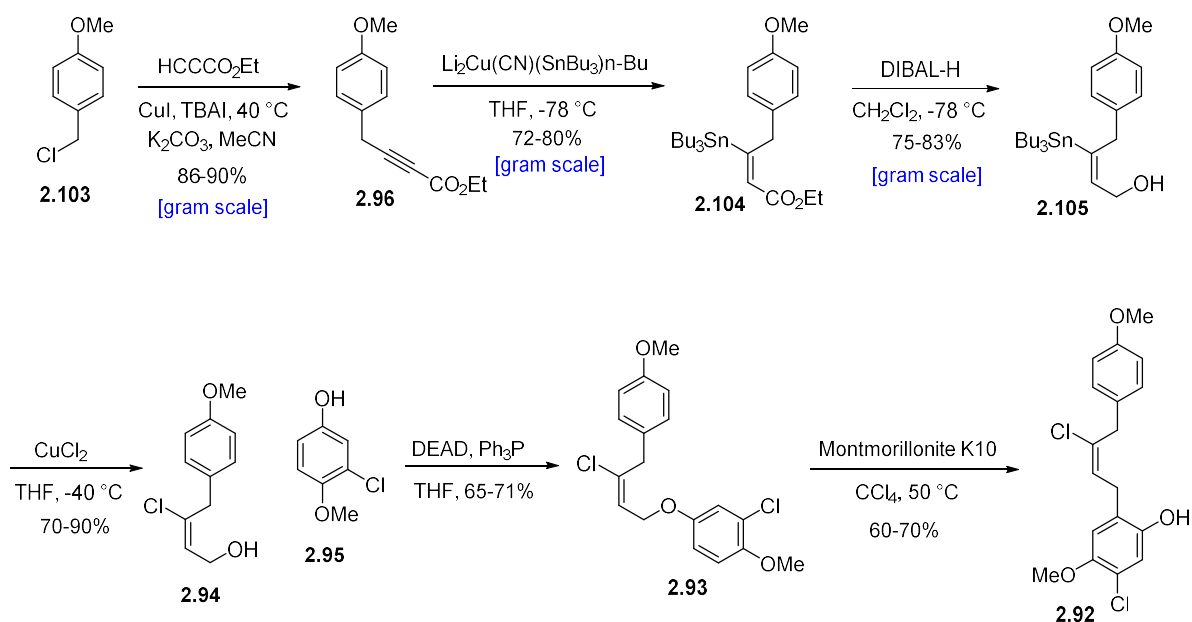
Figure 2.22. Synthesis of hemi-chrysophaentin **2.92.**

As shown above, the substrate needed for the stannylcupration was alkynoate **2.96** (Figure 2.22)**.** Alkynoate **2.96** was accessed in one step from p-methoxybenzyl chloride **2.103** by copper-mediated displacement with ethyl propiolate in 80%.[32] Treatment of alkynoate **2.96** with higher-order cuprate Bu$_3$Sn(Bu)CNCuLi$_2$[31,33,34] afforded stannane **2.104** as single geometric isomer (Figure 2.22). Following stannylcupration, **2.104** was reduced to allylic alcohol **2.105** in 85% yield. The latter was treatment with CuCl$_2$[26] to afford the *E*-chloroalkene **2.94** in 70-90% yield**.**

Treatment of **2.94** and phenol **2.95**[25] under Mitsunobu conditions afforded ether **2.93** in 65% yield. Ether **2.93** is a simplified model system for the proposed O to C migration (Figure 2.22).

Oxygen to carbon (O to C) migrations have been relatively underutilized in the field of synthetic chemistry, however, their use has been shown to be key to the synthesis of prenyl substituted aromatic compounds and macrocyclic peptides.[35] One of the first O to C migrations reported for aromatic substrates was by Yoshizama and co-workers [36] where the treatment of substituted prenyl aryl ether **2.106** with boron trifluoride diethyl etherate afforded O to C migrated product **2.107,** selectively, over Claisen rearrangement products (Figure 2.23). Later work by Dauben and co-workers in 1990 explored the use of silicate-based clays to invoke selectivity for O to C migration over Claisen rearrangement and they found montmorillonite K10 clay catalyzes the O to C migration of prenyl aryl ether **2.108** at room temperature to afford **2.109**. However, Dauben and co-workers discovered if the reaction is heated above 50 °C, further cyclization of the migrated products are possible (Figure 2.23, **2.110**).[37] Dintzner and co-workers [38] further explored the use of silicate-based clays and found that the solvent and temperature can increase the rate of the reaction and affect the selectivity of O to C migration over Claisen rearrangement.

More recently, the Harran group demonstrated the use of acid-catalyzed O to C migrations to rearrange macrocyclic peptides.[39,40] As shown below, the treatment of **2.111** with methanesulfonic acid in nitromethane promoted an O to C migration to form **2.112** in 95% yield. In 2016 Poulsen and co-workers[41] demonstrated that complex allylic ethers such as **2.113** can effectively migrate under Lewis acid conditions such as $BF_3 \cdot Et_2O$, $SnCl_4$, and $FeCl_3$ at low temperatures in dichloromethane (Figure 2.23).
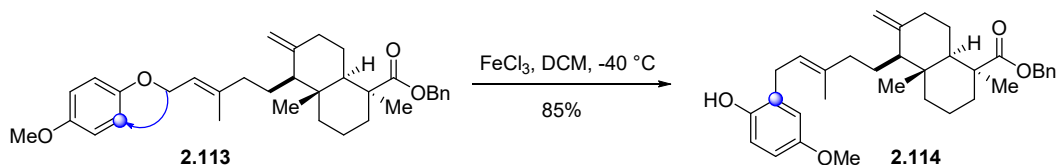
Figure 2.23. Literature examples of O to C migrations.

The examples listed above represent only a few of the reported instances of O to C migrations found in the literature, and based on this work we proposed that we could catalyze the rearrangement of **2.93** to **2.92** with the use of montmorillonite K10 clay or by Lewis acid catalysis. However unlike the previously reported examples, in our proposed O to C migration, either O to C5 or O to C3 migration are possibilities (Figure 2.20, indicated with red and blue arrows) and the

regioisomeric selectivity of O to C migrations have not been previously studied. However, if the O to C migration is not selective it would provide access to two regioisomeric hemi-chrysophaentins which could be used in future biological studies to determine the effect of the substitution pattern around the A-ring has on the observed antimicrobial activity and FtsZ GTPase inhibition. Furthermore, an unselective O to C migration to form 9-dechlorochrysophaentin (**2.51**) would provide two different regioisomeric macrocyclic chrysophaentins which could provide a valuable fragment for biological studies. [3]

To our delight, treatment of ether **2.93** with montmorillonite K10 clay in benzene or dichloromethane provided O to C5 migrated product **2.92** and O to C3 product as a mixture in 60% yield. (Figure 2.22). However, the use of carbon tetrachloride provided the desired C5 isomer **2.92,** exclusively. With the completion of hemi-chrysophaentin **2.92,** we were successfully able to develop a new synthetic route to stereoselectively install the *E*-chloroalkene and found conditions to invoke our proposed late-stage O to C migration which can be adapted to complete the total synthesis of 9-dechlorochrysophaentin (**2.51**) and chrysophaentin A (**2.1**).

With this new synthetic route to access the *E*-chloroalkene, we realized that it could be adapted to synthesize hemi-chrysophaentin (**2.4)** in an improved manner than previously reported.[42] Hemi-chrysophaentin (**2.4**) was originally synthesized by the Wipf group in 12 steps as a mixture of *E/Z* stereoisomers that required super-critical fluid chromatography to separate.[1] Hemi-chrysophaentins **2.4** and **2.18** were found to inhibit the growth of Gram-positive bacteria and the GTPase activity of FtsZ making it a good control compound for future biological studies with 9-dechlorochrysophaentin (**2.51**). We chose to synthesize hemi-chrysophaentin **2.18** over **2.4,** because the previous studies by Bewley and co-workers, determined **2.18** is more active and stable in the GTPase assays.[8]

Therefore, using the chemistry developed for the synthesis of hemi-chrysophaentin **2.92,** we successfully synthesized hemi-chrysophaentin **2.18** in 11 total steps with a longest linear sequence of 7 steps, featuring a stereoselective installation of the *E*-chloroalkene and late-stage Lewis acid-catalyzed O to C migration. This work has recently been published[42] and will only be covered briefly in the context of this document to highlight the optimization of the O to C migration.

Starting with 2,4-dihydroxybenzoic acid (**1.115**), peralkylation with 2-bromopropane followed by reduction with DIABL and treatment with TPP·Cl$_2$ [43] afforded benzylic chloride **2.116** in 80% yield over 3 steps (Figure 2.24). Chloride **2.116** was coupled with ethyl propiolate[32] followed by stannylcupration to afford *E*-stannane **2.117** in 61% yield over the two steps. Enoate **2.117** underwent tin-chloride conversion to the corresponding E-chloroalkene **2.118** in 80% yield. With the *E*-chloroalkene installed, allylic alcohol **2.118** was merged with phenol **2.95**[25] under Mitsunobu conditions to afford **2.119** in 70 % yield. Initial attempts to catalyze the O to C migration with montmorillonite K10, as was used in our synthesis of hemi-chrysophaentin **2.92**, resulted in the isolation of phenol **2.95** as the major product.
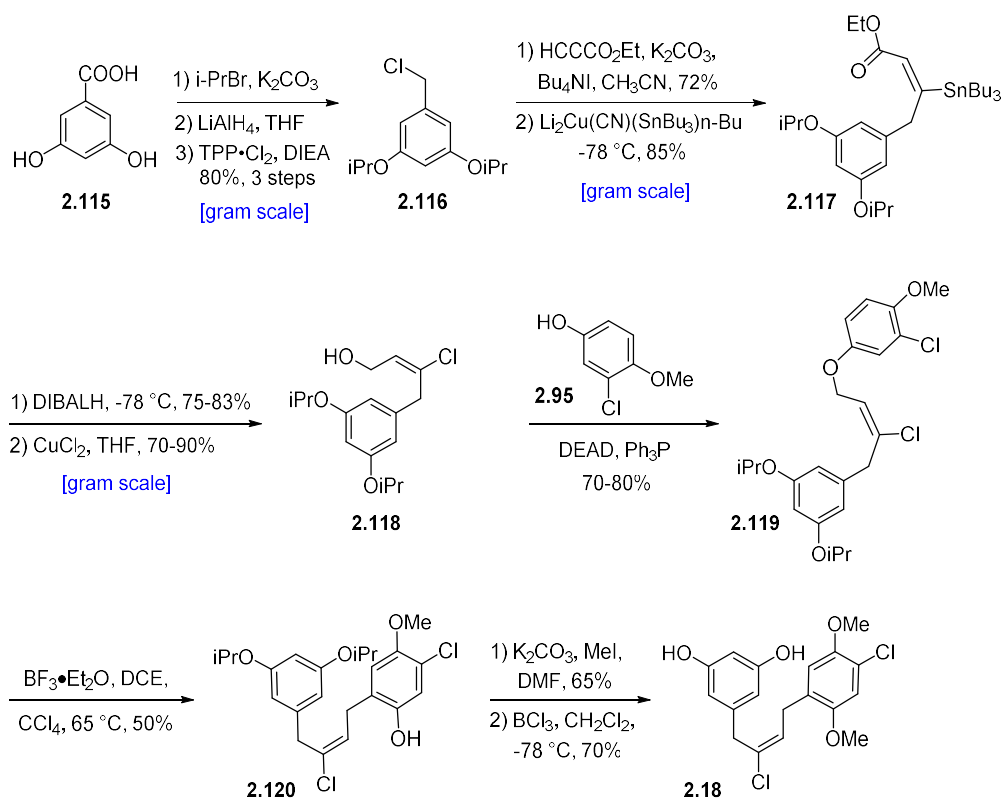
Figure 2.24. An improved synthesis of hemi-chrysophaentin **2.18**.[42]

The formation of phenol **2.95** indicates an intermediate in the O to C migration is being intercepted by advantageous nucleophiles, such as water, cleaving the ether linkage before migration occurs. Montmorillonite clay is known to be hygroscopic and attempts to thoroughly dry montmorillonite K10 at elevated temperatures under vacuum were unsuccessful. Therefore, a screen of Lewis acids was tested to identify new conditions to invoke the O to C migration (Table 2.3).

Catalysis by weak Lewis acids such as AlCl$_3$ and FeCl$_3$ resulted in the recovery of starting ether **2.119** (Table 2.3, entry 2, and 3). However, the use of Sc(OTf)$_3$ resulted in the formation of O to C5 migrated product **2.120** selectively in 24% yield with recovered starting ether **2.119 (**41%) (Table 2.3, entry 5). Increasing the temperature of the reaction resulted in complete consumption of starting ether **2.119.** However, O to C5 product **2.120** was only isolated in 21% yield and the

remaining material was an inseparable mixture of **2.121** and **2.95** (16%) (Table 2.3, entry 6). The

formation of **2.95** and **2.121** indicated that the increase in temperature promotes ether cleavage

and decreases selectivity for **2.120.** Reducing the equivalents of Sc(OTf)$_3$, using a mixture of

carbon tetrachloride in dichloromethane, and reduction of the reaction temperature from 90 °C to

60 °C resulted in complete conversion of **2.119** to O to C5 migrated **2.120** and O to C3 migrated

2.121 in 37% and 31% respectively (Table 2.3, entry 7).

Table 2.3. Hemi-chrysophaentin **2.18** O to C migration optimization.
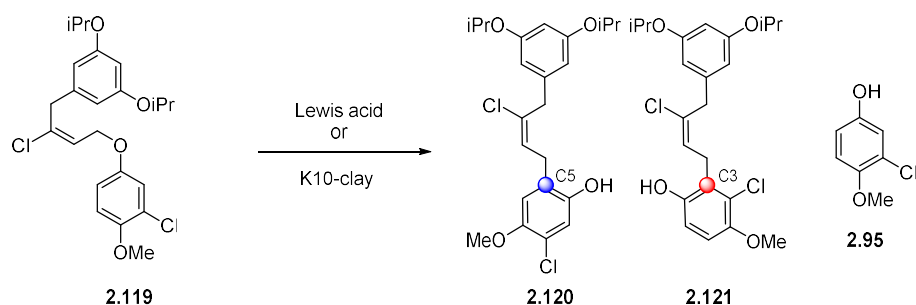
Catalyst (equiv)	Temperature	Solvent	Time	Product (%)
K10 (3 wt%)	60 °C	CCl$_4$	18 h	**2.95** (50%)
Fe^{3+}-K10 (3 wt%)	60 °C	CCl$_4$	18 h	**2.95** (30%)
AlCl$_3$ (1.1)	60 °C	DCE	18 h	**2.119** (80%)
FeCl$_3$ (1.1)	60 °C	DCE	18 h	**2.119** (70%)
Sc(OTf)$_3$ (0.5)	50 °C	CCl$_4$	18 h	**2.120** (24%), **2.119** (41%)
Sc(OTf)$_3$ (0.6)	90 °C	DCE	18 h	**2.120** (21%), **2.121/2.95** (16%)
Sc(OTf)$_3$ (0.25)	60 °C	DCE/CCl$_4$(5:1)	18 h	**2.120** (37%), **2.121** (31%)
BF$_3$·Et$_2$O (2.0)	50 °C	DCE	18 h	**2.120** (45%), **2.121/2.95** (26%)
BF$_3$·Et$_2$O (3.0)	**50 °C**	**DCE/CCl$_4$(5:1)**	**18 h**	**2.120 (57%), 2.121/2.95 (10%)**

Further optimization by switching the Lewis acid catalyst to $BF_3 \cdot Et_2O$ in a 1:5 mixture of carbon tetrachloride in dichloromethane resulted in a 57% yield of the desired O to C5 migrated **2.120** with only 10% formation of **2.121** mixed with **2.95** (Table 2.3, entry 9). Following protection of **2.120** with MeI and deprotection of the isopropyl protecting groups afforded hemi-chrysophaentin **2.18** in a total of 11 steps and as a single geometric isomer. Hemi-chrysophaentin **2.18** will be used as a positive control molecule for biological assays which will be discussed in Chapter 3. Upon the completion of these syntheses, the synthetic route was adapted for the synthesis of the Southern AD fragment of 9-dechlorochrysophaentin (**2.51**).

2.6.3 Synthesis of VU0848354 and VU0848355: Optimization of Southern AD Fragment

Southern AD fragment **2.58** is the remaining fragment needed to complete the synthesis of 9-dechlorochrysophaentin (**2.51**). In order to adapt the stannylcupration installation of the *E*-chloroalkene for the AD fragment, the S_NAr coupling partner needed to be changed from bromide **2.62** to phenol **2.122.** The ester moiety of phenol **2.122** facilitates the installation of an alkynoate moiety needed for the stannylcupration. Phenol **2.122** was generated by acidic esterification of commercial syringic acid in 90% yield. Treatment of phenol **2.122** under standard S_NAr conditions with **2.61** afforded diaryl ether **2.123** in 72% yield. Fortuitously, the ester moiety of the D-ring resulted in selective aryl-migration under Baeyer-Villager conditions affording, after methanolysis, phenol **2.124** in 65% over the two steps (Figure 2.25). Phenol **2.124** was treated with allyl bromide under basic conditions to afford allyl ether **2.125**, which subsequently was irradiated at 200 °C in a microwave reactor on water to afford a 1:1 mixture of regioisomeric Claisen rearrangement products **2.126** and **2.127** in 34 and 32% yield, respectively. Initially, **2.126** and **2.127** were separated and **2.127** was advanced through the synthesis, however, it became

apparent that the loss of material would not facilitate the completion of 9-dechlorochrysophaentin (**2.51**). Therefore, it was discovered that treatment of allyl ether **2.125** at low temperature with boron trichloride promoted Claisen rearrangement favoring our desired regioisomeric product **2.127** in a 2:1 ratio over **2.126,** in 60% yield.
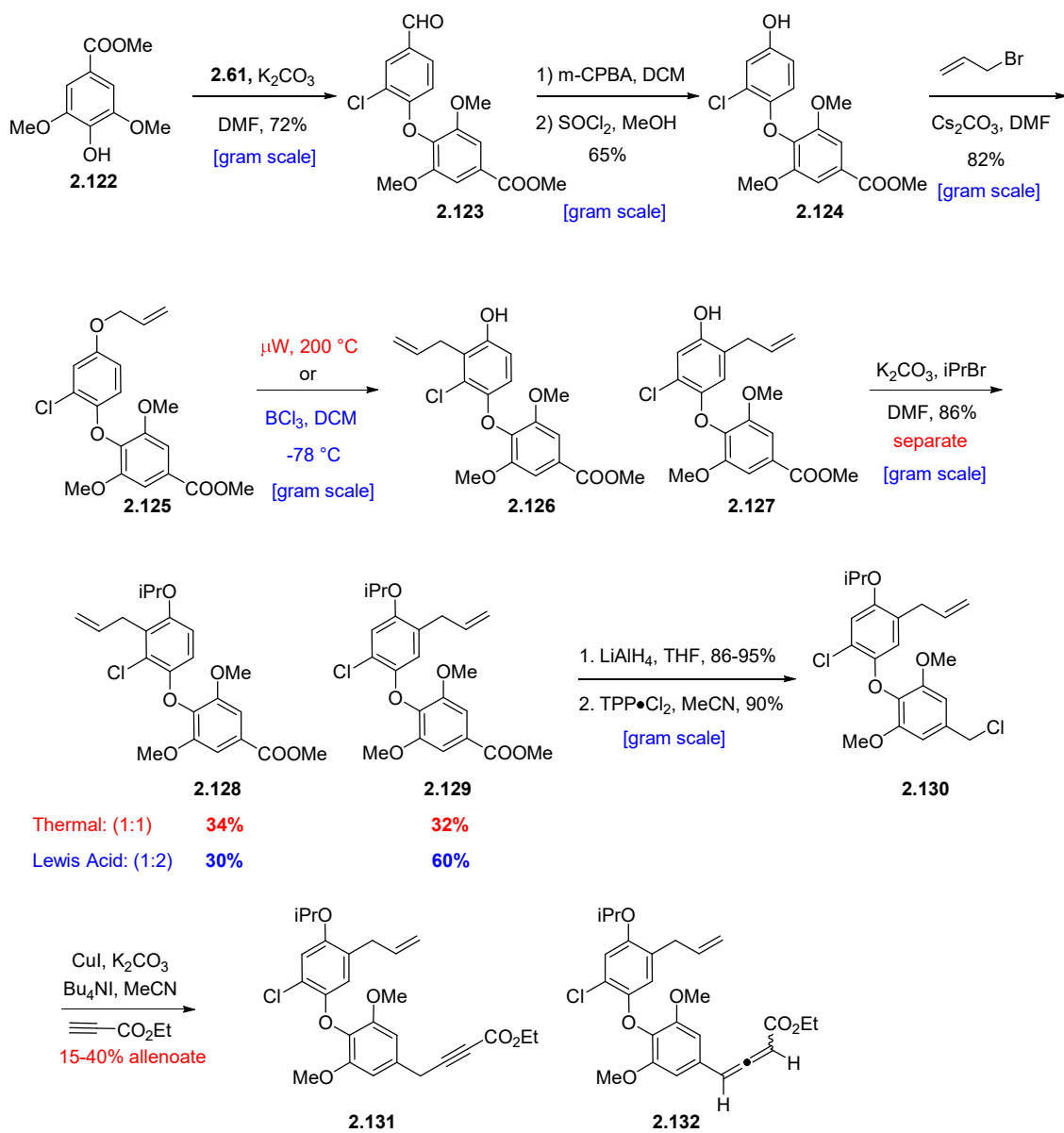

Figure 2.25. Synthesis of AD fragment alkynoate **2.131.**

With our optimized Claisen conditions, **2.126** and **2.127** were protected as the isopropyl ethers **2.128** and **2.129** and separated by column chromatography. Ester of **2.129** was reduced and the intermediate benzylic alcohol was converted to chloride **2.130** with TPP·Cl$_2$.[43] Attempts to displace the latter formed benzylic chloride with ethyl propiolate[32] resulted in a mixture of alkynoate **2.131** and allenoate **2.132** (Figure 2.25). Allenoate **2.132** is presumed to form by base mediated isomerization of alkynoate **2.131** to allenoate **2.132.**

Buchwald and co-workers [44] saw a similar propensity of benzylic alkynes to isomerize to allenes when studying palladium coupling of benzylic chlorides with terminal alkynes. Buchwald and co-workers determined that the equivalents of base, solvent, and temperature played a key role in the formation of allene products and selective formation of alkyne products could be favored, when the reaction was maintained below 65 °C, ran in acetonitrile or THF, with 1.05 equivalents of base.[44] Unfortunately, adapting Buchwald and co-workers' conditions to our copper(I) mediate displacement had no effect favoring alkynoate over allenoate formation. Furthermore, attempts to couple ethyl propiolate under Buchwald and coworkers' palladium conditions[44] were unsuccessful. Therefore, a new multistep sequence to furnish alkynoate **1.131** was needed.

Based on the Wipf's group synthesis of hemi-chrysophaentin (**2.4**),[1] benzylic chloride **2.130** was displaced with ethynyltrimethylsilane to afford alkyne **2.133** in 82% yield (Figure 2.26). Deprotection with catalytic sodium methoxide afforded intermediate terminal alkyne and subsequent treatment with nBuLi followed by carbon dioxide quench and esterification afforded alkynoate **2.131** in 60% yield (Figure 2.26). Alkynoate **2.131** was then treated under stannylcupration conditions[31] to afford *E*-stannane **2.134** as a single geometric isomer. Stannane **2.134** was reduced with DIBAL followed by a tin-chloride exchange with copper (II) chloride[26] to afford Southern AD fragment **2.135** in 15 steps from syringic acid.
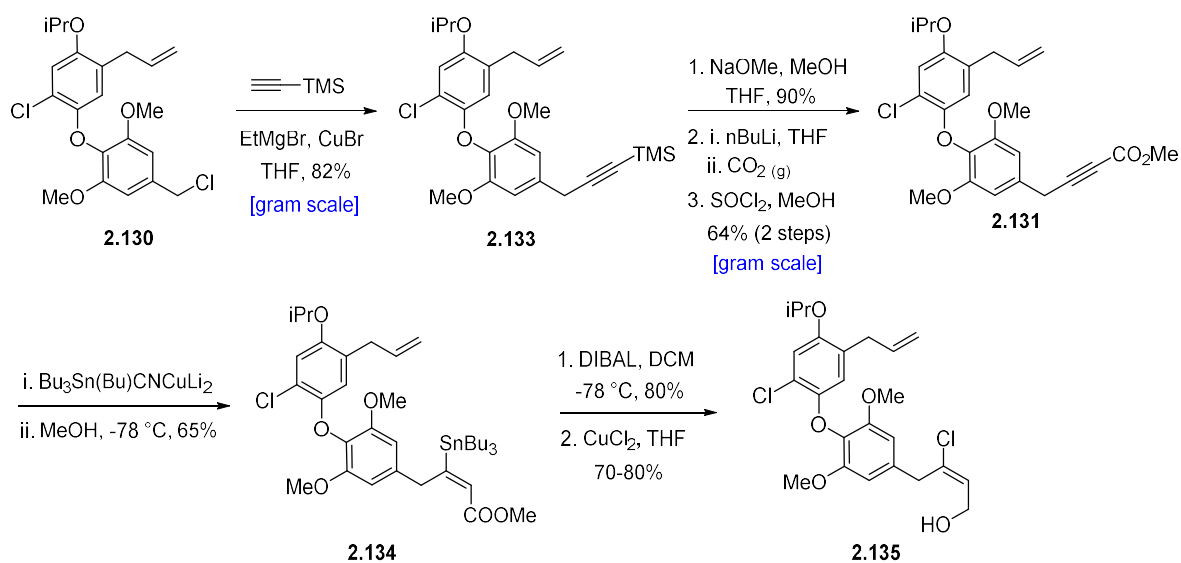
Figure 2.26. Synthesis of AD fragment **2.135.**

Following the completion of AD fragment **2.135,** attention was directed at the merger of Northern BC and Southern AD fragments. BC fragment **2.87** and AD fragment **2.135** were merged under Mitsunobu conditions[45,46] to afford ether **2.136** in 65% yield (Figure 2.27). At this point, we had two distinct options on how to form the macrocyclic core either invoke the O to C migration followed by ring-closing metathesis (RCM) or ring-closing metathesis (RCM) followed by O to C migration. The latter sequence proved more efficient and alkyl aryl ether **2.136** was treated with Grubbs second-generation catalyst to afford **2.138** as an inseparable mixture of *E/Z* stereoisomers.
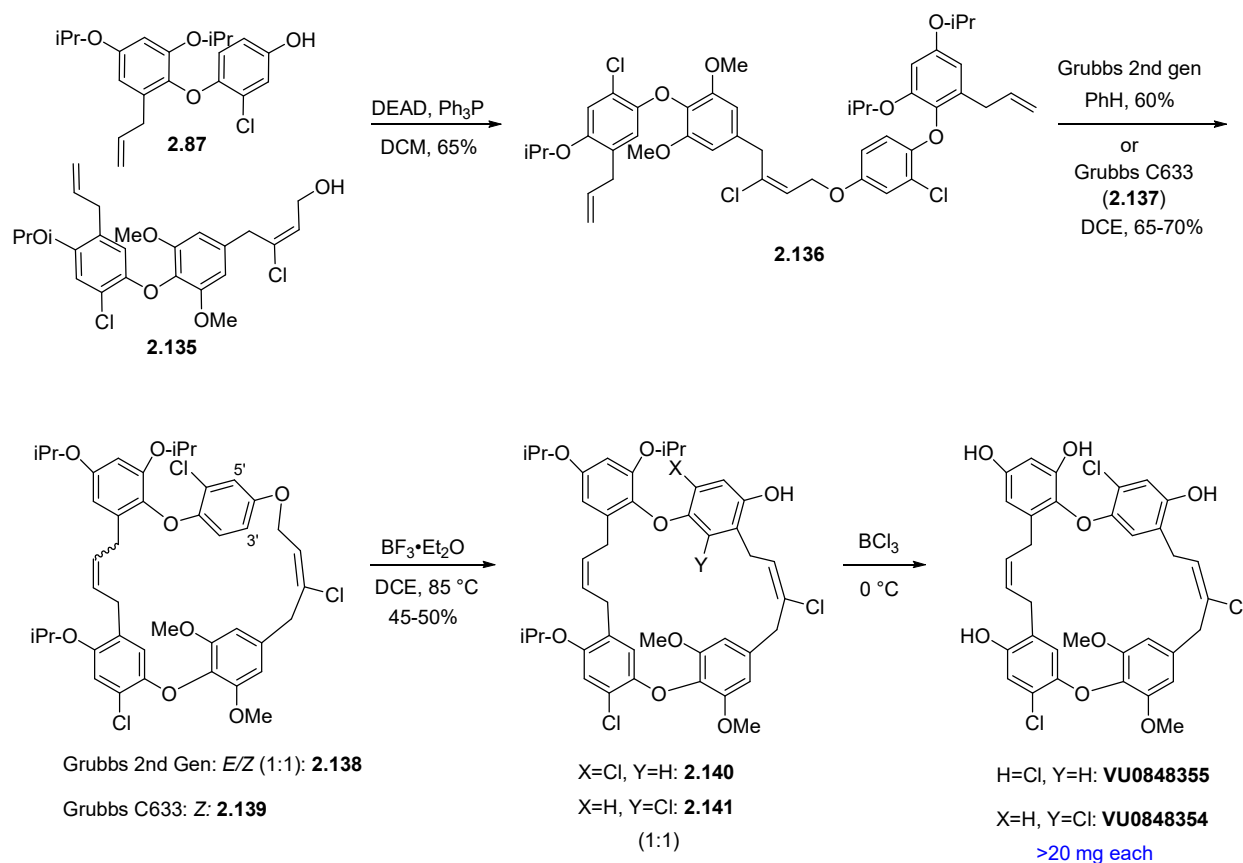
Figure 2.27. Synthesis of 9-dechlorochrysophaentins **VU0848355** and **VU0848354.**

Fortuitously, the use of Grubbs *Z*-selective catalyst (C633)[15,47–49] (**2.137**) provided the desired *Z*-macrocycle **2.139** in 65% yield (Figure 2.27). As mentioned above, treatment of **2.136** with Grubbs second-generation catalyst afforded both the *E*-alkene or *Z*-alkene containing macrocycle, **2.138,** and as depicted below the mechanism of a ring-closing metathesis reaction is a series of [2+2] cycloadditions and cycloreversions which allows for the formation of either *E*-alkene or *Z*-alkene products (Figure 2.28). The first step of a ring-closing metathesis reaction is a [2+2] cycloaddition and cycloreverison that occurs between the catalyst and a substrate alkene to afford intermediate **2.142** (Figure 2.28).[49] Intermediate **2.142** then coordinates another alkene in the substrate and undergoes [2+2] cycloaddition generating ruthenacyclobutane **2.143** or **2.147.**

Sterics and thermodynamics control the formation of the ruthenacyclobutane intermediates **2.143** and **2.147**. Formation of **2.147** results in the *anti*-arrangement of the R-groups which is sterically favored and affords *E*-isomer **2.148** upon cycloreverison. However, if the ruthenacyclobutane forms with the R-groups in a *syn*-relationship to each other, **2.143** which is sterically less favored, upon cycloreverison affords the *Z*-alkene **2.145** (Figure 2.28).[49]
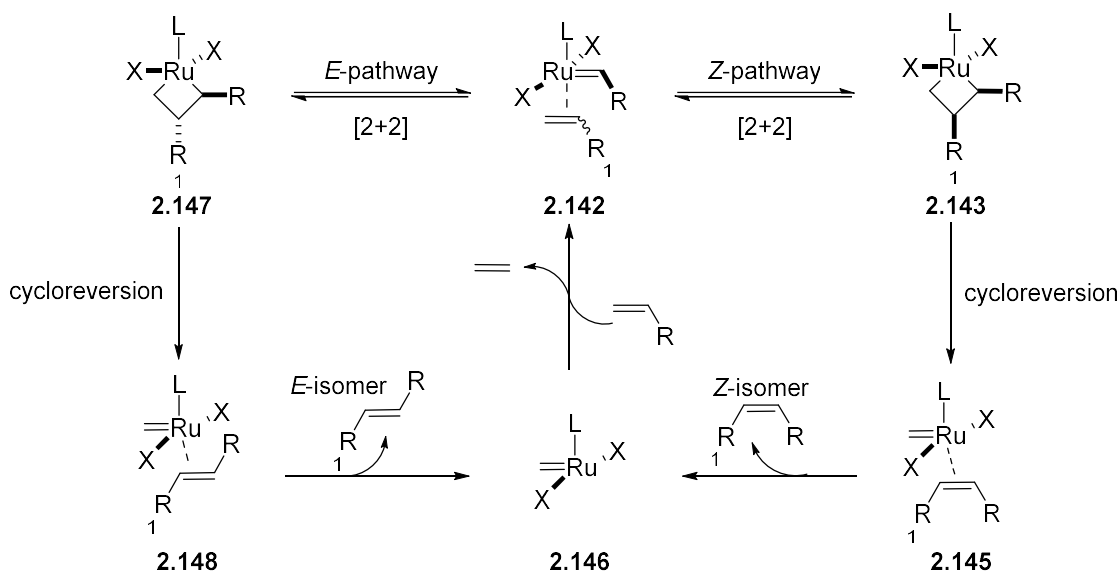
Figure 2.28. Ring-closing metathesis: mechanism of *E/Z* isomer formation, adapted from Montgomery et al.[49]

Grubbs and co-workers found that for traditional cross-metathesis the ratio of *E* to *Z* olefin formation was 9:1, favoring *E*-alkene formation.[15] Based on the selectivity favoring *E*-alkene products, Grubbs and co-workers proposed that to selectively form the *Z*-alkene in a metathesis reaction, a new catalyst would need to designed to limit the olefin coordination to the ruthenium-carbene intermediate **2.142** to occur from only one side, and favor formation of only *syn*-ruthenacycle **2.143**. This hypothesis led to the discovery and synthesis of Grubbs catalyst 633 (**2.137**)[47] (Figure 2.29). Catalyst **2.137** promotes selective *Z*-olefin metathesis reactions by

disfavoring the formation of *anti*-ruthenacycle **2.147** by creating steric interactions with the ruthenium catalyst (Figure 2.29).[47–49]

As depicted below, the formation of the *syn*-ruthenacyclobutane **2.149** is favored due to unfavorable steric interactions of the NHC-ligand mesityl group with the substrate R-groups, if they are arranged in an *anti*-relationship (Figure 2.29, **2.150**). As mentioned above for our system, catalyst **2.137** provided the desired *Z*-alkene product **2.139,** exclusively (Figure 2.30). Confirmation of olefin geometry was accomplished by selective 1D-NOE's between the methylenes adjacent to the newly formed alkene (see appendix for NOE correlation).
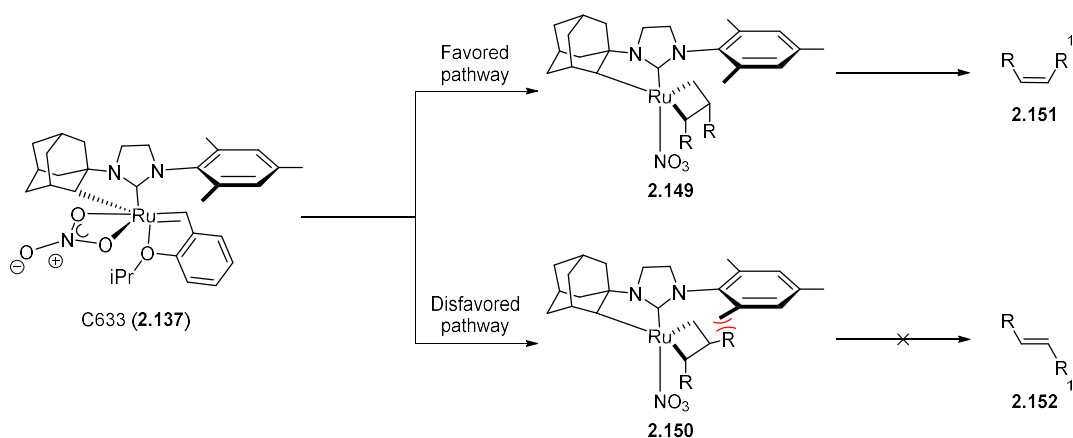
Figure 2.29. Hoveyda-Grubbs (C633) *Z*-selective catalyst model for selectivity.

Following ring-closing metathesis, expanded macrocycle **2.138** was treated with $BF_3 \cdot Et_2O$ at elevated temperatures to promote the O to C migration affording a 1:1 mixture of O to C5' migrated product, **2.140** and O to C3' migrated product, **2.141** (Figure 2.27). Unfortunately, selective formation of either C5' or C3' migrated product could not be achieved. However, following deprotection of **2.140** and **2.141** with BCl_3 afforded **VU0848354** and **VU0848355** (Figure 2.27). Attempts were made to cleave the methyl ethers of **VU0848355** and **VU0848354**

with BBr$_3$, BCl$_3$/Bu$_4$NI, and pyridine-HCl salt to afford 9-dechlorochrysophaentin (**2.51**), but were unsuccessful.

Difficulty in the removal of the methyl ethers was also seen with the previous route by the VICB Synthesis Core, however, we chose to proceed with the methyl ether protected D-ring due to the commercial availability of phenol **2.122** (Figure 2.25). We were hopeful a screen of deprotection conditions would afford 9-dechlorochrysophaentin (**2.51**). Even though we could not deprotect **VU0848354** and **VU0848355,** the 9-dechlorochrysophaentin congeners were used in antimicrobial activity and mechanism of action studies, which will be discussed in Chapter 3.

2.7 Analysis of VU0848355 and VU0848354 Reveals potential Non-canonical Atropisomerism

With the completion of 9-dechlorochrysophaentins **VU0848355** and **VU0848354,** we turned our attention towards their structural analysis using NMR techniques. First, we confirmed the *Z*-geometry of the C8-C9 alkene, installed by the key *Z*-selective RCM reaction. Using NMR we observed complementary nuclear Overhauser enhancements (NOEs) between neighboring allylic methylenes C7 and C10 (1D-NOE correlations are available in appendix). However, most surprising were the differences in proton and carbon signals in **VU0848355** and **VU0848354.**

Recall the O to C migration bifurcated between C3' and C5' leading to **VU0848355** and **VU0848354,** possessing natural and unnatural C-ring substitution patterns. For clarity purposes, we refer to the unnatural C-ring macrocycle as "iso" chrysophaentins. When the ^{1}H NMR of **VU0848355** and **VU0848354** were compared, we were surprised to see resonances in **VU0848355**

corresponding to the O-methyl ether protons to be significantly broadened when compared to the iso-chrysophaentin (**VU0848354**) (Figure 2.30).
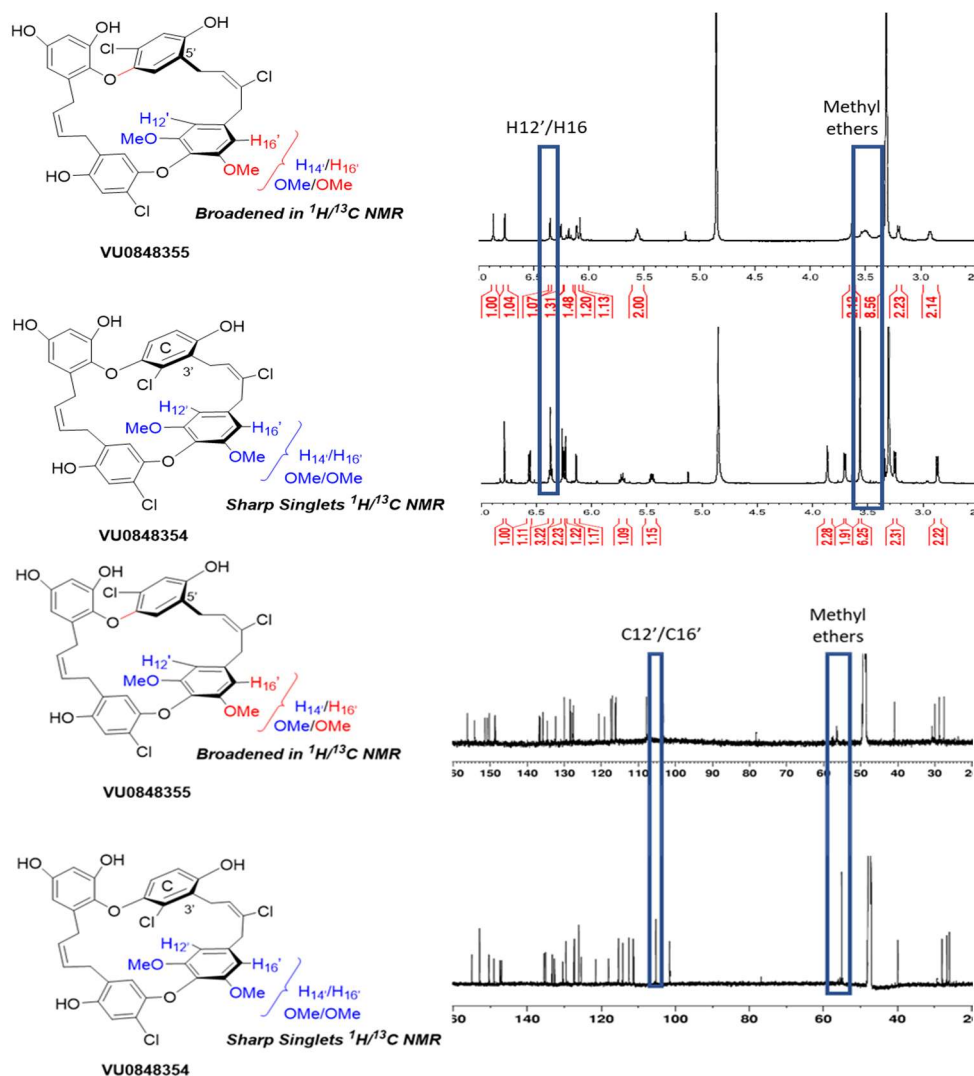
Figure 2.30. ^{1}H and ^{13}C NMR differences for **VU0848355** and **VU0848354.**

Likewise, aromatic proton signals corresponding to H12' and H16' were broadened to the point of being absent in natural isomer (**VU0848355**). In contrast, the ^{1}H NMR of iso-chrysophaentin (**VU0848354**) showed sharp singlets at 3.56 ppm and 6.37 ppm representing the methyl ethers and the protons corresponding to H12 and H16, respectively (Figure 2.30, blue box

highlights proton and carbon spectra differences). The stark difference between the proton spectra of **VU0848355** and **VU0848354** continued upon inspection of their ^{13}C NMR spectra, where the methyl ether carbon peak for **VU0848355** was very broad and almost undetectable at 55.4 ppm, while the carbon spectra of **VU0848354** contained a sharp peak at 55.1 ppm corresponding to the methyl ethers (Figure 2.30, bottom spectra). The carbon peak representing C12' and C16' was also absent in **VU0848355.** The broadness of the methyl ether proton and carbon peaks along with the absence of the proton and carbon peaks representing H12'/C12' and H16'/C16' indicated that **VU0848355** contains a rotational barrier (Figure 2.30).

Rotational barriers in small molecule containing biaryls and macrocyclic natural products have been extensively studied and are an important area of investigation for drug discovery.[50–52] Macrocyclic natural products that contain rotational barriers are frequently isolated as a single atropisomer. Naphthalenophane (**2.153**), longithorone A (**2.154**), vancomycin (**2.155**), cavicurlarin (**2.156**) are all examples of macrocycle-containing unnatural or natural products which incorporate bonds with rotational barriers allowing their isolation as single atropisomers (Figure 2.31).[53] Typically barriers to bond rotation need to be greater than 30 Kcal/mol to be isolable at room temperature.
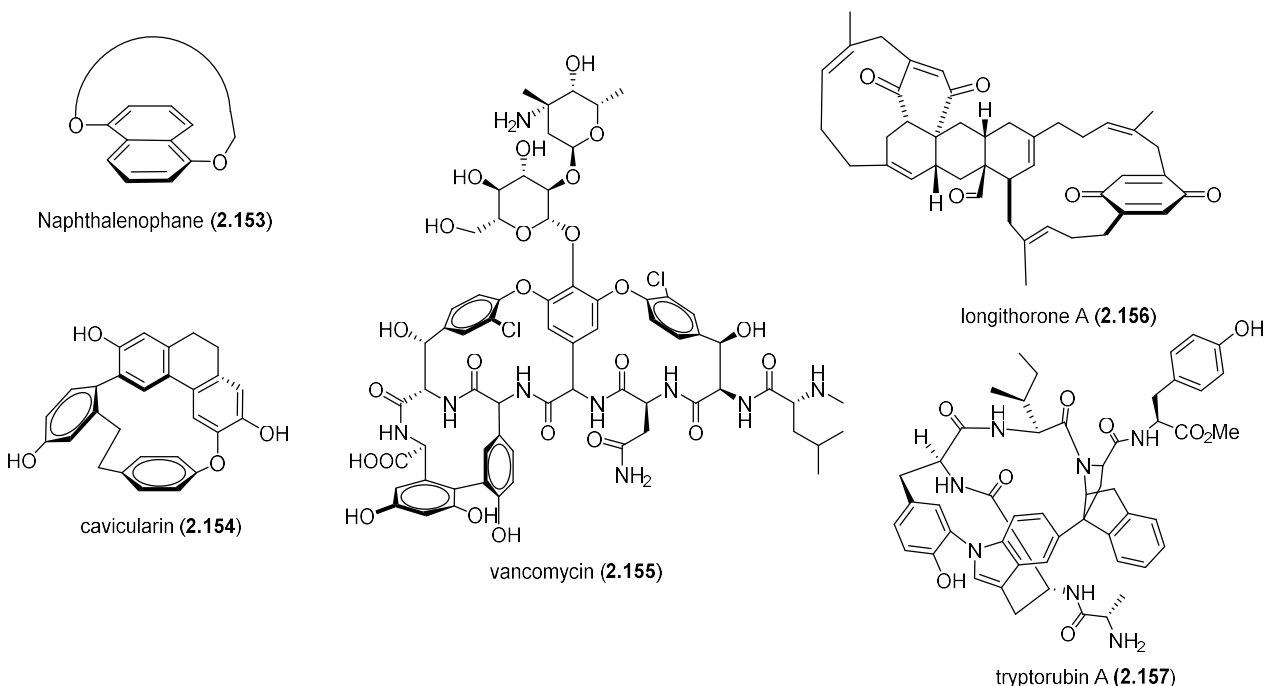
Figure 2.31. Cyclophane and macrocyclic peptide natural products with rotational barriers.

Recently the Baran group published the total synthesis of tryptorubin A (**2.157**)[54] a natural product proposed to exist as a single diastereomer due to "non-canonical" atropoisomerism. Canonical atropisomers are defined as interchangeable by rotation about a single bond such as binaphthol or highly substituted amides. In contrast, non-canonical atropisomers require multiple bond distortions as represented by the rotaxanes. As a non-canonical atropisomer, tryptorubin A (**2.157**) can exist as either bridged-above atropisomer or the bridged-below atropisomer, however, the interconversion would require the bridged ring system (highlighted in blue and green) to thread through the peptide ring (black and light grey) (Figure 2.32). The interconversion would require numerous bond torsions and therefore is not achievable by simple thermal equilibration. Based on this definition, the chrysophaentins could be an example of non-canonical atropisomers as an interchange between enantiomeric conformers would require multiple bond distortions (more than

71

one) (Figure 2.33). This threading or rotation through the macrocycle would require multiple bond torsions similar to tryptorubin A (**2.157**).
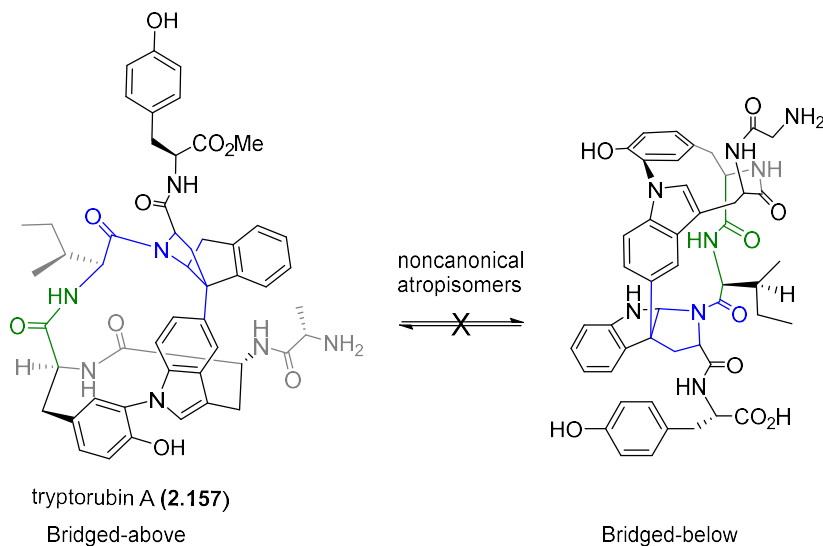
Figure 2.32. Tryptorubin A (**2.157**) non-canonical atropisomers.
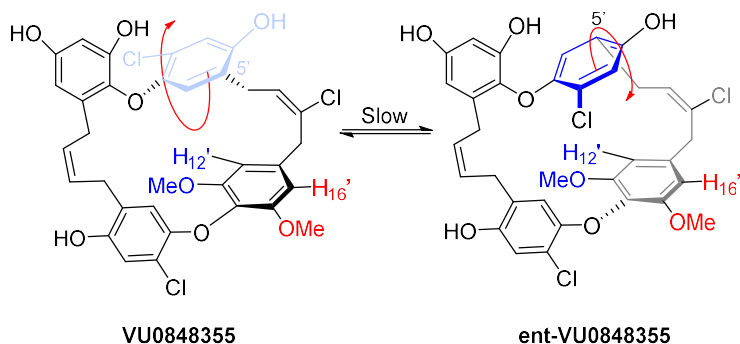
Figure 2.33. Potential non-cononical atropisomers of **VU0848355.**

Providing the bond rearrangement required to interchange between conformers **VU0848355** and **ent-VU0848355** (Figure 2.33) was greater than 30 Kcal these two enantiomeric compounds could be resolved by chiral HPLC. However, attempts to separate the enantiomeric conformers by chiral HPLC under multiple conditions proved unsuccessful (chromatogram available in appendix). This led us to conclude the two conformers (**VU0848355** and **ent-**

VU0848355) slowly interchange at room temperature with a barrier to interconversion between 10 and 25 Kcal. We anticipated variable temperature NMR would support this conclusion. While heating an NMR sample of **VU0848355** to 90 °C did not lead to spectral coalescence, low-temperature NMR experiments did support the slow interconversion of conformers.

Upon cooling an NMR sample of **VU0848355** in CD$_3$OD from room temperature (23 °C) down to -40 °C we observed sharpening of the spectral signals leading to the observation of the previously broadened resonances (O-methyl and aromatic H12'/C12' and H16'/C16' signals) (Figure 2.34). Upon closer inspection and low-temperature HSQC acquisition (available in appendix), it was determined that the new peaks at 3.74 and 3.21 ppm corresponded to the methyl ethers with carbon shifts of 56.4 and 55.2 ppm which is comparable with the carbon shift for the methyl ethers of **VU0848354**.

Similarly, the hydrogens of methylenes at 3.62 ppm and 2.91 ppm at room temperature split into two peaks at 3.84 and 3.41 ppm and 2.87 and 2.92 ppm, respectively at -40 °C. The splitting on the methylene groups provides evidence that the rotational barrier is more complex than simple atropisomerization as seen with binaphthyl and biaryls, and our rotational barrier could be a result of non-canonical atropisomerization. Furthermore, two new peaks also appeared in the aromatic region (6-8 ppm), which corresponded to the missing H12' and H16' protons as confirmed by low-temperature HSQC. The new protons at 6.63 ppm and 5.68 ppm are H12' and H16' and corresponded to carbons with the shifts of 108.2 and 104.4 ppm. These shifts are near the other aromatic carbons and are comparable to the carbon shift of C12'/C16' in **VU0848354** of 106.4 ppm.
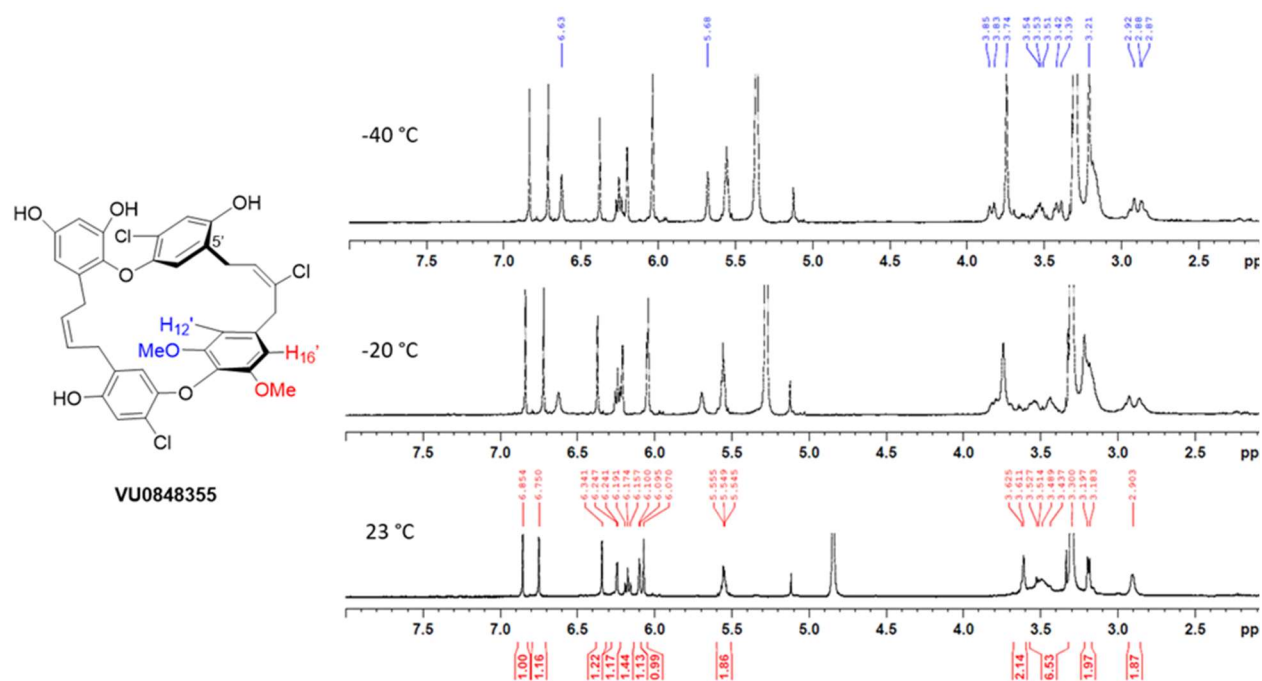
Figure 2.34. Low temperature ^{1}H NMR assignemtn of methyl ethers H12'/H16' of **VU0848355**.

The biological activity of small molecules and natural products is heavily dependent upon the conformations of the molecules and the different overall conformation of two atropisomers can result in completely different biological activity, efficacy, toxicity, off-target effects, and in rare cases completely change the protein target or engagement.[52,61,62] The importance of understanding how molecular conformation and shape of natural products is vital to interpreting their biological activity has been studied extensively for polyketide natural products by Taylor and co-workers.[55,56] Furthermore, Emil Fischer summarized this notion with the lock-and-key analogy of how bioactive molecules interact with protein or biological targets, where the small molecule is the key and the protein structure is the lock.[57] Koshland updated the lock and key model to the induced fit model, which states that an enzyme or ligand will change its shape upon binding to generate a better interaction.[58–60] We hypothesized that the rotational barrier seen with **VU0848355** could be a result of non-canonical atropisomerization, and the difference in conformation of **VU0848355** compared

74

to **VU0848354** could affect interaction with FtsZ and their antimicrobial activity based on the induced fit model.

Boehringer Ingelheim has created a classification system of atropisomers based on computational and experimental analysis of rotational barriers in small molecules.[52,62] Boehringer Ingelheim classified atropisomers based on torsional energy barriers and the half-life of the isomers into three different classes, which can be used to aide in the development of molecules that possess atropisomers.[52,54] Based on their classification system, **VU0848355**, falls into class 2 of atropisomers, which means the atropisomers are interconverting on the timescale of minutes-hours with an energy barrier of ~15-25 kcal. Based on Boehringer Ingelheim's classification system, the molecule should be developed as a mixture, because the atropisomers cannot be isolated from each other. Furthermore, with the knowledge of this small rotation barrier, future synthetic analogs can be synthesized with larger substituents on the C-ring (for example C1-methyl) to further slow the interconversion and allow for the formation and isolation of the two non-canonical atropisomers. The two atropisomers could be used in biological assays to determine the importance of the overall conformation of the chrysophaentins. With the structures of **VU0848355** and **VU0848354** confirmed, the total synthesis of 9-dechlorochrysophaentin (**2.51**) would require a new Southern AD fragment with labile isopropyl protecting groups.

2.8 Chemical Synthesis of 9-dechlorochrysophaentin (2.51)

Cleavage of C13' and C15' methyl ethers of **VU0848355** and **VU0848354** proved unworkable disabling access to 9-dechlorochrysophaentin (**2.51**) by the previously described synthetic route. Therefore, a revised synthesis of AD biaryl **2.135** was needed with the replacement

of the stubborn methyl esters with the more readily cleavable isopropyl ethers. To this end, 4-bromo-3,5-dihydroxybenzoic acid was peralkylated with isopropyl bromide to afford **2.158** in 85% yield (Figure 2.35). Lithium-halogen exchange followed by boronate quench and oxidation afforded S_NAr coupling partner, phenol **2.159** in 60% yield**.** The lithium-halogen exchange was found to be successful only at -100 °C or substantial addition of nBuLi to the ester moiety was observed. Following oxygenation of bromide **2.158,** phenol **2.159** and aldehyde **2.61** were treated under standard S_NAr conditions to form biaryl ether **2.160.** Using the same synthetic sequence used for the synthesis of AD fragment **2.135**, phenol **2.161** was accessed in 65% over two steps (Figure 2.35). The latter was treated with allyl bromide under basic conditions to afford allyl ether **2.162**, which subsequently underwent Claisen rearrangement to afford **2.163** and **2.164,** after protection of the generated phenols with isopropyl bromide. Unfortunately, by exchanging the methyl ether protecting groups to isopropyl protecting groups, the Lewis acid-catalyzed Claisen rearrangement conditions developed previously could no longer be used, as the isopropyl groups are cleaved under Lewis acidic conditions. As the allyl aryl ether Claisen rearrangement results in a mixture of isomers, an alternative path to selectively introduce the allyl group was developed.

Based on literature precedent we anticipated that selective bromination of the A-ring at C5 could be achieved. To our delight, treatment of **2.161** with PTSA and N-bromosuccinimide, [63] followed by protection with isopropyl bromide afforded **2.165** in 72 % yield over the two steps. Bromide **2.165** was then engaged into a Suzuki cross-coupling with pinacol allylboronate to give **2.164** in 85% yield (Figure 2.34).[64,65]
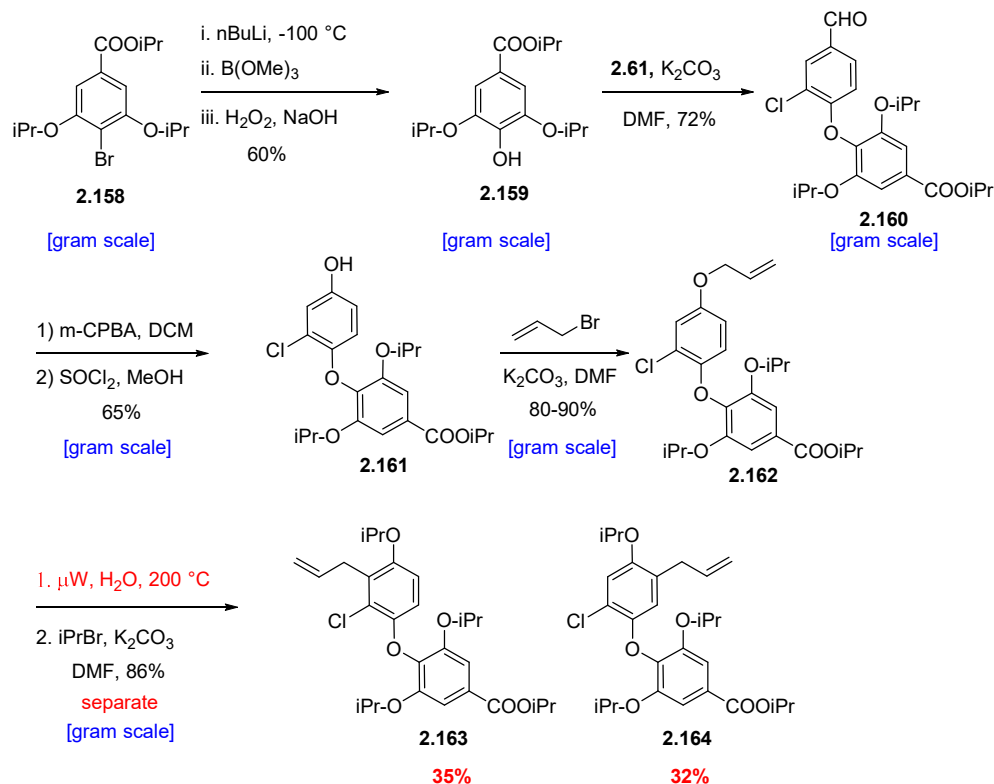
Figure 2.35. Second generation synthesis of AD Fragment **2.168.**

With the C5 allyl group selectively installed, elaboration of the D-ring ester to alkynoate **2.168** could be achieved in a similar fashion as was used for alkynoate **2.131** (Figure 2.27). Reduction with lithium aluminum hydride (LAH) followed by conversion to the benzylic chloride with TPP·Cl$_2$[43] occurred in 80% yield. Homologation of the latter formed benzylic chloride was achieved with ethynyltrimethylsilane.[1] Treatment with catalytic sodium methoxide afforded deprotected alkyne **2.166** in 72% yield over two steps**.** Alkyne **2.166** was deprotonated with nBuLi and subsequently quenched with carbon dioxide to afforded carboxylic acid **2.167** and following esterification gave alkynoate **2.168** in 70% yield over two steps. Alkynoate **2.168** was then converted into AD fragment **2.169** by the previously described sequence (Figure 2.26). The isopropyl protected AD fragment was completed in 17 steps.
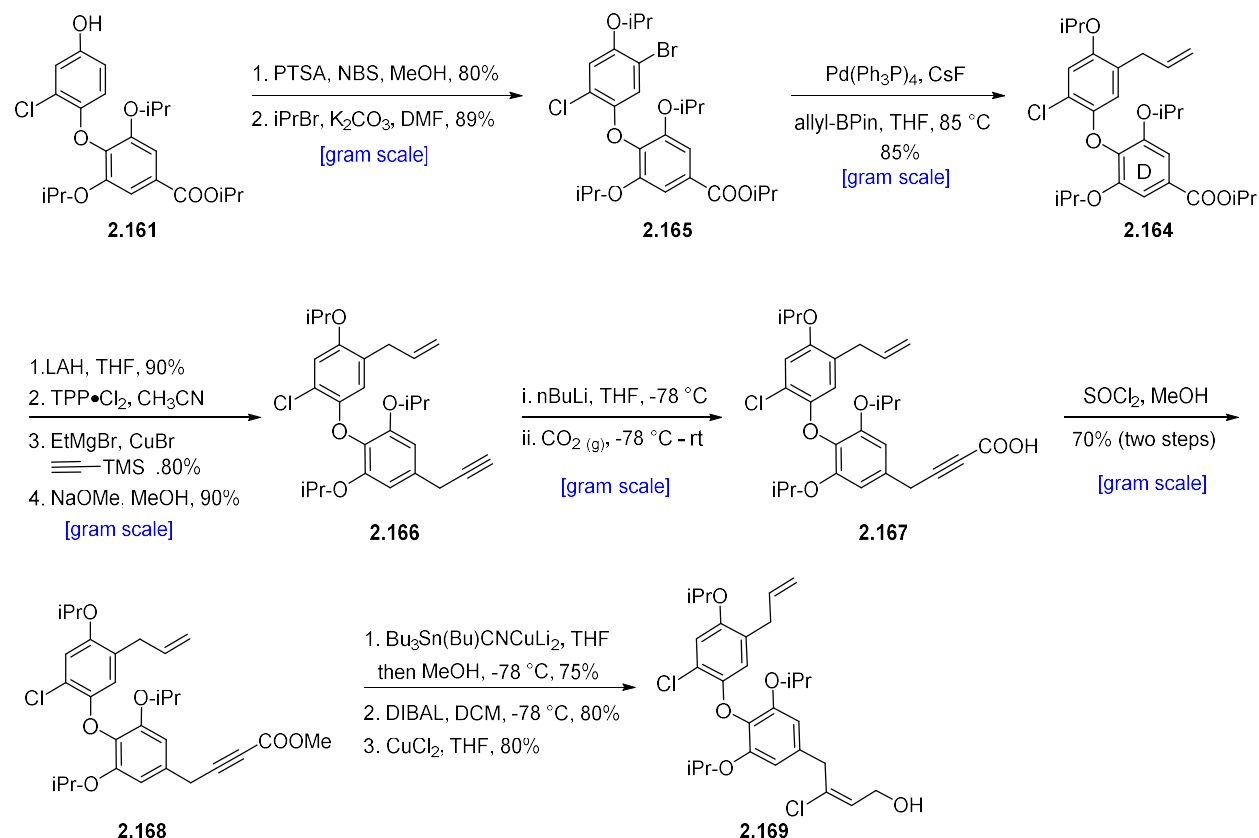
Figure 2.36. Third generation synthesis of AD fragment **2.169:** selective C5-allyl installation**.**

The merging of the biaryl ether fragments **2.87** and **2.169** was accomplished using the previously described sequence (Figure 2.27) starting with Mitsunobu coupling to afford allyl aryl ether **2.170** (Figure 2.37). Ether **2.170** was treated with Grubbs Z-selective catalysis (C633)[15,47–49] to afford macrocycle **2.171** and following treatment with BF$_3$·Et$_2$O and deprotection with BCl$_3$ completed the chemical synthesis of 9-dechlorochrysophaentin (**2.51, VU0849855**) accompanied by iso-9-dechlorochrysophaentin (**2.174, VU0849838**).   9-dechlorochrysophaentin (**2.51**) was completed in 29 total steps, 17 step longest linear sequence and is the closest any groups have been to completing the total synthesis of chrysophaentin A (**2.1**), in which only the C9-chloride group is missing (Figure 2.37).
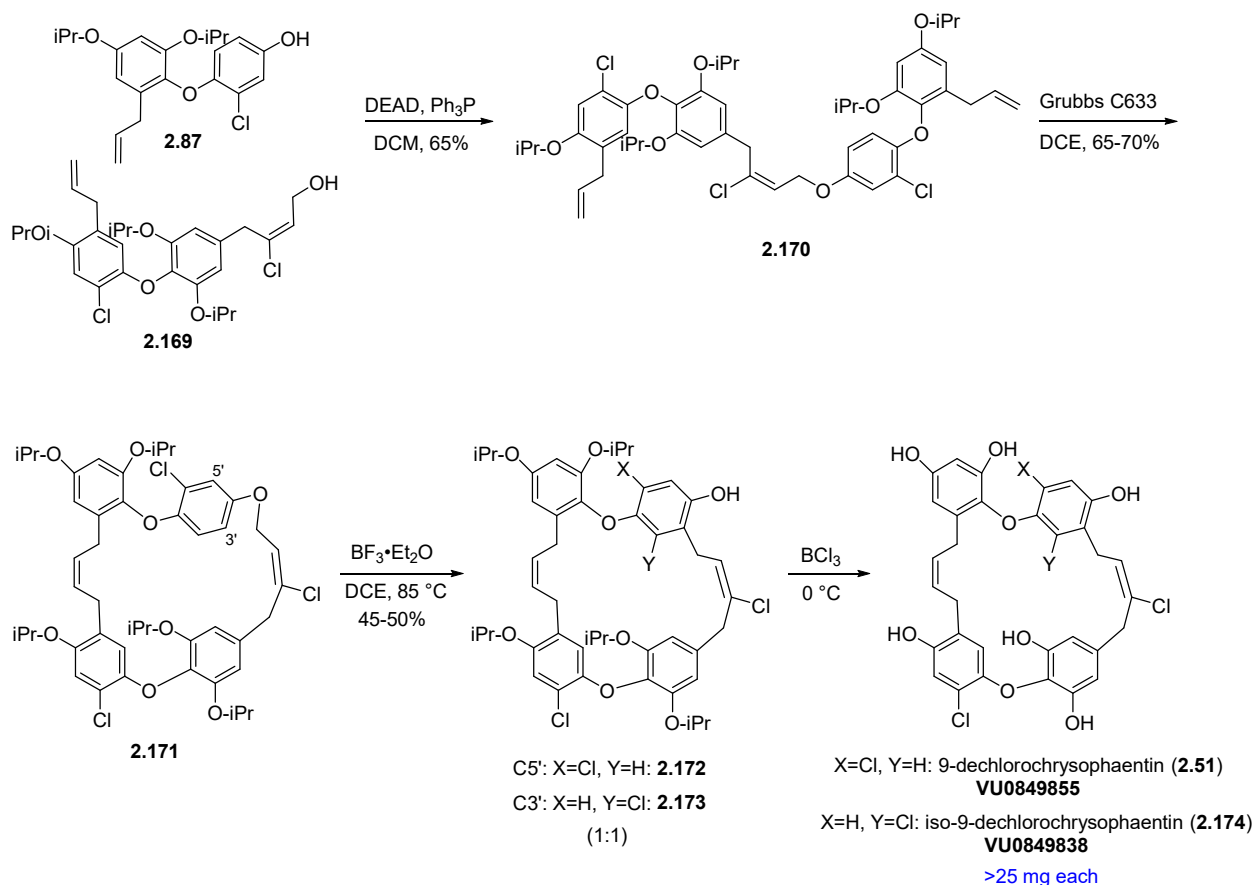
78

Figure 2.37. Synthesis of 9-dechlorochrysophaentins **VU0849838** and **VU0849855.**

Analysis of iso- and 9-dechlorochrysophaentin **(VU0849838** and **VU0849855)** revealed no visible differences in their proton and carbon spectra. The lack of broadening for **VU0849855** indicates that the rotational barrier observed for **VU0848355** is most likely due to the presence of the sterically demanding methyl ethers at C13' and C15'. Nonetheless, there likely is a difference in flexibility of the macrocyclic structures of **VU0848355** and **VU0849855** and unnatural or iso-macrocycle containing **VU0848354** and **VU0849838.** This flexibility difference could still be important for biological target engagement and activity. The difference in macrocycle flexibility and how it affects antimicrobial activity or **VU0848355**, **VU0848354**, **VU0849838**, and **V0849855** will be examined in the context of growth inhibition of Gram-positive bacteria in Chapter 3.

2.9 Conclusions

In conclusion, three groups other than ours have attempted the total synthesis of chrysophaentin A (**2.1**) and chrysophaentin F (**2.2**) and to date, no group has been successful. However, each published route has provided valuable information about the formation of the *E*-chloroalkenes, diaryl ethers, and the macrocyclic core. I have achieved the total synthesis of the most advance chrysophaentin A (**2.1**) analog, 9-dechlorochrysophaentin (**VU0849838),** as well as three other chrysophaentin congeners **VU0849855, VU0848354**, **VU0848355** and an improved synthesis of hemi-chrysophaentin **2.18**.[42] The completion of these syntheses required the development of synthetic routes to stereoselectively install the *E*-chloroalkene (Stannylcupration/tin-chloride exchange), macrocycle formation (O to C migration and *Z*-selective ring-closing metathesis), alkynoate optimization and selective installation of the C5 allyl group. Each problem presented unique opportunities to explore and discover new chemistry and study the reactivity around the chrysophaentin's highly substituted and oxygen-rich aryl rings. However, our total synthesis of 9-dechlorochrysophaentin (**2.51**) is not perfect and future work is needed to further optimize our route to allow for greater throughput of material. In addition, I have synthesized over 20 mg of **VU0848355, VU0848354**, 9-dechlorochrysophaentin (**2.51**), and iso-9-dechlorochrysophaentin (**2.174**) each and this material has been essential for the investigation of the chrysophaentins antimicrobial activity and potential mechanism of action. In Chapters 3 and 4, I will discuss the initial biological activity and mechanism of action studies for **VU0848355, VU0848354**, **VU0849838** and **VU0849855** as well as our recent efforts towards the completion of the first total synthesis of chrysophaentin A (**2.1**).

References:

(1)   Keffer, J. L.; Hammill, J. T.; Lloyd, J. R.; Plaza, A.; Wipf, P.; Bewley, C. A. Geographic Variability and Anti-Staphylococcal Activity of the Chrysophaentins and Their Synthetic Fragments. *Marine Drugs* **2012**, *10* (12), 1103–1125. https://doi.org/10.3390/md10051103.

(2)   Davison, J. R.; Bewley, C. A. Antimicrobial Chrysophaentin Analogs Identified from Laboratory Cultures of the Marine Microalga Chrysophaeum Taylorii. *Journal of Natural Products* **2019**, *82* (1), 148–153. https://doi.org/10.1021/acs.jnatprod.8b00858.

(3)   K. Allred, T.; Manoni, F.; G. Harran, P. Exploring the Boundaries of "Practical": De Novo Syntheses of Complex Natural Product-Based Drug Candidates. *Chemical Reviews* **2017**, *117* (18), 11994–12051. https://doi.org/10.1021/acs.chemrev.7b00126.

(4)   Brockway, A. J.; Grove, C. I.; Mahoney, M. E.; Shaw, J. T. Synthesis of the Diaryl Ether Cores Common to Chrysophaentins A, E, and F. *Tetrahedron Letters* **2015**, *56* (23), 3396–3401. https://doi.org/10.1016/j.tetlet.2015.01.073.

(5)   Vendeville, J.-B.; Matters, R. F.; Chen, A.; Light, M. E.; Tizzard, G. J.; Chai, C. L. L.; Harrowven, D. C. A Synthetic Approach to Chrysophaentin F. *Chemical Communications* **2019**, *55* (33), 4837–4840. https://doi.org/10.1039/C9CC01666J.

(6)   A. Wender, P.; A. Verma, V.; J. Paxton, T.; H. Pillow, T. Function-Oriented Synthesis, Step Economy, and Drug Design. *Accounts of Chemical Research* **2007**, *41* (1), 40–49. https://doi.org/10.1021/ar700155p.

(7)   Hammill, J. T. Syntheses of Peptidic , Natural Product-Inspired , and Heterocyclic Molecules as Biological Probes By. **2013**.

(8)   Keffer, J. L.; Huecas, S.; Hammill, J. T.; Wipf, P.; Andreu, J. M.; Bewley, C. A. Chrysophaentins Are Competitive Inhibitors of FtsZ and Inhibit Z-Ring Formation in Live Bacteria. *Bioorganic & Medicinal Chemistry* **2013**, *21* (18), 5673–5678. https://doi.org/10.1016/j.bmc.2013.07.033.

(9)   Chan, D. M. T.; Monaco, K. L.; Wang, R. P.; Winters, M. P. New N- and O-Arylations with Phenylboronic Acids and Cupric Acetate. *Tetrahedron Letters* **1998**, *39* (19), 2933–2936. https://doi.org/10.1016/S0040-4039(98)00503-6.

(10)   Lam, P. Y. S.; Clark, C. G.; Saubern, S.; Adams, J.; Winters, M. P.; Chan, D. M. T.; Combs, A. New Aryl/Heteroaryl C-N Bond Cross-Coupling Reactions via Arylboronic Acid/Cupric Acetate Arylation. *Tetrahedron Letters* **1998**, *39* (19), 2941–2944. https://doi.org/10.1016/S0040-4039(98)00504-8.

(11)   Evans, D. A.; Katz, J. L.; West, T. R. Synthesis of Diaryl Ethers through the Copper-Promoted Arylation of Phenols with Arylboronic Acids. An Expedient Synthesis of Thyroxine. *Tetrahedron Letters* **1998**, *39* (19), 2937–2940. https://doi.org/10.1016/S0040-4039(98)00502-4.

(12)   Chao, W.; Weinreb, S. M. The First Examples of Ring-Closing Olefin Metathesis of Vinyl Chlorides. *Organic Letters* **2003**, *5* (14), 2505–2507. https://doi.org/10.1021/ol034775z.

(13)   Sashuk, V.; Samojłowicz, C.; Szadkowska, A.; Grela, K. Olefin Cross-Metathesis with Vinyl Halides. *Chemical Communications* **2008**, No. 21, 2468–2470. https://doi.org/10.1039/b801687a.

(14)   Marx, V. M.; Herbert, M. B.; Keitz, B. K.; Grubbs, R. H. Stereoselective Access to Z and e Macrocycles by Ruthenium-Catalyzed Z-Selective Ring-Closing Metathesis and

Ethenolysis. *Journal of the American Chemical Society* **2013**, *135* (1), 94–97. https://doi.org/10.1021/ja311241q.

(15)   Herbert, M. B.; Grubbs, R. H. Z-Selective Cross Metathesis with Ruthenium Catalysts: Synthetic Applications and Mechanistic Implications. *Angewandte Chemie - International Edition*. Wiley-VCH Verlag April 20, 2015, pp 5018–5024. https://doi.org/10.1002/anie.201411588.

(16)   Kumamoto, H.; Onuma, S.; Tanaka, H. Sulfur Extrusion with Tin Radical: Synthesis of 4′,5′ -Didehydro-5′-Deoxy-5′-(Tributylstannyl)Adenosine, an Intermediate for Potential Inhibitors against S-Adenosyl Homocysteine Hydrolase. *Journal of Organic Chemistry* **2004**, *69* (1), 72–78. https://doi.org/10.1021/jo030256y.

(17)   Hawthorne, M. F.; Emmons, W. D.; McCallum, K. S. A Re-Examination of the Peroxyacid Cleavage of Ketones. I. Relative Migratory Aptitudes. *Journal of the American Chemical Society* **1958**, *80* (23), 6393–6398. https://doi.org/10.1021/ja01556a057.

(18)   Ogata, Y.; Sawaki, Y. Kinetics and Mechanism of the Baeyer-Villiger Reaction of Benzaldehydes with Perbenzoic Acids. *Journal of the American Chemical Society* **1972**, *94* (12), 4189–4196. https://doi.org/10.1021/ja00767a025.

(19)   Sandmeyer, T. Ueber Die Ersetzung Der Amid-Gruppe Durch Chlor, Brom Und Cyan in Den Aromatischen Substanzen. *Berichte der deutschen chemischen Gesellschaft* **1884**, *17* (2), 2650–2653. https://doi.org/10.1002/cber.188401702202.

(20)   Sandmeyer, T. Ueber Die Ersetzung Der Amidgruppe Durch Chlor in Den Aromatischen Substanzen. *Berichte der deutschen chemischen Gesellschaft* **1884**, *17* (2), 1633–1635. https://doi.org/10.1002/cber.18840170219.

(21)   Roy, A.; Reddy, K. R.; Mohanta, P. K.; Ila, H.; Junjappa, H. Hydrogen Peroxide/Boric Acid: An Efficient System for Oxidation of Aromatic Aldehydes and Ketones to Phenols. *Synthetic Communications* **1999**, *29* (21), 3781–3791. https://doi.org/10.1080/00397919908086017.

(22)   Krasovskiy, A.; Knochel, P. A LiCl-Mediated Br/Mg Exchange Reaction for the Preparation of Functionalized Aryl- and Heteroarylmagnesium Compounds from Organic Bromides. *Angewandte Chemie - International Edition* **2004**, *43* (25), 3333–3336. https://doi.org/10.1002/anie.200454084.

(23)   Ishiyama, T.; Murata, M.; Miyaura, N. Palladium(0)-Catalyzed Cross-Coupling Reaction of Alkoxydiboron with Haloarenes: A Direct Procedure for Arylboronic Esters. *Journal of Organic Chemistry* **1995**, *60* (23), 7508–7510. https://doi.org/10.1021/jo00128a024.

(24)   Boger, D. L.; Borzilleri, R. M.; Nukui, S.; Beresis, R. T. Synthesis of the Vancomycin CD and DE Ring Systems. *Journal of Organic Chemistry* **1997**, *62* (14), 4721–4736. https://doi.org/10.1021/jo970560p.

(25)   Chuang, K. v; Navarro, R.; Reisman, S. E. Benzoquinone-Derived Sulfinyl Imines as Versatile Intermediates for Alkaloid Synthesis: Total Synthesis of (–)-3-Demethoxyerythratidinone. *Chemical Science* **2011**, *2* (6), 1086. https://doi.org/10.1039/c1sc00095k.

(26)   Kim, G.; Sohn, T. I.; Kim, D.; Paton, R. S. Asymmetric Total Synthesis of (+)-Bermudenynol, a C15 Laurencia Metabolite with a Vinyl Chloride Containing Oxocene Skeleton, through Intramolecular Amide Enolate Alkylation. *Angewandte Chemie - International Edition* **2014**, *53* (1), 272–276. https://doi.org/10.1002/anie.201308077.

(27)   Barbero, A.; Pulido, F. J. Allylstannanes and Vinylstannanes from Stannylcupration of C-C Multiple Bonds. Recent Advances and Applications in Organic Synthesis. *Chemical Society Reviews*. Royal Society of Chemistry November 14, 2005, pp 913–920. https://doi.org/10.1039/b506622k.

(28)   Betzer, J. F.; Delaloge, F.; Muller, B.; Pancrazi, A.; Prunet, J. Radical Hydrostannylation, Pd(0)-Catalyzed Hydrostannylation, Stannylcupration of Propargyl Alcohols and Enynols: Regio- and Stereoselectivities. *Journal of Organic Chemistry* **1997**, *62* (22), 7768–7780. https://doi.org/10.1021/jo9710339.

(29)   Nielsen, T. E.; Cubillo de Dios, M. A.; Tanner, D. Highly Stereoselective Addition of Stannylcuprates to Alkynones. *Journal of Organic Chemistry* **2002**, *67* (21), 7309–7313. https://doi.org/10.1021/jo0259008.

(30)   Lipshutz, B. H.; Ellsworth, E. L.; Dimock, S. H.; Reuter, D. C. Transmetalation Reactions of Higher Order Cyanocuprates: Direct Formation of Trialkyltin Cuprates from Tin Hydrides Which Bypasses Organolithium Intermediates. *Tetrahedron Letters* **1989**, *30* (16), 2065–2068. https://doi.org/10.1016/S0040-4039(01)93712-8.

(31)   Williams, D. R.; Pinchman, J. R. Studies of Neodolastanes — Synthesis of the Tricyclic Core of the Trichoaurantianolides. *Canadian Journal of Chemistry* **2012**, *91* (1), 21–37. https://doi.org/10.1139/v2012-088.

(32)   Davies, K. A.; Abel, R. C.; Wulff, J. E. Operationally Simple Copper-Promoted Coupling of Terminal Alkynes with Benzyl Halides. *Journal of Organic Chemistry* **2009**, *74* (10), 3997–4000. https://doi.org/10.1021/jo900444x.

(33)   Reginato, G.; Capperucci, A.; Degl'Innocenti, A.; Mordini, A.; Pecchi, S. Stannylcupration of γ-Heterosubstituted Acetylenic Esters: A New Route to 4-Stannylated

Five Membered N- and O- Heterocycles. *Tetrahedron* **1995**, *51* (7), 2129–2136. https://doi.org/10.1016/0040-4020(94)01086-F.

(34)   Piers, E.; Morton, H. E. Stereoselective Conjugate Addition of Lithium (Phenylthio)(Trimethylstannyl)Cuprate to, α,β-Acetylenic Esters. Preparation of (E)- and (Z)-4-Lithio-l,3-Pentadienes and Their Reaction with Electrophiles. *Journal of Organic Chemistry* **1980**, *45* (21), 4263–4264. https://doi.org/10.1021/jo01309a053.

(35)   Nasveschuk, C. G.; Rovis, T. The [1,3] O-to-C Rearrangement: Opportunities for Stereoselective Synthesis. *Organic and Biomolecular Chemistry* **2008**, *6* (2), 240–254. https://doi.org/10.1039/b714881j.

(36)   Yoshizawa, T.; Toyofuku, H.; Tachibana, K.; Kuroda, T. REGIOSELECTIVE POLYPRENYL REARRANGEMENT OF POLYPRENYL 2,3,4,5-TETRASUBSTITUTED PHENYL ETHERS PROMOTED BY BORON TRIFLUORIDE. *Chemistry Letters* **1982**, *11* (8), 1131–1134. https://doi.org/10.1246/cl.1982.1131.

(37)   Dauben, W. G.; Cogen, J. M.; Behar, V. Clay Catalyzed Rearrangement of Substituted Allyl Phenyl Ethers: Synthesis of Ortho-Allyl Phenols, Chromans and Coumarans. *Tetrahedron Letters* **1990**, *31* (23), 3241–3244. https://doi.org/10.1016/S0040-4039(00)89033-4.

(38)   Dintzner, M. R.; Morse, K. M.; McClelland, K. M.; Coligado, D. M. Investigation of the Montmorillonite Clay-Catalyzed [1,3] Shift Reaction of 3-Methyl-2-Butenyl Phenyl Ether. *Tetrahedron Letters* **2004**, *45* (1), 79–81. https://doi.org/10.1016/j.tetlet.2003.10.119.

(39)   Lawson, K. È.; Rose, T. E.; Harran, P. G. Template-Induced Macrocycle Diversity through Large Ring-Forming Alkylations of Tryptophan. *Tetrahedron* **2013**, *69* (36), 7683–7691. https://doi.org/10.1016/j.tet.2013.05.060.

(40)   Lawson, K. È.; Rose, T. E.; Harran, P. G. Template-Constrained Macrocyclic Peptides Prepared from Natièe, Unprotected Precursors. *Proceedings of the National Academy of Sciences of the United States of America* **2013**, *110* (40), E3753–E3760. https://doi.org/10.1073/pnas.1311706110.

(41)   Yu, W.; Hjerrild, P.; Overgaard, J.; Poulsen, T. B. A Concise Route to the Strongylophorines. *Angewandte Chemie - International Edition* **2016**, *55* (29), 8294–8298. https://doi.org/10.1002/anie.201602476.

(42)   Fullenkamp, C. R.; Sulikowski, G. A. An Improved Synthesis of Hemichrysophaentin-AB Fragment of Chrysophaentin A. *Tetrahedron Letters* **2020**, 151856. https://doi.org/10.1016/j.tetlet.2020.151856.

(43)   Chehade, K. A. H.; Kiegiel, K.; Isaacs, R. J.; Pickett, J. S.; Bowers, K. E.; Fierke, C. A.; Andres, D. A.; Spielmann, H. P. Photoaffinity Analogues of Farnesyl Pyrophosphate Transferable by Protein Farnesyl Transferase. *Journal of the American Chemical Society* **2002**, *124* (28), 8206–8219. https://doi.org/10.1021/ja0124717.

(44)   Larsen, C. H.; Anderson, K. W.; Tundel, R. E.; Buchwald, S. L. Palladium-Catalyzed Heck Alkynylation of Benzyl Chlorides. *Synlett* **2006**, No. 18, 2941–2946. https://doi.org/10.1055/s-2006-949625.

(45)   Mitsunobu, O.; Yamada, M. Preparation of Esters of Carboxylic and Phosphoric Acid via Quaternary Phosphonium Salts . *Bulletin of the Chemical Society of Japan* **1967**, *40* (10), 2380–2382. https://doi.org/10.1246/bcsj.40.2380.

(46)   Mitsunobu, O.; Yamada, M.; Mukaiyama, T. Preparation of Esters of Phosphoric Acid by the Reaction of Trivalent Phosphorus Compounds with Diethyl Azodicarboxylate in the

Presence of Alcohols. *Bulletin of the Chemical Society of Japan* **1967**, *40* (4), 935–939. https://doi.org/10.1246/bcsj.40.935.

(47)   Keitz, B. K.; Endo, K.; Patel, P. R.; Herbert, M. B.; Grubbs, R. H. Improved Ruthenium Catalysts for Z-Selective Olefin Metathesis. *Journal of the American Chemical Society* **2012**, *134* (1), 693–699. https://doi.org/10.1021/ja210225e.

(48)   Ahmed, T. S.; Grubbs, R. H. A Highly Efficient Synthesis of Z-Macrocycles Using Stereoretentive, Ruthenium-Based Metathesis Catalysts. *Angewandte Chemie - International Edition* **2017**, *56* (37), 11213–11216. https://doi.org/10.1002/anie.201704670.

(49)   Montgomery, T. P.; Johns, A. M.; Grubbs, R. H. Recent Advancements in Stereoselective Olefin Metathesis Using Ruthenium Catalysts. *Catalysts* **2017**, *7* (12), 87. https://doi.org/10.3390/catal7030087.

(50)   Laplante, S. R.; Fader, L. D.; Fandrick, K. R.; Fandrick, D. R.; Hucke, O.; Kemper, R.; Miller, S. P. F.; Edwards, P. J. Assessing Atropisomer Axial Chirality in Drug Discovery and Development. *Journal of Medicinal Chemistry*. American Chemical Society October 27, 2011, pp 7005–7022. https://doi.org/10.1021/jm200584g.

(51)   Piątek, P.; Kalisiak, J.; Jurczak, J. Synthesis and Chiroptical Properties of Two New Planar-Chiral Macrocycles. *Tetrahedron Letters* **2004**, *45* (16), 3309–3311. https://doi.org/10.1016/j.tetlet.2004.02.063.

(52)   LaPlante, S. R.; Edwards, P. J.; Fader, L. D.; Jakalian, A.; Hucke, O. Revealing Atropisomer Axial Chirality in Drug Discovery. *ChemMedChem* **2011**, *6* (3), 505–513. https://doi.org/10.1002/cmdc.201000485.

(53)   Gagnon, C.; Godin, É.; Minozzi, C.; Sosoe, J.; Pochet, C.; Collins, S. K. Biocatalytic Synthesis of Planar Chiral Macrocycles. *Science* **2020**, *367* (6480), 917–921. https://doi.org/10.1126/science.aaz7381.

(54)   Reisberg, S. H.; Gao, Y.; Walker, A. S.; Helfrich, E. J. N.; Clardy, J.; Baran, P. S. Total Synthesis Reveals Atypical Atropisomerism in a Small-Molecule Natural Product, Tryptorubin A. *Science* **2020**, *367* (6476), 458–463. https://doi.org/10.1126/science.aay9981.

(55)   Larsen, E. M.; Wilson, M. R.; Taylor, R. E. Conformation-Activity Relationships of Polyketide Natural Products. *Natural Product Reports*. Royal Society of Chemistry August 1, 2015, pp 1183–1206. https://doi.org/10.1039/c5np00014a.

(56)   E. Taylor, R.; Chen, Y.; Beatty, A.; C. Myles, D.; Zhou, Y. Conformation−Activity Relationships in Polyketide Natural Products: A New Perspective on the Rational Design of Epothilone Analogues. *Journal of the American Chemical Society* **2002**, *125* (1), 26–27. https://doi.org/10.1021/ja028196l.

(57)   Fischer, E. Einfluss Der Configuration Auf Die Wirkung Der Enzyme. *Berichte der deutschen chemischen Gesellschaft* **1894**, *27* (3), 2985–2993. https://doi.org/10.1002/cber.18940270364.

(58)   Koshland, D. E. Correlation of Structure and Function in Enzyme Action. *Science* **1963**, *142* (3599), 1533–1541. https://doi.org/10.1126/science.142.3599.1533.

(59)   Koshland, D. E. Application of a Theory of Enzyme Specificity to Protein Synthesis. *Proceedings of the National Academy of Sciences* **1958**, *44* (2), 98–104. https://doi.org/10.1073/pnas.44.2.98.

(60)   Koshland, D. E. The Key–Lock Theory and the Induced Fit Theory. *Angewandte Chemie International Edition in English* **1995**, *33* (2324), 2375–2378. https://doi.org/10.1002/anie.199423751.

(61)   Toenjes, S. T.; Gustafson, J. L. Atropisomerism in Medicinal Chemistry: Challenges and Opportunities. *Future Medicinal Chemistry*. Future Medicine Ltd. February 1, 2018, pp 409–422. https://doi.org/10.4155/fmc-2017-0152.

(62)   Smyth, J. E.; Butler, N. M.; Keller, P. A. A Twist of Nature-the Significance of Atropisomers in Biological Systems. *Natural Product Reports*. Royal Society of Chemistry November 1, 2015, pp 1562–1583. https://doi.org/10.1039/c4np00121d.

(63)   Georgiev, D.; Saes, B.; Johnston, H.; Boys, S.; Healy, A.; Hulme, A. Selective and Efficient Generation of Ortho-Brominated Para-Substituted Phenols in ACS-Grade Methanol. *Molecules* **2016**, *21* (1), 88. https://doi.org/10.3390/molecules21010088.

(64)   Desurmont, G.; Dalton, S.; Giolando, D. M.; Srebnik, M. Sequential Transformations of 1,3-Dibora Butadienes to Enones or Tetrasubstituted 1,3-Butadienes. *Journal of Organic Chemistry* **1996**, *61* (22), 7943–7946. https://doi.org/10.1021/jo9611125.

(65)   Kotha, S.; Behera, M.; Shah, V. R. A Simple Synthetic Approach to Allylated Aromatics via the Suzuki-Miyaura Cross-Coupling Reaction. *Synlett* **2005**, *2005* (12), 1877–1880. https://doi.org/10.1055/s-2005-871569.

Chapter 3

Antimicrobial Activity and Phenotypic Studies on 9-dechlorochrysophaentin Congeners

3.1 9-dechlorochrysophaentins Inhibition of Growth of Gram-positive Bacteria Including Clinically Relevant Drug-resistant Strains

Upon completion of the syntheses of 9-dechlorochrysophaentins: **VU0848355, VU0848354, VU0849838,** and **VU0849855** we were eager to evaluate their antimicrobial activity against Gram-positive bacteria in comparison to chrysophaentin A (**3.1**). In collaboration with Carole Bewley (NIDDK) our synthetic products were screened against a panel of Gram-positive bacteria including clinically relevant drug-resistant strains, MRSA and VRE. All four 9-dechlorochrysophaentins inhibited the growth of the Gram-positive bacteria with MIC_{50} values in the range of 0.3-8 μg/mL (466 nM to 12 μM) (Table 3.1). Overall, the activity of our 9-dechlorochrysophaentin congeners compared favorably to chrysophaentin A (**3.1**) which Bewley's lab determined to have an MIC50 value of 2 μg/mL or 2.9 μM against the panel of Gram-positive pathogens.

To glean mechanistic insight, FtsZ inhibitors PC190723[1] (**3.3**) and zantrin Z3[2] (**3.2**) were tested alongside our 9-dechlorochrysophaentin congeners. Our synthetic products compared favorably to zantrin Z3 (**3.2**) (5.8 – 11.6 μM) and PC190723 (**3.3**) (1.12 μM). However, our 9-dechlorochrysophaentins demonstrated broader activity against different bacterial strains including E. *faecalis* and B. *subtilis* when compared to PC190723 (**3.3**) (Table 3.1).

Table 3.1. Antimicrobial activity of 9-dechlorochrysophaentins.

Z=H, X=Cl, Y=H: **VU0849855**
Z=H, X=H, Y=Cl: **VU0849838**
Z=H, X=Cl, Y=H: Chrysophaentin A (**3.1**)

H=Cl, Y=H: **VU0848355**
X=H, Y=Cl: **VU0848354**

zantrin Z3 (**3.2**)

PC190723 (**3.3**)

Hemi-chrysophaentin (**3.4**)
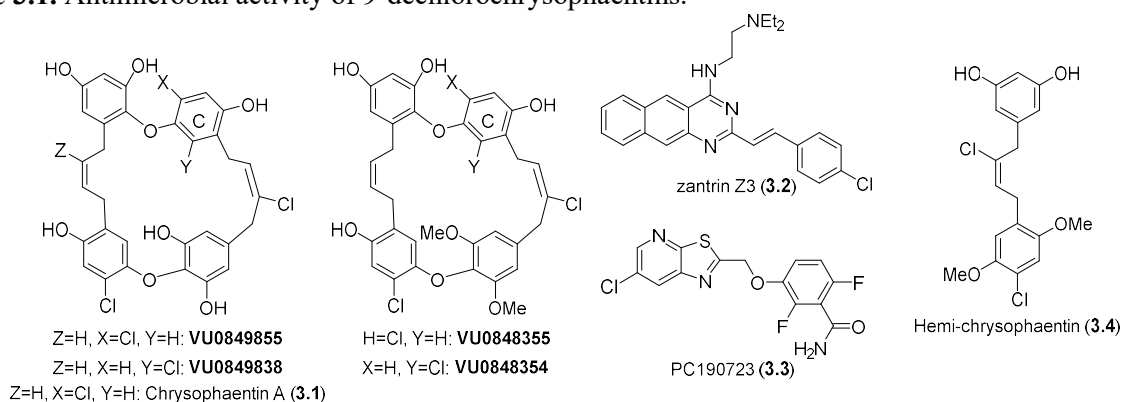
	MIC$_{50}$ (μg/mL)				
	S. aureus	MRSA	*E. faecalis*	VRE	*B. subtilis*
Chrysophaentin A (**3.1**)	2	2	2	2	n/a
VU0848355	4	4	4	8	4.2
VU0848354	**2**	**2**	**2**	**4**	**1.4**
9-dechloro (**VU0849855**)	2.5	2.5	2.5	5	4
Iso-9-dechloro (**VU0849838**)	**1.1**	**1.1**	**0.3**	**2.2**	**2**
Hemi-chrysophaentin (**3.4**)	10	10	5.0	10	n/a
PC190723 (**3.3**)	0.4	0.4	n/a	n/a	n/a
Zantrin Z3 (**3.2**)	2.5	2.5	2.5	5	n/a

Bacterial strains were obtained from the ATCC and have the following identifiers: *S. aureus* 25913; MRSA, methicillin-resistant *S. aureus* 43300; *Enterococcus faecalis* 29212; VRE, vancomycin-resistant-*E. faecalis* 51299; *B. Subtilis*. [a]n/a, no tested.

Interestingly, iso-9-dechlorochrysophaentin (**VU0849838)** was found to be the most potent chrysophaentin (MIC$_{50}$ range of 0.3 to 2.2 μg/mL or 466 nM to 3.4 μM), superior to chrysophaentin A itself. As expected, hemi-chrysophaentin (**3.4**) was 2-5 fold less potent compared to 9-dechlorochrysophaentins. Notably, the observed antimicrobial activity of our synthetic hemi-chrysophaentin (**3.4**) (13-17 μM) was in the range of the activity reported earlier by Wipf and co-workers (11-20 μM).[3] Most intriguing was the apparent two-fold difference in activity between iso-chrysophaentins (**VU0848355** and **VU0849838**) and 9-dechlorochrysophaentins (**VU0848354** and **VU0849855**), the latter differing in substitution pattern at ring C (Table 3.1, bold text). Based
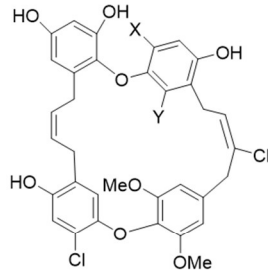
on the NMR data of the unnatural C-ring isomers or iso-chrysophaentins (vide infra), we hypothesize the two-fold difference in activity may be attributed to differences in rotational barriers or flexibility of the cyclophane-like structures. With confirmation that our synthetic 9-dechlorochrysophaentin congeners inhibit the growth of Gram-positive bacteria comparably to chrysophaentin A (**3.1**), we next assayed their ability to inhibit FtsZ GTPase activity in a biochemical assay in the Bewley lab.

3.2 Evaluation of FtsZ Inhibition of 9-dechlorochrysophaentins

As mentioned in Chapter 1, chrysophaentin A (**3.1**) was found to inhibit the GTPase activity of EcFtsZ and SaFtsZ with IC_{50} of 9.9 μM and 67 μM, respectively. Continuing our collaboration with the Bewley lab, inhibition of FtsZ GTPase activity was determined for our synthetic 9-dechlorochrysophaentin congeners using their GTPase biochemical assay. As summarized in Table 3.2, **VU0848355** and **VU0848354** inhibit the FtsZ GTPase activity of SaFtsZ and EcFtsZ with IC_{50} of 30 and 25 μM for SaFtsZ and 50 and 45 μM for EcFtsZ (Table 3.2). Surprisingly, the FtsZ GTPase inhibition was 3-fold weaker than the growth inhibition for **VU0848355** and 12-fold weaker for **VU0848354** in S. *aureus*. Furthermore, **VU0849855** and **VU0849838** also showed a 2.6-fold and 3 to 5-fold weaker GTPase inhibition compared to their growth inhibition in S. *aureus*. The lack of correlation between the GTPase inhibition and observed growth inhibition data was also observed with chrysophaentin A (**3.1**). However, Bewley and co-workers hypothesized that the discrepancies in the data could be the result of a compounding effect FtsZ inhibition has on cell growth, similar to what has been observed for tubulin inhibitors.[4,5] More surprising than the GTPase and growth inhibition discrepancies was the absence of the two-fold

difference in activity observed between **VU0848355** and **VU0848354** and **VU0849855** and **VU0849838.**

Table 3.2. FtsZ GTPase inhibition of 9-dechlorochrysophaentin congeners.

	IC$_{50}$ (µM)	
	SaFtsZ	EcFtsZ
Chrysophaentin A (3.1)	67	9.9
VU0848355	30	50
VU0848354	25	45
9-dechloro (**VU0849855**)	10	9.5
Iso-9-dechloro (**VU0849838**)	10	6.5
Hemi-chrysophaentin (3.4)	40	18
PC190723 (3.3)	--	--
Zantrin Z3 (3.2)	--	20

--, no inhibition observed

Inhibition of GTPase activity of E. *coli* (EcFtsZ) and S. *aureus* (SaFtsZ) was determined colorimetrically using a Malachite Green-molybdate phosphate assay kit (Sigma Aldrich, St. Louis MO).

Based on the trends observed with the inhibition of growth data we would expect **VU0849838** and **VU0848354** to display a two-fold difference in GTPase activity compared to **VU0849855** and **VU0848355,** however, the GTPase inhibition was essentially equivalent between C ring isomers. The well-characterized FtsZ inhibitor PC190723 (**3.3**) showed no inhibition of SaFtsZ or EcFtsZ GTPase activity, while zantrin Z3 (**3.2**) only inhibited the activity of EcFtsZ and not SaFtsZ. The lack of inhibition of SaFtsZ by zantrin Z3 (**3.2**) was quite surprising based on the previous reported activity[2] and confirmation of the GTPase inhibitory activity completed by the Shaw[6] and Bewley groups.[5] One possible explanation for this discrepancy is the variable quality of commercial zantrin Z3.

Our observation of a lack of correlation of antimicrobial activity and the commercially available GTPase colorimetric assay data lead us to seek an alternative, whole-cell or phenotypic assay to further investigate chrysophaentin's mechanism of action. Further supporting this

decision, as mentioned in Chapter 1, PC190723's (**3.3**) reported GTPase activity has proven difficult to reproduce by several labs using the same colorimetric assay.[6,7]

3.3 9-dechlorochrysophaentins Effect on Cell Elongation and FtsZ, FtsA, and PBP2B Localization

As discussed in the conclusion of the last section we judged the commercial FtsZ colorimetric GTPase assay as not very informative or reproducible. Insight into the role of FtsZ in cell division reveals an increasingly complex function in the organization and dynamics of the divisome. This led us to seek a whole-cell assay using microscopy to identify FtsZ inhibition phenotypes upon treatment with chrysophaentins. One such phenotype mentioned in Chapter 1 (Figure 1.7 and 3.9), is the elongation of rod-shaped bacteria (for example B. *subtilis*) on treatment with PC190723. A second phenotype is the intracellular delocalization of FtsZ from the midline, preventing Z-ring formation which can be visualized using fluorescently labeled FtsZ. With this background, we initiated a collaboration with the VanNieuwenhze group at Indiana University.

The first experiment conducted by the Indiana group was the determination of whether our synthetic 9-dechlorochrysophaentins would induce an elongation phenotype in B. *subtilis* as was observed with PC190723. To this end, the treatment of B. *subtilis* with **VU0848354** and **VU0848355 (**5-20 μM) was compared to untreated B. *subtilis* and surprisingly showed no significant difference in cell length (Figure 3.1). In comparison, treatment with PC190723 (**3.3**) showed a significant increase in the overall length of the B. *subtilis* population, indicating inhibition of cell division (Figure 3.1). Next, we examined the effect of our 9-dechlorochrysophaentin congeners on Z-ring and peptidoglycan synthesis.
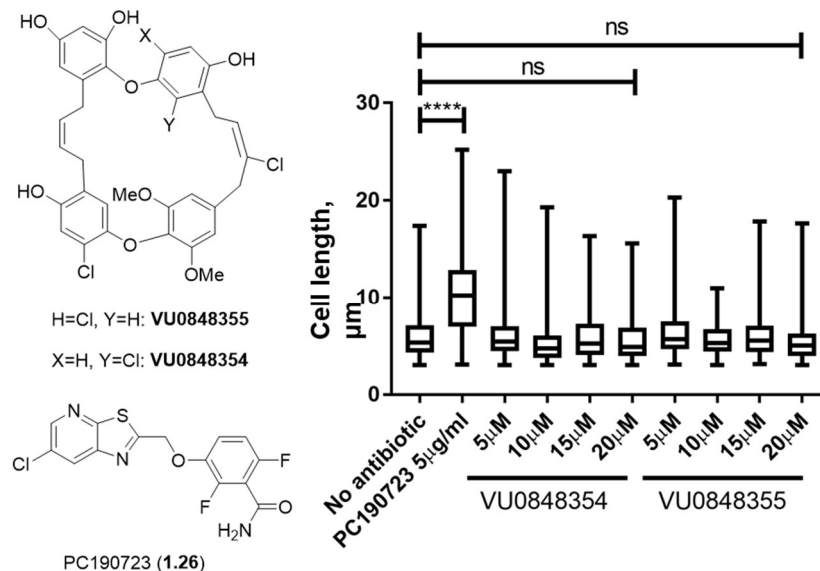
Figure 3.1. Cell lengthening phenotypic analysis.

3.3.1 Evaluation of the Effect of VU0848354 and VU0848355 on FtsZ, FtsA, and PBP2B Localization

FtsZ plays an essential role in bacteria cell division and has been linked to septal peptidoglycan synthesis through protein-protein interactions in the divisome.[8] However, the direct role FtsZ plays in septal peptidoglycan synthesis was unknown until recently. The VanNieuwenhze group developed techniques using super-resolution microscopy and fluorescently-labeled cell division protein fusions to investigate the dynamics of the Z-ring and its role in septal peptidoglycan synthesis. [9,10] Their studies found that FtsZ undergoes a treadmilling-like process powered by the hydrolysis of GTP. GTP-bound FtsZ undergoes polymerization to the leeward end of the Z-ring polymer, followed by hydrolysis of GTP, and then depolymerization of GDP-bound FtsZ on the wayward end of the Z-ring polymers. This polymerization-hydrolysis-depolymerization results in the movement of the Z-ring around the circumference of the bacterial division plane constricting the cellular membrane and coordinating the synthesis of new septal

peptidoglycan (Figure 3.2).[9–11] This treadmilling motion concentrically moves around the division plane forming smaller and smaller circles, which guides in the formation of the septal wall between the two daughter cells.

	Cell membrane
	Peptidoglycan-New
	Peptidoglycan-Old
	PG Synthases
	FtsA
	FtsZ-GDP
	FtsZ-GTP
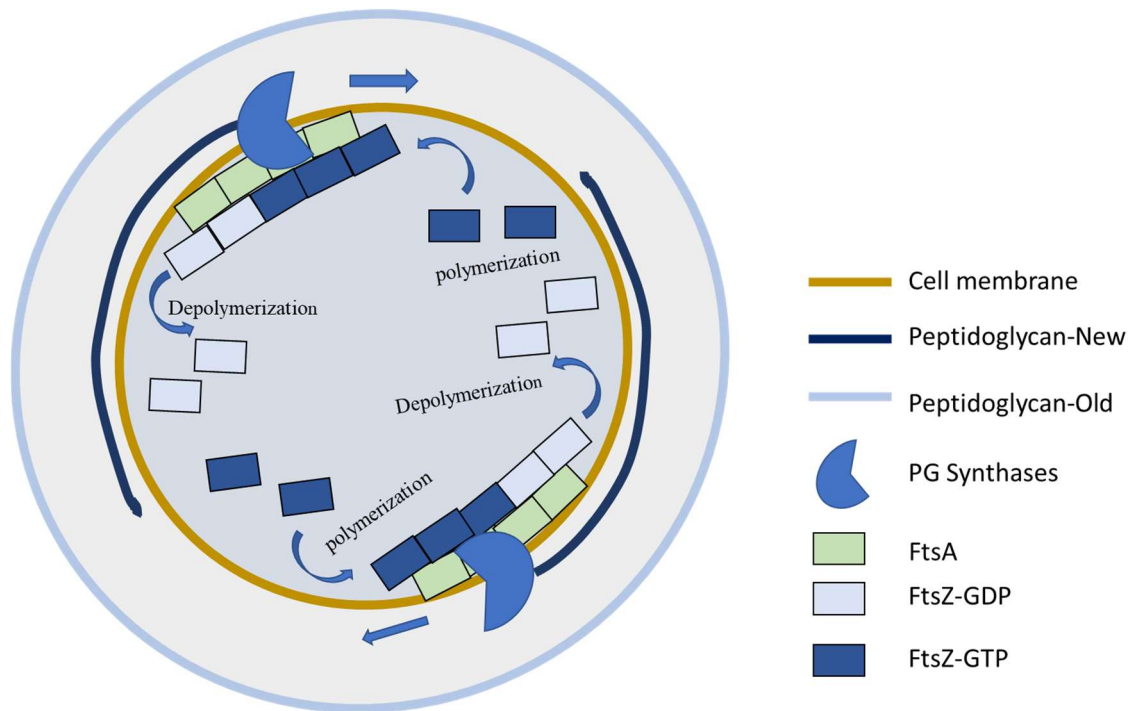
Figure 3.2. FtsZ treadmilling drives septal peptidoglycan synthesis in B. *subtilis*.

The link between the treadmilling motion of FtsZ and peptidoglycan synthases was visualized utilizing super-resolution microscopy with fluorescently labeled protein fusions of FtsZ and PBP2B[11] and peptidoglycan labeling with Fluorescently-labeled D-Amino Acids (FDAAs), which were developed by the VanNieuwenhze group.[10,12] It was determined that the rate and direction of FtsZ treadmilling corresponds to the rate and direction of septal peptidoglycan and inhibition of FtsZ treadmilling resulted in the inhibition of septal peptidoglycan synthesis.[9] The results of this study lead to the conclusion that FtsZ treadmilling directs and controls the motion of septal peptidoglycan synthases during bacterial cell division and FtsZ and PBP2B are working

in concert with each other. Super-resolution microscopy in conjunction with fluorescently-labeled proteins provides a new tool for the investigation of reported FtsZ inhibitors by monitoring their effects on FtsZ treadmilling dynamics. The use of FDAAs labeling allows for the investigation of peptidoglycan synthesis and the effect FtsZ inhibitors might have on septal and peripheral cell wall biosynthesis.

To determine the effect our 9-dechlorochrysophaentin congeners have on FtsZ localization the VanNieuwenhze group expressed fluorescently labeled cell division proteins, FtsZ-mNeonG, FtsA-mNeonG, or PBP2B-mNeonG in B. *subtilis*. The bacteria were then treated with **VU0848354** and **VU0848355** and visualized under fluorescent microscopy to determine the effect treatment had on cell division protein localization. In untreated B. *subtilis,* FtsZ, FtsA, and PBP2B all localize to the midline of the cell, as expected (Figure 3.3, column one). However, B. *subtilis* treated with **VU0848355** and **VU0848354** resulted in the delocalization of FtsZ, FtsA, and PBP2B from the division plane (Figure 3.3, column 2 and 3). FtsZ delocalization itself is expected when inhibited by a small molecule,[6] however traditionally FtsZ will delocalize to discrete foci throughout the cell and not completely disassociate from each other.[5] Thus, treatment with **VU0848355** and **VU0848354** resulted in the complete break-up of the Z-ring and the observed delocalization of FtsZ was equally dispersed throughout the cell with no discrete FtsZ foci (Figure 3.3). The dispersion of FtsA and PBP2B from the midline of the cell has not been previously observed (to the best of our knowledge). For comparison purposes, ampicillin and PC190723 (**3.3**) were also evaluated in the assay. Treatment of B. *subtilis* with PC190723 (**3.3**) and ampicillin showed no delocalization of FtsZ from the midline of the cell (Figure 3.4), indicating the

chrysophaentins mechanism is likely unique compared to FtsZ (PC190723) and peptidoglycan (ampicillin) inhibitors.
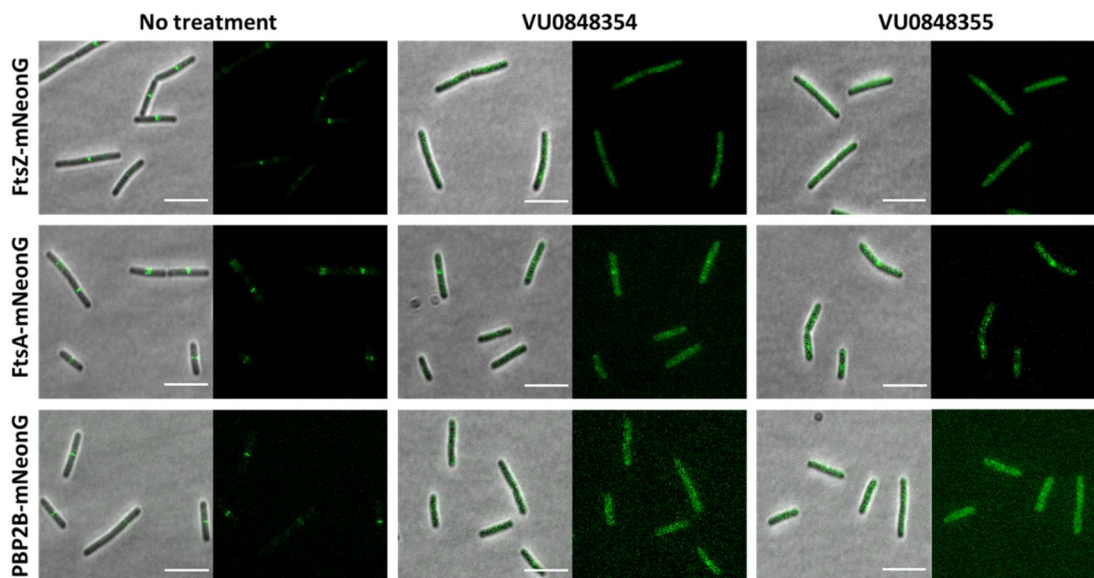
Figure 3.3. Delocalization of FtsZ, FtsA and PBP2B upon treatment with **VU0848355** and **VU0848354.**

The presence of an intact Z-ring upon PC190723 (**3.3**) treatment is interesting, because the original report described the delocalization of FtsZ *in vitro* and bacteria, upon treatment with PC190723 (**3.3**). [1] However, later reports refuted that observation and found that PC190723 (**3.3**) activates FtsZ GTPase activity and stabilizes the Z-ring.[13] Our results seem to agree with the later report of FtsZ stabilization. However, the delocalization of FtsZ, FtsA, and PBP2B from the midline of the cell caused by 9-dechlorochrysophaentins is unprecedented. The major function of the divisome is to orchestrate cell wall biosynthesis, the Indiana group next evaluated the impact of 9-dechlorochrysophaentins on peptidoglycan synthesis.
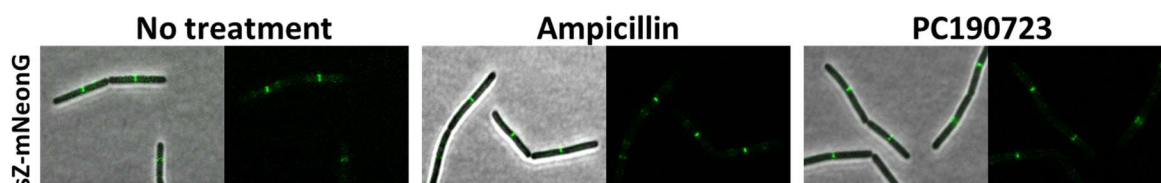
Figure 3.4. FtsZ delocalization for ampicillin and PC190723 (**3.3**).

99

3.3.2 VU0848354 and VU0848355's Effect on Peptidoglycan Synthesis

As outlined above, the VanNieuwenhze group found that FtsZ undergoes a treadmilling-like movement around the division plane forming smaller concentric circles that coincide with septal peptidoglycan synthesis.[9] The link between FtsZ localization, treadmilling movement, and septal peptidoglycan synthesis lead us to hypothesize that the observed dispersion of FtsZ and PBP2B from the midline of the cell should result in the inhibition in septal peptidoglycan synthesis. The Indiana group has reported on the synthesis and application of a library of fluorescently-labeled D-amino acids, which are incorporated into the cell wall and can be visualized with fluorescent microscopy to determine the effect antibiotics have on peptidoglycan synthesis. [10,12]

Using fluorescently-labeled D-alanine (HADA) allowed visualization of peptidoglycan synthesis in B. *subtilis* treated with **VU0848354, VU0848355,** and PC190723 (**3.3**). As reported earlier, the treatment of B. *subtilis* with PC190723 (**3.3**) resulted in limited inhibition of incorporation of fluorescently-labeled D-amino acids, where inhibition of incorporation was only observed at the septum (midline of the cell wall). As mentioned in Chapter 1, the peripheral peptidoglycan is synthesized by an elongation complex controlled by MreB[14] which is thought to be independent of FtsZ, therefore the observed septum inhibition is consistent with inhibition of FtsZ by PC190723 (**3.3**). Treatment with ampicillin, a known peptidoglycan synthesis inhibitor that targets penicillin-binding proteins,[15] resulted in complete inhibition of fluorescence incorporation indicating the complete shutdown of cell wall synthesis at both the septum and periphery (Figure 3.5, square 2). Surprisingly, treatment of B. *subtilis* with **VU0848355** and **VU0848354** resulted in the complete inhibition of incorporation of FDAAs at both the septum and at the peripheral cell wall, similar to the observed phenotype generated with ampicillin treatment (Figure 3.5, squares 4 and 5).
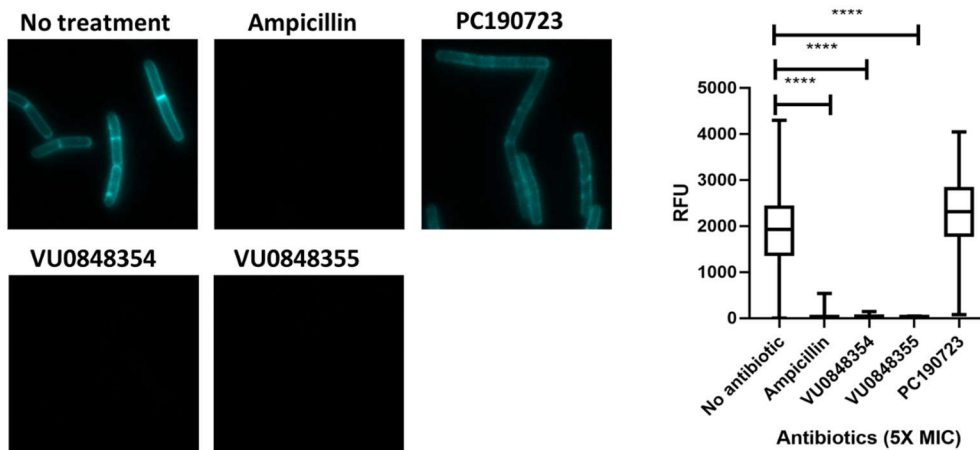
Figure 3.5. FDAAs labeling of B. *subtilis* peptidogylcan.

The fluorescence incorporation can also be represented numerically as the relevant fluorescence units (RFU) as seen in the chart above (Figure 3.5, right panel). **VU0848354** and **VU0848355** inhibit cell wall biosynthesis at both the septum and peripheral of the cell with a similar reduction in RFU compared to peptidoglycan synthesis inhibitor ampicillin (Figure 3.5, right panel). **VU0848354** and **VU0848355's** complete inhibition of peptidoglycan synthesis further supported our hypothesis that the observed delocalization of FtsZ and PBP2B from the midline would inhibit septal peptidoglycan synthesis. However, the observed inhibition of peripheral peptidoglycan was unexpected due to the independent nature of the elongation machinery and division machinery. Collectively, this data supports the notion that the chrysophaentin's mechanism of action is more complex than FtsZ GTPase inhibition and involves both elongation and division. To ensure the validity of the observed peptidoglycan synthesis inhibition assay, positive control vancomycin, and negative controls kanamycin and chloramphenicol, were also tested in the above assay and as expected only the positive control, vancomycin inhibited the incorporation of FDAAs similar to what was observed with ampicillin for **VU0848354** and **VU0848355** (Figure 3.6).
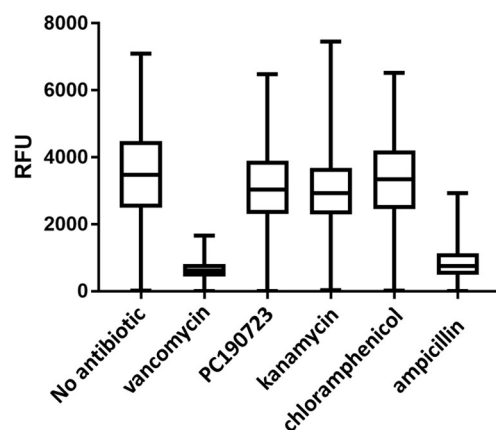
Figure 3.6. Antibiotic effect on FDAAs incorporation.

The ability of our synthetic 9-dechlorochrysophaentin congeners to inhibit cell wall biosynthesis at both the septum and peripheral cell wall and cause the delocalization of divisome proteins FtsZ, FtsA and PBP2B from the division site represents a novel mechanism of the inhibition of cell wall biosynthesis. 9-dechlorochrysophaentin (**VU0849855**) and iso-9-dechlorochrysophaentin (**VU0849838**) also cause the delocalization of FtsZ from the midline of the cell and inhibit peptidoglycan synthesis (Figure 3.7). Current work is in progress to determine the effect **VU0849838** and **VU0849855** have on FtsA and PBP2B localization and filamentous cell phenotype formation.
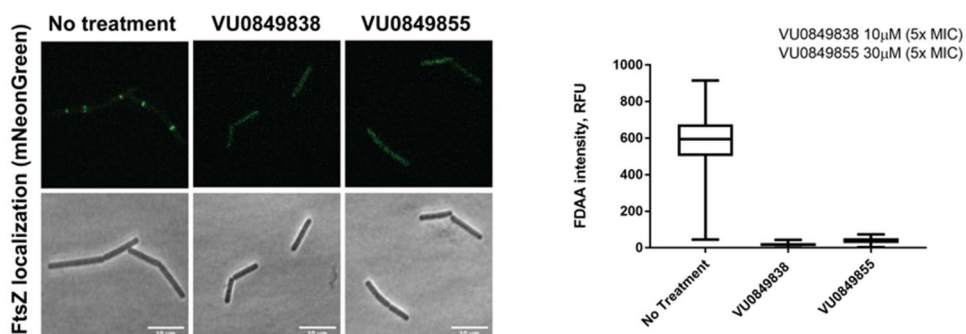
Figure 3.7. VU0849838 and **VU0849855** delocalization of FtsZ and inhibition of peptidoglycan synthesis.

Finally, Bewley and co-workers we able to isolate a few nanograms of chrysophaentin A (**3.1**) for testing in the VanNieuwenhze lab and treatment of B. *subtilis* with chrysophaentin A (**3.1**) also resulted in the complete dispersion of the divisome proteins FtsZ, FtsA and PBP2B from the midline of the cell indicating chrysophaentin A (**3.1**) displays a similar phenotype as our synthetic congeners **VU0848355, VU0848354, VU0849838,** and **VU0849855** (Figure 3.8). However, due to the limited quantity from isolation, the effect on peptidoglycan synthesis could not be determined, but based on our results from our 9-dechlorochrysophaentins, chrysophaentin A (**3.1**) inhibits cell wall biosynthesis.
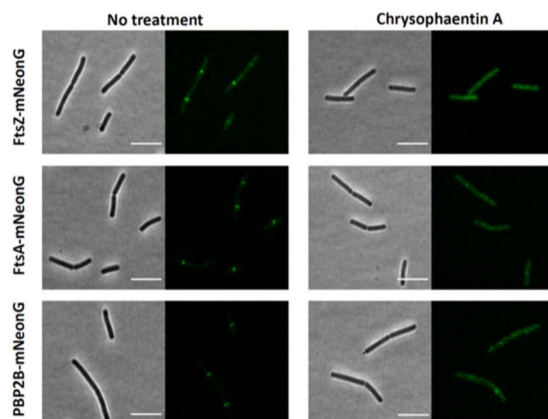
Figure 3.8. Treatment with chrysophaentin A (**3.1**) results in delocalization of FtsZ, FtsA, and PBP2B.

The novel mechanism of the chrysophaentins is unlike any other reported mechanism for peptidoglycan synthesis inhibition or FtsZ inhibition. This preliminary data does not provide enough information to determine the actual protein or proteins that are targeted by the chrysophaentins and further investigation of this novel mechanism of peptidoglycan synthesis is needed. Current work is ongoing studying the effect of **VU0849855** and **VU0849838** on cell elongation and delocalization of FtsA and PBP2B. However, based on this preliminary work it is clear that the antimicrobial mechanism of action for the chrysophaentins is not simply FtsZ inhibition and is more complex in that it modulates both the elongation and division complexes

leading to complete inhibition of cell wall biosynthesis. The following section will outline the formation and regulation of the Z-ring and divisome complexes. While also highlighting key protein-protein interactions with FtsZ and their role in linking FtsZ to peptidoglycan synthesis. Furthermore, based on the literature review of the divisome, I will propose potential protein and protein complex targets that could explain the unique mechanism of cell wall synthesis inhibition caused by chrysophaentin treatment.

3.4 Review of FtsZ's Role, Regulation, and the Protein Components of the Divisome

The discrepancies between the observed growth inhibition and GTPase activity lead to the collaboration with the VanNieuwenhze group where we fortuitously uncovered a novel mechanism of cell wall biosynthesis inhibition induced by the chrysophaentins. However, to fully understand the observed phenotype and how it relates to cell wall biosynthesis inhibition, the role and regulation of FtsZ and how the Z-ring forms and interacts with the individual proteins that make up the divisome is needed. In addition, the connection of divisome proteins to the elongation machinery is needed in order to understand the comprehensive inhibition of peripheral and septal peptidoglycan synthesis.

3.4.1 FtsZ: Filamenting Temperature-Sensitive Mutant Z

As mentioned in Chapter 1, FtsZ, filamenting temperature-sensitive mutant Z, is the most conserved bacterial cell division protein in prokaryotes, with a 40-50% sequence homology throughout bacteria and is essential for bacterial cell division.[16,17] FtsZ has been found to be the first cell division protein to localize to the midline of the cell and marks the plane of division.[16,18]

FtsZ is the prokaryotic homolog of eukaryotic tubulin[19] and similar to tubulin, FtsZ has GTPase activity which drives polymerization of FtsZ monomers into protofilaments. The protofilaments then undergo bundling to form a ring-like structure called the Z-ring (Figure 3.9). The Z-ring acts as a scaffold for the recruitment of the remaining proteins necessary for cell division and these proteins localize to the midline of the cell and form the cell division complex called the divisome.[20] The essential nature of FtsZ to bacterial cell division and its key role in the recruitment of the divisome complex make FtsZ a prime target for the development of new antimicrobials.[2,21,22]
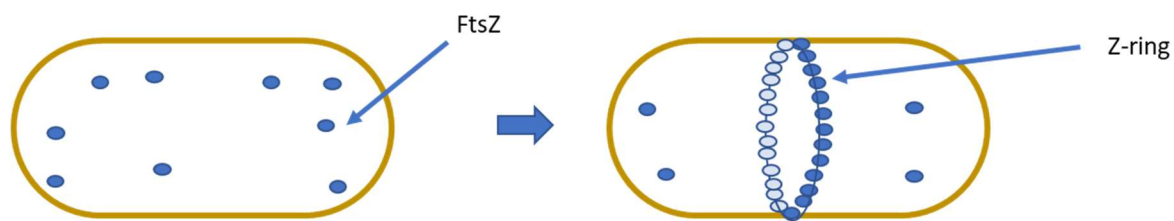
Figure 3.9. FtsZ polymerization and Z-ring formation.

3.4.2 FtsZ's Role in Bacterial Cell Division and Divisome Complex Formation

Bacterial cell division has been extensively studied in E. *coli* and B. *subtilis* and in these systems, cell division starts with nucleoid replication and cell elongation.[18,20,23,24] Cell elongation is controlled by a complex that is separate from the divisome with the recruitment of related proteins under the direction of the bacterial protein MreB.[14] MreB forms a ring-like structure similar to FtsZ, however, its placement is throughout the periphery of the cell and it directs peripheral peptidoglycan synthesis resulting in cell elongation.[14] Following cell elongation and nucleoid replication, FtsZ localizes to the midline of the cell and undergoes a GTP-dependent polymerization to form a ring-like structure called the Z-ring (Figure 3.9).[20]

The Z-ring then organizes essential cell division proteins to form a complex called the divisome. The recruitment of the proteins that make up the cell division machinery are dependent upon FtsZ localization, and regulation of FtsZ is an important checkpoint during cell division.[25] The divisome is made up of more than 15 proteins that have various roles in cell division, from the regulation of Z-ring formation and stabilization, to peptidoglycan synthesis, and septum formation.[20] Following divisome formation, FtsZ hydrolyzes GTP resulting in the bending of FtsZ dimers which make up the Z-ring polymers. The bending of FtsZ is believed to provide the physical force necessary for inner membrane constriction (Figure 3.10, image 3).[27]

Cell elongation and nucleoid segregation: diminish nucleoid occlusion and Min, allowing FtsZ to polymerize

Recruitment of divisome proteins triggers membrane constriction

Septal invagination achieved by Z ring contraction and septal peptidoglycan synthesis

Membrane scission divides inner membrane of daughter cells. Peptidoglycan synthesis is continuous

Amidases hydrolyze peptidoglycan to separate daughter cells

Figure 3.10. Bacterial cell division.

Following inner membrane constriction, septal invagination is achieved by the joint effort of Z-ring constriction and septal peptidoglycan synthesis (Figure 3.10, image 4).[27] Once membrane constriction and septal cell wall synthesis have been completed, membrane scission occurs, separating the inner membranes of the two daughter cells (Figure 3.10, image 5). After membrane

scission, amidases, hydrolyze the septal peptidoglycan between the two daughter cells leading to cell separation, completing the process of cytokinesis (Figure 3.10, image 6).[27]

3.4.3 FtsZ Regulation in Bacteria.

FtsZ is a key recruitment factor for the formation of the divisome and the polymerization of FtsZ monomers is highly regulated by different proteins and cellular signals, throughout the division process. In both E. *coli* and B. *subtilis*, FtsZ polymerization is regulated by three classes of proteins: promoters/stabilizers, cell cycle responsive regulators, and general regulators (Figure 3.11).[18,25] Cell cycle responsive regulators include the UgtP, SulA, and MciZ. In B. *subtilis*, Z-ring "fine-tuning" is carried out by UgtP, which responds to nutrient availability and cell growth.[28]

UgtP's main role is delaying FtsZ polymers from bundling to form the Z-ring until cells reach the correct size for division. UgtP also acts as a metabolic sensor for nutrient availability in B. *subtilis,* ensuring cell division only occurs when enough nutrients are available (Figure 3.11, right panel).[28,29]
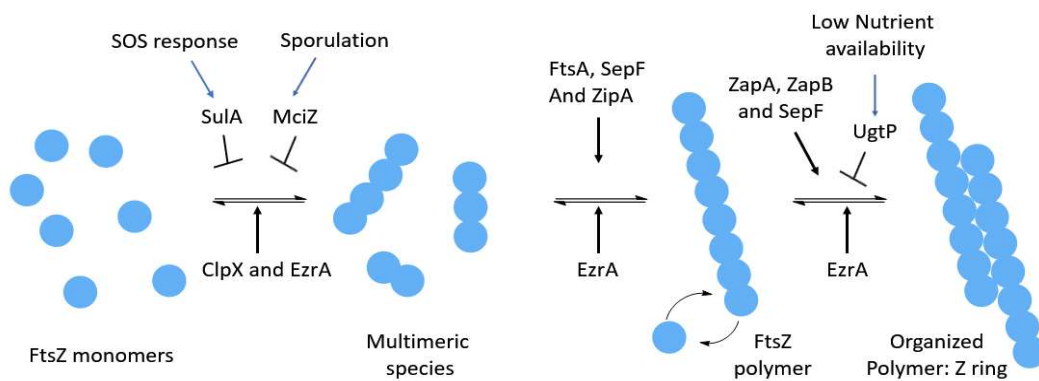
Figure 3.11 Regulation of FtsZ polymerization. Adapted from Adams et al.[18]

Other cell cycle response regulators of FtsZ polymerization are SulA in E. *coli* and MciZ in B. *subtilis.* SulA and MciZ prevent the polymerization of FtsZ monomers to multimeric species, maintaining the FtsZ monomer pool (Figure 3.11, left panel).[18] SulA is activated as part of the SOS response due to DNA damage and promotes the disassembly of the Z-ring.[30,31] In B. *subtilis*, the SOS response activates YneA, which has a similar regulatory role as SulA in E. *coli*.[32] MciZ inhibits Z-ring formation in response to sporulation in B. *subtilis* by capping FtsZ filaments preventing further bundling and annealing of polymers into protofilaments.[33] The Min and nucleoid exclusion systems are also considered cell cycle responsive FtsZ inhibitors and are key for the correct placement of the Z-ring, ensuring Z-ring formation does not occur at the cell poles or over the nucleoids.[34]

General regulators of FtsZ polymerization and Z-ring formation are EzrA, ClpX, SepF, ZapB, and ZapA. EzrA, as mentioned above, works in conjugation with the Min system to aid in the prevention of aberrant FtsZ polymerization and formation of Z-rings at the cell poles.[35] The final known negative regulator of FtsZ polymerization is ClpX. ClpX helps maintain the cytoplasmic monomer pool and prevents the further polymerization of FtsZ monomers into polymers.[36] ClpX is highly conserved in many bacteria indicating that it has an important role in the general regulation of FtsZ polymerization however, the exact mechanism of regulation is not fully understood at this time.

Bacteria have also evolved numerous promoters of Z-ring formation, which many have been discussed above. Proteins that encourage FtsZ polymerization include FtsA, ZipA, ZapA, ZapB, and SepF.[18] The exact mechanism of how these proteins encourage polymerization is unknown, but it is believed that their direct interaction with FtsZ promotes polymer stability and Z-ring formation.[18,23] The regulation of FtsZ is key for the correct positioning of the Z-ring and

correct timing of septum formation. The inhibition of FtsZ results in inhibition of cell division, making it a prime target for novel antimicrobial development. Furthermore, understanding its regulation is key for designing assays to determine the mechanism of action of potential FtsZ inhibitors, like the chrysophaentins. The following section will highlight the divisome formation in E. *coli* and B. *subtilis* and the key protein-interactions that could potentially explain the novel mechanism of action of the chrysophaentins.

3.4.4 E. *coli* and B. *subtilis* Divisome Formation.

FtsZ is the first protein to localize to the midline of the cell and forms the Z-ring which acts a scaffold to recruit and organize up to 15 proteins in E. *coli* and 20 proteins in B. *subtilis*.[28] However, the proteins and the order in which those proteins are recruited to the Z-ring differ between bacterial species. The understanding of the differences between bacterial strains is essential for the development of cross-species active FtsZ inhibitors. E. *coli* and B. *subtilis* divisomes are the most studied and have been found to form in two distinct fashions. In E. *coli*, the divisome forms in a linear sequential manner, while in B. *subtilis* the divisome forms in a two-phase process.[27,37] Outline below, will be a brief description of the order of recruitment and the function of the individual proteins that make up the divisome in E. *coli* and B. *subtilis*.

In E. *coli,* the divisome forms sequentially and linearly where FtsZ localizes to the site of division followed shortly by FtsA, ZapA, and ZipA.[27] FtsA and is a membrane-associated protein that anchors FtsZ to the cellular membrane, while ZipA helps to stabilize the Z-ring at the membrane fusion.[8,18] ZapA is believed to act as an FtsZ protofilament bundler and aides in the polymerization and stability of the FtsZ polymers, which allows for the formation of the Z-ring.

The localization of FtsA, ZapA, and ZipA is dependent on FtsZ localization and these proteins promote the formation and stabilization of the Z-ring (Figure 3.12).[38]
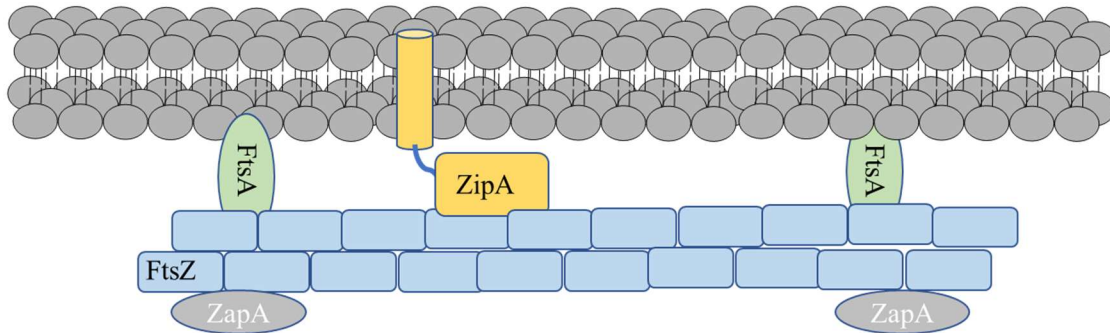
Figure 3.12. FtsZ, FtsA, ZipA and ZapA complex in E. *coli.*

Once the Z-ring is formed and stabilized, FtsE and FtsX localize to the Z-ring simultaneously. However, their function is not completely understood at this time, but are believed to form a conserved ATP-binding transporter complex. This complex functions as a transmembrane regulator of septal peptidoglycan hydrolysis.[25,39,40] The remodeling of old peptidoglycan through hydrolysis is necessary for the synthesis and cross-linking of newly synthesized septal peptidoglycan (Figure 3.13).

The next protein to localize to the Z-ring is FtsK. FtsK is a DNA translocase that has an essential role involved in chromosome segregation.[41] The main role of FtsK is to aid the separation of chromosome dimers which are generated as a result of recombination events between the two growing DNA chains.[41] FtsK in conjugation with a protein complex made up of ZapA, ZapB, and MatP, along with the nucleoid occlusion system coordinate cell division with the separation of the two nucleoids.[17] MatP binds to the Ter region of the chromosomes and through interactions with ZapB and ZapA form a bridge between the chromosomes and Z-ring ensuring nucleoid segregation is complete before membrane constriction and septum formation (Figure 3.13).[25]

Following localization of ZapA, ZapB, MatP, FtsQ localizes to the Z-ring followed shortly by FtsB and FtsL. FtsQ, FtsB, and FtsL form a trimeric protein complex, FtsQBL, which is linked to the Z-ring through interactions with FtsK.[17] FtsQBL is a transmembrane protein complex that is believed to be important in linking the Z-ring to the septal peptidoglycan synthesis machinery. FtsQBL is regulated by FtsK to coordinate septal peptidoglycan synthesis with nucleoid segregation.[17] Following the localization of FtsQBL, is the localization of FtsW.
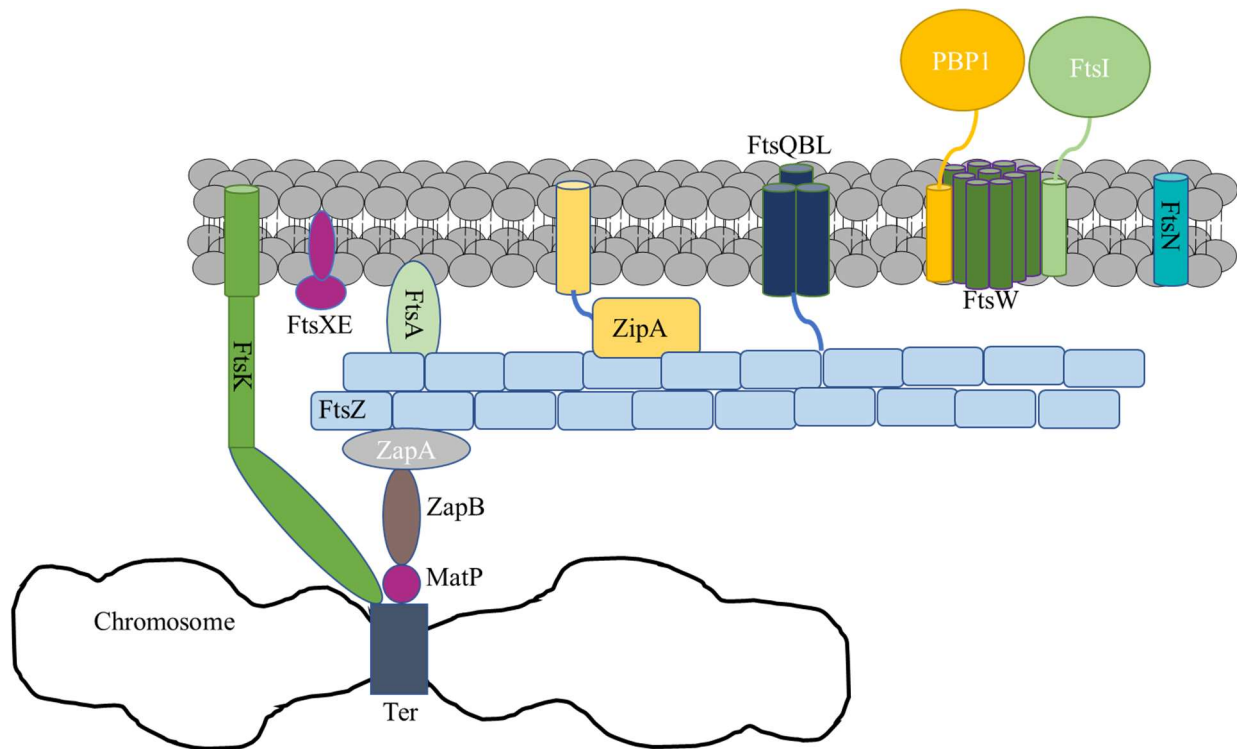
Figure 3.13. E. *Coli* divisome, adapted from Wang et al.[25]

FtsW was originally hypothesized to translocate the peptidoglycan precursor lipid II across the cytoplasmic membrane.[42] However, it has recently been discovered to be responsible for septal peptidoglycan synthesis. FtsW works in conjunction with a class b penicillin-binding protein (PBP) partner, FtsI (PBP3), which localizes to the divisome shortly after FtsW.[43] FtsW-FtsI

complex coordinates the early stages of septal peptidoglycan synthesis in connection with FtsZ treadmilling,[43] which was discussed above. Following FtsW and FtsI localization, the last essential divisome protein, FtsN localizes to the divisome and triggers the start of septal peptidoglycan synthesis.[44] FtsN's exact function is unknown, but it possesses a murein binding domain and interacts with FtsQ, FtsW, and FtsI, which are all involved with septal peptidoglycan synthesis and indicates its role could be involved in the regulation or control of septal peptidoglycan synthesis.

As mentioned previously, septal peptidoglycan synthesis in conjunction with Z-ring constriction is responsible for septum formation. The final two proteins to localize to the midline of the cell, AmiC, and EnvC, are not technically apart of the divisome but are murein hydrolases that are required for the degradation of the new septal wall that is formed between the two daughter cells. AmiC and EnvC hydrolyze the septal wall allowing for the separation of two new daughter cells.[45] Overall, the E. *coli* divisome complex formation can be thought of as a linear process that starts with the localization of FtsZ to the midline of the cell and following polymerization and stabilization by FtsA, ZipA, and ZapA, the Z-ring then recruits the other remaining divisome proteins sequentially. The formation of the divisome in B. *subtilis* is quite different and will be discussed in the following section.

The formation of the divisome complex in B. *subtilis* happens in two phases instead of the sequential, linear pathway as is seen in E. *coli*.[37] In B. *subtilis*, FtsZ localizes to the midline of the cell concurrently with FtsA, ZapA, SepF, and EzrA (Figure 3.14). The localization of these five proteins to the midline is the first phase of divisome formation in B. *subtilis*.[37] It is believed that these proteins localize interdependent of each other, but dependent upon FtsZ localization. As mentioned above for E. *coli*, FtsA anchors FtsZ to the membrane, and ZapA stabilizes and bundles FtsZ polymers allowing for the formation of the Z-ring. SepF is believed to have a redundant role

similar to FtsA and is not essential for cell division.[38] EzrA, is a membrane-associated protein that acts as a negative regulator of Z-ring assembly and is distributed throughout the cellular membrane during cell elongation to prevent aberrant Z-ring formation.[35] Once cell elongation is complete, EzrA is recruited by FtsZ to the midline of the cell and is down-regulated by other divisome proteins to allow FtsZ polymerization and Z-ring formation. EzrA's negative regulation works in connection with the Min-system to prevent aberrant Z-ring formation at the poles of the cell and with the nucleoid exclusion (NO) system to prevent Z-ring formation over the nucleoids.[18] EzrA also has a role in coordinating cell elongation with cell division, however, this link is not fully understood (Figure 3.14).
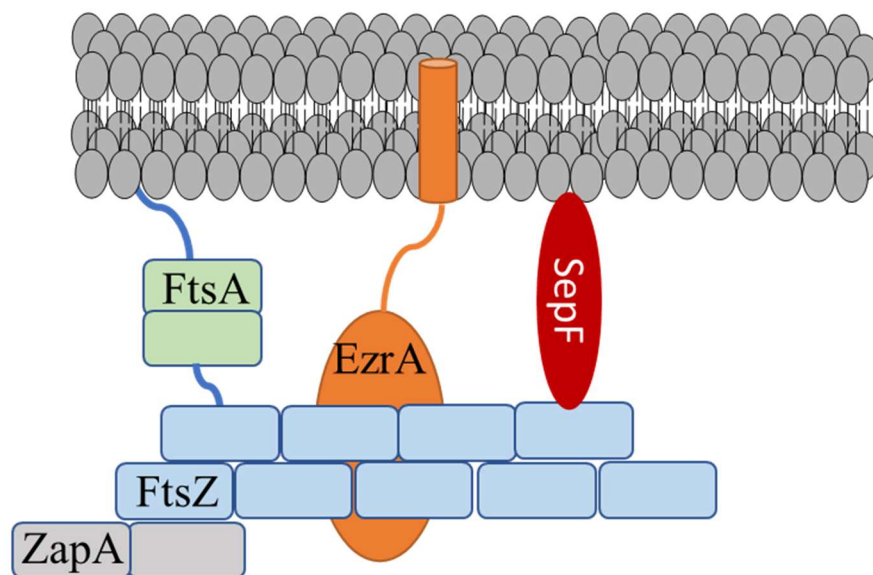
Figure 3.14. First phase of B. *subitilis* divisome formation.

The second stage of divisome formation in B. *subtilis* occurs with a time delay of at least 20% of the cell cycle and consist of the recruitment of membrane-bound proteins GpsB, DivIVA, DivIB, DivIC, FtsL, PBP1, PBP2B and FtsW (Figure 3.15).[37] GpsB, is essential for the shuttling of PBP1 between the elongation machinery and the divisome, ensuring cell wall synthesis is

occurring at the correct location.[46] GpsB has also been attributed to the stabilization of the FtsZ protofilaments which make up the Z-ring.[47] DivIVA, is believed to aid in the spatial and topological placement of the Z-ring and mutation in the DivIVA gene result in minicells and misplaced Z-rings.[48] DivIB and DivIC are homologs to E. *coli* FtsQ and FtsB, which as mentioned above, form a trimeric protein complex which is important in linking the Z-ring to septal peptidoglycan synthesis. FtsW and its class b penicillin-binding protein (PBP) partner, PBP2B in B. *subtilis*, form a complex and are essential for septal peptidoglycan synthesis.[37] The remaining localization of divisome proteins in B. *subtilis* is not well understood and is thought to occur shortly after FtsW localization.
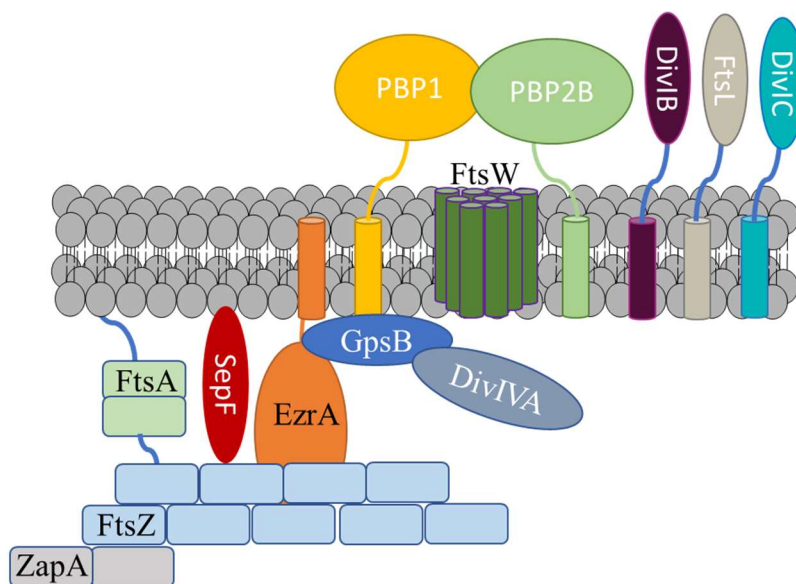
Figure 3.15. Second phase of B. *subtilis* divisome formation.

However, recently the formation of the divisome in E. *coli* as a linear and sequential process has been disputed and some evidence has suggested that the formation is more similar to B. *subtilis* in which the divisome forms by sequential localization of three subcomplexes which localize independently of each other.[27,49] However, the key differences between E. *coli* and B.

subtilis divisomes are in the different proteins that make up their respective divisomes and how these proteins interact with FtsZ. The targeting of FtsZ with new antimicrobials will require a fundamental knowledge of the key interactions between FtsZ and the proteins that make up the divisome. The understanding of these key interactions can influence and direct mechanism of action studies for chrysophaentin A (**3.1**) and aid in ruling out other potential mechanisms of action. One area of research that has recently expanded our knowledge of bacterial cell division is the use of super-resolution microscopy in conjugation with fluorescently labeled proteins fusions which have allowed for the tracking of individual proteins that make up the divisome and the order in which they localize.

3.5   Potential Protein Targets of the Chrysophaentins.

As highlighted above our synthetic 9-dechlorochrysophaentin congeners did not exhibit the expected mechanism of FtsZ GTPase inhibition, but inhibit peptidoglycan synthesis. The unique aspect of the observed phenotype is the dispersion of FtsZ, FtsA, and PBP2B resulting in the inhibition of cell division and peptidoglycan synthesis. In an attempt to elucidate the potential target of the chrysophaentins, the Skaar lab (Vanderbilt University) attempted to generate resistant mutants in B. *subtilis* to our synthetic chrysophaentins. However, these attempts were unsuccessful, and further attempts to gain insights into the mechanism of action through testing the Nebraska Transposon Mutant Library provided two interesting hits, LytH and GpsB/DivIVA.

The first interesting hit, LytH, is a presumed amidase that is important for peptidoglycan hydrolysis. Walker and co-workers recently reported that LytH is involved in the regulation of peptidoglycan synthesis and the deletion of the LytH caused deregulated cell growth and

division.[50] Typically, as mentioned above for AmiC and EnvC, amidases hydrolyze peptidoglycan to allow for the synthesis and incorporation of new peptidoglycan and to hydrolyze septal peptidoglycan to allow for daughter cell separation.[45] However, Walker and co-workers discovered that LytH forms a protein complex with ActH and this protein complex spatially regulates cell wall synthesis by controlling the density of cell wall synthesis sites within S. *aureus*.[50] We do not propose that LytH is the protein target of the chrysophaentins, because deletion of LytH leads to an increase in peptidoglycan synthesis.[50] However, the discovery that amidases can regulate cell division and growth is intriguing in the context of the chrysophaentins. Treatment with **VU0848355** and **VU0848354** results in the inhibition of peptidoglycan synthesis and cell division, the same two processes that LytH was found to regulate. These results support the idea that there could be another amidase, that has not been characterized similar to LytH, that also has a regulatory role both peripheral and septal peptidoglycan synthesis, which could potentially explain our observed mechanism of cell wall synthesis and division inhibition.

The second interesting hit from the transposon screen was the cell cycle protein GpsB/DivIVA proteins. As mentioned above, GpsB is essential for the shuttling of PBP1 between the elongation machinery and the divisome, ensuring cell wall synthesis is occurring at the correct location and for stabilizing the Z-ring.[46,47] GpsB's shuttling of PBP1 from the elongation machinery to divisome, effectively regulates the location of cell wall synthesis. The protein complex that is shuttled between the elongation machinery and divisome consists of GpsB, EzrA, and PBP1.[53] EzrA is a regulatory protein that inhibits the polymerization of FtsZ and is recruited to the divisome after nucleoid separation to allow for FtsZ polymerization.

If the chrysophaentins were targeting the elongation-division PBP1 shuttling complex, it could result in negative regulation of FtsZ polymerization and the observed delocalization of FtsA

and PBP2B. The delocalization of PBP2B and FtsZ would result in the inhibition of septal peptidoglycan synthesis. Interaction of the chrysophaentins with this complex could also result in the dysregulation of PBP1, which the main peptidoglycan synthase and this could explain the observed peripheral cell wall synthesis inhibition. GpsB has been found to interact with DivIVA which is believed to aid in the spatial and topological placement of the Z-ring.[48] The complex protein-protein interaction of the GpsB/EzrA/PBP1 with FtsZ and DivIVA and their essential roles in the regulation of cell wall synthesis at both periphery and septum provides evidence that this protein complex could be a potential target for the chrysophaentins.

Other proteins besides GpsB/EzrA complex and cell wall amidases that could explain the mechanism of the chrysophaentins are, PBP2B, FtsW/FTsQBL, MreB, and general cell growth regulation induced by SOS response and membrane potential. PBP2B has been shown to be responsible for septal peptidoglycan synthesis by the VanNieuwenhze group,[9,12] however recent studies have shown it is also involved with the elongation machinery in pneumococcal bacteria.[52] Work by den Blaauwen[53] has demonstrated the colocalization of the elongasome and divisome complexes to the midline of E. *coli* and this colocalization is required for the initiation of new cell pole synthesis. The colocalization and presence of PBP2B in both the elongasome and divisome provide evidence that it could be responsible for the observed phenotype. However, binding of the chrysophaentins to PBP2B by itself would not account for the dispersion of FtsZ and FtsA. FtsZ has been shown to still polymerize into the Z-ring and cell membrane invagination still occurs in the absence of PBP2B in B. *subtilis*.[54] The independent polymerization and treadmilling of the Z-ring in the absence of PBP2B was also observed in studies by the VanNieuwenhze group,[9] indicating the mechanism of the chrysophaentins most likely is not inhibition of PBPs. However,

the proteins which interact and coordinate the activity of PBPs with the Z-ring could be potential targets of the chrysophaentins, such as FtsW and FtsQBL protein complex.

FtsW and FtsQBL (DivIB/DivIC/FtsL) complexes link FtsZ to PBPs and coordinate cell wall synthesis with Z-ring treadmilling.[38,42,43] FtsW, as mentioned, above works with FtsI (PBP3) in E. *coli* to coordinate cell wall synthesis with the Z-ring. However, there is little literature evidence of the effects of FtsW inhibition or depletion have on cell growth and division. FtsQBL complex (E. *coli*) or DivIB/DivIC/FtsL (B. *subtilis*) are essential proteins for cell growth and viability and also aid in the coordination of cell wall synthesis to the Z-ring. The FtsQBL complex has been shown to interact with PBP2B to remodel and synthesize new peptidoglycan.[38] Inhibition or break up of protein-protein interactions of this complex could result in the inhibition of cell wall synthesis. However, the inhibition of the FtsQBL complex's effect on FtsZ localization is not known at this time.

The final potential protein target of the chrysophaentins that will be discussed is MreB. MreB is an actin-like protein that forms a complex ring-like structure at the peripheral cell wall and coordinates cell elongation or growth.[14] It could be possible that the chrysophaentins interaction with both FtsZ and MreB protein complexes effectively shutting down both cell elongation and division. Bewley and co-workers have already demonstrated the chrysophaentin A (**3.1**) binds to FtsZ through STD NMR studies.[4] However, the chrysophaentins possess weak GTPase inhibition activity, indicating that their mechanism of action is distinct from the GTP-dependent polymerization and treadmilling of the Z-ring and the chrysophaentins could block key protein-protein interactions of FtsZ and MreB which stabilize their ring-like scaffold resulting in destabilization and inhibition of cell division and elongation. It should be noted that the chrysophaentins could be enacting their mechanism through cellular processes other than direct

protein binding. DNA damage results in the induction of the SOS response and production of SulA in E. *coli* and YneA in B. *subtilis*, these proteins directly inhibit FtsZ polymerization and cell growth.[30,31]

Furthermore, Hamoen and co-workers have found membrane potential is important for cell division and elongation machinery localization. Their study demonstrated that MreB and FtsA delocalize throughout the cell when membrane potential is disturbed.[55] However, FtsZ and PBP2B localization were not affected in B. *subtilis*. The above highlighted potential mechanisms are just hypotheses based on information in the literature that was highlighted previously in this chapter.

3.6 Conclusion

In summary, we have shown that the chrysophaentins mechanism of action is more complex than inhibition of the GTPase activity of FtsZ and the chrysophaentins have a novel mechanism of cell wall synthesis inhibition through the dispersion of divisome proteins FtsZ, FtsA, and PBP2B from the midline in B. *subtilis*. The observed phenotype is distinct from reported FtsZ inhibitors, PC190723 (**3.3**), and cell wall synthesis inhibitors, vancomycin, and ampicillin.[9] However, as outlined above the divisome formation and the protein interactions within the divisome are quite complex and to determine the mechanism of action for the chrysophaentins will require an extensive investigation of the divisome proteins and their effects on cell wall synthesis and division. Furthermore, the elimination of innate cellular regulatory mechanisms, such as SOS response, will need to be ruled out as well. Overall, these results indicate the importance of studying natural products with antimicrobial activity, and further highlight the importance of

completing a total synthesis of chrysophaentin A (**1.1**) to elucidate its novel mechanism of cell wall synthesis inhibition and to determine its therapeutic potential.

References:

(1)   Haydon, D. J.; Stokes, N. R.; Ure, R.; Galbraith, G.; Bennett, J. M.; Brown, D. R.; Baker, P. J.; Barynin, V. v.; Rice, D. W.; Sedelnikova, S. E.; et al. An Inhibitor of FtsZ with Potent and Selective Anti-Staphylococcal Activity. *Science* **2008**, *321* (5896), 1673–1675. https://doi.org/10.1126/science.1159961.

(2)   Margalit, D. N.; Romberg, L.; Mets, R. B.; Hebert, A. M.; Mitchison, T. J.; Kirschner, M. W.; RayChaudhuri, D. Targeting Cell Division: Small-Molecule Inhibitors of FtsZ GTPase Perturb Cytokinetic Ring Assembly and Induce Bacterial Lethality. *Proceedings of the National Academy of Sciences of the United States of America* **2004**, *101* (32), 11821–11826. https://doi.org/10.1073/pnas.0404439101.

(3)   Keffer, J. L.; Hammill, J. T.; Lloyd, J. R.; Plaza, A.; Wipf, P.; Bewley, C. A. Geographic Variability and Anti-Staphylococcal Activity of the Chrysophaentins and Their Synthetic Fragments. *Marine Drugs* **2012**, *10* (12), 1103–1125. https://doi.org/10.3390/md10051103.

(4)   Plaza, A.; Keffer, J. L.; Bifulco, G.; Lloyd, J. R.; Bewley, C. A. Chrysophaentins A−H, Antibacterial Bisdiarylbutene Macrocycles That Inhibit the Bacterial Cell Division Protein FtsZ. *Journal of the American Chemical Society* **2010**, *132* (26), 9069–9077. https://doi.org/10.1021/ja102100h.

(5)   Keffer, J. L.; Huecas, S.; Hammill, J. T.; Wipf, P.; Andreu, J. M.; Bewley, C. A. Chrysophaentins Are Competitive Inhibitors of FtsZ and Inhibit Z-Ring Formation in Live

Bacteria. *Bioorganic & Medicinal Chemistry* **2013**, *21* (18), 5673–5678. https://doi.org/10.1016/j.bmc.2013.07.033.

(6)   E. Anderson, D.; B. Kim, M.; T. Moore, J.; E. O'Brien, T.; A. Sorto, N.; I. Grove, C.; L. Lackner, L.; B. Ames, J.; T. Shaw, J. Comparison of Small Molecule Inhibitors of the Bacterial Cell Division Protein FtsZ and Identification of a Reliable Cross-Species Inhibitor. *ACS Chemical Biology* **2012**, *7* (11), 1918–1928. https://doi.org/10.1021/cb300340j.

(7)   Khare, S.; Hsin, J.; Sorto, N. A.; Nepomuceno, G. M.; Shaw, J. T.; Shi, H.; Huang, K. C. FtsZ-Independent Mechanism of Division Inhibition by the Small Molecule PC190723 in Escherichia Coli. *Advanced Biosystems* **2019**, *3* (11), 1900021. https://doi.org/10.1002/adbi.201900021.

(8)   Lutkenhaus, J.; Pichoff, S.; Du, S. Bacterial Cytokinesis: From Z Ring to Divisome. *Cytoskeleton* **2012**, *69* (10), 778–790. https://doi.org/10.1002/cm.21054.

(9)   Bisson-Filho, A. W.; Hsu, Y. P.; Squyres, G. R.; Kuru, E.; Wu, F.; Jukes, C.; Sun, Y.; Dekker, C.; Holden, S.; VanNieuwenhze, M. S.; et al. Treadmilling by FtsZ Filaments Drives Peptidoglycan Synthesis and Bacterial Cell Division. *Science* **2017**, *355* (6326), 739–743. https://doi.org/10.1126/science.aak9973.

(10)   Hsu, Y.-P.; Rittichier, J.; Kuru, E.; Yablonowski, J.; Pasciak, E.; Tekkam, S.; Hall, E.; Murphy, B.; Lee, T. K.; Garner, E. C.; et al. Full Color Palette of Fluorescent D-Amino Acids for in Situ Labeling of Bacterial Cell Walls †. **2017**. https://doi.org/10.1039/c7sc01800b.

(11)   Yang, X.; Lyu, Z.; Miguel, A.; McQuillen, R.; Huang, K. C.; Xiao, J. GTPase Activity-Coupled Treadmilling of the Bacterial Tubulin FtsZ Organizes Septal Cell Wall Synthesis. *Science* **2017**, *355* (6326), 744–747. https://doi.org/10.1126/science.aak9995.

(12)   Kuru, E.; Tekkam, S.; Hall, E.; Brun, Y. v.; van Nieuwenhze, M. S. Synthesis of Fluorescent D-Amino Acids and Their Use for Probing Peptidoglycan Synthesis and Bacterial Growth in Situ. *Nature Protocols* **2015**, *10* (1), 33–52. https://doi.org/10.1038/nprot.2014.197.

(13)   Andreu, J. M.; Schaffner-Barbero, C.; Huecas, S.; Alonso, D.; Lopez-Rodriguez, M. L.; Ruiz-Avila, L. B.; Núñez-Ramírez, R.; Llorca, O.; Martín-Galiano, A. J. The Antibacterial Cell Division Inhibitor PC190723 Is an FtsZ Polymer-Stabilizing Agent That Induces Filament Assembly and Condensation. *Journal of Biological Chemistry* **2010**, *285* (19), 14239–14246. https://doi.org/10.1074/jbc.M109.094722.

(14)   Mirouze, N.; Ferret, C.; Yao, Z.; Chastanet, A.; Carballido-López, R. MreB-Dependent Inhibition of Cell Elongation during the Escape from Competence in Bacillus Subtilis. *PLoS Genetics* **2015**, *11* (6). https://doi.org/10.1371/journal.pgen.1005299.

(15)   Raynor, B. D. Penicillin and Ampicillin. *Primary Care Update for Ob/Gyns* **1997**, *4* (4), 147–152. https://doi.org/10.1016/S1068-607X(97)00012-7.

(16)   Lutkenhaus, J.; Addinall, S. G. BACTERIAL CELL DIVISION AND THE Z RING. *Annual Review of Biochemistry* **1997**, *66* (1), 93–116. https://doi.org/10.1146/annurev.biochem.66.1.93.

(17)   Vedyaykin, A. D.; Ponomareva, E. v.; Khodorkovskii, M. A.; Borchsenius, S. N.; Vishnyakov, I. E. Mechanisms of Bacterial Cell Division. *Microbiology (Russian*

Federation). Pleiades Publishing May 1, 2019, pp 245–260. https://doi.org/10.1134/S0026261719030159.

(18)   Adams, D. W.; Errington, J. Bacterial Cell Division: Assembly, Maintenance and Disassembly of the Z Ring. *Nature Reviews Microbiology*. 2009, pp 642–653. https://doi.org/10.1038/nrmicro2198.

(19)   Nogales, E.; Downing, K. H.; Amos, L. A.; Löwe, J. Tubulin and FtsZ Form a Distinct Family of GTPases. *Nature Structural Biology* **1998**, *5* (6), 451–458. https://doi.org/10.1038/nsb0698-451.

(20)   Haeusser, D. P.; Margolin, W. Splitsville: Structural and Functional Insights into the Dynamic Bacterial Z Ring. *Nature Reviews Microbiology*. Nature Publishing Group May 1, 2016, pp 305–319. https://doi.org/10.1038/nrmicro.2016.26.

(21)   Kusuma, K. D.; Payne, M.; Ung, A. T.; Bottomley, A. L.; Harry, E. J. FtsZ as an Antibacterial Target: Status and Guidelines for Progressing This Avenue. *ACS Infectious Diseases* **2019**, *5* (8), 1279–1294. https://doi.org/10.1021/acsinfecdis.9b00055.

(22)   Hurley, K. A.; Santos, T. M. A.; Nepomuceno, G. M.; Huynh, V.; Shaw, J. T.; Weibel, D. B. Targeting the Bacterial Division Protein FtsZ. *Journal of Medicinal Chemistry*. American Chemical Society August 11, 2016, pp 6975–6998. https://doi.org/10.1021/acs.jmedchem.5b01098.

(23)   Errington, J.; Daniel, R. A.; Scheffers, D.-J. Cytokinesis in Bacteria. *Microbiology and Molecular Biology Reviews* **2003**, *67* (1), 52–65. https://doi.org/10.1128/mmbr.67.1.52-65.2003.

(24)   Margolin, W. FtsZ and the Division of Prokaryotic Cells and Organelles. *Nature Reviews Molecular Cell Biology*. Nature Publishing Group November 14, 2005, pp 862–871. https://doi.org/10.1038/nrm1745.

(25)   Wang, M.; Fang, C.; Ma, B.; Luo, X.; Hou, Z. Regulation of Cytokinesis: FtsZ and Its Accessory Proteins. *Current Genetics*. Springer Verlag June 17, 2019, pp 43–49. https://doi.org/10.1007/s00294-019-01005-6.

(26)   Erickson, H. P. Modeling the Physics of FtsZ Assembly and Force Generation. *Proceedings of the National Academy of Sciences of the United States of America* **2009**, *106* (23), 9238–9243. https://doi.org/10.1073/pnas.0902258106.

(27)   Goehring, N. W.; Beckwith, J. Diverse Paths to Midcell: Assembly of the Bacterial Cell Division Machinery. *Current Biology*. Cell Press July 12, 2005. https://doi.org/10.1016/j.cub.2005.06.038.

(28)   Weart, R. B.; Lee, A. H.; Chien, A. C.; Haeusser, D. P.; Hill, N. S.; Levin, P. A. A Metabolic Sensor Governing Cell Size in Bacteria. *Cell* **2007**, *130* (2), 335–347. https://doi.org/10.1016/j.cell.2007.05.043.

(29)   Monahan, L. G.; Hajduk, I. v.; Blaber, S. P.; Charles, I. G.; Harry, E. J. Coordinating Bacterial Cell Division with Nutrient Availability: A Role for Glycolysis. *mBio* **2014**, *5* (3). https://doi.org/10.1128/mBio.00935-14.

(30)   Dajkovic, A.; Mukherjee, A.; Lutkenhaus, J. Investigation of Regulation of FtsZ Assembly by SulA and Development of a Model for FtsZ Polymerization. *Journal of Bacteriology* **2008**, *190* (7), 2513–2526. https://doi.org/10.1128/JB.01612-07.

(31) Trusca, D.; Scott, S.; Thompson, C.; Bramhill, D. Bacterial SOS Checkpoint Protein SulA Inhibits Polymerization of Purified FtsZ Cell Division Protein. *Journal of Bacteriology* **1998**, *180* (15), 3946–3953. https://doi.org/10.1128/jb.180.15.3946-3953.1998.

(32) Mo, A. H.; Burkholder, W. F. YneA, an SOS-Induced Inhibitor of Cell Division in Bacillus Subtilis, Is Regulated Posttranslationally and Requires the Transmembrane Region for Activity. *Journal of Bacteriology* **2010**, *192* (12), 3159–3173. https://doi.org/10.1128/JB.00027-10.

(33) Bisson-Filho, A. W.; Discola, K. F.; Castellen, P.; Blasios, V.; Martins, A.; Sforça, M. L.; Garcia, W.; Zeri, A. C. M.; Erickson, H. P.; Dessen, A.; et al. FtsZ Filament Capping by MciZ, a Developmental Regulator of Bacterial Division. *Proceedings of the National Academy of Sciences of the United States of America* **2015**, *112* (17), E2130–E2138. https://doi.org/10.1073/pnas.1414242112.

(34) Rowlett, V. W.; Margolin, W. The Min System and Other Nucleoid-Independent Regulators of Z Ring Positioning. *Frontiers in Microbiology*. Frontiers Media S.A. 2015. https://doi.org/10.3389/fmicb.2015.00478.

(35) Haeusser, D. P.; Schwartz, R. L.; Smith, A. M.; Oates, M. E.; Levin, P. A. EzrA Prevents Aberrant Cell Division by Modulating Assembly of the Cytoskeletal Protein FtsZ. *Molecular Microbiology* **2004**, *52* (3), 801–814. https://doi.org/10.1111/j.1365-2958.2004.04016.x.

(36) Weart, R. B.; Nakano, S.; Lane, B. E.; Zuber, P.; Levin, P. A. The ClpX Chaperone Modulates Assembly of the Tubulin-like Protein FtsZ. *Molecular Microbiology* **2005**, *57* (1), 238–249. https://doi.org/10.1111/j.1365-2958.2005.04673.x.

(37)   Gamba, P.; Veening, J. W.; Saunders, N. J.; Hamoen, L. W.; Daniel, R. A. Two-Step Assembly Dynamics of the Bacillus Subtilis Divisome. *Journal of Bacteriology* **2009**, *191* (13), 4186–4194. https://doi.org/10.1128/JB.01758-08.

(38)   Lock, R. L.; Harry, E. J. Cell-Division Inhibitors: New Insights for Future Antibiotics. *Nature reviews. Drug discovery*. Nature Publishing Group April 1, 2008, pp 324–338. https://doi.org/10.1038/nrd2510.

(39)   Schmidt, K. L.; Peterson, N. D.; Kustusch, R. J.; Wissel, M. C.; Graham, B.; Phillips, G. J.; Weiss, D. S. A Predicted ABC Transporter, FtsEX, Is Needed for Cell Division in Escherichia Coli. *Journal of Bacteriology* **2004**, *186* (3), 785–793. https://doi.org/10.1128/JB.186.3.785-793.2004.

(40)   Reddy, M. Role of FtsEX in Cell Division of Escherichia Coli: Viability of FtsEX Mutants Is Dependent on Functional SufI or High Osmotic Strength. *Journal of Bacteriology* **2007**, *189* (1), 98–108. https://doi.org/10.1128/JB.01347-06.

(41)   Crozat, E.; Rousseau, P.; Fournes, F.; Cornet, F. The FtsK Family of DNA Translocases Finds the Ends of Circles. *Journal of Molecular Microbiology and Biotechnology*. S. Karger AG April 16, 2014, pp 396–408. https://doi.org/10.1159/000369213.

(42)   Mohammadi, T.; van Dam, V.; Sijbrandi, R.; Vernet, T.; Zapun, A.; Bouhss, A.; Diepeveen-de Bruin, M.; Nguyen-Distèche, M.; de Kruijff, B.; Breukink, E. Identification of FtsW as a Transporter of Lipid-Linked Cell Wall Precursors across the Membrane. *The EMBO Journal* **2011**, *30* (8), 1425–1432. https://doi.org/10.1038/emboj.2011.61.

(43)   Taguchi, A.; Welsh, M. A.; Marmont, L. S.; Lee, W.; Sjodt, M.; Kruse, A. C.; Kahne, D.; Bernhardt, T. G.; Walker, S. FtsW Is a Peptidoglycan Polymerase That Is Functional Only

in Complex with Its Cognate Penicillin-Binding Protein. *Nature Microbiology*. Nature Publishing Group April 1, 2019, pp 587–594. https://doi.org/10.1038/s41564-018-0345-x.

(44)   den Blaauwen, T.; Luirink, J. Checks and Balances in Bacterial Cell Division. **2019**, No. February, 1–5. https://doi.org/10.1128/mBio.01912-18.

(45)   Priyadarshini, R.; de Pedro, M. A.; Young, K. D. Role of Peptidoglycan Amidases in the Development and Morphology of the Division Septum in Escherichia Coli. *Journal of Bacteriology* **2007**, *189* (14), 5334–5347. https://doi.org/10.1128/JB.00415-07.

(46)   Cleverley, R. M.; Rutter, Z. J.; Rismondo, J.; Corona, F.; Tsui, H. C. T.; Alatawi, F. A.; Daniel, R. A.; Halbedel, S.; Massidda, O.; Winkler, M. E.; et al. The Cell Cycle Regulator GpsB Functions as Cytosolic Adaptor for Multiple Cell Wall Enzymes. *Nature Communications* **2019**, *10* (1), 1–17. https://doi.org/10.1038/s41467-018-08056-2.

(47)   du Toit, A. Time to Split. *Nature Reviews Microbiology*. Nature Publishing Group December 1, 2018, pp 716–717. https://doi.org/10.1038/s41579-018-0108-y.

(48)   Edwards, D. H.; Errington, J. The Bacillus Subtilis DivIVA Protein Targets to the Division Septum and Controls the Site Specificity of Cell Division. *Molecular Microbiology* **1997**, *24* (5), 905–915. https://doi.org/10.1046/j.1365-2958.1997.3811764.x.

(49)   Goehring, N. W.; Gonzalez, M. D.; Beckwith, J. Premature Targeting of Cell Division Proteins to Midcell Reveals Hierarchies of Protein Interactions Involved in Divisome Assembly. *Molecular Microbiology* **2006**, *61* (1), 33–45. https://doi.org/10.1111/j.1365-2958.2006.05206.x.

(50)   Do, T.; Schaefer, K.; Santiago, A. G.; Coe, K. A.; Fernandes, P. B.; Kahne, D.; Pinho, M. G.; Walker, S. Staphylococcus Aureus Cell Growth and Division Are Regulated by an Amidase That Trims Peptides from Uncrosslinked Peptidoglycan. *Nature Microbiology*.

Nature Research February 1, 2020, pp 291–303. https://doi.org/10.1038/s41564-019-0632-1.

(51)   Claessen, D.; Emmins, R.; Hamoen, L. W.; Daniel, R. A.; Errington, J.; Edwards, D. H. Control of the Cell Elongation–Division Cycle by Shuttling of PBP1 Protein in Bacillus Subtilis. *Molecular Microbiology* **2008**, *68* (4), 1029–1046. https://doi.org/10.1111/j.1365-2958.2008.06210.x.

(52)   Straume, D.; Stamsås, G. A.; Berg, K. H.; Salehian, Z.; Håvarstein, L. S. Identification of Pneumococcal Proteins That Are Functionally Linked to Penicillin-Binding Protein 2b (PBP2b). *Molecular Microbiology* **2017**, *103* (1), 99–116. https://doi.org/10.1111/mmi.13543.

(53)   van der Ploeg, R.; Verheul, J.; Vischer, N. O. E.; Alexeeva, S.; Hoogendoorn, E.; Postma, M.; Banzhaf, M.; Vollmer, W.; den Blaauwen, T. Colocalization and Interaction between Elongasome and Divisome during a Preparative Cell Division Phase in *Escherichia Coli*. *Molecular Microbiology* **2013**, *87* (5), 1074–1087. https://doi.org/10.1111/mmi.12150.

(54)   Daniel, R. A.; Harry, E. J.; Errington, J. Role of Penicillin-Binding Protein PBP 2B in Assembly and Functioning of the Division Machinery of Bacillus Subtilis. *Molecular Microbiology* **2000**, *35* (2), 299–311. https://doi.org/10.1046/j.1365-2958.2000.01724.x.

(55)   Strahl, H.; Hamoen, L. W. Membrane Potential Is Important for Bacterial Cell Division. *Proceedings of the National Academy of Sciences of the United States of America* **2010**, *107* (27), 12281–12286. https://doi.org/10.1073/pnas.1005485107

Chapter 4
Current Progress and Future Directions Towards the Total Syntheses of Chrysophaentin A and Chrysophaentin F

4.1 Introduction

Upon the completion of our 9-dechlorochrysophaentins, attention was directed towards the completion of the first total synthesis of chrysophaentin A (**4.1**). In order to accomplish the total synthesis, an approach enabling the incorporation of the C9 chloride would need to be developed. The most direct strategy would be to achieve a *Z*-selective RCM reaction with an RCM substrate incorporating a C9 chloro group. While we were cognizant of the difficulty of achieving such an RCM reaction, screening of catalysts was justified given the directness of such a route. To this end, we aimed to prepare RCM substrate **4.3** in order to achieve ring-closing metathesis to afford expanded macrocycle **4.2,** with the *E*-alkene geometry. Macrocycle **4.2** is only a few steps away from chrysophaentin A (**4.1**) (Figure 4.1). The synthesis of ether **4.2** would utilize the same
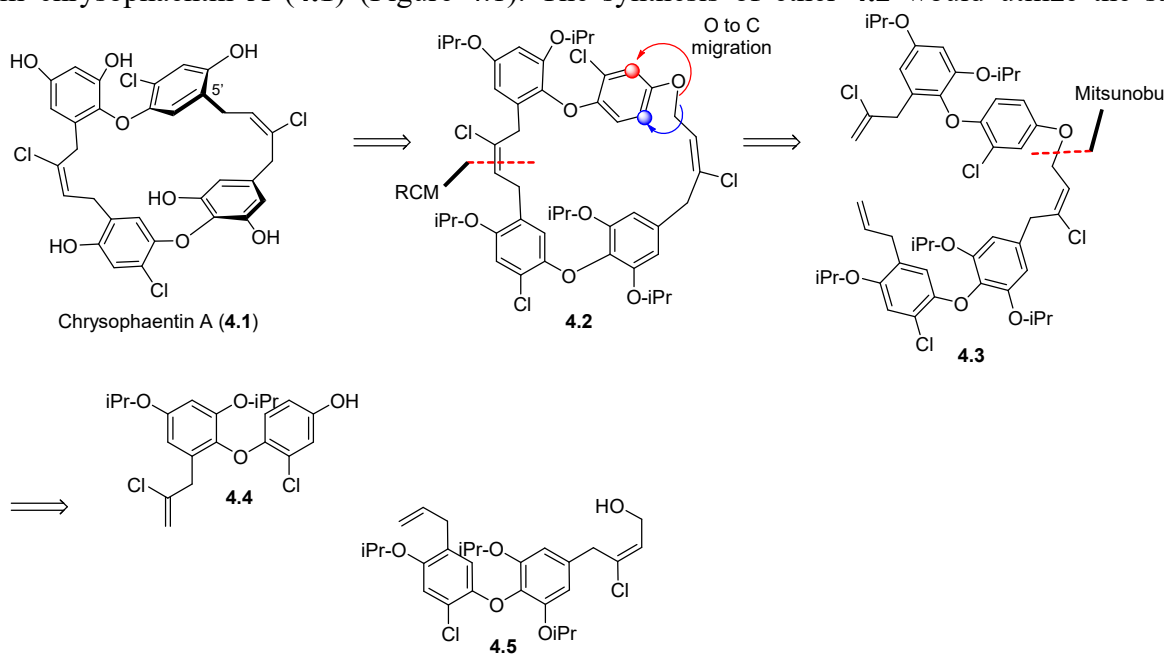
Figure 4.1. Retrosynthetic analysis of chrysophaentin A (**4.1**).

129

synthetic route used for the synthesis of **VU0849855** and **VU0849838**, with modification of the Northern BC fragment to include the C9-chloride.

4.2 Synthesis of C9-Chloro Ring-closing Metathesis Substrate

The C9-chloride BC fragment **4.4** was synthesized in ten steps utilizing the same synthetic route for our previous BC fragment with two slight modifications, allylation with 2,3-dichloropropene and acetylation of phenol **4.13** to facilitate the diatization-Sandmeyer reaction (Figure 4.2).
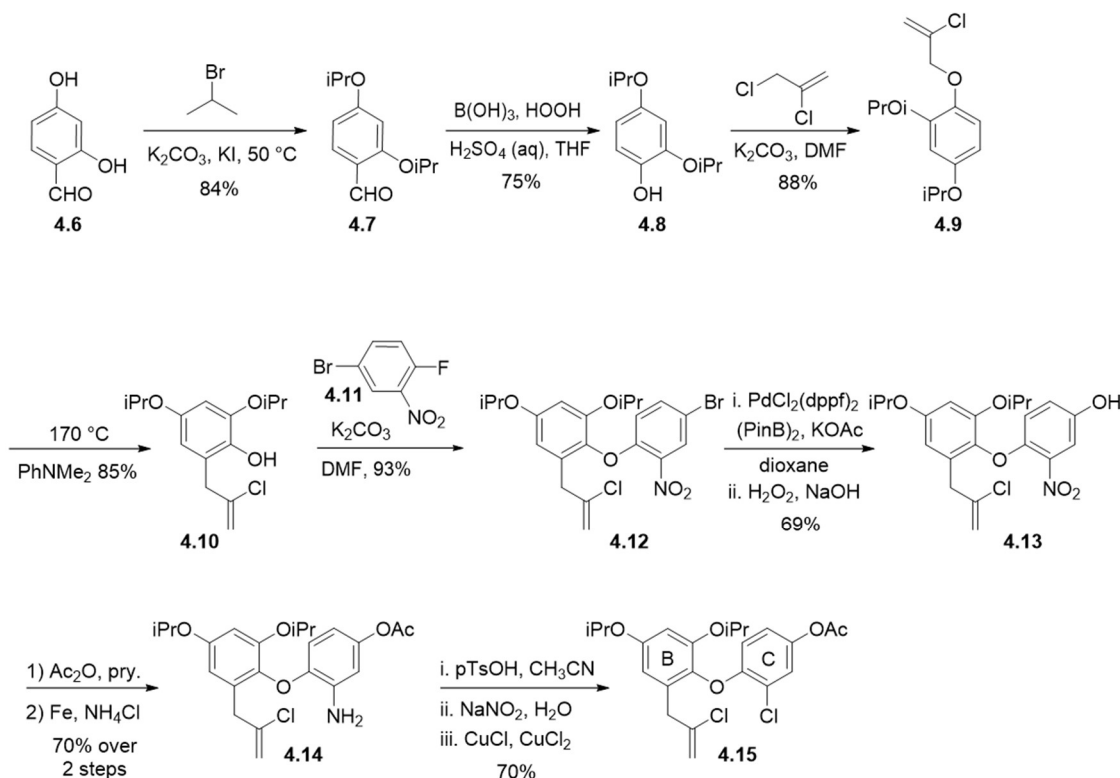
Figure 4.2. Synthesis of C9-chloro BC fragment.

The substitution of 2,3-dichloropropene allowed for the incorporation of the C9-chloride by way of a Claisen rearrangement to afford phenol **4.10**. Phenol **4.10** was treated under standard

S$_N$Ar conditions to afford biaryl ether **4.12**. Suzuki-Miyaura coupling followed by oxidation afforded phenol **4.13**, which was subsequently protected as the acetate. The acetate group was necessary to increase the yields for the diatization-Sandmeyer reaction. Following reduction of the nitro moiety to the aniline **4.14** and treatment under diatization-Sandmeyer conditions afforded acetate protected C9-chloro BC fragment **4.15** in 70% yield.

Upon completion of the C9-chloro-BC fragment **4.4**, attention was turned towards the merger of AD fragment **4.5** and BC fragment **4.4**. The Northern BC fragment was deprotected and merged with Southern AD fragment **4.5** under standard Mitsunobu conditions to afford alkyl ether **4.3** in 65% yield. We anticipated a screen of ring-closing metathesis catalysts would afford macrocycle **4.2.** Treatment of **4.2** under O to C migration conditions followed by deprotection would afford chrysophaentin A (**4.1**) (Figure 4.3).
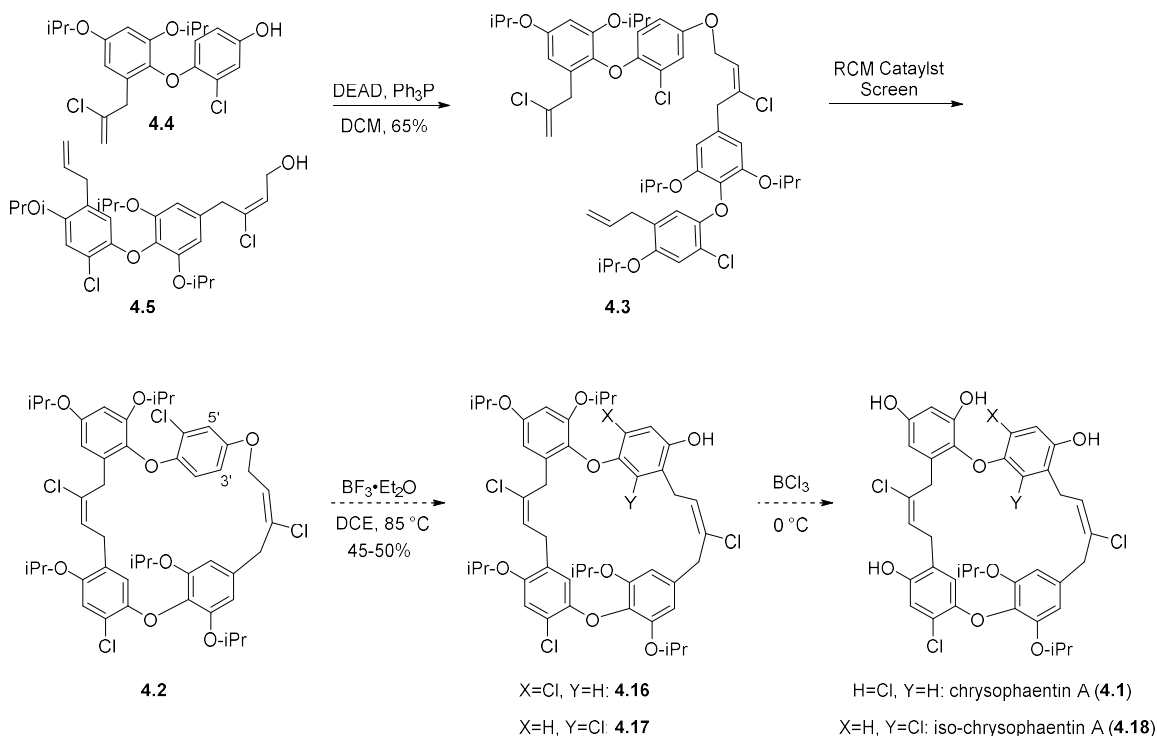
Figure 4.3. Synthesis of C9-chloro RCM substrate.

In collaboration with the Grubbs group at Caltech, a small library of Z-selective[1–3] and stereoretentive catalyst[4–7] were screened against **4.3** in an attempt to invoke the proposed ring-closing metathesis. The initial screen with Z-selective catalyst: **4.19** and **4.20** did not afford macrocycle **4.2**. Therefore, catalyst **4.21,** which initiates the reaction at a faster rate was tried, however, macrocycle formation was still not observed (Figure 4.4).
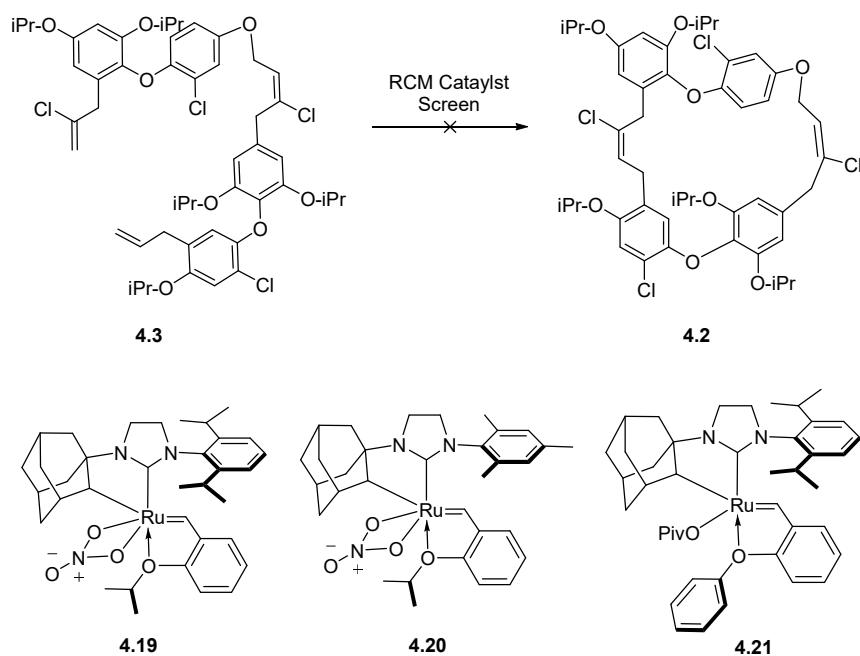
Figure 4.4. Z-selective RCM catalyst screen.

In addition, they attempted to utilize a stereoretentive approach to access expanded macrocycle **4.2.** Catalyst **4.22** was reacted with **4.3** in the presence of 3-hexene to selectively form Z-hexene intermediate **4.25.** The Z-intermediate **4.25** was subsequently treated with catalyst **4.23** or **4.24.** These catalysts have been demonstrated to invoke ring-closing metathesis and cross-metathesis reactions with retention of the substrate alkene geometry.[4–7] However, the treatment of **4.25** with either catalyst did afford any of the desired product (Figure 4.5). Based on these results

we concluded that a ring-closing metathesis with the C9-chloride is not feasible and therefore a new substrate containing a C9-functional group that is compatible with ring-closing metathesis reactions and can be converted to the C9-chloride was necessary.
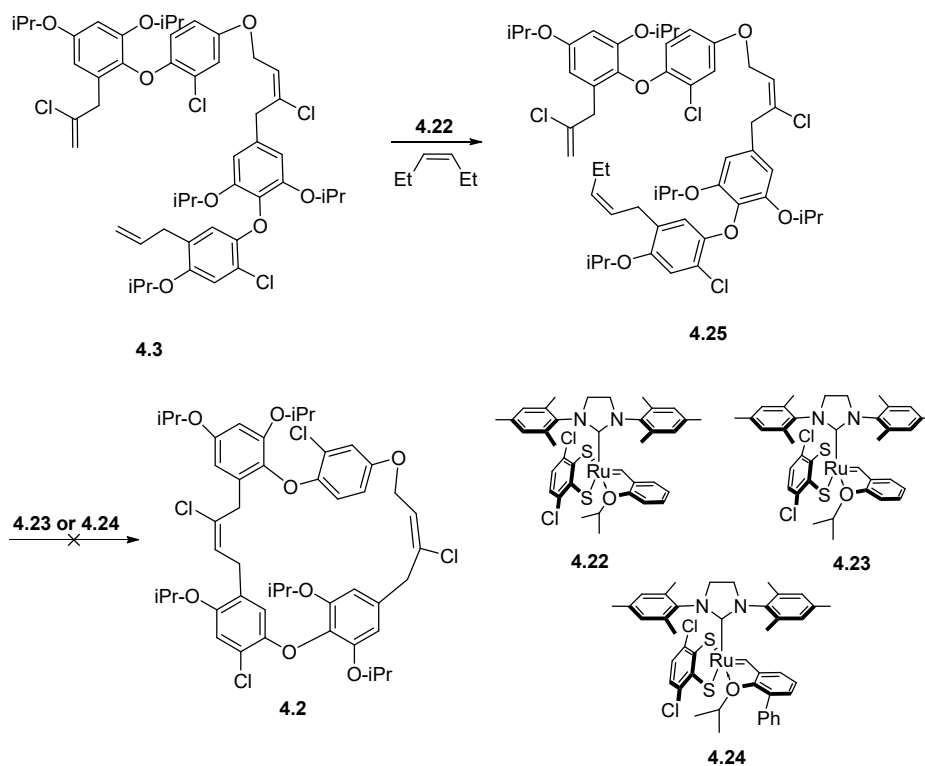
Figure 4.5. Stereoretentive RCM approach.

4.3 Vinyl Metal RCM: Progress Towards the Total Synthesis of Chrysophaentin A (4.1) and Chrysophaentin F (4.40)

Based on the difficultly of the ring-closing metathesis with the C9-chloride installed, we proposed to synthesize new RCM substrates with different vinyl metals which could be converted to the chloride following ring-closing metathesis. Vinyl silanes,[8] siloxanes,[9,10,] and boranes[7,11]

have been shown to be compatible with ring-closing metathesis reactions and Schreiber and co-workers have shown siloxanes selectively form the *syn*-relationship between the two alkyl groups.[9,10] We anticipated after Mitsunobu coupling of AD Fragment **4.5** with alkynyl BC fragment **4.28,** that the intermediate alkynyl ether could be hydrometallated (Figure 4.6, highlighted in green) to afford ring-closing metathesis substrate **4.26.** Following ring-closing metathesis of **4.26** (Figure 4.6, highlighted in blue) the intermediate alkenyl metal could undergo metal-chloride exchange to afford the C9-chloride expanded macrocycle **4.2** (Figure 4.6, highlighted in pink), which is two steps from chrysophaentin A (**4.1).**
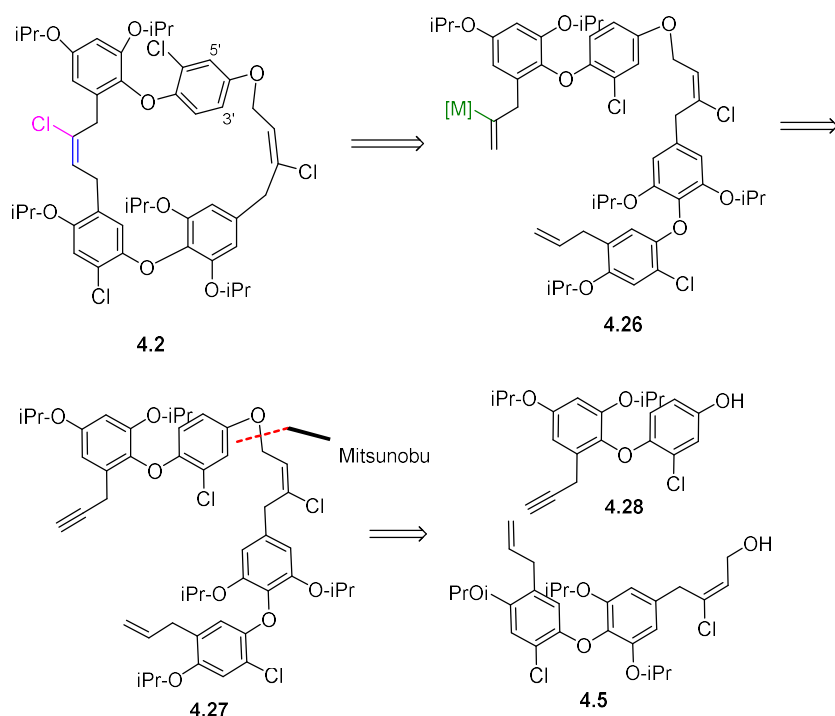
Figure 4.6. Vinyl Metal RCM retrosynthetic analysis.

We anticipated that alkyne **4.28** could arise from the derivatization of the allyl group of our current BC fragment **4.29** (Figure 4.7, panel A). Derivatization of BC fragment **4.29** proved quite difficult and attempts at functionalization resulted in, complete decomposition, of the **4.29.**

Therefore, we proposed to synthesized phenol **4.30**, which could then be used in our established BC fragment synthetic route to access alkynyl BC fragment **4.28** (Figure 4.7, panel B).

A. Derivitization of BC fragment **4.29** to alkynyl BC fragment **4.28.**
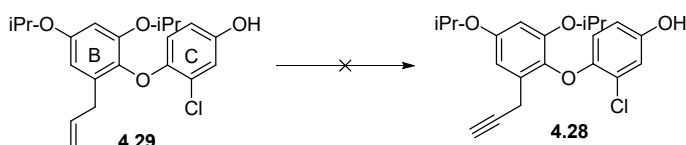
B. Retrosynthetic analysis of alkynyl BC fragment **4.28.**
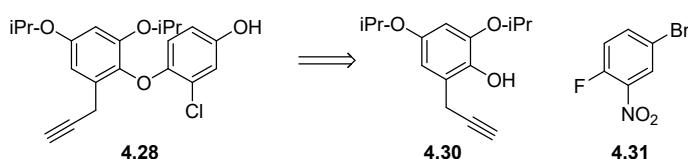
C. Synthesis of alkynyl BC fragment **4.28.**
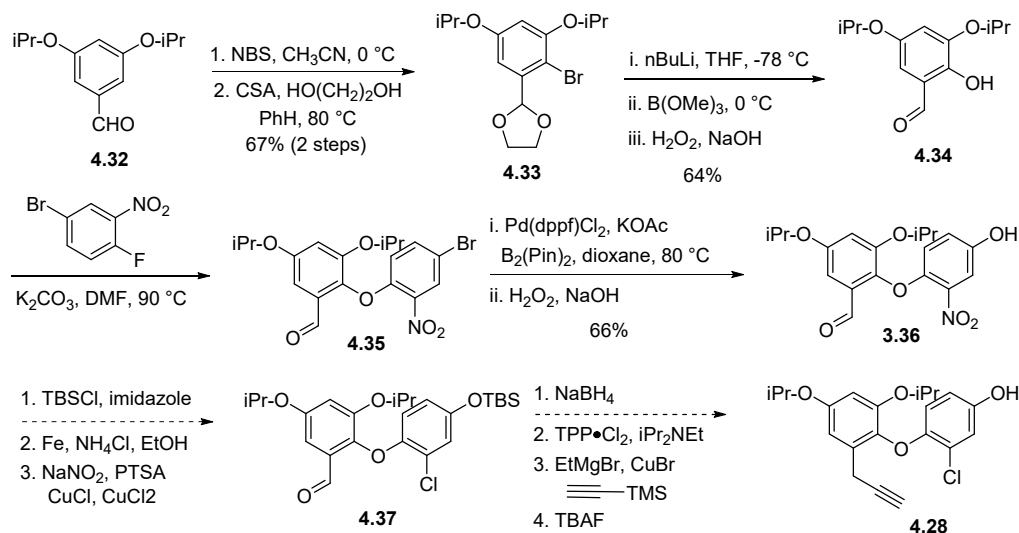
Figure 4.7. Analysis and synthesis of alkynyl BC fragment **4.34.**

Starting with 3,5-dihydroxybenzaldehye (**4.37**), peralkylation with isopropyl bromide followed by bromination with NBS, and acetal formation afforded bromide **4.33** in 60% over three steps (Figure 4.7, panel C). The latter underwent lithium-halogen exchange followed borylation

and oxidation to afford phenol **4.34.** The acetal group was deprotected upon neutralization of the oxidation step and could not be reinstalled. However, aldehyde **4.34** was treated under standard S_NAr conditions with bromide **4.31** to afford biaryl **4.35.** The latter underwent Suzuki-Miyaura coupling and oxidation to afford phenol **4.36** in 66% yield**.**

To complete the synthesis of alkynyl-BC fragment **4.28,** phenol **4.41** will need to be protected, followed by reduction of the nitro moiety and diatization-Sandmeyer to afford chloride **4.37.** Chloride **4.37** we anticipate can be converted to the alkyne by way of reduction to the corresponding benzylic alcohol, which upon treatment with TPP·Cl$_2$ would afford an intermediate benzylic chloride. The latter generated chloride can be displaced with Ethynyltrimethylsilane to afford alkynyl BC fragment **4.28**, after deprotection (Figure 4.6, panel C).

Upon completion of **4.28**, merger under Mitsunobu conditions with **4.5** would afford alkyl ether **4.27**. Treatment of alkyne **4.27** with Trost's ruthenium catalyst[10] and triethoxysilane would afford **4.38**. Treatment of **4.38** with Grubbs second-generation or Hoveyda-Grubbs catalyst C571[10] would afford expanded macrocycle **4.36,** as the *E*-siloxane exclusively. Following treatment of **4.36** with NCS or CuCl$_2$ would afford expanded macrocycle **4.2.** Treatment of **4.2** with Lewis acidic conditions to invoke an O to C migration and deprotection with BCl$_3$ would complete the first total synthesis of chrysophaentin A (**4.1**) and iso-chrysophaentin A (**4.37**) (Figure 4.8).

Also, if the silylation or ring-closing metathesis of **4.38** is unsuccessful, alkyne **4.27** can be functionalized as the α-boronate based on work by Prabhu[12] and Hoveyda[13] to afford **4.39.** Treatment of **4.39** with Grubbs' ruthenium or Hoveyda's molybdenum metathesis catalysts [5,11] would result in expanded macrocycle **4.2**, after treatment with CuCl$_2$.[14] This reaction sequence would provide an alternative to the above outline alkenyl siloxane approach to give access to chrysophaentin A (**4.1**) (Figure 4.8).
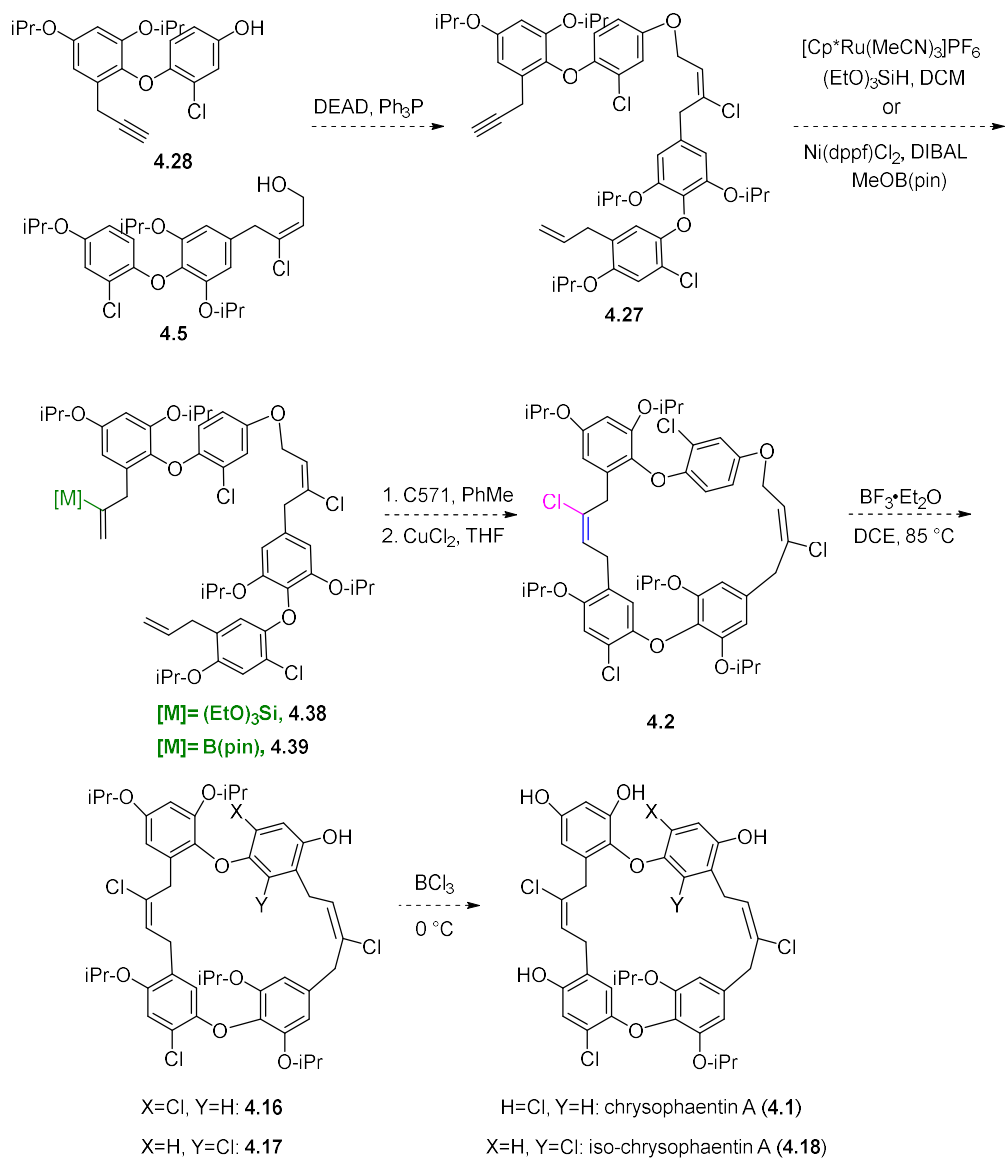
Figure 4.8. Proposed synthesis of Chrysophaentin A **(4.1)**.

4.4 Progress Towards the Total Synthesis of Chrysophaentin F (4.40)

In addition to chrysophaentin A (**4.1**), the proposed alkyne hydrometallation-ring closing metathesis reaction sequence outlined above can be adapted for the total synthesis of chrysophaentin F (**4.40**) (Figure 4.9). Fortuitously, minor modification of our established AD fragment **4.5** would provide alkyne **4.43.** Merger of **4.43** with AD fragment **4.5** followed by hydrometallation would afford C9-siloxane **4.42.** Treatment with **4.42** under ring-closing metathesis conditions would afford expanded macrocycle **4.41.** Siloxane-chloride exchange with CuCl2, followed by rearrangement under Lewis acidic conditions and deprotection would afford chrysophaentin F (**4.40**) (Figure 4.9).
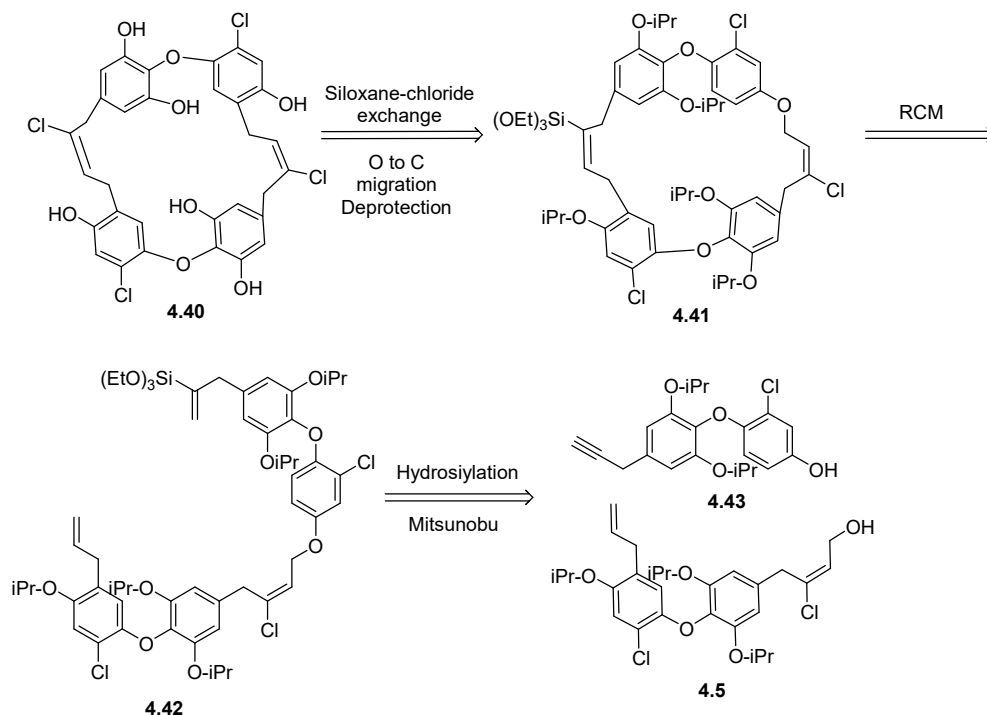
Figure 4.9. Retrosynthetic analysis of chrysophaentin F (**4.40**).

Starting with phenol **4.44,** an intermediate along the synthetic pathway of AD fragment **4.5**, protection as the TBS-ether and reduction of the ester and subsequent conversion of the intermediate benzylic alcohol with TPP·Cl$_2$ afforded benzylic chloride **4.45** in 62% yield over the three steps (Figure 4.10). Benzylic chloride **4.45** was homologated with Ethynyltrimethylsilane, followed by deprotection to afford alkynyl AD fragment **4.43.** Merger of the AD fragment **4.5** and alkynyl AD fragment **4.43** afforded **4.46** in 86% yield. The latter was functionalized with Trost's ruthenium catalyst[15] with triethoxysilane to afford C9-siloxane **4.42.**
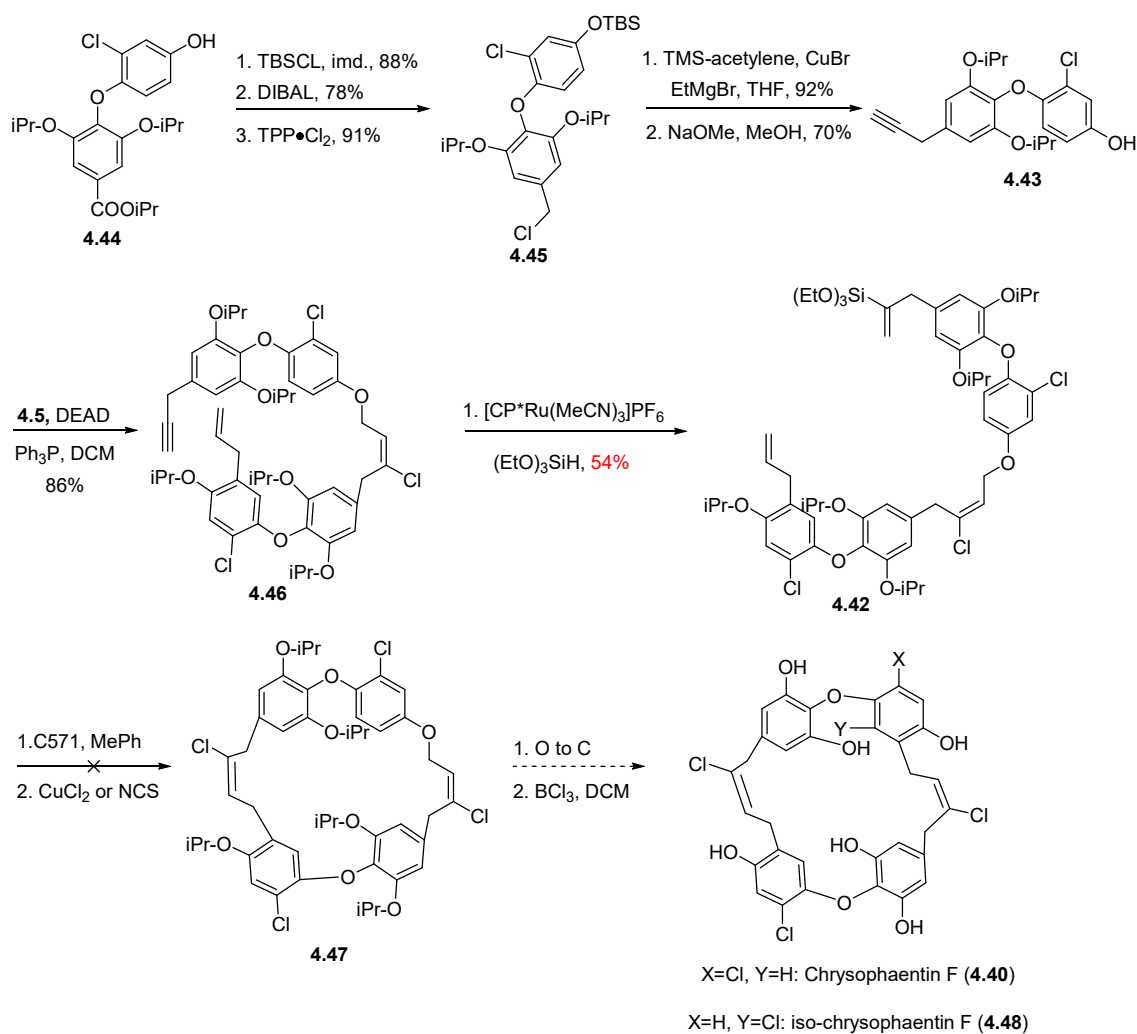
Figure 4.10. Synthesis of Chrysophaentin F **(4.40).**

139

Unfortunately, the treatment of **4.42** with Hoveyda-Grubbs catalyst C571, did not yield any macrocyclic product. Further attempts to achieve the ring-closing metathesis of C9-siloxane and functionalization of alkyne **4.46** as the C9-alkenylboronate has not been attempted. In conclusion, we have developed a route to potentially access chrysophaentin A (**4.1**) and chrysophaentin F (**4.40**) via alkyne hydrometallation-ring closing metathesis-chlorination sequence. In order to complete the first total synthesis of chrysophaentin A (**4.1**) and chrysophaentin F (**4.40**), optimization of ring-closing metathesis conditions and hydrometallation of alkynes **4.28** and **4.43** are needed.

4.5 Conclusion

The future for the chrysophaentins is promising. We have completed the synthesis of four 9-dechlorochrysophaentin analogs which display a novel mechanism of cell wall synthesis inhibition, designed an improved synthesis of hemi-chrysophaentin, and are currently only a few steps away from the completion of the first total syntheses of chrysophaentin A (**4.1**) and chrysophaentin F (**4.40**). Currently, our lab proposes to scale up the synthesis of 9-dechlorochrysophaentins **VU0849855** and **VU0849838** to investigate the novel mechanism of cell wall synthesis inhibition and determine the efficacy of our synthetic congeners in *vivo*.

This work will set up future investigations studying the rotational barrier and the effect it has on the chrysophaentins antimicrobial activity. Furthermore, SAR studies around the chrysophaentin core will be initiated. The work outlined in this thesis highlights the complexity of the total synthesis of the chrysophaentins presents, and highlights our work towards the most advanced chrysophaentin derivative to date. Furthermore, this work reinforces the importance of

studying natural products as new antimicrobials due to the fortuitous discovery of a novel mechanism of cell wall synthesis inhibition. The chrysophaentins are a promising new antimicrobial natural product that will aid in our study and understanding of cell wall synthesis and its link with cell growth and division. The work on **VU0849855** and **VU0849838** is currently being written up and will be published in due course. The investigation into **VU0848355**'s rotational barrier is still in progress and hopefully, the synthesis of novel sterically encumbering analogs will allow for the separation and evaluation of potential non-canonical atropisomers antimicrobial activity. Overall, this project has generated the most advanced chrysophaentin congeners to date and discovered their unique and novel mechanism of action as cell wall synthesis inhibitors.

References:

(1)   Herbert, M. B.; Grubbs, R. H. Z-Selective Cross Metathesis with Ruthenium Catalysts: Synthetic Applications and Mechanistic Implications. *Angewandte Chemie - International Edition*. Wiley-VCH Verlag April 20, 2015, pp 5018–5024. https://doi.org/10.1002/anie.201411588.

(2)   Keitz, B. K.; Endo, K.; Patel, P. R.; Herbert, M. B.; Grubbs, R. H. Improved Ruthenium Catalysts for Z-Selective Olefin Metathesis. *Journal of the American Chemical Society* **2012**, *134* (1), 693–699. https://doi.org/10.1021/ja210225e.

(3)   Marx, V. M.; Herbert, M. B.; Keitz, B. K.; Grubbs, R. H. Stereoselective Access to Z and e Macrocycles by Ruthenium-Catalyzed Z-Selective Ring-Closing Metathesis and

Ethenolysis. *Journal of the American Chemical Society* **2013**, *135* (1), 94–97. https://doi.org/10.1021/ja311241q.

(4)   Ahmed, T. S.; Grubbs, R. H. A Highly Efficient Synthesis of Z-Macrocycles Using Stereoretentive, Ruthenium-Based Metathesis Catalysts. *Angewandte Chemie - International Edition* **2017**, *56* (37), 11213–11216. https://doi.org/10.1002/anie.201704670.

(5)   Montgomery, T. P.; Johns, A. M.; Grubbs, R. H. Recent Advancements in Stereoselective Olefin Metathesis Using Ruthenium Catalysts. *Catalysts* **2017**, *7* (12), 87. https://doi.org/10.3390/catal7030087.

(6)   M. Johns, A.; S. Ahmed, T.; W. Jackson, B.; H. Grubbs, R.; L. Pederson, R. High Trans Kinetic Selectivity in Ruthenium-Based Olefin Cross-Metathesis through Stereoretention. *Organic Letters* **2016**, *18* (4), 772–775. https://doi.org/10.1021/acs.orglett.6b00031.

(7)   Müller, D. S.; Baslé, O.; Mauduit, M. A Tutorial Review of Stereoretentive Olefin Metathesis Based on Ruthenium Dithiolate Catalysts. *Beilstein Journal of Organic Chemistry*. Beilstein-Institut Zur Forderung der Chemischen Wissenschaften December 7, 2018, pp 2999–3010. https://doi.org/10.3762/bjoc.14.279.

(8)   Pietraszuk, C.; Marciniec, B.; Fischer, H. Cross-Metathesis of Vinylsilanes with Styrene Catalyzed by Ruthenium−Carbene Complexes. *Organometallics* **2000**, *19* (5), 913–917. https://doi.org/10.1021/om9909901.

(9)   Wang, Y.; Jimenez, M.; Sheehan, P.; Zhong, C.; Hung, A. W.; Tam, C. P.; Young, D. W. Selective Access to Trisubstituted Macrocyclic e - And Z-Alkenes from the Ring-Closing Metathesis of Vinylsiloxanes. *Organic Letters* **2013**, *15* (6), 1218–1221. https://doi.org/10.1021/ol400134d.

(10)   Wang, Y.; Jimenez, M.; Hansen, A. S.; Raiber, E. A.; Schreiber, S. L.; Young, D. W. Control of Olefin Geometry in Macrocyclic Ring-Closing Metathesis Using a Removable Silyl Group. *Journal of the American Chemical Society* **2011**, *133* (24), 9196–9199. https://doi.org/10.1021/ja202012s.

(11)   Renaud, J.; G. Ouellet, S. Novel Synthesis of Cyclic Alkenylboronates via Ring-Closing Metathesis. *Journal of the American Chemical Society* **1998**, *120* (31), 7995–7996. https://doi.org/10.1021/ja980958i.

(12)   Ojha, D. P.; Prabhu, K. R. Pd-Catalyzed Hydroborylation of Alkynes: A Ligand Controlled Regioselectivity Switch for the Synthesis of α- Or β-Vinylboronates. *Organic Letters* **2016**, *18* (3), 432–435. https://doi.org/10.1021/acs.orglett.5b03416.

(13)   Gao, F.; Hoveyda, A. H. α-Selective Ni-Catalyzed Hydroalumination of Aryl- and Alkyl-Substituted Terminal Alkynes: Practical Syntheses of Internal Vinyl Aluminums, Halides, or Boronates. *Journal of the American Chemical Society* **2010**, *132* (32), 10961–10963. https://doi.org/10.1021/ja104896b.

(14)   Le, H.; Kyne, R. E.; Brozek, L. A.; Morken, J. P. Catalytic Enantioselective Allyl-Allyl Cross-Coupling with a Borylated Allylboronate. *Organic Letters* **2013**, *15* (7), 1432–1435. https://doi.org/10.1021/ol400088g.

(15)   Trost, B. M.; Ball, Z. T. Markovnikov Alkyne Hydrosilylation Catalyzed by Ruthenium Complexes. *Journal of the American Chemical Society*. American Chemical Society December 19, 2001, pp 12726–12727. https://doi.org/10.1021/ja0121033.

Appendix:

A1. General Procedure: All non-aqueous reactions were performed in flame-dried or oven-dried round-bottomed flasks under an atmosphere of argon. Stainless steel syringes or cannula were used to transfer air- and moisture-sensitive liquids. Reaction temperatures were controlled using a thermocouple thermometer and analog hotplate stirrer and monitored using liquid-in-glass thermometers. Reactions were conducted at room temperature (approximately 21-23 °C) unless otherwise noted. Flash column chromatography was conducted using silica gel 230-400 mesh. Reactions were monitored by analytical thin-layer chromatography, using EMD Silica Gel 60 F254 glass-backed pre-coated silica gel plates. The plates were visualized with UV light (254 nm) and stained with potassium permanganate or *p*- anisaldehyde-sulfuric acid followed by charring. Yields were reported as isolated, spectroscopically pure compounds.

A2. Materials: Solvents and chemicals were purchased from Sigma-Aldrich, Acros Organics, TCI and/or Alfa Aesar and used without further purification. Solvents were purchased from Fisher Scientific. Dry dichloromethane (CH_2Cl_2) was collected from an MBraun MB-SPS solvent system. Dichloroethane (DCE) was distilled from calcium hydride and stored over 4 Å molecular sieves. Triethylamine, N,N-dimethylformamide (DMF), and dimethyl sulfoxide (DMSO) were used as received in a bottle with a Sure/Seal. N,N-diisopropylethylamine was distilled from calcium hydride and stored over KOH. $BF_3 \cdot Et_2O$ was distilled prior to use from calcium hydride. Deuterated solvents were purchased from Cambridge Isotope Laboratories.

A3. Instrumentation: Preparative reverse phase HPLC (Gilson) was performed using a Phenomenex Gemini column (5 microns, 110 Å, 50 x 21.20 mm, flow rate 30 mL/min) with UV/Vis detection. Infrared spectra were obtained as thin films on NaCl plates using a Thermo Electron IR100 series instrument and are reported in terms of frequency of absorbance (cm^{-1}). ^1H NMR spectra were recorded on Bruker 400 or 600 MHz spectrometers and are reported relative to internal chloroform (^1H, δ 7.26), methanol (^1H, δ 3.31), and DMSO (^1H, δ 2.50). Data for ^1H NMR spectra are reported as follows: chemical shift (δ ppm), multiplicity (s = singlet, d = doublet, t = triplet, dd = doublet of doublet, ddd = doublet of doublet of doublet, m = multiplet, br=broad), coupling constants (Hz), and integration. ^{13}C NMR was recorded on Bruker 100 or 150 MHz spectrometers and are reported relative to internal chloroform (^{13}C, δ 77.1), methanol (^{13}C, δ 49.2), and DMSO (^{13}C, δ 40.3). Low-resolution mass spectra were acquired on an Agilent Technologies Series 1200 single quad ChemStation autosampler system using electrospray ionization (ESI) in positive mode. High-resolution mass spectra (HRMS) were obtained from the Department of Chemistry and Biochemistry, University of Notre Dame Mass Spectrometry Center, or the Mass Spectrometry Research Center at Vanderbilt University.

A4. Compound Preparation:
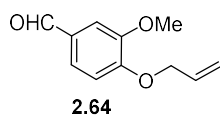
2.64 To a solution of vanillin (2.50 g, 16.43 mmol) in DMF (32 mL) was added K$_2$CO$_3$ (5.67 g, 41.07 mmol, 2.5 equiv) and allyl bromide (2.84 mL, 32.5 mmol, 2 equiv). The reaction mixture was maintained at room temperature for 18 h, before dilution with water (150 mL). The reaction mixture was extracted with ethyl acetate (3 x 50 mL), washed with water (2 x 100 mL) and brine (150 mL), dried (MgSO$_4$), filtered and concentrated *in vacuo*. The crude residue was purified by flash column chromatography (gradient 0 to 15% EtOAc in hexanes) to afford 2.93 g (93%) of **2.64** as a yellow oil: ^{1}H NMR (400 MHz, CDCl$_3$) δ 9.46 (s, 1H), 7.02 (dd, J = 9.9 Hz, 1.8 Hz, 1H), 6.58 (d, J = 8.3 Hz, 1H), 5.77-5.67 (m, 1H), 5.09 (dd, J = 17 Hz, 1.5 Hz, 1H), 4.95 (dd, J = 10 Hz, 1.3 Hz, 1H), 4.27 (d, J = 6.0 Hz, 2H), 3.51 (s, 3H); ^{13}C NMR (100 MHz, CDCl$_3$) δ 189.7, 152.6, 149.0, 131.7, 129.4, 125.4, 117.5, 117.4, 111.2, 108.6, 68.7, 54.9.
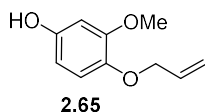
2.65 To a suspension of boric acid (9.19 g, 148 mmol, 5 equiv) in THF (50 mL) was added sulfuric acid (4.28 mL, 2.7 equiv) and H$_2$O$_2$ (10 mL, 30% w/v, 3.2 equiv). The suspension was maintained at room temperature for 30 min before the addition of **2.64** (5.72 g, 29.7 mmol) as a solution in THF (35 mL). The suspension was maintained at room temperature for 5 h, before cooling to 0 °C. The cooled solution was neutralized with saturated aq NaHCO$_3$ (~ 100 mL) and extracted with EtOAc (3 x 100 mL). The extracts were washed with water (100 mL) and brine (100 mL), dried (MgSO$_4$), filtered and concentrated *in vacuo*. The crude residue was purified by flash column chromatography (silica gel, gradient, 0 to 40% EtOAc in hexanes) to afford 3.35 g (61%) of **2.65** as a white solid: ^{1}H NMR (400 MHz, CDCl$_3$) δ 6.74 (d, J = 8.6 Hz, 1H), 6.46 (d, J = 2.8 Hz, 1H), 6.32 (dd, J = 8.6 Hz, 2.8 Hz, 1H), 6.09-5.99 (m, 1H), 5.34 (dd, J = 17 Hz, 1.5 Hz, 1H), 5.22 (dd, J = 10 Hz, 1.4 Hz, 1H), 4.50 (d, J = 5.6 Hz, 2H), 3.75 (s, 3H); ^{13}C NMR (100 MHz, CDCl$_3$) δ 150.9, 150.6, 141.7, 133.7, 117.9, 115.7, 106.2, 100.9, 71.2, 55.8.
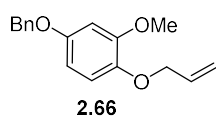
2.66 To a solution of **2.65** (2.03 g, 11.3 mmol) in DMF (23 mL) was added K$_2$CO$_3$ (4.67 g, 33.8 mmol, 3 equiv) and benzyl bromide (2.7 mL, 22.5 mmol, 2 equiv). The reaction mixture was maintained at room temperature for 18 h, before dilution with water (100 mL) and extraction with EtOAc (3 x 30 mL). The extracts were washed with water (2 x 100 mL) and brine (100 mL), dried (MgSO$_4$), filtered and concentrated *in vacuo*. The crude residue was purified by flash column chromatography (silica gel, gradient 0 to 30% EtOAc in hexanes) to afford 2.17 g (71%) of **2.66** as a white solid: ^{1}H NMR (400 MHz, CDCl$_3$) δ 7.45 (d, *J* = 7.2 Hz, 2H), 7.40 (t, *J* = 7.1 Hz, 2H), 7.34 (d, *J* = 7.1 Hz, 1H), 6.82 (d, *J* = 8.7 Hz, 1H), 6.62 (d, *J* = 2.7 Hz, 1H), 6.45 (dd, *J* = 8.7 Hz, 2.8 Hz, 1H), 6.14-6.05 (m, 1H), 5.40 (dd, *J* = 17 Hz, 1.5 Hz, 1H), 5.28 (dd, *J* = 10 Hz, 1.3 Hz, 1H), 5.0 (s, 2H), 4.56 (d, *J* = 5.5 Hz, 2h), 3.85 (s, 3H); ^{13}C NMR (100 MHz, CDCl$_3$) δ 153.9, 150.6, 142.5, 137.2, 133.8, 128.6, 128.0, 127.6, 117.8, 114.8, 104.2, 101.4, 70.9, 70.6, 55.9.
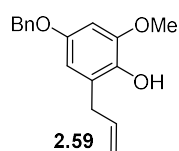
2.59 A solution of **2.66** (1.60 g, 5.92 mmol) in N,N-diethylanline (15 mL) was added to a sealed µW vial and irradiated at 190 °C for 5 h and 30 min. The reaction mixture was diluted with diethyl ether (30 mL) and washed with 1 N HCl (3 x 30 mL), water (20 mL) and brine (20 mL). The washed extracts were dried (MgSO$_4$), filtered and concentrated *in vacuo*. The crude residue was purified by flash column chromatography (silica gel, gradient 0 to 8% EtOAc in hexanes) to afford 1.28 g (80%) of **2.59** as a white solid: ^{1}H NMR (400 MHz, CDCl$_3$) δ 7.48 (d, *J* = 7.1 Hz, 2H), 7.42 (t, *J* = 7.4 Hz, 2H), 7.37 (d, *J* = 7.0 Hz, 1H), 6.51 (d, *J* = 3.3 Hz, 1H), 6.45 (d, *J* = 3.3 Hz, 1H), 6.10-6.00 (m, 1H), 5.41 (s, 1H, exchanges with D$_2$O), 5.17-5.11 (m, 2H), 5.03 (s, 2H), 3.86 (s, 3H), 3.45 (d, *J* = 7.0 Hz, 2H); ^{13}C NMR (100 MHz, CDCl$_3$) δ 152.1, 146.9, 137.7, 137.3, 136.5, 128.7, 127.9, 127.6, 125.7, 115.6, 106.8, 98.2, 70.7, 56.0, 34.1.
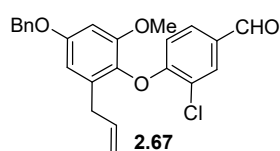
2.67 To a solution of **2.59** (1.52 g, 5.62 mmol) in acetonitrile (18 mL) was added Cs$_2$CO$_3$ (3.7 g, 11.2 mmol, 2 equiv) and 3-chloro-4-fluorobenzaldehyde (1.34 g, 8.43 mmol, 1.5 equiv). The reaction mixture was maintained at room temperature for 18 h, before dilution with water (75 mL). The diluted

solution was extracted with EtOAc (3 x 35 mL), washed with water (100 mL) and brine (100 mL), dried (MgSO$_4$), filtered and concentrated *in vacuo*. The crude residue was purified by flash column chromatography (silica gel, gradient 0 to 10 % EtOAc in hexanes) to afford 1.5 g (65%) of **2.67** as an off-white solid: ^{1}H NMR (400 MHz, CDCl$_3$) δ 9.85 (s, 1H), 7.96 (d, J = 1.9 Hz, 1H), 7.60 (dd, J = 8.5 Hz, 2.0 Hz, 1H), 7.47 (d, J = 7.15 Hz, 2H), 7.42 (t, J = 7.7 Hz, 2H), 7.37 (d, J = 7.15 Hz, 1 H), 6.63 (d, J = 8.4 Hz, 1H), 6.56 (d, J = 2.9 Hz, 1H), 6.52 (d, J = 2.9 Hz, 1H), 5.86-5.78 (m, 1H), 5.07 (s, 2H), 5.05-4.98 (m, 2H), 3.72 (s, 3H), 3.27 (d, J = 6.7 Hz, 2H); 189.7, 159.0, 157.3, 152.6, 136.7, 135.5, 134.6, 134.2, 131.8, 131.1, 129.7, 128.7, 128.2, 127.7, 123.2, 116.8, 114.5, 106.6, 99.4, 70.5, 56.0, 34.4.
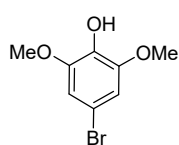
2.62 To a -40 °C solution of 2,6-dimethoxyphenol (5.00 g 32.4 mmol) in chloroform (45 mL) was added a solution of NaH (8.00 mg, 1 mol %) dissolved in MeOH (400 µL). The reaction mixture was allowed to stir for ten minutes before cooling to -78 °C. NBS (6.12 g, 34.3 mmol, 1.06 equiv) was added portion-wise (4 portions) over 20 min at -78 °C and the reaction was maintained at -78 °C for 5 h. The reaction was quenched by the addition of saturated aq NaHCO$_3$ (100 mL), extracted with EtOAc (3 x 50 mL), washed with saturated aq NaHCO$_3$ (2 x 100 mL) and brine (100 mL), dried (MgSO$_4$), filtered and concentrated *in vacuo*. The crude residue was purified by flash column chromatography (silica gel, gradient 0 to 30% EtOAc in hexanes) to afford 5.77 g (76%) of **2.62** as a white solid: ^{1}H NMR (400 MHz, CDCl$_3$) δ 6.72 (s, 2 H), 5.44 (s, 1H, exchanges with D$_2$O), 3.88 (s, 6H); ^{13}C NMR (100 MHz, CDCl$_3$) δ 147.7, 134.1, 111.1, 108.6, 56.5.
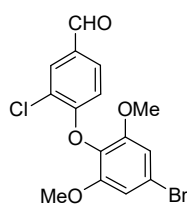
2.68 To a solution of **2.62** (1.86 g, 8.02 mmol) in CH$_3$CN (40 mL) was added Cs$_2$CO$_3$ (3.66 g, 11.23 mmol, 1.4 equiv) followed by 3-chloro-4-fluorobenzaldehyde (1.53 g, 9.62 mmol, 1.2 equiv). The reaction mixture was maintained at room temperature for 24 h, then diluted with water (100 mL). The crude reaction was extracted with EtOAc (3 x 50 mL), washed with water (100 mL) and brine (100 mL), dried (MgSO$_4$), filtered and concentrated *in vacuo*. The crude residue was purified by flash column chromatography (silica gel, gradient 0 to 20% EtOAc in hexanes) to afford 2.08 g (70%) of **2.68** as a yellow solid: ^{1}H NMR (400 MHz, CDCl$_3$) δ 9.88 (s, 1H), 7.96 (d, J = 1.7 Hz, 1H), 7.61 (dd, J = 8.5 Hz, 1.7 Hz, 1H), 6.83 (s, 2H), 6.64 (d, J = 8.5 Hz, 1H), 3.77

(s, 6H); ^{13}C NMR (100 MHz, CDCl$_3$) δ 189.7, 158.5, 153.4, 131.9, 131.5, 130.4, 129.7, 123.5, 119.4, 114.3, 109.2, 56.6.
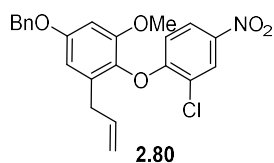
2.80 To a solution of **2.59** (0.757 g, 2.8 mmol) in acetonitrile (19 mL) was added potassium hydroxide (0.196 g, 3.5 mmol, 1.25 equiv) and 3-chloro-4-fluoronitrobenzene (**2.79)** (0.492 g, 2.8 mmol, 1 equiv). The reaction mixture was heated and maintained at 40 °C for 18 h. The mixture was allowed to cool to room temperature before being diluted with water (25 mL). The reaction mixture was extracted with EtOAc (3 x 30 mL), washed with brine (100 mL), dried (MgSO$_4$), filtered and concentrated *in vacuo*. The crude residue was purified by flash column chromatography (silica gel, gradient 0 to 1% EtOAc in hexanes) to afford 1.05 g (88%) of **2.80** as a yellow oil: ^{1}H NMR (400 MHz, CDCl$_3$) δ 8.35 (d, *J* = 2.8 Hz, 1H), 7.98 (dd, *J* = 9.0 Hz, 2.7 Hz, 1H), 7.46 (d, *J* = 7.0 Hz, 2H), 7.42 (t, *J* = 7.3 Hz, 2H), 7.36 (d, *J* = 7.1 Hz, 1H), 6.59 (d, *J* = 9.0 Hz, 1H), 6.56 (d, *J* = 2.7 Hz, 1H), 6.51 (d, *J* = 2.7 Hz, 1H), 5.86-5.76 (m, 1H), 5.07 (s, 2H), 5.04-4.98 (m, 2H), 3.72 (s, 3H), 3.26 (d, *J* = 6.5 Hz, 2H); ^{13}C NMR (100 MHz, CDCl$_3$) δ 159.1, 157.3, 152.2, 141.8, 136.4, 135.2, 134.4, 133.8, 128.6, 128.1, 127.6, 126.1, 123.4, 122.5, 116.7, 113.8, 106.5, 99.2, 70.4, 55.8, 34.3.
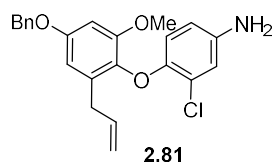
2.81 To a suspension of iron powder (0.412 g, 7.39 mmol, 3 equiv) in EtOH (11.7 mL) and water (5 mL) was added NH$_4$Cl (1.19 g, 22.19 mmol, 9 equiv). The suspension was heated and maintained at 45 °C for 20 min (reddish-orange color), then **2.80** (1.05 g, 2.46 mmol) in CH$_3$CN (10 mL) was added. The reaction mixture was heated and maintained at 100 °C for 1 h. The reaction mixture was allowed to cooled to room temperature, before dilution with water (100 mL). The reaction mixture was extracted with EtOAc (3 x 25 mL), washed with brine (100 mL), dried (MgSO$_4$), filtered and concentrated *in vacuo*. The crude residue was purified by flash column chromatography (silica gel, gradient 0 to 20 % EtOAc in hexanes) to afford 0.850 g (87%) of **2.81** as a yellow oil: ^{1}H NMR (400 MHz, (CD$_3$)$_2$SO) δ 7.47 (d, *J* = 7.1 Hz, 2H), 7.40 (t, *J* = 7.6 Hz, 2H), 7.34 (d, *J* = 7.6 Hz, 1H), 6.67 (t, *J* = 2.7 Hz, 1H), 6.50 (d, *J* = 2.7 Hz, 1H), 6.33 (dd, *J* = 8.7 Hz, 2.6 Hz, 1H), 6.14 (d, *J* = 8.8 Hz, 1H), 5.83-5.73 (m, 1H), 5.07 (s, 2H), 5.00-4.86 (m, 2H), 4.03 (s, 2H, exchanges with D$_2$O), 3.69 (s, 3H), 3.15 (d, *J* = 7.2 Hz, 2H); ^{13}C NMR (100 MHz,

(CD₃)₂SO) δ155.0, 152.9, 144.4, 143.79, 143.75, 136.9, 136.0, 143.7, 134.1, 128.4, 127.1, 120.4, 116.2, 114.9, 114.8, 113.2, 106.6, 99.1, 69.6, 55.8, 33.7.
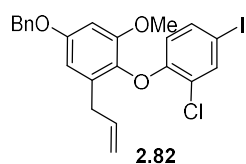
2.82 To a 0 °C solution of **2.81** (2.61 g, 6.59 mmol) in CH₃CN (65 mL) was added p-TsOH (3.76 g, 19.7 mmol, 3 equiv). The reaction mixture was maintained at 0 °C for 15 min, then a solution of NaNO₂ (1.00g, 14.5 mmol, 2.2 equiv) and KI (2.74 g, 16.48 mmol, 2.5 equiv) in water (3 mL) was added dropwise over 1 h. Upon completion of the addition, the reaction was maintained at 0 °C for 1 h, then allowed to slowly warm to room temperature and maintained for 3 h. The reaction was quenched by the addition of saturated aq Na₂S₂O₃ (30 mL) and extracted with EtOAc (3 x 30 mL). The extracts were washed with brine (100 mL), dried (MgSO₄), filtered and concentrated *in vacuo*. The crude residue was purified by flash column chromatography (silica gel, gradient 0 to 10 %) to afford 2.55 g (76%) of **2.82** as a yellow oil: ¹H NMR (400 MHz, CDCl₃) δ 7.71 (d, *J* = 2.1 Hz, 1 H), 7.46 (d, *J* = 7.4 Hz, 2H), 7.41 (t, *J* = 7.2 Hz, 2H), 7.36 (d, *J* = 7.2 Hz, 1H), 7.33 (dd, *J* = 8.6 Hz, 2.1 Hz, 1H), 6.52 (d, *J* = 2.8 Hz, 1H), 6.48 (d, *J* = 2.8 Hz, 1H), 6.25 (d, *J* = 8.6 Hz, 1H), 5.88-5.78 (m, 1H), 5.05 (s, 2H), 5.02-4.99 (m, 2H), 3.71 (s, 3H), 3.25 (d, *J* = 6.7 Hz, 2H); ¹³C NMR (100 MHz, CDCl₃) δ 157.0, 154.4, 152.9, 138.3, 136.8, 136.3, 135.7, 134.8, 134.5, 128.7, 128.2, 127.8, 123.4, 116.7, 116.3, 106.5, 99.4, 82.8, 70.5, 56.1, 34.4.
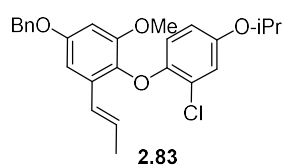
2.83 To a solution of **2.82** (100 mg, 0.197 mmol) in isopropanol (0.500 mL) was added CuI (4.00 mg, 0.019 mmol, 10 mol%), 1,10-phenanthroline (7.00 mg, 0.039 mmol, 20 mol%) and Cs₂CO₃ (90.0 mg, 0.275 mmol, 1.4 equiv). The reaction mixture was heated and maintained at 100 °C for 24 h, then allowed to cool to room temperature. The crude residue was filtered through a plug of celite and concentrated *in vacuo*. The crude residue was purified by flash column chromatography (silica gel, gradient 0 to 40% EtOAc in hexanes) to afford 36.0 mg (60%) of **2.83** as a white film: ¹H NMR (400 MHz, CDCl₃) δ 7.47 (d, *J* = 7.4 Hz, 2H), 7.42 (t, *J* = 7.48 Hz, 2H), 7.36 (d, *J* = 7.4 Hz, 1H), 6.98 (d, *J* = 2.8 Hz, 1H), 6.73 (d, *J* = 2.8 Hz, 1H), 6.59 (dd, *J* = 8.9 Hz, 2.7Hz, 1H), 6.53-6.49 (m, 2H), 6.39 (d, *J* = 9.0 Hz, 1H), 6.29-6.20 (m, 1H), 5.07 (s, 2H), 4.40 (m, 1H), 3.71 (s, 3H), 1.82 (dd, *J* = 6.7 Hz, 1.4Hz, 3H), 1.31 (d, *J* = 6.0 Hz, 6H); ¹³C NMR (100 MHz, CDCl₃) δ 156.6, 153.4,

152.5, 148.7, 136.9, 134.9, 132.7, 128.7, 128.4, 128.2, 127.8, 124.7, 122.1, 118.0, 115.3, 115.1, 101.9, 100.1, 71.1, 70.5, 56.2, 22.1, 18.9.
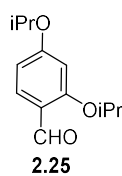
2.25 To a suspension of 2,4-dihydroxybenzaldehyde (**2.24**) (10.0 g, 72.4 mmol), K_2CO_3 (30.0 g, 217 mmol, 3.00 equiv), KI (310 g, 217 mmol, 3.0 equiv) in DMF (200 mL) was added 2-bromopropane (270 mL, 289 mmol, 4.0 equiv). The reaction mixture was heated and maintained at 50 °C for 18 h, and then allowed to cool to room temperature. The mixture was diluted with EtOAc (200 mL), washed with water (2 x 150 mL) and brine (150 mL), dried (MgSO$_4$), filtered and concentrated *in vacuo*. The residue was purified by flash column chromatography (silica gel, gradient elution, 0-10% EtOAc in hexanes) to afford 15.1 g (94%) of **2.25** as a yellow-orange oil: ^{1}H NMR (400 MHz, CDCl$_3$) δ 10.3 (s, 1H), 7.79 (d, $J = 8.7$ Hz, 1H), 6.50 (dd, $J = 8.7, 2.0$ Hz, 1H), 6.41 (d, $J = 2.0$ Hz, 1H), 4.62 (m, 2H), 1.32 (d, $J = 6.0$ Hz, 6H), 1.29 (d, $J = 6.0$ Hz, 6H); ^{13}C NMR (100 MHz, CDCl$_3$) δ 188.5, 164.5, 162.3, 130.1, 119.5, 106.9, 101.2, 70.9, 70.2, 21.9. NMR data corresponded to literature value.[1]
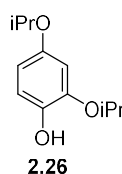
2.26 To a suspension of boric acid (103 g, 167 mmol, 5.0 equiv) in THF (100 mL) was added conc. H$_2$SO$_4$ (4.80 mL, 902 mmol, 1.80 equiv) followed by a solution of H$_2$O$_2$ (110 mL, 107 mmol, aqueous 30%, 3.20 equiv). After the mixture was stirred for 30 min, a solution of aldehyde **2.25** (7.43 g, 33.4 mmol) in THF (100 mL) was added and stirring was continued for 5 h. The suspension was filtered to remove excess salts. The filtrate was cooled to 0 °C and neutralized with saturated aq NaHCO$_3$ (~100 mL). The mixture was extracted with EtOAc (3 x 100 mL), and the combined organic extracts were washed with brine (100 mL), dried (MgSO$_4$), filtered and concentrated *in vacuo*. The residue was purified by flash column chromatography (silica gel, gradient elution, 0-10% EtOAc in hexanes) to afford 7.4 g (86%) of **2.26** as a yellow oil: ^{1}H NMR (400 MHz, CDCl$_3$) δ 6.82 (d, $J = 8.7$ Hz, 1H), 6.50 (d, $J = 2.5$ Hz, 1H), 6.40 (dd, $J = 8.7, 2.5$ Hz, 1H), 5.47 (s, 1H, exchanges with D$_2$O), 4.54-4.51 (m, 1H) 4.41-4.38 (m, 1H), 1.35 (d, $J = 6.0$ Hz, 6H), 1.30 (d, $J = 6.0$ Hz, 6H); ^{13}C NMR (100 MHz, CDCl$_3$) δ 151.4, 145.0, 140.9, 114.2, 107.9, 104.2, 71.6, 71.0, 22.1. NMR data corresponded to literature values.[1]
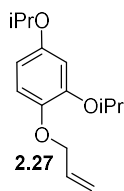
2.27 To a solution of phenol **2.26** (7.99 g, 379 mmol) in DMF (82.0 mL) was added K$_2$CO$_3$ (131 g, 94.9 mmol, 2.50 equiv) followed by allyl bromide (6.57 mL, 75.9 mmol, 2.00 equiv). The suspension was allowed to stir for 18 h, diluted with water (100 mL) and extracted with EtOAc (3 x 100 mL). The combined organic extracts were washed with water (3 x 100 mL) and brine (100 mL), dried (MgSO$_4$), filtered, and concentrated *in vacuo*. The residue was purified by flash column chromatography (silica gel, gradient elution, 0-20% EtOAc in hexanes) to afford 8.65 g (91%) of **2.27** as a yellow oil: ^{1}H NMR (400 MHz, CDCl$_3$) δ 6.82 (d, *J* = 8.7 Hz, 1H), 6.52 (d, *J* = 2.8 Hz, 1H), 6.41 (dd, *J* = 8.7, 2.8 Hz, 1H), 6.17-6.02 (m, 1H), 5.38 (dd, *J* = 17.2, 1.6 Hz, 1H), 5.23 (dd, *J* = 10.1, 1.5 Hz, 1H) 4.51 (m, 2H) 4.49-4.39 (m, 2H), 1.35 (d, *J* = 6.0 Hz, 6H), 1.31 (d, *J* = 6.0 Hz, 6H); ^{13}C NMR (100 MHz, CDCl$_3$) δ 153.0, 149.2, 143.9, 134.3, 117.1, 116.9, 107.6, 106.9, 71.8, 71.4, 70.7, 22.3, 22.2. NMR data corresponded to literature values.[1]
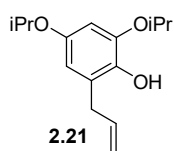
2.21 Allyl ether **2.27** (8.65 g, 34.5 mmol) was added to a microwave vial, neat. The vial was sealed, and heated and maintained at 185 °C in a reaction block for 18 h. The vial was then allowed to cool to room temperature, the crude residue was purified by flash column chromatography (silica gel, gradient elution, 0-15% EtOAc in hexanes) to afford 7.65 g (92%) of phenol **2.21** as a yellow oil: ^{1}H NMR (400 MHz, CDCl$_3$) δ 6.40 (d, *J* = 2.7 Hz, 1H), 6.33 (d, *J* = 2.7 Hz, 1H), 6.06-5.97 (m, 1H), 5.48 (s, 1H, exchanges with D$_2$O), 5.14-5.06 (m, 2H), 4.53 (m, 1H), 4.42 (m, 1H), 3.41 (d, *J* = 7.0 Hz, 2H), 1.36 (d, *J* = 6.0 Hz, 6H), 1.32 (d, *J* = 6.0 Hz, 6H); ^{13}C NMR (100 MHz, CDCl$_3$): 150.7, 144.8, 138.7, 136.7, 125.8, 115.5, 109.0, 101.8, 71.6, 70.8, 34.1, 22.23, 22.20. NMR data corresponded to literature values.[1]
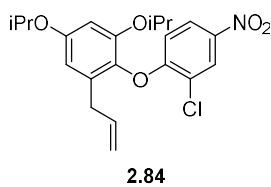
2.84 To a solution of phenol **2.21** (9.62 g, 38.4 mmol) in CH$_3$CN (75.0 mL) was added KOH (2.8 g, 49.96 mmol, 1.3 equiv) and 3-chloro-4-fluoronitrobenzene (**2.79**) (6.62 g, 37.6 mmol, 0.98 equiv). The suspension was heated and maintained at 45 °C for 18 h (judged complete by TLC). The reaction mixture was allowed to cool to room temperature before being diluted with water (150 mL). The solution was extracted with ether (3 x 100 mL), washed with saturated aq NH$_4$Cl (200 mL), water (2 x 200 mL) and brine (250 mL), dried (MgSO$_4$), filtered and concentrated *in vacuo*. The residue was purified by flash column chromatography (silica gel,

gradient elution, 0-4% EtOAc in hexanes) to afford 12. 0 g (73 %) of **2.84** as a yellow oil: ^{1}H NMR (400 MHz, CDCl$_3$) δ 8.34 (d, J = 2.8 Hz, 1H), 7.97 (dd, J = 9.0 Hz, 2.8 Hz, 1H), 6.64 (d, J = 9.0 Hz, 1H), 6.43 (d, J = 2.8 Hz, 1H), 6.41 (d, J = 2.8 Hz, 1H), 5.88-5.78 (m, 1H), 5.04-4.97 (m, 2H), 4.57-4.48 (m, 1H), 4.42-4.36 (m, 1H), 3.27 (d, J = 6.7 Hz, 2H), 1.36 (d, J = 6.0 Hz, 6H), 1.13 (d, J =6.0 Hz, 6H); ^{13}C NMR (100 MHz, CDCl$_3$) δ 159.6, 156.3, 150.4, 141.8, 135.6, 135.2, 134.5, 126.1, 123.3, 122.8, 116.7, 114.6, 108.3, 103.0, 71.7, 70.4, 34.6, 22.1, 21.9.
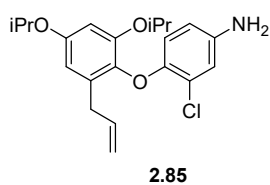
2.85 To a solution of **2.84** (2.87 g, 7.08 mmol) in EtOH (35 mL) was added SnCl$_2$ (7.9 g, 35.4 mmol, 5 equiv) as a solution in conc. HCl (5 mL). The reaction mixture was heated and maintained at reflux for three hours. The mixture was allowed to cool to room temperature before being quenched by the addition of saturated aq NaHCO$_3$ (200 mL). The reaction mixture was extracted with Et$_2$O (3 x 40 mL), washed with brine (100 mL), dried (MgSO$_4$), filtered and concentrated *in vacuo*. The crude residue was purified by flash column chromatography (silica gel, gradient elution, 0-40% EtOAc in hexanes) to afford 2.17 g (82%) of **2.85** as a yellow oil: ^{1}H NMR (400 MHz, CDCl$_3$) δ 6.72 (s, 1H), 6.41 (d, J = 2.7 Hz, 1H), 6.39 (d, J = 2.7 Hz, 1H), 6.33 (s, 2H), 5.92-5.81 (m, 1H), 5.05-4.97 (m, 2H), 4.51-4.45 (m, 1H), 4.43-4.37 (m, 1H), 3.47 (s, 2H, exchanges with D$_2$O), 3.29 (d, J = 6.7 Hz, 2 H), 1.33 (d, J = 6.0 Hz, 6H), 1.13 (d, J = 6.0 Hz, 6H); ^{13}C NMR (100 MHz, CDCl$_3$) δ 155.1, 151.0, 147.2, 141.0, 137.1, 136.3, 134.9, 122.3, 116.7, 116.1, 115.7, 114.0, 103.6, 71.5, 70.2, 34.3, 22.0, 21.9.
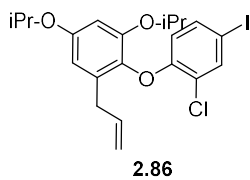
2.86 To a 0 °C solution of **2.85** (1g, 2.66 mmol) in CH$_3$CN (27.0 mL) was added p-TsOH (1.52 g, 7.98 mmol, 3 equiv). The reaction mixture was allowed to stir for 10 min before the addition of NaNO$_2$ (0.422 g, 6.12 mmol, 2.3 equiv) and KI (1.10 g, 6.65 mmol, 2.5 equiv) as a solution in water (1.33 mL) dropwise over 1 h. The reaction mixture was allowed to slowly warm to room temperature and was maintained for 4 h. Upon completion as judged by TLC, the reaction mixture was quenched with saturated aq Na$_2$S$_2$O$_3$ (20 mL), extracted with EtOAc (3 x 20 mL), washed with brine (50 mL), dried (MgSO$_4$), filtered and concentrated *in vacuo*. The crude residue was purified by flash column chromatography (silica gel, gradient, 0 to 2% EtOAc in hexanes) to afford 0.750 g (58%) of **2.86** as a yellow oil: ^{1}H NMR (400 MHz, CDCl$_3$) δ 7.69 (d, J = 2.2 Hz, 1H), 7.31 (dd,

J = 8.6 Hz, 2.0 Hz, 1H), 6.41 (d, *J* = 2.8 Hz, 1H), 6.39 (d, *J* = 2.8 Hz, 1H), 6.29 (d, *J* = 8.6 Hz, 1H), 5.90-5.79 (m, 1H), 5.07-4.97 (m, 2H), 4.55-4.46 (m, 1H), 4.42-4.36 (m, 1H), 3.26 (d, *J* = 6.9 Hz, 2H), 1.35 (d, *J* = 6.0 Hz, 6H), 1.14 (d, *J* = 6.0 Hz, 6 H); ^{13}C NMR (100 MHz, CDCl$_3$) δ 155.6, 154.5, 150.6, 137.9, 135.9, 135.87, 135.83, 134.6, 123.4, 116.8, 116.4, 108.3, 103.3, 82.5, 71.5, 70.1, 34.4, 22.1, 21.9.
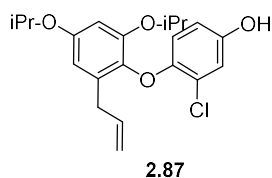
2.87 To a -78 °C solution of **2.86** (100 mg, 0.205 mmol) in THF (1 mL) was added nBuLi (97.0 μL, 1 equiv, 2.1 M in hexanes) dropwise. The reaction mixture was maintained at -78 °C for 15 min, then placed in an ice bath and maintained at 0 °C for 1 h. B(OMe)$_3$ (50.0 μL, 0.410 mmol, 2 equiv) was added and the reaction mixture was allowed to warm to room temperature and stir for 1.5 h, before the addition of H$_2$O$_2$ (100 μL) and NaOH (205 μL, 1M). The solution was maintained at room temperature for 30 min, then neutralized with HCl (~215 mL, 1N HCl). The solution was extracted with EtOAc (3 x 5 mL), washed with water (10 mL) and brine (10 mL), dried (MgSO$_4$), filtered and concentrated *in vacuo*. The crude residue was purified by flash column chromatography (silica gel, gradient 0 to 10% EtOAc in hexanes) to afford 31.0 mg (40%) of **2.87** as a yellow oil: R$_f$ 0.24 (DCM); ^{1}H NMR (400 MHz, CDCl$_3$) δ 6.91 (d, *J* = 2.9 Hz, 1H), 6.48 (dd, *J* = 8.9, 2.9 Hz, 1H), 6.41 (m, 2H), 6.38 (d, *J* = 8.9 Hz, 1H), 5.92-5.83 (m, 1H), 5.06-4.99 (m, 2H), 4.83 (s, 1H, exchanges with D$_2$O), 4.51-4.48 (m, 1H), 4.42-4.39 (m, 1H), 3.29 (d, *J* = 6.8 Hz, 2H), 1.34 (d, *J* = 6.0 Hz, 6H), 1.13 (d, *J* = 6.0 Hz, 6H); ^{13}C NMR (100 MHz, CDCl$_3$) δ 155.2, 151.0, 149.9, 148.8, 137.2, 136.3, 135.1, 122.4, 117.1, 116.3, 115.5, 114.1, 108.8, 103.9, 71.8, 70.5, 34.5, 22.2, 22.0; LRMS calculated for C$_{21}$H$_{25}$ClO$_4^+$ [M+H]$^+$ m/z 377.1, measured LC/MS (ESI) R$_t$ 1.29 min, m/z 377.4 [M+H]$^+$.

2.89 To a solution of phenol **2.21** (9.45 g, 38.7 mmol) in DMF (75.0 mL) was added K$_2$CO$_3$ (105 g, 754 mmol, 2.00 equiv) and 4-bromo-1-fluoro-2-nitrobenzene (**2.88**) (8.30 g, 37.7mmol, 2.00 equiv). The suspension was heated and maintained at 80 °C for 48 h (judged complete by LCMS analysis). The reaction mixture was allowed to cool to room temperature before being diluted with water (150 mL) and the solution was extracted with ether (3 x 100 mL). The combined organic extracts were washed

with saturated aq NH$_4$Cl (200 mL), water (2 x 200 mL) and brine (250 mL), dried (MgSO$_4$), filtered and concentrated *in vacuo*. The residue was purified by flash column chromatography (silica gel, gradient elution, 0-0.4-1% EtOAc in hexanes) to afford 164 g (95%) of biaryl ether **2.89** as an orange oil: R$_f$ 0.54 (9:1 hexanes/EtOAc); IR (thin-film): 3081, 2978, 1601, 1531 cm^{-1}; ^{1}H NMR (400 MHz, CDCl$_3$) δ 8.02 (d, *J* = 2.4 Hz, 1H), 7.44 (dd, *J* = 8.9, 2.4 Hz, 1H), 6.61 (d, *J* = 8.9 Hz, 1H), 6.40 (s, 2H), 5.87-5.80 (m, 1H), 5.04-4.96 (m, 2H), 4.51 (m, 1H), 4.38 (m, 1H), 3.31 (d, *J* = 7.0 Hz, 2H), 1.33 (d, *J* = 6.0 Hz, 6H), 1.11 (d, *J* = 6.0 Hz, 6H); ^{13}C NMR (100 MHz, CDCl$_3$) δ 156.1, 151.6, 150.4, 139.6, 136.3, 135.7, 134.9, 134.7, 127.9, 118.4, 116.6, 112.4, 108.3, 103.0, 71.6, 70.3, 34.5, 22.1, 21.9; LRMS calculated for C$_{21}$H$_{24}$BrO$_5$$^+$ [M+H]$^+$ m/z 450.0, measured LC/MS (ESI) R$_t$ 1.06 min, m/z 450.0 [M+H]$^+$.

2.90 To a degassed (argon purge for 20 min) solution of aryl bromide **2.89** (164 g, 364 mmol) and bis(pinacolato)diboron (112 g, 43.7 mmol, 1.20 equiv) in 1,4-dioxanes (145 mL) was added potassium acetate (7.10 g, 72.8 mmol, 2.00 equiv) and Pd(dppf)Cl$_2$ (800 mg, 1.09 mmol, 3.00 mol %). The reaction mixture was heated and maintained at 80 °C for 18 h (judged complete by LCMS). The reaction was cooled to 0 °C before solutions of H$_2$O$_2$ (9.33 mL, 911 mmol, aqueous 30%, 2.50 equiv) and a 1M NaOH (911 mL, 911 mmol, 2.50 equiv) were added. The reaction was allowed to warm to room temperature and stir for 20 min. The crude reaction mixture was acidified with 1 N HCl (105 mL) and extracted with EtOAc (3 x 200 mL). The combined organic extracts were washed with saturated aq NaHCO$_3$ (150 mL), water (200 mL) and brine (200 mL), dried (MgSO$_4$), filtered, and concentrated *in vacuo*. The residue was purified by flash column chromatography (silica gel, gradient elution, 0-20% EtOAc in hexanes) to afford 11.2 g (79%) of phenol **2.90** as an orange oil: R$_f$ 0.37 (2:1 hexanes/EtOAc); IR (thin-film): 3443, 2978, 2930, 1596, 1529, 1478, 1346, 1209, 1116 cm^{-1}; ^{1}H NMR (400 MHz, CDCl$_3$) δ 7.39 (d, *J* = 3.0 Hz, 1H), 6.85 (dd, *J* = 9.0, 3.0 Hz, 1H), 6.56 (d, *J* = 8.8 Hz, 1H), 6.41 (s, 2H), 5.86-5.81 (m, 1H), 5.04-4.97 (m, 2H), 4.54-4.48 (m, 1H), 4.40-434 (m, 1H), 3.32 (d, *J* = 7.0 Hz, 2H), 1.34 (d, *J* = 6.0 Hz, 6H), 1.08 (d, *J* = 6.0 Hz, 6H); ^{13}C NMR (100 MHz, CDCl3): 155.5, 150.6, 149.6, 146.6, 138.8, 136.2, 135.9, 135.0, 121.6, 117.7, 116.6, 111.7, 108.9, 103.6, 71.8, 70.8, 34.4, 22.1, 21.8; LRMS calculated for C$_{21}$H$_{25}$NO$_6$$^+$ [M+H]$^+$ m/z 388.1, measured LC/MS (ESI) R$_t$ 1.25 min, m/z 388.0 [M+H]$^+$.
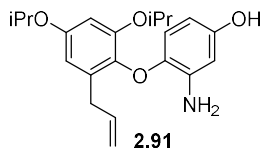
2.91 A suspension of iron powder (4.79 g, 86.0 mmol, 3.00 equiv) and ammonium chloride (13.8 g, 258 mmol, 9.00 equiv) in ethanol (136 mL) and water (53.0 mL) was heated to 45 °C for 15 min (rust orange in color), before a solution of **2.90** (11.1 g, 28.6 mmol) in CH$_3$CN (136 mL) was added. The reaction mixture was heated and maintained at reflux, until judged complete by TLC analysis (ca. 2 h), the reaction was allowed to cool to room temperature and quenched with saturated aq NaHCO$_3$ (100 mL). The quenched reaction mixture was extracted with EtOAc (3 x 150 mL), washed with saturated aq NH$_4$Cl (2 x 100 mL) and brine (150 mL), dried (MgSO$_4$), filtered and concentrated *in vacuo*. The crude residue was purified by flash column chromatography (silica gel, gradient elution, 0-35% EtOAc in hexanes) to afford 8.08 g (80%) of aniline **2.91** as a red foam: R$_f$ 0.51 (DCM/MeOH: 9:1); ^{1}H NMR (400 MHz, CDCl$_3$) δ 6.41 (d, *J* = 2.8 Hz, 1H), 6.37 (d, *J* = 2.8 Hz, 1H), 6.28 (d, *J* = 2.8 Hz, 1H), 6.22 (d, *J* = 8.6 Hz, 1H), 6.0 (dd, *J* = 8.6, 2.8 Hz, 1H), 5.91-5.84 (m, 1H), 5.05-4.99 (m, 2H), 4.51-4.48 (m, 1H), 4.40-4.37 (m, 1H), 3.29 (d, *J* = 6.6 Hz, 2H), 1.34 (d, *J* = 6.0 Hz, 6H), 1.12 (d, *J* = 6.0 Hz, 6H); ^{13}C NMR (100 MHz, CDCl$_3$) δ 155.0, 151.2, 150.6, 141.3, 137.6, 137.1, 136.6, 135.0, 116.1, 114.4, 108.3, 104.2, 103.2, 103.1, 71.3, 70.4, 34.5, 22.2, 22.0; LRMS calculated for C$_{21}$H$_{27}$NO$_4^+$ [M+H]$^+$ m/z 358.2, measured LC/MS (ESI) R$_t$ 1.01 min, m/z 358.4 [M+H]$^+$.
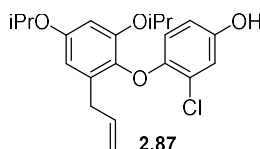
2.87 To a degassed (argon purge for 20 min), 0 °C solution of **2.91** (7.87 g, 22.0 mmol) in CH$_3$CN (440 mL) was added p-TSA (12.5 g, 66.0 mmol, 3.00 equiv). The reaction mixture was maintained at 0 °C for 10 min, then NaNO$_2$ (3.03 g, 44.0 mmol, 2.00 equiv) was added as a solution in water (22 mL) dropwise over 45 min. The reaction mixture was maintained at 0 °C for 5 min, then CuCl (43.5 g, 440 mmol, 20.0 equiv) and CuCl$_2$ (88.0 g, 660 mmol, 30.0 equiv) were added. The slurry was allowed to stir at 0 °C for 30 min, then the reaction mixture was allowed to warm to room temperature and continue to stir for 6 h (judged complete by LCMS). Saturated aq NH$_4$Cl (1500 mL) was added and the reaction mixture was extracted with EtOAc (4 x 500 mL). The combined organic extracts were washed with saturated aq NH$_4$Cl (2 x 500 mL) and brine (600 mL). The organic extracts were dried (MgSO$_4$), filtered and concentrated *in vacuo*. The crude residue was purified by flash column chromatography (silica gel, DCM) to afford 4.14 g (50%) of aryl chloride **2.87** as yellow oil: R$_f$ 0.24 (DCM); ^{1}H NMR (400 MHz, CDCl$_3$) δ 6.91 (d, *J* = 2.9 Hz, 1H), 6.48 (dd, *J* = 8.9, 2.9 Hz,

1H), 6.41 (m, 2H), 6.38 (d, J = 8.9 Hz, 1H), 5.92-5.83 (m, 1H), 5.06-4.99 (m, 2H), 4.83 (s, 1H, exchanges with D_2O), 4.51-4.48 (m, 1H), 4.42-4.39 (m, 1H), 3.29 (d, J = 6.8 Hz, 2H), 1.34 (d, J = 6.0 Hz, 6H), 1.13 (d, J = 6.0 Hz, 6H); ^{13}C NMR (100 MHz, CDCl$_3$) δ 155.2, 151.0, 149.9, 148.8, 137.2, 136.3, 135.1, 122.4, 117.1, 116.3, 115.5, 114.1, 108.8, 103.9, 71.8, 70.5, 34.5, 22.2, 22.0; LRMS calculated for $C_{21}H_{25}ClO_4^+$ [M+H]$^+$ m/z 377.1, measured LC/MS (ESI) R$_t$ 1.29 min, m/z 377.4 [M+H]$^+$.

2.96 A solution of **2.103** (0.896 mL, 6.39 mmol) in CH$_3$CN (18.0 mL) was added K$_2$CO$_3$ (0.882 g, 6.39 mmol, 1 equiv), CuI (1.21 g, 6.39 mmol, 1 equiv) and tetrabutylammonium iodide (2.36 g, 6.39 mmol, 1 equiv). The reaction mixture was heated to 40 °C, then ethyl propiolate (1.3 mL, 12.77 mmol, 2 equiv) was added. The reaction mixture was maintained at 40 °C for 24 h, before allowing to cool to room temperature. The reaction was quenched with saturated aq NH$_4$Cl (10 mL), extracted with ethyl acetate (3 x 10 mL), washed with water (25 mL) and brine (25 mL), dried (MgSO$_4$), filtered and concentrated *in vacuo*. The crude residue was purified by flash column chromatography (silica gel, gradient 2.5 to 5% EtOAc in hexanes) to afford 1.2 g (86%) of **2.96** as a yellow oil: R$_f$: 0.35 (4:1 hexanes/EtOAc); ^{1}H NMR (400 MHz, CDCl$_3$) δ 7.24 (d, J = 8.7 Hz, 2H), 6.85 (d, J = 8.7 Hz, 2H), 4.23 (q, J = 7.1 Hz, 2H), 3.80 (s, 3H), 3.68 (s, 2H), 1.31 (t, J = 7.1 Hz, 3H); ^{13}C NMR (100 MHz, CDCl$_3$) δ 158.6, 153.67, 128.9, 125.9, 114.1, 113.7, 86.6, 74.5, 61.8, 55.2, 24.0, 13.9.
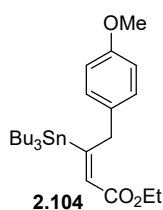
2.104 To a -78 °C suspension of CuCN (0.561 g, 6.27 mmol, 1.2 equiv) in THF (20 mL) was added nBuLi (5.5 mL, 12.54 mmol, 2.4 equiv) dropwise. Let stir for 5 min, then warm to -40 °C for five min, before cooling to -78 °C. Repeat the warming and cooling cycle until homogenous solution persists (ca. 3 cycles). Bu$_3$SnH (3.37 mL, 12.54 mmol, 2.4 equiv) was added dropwise over 10 min. The solution was maintained at -78 °C for 45 min (bright yellow solution), then MeOH (0.568 µl, 14.05 mmol, 2.69 equiv) was and allowed to stir for 10 min, before the addition of **2.96** (1.14 g, 5.22 mmol) as a solution in THF (10 mL) dropwise over 20 minutes. The reaction mixture was maintained at -78 °C for 2 h. The reaction mixture was quenched with NH$_4$Cl (15 mL) at -78 °C and allowed to slowly warm to room temperature for one hour. The reaction mixture was extracted with EtOAc (3 x 15 mL), washed with NH$_4$Cl (2 x 25 mL) and brine (30 mL), dried (MgSO$_4$), filtered and concentrated *in*

vacuo. The crude residue was purified by flash column chromatography (silica gel, gradient 0 to 4% EtOAc in hexanes) to afford 2.11 g (80%) as a clear oil: R_f: 0.65 (4:1 hexanes/EtOAc); ^{1}H NMR (400 MHz, CDCl$_3$) δ 7.0 (d, J = 8.6 Hz, 2 H), 6.81 (d, J = 8.6 Hz, 2H), 6.05 (s, J_{Sn-H} = 31 Hz, 1H), 4.28-4.14 (m, 4H), 3.77 (s, 3H), 1.34-1.29 (m, 8 H), 1.25-1.19 (m, 8H), 0.85 (t, J = 7.2 Hz, 9H), 0.72 (m, 5 H); ^{13}C NMR (100 MHz, CDCl$_3$) δ 171.2, 164.7, 158.3, 131.5, 130.2, 127.8, 113.9, 59.8, 55.2, 40.0, 28.9, 27.4, 14.4, 13.6, 10.0.
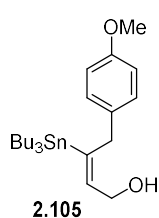
2.105 To a -78 °C solution of **2.104** (2.1 g, 4.12 mmol) in DCM (83 mL) was added DIBAL (10 mL, 10.3 mmol, 2.5 equiv, 1M solution in DCM) slowly over 5 min. The solution was maintained at -78 °C for 1 h, then allowed to warm to -15 °C for 20 min. The reaction mixture was quenched with saturated aq Rochelle's salt (40 mL) and allowed to warm to room temperature and was vigorously stirred for 12 h. The layers were separated and the aqueous layer was extracted with Et$_2$O (3 x 20 mL), washed with brine (25 mL), dried (Na$_2$SO$_4$), filtered and concentrated *in vacuo*. The crude residue was purified by flash column chromatography (silica gel (buffered 2% Et$_3$N) gradient, 0 to 10% EtOAc in hexanes) to afford 1.57 g (81%) of **2.105** as a clear oil: R_f: 0.25 (4:1 hexanes/EtOAc); ^{1}H NMR (400 MHz, CDCl$_3$) δ 7.0 (d, J = 8.6 Hz, 2H), 6.80 (d, J = 8.6 Hz, 2H), 5.88 (t, J = 6.21 Hz, J_{Sn-H} = 33 Hz, 1H), 4.35 (d, J = 6.1 Hz, 2H), 3.77 (s, 3H), 3.58 (s, J_{Sn-H} = 28 Hz, 2 H), 1.34-1.28 (m, 6H), 1.26-1.19 (m, 6H), 0.83 (t, J = 7.2 Hz, 9 H), 0.68 (m, 6H); ^{13}C NMR (100 MHz, CDCl$_3$) δ 158.2, 147.0, 139.4, 132.3, 129.8, 113.9, 59.2, 55.3, 38.4, 29.0, 27.5, 13.7, 9.6.
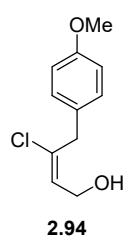
2.94 To a 0°C solution of **2.105** (0.770 g, 1.65 mmol) in THF (100 mL) was added CuCl$_2$ (4.41 g, 32.8 mmol, 20 equiv). The reaction slurry was allowed to slowly warm to room temperature and was maintained for 24 h. The reaction was quenched by the addition of saturated aq NH$_4$Cl (50 mL), extracted with Et$_2$O (3 x 40 mL), washed with saturated aq NH$_4$Cl (2 x 50 mL) and brine (50 mL), dried (Na$_2$SO$_4$), filtered and concentrated *in vacuo*. The crude residue was purified by flash column chromatography (silica gel, gradient 0 to 20 %) to afford 0.275 g (78%) as a yellow oil: R_f: 0.33 (4:1 hexanes/EtOAc); ^{1}H NMR (400 MHz, CDCl$_3$) δ 7.16 (d, J = 8.7 Hz, 2H), 6.87 (d, J = 8.7 Hz, 2H), 5.98 (t, J = 7.2 Hz, 1H), 4.29 (d, J = 7.3 Hz, 2H), 3.80 (s, 3H), 3.68 (s, 2H).
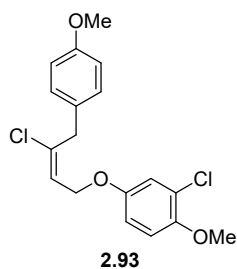
2.93 To a 0 °C solution of **2.94** (0.500 g, 2.35 mmol), triphenylphosphine (0.925 g, 3.53 mmol, 1.5 equiv) and 3-chloro-4-methoxy (**2.95**) (0.600 mg, 4 mmol, 1.5 equiv) in THF (5 mL) was added DEAD (1.61 mL, 4 mmol, 1.5 equiv, 40% w/V in toluene) dropwise over 8 min. The reaction mixture was maintained at 0 °C for 15 min, then allowed to warm to room temperature and was maintained for 4 h. The reaction mixture was diluted with saturated aq NaHCO$_3$ (5 mL), extracted with EtOAc (3 x 10 mL), washed with brine (15 mL), dried (MgSO$_4$), filtered and concentrated *in vacuo*. The crude residue was purified by flash column chromatography (silica gel, gradient 0 to 10% EtOAc in hexanes) to afford 0.587 g (71%) of **2.93** as a yellow oil: R$_f$ 0.66 (4:1 hexanes/EtOAc); ^{1}H NMR (400 MHz, CDCl$_3$) δ 7.16 (d, J = 8.7 Hz, 2H), 6.98 (d, J = 2.91 Hz, 1H), 6.88-6.86 (m, 3H), 6.79 (dd, J = 9.0 Hz, 2.9Hz, 1H), 6.05 (t, J = 7.0 Hz, 1H), 4.57 (d, J = 7.0 Hz, 2H), 3.87 (s, 3H), 3.81 (s, 3H), 3.71 (s, 2H).
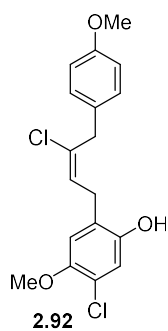
2.92 To a solution of **2.94** (30 mg, 0.080 mmol) in CCl$_4$ (1.7 mL) was added montmorillonite K10 (90 mg) and the slurry was heated and maintained at 50 °C for 18 h. The reaction mixture was allowed to cool to room temperature, filtered through celite and concentrated *in vacuo*. The crude residue was purified by flash column chromatography (silica gel, gradient 0 to 10% EtOAc in hexanes) to afford 22.0 mg (70%) of **2.92** as a white film: R$_f$ 0.45 (4:1 hexanes/EtOAc); ^{1}H NMR (400 MHz, CDCl$_3$) δ 7.17 (d, J = 8.6 Hz, 2 H), 6.86 (d, J = 8.6 Hz, 2H), 6.83 (s, 1H), 6.67 (s, 1H), 5.90 (t, J = 7.8 Hz, 1H), 4.68 (s, 1H, exchanges with D$_2$O), 3.81 (s, 3H), 3.80 (s, 3H), 3.76 (s, 2H).
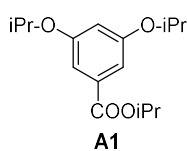
A1 To a solution of 3,5-dihydroxybenzoic acid (**2.115**) (5.00 g, 32.4 mmol) in DMF (81.0 mL) was added K$_2$CO$_3$ (17.9 g, 129 mmol, 4.00 equiv) and tetrabutylammonium iodide (1.50 g, 9.73 mmol, 30.0 mol %). The suspension was heated to 50 °C, 2-bromopropane (12.1 mL, 129 mmol, 4.00 equiv) was added and mixture was maintained at 50 °C until judge complete by TLC (ca. for 48 h). The reaction was allowed to cool to room temperature and diluted with water (100 mL). The reaction mixture was extracted with ether (3 x 150 mL). The combined organic extracts were washed with water (2 x 100 mL), saturated aq NH$_4$Cl (2 x 100 mL) and brine (100 mL). The washed extracts were dried (MgSO$_4$), filtered

158

and concentrated *in vacuo*. The crude residue was purified by flash column chromatography (silica gel, gradient elution, 0-20% EtOAc in hexanes) to afford 8.17 g (90%) of ester **A1** as a clear oil: R_f 0.6 (9:1 hexanes/EtOAc); IR (thin-film) 2923, 1714, 1594, 1456 cm^{-1}; ^{1}H NMR (400 MHz, CDCl$_3$) δ 7.14 (d, J = 2.4 Hz, 2H), 6.59 (t, J = 2.4 Hz, 1H), 5.24-5.17 (m, 1H), 4.59-53 (m, 2H), 1.32 (m, 18 H); ^{13}C NMR (100 MHz, CDCl$_3$) δ 166.0, 158.9, 132.8, 108.9, 108.5, 70.1, 68.4, 22.0, 21.9; LRMS calculated for C$_{16}$H$_{24}$O$_4$$^+$ [M+H]$^+$ m/z 281.1, measured LC/MS (ESI) R_t 0.78 min, m/z 281.6 [M+H]$^+$.

A2 To a suspension of LAH (674 mg, 17.7 mmol, 1.00 equiv) in THF (30.0 mL) was added, a solution of ester **A1** (4.98 g, 17.76 mmol) in THF (30.0 mL) dropwise. The reaction mixture was allowed to stir at room temperature for 1 h. The reaction mixture was cooled to 0 °C and diluted with ether (30.0 mL). The reaction was quenched by the sequential addition of water (0.674 mL), NaOH (aqueous 10 % w/v, 0.674 mL) and water (1.80 mL). The mixture was allowed to warm to room temperature and maintained for 15 min, before the addition of MgSO$_4$. The mixture was filtered and the filtrate concentrated *in vacuo.* The crude residue was purified by flash column chromatography (silica gel, gradient elution, 0-30% EtOAc in hexanes) to afford 3.5 g (88%) of alcohol **A2** as a clear oil: R_f 0.42 (4:1 hexanes/EtOAc); IR (thin-film) 3393, 2977, 1598, 1497 cm^{-1}; ^{1}H NMR (400 MHz, CDCl$_3$) δ 6.46 (d, J = 2.4 Hz, 2H), 6.34 (t, J = 2.4 Hz, 1H), 4.54-4.47 (m, 4H), 2.62 (s, 1H, exchanges with D$_2$O), 1.30 (d, J = 6.0 Hz, 12H); ^{13}C NMR (100 MHz, CDCl$_3$): δ 159.2, 143.4, 106.4, 102.9, 69.9, 65.1, 22.0; LRMS calculated for C$_{13}$H$_{20}$O$_3$$^+$ [M+H]$^+$ m/z 225.1, measured LC/MS (ESI) R_t 0.14 min, m/z 225.6 [M+H]$^+$.
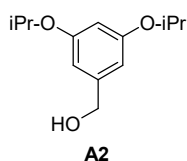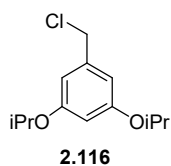
2.116 To a 0 °C solution of alcohol **A2** (2.39 g, 10.7 mmol) in acetonitrile (27.0 mL) was added diisopropylethylamine (3.72 mL, 21.4 mmol, 2.00 equiv) followed by the addition of triphenylphosphine dichloride (8.91 g, 26.7 mmol, 2.50 equiv). The reaction mixture was maintained at 0 °C until judged complete by TLC (ca. 30 min). The crude reaction mixture was loaded directly onto silica gel column and purified by flash column chromatography (gradient elution, 0-10% EtOAc in hexanes) to afford 2.38 g (92%) of **2.116** as a clear oil: R_f 0.72 (4:1 hexanes/EtOAc); IR (thin-film) 2977, 1598, 1458, 1329 cm^{-1}; ^{1}H NMR (400 MHz, CDCl$_3$) δ 6.52 (d, J = 2.4 Hz, 2H), 6.40 (t, J = 2.4 Hz, 1H), 4.57-4.52 (m , 2H),

4.50 (s, 2H), 1.35 (d, J = 6.0 Hz, 12H); ^{13}C NMR (100 MHz, CDCl$_3$): δ 159.3, 139.4, 108.1, 103.7, 70.0, 46.5, 22.1; LRMS calculated for C$_{13}$H$_{19}$ClO$_2^+$ [M+H]$^+$ m/z 243.1, measured LC/MS (ESI) R$_t$ 0.60 min, m/z 243.4 [M+H]$^+$.
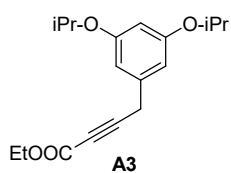
A3 To a solution of chloride **2.116** (2.87 g, 11.8 mmol) in acetonitrile (33.0 mL) was added CuI (2.25 g, 11.8 mmol, 1.00 equiv), K$_2$CO$_3$ (1.63 g, 11.8 mmol, 1.00 equiv) and tetrabutylammonium iodide (4.36 g, 11.8 mmol, 1.00 equiv). The reaction mixture was heated to 40 °C and neat ethyl propiolate (2.40 mL, 23.6 mmol, 2.00 equiv) was added. The reaction was maintained at 40 °C for 24 h, quenched by the addition of saturated aq NH$_4$Cl (20 mL) and extracted with EtOAc (3 x 20 mL). The combined organic extracts were washed with brine (30 mL), dried (MgSO$_4$), filtered and concentrated *in vacuo.* The crude residue was purified by flash column chromatography (silica gel, gradient elution, 0-10%, EtOAc in hexanes) to afford 2.75 g (76%) of alkynoate **A3** as a clear oil: R$_f$ 0.71 (4:1 hexanes/EtOAc); IR (thin-film) 2979, 2238, 1711, 1598 cm^{-1}; ^{1}H NMR (400 MHz, CDCl$_3$): δ 6.42 (d, *J* = 2.0 Hz, 2H), 6.32 (t, *J* = 2.4 Hz, 1H), 4.53-4.47 (m, 2H), 4.21 (q, *J* = 7.2 Hz, 2H), 3.63 (s, 2H), 1.31-1.27 (m, 15H); ^{13}C NMR (100 MHz, CDCl$_3$): δ 159.3, 153.6, 136.1, 107.8, 102.3, 86.1, 74.8, 69.8, 61.8, 25.1, 22.0, 14.0; LRMS calculated for C$_{18}$H$_{25}$O$_4^+$ [M+H]$^+$ m/z 305.1, measured LC/MS (ESI) R$_t$ 0.70 min, m/z 305.4 [M+H]$^+$; HRMS (APCI-orbitrap MS) calculated for C18H25O4$^+$ [M+H]$^+$ m/z 305.1747, measured 305.174.
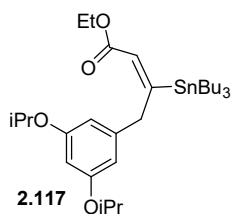
2.117 To a -78 °C suspension of CuCN (349 mg, 3.90 mmol, 1.20 equiv) in THF (13.0 mL) was added a solution of n-BuLi (3.39 mL, 7.80 mmol, 2.3 M, 2.40 equiv) dropwise. The mixture was warmed to -40 °C maintained for 10 min, and then cooled to -78 °C. The warming and cooling process was repeated until a homogenous solution is obtained (ca. 3 cycles). To the -78 °C solution was added tributyltin hydride (2.09 mL, 7.80 mmol, 2.40 equiv) dropwise and the reaction was maintained at -78 °C for 30 min (bright yellow solution). A solution of alkynoate **A3** (990 mg, 3.25 mmol) in MeOH (9.25 mL, 9.07 mmol, 0.98 M in THF, 2.79 equiv) was added dropwise over 10 min. The reaction was maintained at -78 °C for 1.5 h, then quenched at -78 °C by the addition of saturated aq NH$_4$Cl (10 mL). The reaction mixture was allowed to warm to room temperature and stir until the aqueous phase achieved a deep blue (ca. 2 h). The mixture was extracted with

ether (3 x 20 mL). The combined organic extracts were washed with saturated aq NH$_4$Cl (10 mL) and brine (10 mL), dried (MgSO$_4$), filtered, and concentrated *in vacuo.* The crude residue was purified by flash column chromatography (Silica gel/K$_2$CO$_3$ (10:1); gradient elution, 0-4 % EtOAc in hexanes) to afford 1.78 g (92%) of stannane **2.117** as a clear oil: R$_f$ 0.63 (9:1 hexanes/EtOAc); IR (thin-film) 2923, 2335, 1714, 1594 cm^{-1}; ^{1}H NMR (400 MHz, CDCl$_3$) δ 6.27 (m, 3H), 6.04 (s, 1H), 4.50-4.46 (m, 2H), 4.22-4.17 (m, 4H), 1.36-1.30 (m, 22H), 1.29 -1.20 (m, 6H), 0.90-0.83 (m, 9H), 0.77-0.72 (m, 5H); ^{13}C NMR (100 MHz, CDCl$_3$) δ 170.6, 164.7, 159.2, 141.7, 128.1, 109.2, 101.7, 69.7, 59.8, 41.1, 28.9, 27.4, 22.2, 14.4, 13.7, 10.1; HRMS (APCI-orbitrap MS) calculated for C$_{30}$H$_{54}$O$_4$Sn$^+$ [M+H]$^+$ 597.2960, measured 597.2961.
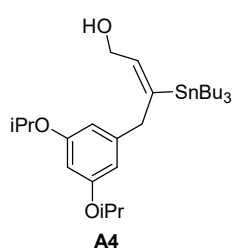
A4 To a -78 °C solution of enoate **2.117** (1.70 g, 2.85 mmol) in DCM (20.0 mL) was added a solution of DIBAL (5.70 mL, 5.70 mmol, 1 M in hexanes, 2.0 equiv) dropwise. The reaction mixture was maintained at -78 °C for 1 h, then an additional equivalent of DIBAL (2.85 mL, 2.85 mmol, 1 M in hexanes, 1.00 equiv) was added. The reaction solution was warmed to -15 °C and maintained at that temperature for 20 min. The reaction was quenched by the addition of saturated aq Rochelle's salt (20 mL). The biphasic solution was stirred at room temperature for 2 h. The reaction mixture was extracted with DCM (3 x 25 mL), the organic extracts were combined, washed with brine (20 mL), dried (Na$_2$SO$_4$), filtered and concentrated *in vacuo*. The crude residue was purified by flash column chromatography (silica gel (2% Et$_3$N buffered); gradient elution, 0-20% EtOAc in hexanes) to afford 1.18 g (75%) of alcohol **A4** as a clear oil: R$_f$ 0.36 (9:1 hexanes/EtOAc); IR (thin-film) 3332, 2922, 1595 cm^{-1}; ^{1}H NMR (400 MHz, CDCl$_3$) δ 6.27 (d, *J* = 2.4 Hz, 1H), 6.24 (m, 2H), 5.90 (t, *J* = 6.4 Hz, 1H), 4.51-4.44 (m, 2H), 4.34 (d, *J* = 6.4 Hz, 2H), 3.55 (s, 2H), 1.37-1.30 (m, 18H), 1.27-1.20 (7H), 0.86-0.82 (m, 9H), 0.74-0.72 (m, 5H); ^{13}C NMR (100 MHz, CDCl$_3$) δ 159.2, 146.4, 142.4, 139.7, 108.8, 101.5, 69.8, 59.3, 39.5, 29.1, 27.5, 22.2, 13.7, 9.7; HRMS (ESI-orbitrap MS) calculated for C$_{28}$H$_{51}$O$_3$Sn$^+$ [M+H]$^+$ m/z 555.2855, measured 555.2856.
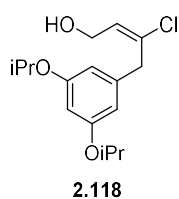
2.118 To a 0°C solution of stannane **A4** (1.04 g, 1.87 mmol) in THF (37.0 mL) was added CuCl$_2$ (5.00 g, 37.6 mmol, 20.0 equiv). The reaction mixture was allowed to slowly warm to room temperature and stir for 18 h. The reaction was quenched by the addition of saturated aq NH$_4$Cl (20.0 mL). The reaction mixture was extracted with diethyl ether (3 x 40.0 mL), washed with saturated aq NH$_4$Cl (2 x 20.0 mL) and brine (20.0 mL), dried (MgSO$_4$), filtered and concentrated *in vacuo*. The crude residue was purified by flash column chromatography (silica gel/K$_2$CO$_3$ (10:1); gradient elution, 0-30% EtOAc in hexanes) to afford 558 mg (80%) of **2.118** as a clear oil: R$_f$ 0.30 (4:1 hexanes/EtOAc); IR (thin-film) 3400, 2976, 1597, 1458 cm^{-1}; ^{1}H NMR (400 MHz, CDCl$_3$) 6.33 (m, 3H), 5.99 (t, J = 7.2 Hz, 1H), 4.54-4.48 (m, 2H), 4.27-4.24 (m, 2H), 3.64 (s, 2H), 1.32 (d, J = 6.0 Hz, 12H); ^{13}C NMR (100 MHz, CDCl$_3$) δ 159.2, 138.9, 136.3, 128.0, 108.4, 102.0, 69.9, 59.1, 40.4, 22.1; LRMS calculated for C$_{16}$H$_{24}$ClO$_3^+$ [M+H]$^+$ m/z 299.1, measured LC/MS (ESI) R$_t$ 0.23 min, m/z 299.6 [M+H]$^+$; HRMS (APCI-orbitrap MS) calculated for C$_{16}$H$_{24}$ClO$_3^+$ [M+H]$^+$ m/z 299.1408, measured 299.1409.
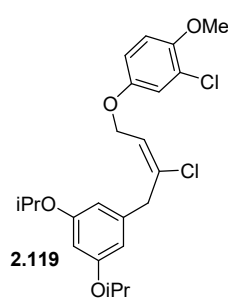
2.119 To a 0 °C solution of alcohol **2.118** (181 mg, 0.608 mmol), 3-chloro-4-methoxyphenol (**2.95**)[2] (145 mg, 0.913 mmol, 1.50 equiv) and triphenylphosphine (239 mg, 0.913 mmol, 1.50 equiv) in DCM (3.0 mL) was added a solution of diethyl azodicarboxylate (0.415 mL, 0.913 mmol, 40 % solution in toluene, 1.50 equiv) at a rate of ca. 1 drop per minute. The reaction was maintained at 0 °C for 30 min, allowed to warm to room temperature and stir for 15 min. When judged complete by TLC (ca. 15-20 min), the reaction was loaded directly onto column and purified by flash column chromatography (silica gel, gradient elution, 0-10% EtOAc in hexanes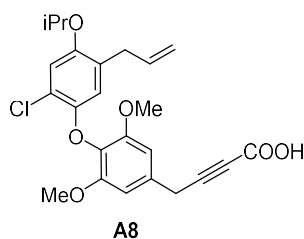) to afford 212 mg (79%) of ether **2.119** as a yellow oil: R$_f$ 0.58 (4:1 hexanes/EtOAc); IR (thin-film) 2976, 1597, 1497, 1459 cm^{-1}; ^{1}H NMR (400 MHz, CDCl$_3$) 6.98 (d, J = 2.8 Hz, 1H), 6.86 (d, J = 9.2 Hz, 1H), 6.77 (dd, J = 9.2, 2.8 Hz, 1H), 6.36-6.33 (m, 3H), 6.07 (t, J = 7.0 Hz, 1H), 4.55 (d, J = 7.2 Hz, 2H), 4.50 (m, 2H), 3.86 (s, 3H), 3.68 (s, 2H), 1.32 (d, J = 6.0 Hz, 12H); ^{13}C NMR (100 MHz, CDCl$_3$) δ 159.3, 152.5, 150.0, 138.5, 138.2, 124.1, 123.2, 117.4, 113.9, 113.2, 108.4, 102.2, 69.9, 64.9, 56.8, 40.8, 22.2; LRMS calculated for C$_{23}$H$_{29}$O$_4^+$ [M+H]$^+$ m/z 439.1, measured LC/MS (ESI) R$_t$ 0.96 min, m/z 439.5 [M+H]$^+$; HRMS (ESI-orbitrap MS) calculated for C$_{23}$H$_{29}$Cl$_2$O$_4$+ [M+H]$^+$ m/z 439.1437, measured 439.1443.
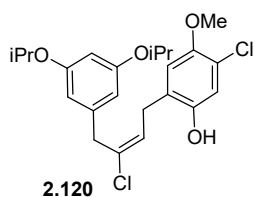
2.120 To a solution of ether **2.119** (68.0 mg, 0.155 mmol) in carbon tetrachloride (4.56 mL) and DCE (400 µL) was added a solution of BF$_3$·Et$_2$O (698 µL, 0.467 mmol, 0.67 M in DCE, 3.00 equiv). The reaction mixture was heated and maintained at 65 °C for 18 h. The reaction was allowed to cool to room temperature before being quenched by the addition of saturated aq NaHCO$_3$ (5 mL). The reaction mixture was extracted with EtOAc (3 x 10 mL). The combined organic extracts were washed with brine (10 mL), dried (Na$_2$SO$_4$), filtered and concentrated *in vacuo*. The crude residue was purified by flash column chromatography (silica gel, gradient elution, 0-15% EtOAc in hexanes) to give 39.0 mg (57%) of phenol **2.120** as a clear oil: R$_f$ 0.51 (4:1 hexanes/EtOAc); IR (thin-film) 3385, 2977, 1596, 1497 cm^{-1}; ^{1}H NMR (400 MHz, CDCl$_3$) δ 6.82 (s, 1H), 6.68 (s, 1H), 6.36 (d, J = 2.0 Hz, 2H), 6.32 (d, J = 2.0 Hz, 1H), 5.93 (t, J = 8.0 Hz, 1H), 4.72 (s, 1H, exchanges with D$_2$O), 4.50-4.45 (m, 2H), 3.81 (s, 3H), 3.73 (s, 2H), 3.45 (d, J = 8.0 Hz, 2H), 1.31 (d, J = 6.0 Hz, 12H); ^{13}C NMR (100 MHz, CDCl$_3$) δ 159.2, 149.6, 147.3, 139.3, 133.5, 126.6, 125.3, 120.7, 117.5, 114.2, 108.5, 102.0, 70.0, 57.0, 40.1, 29.4, 22.2; HRMS (APCI-orbitrap MS) calculated for C$_{23}$H$_{27}$Cl$_2$O$_4^-$ [M-H]$^-$ m/z 437.1292, measured 437.1285.
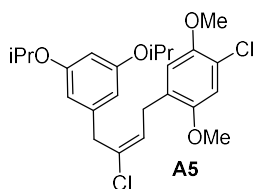
A5 To a solution of phenol **2.120** (31.0 mg, 0.0700 mmol) in acetone (1.00 mL) was added K$_2$CO$_3$ (20.0 mg, 0.141 mmol, 2.00 equiv) and iodomethane (15.0 µL, 0.210 mmol, 3.00 equiv). The reaction mixture was heated and maintained at 55 °C for 3 h, allowed to cool room temperature and quenched with water (3 mL). The crude mixture was extracted with EtOAc (3 x 5 mL), washed with brine (5 mL), dried (Na$_2$SO$_4$), filtered and concentrated *in vacuo*. The crude residue was purified by flash column chromatography (silica gel, gradient elution, 0-13% EtOAc in hexanes) to give 35.0 mg (60%) of **A5** as clear oil: R$_f$ 0.48 (9:1 hexanes/EtOAc); IR (thin-film) 2975, 1596, 1496, 1457 cm^{-1}; ^{1}H NMR (CDCl3, 400 MHz) δ 6.89 (s, 1H), 6.72 (s, 1H), 6.36 (d, J = 2.12 Hz, 2H), 6.32 (m, 1H), 5.91 (t, J = 7.8 Hz, 1H), 4.49-4.43 (m, 2H), 3.82 (s, 3H), 3.78 (s, 3H), 3.72 (s, 2H), 3.45 (d, J = 7.9 Hz, 2H), 1.31 (d, J = 6.0 Hz, 12 H); ^{13}C NMR (100 MHz, CDCl3) δ 159.2, 151.4, 149.1, 139.4, 133.0, 127.1, 127.0, 120.6, 114.4, 113.0, 108.4, 101.8, 69.8, 57.0, 56.1, 40.0, 29.4, 22.1; HRMS (APCI-orbitrap MS) calculated for C$_{24}$H$_{31}$Cl$_2$O$_4^+$ [M+H]$^+$ m/z 453.1594, measured 453.1602.
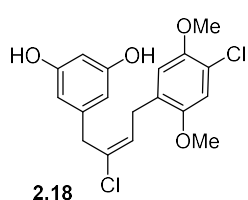
Hemi-chrysophaentin (2.18) To a -78 °C solution of ether **A6** (17.0 mg, 0.037 mmol) in DCM (2 mL) was added a solution of boron trichloride (112 µL, 0.112 mmol, 1 M in DCM, 3 equiv). The reaction mixture was allowed to warm to 0 °C and maintained for 30 min. Then the reaction was allowed to warm to room temperature and was maintained for 3 h. Upon completion as judge by TLC (ca. 3-4 h), the reaction was quenched by the addition of saturated aq NaHCO$_3$ (5 mL) and allowed to stir at room temperature for 10 min, before being acidified with 1 N HCl (6 mL). The reaction mixture was extracted EtOAc (3 x 5 mL), the combined organic extracts were washed with brine (5 mL) and dried (MgSO$_4$). Following filtration, the solution was concentrated *in vacuo*. The crude residue was purified by flash column chromatography (silica gel, gradient elution, 0-10 % methanol in DCM) to afford 9.0 mg (70%) of **2** as an off-white film: R$_f$ 0.74 (9:1 DCM/methanol); ^{1}H NMR (400 MHz, CDCl$_3$) δ 6.88 (s, 1H), 6.70 (s, 1H), 6.31 (d, *J* = 2.00 Hz, 2H), 6.23 (app t, *J* = 2.0 Hz, 1H), 5.89 (t, *J* = 8.0 Hz, 1H), 4.93 (br s, 2H, exchanges with D$_2$O), 3.81 (s, 3H), 3.77 (s, 3H), 3.68 (s, 2H), 3.42 (d, *J* = 6.0 Hz, 2H); ^{13}C NMR (100 MHz, CDCl$_3$): 157.0, 151.5, 149.1, 140.4, 132.5, 127.4, 127.0, 120.8, 114.6, 113.1, 108.3, 101.4, 57.1, 56.1, 39.6, 29.5; HRMS (ESI-orbitrap MS) calculated for C$_{23}$H$_{27}$Cl$_2$O$_4$[−] [M-H][−] m/z 367.0509, measured 367.0509. NMR data are consistent with reported values.[3]
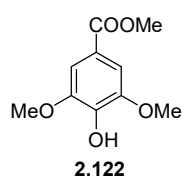
2.122 To a suspension of 4-hydroxy-3,5-dimethoxybenzoic acid (5.0 g, 25.2 mmol) in methanol (51 mL) was added thionyl chloride (1.38 mL, 18.9 mmol, 0.75 equiv) dropwise. The reaction mixture was heated and maintained at 50 °C for 18 h. The reaction mixture was allowed to cool to room temperature before the addition of silica gel (ca. 10 g). The slurry was concentrated *in vacuo* and loaded onto a silica gel column and purified by column chromatography (gradient, 20 to 50% EtOAc in hexanes) to afford 5.11 g (96%) of **2.128** as a white solid: ^{1}H NMR (400 MHz, CDCl$_3$) δ 7.32 (s, 2H), 5.93 (s, 1H), 3.94 (s, 6H), 3.90 (s, 3H); ^{13}C NMR (100 MHz, CDCl$_3$): 166.9, 146.8, 139.3, 121.2, 106.7, 56.5, 52.2. NMR data corresponded to reported literature values.[4]
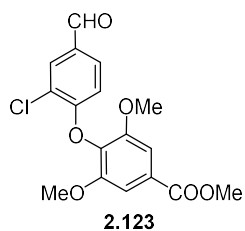
2.123 To a solution of phenol **2.122** (4.97 g, 23.4 mmol) in DMF (78 mL) was added K$_2$CO$_3$ (6.47 g, 46.8 mmol, 2 equiv) followed by 3-chloro-4-fluorobenzaldehyde (**2.61**) (3.71 g, 23.4 mmol, 1 equiv). The reaction mixture was heated and maintained at 120 ºC for 24 h. The suspension was allowed to cool to room temperature and diluted with water (200 mL). The reaction mixture was extracted with EtOAc (3 x 25 mL), washed with saturated aq NH$_4$Cl (2 x 50 mL) and brine (30 mL). The organic layers were dried (MgSO$_4$), filtered and concentrated *in vacuo*. The crude solid was recrystallized from hot methanol/water (~1:10) to afford 6.1 g (75%) of **2.123** as a white solid: R$_f$ 0.25 (4:1 hexanes/EtOAc); IR (thin-film): 2951, 2842, 1708, 1596, 1239 cm^{-1}; ^{1}H NMR (400 MHz, CDCl$_3$) δ 9.87 (s, 1H), 7.97 (d, J = 2.0 Hz, 1H), 7.60 (dd, J = 8.5 Hz, 2.0 Hz, 1H), 7.39 (s, 2H), 6.62 (d, J = 8.5 Hz, 1 H), 3.96 (s, 3H), 3.84 (s, 6 H); ^{13}C NMR (100 MHz, CDCl$_3$): 189.8, 166.4, 158.5, 152.8, 135.0, 132.0, 131.7, 129.7, 128.4, 123.7, 114.6, 106.9, 56.6, 52.6; LRMS calculated for C$_{17}$H$_{16}$ClO$_6$$^+$ [M+H]$^+$ m/z 351.0, measured LC/MS (ESI) R$_t$ 0.332 min, m/z 351.4 [M+H]$^+$.

2.124 To a 0 °C solution of aldehyde **2.123** (7.65 g, 21.8 mmol) in DCM (110 mL) was added mCPBA (10.7 g, 46.9 mmol, 2 equiv) in three portions over 15 minutes, after which the reaction was allowed to warm to room temperature and stir for 7 h. The reaction was quenched by the addition of saturated aq Na$_2$S$_2$O$_3$ (100 mL) and saturated aq NaHCO$_3$ (100 mL), followed by extraction with Et$_2$O (3 x 100 mL). The combined organic extracts were washed with saturated aq NaHCO$_3$ (2 x 100 mL), water (100 mL) and brine (100 mL), dried (MgSO$_4$), filtered, and concentrated *in vacuo*. The crude formate was dissolved in MeOH (40 mL, 0.5 M) and THF (10 mL), then thionyl chloride (1.31 mL, 16.1 mmol, 0.75 equiv) was added dropwise. The solution was maintained at room temperature for 7 h, before the addition of silica gel (ca. 10 g). The mixture was concentrated *in vacuo* and purified by column chromatography (DCM) to afford 6.03 g (82%) of **2.124** as a white solid: R$_f$: 0.23 (2:1 hexanes/EtOAc); IR (thin-film): 3327, 2944, 1672, 1596 cm^{-1}; ^{1}H NMR (400 MHz, (CD$_3$)$_2$CO) δ 8.30 (s, 1H, exchanges with D$_2$O), 7.39 (s, 2H), 6.93 (d, J = 2.8 Hz, 1H), 6.60 (dd, J = 8.8, 2.8 Hz, 1H), 6.40 (d, J = 9.2 Hz, 1H), 3.90 (s, 3H), 3.82 (s, 6H); ^{13}C (100 MHz, (CD$_3$)$_2$CO) δ 166.7, 154.1, 153.2, 147.9, 137.3, 128.2, 122.6, 117.5, 116.0, 115.1,

107.6, 56.7, 52.5; LRMS calculated for $C_{16}H_{16}ClO_6^+$ [M+H]$^+$ m/z 339.0, measured LC/MS (ESI) R_t 0.973 min, m/z 339.3 [M+H]$^+$.

2.125

2.125 To a solution of phenol **2.124** (4.02 g, 11.8 mmol) in DMF (47 mL) was added Cs_2CO_3 (5.80 g, 17.8 mmol, 1.5 equiv) and Bu$_4$NI (0.438 g, 1.18 mmol, 0.1 equiv). The suspension was allowed to stir for 10 min before allyl bromide (1.34 mL, 15.4 mmol, 1.5 equiv) was added. The reaction mixture was maintained at room temperature for 18 h, before dilution with water (100 mL) and extraction with EtOAc (3 x 50 mL). The combined organic layers were washed with water (2 x 100 mL) and brine (100 mL), dried (MgSO$_4$), filtered and concentrated *in vacuo.* The crude residue was purified by column chromatography (gradient, 0 to 15 %, EtOAc in hexanes) to afford 4.13 g (92%) of **2.125** as a white solid: R$_f$: 0.28 (4:1 hexanes/EtOAc); IR (thin film): 1720; ^{1}H NMR (400 MHz, CDCl$_3$) δ 7.36 (s, 2H), 6.9 (d, J= 2.9 Hz, 1H), 6.62 (dd, J= 9.0, 2.9 Hz, 1H), 6.45 (d, J= 9.0 Hz, 1H), 6.02 (m, 1H), 5.40 (dd, J= 16 Hz, 1.5 Hz, 1H), 5.28 (dd, J= , 1H), 4.46 (d, J=3.8 Hz, 2H), 3.94 (s, 3H), 3.83 (s, 6H); ^{13}C NMR (100 MHz, CDCl$_3$) δ 166.6, 153.7, 153.1, 148.1, 136.9, 133.1, 127.2, 122.8, 117.9, 116.7, 115.3, 113.9, 107.0, 69.6, 56.6, 52.5; LRMS calculated for $C_{19}H_{20}ClO_6^+$ [M+H]$^+$ m/z 379.0, measured LC/MS (ESI) R$_t$ 1.18 min, m/z 379.3 [M+H]$^+$.

2.128   **2.129**

2.128/2.129 To a -78 °C solution of allyl ether **2.125** (3.5 g, 9.24 mmol) in DCM (92 mL) was added BCl$_3$ (15 mL, 15 mmol, 1 M in DCM, 1.6 equiv) dropwise over 5 min. The reaction mixture was maintained at -78 °C for 1 h, then warmed to 0 °C for one hour. Upon completion of the reaction, as determined by TLC (ca. 2 h), the reaction was quenched by the addition of saturated aq NaHCO$_3$ (100 mL). The solution was extracted with DCM (3 x 50 mL) and the combined organic layers were washed with brine (50 mL), dried (MgSO$_4$), filtered and concentrated *in vacuo.* The crude mixture of regioisomers was dissolved in DMF (27 mL), followed by the addition of cesium carbonate (6.00 g, 18.3 mmol, 2 equiv), Bu$_4$NI (0.663 g, 1.84 mmol, 0.2 equiv) and 2-bromopropane (3.45 mL, 36.7 mmol, 4 equiv). The reaction mixture was maintained at room

temperature for 18 h, before dilution with water (100 mL) and extraction with diethyl ether (3 x 50 mL). The combined extracts were washed with saturated aq NH$_4$Cl (75 mL) and brine (75 mL), dried (MgSO$_4$), filtered, and concentrated *in vacuo*. The crude residue was purified by Teledyne ISCO column chromatography (column: 80 g, gradient, 0 to 10 % EtOAc in hexanes) to afford 882 mg (30%) of **6** and 1.92 g (60%) of **5** as white amorphous solids:

2.128 R$_f$: 0.30 (4:1 hexanes/EtOAc); IR (thin-film): 2974, 1721, 1595, 1464, 1341 cm^{-1}; ^{1}HNMR (400 MHz, CDCl$_3$) δ 7.37 (s, 2 H), 6.59 (d, J = 9.0 Hz, 1H), 6.33 (d, J = 9.0Hz, 1H), 5.96-5.87 (m, 1H), 5.10 (dd, J = 17 Hz, 1.8 Hz, 1H), 5.02 (dd, J = 10 Hz, 1.8 Hz, 1H), 4.41 (m, 1H), 3.94 (s, 3 H), 3.82 (s, 6H), 3.61 (d, J = 6.0 Hz, 2H), 1.29 (d, J = 6.0 Hz, 6H); ^{13}C NMR (100 MHz, CDCl$_3$): 153.5, 150.8, 148.4, 138.6, 135.3, 132.1, 129.3, 123.4, 115.4, 112.0, 111.7, 104.1, 71.2, 65.4, 56.4, 31.9, 22.3; LRMS calculated for C$_{22}$H$_{26}$ClO$_6^+$ [M+H]$^+$ m/z 421.1, measured LC/MS (ESI) R$_t$ 0.871 min, m/z 421.6 [M+H]$^+$.

2.129 R$_f$: 0.42 (4:1 hexanes/EtOAc); IR (thin-film): 2965, 1719, 1597, 1477 cm^{-1}; ^{1}H NMR (400 MHz, CDCl$_3$) δ 7.35 (s, 2H), 6.90 (s, 1H), 6.32 (s, 1 H), 5.83-5.73 (m, 1H), 4.92-4.87 (m, 2H), 4.43-4.40 (m, 1H), 3.92 (s, 3H), 3.81 (s, 6H), 3.18 (d, J = 6.4 Hz, 2H), 1.30 (d, J = 6.0 Hz, 6 H); ^{13}C NMR (100 MHz, CDCl$_3$) δ 166.6, 153.0, 150.5, 147.3, 136.9, 136.5, 129.1, 127.0, 119.8, 116.2, 115.6, 115.5, 107.0, 71.3, 56.5, 52.3, 34.0, 22.1; LRMS calculated for C$_{22}$H$_{26}$ClO$_6^+$ [M+H]$^+$ m/z 421.1, measured LC/MS (ESI) R$_t$ 0.845 min, m/z 421.6 [M+H]$^+$.

A6 To a three-neck round bottom with a condenser, addition funnel and septum was added LAH (186 mg, 4.91 mmol, 1 equiv) in THF (20 mL). The suspension was heated to reflux for 15 minutes, then allowed to cool to room temperature before the dropwise addition of ester **2.129** (2.07 g, 4.91 mmol, 1 equiv) as a solution in THF (20 mL). The reaction mixture was maintained at room temperature for 1 h, before being cooled to 0 °C and diluted with Et$_2$O (30 mL). Water (186 μL), NaOH (15%, 186 μL) and then water (500 μL) were added in that order, slowly. The solution was allowed to warm to room temperature and stir for 15 minutes before the addition of MgSO$_4$ (ca. 300 mg). The mixture was stirred for 15 minutes, then filtered and concentrated *in vacuo*. The crude residue was purified by column chromatography (gradient, 0 to 30% EtOAc in hexanes) to afford 1.84 g (>95%) of **A6** as a white solid: R$_f$: 0.15 (2:1 hexanes/EtOAc); IR(thin-

film): 3398, 2967, 1599, 1480 cm^{-1}; ^{1}H NMR (400 MHz, CDCl$_3$) δ 6.90 (s, 1H), 6.63 (s, 2H), 6.33 (s, 1H), 5.83-5.76 (m, 1H), 4.92-4.87 (m, 2H), 4.64 (s, 2H), 4.39 (m, 1H), 3.74 (s, 6H), 3.17 (d, J = 6.0 Hz, 2H), 1.29 (d, J = 6.0 Hz, 6 H); ^{13}C NMR (100 MHz, CDCl$_3$): 153.2, 150.2, 147.7, 138.6, 136.7, 131.8, 129.1, 119.4, 116.0, 115.7, 115.3, 104.0, 71.4, 65.2, 56.3, 34.12; LRMS calculated for C$_{21}$H$_{26}$ClO$_5$$^+$ [M+H]$^+$ m/z 393.1, measured LC/MS (ESI) R$_t$ 0.550 min, m/z 393.4 [M+H]$^+$.
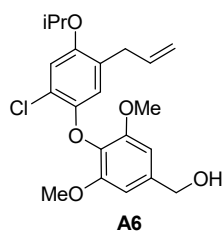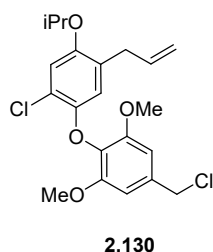
2.130 To a solution of alcohol **A6** (1.7 g, 4.32 mmol) in CH$_3$CN (27 mL) was added iPr$_2$NEt (1.2 mL, 6.92 mmol, 1.6 equiv). The reaction mixture was cooled to 0 °C before the addition of triphenylphosphine dichloride (2.16 g, 6.49 mmol, 1.5 equiv). The mixture was maintained at 0 °C for 30 min or until judged complete by TLC (ca. 25 to 40 min). Upon completion the reaction mixture was loaded directly onto a silica gel packed column and purified (gradient, 0 to 10%, EtOAc in hexanes) to afford 1.7 g (96%) of **2.130** as a white solid: R$_f$: 0.71 (2:1 hexanes/EtOAc); IR (thin-film): 2968, 1598, 1482 cm^{-1}; ^{1}H NMR (400 MHz, CDCl$_3$) δ 6.91 (s, 1H), 6.68 (s, 2H), 6.35 (s, 1H), 5.89-5.78 (m, 1H), 4.94-4.89 (m, 2H), 4.59 (s, 2H), 4.42 (m, 1H), 3.78 (s, 6H), 3.19 (d, J = 6.0 Hz), 1.31 (d, J = 6.0 Hz, 6H); ^{13}C NMR (100 MHz, CDCl$_3$): 153.4, 150.5, 147.6, 136.8, 134.8, 132.9, 129.1, 119.7, 116.2, 115.7, 115.4, 106.1, 71.4, 56.5, 46.8, 34.2, 22.3; LRMS calculated for C$_{21}$H$_{25}$Cl$_2$O$_4$$^+$ [M+H]$^+$ m/z 411.1, measured LC/MS (ESI) R$_t$ 0.871 min, m/z 411.4 [M+H]$^+$.

2.131/2.132 To a solution of **2.130** (102 mg, 0.248 mmol) in CH$_3$CN (1 mL) was added K$_2$CO$_3$ (34.0 mg, 0.248 mmol, 1 equiv), CuI (52 mg, 0.273 mmol, 1.1 equiv) and Bu$_4$NI (91.6 mg, 0.248 mmol, 1 equiv). The reaction mixture was heated to 50 °C and maintained for 5 min followed by the addition of ethyl propiolate (54.0 μL, 0.496 mmol, 2 equiv). The reaction was maintained at 50 °C for 18 h, then was allowed to cool to room temperature. The reaction mixture was filtered through a plug of celite and filtrate was concentrated *in vacuo*. The crude residue was purified by flash column chromatography (silica gel, gradient 0 to 15% EtOAc in hexanes) to afford 107 mg (90%) of **2.131** and **2.132** as a yellow oil:

R$_f$ 0.3 (4:1 hexanes/EtOAc); ^{1}H NMR (400 MHz, CDCl$_3$) δ 6.90 (s, 1H), 6.60 (s, 2H), 6.33 (s, 1H), 5.85-5.80 (m, 1H), 4.94-4.89 (m, 2 H), 4.41 (sept , J = 6.0 Hz, 1H), 4.25 (q, J = 7.1 Hz, 2H), 3.77 (s, 6H), 3.75 (s, 2H), 3.19 (d, J = 6.5 Hz, 2H), 1.30 (d, J = 6.0 Hz, 6H); ^{13}C NMR (100 MHz, CDCl$_3$) δ 153.7, 153.4, 150.3, 147.6, 136.7, 131.8, 131.5, 129.1, 119.5, 116.0, 115.6, 115.3, 105.5, 85.9, 71.3, 62.0, 56.4, 34.1, 25.3, 22.2, 14.1; Dialogistic ^{1}H/^{13}C peaks for allenoate **2.132:** ^{1}H NMR (400 MHz, CDCl$_3$) δ 6.58 (s, 2H), 6.34 (s, 1H), 6.06 (d, J = 6.3 Hz, 1H); ^{13}C NMR (100 MHz, CDCl$_3$) δ 214.6, 99.0, 92.3.

2.133

2.133 To a 0 °C solution of freshly distilled TMS-acetylene (3.50 mL, 25.4 mmol, 5 equiv) in THF (31.0 mL) was added EtMgBr (11.2 mL, 20.2 mmol, 1.80 M in THF, 4 equiv) dropwise. The solution was allowed to warm to room temperature and maintained for 1 h. Then Cu(I)Br (0.868 g, 6.07 mmol, 1.2 equiv) was added. The resulting suspension was maintained at room temperature for 1 h, before the addition of chloride **2.130** (2.08 g, 5.06 mmol) in THF (20 mL). The reaction mixture was heated and maintained at 65 °C for 24 h. The reaction mixture was allowed to cool to room temperature, before the addition of saturated aq NH$_4$Cl (20 mL) and extraction with Et$_2$O (3 x 30 mL). The combined organic extracts were washed with saturated aq NH$_4$Cl (2 x 40 mL) and brine (45 mL). The washed extracts were dried (MgSO$_4$), filtered, and concentrated *in vacuo*. The residue was purified by flash column chromatography (gradient, 0 to 2 %, EtOAc in hexanes) to afford 1.89 g (80%) of **2.133** as a white solid: R$_f$: 0.42 (9:1 hexanes/EtOAc); IR (thin-film): 2967, 2176, 1598, 1488 cm^{-1}; ^{1}H NMR (400 MHz, CDCl$_3$) δ 6.91 (s, 1H), 6.67 (s, 2H), 6.36 (s, 1H), 5.86-5.79 (m,1H), 4.94-4.89 (m, 1H), 4.41 (m, 1H), 3.78 (s, 6H), 3.67 (s, 2H), 3.2 (d, J = 6 Hz, 2H), 1.30 (d, J = 6.0 Hz, 6H), 0.23 (s, 9H); ^{13}C NMR (100 MHz, CDCl$_3$) δ 153.1, 150.2, 147.8, 136.7, 133.7, 131.2, 128.9, 119.5, 116.0, 115.6, 115.3, 105.2, 104.1, 87.7, 71.3, 56.2, 34.1, 26.4, 22.2, 0.11; LRMS calculated for C$_{26}$H$_{34}$ClO$_4$Si$^+$ [M+H]$^+$ m/z 473.1, measured LC/MS (ESI) R$_t$ 1.21 min, m/z 473.6 [M+H]$^+$.

A7 To a solution of alkyne **2.133** (435 mg, 0.919 mmol) in MeOH (9 mL) and THF (0.919 mL) was added NaOMe (90 μL, 0.138 mmol, 1.52 M in MeOH, 0.15 equiv) dropwise. The solution was maintained at room temperature for 4 h before being concentrated *in vacuo*. The crude residue was purified by flash column chromatography (gradient, 0 to 3%, EtOAc in hexanes) to afford 350 mg (95%) of **A7** as a white solid: R_f: 0.41 (9:1 hexanes/EtOAc); IR (thin-film) 3292, 2973, 2251, 2118, 1597 cm^{-1}; ^{1}H NMR (400 MHz, CDCl3) δ 6.91 (s, 1H) 6.65 (s, 2H), 6.35 (s, 1H), 6.87-5.77 (m,1H), 4.91 (m, 2H), 4.41 (m, 1H), 3.78 (s, 6H), 3.62 (d, J = 2.6 Hz, 2H), 3.19 (d, J = 6Hz, 2H), 2.25 (t, J =2.6 Hz, 1H), 1.31 (d, J = 6.0 Hz, 6H), 0.23 (s, 9H); ^{13}C NMR (100 MHz, CDCl3) δ 153.3, 150.3, 147.8, 136.8, 133.5, 131.5, 129.1, 119.5, 116.1, 115.7, 115.3, 105.4, 81.8, 71.4, 71.0, 56.4, 34.2, 25.2, 22.3; LRMS calculated for $C_{23}H_{26}ClO_4^+$ [M+H]$^+$ m/z 401.1, measured LC/MS (ESI) R_t 0.880 min, m/z 401.6 [M+H]$^+$.

A8 To a -78 °C solution of **A7** (0.669 g, 1.66 mmol) in THF (20 m) was added n-BuLi (0.842 mL, 1.68 mmol, 1.05 equiv) dropwise over 5 min. The reaction mixture was maintained at -78 °C for 5 min, then $CO_{2\,(g)}$ was bubbled through the mixture for 10 min. The reaction was allowed to slowly warm to room temperature over 2 h, while under an atmosphere of $CO_{2\,(g)}$. Upon completion as judged by LCMS (ca. 2.5 h), the reaction was quenched with 1 N HCl (15 mL) and extracted with Et$_2$O (3 x 20 mL), the organic extracts were combined, washed with brine (25 mL), dried (MgSO$_4$), and concentrated *in vacuo*. The crude oil as purified by column chromatography (gradient, 0 to 20% MeOH in DCM) to afford 0.590 g (80%) of **A8** as a yellow foam: R_f: 0.48 (4:1 DCM/MeOH); IR (thin-film): 3424, 2970, 2237, 1687, 1613, 1482 cm^{-1}; ^{1}H NMR (400 MHz, CDCl$_3$) δ 9.61 (bs, 1H), 6.90 (s, 1H), 6.59 (s, 2H), 6.33 (s, 1H), 5.84-5.78 (m, 1H), 4.94-4.89 (m, 2 H), 4.41 (m, 1H), 3.77 (s, 8H), 3.29 (d, J = 6.4 Hz, 2H), 1.30 (d, J = 6.0 Hz, 6 H); ^{13}C NMR (100 MHz, CDCl$_3$): 157.6, 153.5, 150.4, 147.7, 136.7, 132.0, 131.1, 129.2, 119.6, 116.1, 115.8, 115.4, 105.6, 89.1, 71.5, 56.5, 34.2, 25.5, 22.3; LRMS calculated for $C_{23}H_{26}ClO_4^+$ [M+H]$^+$ m/z 445.1, measured LC/MS (ESI) R_t 0.705 min, m/z 445.6 [M+H]$^+$.

2.131 To a solution of acid **A9** (0.550 mg, 1.24 mmol, 1 equiv) in MeOH (3.00 mL) was added SOCl$_2$ (50.0 μL, 0.620 mmol, 0.5 equiv). The reaction mixture was maintained at room temperature, until judged complete by TLC (ca. 5 h), before concentration *in vacuo*. The crude residue was purified by column chromatography (gradient, 0 to 20%, EtOAc in hexanes) to afford 0.460 g (80%) of **2.131** as a yellow foam: R$_f$: 0.27 (4:1 hexanes/EtOAc); IR (thin-film): 2963, 2240, 1714, 1598, 1482 cm^{-1}; ^{1}H NMR (400 MHz, CDCl$_3$) δ 6.90 (s, 1H), 6.59 (s, 2H), 6.32 (s, 1H), 5.86-5.76 (m, 1 H), 4.92 (m, 2H), 4.41 (m, 1H), 3.80 (s, 3 H), 3.77 (s, 6 H), 3.75 (s, 2H), 3.19 (d, *J* = 6.8 Hz, 2 H), 1.30 (d, *J* = 6.0 Hz, 6 H); ^{13}C NMR (100 MHz, CDCl$_3$): 154.2, 153.5, 150.4, 147.7, 136.8, 132.0, 131.4, 129.1, 119.6, 116.1, 115.7, 115.4, 105.6, 86.5, 74.9, 71.4, 56.5, 52.8, 34.2, 25.4, 22.3; LRMS calculated for C$_{25}$H$_{28}$ClO$_6^+$ [M+H]$^+$ m/z 459.1, measured LC/MS (ESI) R$_t$ 0.870 min, m/z 459.6 [M+H]$^+$.

2.134 To a suspension of Cu(I)CN (0.112 g, 1.26 mmol, 1.2 equiv) in THF (5.0 mL) at -78 °C was added n-BuLi (1.26 mL, 2.53 mmol, 2.4 equiv, 2 M in hexanes) dropwise. The suspension was warmed to - 40 °C for ten minutes and then cooled to -78 °C, this warming and cooling process was repeated until the reaction solution is homogenous (ca. 3 cycles). Once homogenous, Bu$_3$SnH (0.680 mL, 2.53 mmol, 2.4 equiv) was added dropwise over 5 min and the reaction was stirred at -78 °C for 25 minutes (bright yellow solution). Once the solution is bright yellow, **2.131** (0.485 g, 1.05 mmol) was added as a solution in MeOH (4.6 mL, 2.74 mmol, 2.6 equiv, 0.65 M in THF) over ten minutes. The reaction mixture was maintained at -78 °C until judged complete by TLC (ca. 2 h), and quenched at -78 °C with saturated aq NH$_4$Cl (6 mL). The reaction mixture was allowed to slowly warm to room temperature and maintained until the aqueous layer is deep blue in color. The reaction was extracted with Et$_2$O (3 x 15 mL) and the organic extracts were combined and washed with saturated aq NH$_4$Cl (2 x 20 mL) and brine (20 mL). The washed extracts were dried (MgSO$_4$), filtered and concentrated *in vacuo*. The crude residue was purified by flash column chromatography (10:1 Silica gel/K$_2$CO$_3$ packing material: gradient, 0 to 3% EtOAc in hexanes) to afford 0.480 g (61%) of **2.134** as a clear oil: R$_f$: 0.41 (4:1 hexanes/EtOAc); IR (thin-film): 2926, 1711, 1593, 1490 cm^{-1}; ^{1}H NMR (400 MHz, CDCl$_3$) δ 6.90 (s, 1H), 6.46 (s, 2H), 6.34 (s, 1H), 6.12 (s, 1H), 5.84-5.76 (m, 1 H), 4.90 (m,

2 H), 4.41 (m, 1H), 4.27 (s, 2H), 3.76 (s, 3 H), 3.74 (s, 6 H), 3.17 (d, J = 6.4 Hz, 2H), 1.40-1.30 (m, 6 H), 1.30 (d, J = 6.0 Hz, 6H), 1.28-1.22 (m, 7 H), 0.86 (t, J = 7.4 Hz, 9 H), 0.80-0.77 (m, 5 H); ^{13}C NMR (100 MHz, CDCl$_3$) δ 170.9, 165.0, 153.2, 150.2, 147.9, 136.9, 136.8, 131.4, 129.0, 128.1, 119.5, 116.1, 115.7, 115.2, 106.7, 71.3, 56.3, 51.1, 41.3, 34.3, 29.0, 27.4, 22.3, 13.7, 10.4; LRMS calculated for C$_{37}$H$_{56}$ClO$_6$Sn$^+$ [M+H]$^+$ m/z 751.2, measured LC/MS (ESI) R$_t$ 1.40 min, m/z 751.2 [M+H$^+$.

A9 To a -78 °C solution of **2.134** (0.267 mg, 0.331 mmol) in DCM (7 mL) was added DIABL (0.828 mL, 0.828 mmol, 2.5 equiv, 1 M in hexanes), the solution was maintained at -78 °C for 1 h, then DIBAL (0.331 mL, 0.331 mmol, 1 equiv, 1 M in hexanes) was added. The solution was warmed and maintained at − 15 °C for 20 minutes, before addition of saturated aq Rochelle's salt (10 mL). The biphasic solution was maintained at room temperature overnight with vigorous stirring. The layers were separated and the aqueous layer was extracted with DCM (3 x 15 mL). The combined organic was washed with brine (30 mL), dried (Na$_2$SO4), filtered and concentrated *in vacuo*. The crude residue was purified by column chromatography (gradient, EtOAc in hexanes: 0-30%) to afford 191 mg (80%) of **A9** as a yellow oil: R$_f$: 0.2 (4:1 hexanes/EtOAc); IR (thin-film): 3376, 2930, 1592, 1481 cm^{-1}; ^{1}H NMR (400 MHz, CDCl$_3$) δ 6.89 (s, 1H), 6.42 (s, 2H), 6.34 (s, 1H), 5.96 (t, J = 6.1 Hz, 1H), 5.84-5.77 (m,1H), 4.90 (m, 2H), 4.41 (m, 3H), 3.75 (s, 3 H), 3.65 (s, 2H), 3.18 (d, J = 6 Hz, 2H), 1.43-1.23 (m, 19 H), 0.88-0.77 (m, 14H); ^{13}C NMR (100 MHz, CDCl$_3$) δ 153.2, 150.3, 147.9, 146.3, 137.8, 136.8, 131.3, 129.1, 119.6, 116.2, 115.8, 115.3, 106.3, 71.4, 59.3, 56.4, 39.7, 34.4, 29.2, 27.5, 22.3, 13.8, 10.0; LRMS calculated for C$_{26}$H$_{56}$ClO$_5$Sn$^+$ [M+H]$^+$ m/z 723.2, measured LC/MS (ESI) R$_t$ 1.43 min, m/z 705.6 [M-H$_2$O]$^+$.

2.135 To a 0 °C solution of **A9** (317 mg, 0.439 mmol, 1 equiv) in THF (9.0 mL) was added CuCl$_2$ (1.18g, 8.78 mmol, 20 equiv). The reaction mixture was allowed to slowly warm to room temperature and maintained until completion, as judged by TLC (ca. 18 h). The reaction was quenched by the addition of saturated aq NH$_4$Cl (20 mL). The solution was extracted with diethyl ether (3 x 30 mL), washed with saturated aq NH$_4$Cl (2 x 30 mL) and brine (40 mL),

dried (Na$_2$SO$_4$), filtered and concentrated *in vacuo*. The crude residue was purified by flash column chromatography (gradient, 0 to 30% EtOAc in hexanes) to afford 154 mg (75%) of **2.135** as a clear oil: R$_f$ 0.2 (3:1 hexanes/EtOAc,); IR (thin-film): 3404, 2972, 1597, 1488 cm^{-1}; ^{1}H NMR (400 MHz, CDCl$_3$) δ 6.90 (s, 1H), 6.53 (s, 2H), 6.34 (s, 1H), 6.05 (t, *J* = 7.3 Hz, 1H), 5.81-5.77 (m, 1H), 4.93-4.89 (m, 2H), 4.41 (m, 1H), 4.30 (d, *J* = 7.3 Hz, 2H), 3.76 (s, 6 H), 3.73 (s, 2 H), 3.19 (d *J* = 6.4 Hz, 2 H), 1.30 (d, *J* = 6.0 Hz, 6 H); ^{13}C NMR (100 MHz, CDCl$_3$) δ 153.3, 150.3, 147.8, 136.78, 136.70, 134.2, 131.9, 129.1, 128.0, 119.6, 116.2, 115.8, 115.4, 106.2, 71.44, 59.1, 56.5, 40.6, 34.2, 22.3; LRMS calculated for C$_{24}$H$_{29}$Cl$_2$O$_5$$^+$ [M+H]$^+$ m/z 467.1, measured LC/MS (ESI) R$_t$ 0.752 min, m/z 449.6 [M-H$_2$O]$^+$.
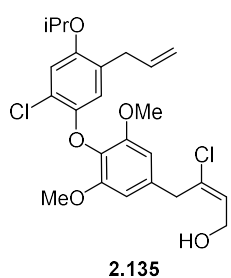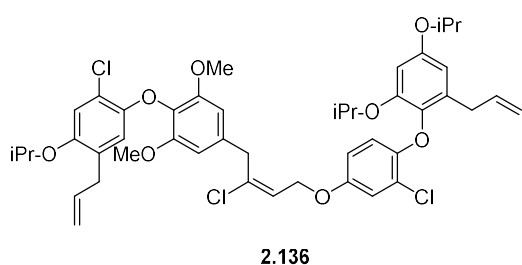
2.136

2.136 To a 0 °C solution of alcohol **2.135** (175 mg, 0.374 mmol), phenol **2.87** (211 mg, 0.561 mmol, 1.50 equiv) and Ph$_3$P (147 mg, 0.561 mmol, 1.50 equiv) in DCM (2.00 mL) was added a solution of diethyl azodicarboxylate (0.478 mL, 1.05 mmol, 40 wt. % in toluene, 1.50 equiv) at a rate of ca. 1 drop every 2 min. Following the addition, the reaction mixture was maintained at 0 °C for 30 min, then was allowed to warm to room temperature and maintained until judged complete by TLC (ca. 15 - 30 min). The reaction mixture was loaded directly onto a silica gel column and purified (silica gel, gradient elution, 0-10% EtOAc in hexanes) to afford 233 mg (75%) of ether **2.136** as a white foam: R$_f$ 0.56 (3:1 hexanes/EtOAc); IR (thin-film): 3068, 2971, 1595, 1478 cm^{-1}; ^{1}H NMR (400 MHz, CDCl$_3$) δ 7.01 (d, J = 2.9 Hz, 1H), 6.91 (s, 1H), 6.62 (dd, J = 9.0, 2.9 Hz, 1H), 6.54 (s, 2H), 6.48 (d, J = 9.0 Hz, 1H), 6.42 (m, 2H), 6.36 (s, 1H), 6.12 (t, J = 7.0 Hz, 1H), 5.91-5.77 (m, 2H), 5.07-5.00 (m, 2H), 4.93-4.89 (m, 2H), 4.58 (d, J = 7.0 Hz, 2H), 4.54-4.47 (m, 1H), 4.44-4.38 (m, 2H), 3.77 (s, 2 H), 3.74 (s, 6H), 3.30 (d, J = 6.7 Hz, 2H), 3.20 (d, J = 6.4 Hz, 2H), 1.34 (d, J = 6.0 Hz, 6H), 1.31 (d, J = 6.0 Hz, 6H) 1.14 (d, J = 6.0 Hz, 6H); ^{13}C NMR (100 MHz, CDCl3) δ 155.4, 153.3, 152.6, 151.0, 150.2, 149.2, 147.7, 138.4, 136.8, 136.6, 136.2, 134.9, 133.8, 131.8, 129.0, 124.1, 122.5, 119.5, 116.4, 116.3, 116.1, 115.7, 115.6, 115.4, 113.7, 108.5, 106.2, 103.6, 71.6, 71.3, 70.3, 64.7, 56.4, 40.8, 34.4, 34.1, 22.2, 22.1, 22.0; LRMS calculated for C$_{45}$H$_{51}$Cl$_3$O$_8$$^+$ [M+H]$^+$ m/z 825.2, measured LC/MS (ESI) R$_t$ 1.22 min, m/z 825.6 [M+H]$^+$.

2.139 To a degassed solution of diene **2.136** (55.0 mg, 0.066 mmol) in DCE (21.0 mL) was added a solution of Grubbs C633 catalyst (**2.137**) (ca. 9 mg, 0.014 mmol, 16.0 mol %) in DCE (1.00 mL). The solution was frozen and placed under vacuum (ca. 0.01 torr) for ca. 10 min, the reaction vessel was sealed under vacuum and allowed to slowly warm to room temperature. Once the flask was at room temperature, the reaction was heated and maintained at 60 °C for 24 h. The reaction was allowed to cool to room temperature and quenched by the addition of ethyl vinyl ether (100 µL). The solution was concentrated *in vacuo* and purified by flash column chromatography (silica gel, gradient elution, 0-10% EtOAc in hexanes) to afford 39.0 mg (74%) of macrocycle **2.139** as a white foam: R_f 0.48 (3:1 hexanes/EtOAc); IR (thin-film): 2975, 2930, 1594, 1483, 1382 cm^{-1}; ^{1}H NMR (400 MHz, CDCl$_3$) δ 6.96 (d, J = 2.8 Hz, 1H), 6.87 (s, 1H), 6.59 (dd, J = 9.0, 2.9 Hz, 1H), 6.38 (m, 2H), 6.36 (s, 2H), 6.32 (d, J = 2.7 Hz, 2H), 6.14 (s, 1H), 6.10 (t, J = 6.7 Hz, 1H), 5.55-5.51 (m, 1H), 5.40-5.33 (m, 1H), 4.56 (d, J = 6.8 Hz, 2H), 4.45-4.38 (m, 3H), 3.77 (s, 2H), 3.67 (s, 6H), 3.26 (d, J = 7.2 Hz, 2H), 3.08 (d, J = 7.2 Hz, 2H), 1.34 (d, J = 6.0, 6H), 1.31 (d, J = 6.0 Hz, 6H), 1.14 (d, J = 6.0 Hz, 6H); ^{13}C NMR (100 MHz, CDCl$_3$) δ 155.6, 153.4, 152.5, 151.0, 150.3, 149.5, 147.5, 137.0, 136.3, 135.5, 133.6, 131.5, 129.7, 129.1, 127.5, 125.8, 122.5, 119.2, 118.2, 115.6, 115.37, 115.31, 114.2, 108.5, 105.7, 104.0, 71.9, 71.1, 70.4, 66.0, 56.4, 40.8, 28.9, 27.5, 22.3, 22.2, 22.1; LRMS calculated for C$_{43}$H$_{47}$Cl$_3$O$_8$$^+$ [M+H]$^+$ m/z 797.2, measured LC/MS (ESI) R_t 1.10 min, m/z 797.6 [M+H]$^+$.
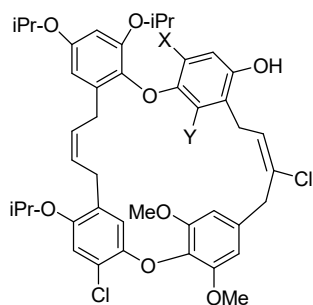
X=Cl, Y=H: **2.140**
X=H, Y=Cl: **2.141**

Phenols 2.140 and 2.141 To a solution of **2.139** (67.0 mg, 0.084 mmol) in DCE (16.0 mL) was added BF$_3$·Et$_2$O (502 µL, 0.251 mmol, 0.5 M in DCE, 3.00 equiv) dropwise. The reaction was heated and maintained at 70 °C for 2 h. The reaction was allowed to cool to room temperature and quenched by the addition of brine (10 mL). The reaction mixture was extracted with EtOAc (3 x 10 mL), and the combined organic extracts washed with brine (15 mL). The washed organic extracts were dried (MgSO$_4$), filtered and concentrated *in vacuo* to afford the ~27.0 mg (40%) of an inseparable mixture of phenols **2.140** and **2.141,** which were used, as is, in the

174

subsequent step: R_f 0.41 (3:1 hexanes/EtOAc); LRMS calculated for $C_{43}H_{47}Cl_3O_8^+$ [M+H]$^+$ m/z 797.2, measured LC/MS (ESI) R_t 1.00 min, m/z 796.2 [M+H]$^+$.
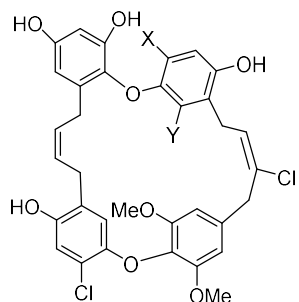
X=Cl, Y=H: **VU0848355**

X=H, Y=Cl: **VU0848354**

VU0848355 and VU0848354 To a -78 °C solution of phenols **2.140** and **2.141** (24.0 mg, 0.030 mmol) in DCM (1.00 mL) was added a solution of BCl$_3$ (120 μL, 0.120 mmol, 1 M in DCM, 4.00 equiv) dropwise. The reaction mixture was allowed to warm to room temperature slowly over 1 h and maintained at room temperature until judged complete by TLC (ca. 2-4 h). The reaction was diluted with brine (2 mL) and extracted with EtOAc (4 x 10 mL). The combined organic extracts were washed with brine (5 mL), dried (Na$_2$SO$_4$), filtered, and concentrated *in vacuo*. The crude residue (~17 mg) was purified by Gilson preparative HPLC (13-80% CH$_3$CN in H$_2$O, over 6 min) to afford 7.00 mg (35%) of **VU0848355** and 8 mg (40%) of **VU0848354**.

VU0848355: R_f 0.31 (10% methanol/DCM); ^{1}H NMR (400 MHz, CD$_3$OD) δ 6.86 (s, 1H), 6.76 (s, 1 H), 6.35 (s, 1H), 6.25 (d, *J* = 2.8 Hz, 1H), 6.18 (t, *J* = 8.6 Hz, 1H), 6.10 (d, *J* = 2.8 Hz, 1H), 6.08 (s, 1H), 5.56-5.55 (m, 2H), 3.62 (s, 2H), 3.53-3.50 (m, 8H), 3.19 (d, *J* = 6.8 Hz, 2H) 2.91 (apt d, *J* = 4.4 Hz, 2H); ^{13}C NMR (150 MHz, CD$_3$OD) 156.1, 154.3, 151.4, 150.7, 150.2, 148.7, 148.6, 136.7, 136.4, 135.8, 134.6, 132.3, 129.9, 128.39, 128.34, 127.8, 127.4, 120.6, 119.1, 117.4, 116.9, 116.2, 116.0, 107.7, 103.2, 56.4, 56.2, 40.8, 29.9, 28.7, 27.5; LRMS calculated for $C_{34}H_{29}Cl_3O_8^+$ [M+H]$^+$ m/z 671.1, measured LC/MS (ESI) R_t 1.16 min, m/z 671.4 [M+H]$^+$.

VU0848354: R_f 0.24 (10% methanol/DCM); ^{1}H NMR (600 MHz, CD$_3$OD) δ 6.78 (s, 1H), 6.56 (d, J = 9.0 Hz, 1H), 6.37 (m, 3H), 6.26-6.25 (m, 2H), 6.23 (s,1H), 6.13 (d, *J* = 3.0 Hz, 1H), 5.73-5.70 (m, 1H), 5.47-5.43 (m, 1H), 3.86 (s, 2H), 3.70 (d, *J* = 7.8 Hz, 2H), 3.56 (s, 6H), 3.25 (d, *J* = 7.8 Hz, 2H), 2.86 (d, J = 7.2 Hz, 2H); ^{13}C NMR (150 MHz,) δ 154.9, 152.8, 150.4, 150.2, 148.9, 147.2, 146.9, 135.4, 135.1, 133.2, 132.6, 130.3, 129.5, 127.3, 126.0, 125.4, 121.4, 118.0, 115.3, 114.2, 112.5, 111.3, 106.9, 105.3, 101.5, 55.1, 41.0, 27.9, 26.7, 26.0; LRMS calculated for $C_{34}H_{29}Cl_3O_8^+$ [M+H]$^+$ m/z 671.1, measured LC/MS (ESI) R_t 1.23 min, m/z 671.4 [M+H]$^+$.
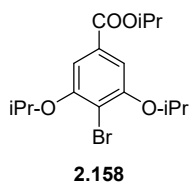
2.158 To a solution of 4-bromo-3,5-dihydroxybenzoic acid (40.0 g, 171 mmol) in DMF (600 mL) was added potassium carbonate (94.8 g, 686 mmol, 4.00 equiv), tetrabutylammonium iodide (6.00 g, 17.6 mmol, 10.0 mol %), and 2-bromopropane (75.0 mL, 858 mmol, 5.00 equiv). The suspension was heated and maintained at 50 °C for 72 h. Upon completion, as judged by TLC (ca. 48-72 h), the reaction mixture was allowed to cool to room temperature, diluted with water (600 mL) and extracted with EtOAc (3 x 400 mL). The combined organic extracts were washed with brine (3 x 200 mL), dried (MgSO$_4$), filtered and concentrated *in vacuo*. The crude residue was purified by flash column chromatography (silica gel, gradient elution, 0-20%, EtOAc in hexanes) to afford 57.3 g (92%) of ester **2.158** as a yellow oil: R$_f$ 0.80 (2:1 hexanes/EtOAc); IR (thin-film): 2975, 1716, 1580 cm^{-1}; ^{1}H NMR (400 MHz, CDCl$_3$) δ 7.20 (s, 2H), 5.24-5.18 (m, 1H), 4.65-4.59 (m, 2H), 1.38-1.34 (m, 18H); ^{13}C NMR (100 MHz, CDCl$_3$) δ 165.6, 155.8, 130.6, 110.7, 108.6, 72.3, 68.8, 22.0, 21.9; LRMS calculated for C$_{16}$H$_{23}$BrO$_4^+$ [M+H]$^+$ m/z 359.0, measured LC/MS (ESI) R$_t$ 0.941 min, m/z 359.4 [M+H]$^+$.
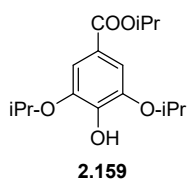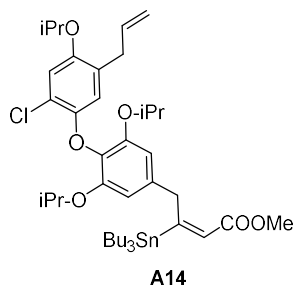
2.159 To a -90 °C solution of bromide **2.158** (59.4 g, 165 mmol) in THF (470 mL) was added a solution of n-BuLi (72.0 mL, 173 mmol, 2.4 M in hexanes, 1.05 equiv) dropwise over 1 h. The reaction mixture was maintained at -90 °C for 1 h, then B(OMe)$_3$ (36.9 mL, 331 mmol, 2.00 equiv) was added over 10 min. The reaction mixture was allowed to slowly warm to room temperature and maintained for 18 h. Solutions of H$_2$O$_2$ (55.0 mL, 529 mmol, aqueous 30%, 3.00 equiv) and NaOH (165 mL, 165 mmol, 1 M, 1.00 equiv) were added. The mixture was allowed to stir for 20 min, neutralized with 1M HCl (165 mL) and extracted with ether (3 x 250 mL). The organic layers were combined, washed with brine (400 mL), dried (MgSO$_4$), filtered and concentrated *in vacuo*. The crude residue was purified by flash column chromatography (silica gel, gradient elution, 0-10% EtOAc in hexanes) to afford 29.6 g (60%) of **2.159** as a yellow oil: R$_f$ 0.39 (4:1 hexanes/EtOAc); IR (thin-film): 3414, 1699 cm^{-1}; ^{1}H NMR (400 MHz, CDCl$_3$) δ 7.27 (s, 2H), 6.06 (s, 1H, exchanges with D$_2$O), 5.21-5.17 (m, 1H); 4.63-4.58 (m, 2H); 1.34-1.32 (m, 18H); ^{13}C NMR (150 MHz, CDCl$_3$) δ 165.9, 144.9, 141.8, 121.6, 110.0, 72.1, 68.1, 22.1, 21.9; LRMS calculated for C$_{16}$H$_{24}$O$_5^+$ [M+H]$^+$ m/z 297.1, measured LC/MS (ESI) R$_t$ 0.550 min, m/z 297.5 [M+H]$^+$.
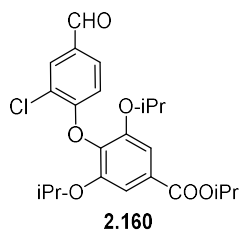
2.160 To a solution of **2.159** (14.5 g, 48.8 mmol) in DMF (122 mL,) was added K$_2$CO$_3$ (13.5 g, 97.6 mmol, 2.00 equiv) followed by 3-chloro-4-fluorobenzaldehyde (**2.61**) (7.74 g, 48.8 mmol, 1.00 equiv). The resulting suspension was heated and maintained at 120 °C for 18 h. Upon completion, as judged by LCMS analysis (ca. 16-18 h), the reaction was allowed to cool to room temperature and diluted with water (200 mL). The crude reaction mixture was extracted with EtOAc (3 x 200 mL). The combined organic extracts were washed with water (2 x 200 mL) and brine (2 x 200 mL), dried (MgSO$_4$), filtered, and concentrated *in vacuo*. The resulting residue was purified by flash column chromatography (silica gel, gradient elution, 0-10% EtOAc in hexanes) to afford 19.8 g (90%) of biaryl ether **2.160** as a yellow oil: R$_f$ 0.44 (4:1 hexanes/EtOAc); IR (thin-film) 2979, 2933, 1706, 1589, 1479, 1369, 1243 cm^{-1}; ^{1}H NMR (400 MHz, CDCl$_3$) δ 9.85 (s, 1H), 7.96 (d, J = 2.0 Hz, 1H), 7.58 (dd, J = 8.0, 2.0 Hz, 1H), 7.32 (s, 2H), 6.64 (d, J = 8.0 Hz, 1H), 5.27-5.21 (m, 1H), 4.58-4.52 (m, 2H), 1.38 (d, J = 6.4 Hz, 6H); 1.20 (d, J = 6.4 Hz, 12H); ^{13}C NMR (100 MHz, CDCl$_3$) δ 189.8, 165.5, 158.9, 151.2, 138.5, 131.7, 131.4, 129.4, 128.6, 123.9, 115.5, 110.2, 72.4, 68.9, 22.07, 22.04; LRMS calculated for C$_{23}$H$_{27}$ClO$_6^+$ [M+H]$^+$ m/z 435.1, measured LC/MS (ESI) R$_t$ 0.955 min, m/z 435.0.
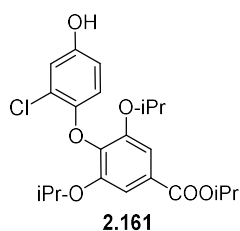
2.161 To a 0 °C solution of aldehyde **2.160** (8.34 g, 19.2 mmol) in DCM (100 mL) was added m-CPBA (6.60 g, 38.4 mmol, 2.00 equiv) in three portions over 15 min. The reaction mixture was allowed to warm to room temperature and maintained for 7 h, or as judged complete by LCMS (ca. 7-8 h). The reaction was quenched by the addition of saturated aq sodium thiosulfate (100 mL) and saturated aq NaHCO$_3$ (100 mL). The reaction mixture was extracted with Et$_2$O (3 x 75 mL) and the combined organic extracts washed with saturated aq NaHCO$_3$ (3 x 100 mL) and brine (200 mL). The washed extracts were dried (MgSO$_4$), filtered and concentrated *in vacuo*. The crude formate was dissolved in MeOH (50 mL) and thionyl chloride (251 μL, 3.44 mmol, 15.0 mol %) was added. The solution was maintained at room temperature for 5 h or until judged complete by LCMS analysis. Upon completion, silica gel (~10.0 g) was added and the reaction mixture was concentrated *in vacuo*. The silica was dry loaded and purified by flash column chromatography (silica gel, gradient elution, 0-20% EtOAc in hexanes) to afford 4.75 g (60%) of **2.161** as a yellow oil: R$_f$ 0.45 (4:1 EtOAc/hexanes); IR (thin-film): 3397, 2980, 1693, 1593 cm^{-1}; ^{1}H NMR (400

177

MHz, CDCl$_3$) δ 7.31 (s, 2H), 6.92 (d, J = 2.8 Hz, 1H), 6.51 (dd, J = 8.0, 2.8 Hz, 1H), 6.42 (d, J = 8.0 Hz, 1H), 6.16 (s, 1H, exchanges with D$_2$O), 5.29-5.20 (m, 1H), 4.58-4.48 (m, 2H), 1.38 (d, J = 6.0 Hz, 6H), 1.19 (d, J = 6 Hz, 12H); ^{13}C NMR (100 MHz, CDCl$_3$) δ 166.4, 151.4, 151.0, 148.1, 140.8, 127.1, 123.3, 117.0, 116.7, 114.1, 110.7, 72.3, 69.2, 22.0; LRMS calculated for C$_{22}$H$_{27}$ClO$_6$$^+$ [M+H]$^+$ m/z 423.1, measured LC/MS (ESI) R$_t$ 0.742 min, m/z 423.6 [M+H]$^+$.

2.162

2.162 To a solution of phenol **2.161** (4.7 g, 11.11 mmol) in DMF (37 mL) was added cesium carbonate (7.23 g, 22.2 mmol, 2 equiv) and tetrabutylammonium iodide (0.400 g, 1.11 mmol, 0.1 equiv), followed by allyl bromide (1.69 mL, 19.4 mmol, 1.8 equiv). The reaction mixture was allowed to stir at room temperature for 18 h. The reaction was then diluted with water (100 mL) and extracted with EtOAc (3 x 40 mL). The combined organic extracts were washed with aqueous satd. NH$_4$Cl (100 mL), brine (100 mL), dried (MgSO$_4$), filtered and concentrated *in vacuo*. The crude residue was purified by flash column chromatography (gradient, 0 to 10% EtOAc/hexanes) to afford 4.65 g, (90%) of **2.162** as a yellow oil: R$_f$ 0.58 (4:1 EtOAc/hexanes); IR (thin-film): 3082, 2989, 1727, 1602, 1494 cm^{-1}; ^{1}H NMR (CDCl$_3$, 400 MHz) δ 7.31 (s, 2 H), 6.98 (d, J = 2.8 Hz, 1H), 6.60 (dd, J = 8.8, 2.8 Hz, 1H), 6.50 (d, J = 8.8 Hz, 1H), 6.02-5.95 (m, 1H), 5.36 (dd, J = 17.2, 0.8 Hz, 1 H), 5.26-5.21 (m, 2H), 4.55 (m, 2 H), 4.45 (d, J = 5.2 Hz, 2 H), 1.36 (d, J = 6.4 Hz, 6 H), 1.20 (d J = 6.0 Hz, 12 H); ^{13}C NMR (CDCl$_3$, 100 MHz) δ 165.6, 153.5, 151.3, 148.5, 140.5, 133.0, 127.4, 123.3, 117.6, 116.4, 116.3, 113.6, 110.5, 72.0, 69.4, 68.6, 21.97, 21.95; LRMS calculated for C$_{25}$H$_{31}$ClO$_6$$^+$ [M+H]$^+$ m/z 463.1, measured LC/MS (ESI) R$_t$ 1.03 min, m/z = 463.6 [M+H]$^+$.
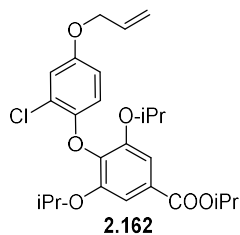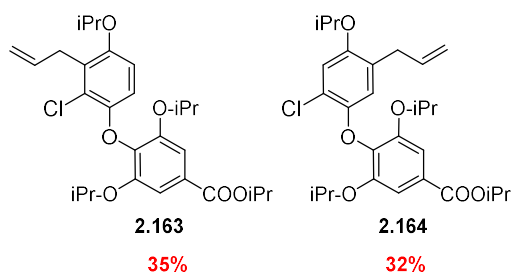
2.163
35%

2.164
32%

2.163 and **2.164** Allyl ether **2.162** (4.01 g, 8.64 mmol, 1 equiv) was added to a μW vial with degassed water (8.6 mL, 1 M). The tube was sealed and irradiated in a Biotage microwave reactor at 195 °C for 7 h. The crude reaction mixture was extracted with EtOAc (3 x 10 mL), washed with brine (20 mL), and dried (MgSO$_4$). The dried extracts were filtered and concentrated *in vacuo.* The crude reaction mixture (3.76 g, 8.12 mmol) in DMF (20 mL, 0.4 M) was added Cs$_2$CO$_3$ (8.00 g, 24.3 mmol, 3 equiv), potassium iodide

(4.04 g, 24.36 mmol, 3 equiv) and 2-bromopropane (2.28 mL, 24.3 mmol, 3 equiv). The suspension was heated to 50 °C and maintained for 18 h. The reaction mixture was allowed to cool to room temperature, diluted with water (80 mL), and extracted with Et$_2$O (3 x 45 mL). The combined organic extracts were washed with brine (100 mL), dried (MgSO$_4$), filtered and concentrated *in vacuo*. The crude mixture was purified by flash column chromatography (gradient, 0 to 5% EtOAc/hexanes) to afford 1.39 g (32%) of **2.164** and 1.45 g (35%) of **2.163** as yellow oils:

2.164: R$_f$ 0.46 (9:1 hexanes/EtOAc); IR (neat) 2977, 2253, 1722, 1588 cm^{-1}; ^{1}H NMR (400 MHz, CDCl$_3$) δ 7.30 (s, 2H), 6.90 (s, 1H), 6.38 (s, 1H), 5.81-5.74 (m, 1H), 5.24 (m, 1H), 4.93-4.89 (m, 2H), 4.56 (m, 2H), 4.43 (m, 1H), 3.17 (d, *J* = 6.8 Hz, 2 H); ^{13}C NMR (100 MHz, CDCl$_3$) δ 165.8, 151.4, 150.5, 148.0, 140.7, 136.5, 129.2, 127.3, 120.5, 117.6, 115.7, 115.5, 110.5, 72.0, 71.4, 68.7, 34.1, 22.1, 22.0; ; LRMS calculated for C$_{28}$H$_{37}$ClO$_6^+$ [M+H]$^+$ m/z 505.2, measured LC/MS (ESI) R$_t$ 1.23 min, m/z = 505.6, [M+H]$^+$.

2.163: R$_f$ 0.44 (9:1 hexanes/EtOAc); IR (neat) 2977, 2252, 1710, 1588 cm^{-1}; ^{1}H NMR (400 MHz, CDCl$_3$) δ 7.31 (s, 2H), 6.56 (d, *J* = 9.2 Hz, 1H), 6.40 (d, *J* = 9.2 Hz, 1H), 6.01-5.91 (m, 1H), 5.23 (m, 1H), 5.07 (dd, *J* = 17.2 Hz, 1.6 Hz, 1H), 5.00 (dd, *J* = 10 Hz, 1.6 Hz, 1H), 4.56 (m, 2H), 4.41 (m, 1H), 3.61 (d, *J* = 6.0 Hz, 2H), 1.37 (d, *J* = 6.0 Hz, 6 H), 1.28 (d, *J* = 6.0 Hz, 6H), 1.19 (d, *J* = 6.0 Hz, 12 H); ^{13}C NMR (100 MHz, CDCl$_3$) δ 165.8, 151.4, 151.0, 148.6, 141.6, 135.2, 129.1, 127.3, 124.3, 115.2, 113.4, 112.1, 110.8, 72.1, 71.2, 68.66, 31.8, 22.1, 22.06, 22.04; LRMS calculated for C$_{28}$H$_{37}$ClO$_6^+$ [M+H]$^+$ m/z 505.2, measured LCMS (ESI) R$_t$ 1.25 min, m/z = 505.6, [M+H]$^+$; HRMS.
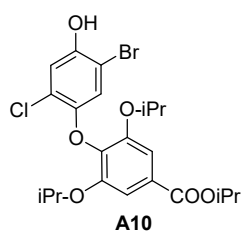
A10 To a solution of phenol **2.161** (4.00 g, 9.50 mmol) in methanol (24.0 mL) maintained in the dark was added a solution of NBS (1.68 g, 9.50 mmol, 1.01 equiv) in methanol (57.0 mL) over 30 min. After the completion of the addition, the reaction was maintained at room temperature until judged complete by LCMS analysis (ca. 5-10 min), then concentrated *in vacuo*. The crude residue was purified by column chromatography (silica gel, DCM) to afford 2.80 g (60%) of bromide **A10** as a white solid: R$_f$: 0.45 (4:1 hexanes/EtOAc), IR (thin-film): 3376, 2977, 1696, 1590 cm^{-1}; ^{1}H NMR (400 MHz, CDCl$_3$) δ 7.32 (s, 2H), 7.10 (s, 1H), 6.67 (s, 1H), 5.34 (s, 1H,

exchanges with D$_2$O), 5.28-5.22 (m, 1H), 4.61-4.55 (m, 2H), 1.39 (d, J = 6.4 Hz, 6H), 1.24 (d, J = 6.0 Hz, 12H); ^{13}C NMR (100 MHz, CDCl$_3$) δ 165.8, 151.3, 148.4, 147.5, 139.9, 127.9, 123.5, 118.8, 117.0, 110.3, 107.4, 72.2, 68.9, 22.0; LRMS calculated for C$_{22}$H$_{26}$BrClO$_6^+$ [M+H]$^+$ m/z 501.0, measured LC/MS (ESI) R$_t$ 0.869 min, m/z 501.5 [M+H]$^+$.
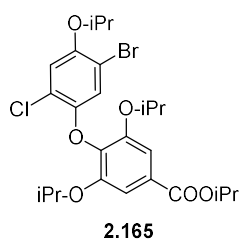
2.165

2.165 To a solution of phenol **A10** (3.50 g, 7.00 mmol) in DMF (2.50 mL) was added potassium carbonate (1.90 g, 14.0 mmol, 2.00 equiv), Bu$_4$NI (510 mg, 1.40 mmol, 10.0 mol %) and 2-bromopropane (1.30 mL, 14.0 mmol, 2.00 equiv). The reaction was maintained at room temperature for 18 h, before dilution with water (15.0 mL). The reaction mixture was extracted with ether (3 x 15 mL), washed with saturated aq NH$_4$Cl (15 mL) and brine (15 mL), dried (MgSO$_4$), filtered and concentrated *in vacuo*. The crude residue was purified by column chromatography (silica gel, gradient elution, 0-10% EtOAc in hexanes) to afford 3.30 g (87%) of **2.165** as a white solid: R$_f$ 0.45 (4:1 hexanes/EtOAc); IR (thin-film): 2979, 1714, 1591, 1474 cm^{-1}; ^{1}H NMR (400 MHz, CDCl$_3$) δ 7.31 (s, 2H), 7.00 (s, 1H), 6.75 (s, 1H), 5.28-5.21 (m, 1H), 4.61-4.55 (m, 2H), 4.47-4.41 (m, 1H), 1.38 (d, J = 6.4 Hz, 6H), 1.36 (d, J = 6.0 Hz, 6H), 1.23 (d, J = 6.0 Hz, 12H); ^{13}C NMR (100 MHz, CDCl$_3$) δ 165.7, 151.2, 149.7, 148.8, 139.7, 127.9, 122.2, 120.4, 118.4, 112.1, 110.2, 73.8, 72.0, 68.8, 22.1, 22.0; LRMS calculated for C$_{25}$H$_{32}$BrClO$_6^+$ [M+H]$^+$ m/z 543.1, measured LC/MS (ESI) R$_t$ 1.18 min, m/z 543.6 [M+H]$^+$.
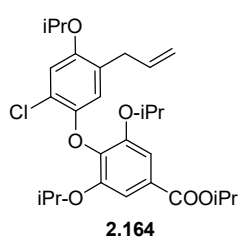
2.164

2.164 To a degassed solution of bromide **2.165** (2.57 g, 4.72 mmol), cesium fluoride (2.86 g, 18.8 mmol, 4.00 equiv) and allyl-Bpin (1.42 mL, 7.55 mmol, 1.60 equiv) in THF (20.0 mL) was added Pd(Ph$_3$P)$_4$ (382 mg, 0.330 mmol, 7.00 mol%). The reaction mixture was heated and maintained at 85 °C for 7 h, then allowed to cooled to room temperature. The reaction mixture was diluted with ether (20 mL) followed by water (30 mL), and extracted with ether (3 x 10 mL). The extracts were combined, washed with saturated aq NH$_4$Cl (2 x 10 mL) and brine (15 mL), dried (MgSO$_4$), filtered and concentrated *in vacuo*. The crude residue was purified by column chromatography (silica gel, gradient elution, 0-5% EtOAc in hexanes) to afford 2.15 g (86%) of **2.164** as a clear oil: R$_f$ 0.46 (9:1 hexanes/EtOAc); IR (neat) 2977, 2253, 1722, 1588 cm^{-1}; ^{1}H NMR (400 MHz, CDCl$_3$) δ 7.30 (s, 2H), 6.90 (s, 1H), 6.38 (s, 1H), 5.81-5.74 (m, 1H), 5.24 (m, 1H),

4.93-4.89 (m, 2H), 4.59-4.53 (m, 2H), 4.44-4.41 (m, 1H), 3.17 (d, $J = 6.8$ Hz, 2H), 1.38 (d, $J = 6.0$ Hz, 6H), 1.30 (d, $J = 6.0$ Hz, 6H), 1.20 (d, $J = 6.0$ Hz, 12H); ^{13}C NMR (100 MHz, CDCl$_3$) δ 165.8, 151.4, 150.5, 148.0, 140.7, 136.4, 129.2, 127.3, 120.5, 117.6, 115.7, 115.5, 110.5, 72.0, 71.4, 68.7, 34.1, 22.1, 22.0; LRMS calculated for C$_{28}$H$_{37}$ClO$_6$$^+$ [M+H]$^+$ m/z 505.2, measured LC/MS (ESI) R$_t$ 1.23 min, m/z 505.6 [M+H]$^+$.

A11 To a solution of ester **2.164** (1.52 g, 3.00 mmol) in DCM (15.0 mL) at -78 °C was added DIBALH (7.52 mL, 7.52 mmol, 1 M in hexanes, 2.50 equiv) dropwise. The reaction was maintained at -78 °C for 1 h, allowed to warm to -10 °C and stir for an additional 20 min, then slowly quenched by the addition of saturated aq Rochelle's salt (20.0 mL). The biphasic solution was allowed to stir at room temperature for 18 h. The reaction was extracted with DCM (3 x 25 mL). The combined organic extracts were washed with brine (40 mL), dried (MgSO$_4$), filtered and concentrated *in vacuo*. The crude residue was purified by flash column chromatography (silica gel, gradient elution, 0-20% EtOAc in hexanes) to afford 1.08 g (80%) of **A11** as a clear oil: R$_f$ 0.25 (2:1 hexanes/EtOAc); IR (thin-film) 3403, 3077, 2363, 1640, 1593 cm^{-1}; ^{1}H NMR δ 6.89 (s, 1H), 6.59 (s, 2H), 6.39 (s, 1H), 5.80-5.73 (m, 1H), 4.90-4.86 (m, 2H), 4.56 (s, 2H), 4.49-4.38 (m, 4H), 3.15 (d, $J = 6.4$ Hz, 2H), 2.82 (s, 1H, exchanges with D$_2$O), 1.26 (d, $J = 6.0$ Hz, 6H), 1.15 (d, $J = 6.0$ Hz, 12H); ^{13}C NMR (100 MHz, CDCl$_3$) δ 151.5, 150.0, 148.2, 138.0, 136.4, 135.6, 128.9, 120.0, 117.2, 115.6, 115.3, 107.8, 71.7, 71.3, 64.9, 34.1, 22.04, 22.02; LRMS calculated for C$_{25}$H$_{33}$ClO$_5$$^+$ [M+H]$^+$ m/z 449.2, measured LC/MS (ESI) R$_t$ 0.895 min, m/z 449.0 [M+H]$^+$.
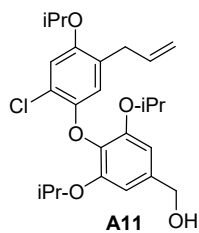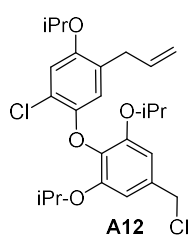
A12 To a solution of alcohol **A11** (2.57 g, 6.54 mmol) in acetonitrile (32.0 mL) was added diisopropylethylamine (1.13 mL, 19.6 mmol, 3.00 equiv). The solution was cooled to 0 °C, maintained for 10 min before triphenylphosphine dichloride (7.62 g, 22.8 mmol, 3.50 equiv) was added in one portion. The reaction mixture was maintained at 0 °C for 30 min, at which time it was judged complete by TLC (20-30 min). The reaction mixture was loaded directly on to a silica gel column for purification (gradient elution, 0-20%, EtOAc in hexanes) to afford 2.40 g (90%) of chloride **A12** as a white solid: R$_f$ 0.64 (9:1 hexanes/EtOAc); IR (thin-film): 2977, 1594, 1487 cm^{-1}; ^{1}H NMR (400 MHz, CDCl$_3$) δ 6.92 (s, 1H), 6.66 (s, 2H), 6.43 (s, 1H), 5.81-5.76 (m, 1H), 4.94-4.90 (m, 2H), 4.52 (s,

2H), 4.51-4.47 (m, 2H), 4.41-4.39 (m, 1H), 3.20 (d, $J = 6.4$ Hz, 2H), 1.28 (d, $J = 6.0$ Hz, 6H), 1.17 (d, $J = 6.0$ Hz, 12 H); ^{13}C NMR (150 MHz, CDCl$_3$) δ 151.5, 150.0, 148.0, 136.3, 136.2, 134.0, 128.8, 120.0, 117.2, 115.3, 115.2, 109.3, 71.5, 71.1, 46.4, 33.9, 21.9, 21.8; LRMS calculated for $C_{25}H_{32}Cl_2O_4^+$ [M+H]$^+$ m/z 467.1, measured LC/MS (ESI) R_t 1.13 min, m/z 467.0 [M+H]$^+$.
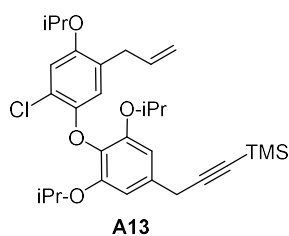
A13 To freshly distilled ethynyltrimethylsilane (1.94 mL, 13.9 mmol, 5.00 equiv) in THF (5.00 mL) at 0 °C was added ethylmagnesium chloride (5.56 mL, 11.1 mmol, 2 M in THF, 4.00 equiv) dropwise. The reaction was allowed to warm to room temperature and maintained for 1 h and CuBr (596 mg, 4.17 mmol, 1.50 equiv) was then added. The suspension was maintained at room temperature for an additional hour, before the addition of chloride **A12** (1.30 g, 2.78 mmol) as a solution in THF (10 mL). The reaction mixture was heated and maintained at 65 °C for 24 h. Upon completion of the reaction as judged by TLC (ca. 24 h) the reaction was allowed to cool to room temperature and quenched by the addition of saturated aq NH$_4$Cl (15 mL). The reaction mixture was extracted with ether (3 x 25 mL). The combined organic extracts were washed with saturated aq NH$_4$Cl (2 x 25 mL), brine (25 mL), dried (MgSO$_4$), filtered and concentrated *in vacuo*. The crude residue was purified by flash column chromatography (silica gel, gradient elution, 0-2% EtOAc in hexanes) to afford 1.35 g (92%) of alkyne **A13** as a yellow oil: R_f 0.72 (9:1 hexanes/EtOAc); IR (thin-film): 2177, 1594, 1486 cm^{-1}; ^{1}H NMR (400 MHz, CDCl$_3$) δ 6.90 (s, 1H), 6.64 (s, 2H), 6.41 (s, 1H), 5.85-5.75 (m, 1H), 4.94-4.90 (m, 2H), 4.51-4.40 (m, 3H), 3.62 (s, 2H), 3.19 (d, $J = 6.4$ Hz, 2H), 1.30 (d, $J = 6.0$ Hz, 6H), 1.20 (d, $J = 6.0$ Hz, 12H), 0.21 (s, 9H); ^{13}C NMR (100 MHz, CDCl$_3$) δ 151.5, 150.0, 148.3, 136.5, 135.1, 132.9, 129.0, 120.0, 117.2, 115.6, 115.3, 109.0, 104.3, 87.4, 71.7, 71.3, 34.2, 26.2, 22.15, 22.12, 0.12; LRMS calculated for $C_{30}H_{41}ClO_4Si^+$ [M+H]$^+$ m/z 529.2, measured LC/MS (ESI) R_t 1.39 min, m/z 529.0 [M+H]$^+$.
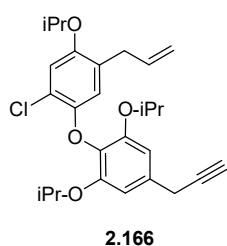
2.166 To a solution of **A13** (1.35 g, 2.55 mmol) in MeOH (7.00 mL) and THF (0.700 mL) was added a solution of NaOMe (0.165 mL, 0.142 mmol, 0.86 M in MeOH, 5.00 mol %). The reaction was allowed to stir at room temperature until judge complete by TLC (ca. 5 h), then concentrated *in vacuo*. The crude residue was purified by flash column chromatography (silica gel, gradient

elution, 0-4% EtOAc in hexanes) to afford 1.03 g (88%) of **2.166** as a yellow oil: R_f 0.58 (9:1 hexanes/EtOAc); IR (neat) 3297, 1593, 1484 cm^{-1}; ^{1}H NMR (400 MHz, CDCl$_3$) δ 6.90 (s, 1H), 6.62 (s, 2H), 6.40 (s, 1H), 5.83-5.74 (m, 1H), 4.93-4.90 (m, 2H), 4.52-4.46 (m, 2H), 4.43-4.40 (m, 1H), 3.57 (d, J = 2.4 Hz, 2H), 3.18 (d, J = 6.4 Hz, 2H), 2.22 (t, J = 2.8 Hz, 1H), 1.30 (d, J = 6.0 Hz, 6H), 1.19 (d, J = 6.0 Hz, 12H); ^{13}C NMR (100 MH, CDCl$_3$) δ 151.7, 150.2, 148.4, 136.7, 135.5, 132.7, 129.1, 120.1, 117.3, 115.7, 115.4, 109.3, 81.9, 72.0, 71.5, 70.8, 34.2, 25.0, 22.26, 22.21; LRMS calculated for C$_{27}$H$_{33}$ClO$_4$$^+$ [M+H]$^+$ m/z 457.2, measured LC/MS (ESI) R_t 1.12 min, m/z 457.0 [M+H]$^+$.

2.167

2.167 A solution of alkyne **2.166** (1.01 g, 2.21 mmol) in THF (30.0 mL) was cooled to -78 °C and a solution of n-BuLi (0.930 mL, 2.23 mmol, 2.4 M in hexanes, 1.01 equiv) added dropwise over 10 min. The reaction mixture was allowed to stir at -78 °C for 5 min, then carbon dioxide was bubbled through the solution while it was allowed to slowly warm to room temperature over 2 h. The reaction was maintained at room temperature until judge complete by LCMS (ca. 1 h), followed by acidification with 1M HCl (3 mL, 1 M). The acidified reaction mixture was extracted with EtOAc (4 x 20 mL), the organic extracts were combined, dried (MgSO$_4$), filtered and concentrated *in vacuo*. The crude residue was purified by flash column chromatography (silica gel, gradient elution, 0-30% MeOH in DCM) to afford 0.962 g (87%) of carboxylic acid **2.167** as an off-white foam: R_f 0.46 (4:1 DCM/Methanol); IR (thin-film): 3411-3074, 2985, 2243, 1710, 1061 cm^{-1}; ^{1}H NMR (400 MHz, CDCl$_3$) δ 9.83 (br s, 1H, exchanges with D$_2$O), 6.90 (s, 1H), 6.57 (s, 2H), 6.38 (s, 1H), 5.82-5.75 (m, 1H), 4.91-489 (m, 2H), 4.52-4.40 (m, 3H), 3.71 (s, 2H), 3.18 (d, J = 6.4 Hz, 2H), 1.30 (d, J = 6.0 Hz, 6H), 1.18 (d, J = 6.0 Hz, 12H); ^{13}C NMR (100 MHz, CDCl$_3$)[4] δ 151.9, 150.2, 148.3, 136.6, 135.8, 130.5, 129.2, 120.1, 117.3, 115.8, 115.5, 109.4, 72.1, 71.5, 34.2, 25.3, 22.2, 22.1; LRMS calculated for C$_{28}$H$_{33}$ClO$_6$$^+$ [M+H]$^+$ m/z 501.2, measured LC/MS (ESI) R_t 0.895 min, m/z 501.5 [M+H]$^+$.
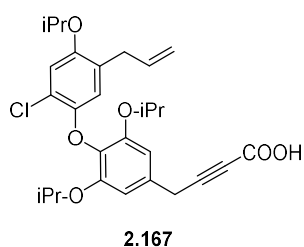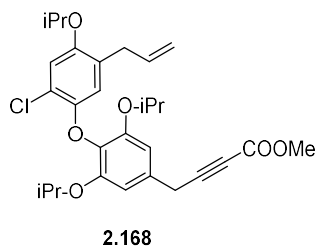
2.168 To a solution of carboxylic acid **2.167** (953 mg, 1.90 mmol, 1.00 equiv) in MeOH (5.00 mL) was added thionyl chloride (69.0 μL, 0.951 mmol, 0.500 equiv). The reaction was allowed to stir at room temperature for 4 h, then concentrated *in vacuo.* The crude residue was purified by flash column chromatography (silica gel, gradient elution, 0-20% EtOAc in hexanes) to afford 0.891 g (91%) of methyl ester **2.168** as a white foam: R_f 0.5 (4:1 hexanes/EtOAc); IR (thin-film): 3072, 2977, 2240, 1716, 1594 cm^{-1}; ^{1}H NMR (400 MHz, CDCl$_3$) δ 6.89 (s, 1H), 6.57 (s, 2H), 6.38 (s, 1H), 5.82-5.75 (m, 1H), 4.50-4.40 (m, 3H), 3.79 (s, 3H), 3.70 (s, 2H), 3.18 (d, *J* = 6.88 Hz, 2H), 1.30 (d, *J* = 6.0 Hz, 6H), 1.19 (d, *J* = 6.0 Hz, 12H); ^{13}C NMR (100 MHz, CDCl$_3$) δ 154.2, 151.9, 150.2, 148.3, 136.6, 135.8, 130.7, 129.2, 120.1, 117.3, 115.7, 115.4, 109.4, 86.7, 74.8, 72.0, 71.5, 52.8, 34.2, 25.2, 22.2, 22.1; LRMS calculated for C$_{29}$H$_{35}$ClO$_6$$^+$ [M+H]$^+$ m/z 515.2, measured LC/MS (ESI) R_t 1.10 min, m/z 515.6 [M+H]$^+$.

A14 To suspension of CuCN (200 mg, 2.24 mmol, 1.20 equiv) in THF (7.50 mL) at -78 °C was added a solution of n-BuLi (1.87 mL, 4.49 mmol, 2.4 M in hexanes, 2.40 equiv) dropwise. The mixture was warmed to -40 °C, maintained for 10 min and then cooled to -78 °C. The warming and cooling process are repeated until a homogenous solution is obtained (ca. 3 cycles), to the -78 °C solution, neat Bu$_3$SnH (1.20 mL, 4.49 mmol, 2.40 equiv) was then added dropwise and the reaction was maintained at -78 °C for 35 minutes (bright yellow solution). A solution of alkynoate **2.168** (890 mg, 1.72 mmol) in MeOH (7.40 mL, 4.79 mmol, 0.65 M in THF, 2.79 equiv) was then added dropwise over 10 min. The reaction mixture was maintained at -78 °C until judged complete by TLC (ca. 1.5 h), then quenched at -78 °C with saturated aq NH$_4$Cl (10 mL). The reaction mixture was allowed to warm to room temperature and stirred until the aqueous layer achieved a deep blue color (ca. 2 h). The reaction was extracted with ether (3 x 25 mL), the combined organic extracts were washed with saturated aq NH$_4$Cl (2 x 15 mL) and brine (10 mL). The washed extracts were dried (MgSO$_4$), filtered and concentrated *in vacuo*. The crude residue was purified by flash column chromatography (Silica gel/K$_2$CO$_3$ (10:1); gradient elution, 0-3% EtOAc in hexanes) to afford 1.10 g (77%) of **A14** as a clear oil: R_f 0.73 (4:1 hexanes/EtOAc); IR (thin-film): 3073, 2926, 1715, 1593, 1488 cm^{-1}; ^{1}H NMR (400 MHz, CDCl$_3$) δ 6.89 (s, 1H), 6.42 (s, 2H), 6.39 (s, 1H), 6.11 (s, J_{Sn-H} = 30 Hz, 1H), 5.84-5.74 (m, 1H), 4.93-4.89

(m, 2H), 4.46-4.39 (m, 3H), 4.20 (s, J_{Sn-H} = 27 Hz, 2H), 3.75 (s, 3H), 3.17 (d, J = 6.4 Hz, 2H), 1.404-137 (m, 6H), 1.37 (d, J = 6.0 Hz, 6H), 1.28-1.22 (m, 7H), 1.17 (d, J = 6.0 Hz, 12H), 0.88-0.84 (app t, J = 7.2 Hz, 9H), 0.81-0.77 (m, 5H); ^{13}C NMR (100 MHz, CDCl$_3$) δ 170.9, 165.0, 151.7, 150.1, 148.5, 136.7, 136.0, 135.3, 129.1, 128.0, 120.1, 117.4, 115.8, 115.3, 110.5, 71.8, 71.5, 51.1, 41.1, 34.4, 29.0, 27.4, 22.2, 13.7, 10.3; HRMS (ESI-orbitrap MS) calculated for C$_{41}$H$_{63}$ClO$_6$Sn$^+$ [M+H]$^+$ m/z = 807.3408, measured 807.3431.

A15

A15 To -78 °C solution of enoate **A14** (1.05 g, 1.30 mmol) in DCM (26.0 mL) was added a solution of DIBAL (3.25 mL, 3.25 mmol, 1M in hexanes, 2.50 equiv). The reaction mixture was maintained at -78 °C for 1 h, then an additional equivalent of DIBAL (1.30 mL, 1.30 mmol, 1M in hexanes, 1.00 equiv) was added. The reaction was maintained at -78 °C for 10 min, then allowed to warm to -10 °C for 20 min. The reaction was quenched slowly by the addition of saturated aq Rochelle's salt (15 mL) and the biphasic solution was allowed to stir for 18 h. The reaction mixture was extracted with DCM (3 x 25 mL) and the combined organic extracts were washed with brine (30 mL). The washed extracts were dried (MgSO$_4$), filtered and concentrated *in vacuo*. The crude residue was purified by flash column chromatography (silica gel (2% Et$_3$N buffered); gradient elution, 0-30% EtOAc in hexanes) to afford 0.838 g (82%) of alcohol **A15** as a clear oil: R$_f$ 0.20 (9:1 hexane/EtOAc); IR(thin-film): 3419, 3070, 2925,1590, 1474 cm^{-1}; ^{1}H NMR (400 MHz, CDCl$_3$) δ 6.89 (s, 1H), 6.39 (s, 3H), 5.95 (t, J = 6.1 Hz, J_{Sn-H} = 33 Hz, 1H), 5.84-5.74 (m, 1H), 4.93-4.88 (m, 2H), 4.47-4.40 (m, 3H), 4.35 (app t, J = 5.1 Hz, 2H), 3.60 (s, J_{Sn-H} = 27 Hz, 2H), 3.17 (d, J = 6.4 Hz, 2H), 1.45-1.37 (m, 7H), 1.30 (d, J = 6.0 Hz, 6H), 1.29-1.21 (m, 6H), 1.18 (d, J = 6.0 Hz, 12H), 0.86 (t, J = 7.2 Hz, 9H), 0.79-0.74 (m, 5H); ^{13}C NMR (100 MHz, CDCl$_3$) δ 151.6, 150.1, 148.4, 146.3, 140.1, 136.9, 136.7, 135.1, 129.1 ,120.1, 117.3, 115.8, 115.3, 110.5, 110.2, 71.9, 71.5, 59.3, 39.5, 34.3, 29.2, 27.5, 13.8, 9.9; HRMS (ESI-orbitrap MS) calculated for C$_{40}$H$_{63}$ClO$_5$Sn$^+$ [M+H]$^+$ 779.3459, measured 761.3375 [M-H$_2$O]$^+$.

2.169 To a 0 °C solution of stannane **A18** (779 mg, 1.00 mmol) in THF (20.0 mL) was added CuCl₂ (2.69 g, 20.0 mmol, 20.0 equiv). The reaction mixture was allowed to warm to room temperature and maintained for 18 h, or until judged complete by TLC analysis (ca. 18-24 h). The suspension was quenched with saturated aq NH₄Cl (25 mL) and extracted with ether (3 x 25 mL). The combined organic extracts were washed with saturated aq NH₄Cl (2 x 20 mL) and brine (20 mL). The washed extracts were dried (Na₂SO₄), filtered, and concentrated *in vacuo*. The crude residue was purified by flash column chromatography (Silica gel/K₂CO₃ (10:1), gradient elution, 0-30% EtOAc in hexanes) to afford 0.458 g (85%) of chloride **2.169** as a clear oil: R_f 0.25 (4:1 hexanes/EtOAc); IR (thin-film): 3417, 2977, 2358, 1644, 1594 cm⁻¹; ¹H NMR (400 MHz, CDCl₃) δ 6.90 (s, 1H), 6.50 (s, 2H), 6.39 (s, 1H), 6.0 (t, *J* = 7.2 Hz, 1H), 5.81-5.74 (m, 1H), 4.93-4.89 (m, 2H), 4.50-4.40 (m, 3H), 4.26 (d, *J* = 7.2 Hz, 2H), 3.67 (s, 2H), 3.18 (d, *J* = 6.4 Hz, 2H), 1.30 (d, *J* = 6.0 Hz, 6H), 1.18 (d, *J* = 6.0 Hz, 12H); ¹³C NMR (100 MHz, CDCl₃) δ 151.6, 150.2, 148.3, 136.7, 136.6, 135.7, 133.6, 129.1, 127.9, 120.1, 117.3, 115.8, 115.5, 110.3, 72.0, 71.5, 59.1, 40.4, 34.1, 22.2, 22.1; ; LRMS calculated for C₂₈H₃₆Cl₂O₅ [M+Na] m/z 545.2, measured LC/MS (ESI) R_t 1.01 min, m/z 545.6 [M+Na].

2.170 To a 0 °C solution of alcohol **2.169** (368 mg, 0.704 mmol), phenol **2.87** (395 mg, 1.05 mmol, 1.50 equiv) and Ph₃P (277 mg, 1.05 mmol, 1.50 equiv) in DCM (3.50 mL) at was added a solution of diethyl azodicarboxylate (478 μL, 1.05 mmol, 40 wt. % in toluene, 1.50 equiv) at a rate of ca. 1 drop every 2 min. Following the addition, the reaction mixture was maintained at 0 °C for 30 min, allowed to warm to room temperature and maintained until judged complete by TLC (ca. 15 - 30 min). The reaction mixture was loaded directly onto a silica gel column and purified (gradient elution, 0-10% EtOAc in hexanes) to afford 430 mg (69%) of ether **2.170** as a yellow oil: R_f 0.56 (4:1 hexanes/EtOAc); IR (thin-film): 3073, 2976, 2927, 1739, 1640, 1594 cm⁻¹; ¹H NMR (400 MHz, CDCl₃) δ 6.99 (d, *J* = 2.8 Hz, 1H), 6.90 (s, 1H), 6.61 (dd, *J* = 9.0, 2.8 Hz, 1H), 6.51 (s, 2H), 6.46 (d, *J* = 9.0 Hz, 1H), 6.40 (m, 3H), 6.09 (t, *J* = 7.0 Hz, 1H), 5.91-5.72 (m, 2H), 5.06-5.02 (m, 2H), 4.93-4.88 (m, 2H), 4.55 (d, *J* = 7.0 Hz, 2H), 4.51-4.37 (m, 5H), 3.71 (s, 2H), 3.29 (d, *J* = 6.6 Hz, 2H), 3.18 (d, *J* = 6.6

Hz, 2H), 1.34 (d, J = 6.0 Hz, 6H), 1.30 (d, J = 6.0 Hz, 6H), 1.17 (d, J = 6.0 Hz, 12H), 1.14 (d, J = 6.0 Hz, 6H); ^{13}C NMR (100 MHz, CDCl$_3$) δ 155.4, 152.7, 151.7, 151.0, 150.2, 149.2, 148.4, 138.7, 136.9, 136.6, 136.3, 135.8, 135.0, 133.1, 129.2, 123.9, 122.5, 120.1, 117.3, 116.5, 116.3, 115.8, 115.58, 115.52, 113.6, 110.3, 108.6, 103.7, 72.0, 71.7, 71.5, 70.3, 64.8, 40.7, 34.5, 34.2, 29.8, 22.26, 22.22, 22.1, 22.0; LRMS calculated for C$_{49}$H$_{59}$Cl$_3$O$_8^+$ [M+H]$^+$ m/z 881.3, measured LC/MS (ESI) R$_t$ 1.38 min, m/z 881.5 [M+H]$^+$.

2.171

2.171 To a degassed solution of diene **2.170** (76.0 mg, 0.086 mmol) in DCE (21.0 mL) was added a solution of Grubbs C633 catalyst (9.00 mg, 0.0140 mmol, 16 mol %) in DCE (1.00 mL). The solution was frozen and placed under vacuum (ca. 0.01 torr) for ca. 10 min, the reaction vessel was sealed under vacuum and allowed to slowly warm to room temperature. Once the flask was at room temperature, the reaction was heated and maintained at 60 °C for 24 h. The reaction was allowed to cool to room temperature and quenched by the addition of ethyl vinyl ether (100 µL). The solution was concentrated *in vacuo* and purified by flash column chromatography (silica gel, gradient elution, 0-10% EtOAc in hexanes) to afford 43.0 mg (59%) of macrocycle **11** as a white foam: R$_f$ 0.4 (4:1 hexanes/EtOAc); IR (thin-film): 3051, 2976, 2927, 1734, 1647, 1594 cm^{-1}; ^{1}H NMR (400 MHz, CDCl$_3$) δ 6.89 (d, J = 2.7 Hz, 1H), 6.86 (s, 1H), 6.53 (dd, J = 9.0, 2.7 Hz, 1H), 6.55-6.36 (m, 5H), 6.13-6.11 (m, 2H), 5.41-5.33 (m, 2H), 4.48 (d, J = 6.8 Hz, 2H), 4.46-4.34 (m, 5H), 3.74 (s, 2H), 3.28 (d, J = 6.6 Hz, 2H), 2.98 (d, J = 6.0 Hz, 2H), 1.32 (app dd, J = 6.0, 2.17 Hz, 12H), 1.24 (d, J = 6.0 Hz, 6H), 1.14 (d, J = 6.0 Hz, 6H), 1.07 (d, J = 6.0 Hz, 6H); ^{13}C NMR (100 MHz, CDCl$_3$) δ 155.5, 152.5, 151.8, 151.1, 150.2, 149.4, 148.0, 136.9, 136.3, 135.6, 135.4, 133.0, 129.8, 129.3, 127.1, 125.6, 122.3, 119.6, 117.6, 116.9, 115.5, 115.3, 113.9, 109.8, 108.6, 103.9, 72.1, 71.9, 71.3, 70.3, 65.7, 41.0, 28.9, 27.8, 22.3, 22.24, 22.21, 22.1; LRMS calculated for C$_{47}$H$_{55}$Cl$_3$O$_8^+$ [M+H]$^+$ m/z 854.3, measured LC/MS (ESI) R$_t$ 1.48 min, m/z 854.6 [M+H]$^+$.

C5': X=Cl, Y=H: **2.172**
C3': X=H, Y=Cl: **2.173**

Phenols 2.172 and 2.173 To a solution of ether **2.171** (41.0 mg, 0.048 mmol, 1.00 equiv) in DCE (3.20 mL) was added BF$_3$·Et$_2$O (0.383 μL, 0.191 mmol, 0.5 M in DCE, 3.00 equiv) dropwise. The reaction was heated and maintained at 70 °C for 2 h, the reaction was allowed to cool to room temperature and quenched with brine (5 mL). The reaction was extracted with EtOAc (3 x 5 mL), washed with brine (10 mL), dried (MgSO$_4$), filtered, and concentrated *in vacuo*. The crude residue ~19 mg (45%) of an inseparable mixture of phenols **2.172** and **2.173** was used in the subsequent step as-is: R$_f$ 0.27 (4:1 hexanes/EtOAc); LRMS calculated for C$_{47}$H$_{55}$Cl$_3$O$_8{}^+$ [M+H]$^+$ m/z 853.3, measured LC/MS (ESI) R$_t$ 1.40 min, m/z 853.0 [M+H]$^+$.

X=Cl, Y=H: 9-dechlorochrysophaentin
VU0849855
X=H, Y=Cl: iso-9-dechlorochrysophaentin
VU0849838

VU0849855 and VU0849838 To a -78 °C solution of phenols **2.172** and **2.173** (24.0 mg, 0.028 mmol) in DCM (2.80 mL) was added a solution of BCl$_3$ (0.244 mL, 0.244 mmol, 1 M in DCM, 7.00 equiv) dropwise. The reaction mixture was allowed to warm to room temperature over 1 h and maintained until judged complete by TLC (ca. 2-4 h). The reaction was diluted with brine (2 mL) and extracted with EtOAc (4 x 5 mL). The combined organic extracts were washed with brine (5.00 mL), dried (Na$_2$SO$_4$), filtered, and concentrated *in vacuo*. The crude residue (~16 mg) was purified by Gilson preparative HPLC (30-455% CH$_3$CN in H$_2$O, over 8 min) to afford 5.00 mg (27%) of **VU0849855** and 6.00 mg (33%) of **VU0849838**:

VU0849855: R$_f$ 0.55 (5:1 DCM/methanol); ^{1}H NMR (600 MHz, CD$_3$OD) δ 6.85 (s, 1H), 6.78 (s, 1H), 6.29 (s, 1H), 6.25 (d, *J* = 3 Hz, 2H), 6.10-6.05 (m, 4H), 5.60-5.56 (m, 1H), 5.49-5.46 (m, 1H), 3.52 (s, 2H), 3.28 (d, *J* = 6.7 Hz, 2H), 3.22 (d, *J* = 8.0 Hz, 2H), 3.01 (d, *J* = 7.2 Hz, 2H); ^{13}C NMR (150 MHz, CD$_3$OD) δ 155.8, 151.5, 151.3, 150.6, 150.3, 148.8, 148.3, 136.7, 136.3, 135.0, 134.8, 130.2, 130.0, 128.1, 128.0, 127.8, 127.4, 120.8, 119.4, 117.3, 117.0, 116.6, 116.4, 109.2, 108.0, 103.1, 40.3, 30.3, 28.6, 28.0; LCMS (ESI) R$_t$ 1.39 min, 1.04 min, m/z = 643.0 [M+H]$^+$; HRMS (ESI-orbitrap MS) calculated for C$_{32}$H$_{25}$Cl$_3$O$_8{}^+$ [M+H]$^+$ m/z 643.0688, measured 643.0713.

VU0849838: R_f 0.47 (5:1 DCM/methanol); ^{1}H NMR (600 MHz, CD$_3$OD) δ 6.80 (s, 1H), 6.55 (d, J = 9.0 Hz, 1H), 6.46 (s, 1H), 6.29-6.28 (m, 3H), 6.26 (d, J = 2.6 Hz, 1H), 6.17-6.14 (m, 2H), 5.77-5.73 (m, 1H), 5.46-5.41 (m, 1H), 3.78 (s, 2H), 3.64 (d, J = 7.7 Hz, 2H), 3.25 (d, J = 7.7 Hz, 2H), 2.96 (d, J = 7.6 Hz, 2H); ^{13}C NMR (150 MHz, CD$_3$OD) δ 156.3, 151.9, 151.5, 150.5, 148.6, 148.1, 137.0, 136.6, 136.5, 134.5, 133.8, 130.3, 130.0, 128.5, 128.2, 127.3, 126.9, 123.2, 119.7, 116.9, 116.4, 113.9, 113.4, 109.2, 108.4, 102.6, 40.9, 28.9, 28.2, 28.1; LCMS (ESI) R_t 1.09 min, m/z = 643.0 [M+H]$^+$; HRMS (ESI-orbitrap MS) calculated for C$_{32}$H$_{25}$Cl$_3$O$_8$$^+$ [M+H]$^+$ m/z 643.0688, measured 643.0711.
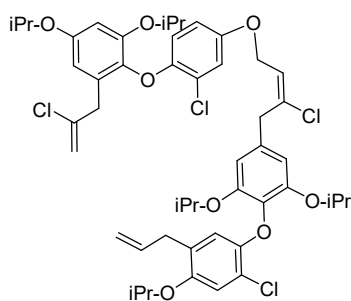
4.3

4.3 To a 0 °C solution of alcohol **4.5** (94.0 mg, 0.704 mmol), phenol **4.4** (110 mg, 0.269 mmol, 1.50 equiv) and Ph$_3$P (71.0 mg, 0.269 mmol, 1.50 equiv) in DCM (1.0 mL) at was added a solution of diethyl azodicarboxylate (119 µL, 0.269 mmol, 40 wt. % in toluene, 1.50 equiv) at a rate of ca. 1 drop every 2 min. Following the addition, the reaction mixture was maintained at 0 °C for 30 min, allowed to warm to room temperature and maintained until judged complete by TLC (ca. 15 - 30 min). The reaction mixture was loaded directly onto a silica gel column and purified (gradient elution, 0-10% EtOAc in hexanes) to afford 123 mg (75%) of ether **4.3** as a white foam: ^{1}H NMR (400 MHz, CDCl$_3$) δ 6.99 (d, J = 3.0 Hz, 1H), 6.90 (s, 1H), 6.61 (dd, J = 9.0, 3.0 Hz, 1H), 6.52 (s, 2H), 6.49-6.46 (m, 2H), 6.40 (s, 1H), 6.09 (t, J = 7.2 Hz, 1H), 5.81-5.73 (m, 1H), 5.19 (s, 1H), 5.15 (s, 1H), 4.93-4.89 (m, 2H), 4.56 (d, J = 7.0 Hz, 2H), 4.53-4.39 (m, 5H), 3.71 (s, 2H), 3.60 (s, 2H), 3.18 (d, J = 6.6 Hz, 2H), 1.36 (d, J =6.0 Hz, 6H), 1.31 (d, J = 6.0 Hz, 6H), 1.17 (d, J = 6.0 Hz, 12H), 1.13 (d, J = 6.0 Hz, 6H); ^{13}C NMR (100 MHz, CDCl$_3$) δ 155.3, 152.8, 151.7, 151.0, 150.1, 149.0, 148.3, 140.1, 138.7, 137.2, 136.6, 135.8, 133.1, 131.6, 129.1, 123.9, 122.5, 120.1, 117.3, 116.5, 115.7, 115.5, 114.4, 113.6, 110.3, 108.3, 104.4, 71.9, 71.56, 71.52, 70.4, 64.8, 49.6, 39.6, 34.1, 22.2, 22.1, 21.9.

A5. References:

(1)   Brockway, A. J.; Grove, C. I.; Mahoney, M. E.; Shaw, J. T. Synthesis of the Diaryl Ether Cores Common to Chrysophaentins A, E, and F. *Tetrahedron Letters* **2015**, *56* (23), 3396–3401. https://doi.org/10.1016/j.tetlet.2015.01.073.

(2)   Chuang, K. v; Navarro, R.; Reisman, S. E. Benzoquinone-Derived Sulfinyl Imines as Versatile Intermediates for Alkaloid Synthesis: Total Synthesis of (–)-3-Demethoxyerythratidinone. *Chemical Science* **2011**, *2* (6), 1086. https://doi.org/10.1039/c1sc00095k.

(3)   Keffer, J. L.; Hammill, J. T.; Lloyd, J. R.; Plaza, A.; Wipf, P.; Bewley, C. A. Geographic Variability and Anti-Staphylococcal Activity of the Chrysophaentins and Their Synthetic Fragments. *Marine Drugs* **2012**, *10* (12), 1103–1125. https://doi.org/10.3390/md10051103.

(4)   Hristea, E. N.; Covaci-Cîmpeanu, I. C.; Ioniţă, G.; Ioniţă, P.; Draghici, C.; Caăproiu, M. T.; Hillebrand, M.; Constantinescu, T.; Balaban, A. T. Reactions of 2,2-Diphenyl-1-Picrylhydrazyl (DPPH) with Two Syringylic Phenols or One Aroxide Derivative. *European Journal of Organic Chemistry* **2009**, *2009* (5), 626–634. https://doi.org/10.1002/ejoc.200800735.

A6. NMR Spectra of Prepared Intermediates:
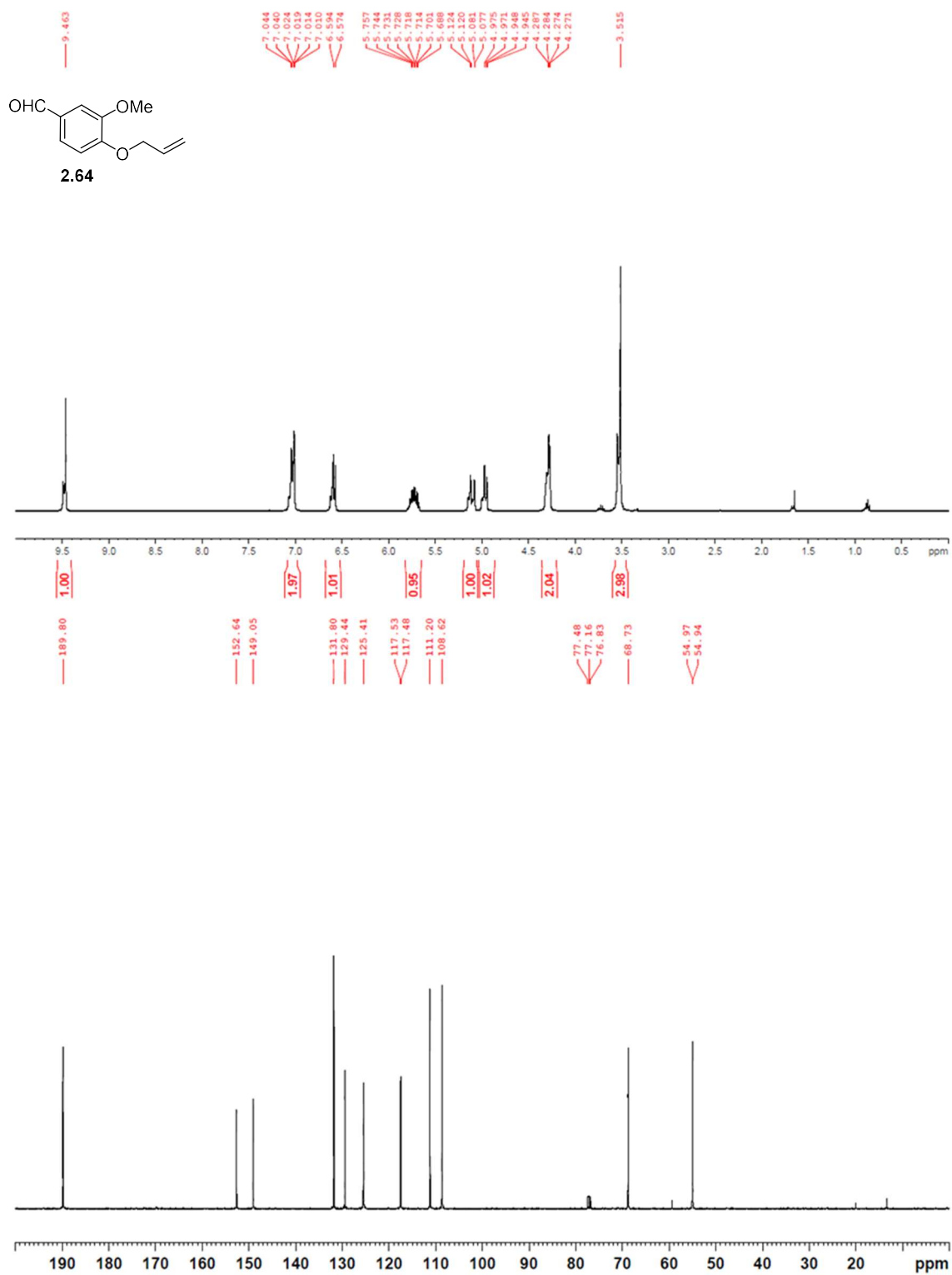
Figure A.1. ^{1}H NMR (400 MHz, CDCl$_3$) and ^{13}C NMR (100 MHz, CDCl$_3$) of **2.64.**
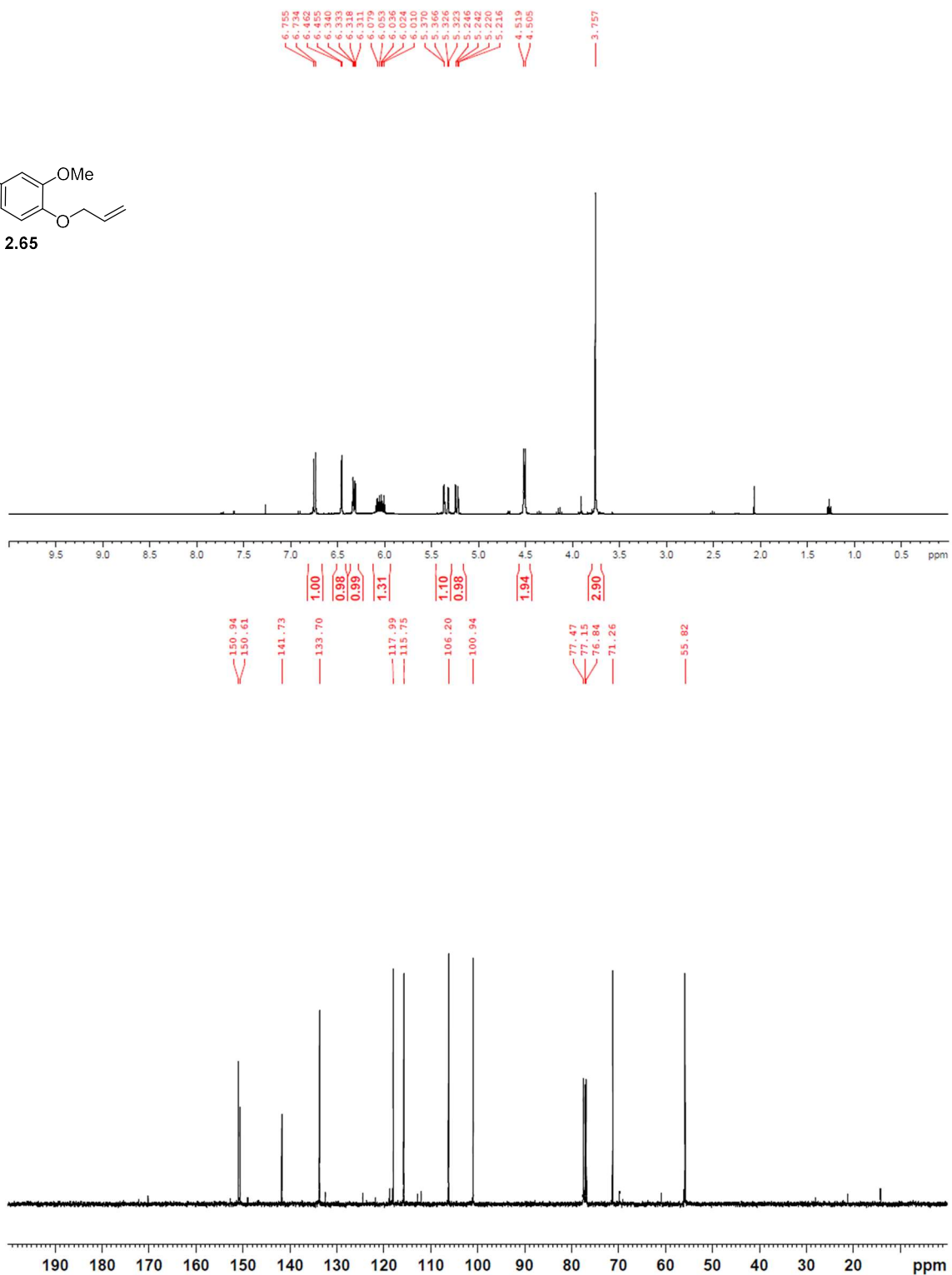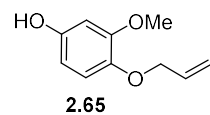
Figure A.2. ^{1}H NMR (400 MHz, CDCl$_3$) and ^{13}C NMR (100 MHz, CDCl$_3$) of **2.65**.
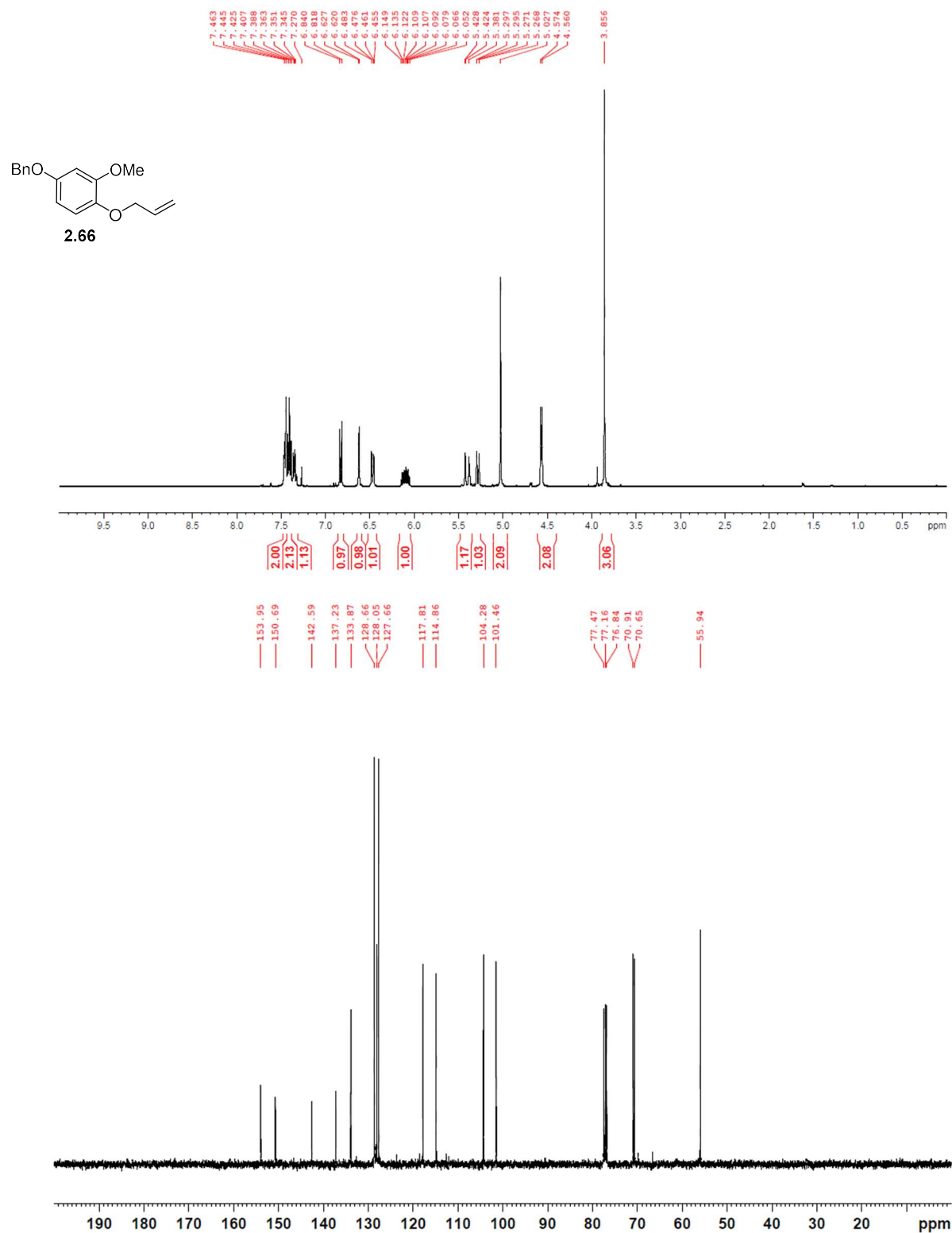
Figure A.3. ^{1}H NMR (400 MHz, CDCl$_3$) and ^{13}C NMR (100 MHz, CDCl$_3$) of **2.66**.
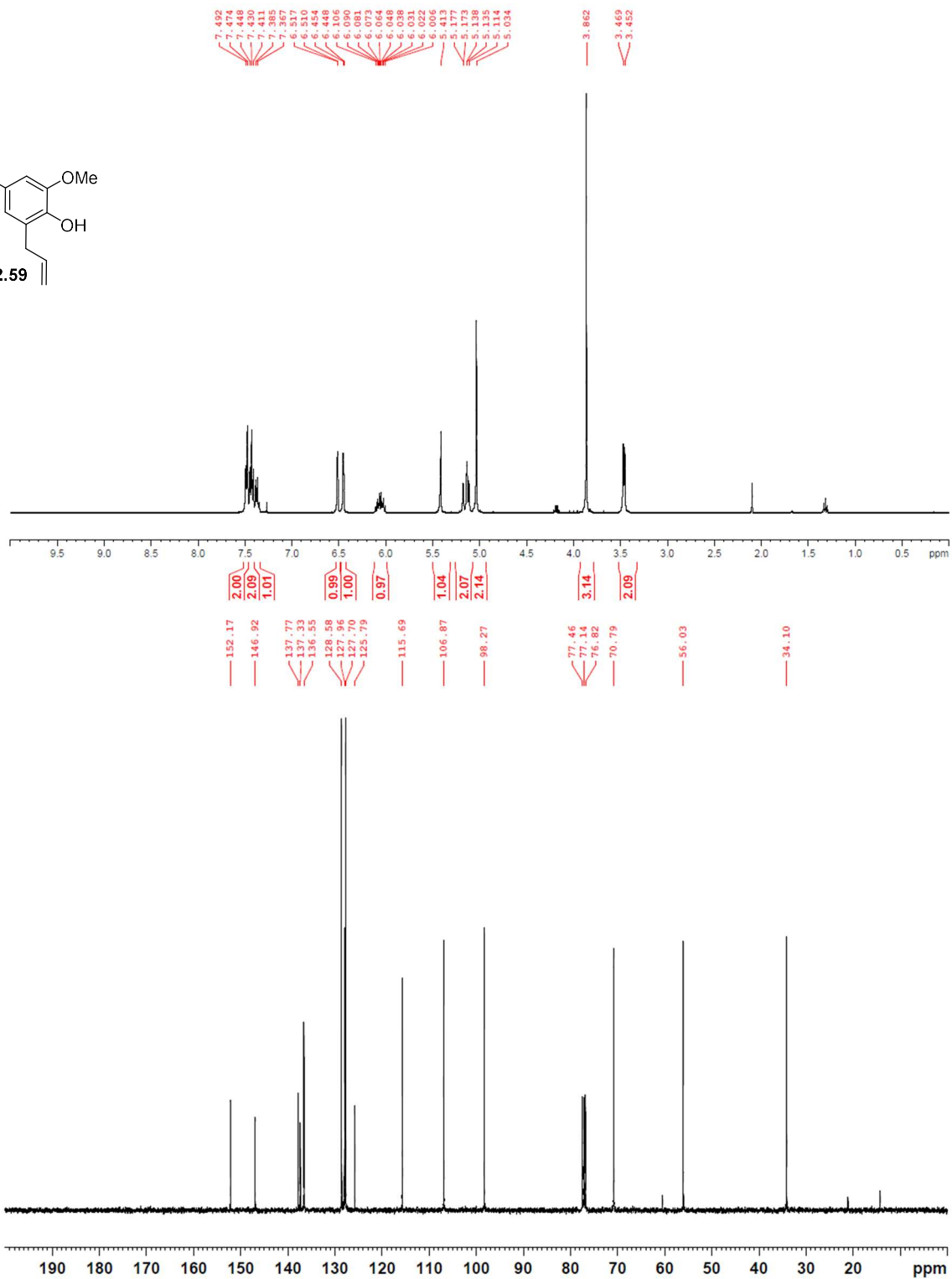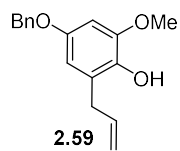
Figure A.4. ^{1}H NMR (400 MHz, CDCl$_3$) and ^{13}C NMR (100 MHz, CDCl$_3$) of **2.59.**
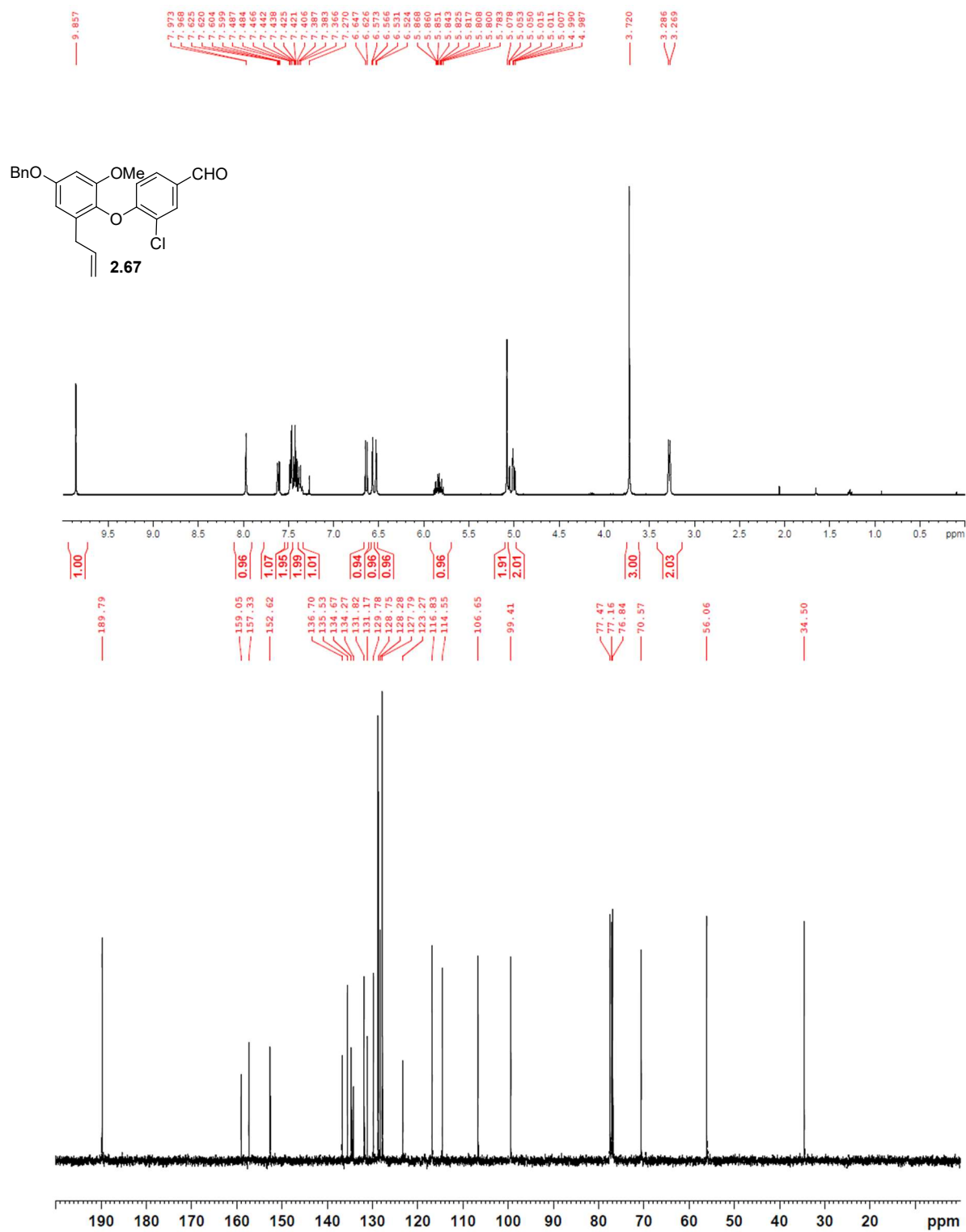
Figure A.5. ^{1}H NMR (400 MHz, CDCl3) and ^{13}C NMR (100 MHz, CDCl3) of **2.67.**
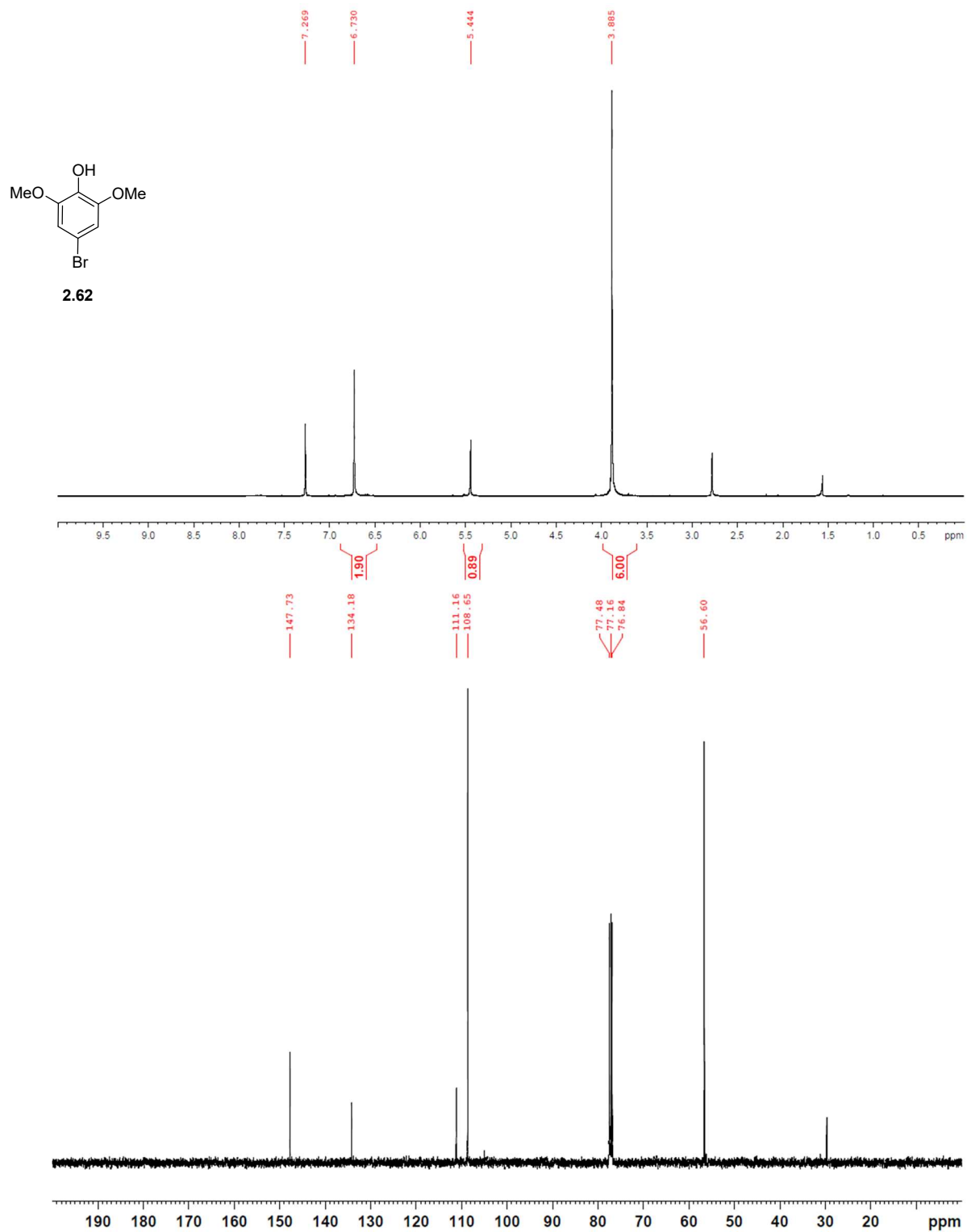
Figure A.6. ^{1}H NMR (400 MHz, CDCl$_3$) and ^{13}C NMR (100 MHz, CDCl$_3$) of **2.62.**
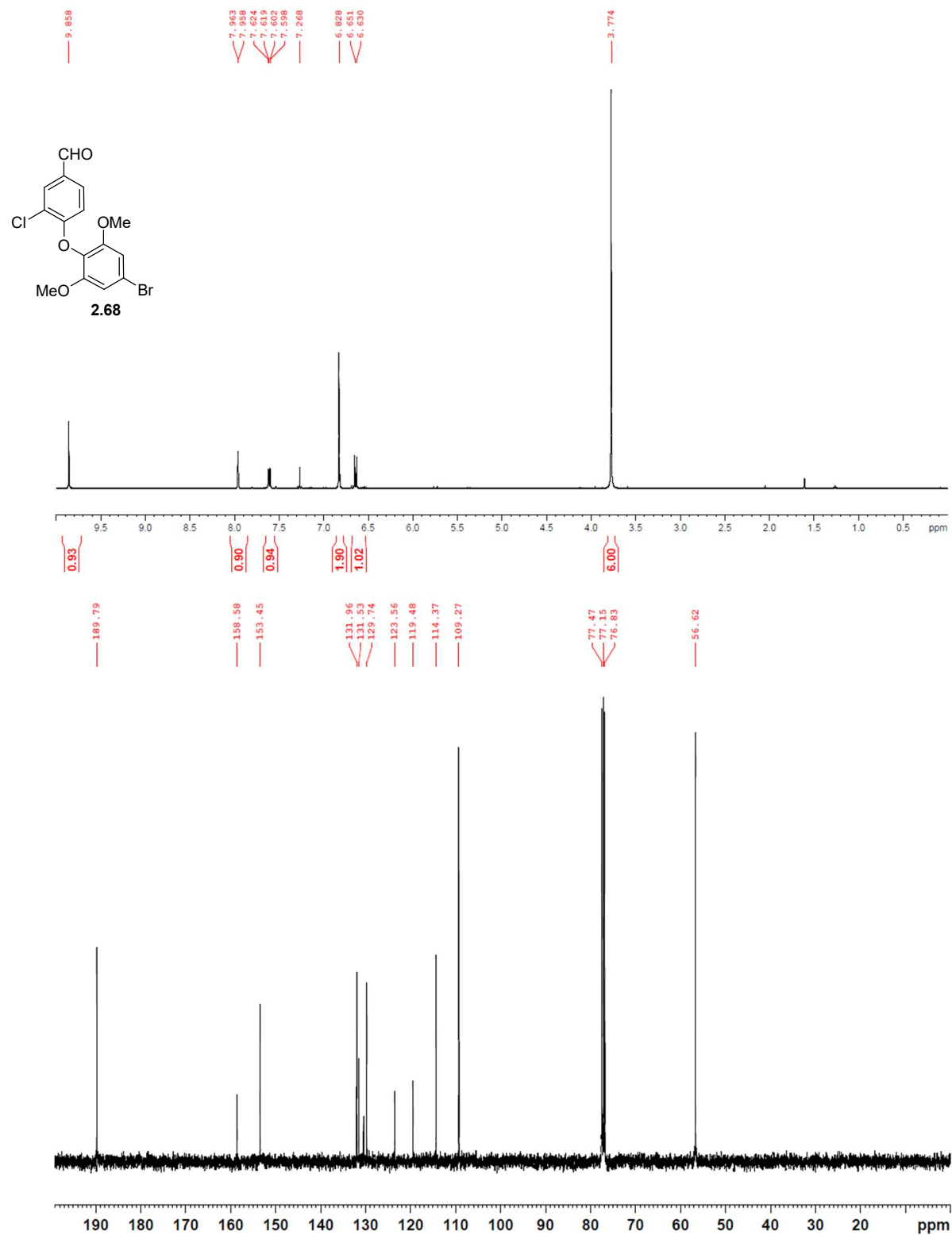
Figure A.7. ^{1}H NMR (400 MHz, CDCl$_3$) and ^{13}C NMR (100 MHz, CDCl$_3$) of **2.68.**
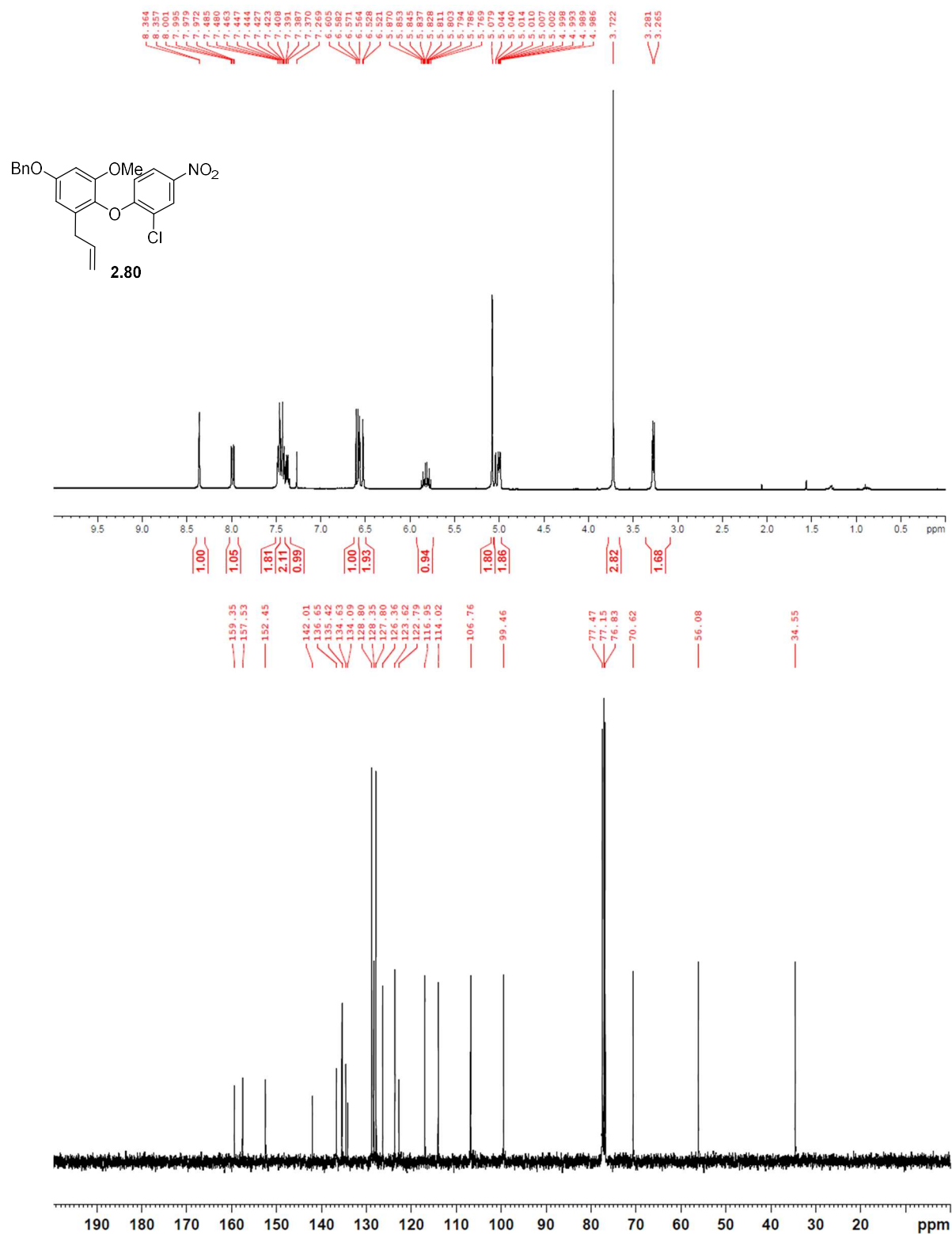
Figure A.8. ^{1}H NMR (400 MHz, CDCl$_3$) and ^{13}C NMR (100 MHz, CDCl$_3$) of **2.80.**
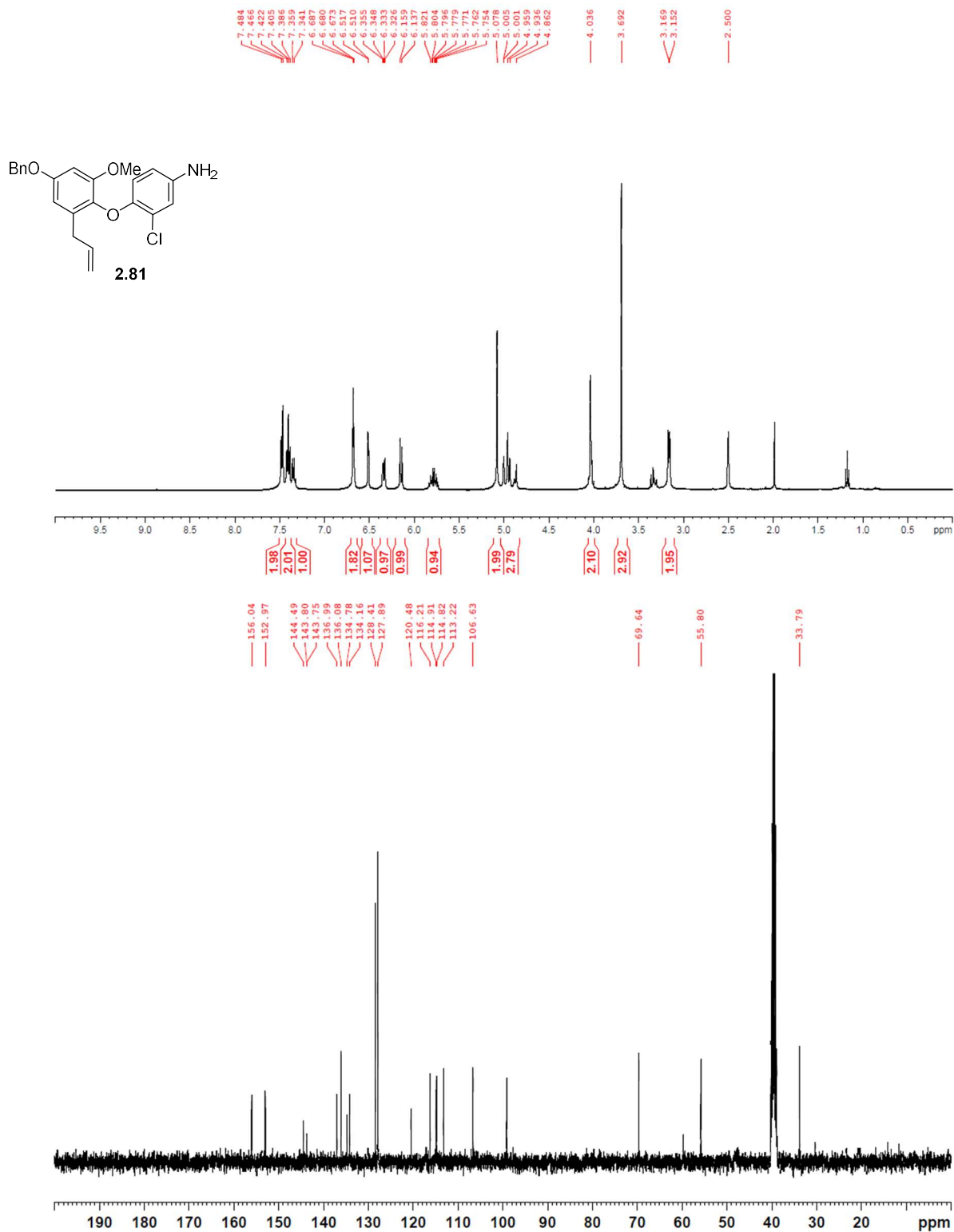
Figure A.9. ^{1}H NMR (400 MHz, (CD$_3$)$_2$SO) and ^{13}C NMR (100 MHz, (CD$_3$)$_2$SO) of **2.81.**
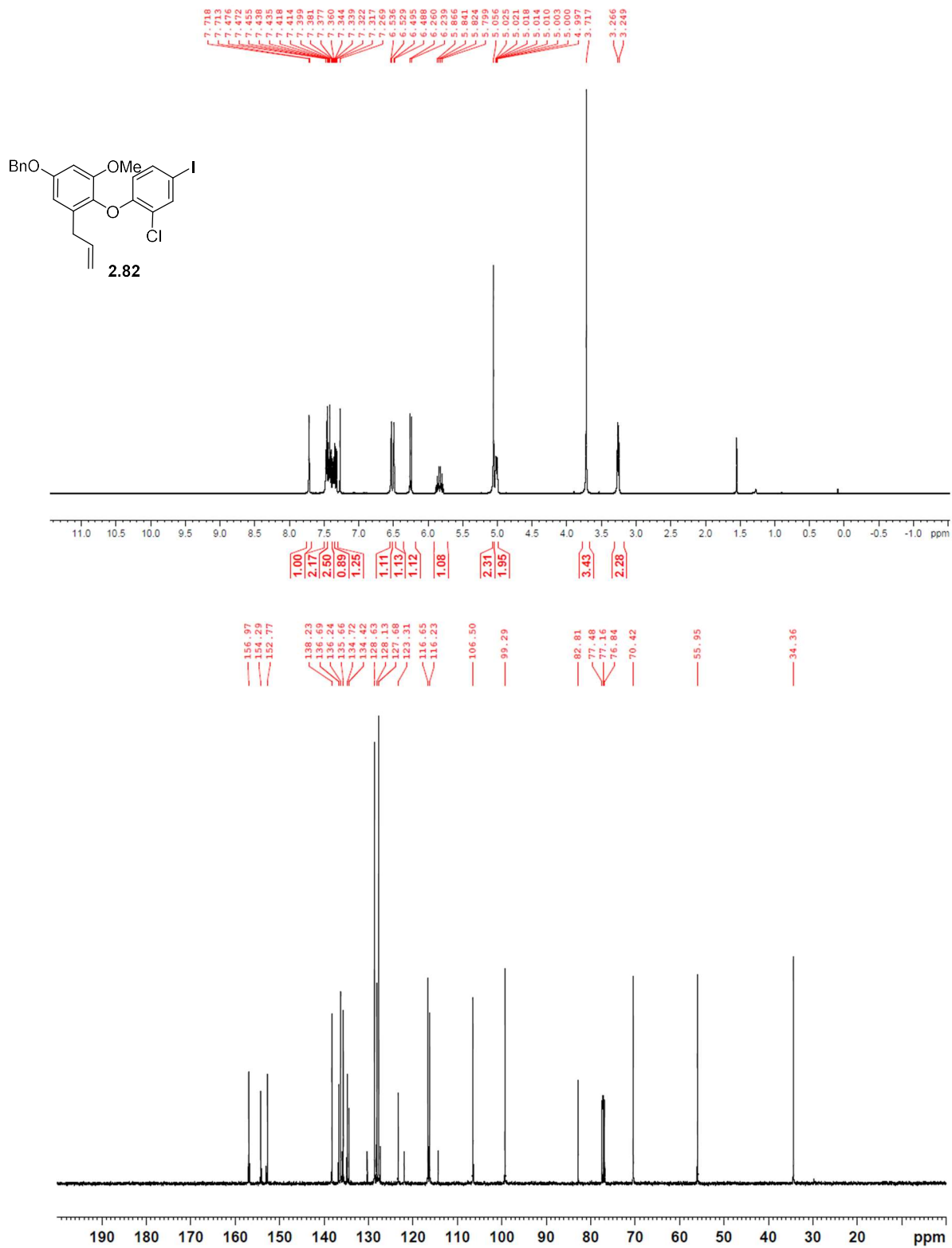
Figure A.10. ^{1}H NMR (400 MHz, CDCl$_3$) and ^{13}C NMR (100 MHz, CDCl$_3$) of **2.82**.
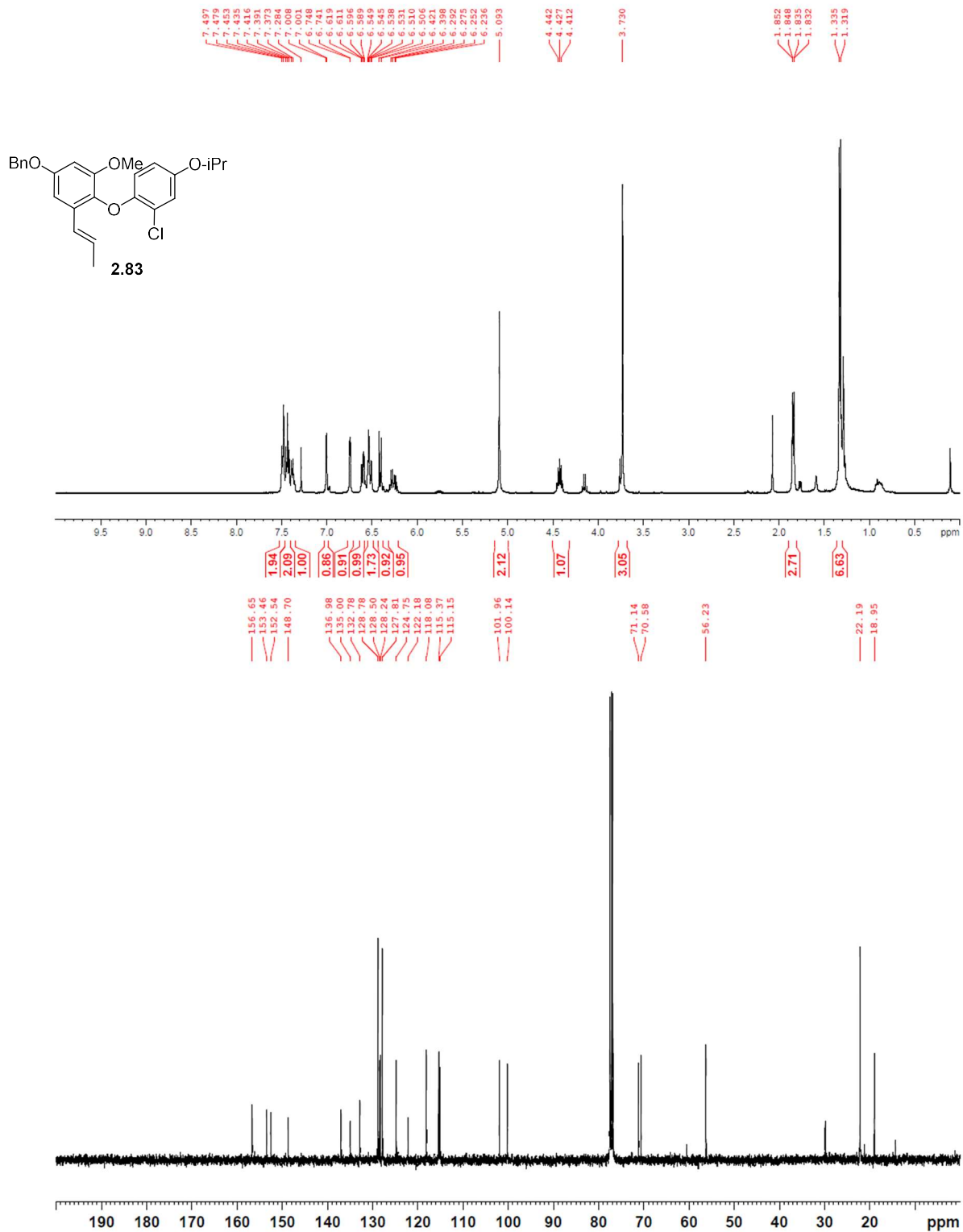
Figure A.11. ^{1}H NMR (400 MHz, CDCl$_3$) and ^{13}C NMR (100 MHz, CDCl$_3$) of **2.83.**
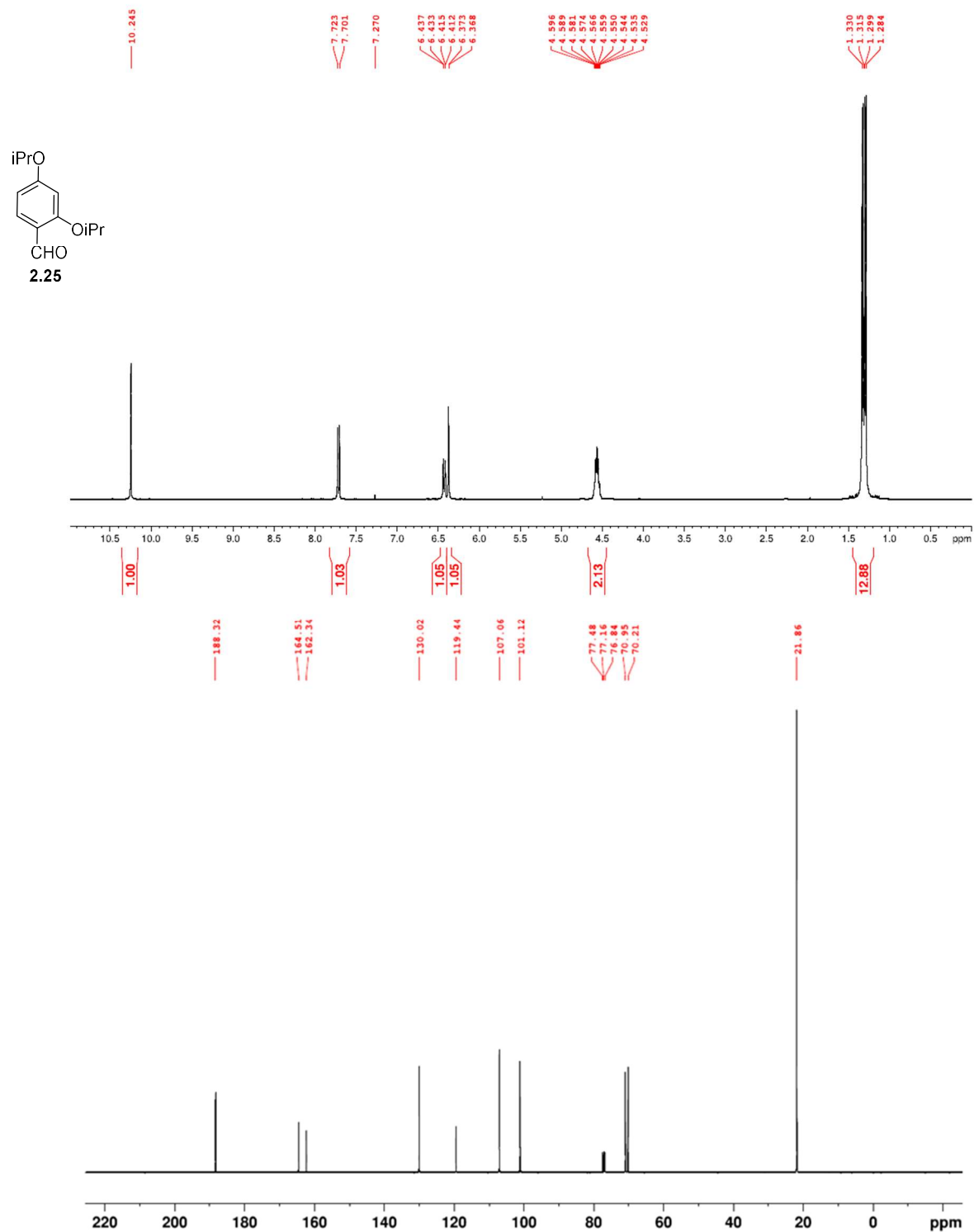
Figure A.12. ^{1}H NMR (400 MHz, CDCl3) and ^{13}C NMR (100 MHz, CDCl3) of **2.25.**
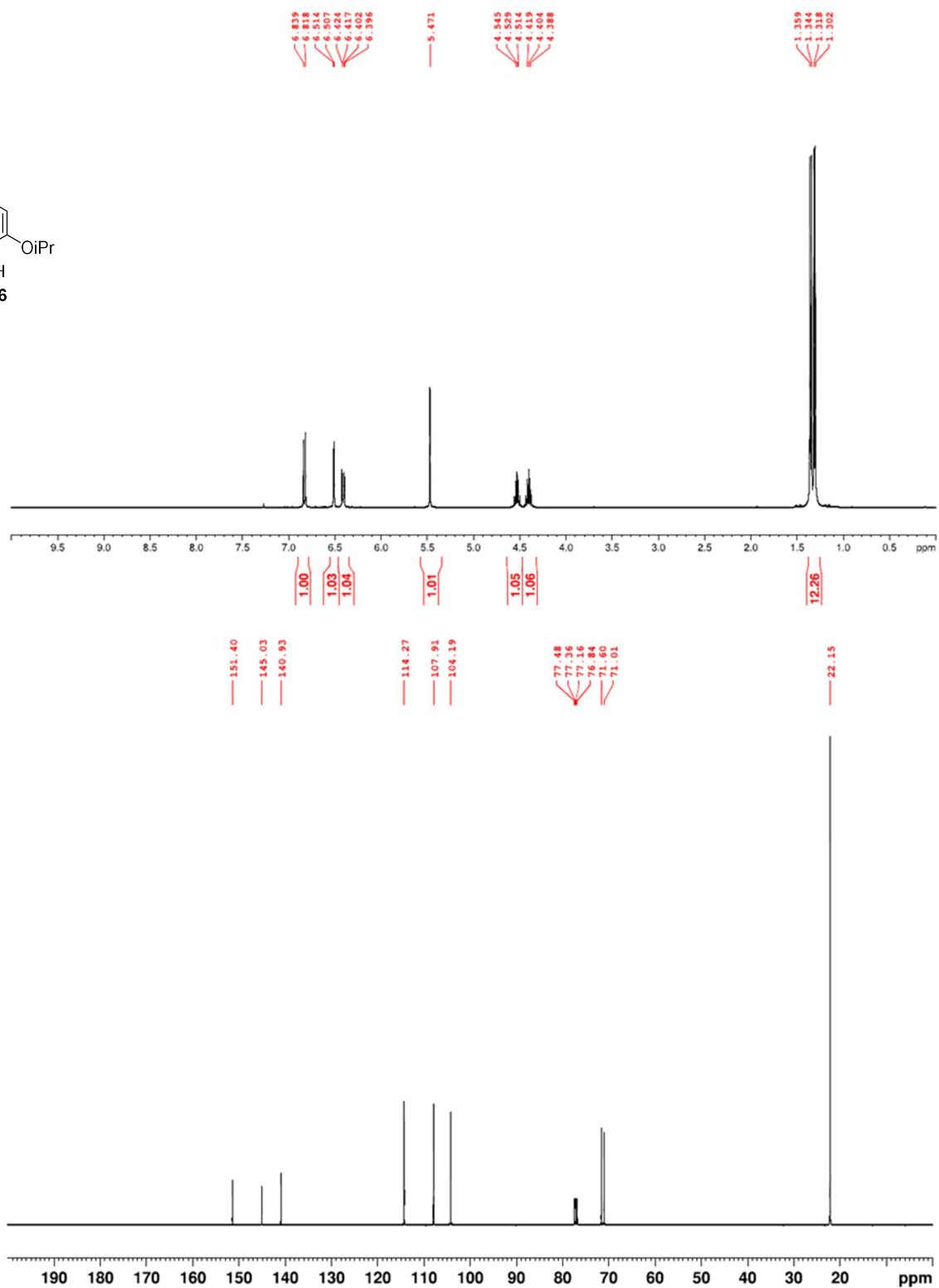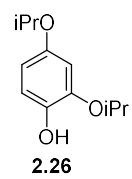
Figure A.13. ¹H NMR (400 MHz, CDCl₃) and ¹³C NMR (100 MHz, CDCl₃) of **2.26.**
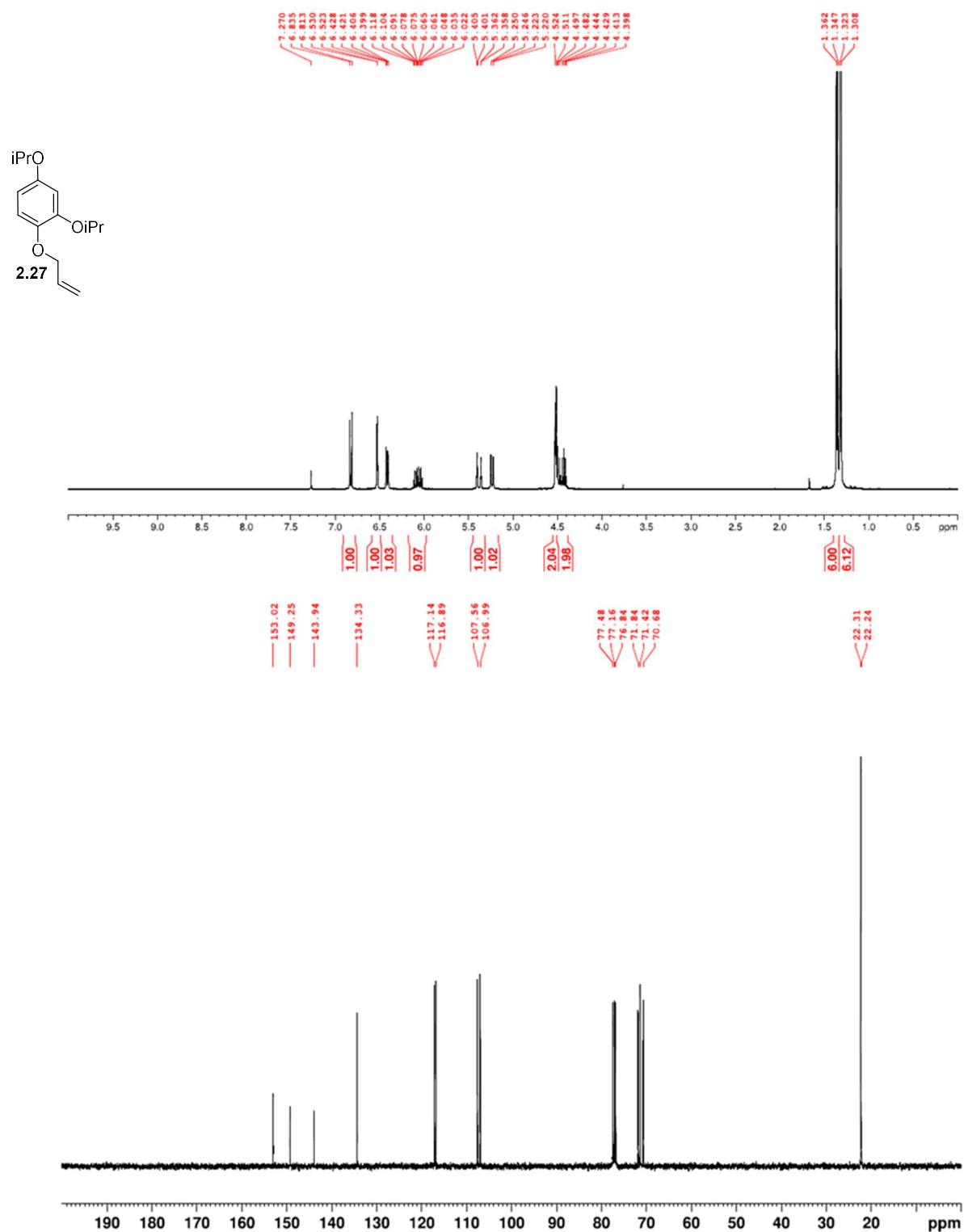
Figure A.14. ^{1}H NMR (400 MHz, CDCl$_3$) and ^{13}C NMR (100 MHz, CDCl$_3$) of **2.27.**
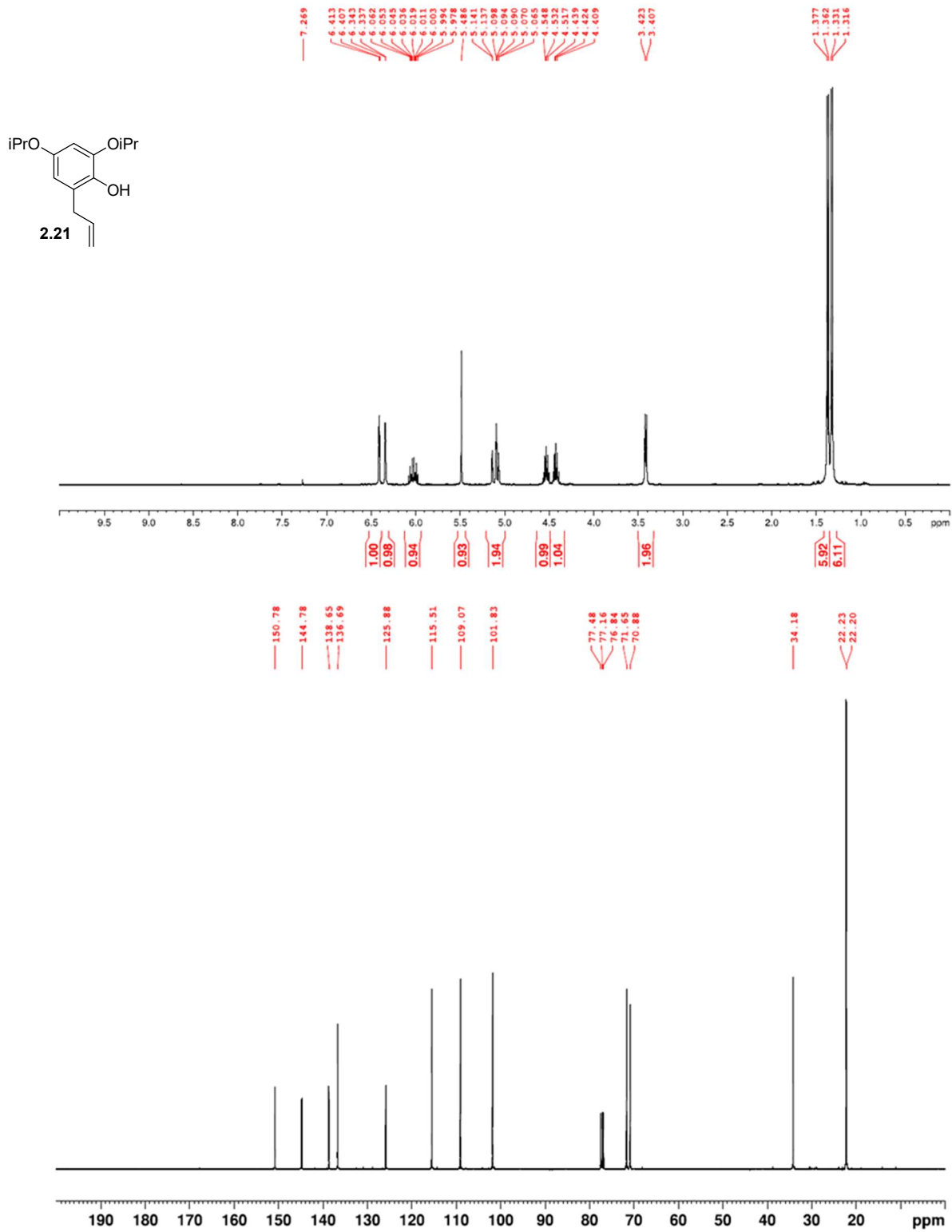
Figure A.15. ^{1}H NMR (400 MHz, CDCl$_3$) and ^{13}C NMR (100 MHz, CDCl$_3$) of **2.21.**
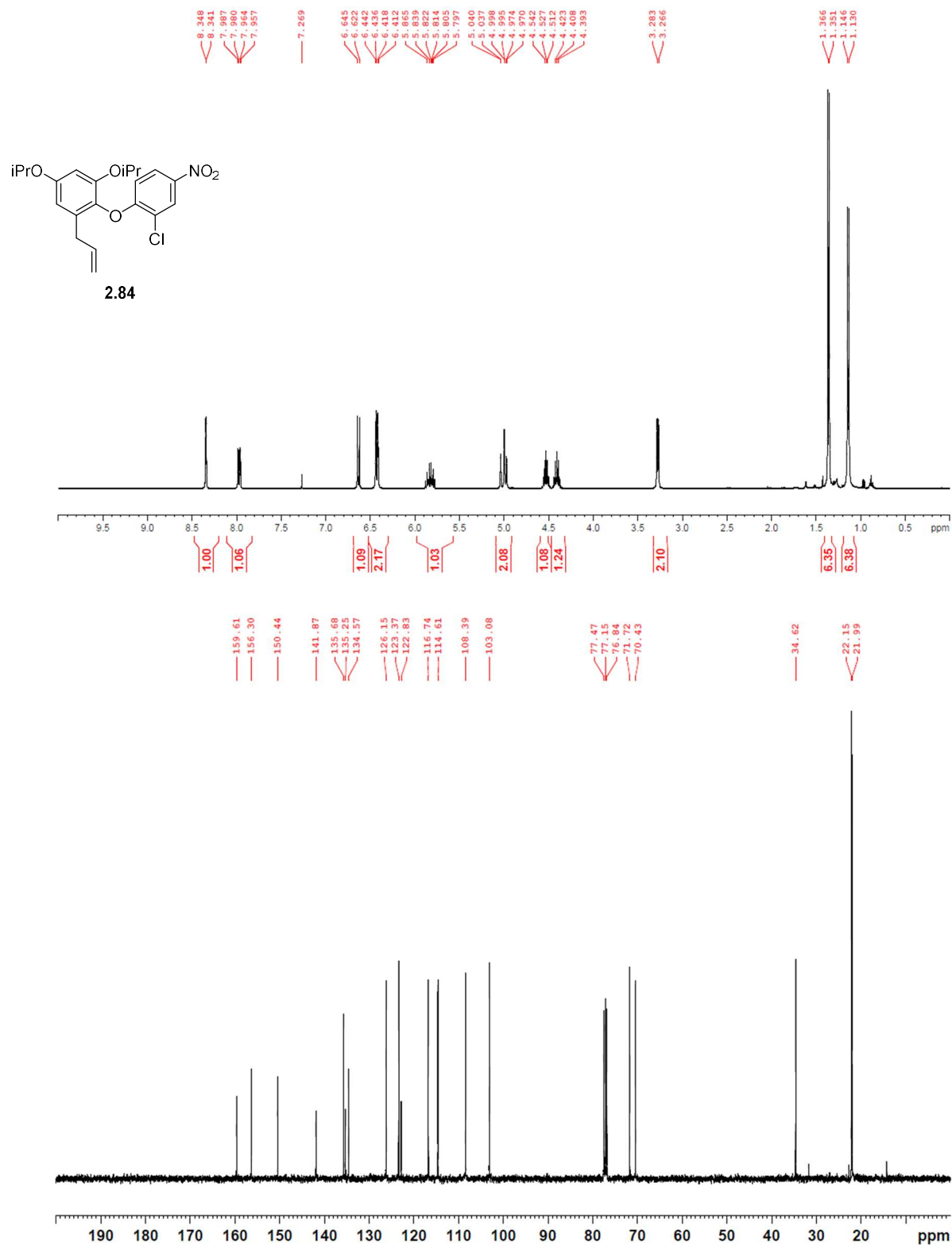
Figure A.16. ^{1}H NMR (400 MHz, CDCl$_3$) and ^{13}C NMR (100 MHz, CDCl$_3$) of **2.84.**
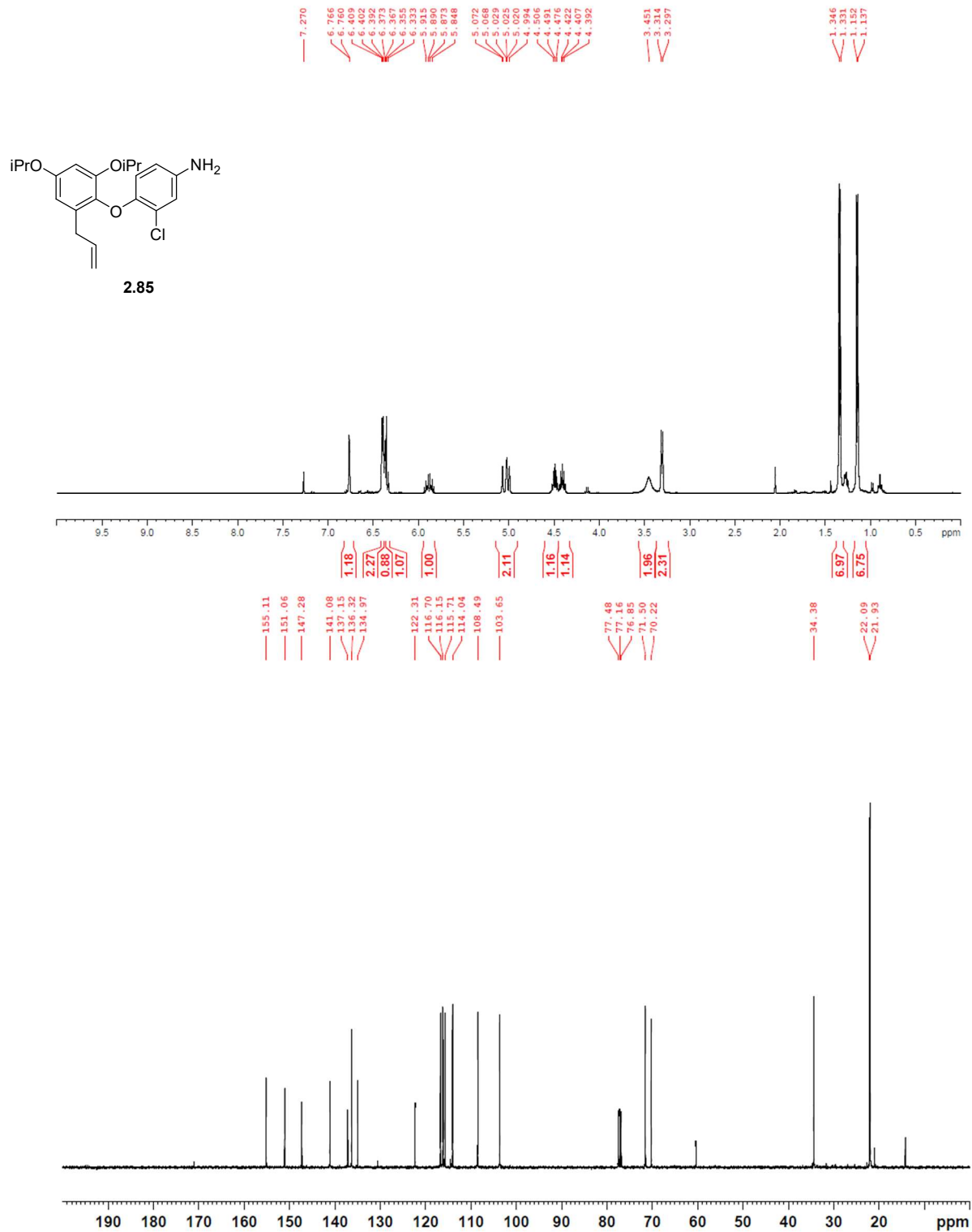
Figure A.17. ^{1}H NMR (400 MHz, CDCl$_3$) and ^{13}C NMR (100 MHz, CDCl$_3$) of **2.85.**
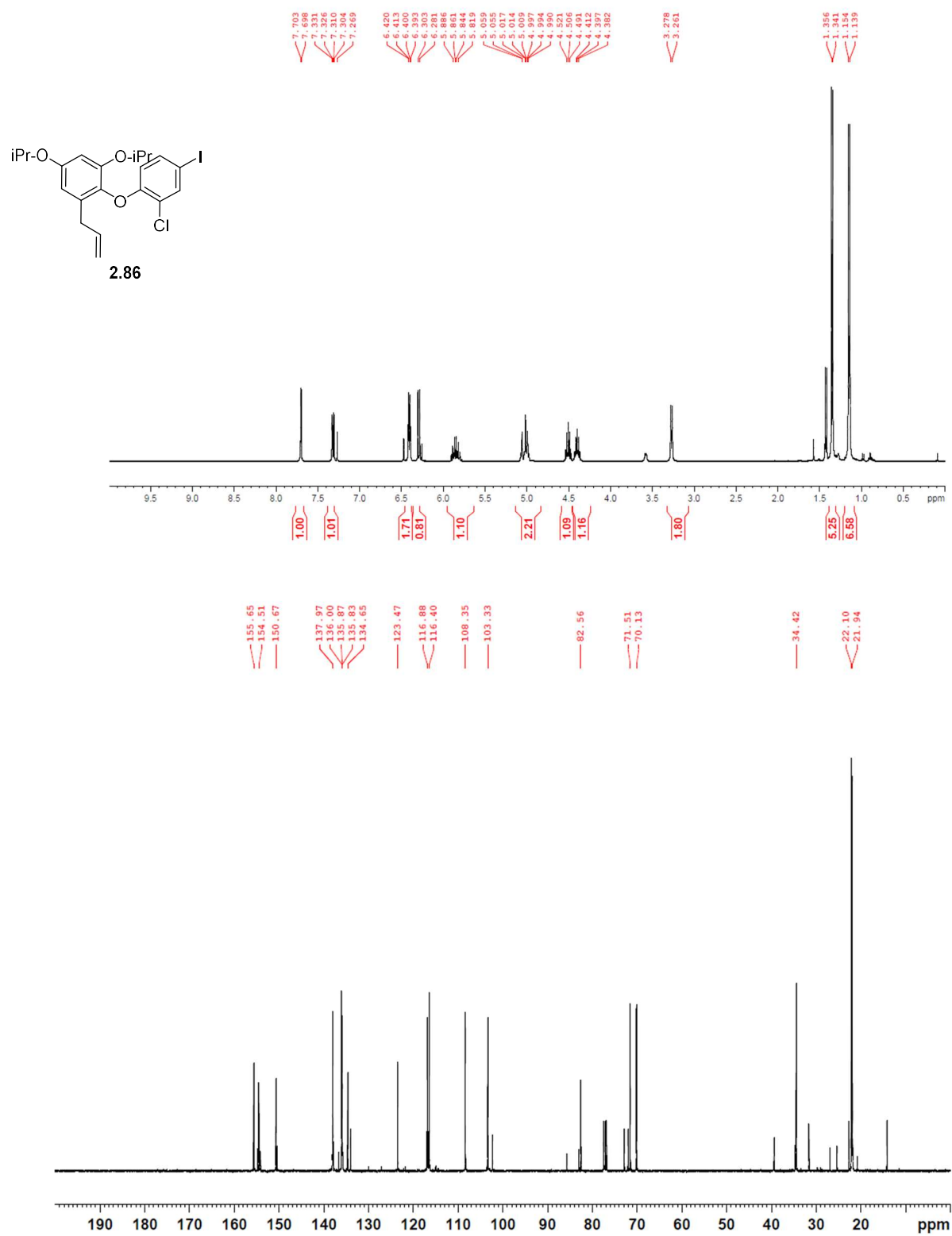
Figure A.18. ^{1}H NMR (400 MHz, CDCl$_3$) and ^{13}C NMR (100 MHz, CDCl$_3$) of **2.86.**
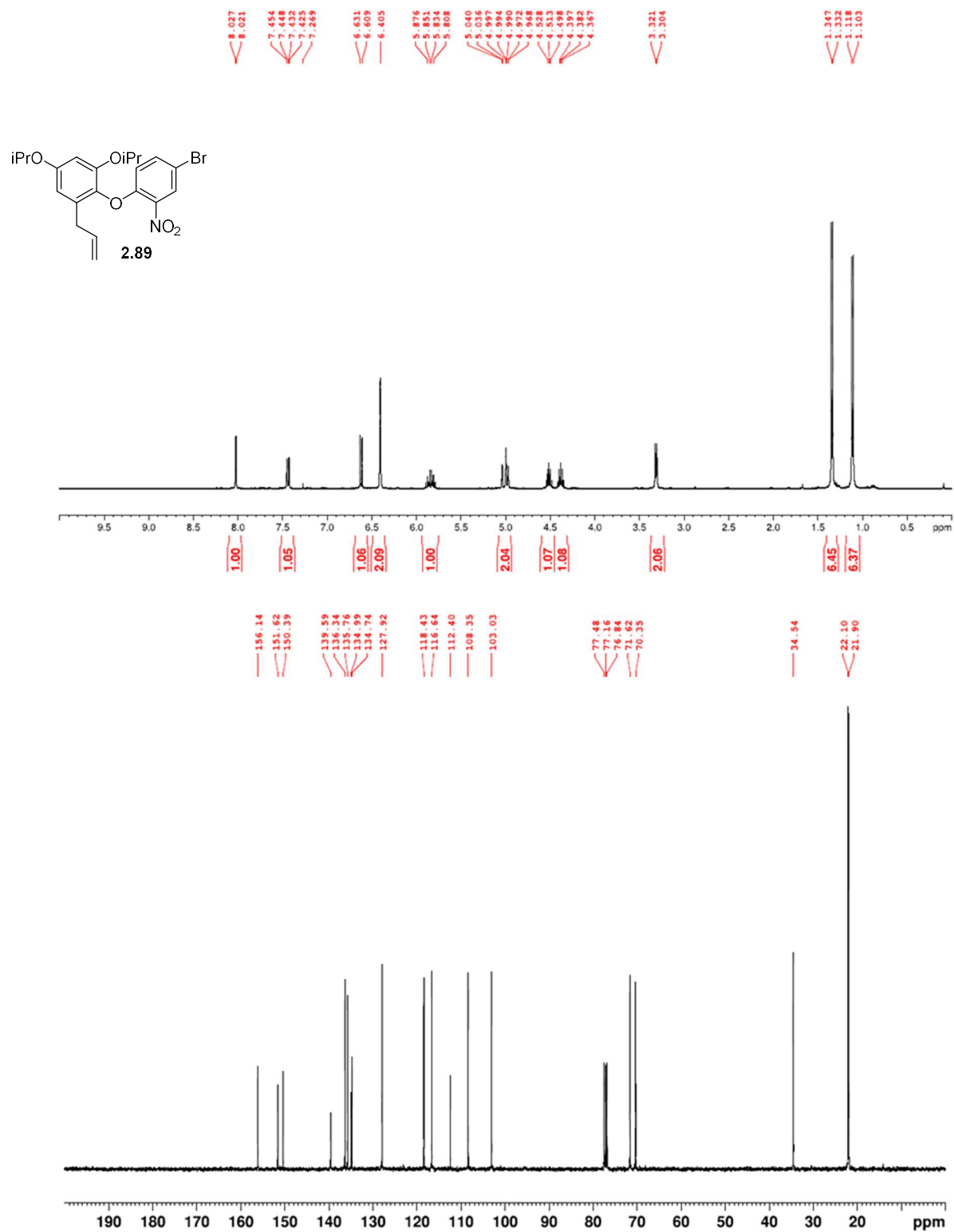
Figure A.19. ^1H NMR (400 MHz, CDCl$_3$) and ^{13}C NMR (100 MHz, CDCl$_3$) of **2.89.**
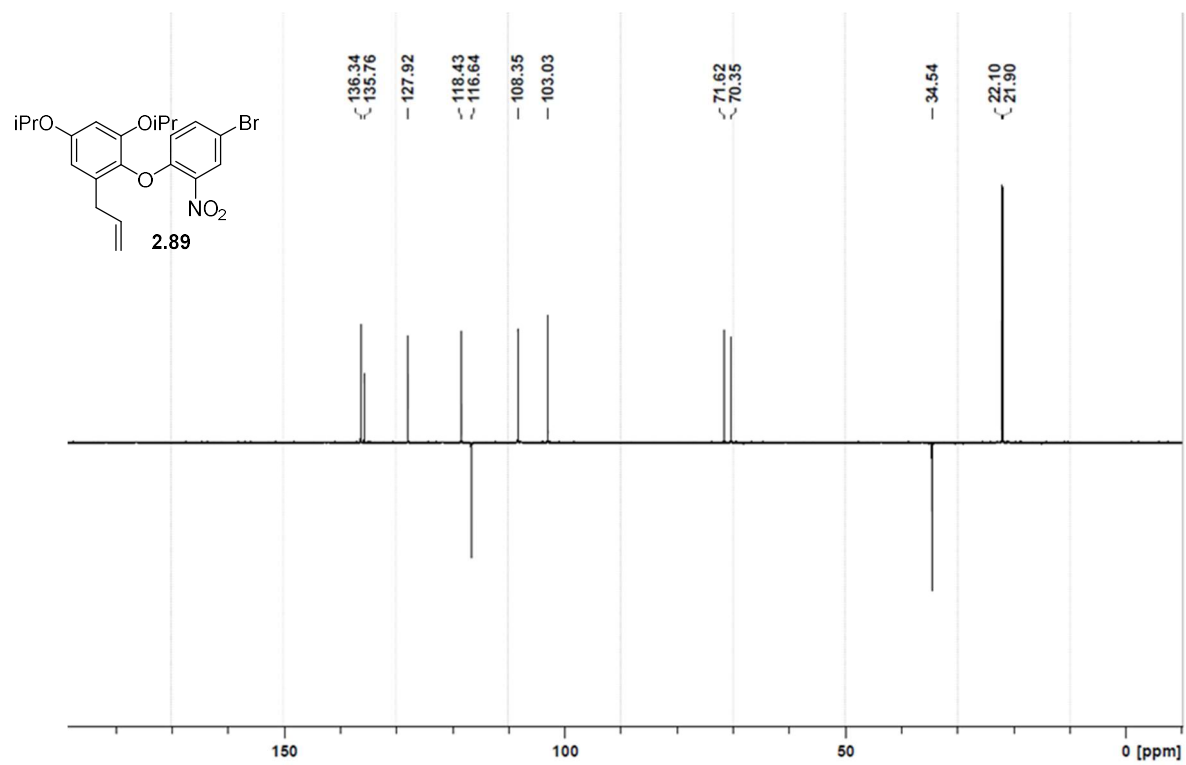
Figure A.20. DEPT-135 (CDCl₃) of **2.89.**

Figure A.21. ^{1}H NMR (400 MHz, CDCl$_3$) and ^{13}C NMR (100 MHz, CDCl$_3$) of **2.90.**
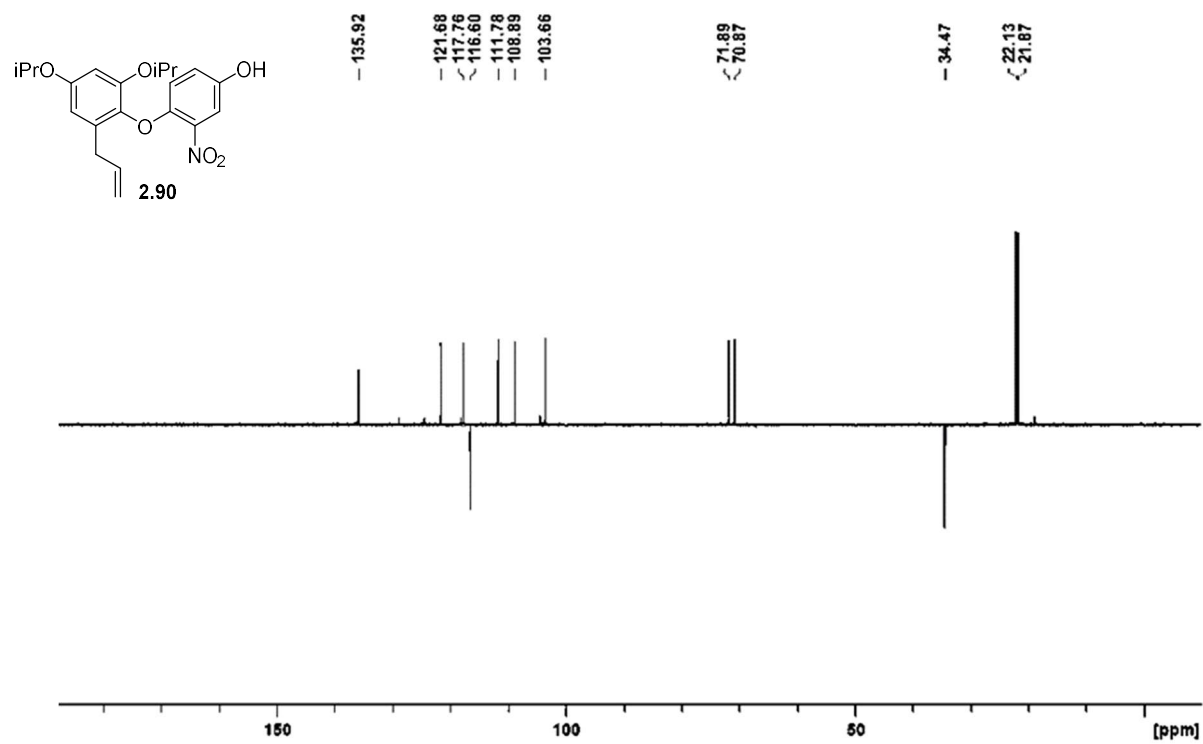
Figure A.22. DEPT-135 (CDCl₃) of **2.90.**
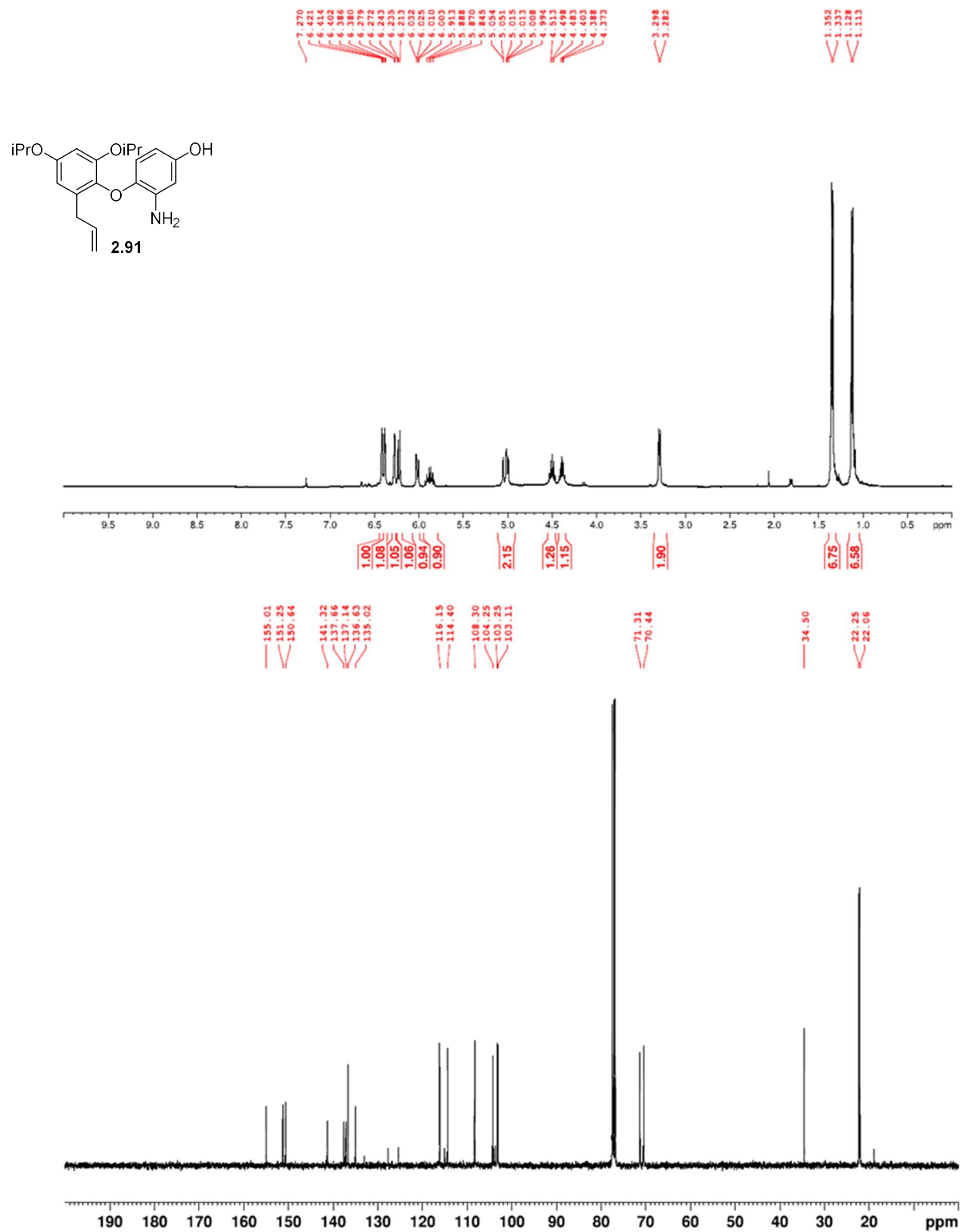
Figure A.23. ^{1}H NMR (400 MHz, CDCl$_3$) and ^{13}C NMR (100 MHz, CDCl$_3$) of **2.91.**
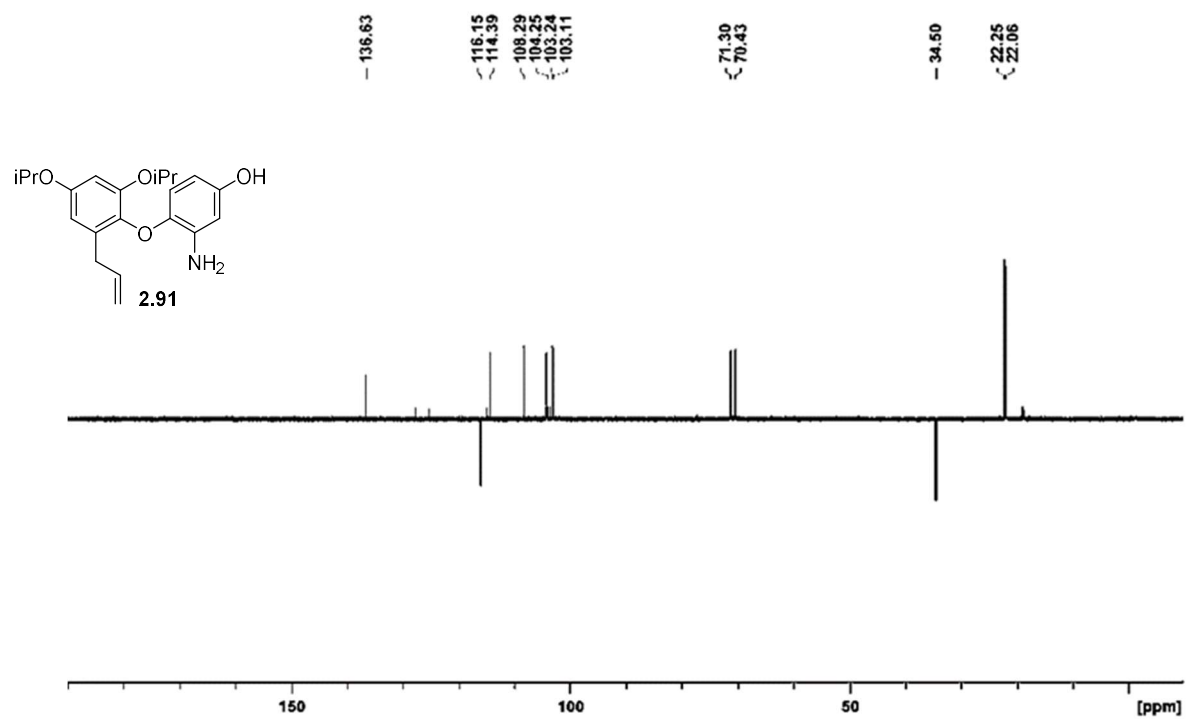
Figure A.24. DEPT-135 (CDCl$_3$) of **2.91.**
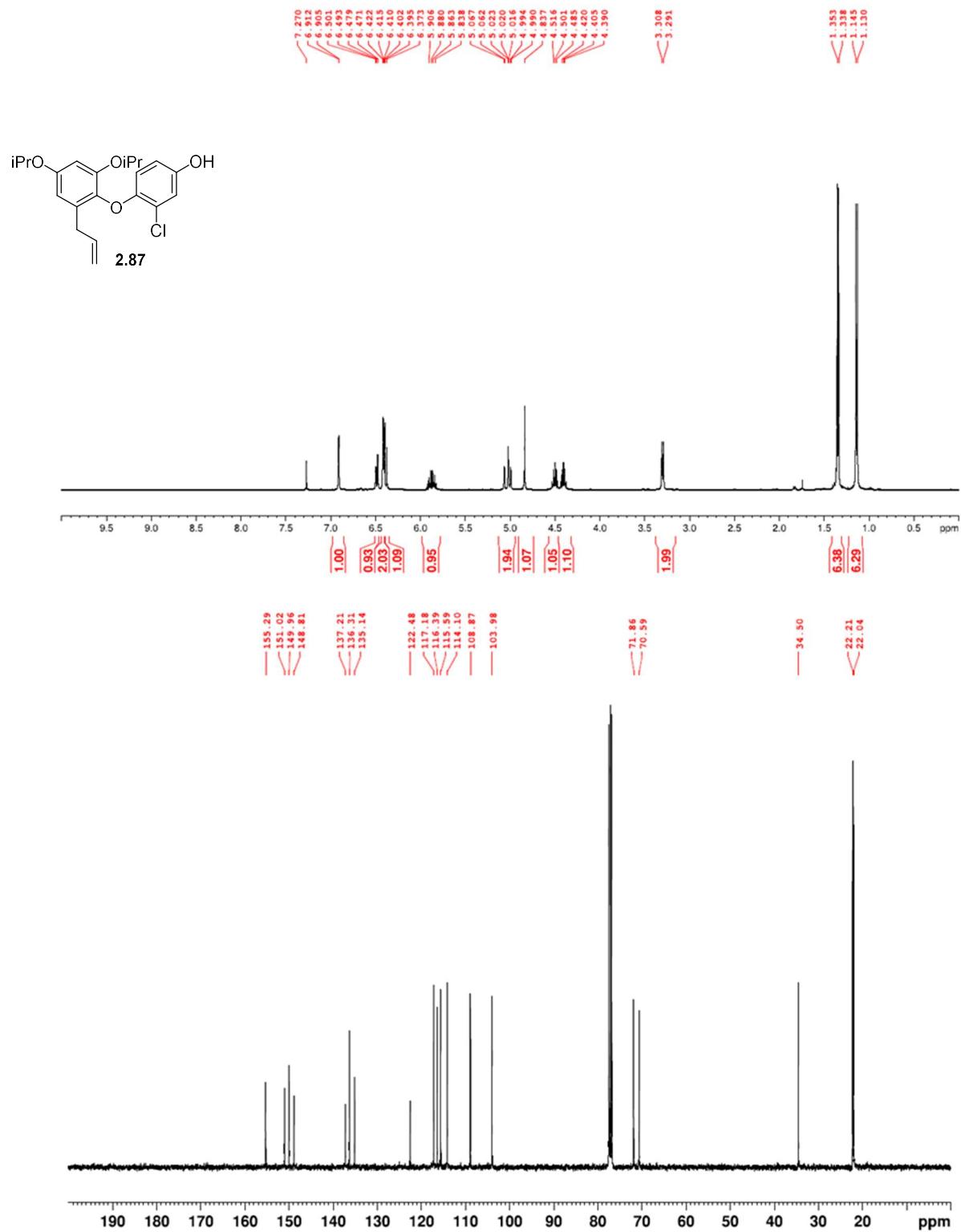
Figure A.25. ^{1}H NMR (400 MHz, CDCl$_3$) and ^{13}C NMR (100 MHz, CDCl$_3$) of **2.87.**
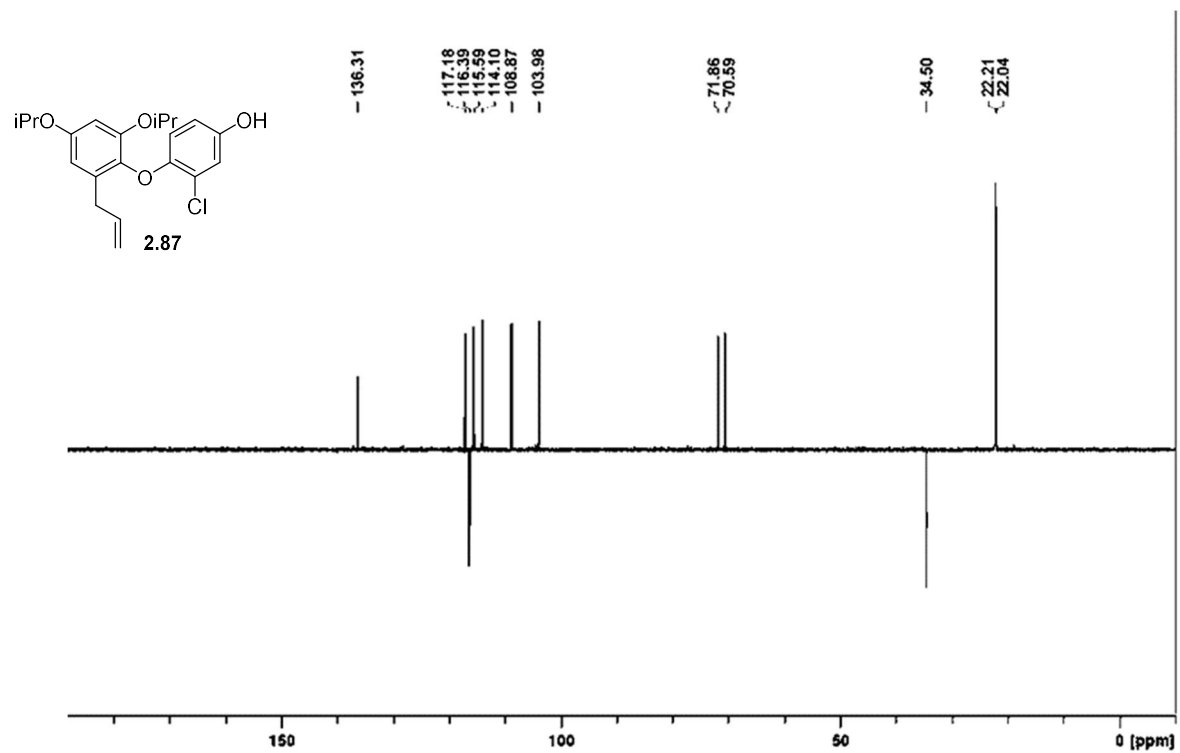
Figure A.26. DEPT-135 (CDCl$_3$) of **2.87**.
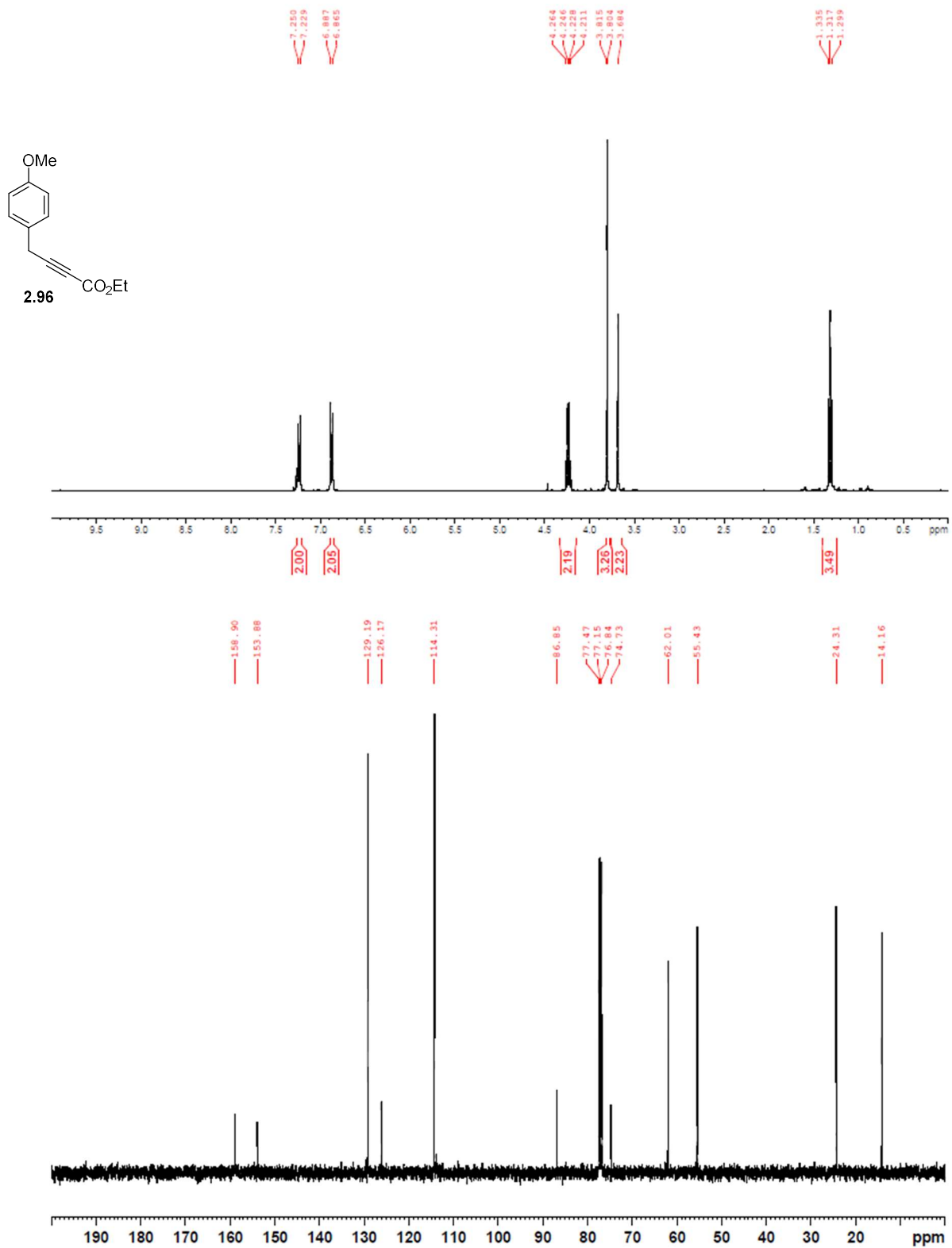
Figure A.27. ^{1}H NMR (400 MHz, CDCl$_3$) and ^{13}C NMR (100 MHz, CDCl$_3$) of **2.96.**
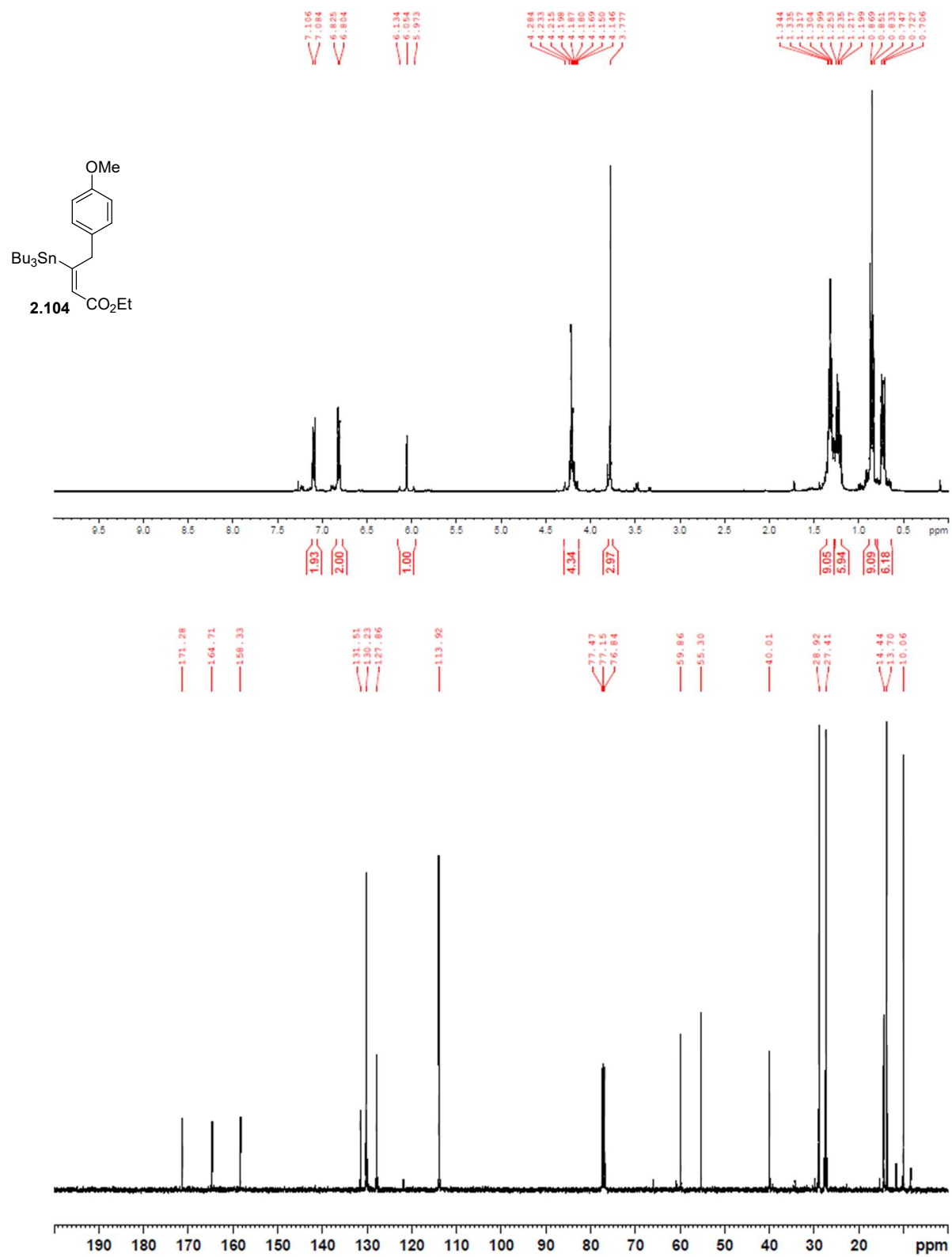
Figure A.28. ^{1}H NMR (400 MHz, CDCl$_3$) and ^{13}C NMR (100 MHz, CDCl$_3$) of **2.104**.
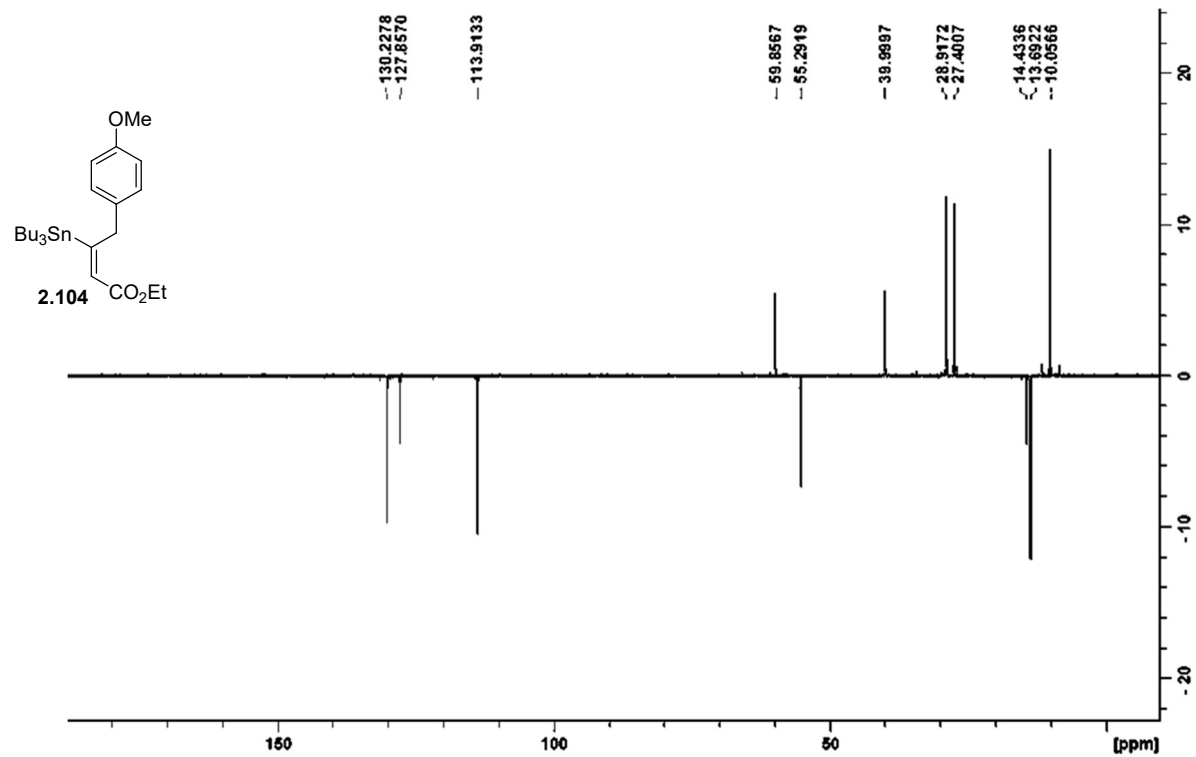
Figure A.29. DEPT-135 (CDCl$_3$) of **2.104.**
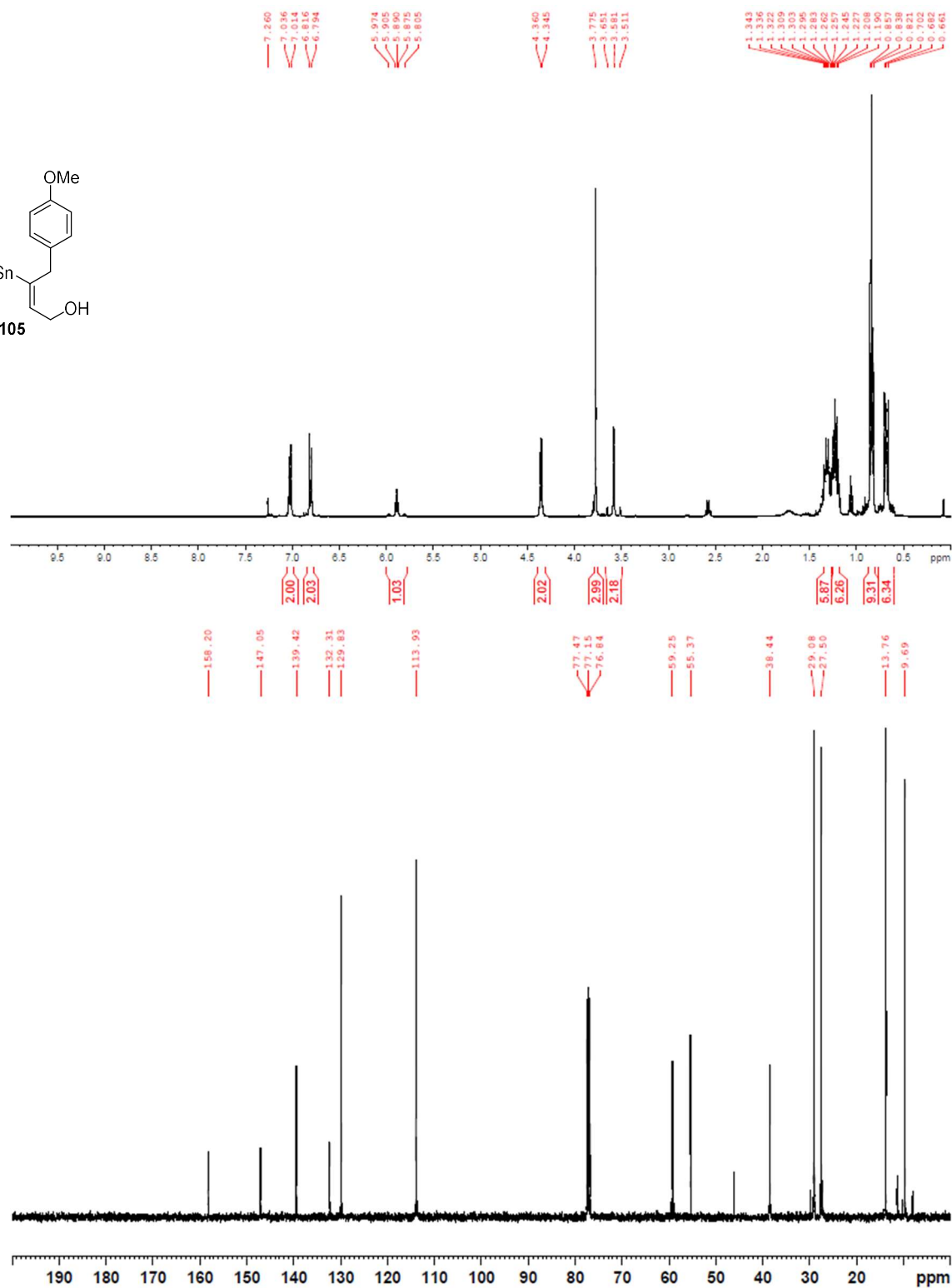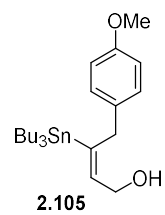
Figure A.30. ^{1}H NMR (400 MHz, CDCl$_3$) and ^{13}C NMR (100 MHz, CDCl$_3$) of **2.105.**
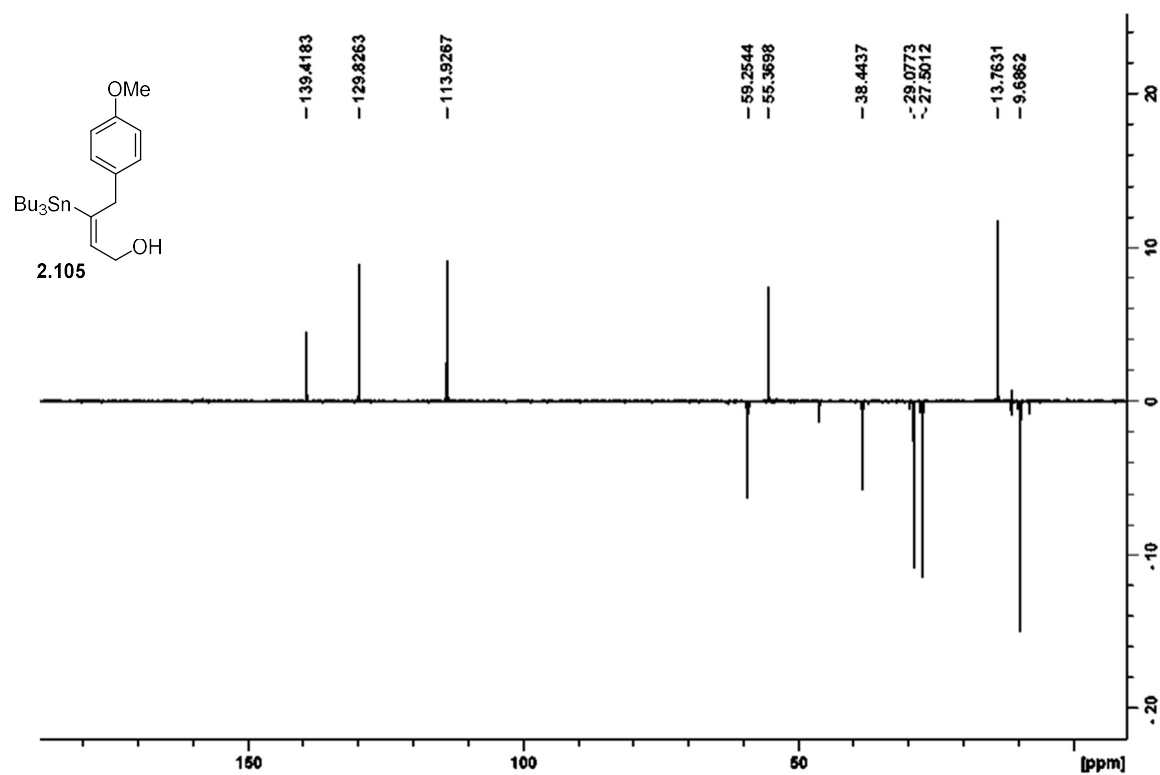
Figure A.31. DEPT-135 (CDCl₃) of **2.105.**
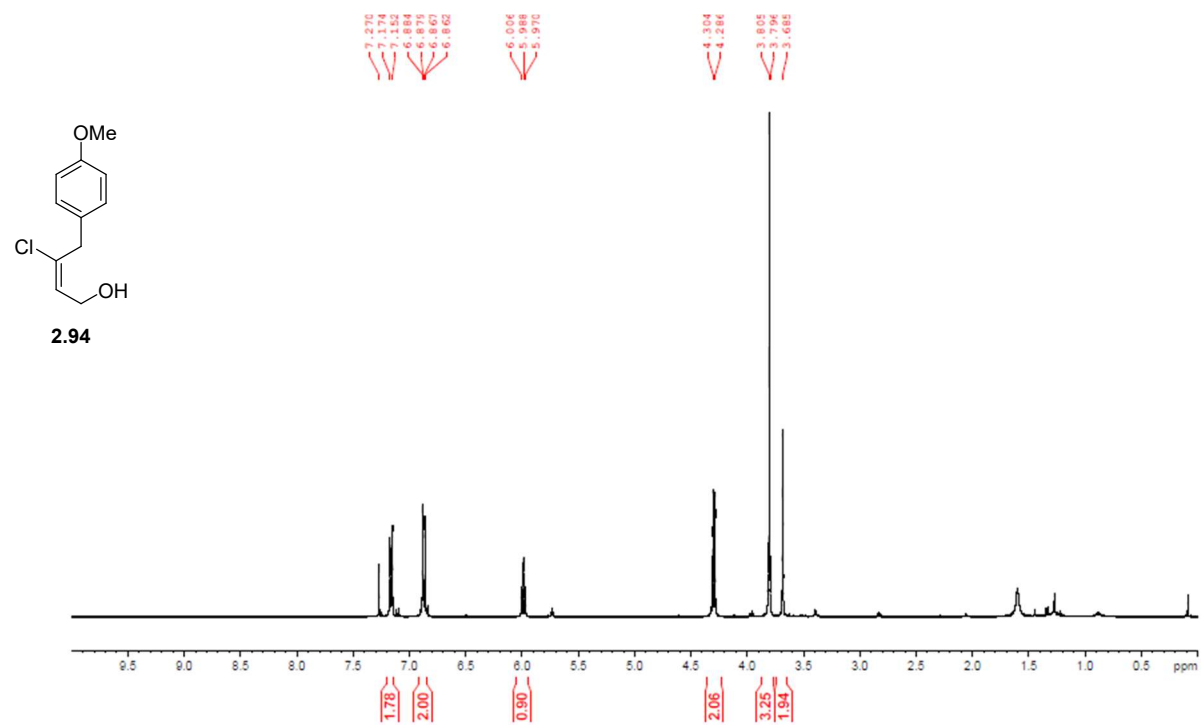
Figure A.32. ¹H NMR (400 MHz, CDCl₃) of **2.94**.
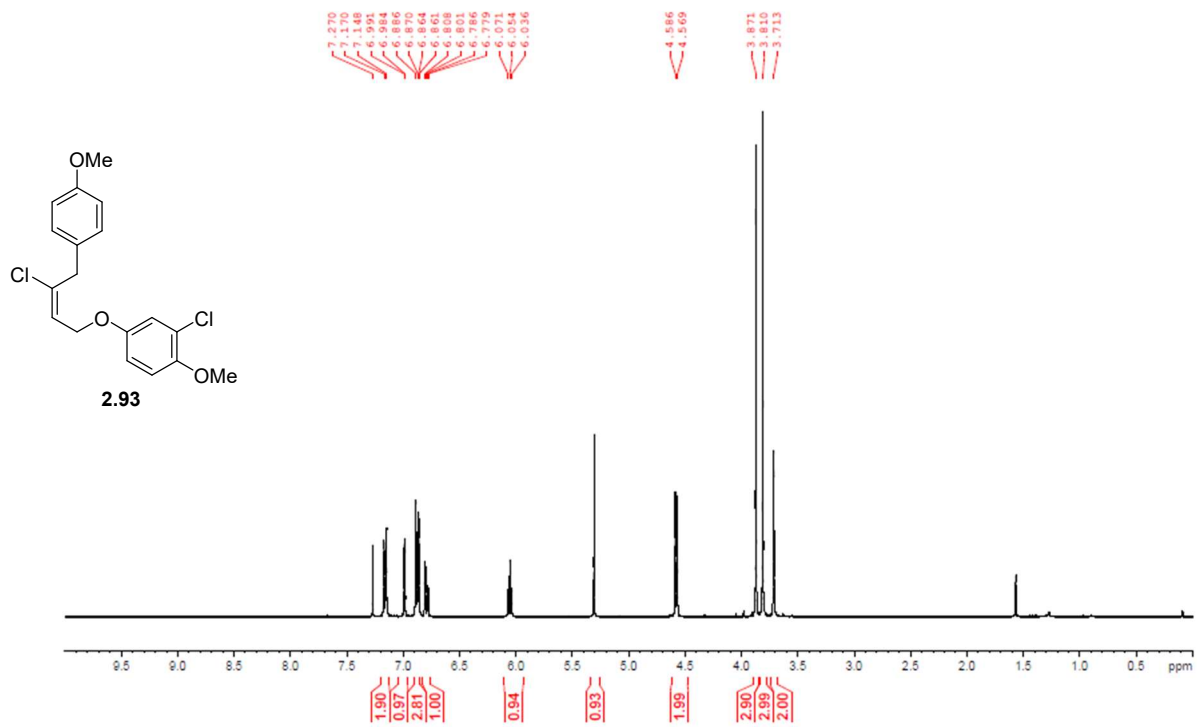
Figure A.33. ^{1}H NMR (400 MHz, CDCl$_3$) of **2.93.**
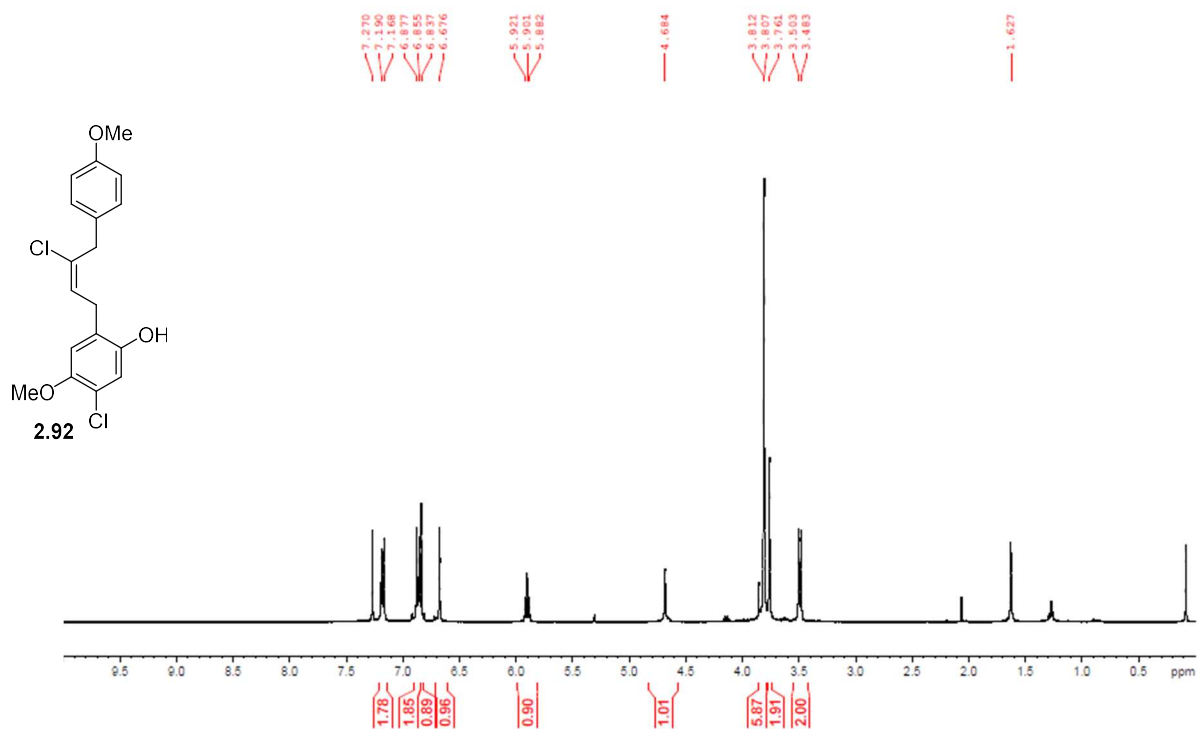
Figure A.34. ^{1}H NMR (400 MHz, CDCl$_3$) of **2.92.**

222
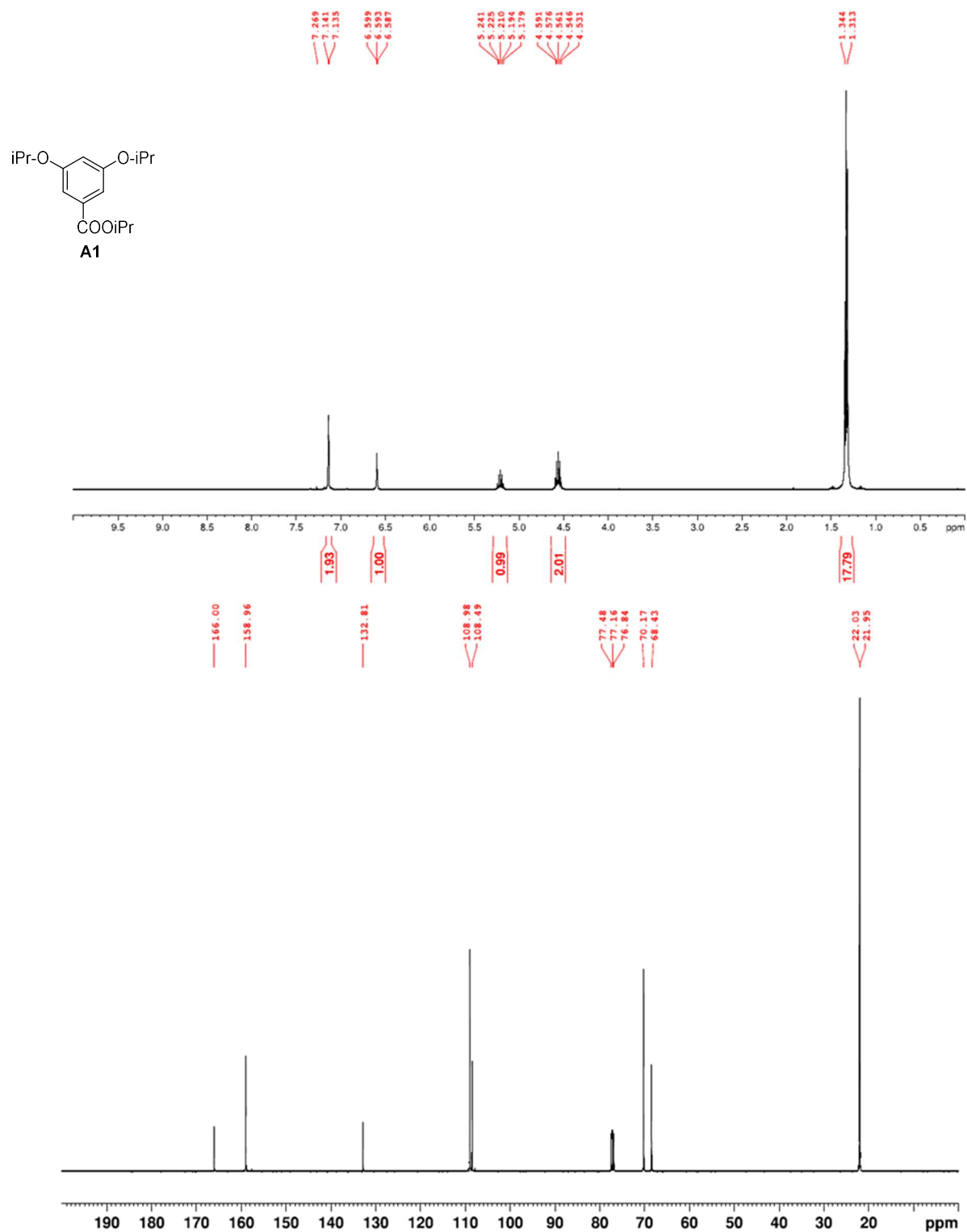
Figure A.35. ^{1}H NMR (400 MHz, CDCl$_3$) and ^{13}C NMR (100 MHz, CDCl$_3$) of **A1.**
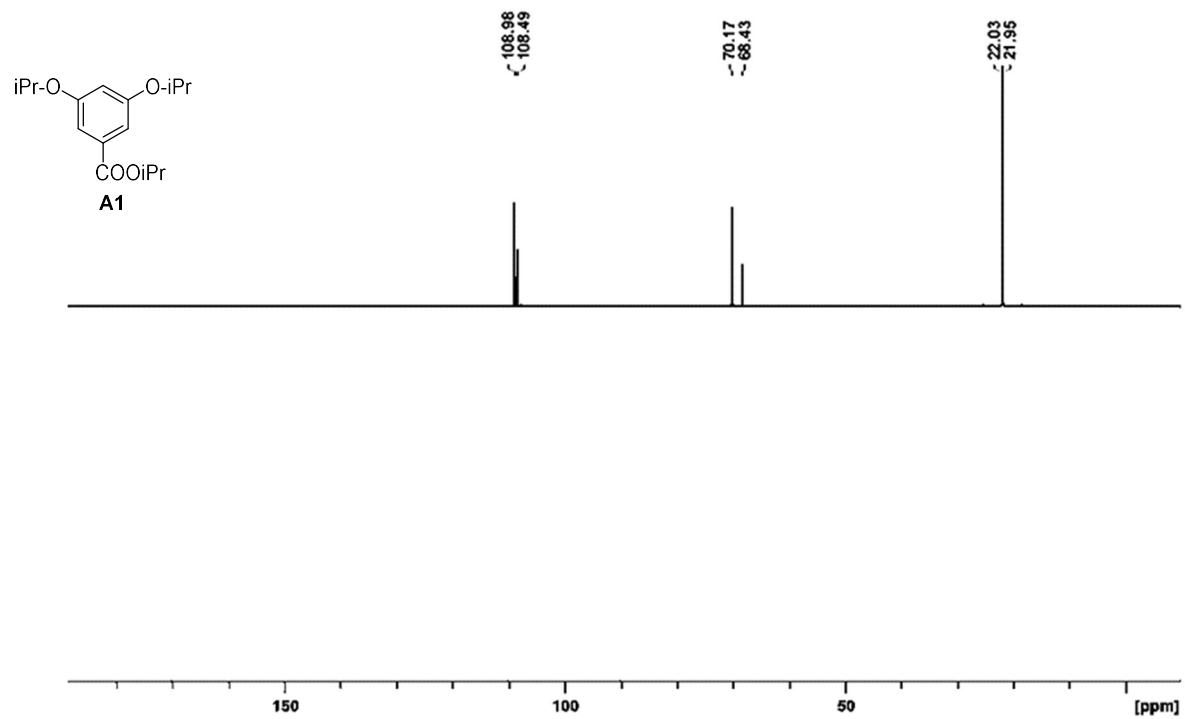
Figure A.36. DEPT-135 (CDCl$_3$) of **A1.**
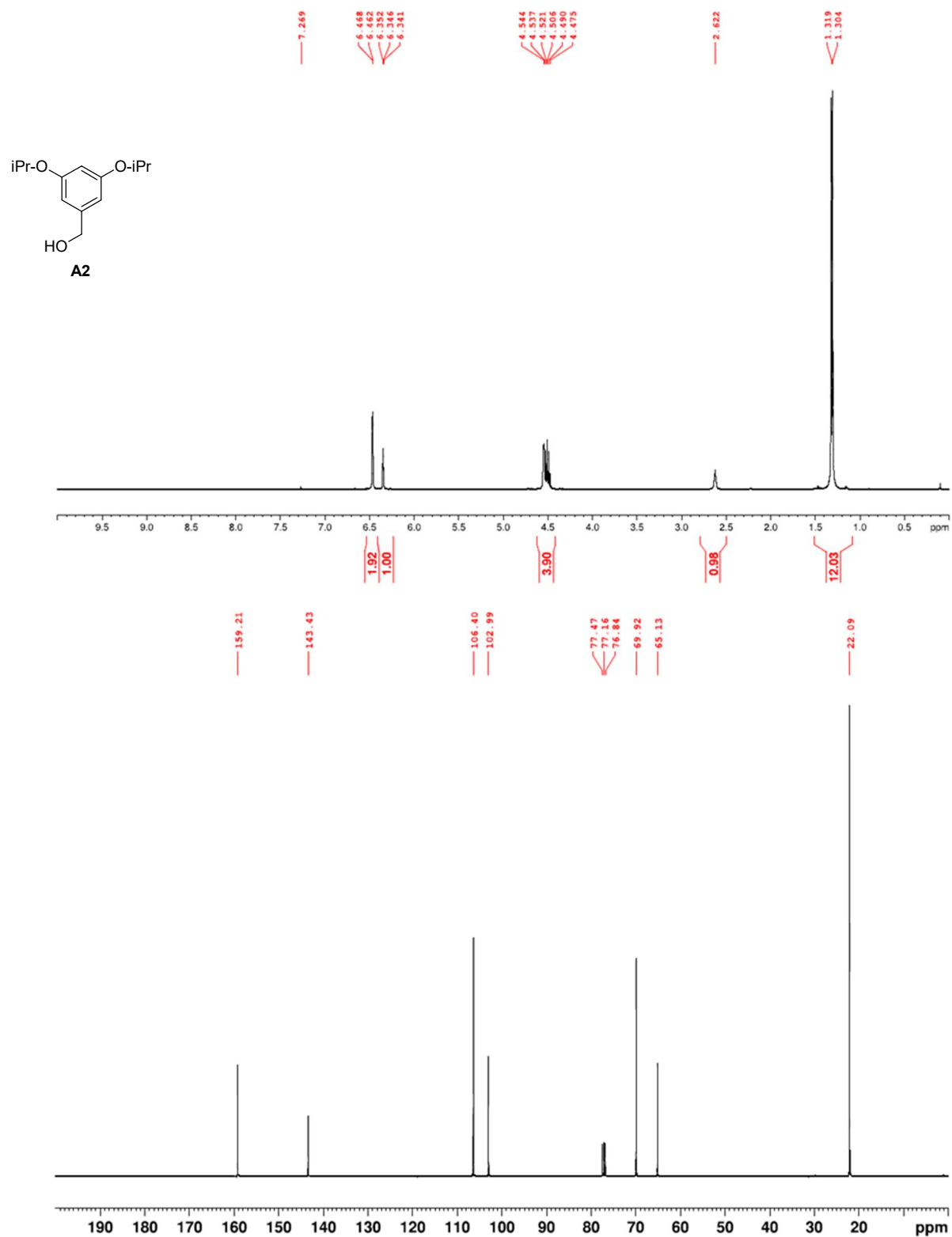
Figure A.37. ^{1}H NMR (400 MHz, CDCl$_3$) and ^{13}C NMR (100 MHz, CDCl$_3$) of **A2.**
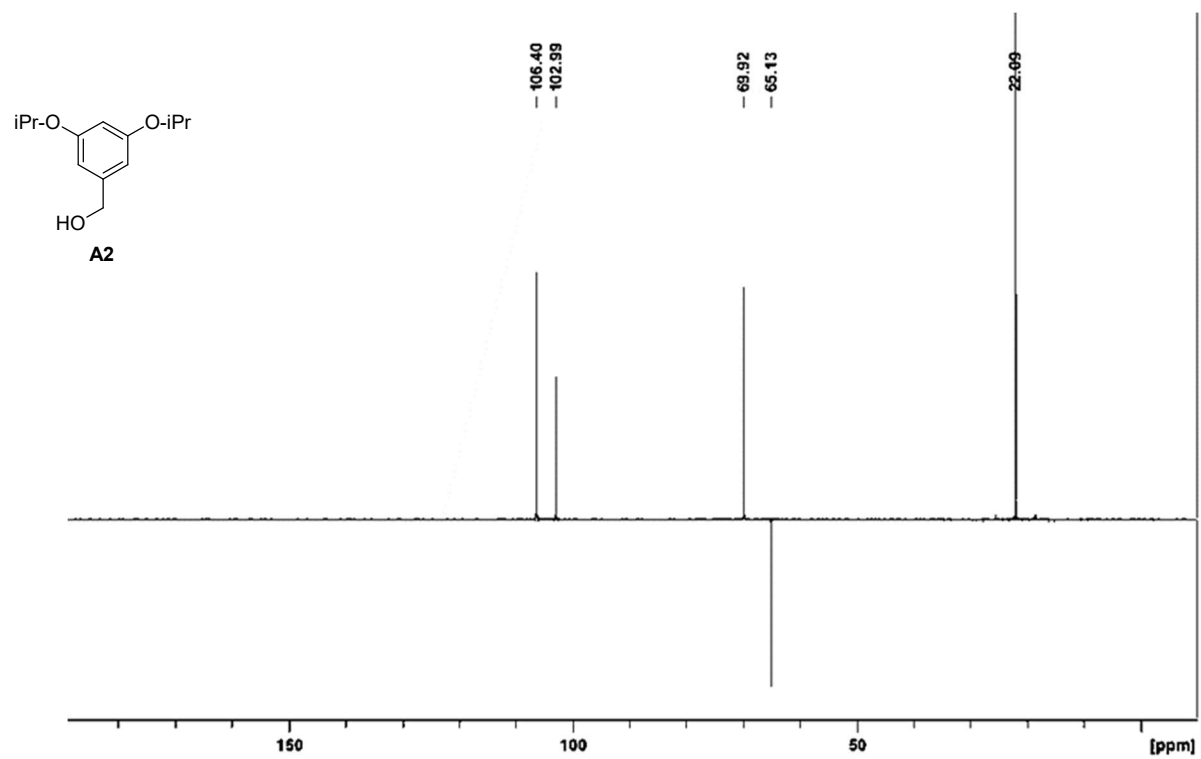
Figure A.38. DEPT-135 (CDCl₃) of **A2.**
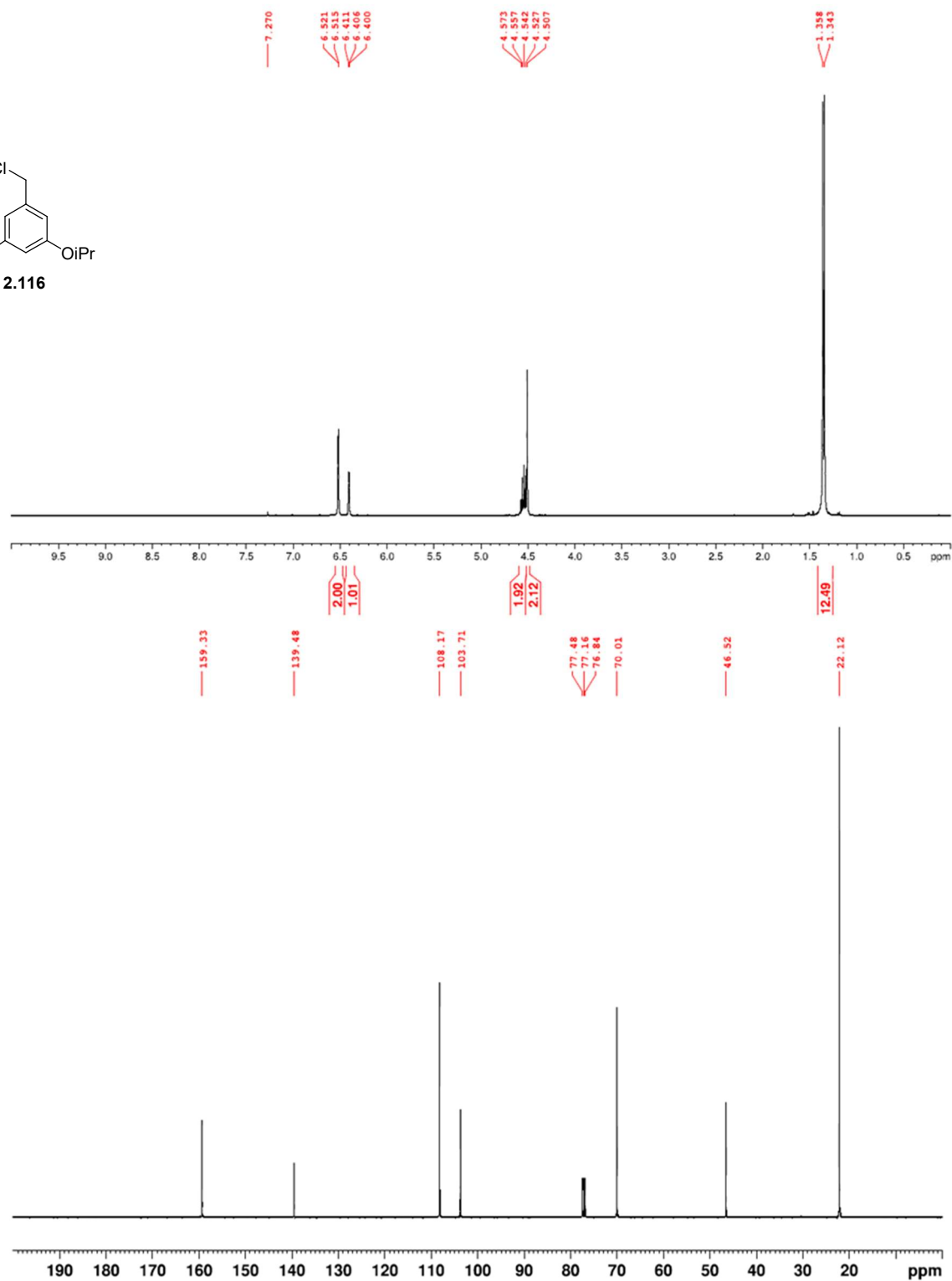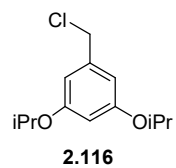
Figure A.39. ^{1}H NMR (400 MHz, CDCl$_3$) and ^{13}C NMR (100 MHz, CDCl$_3$) of **2.116.**
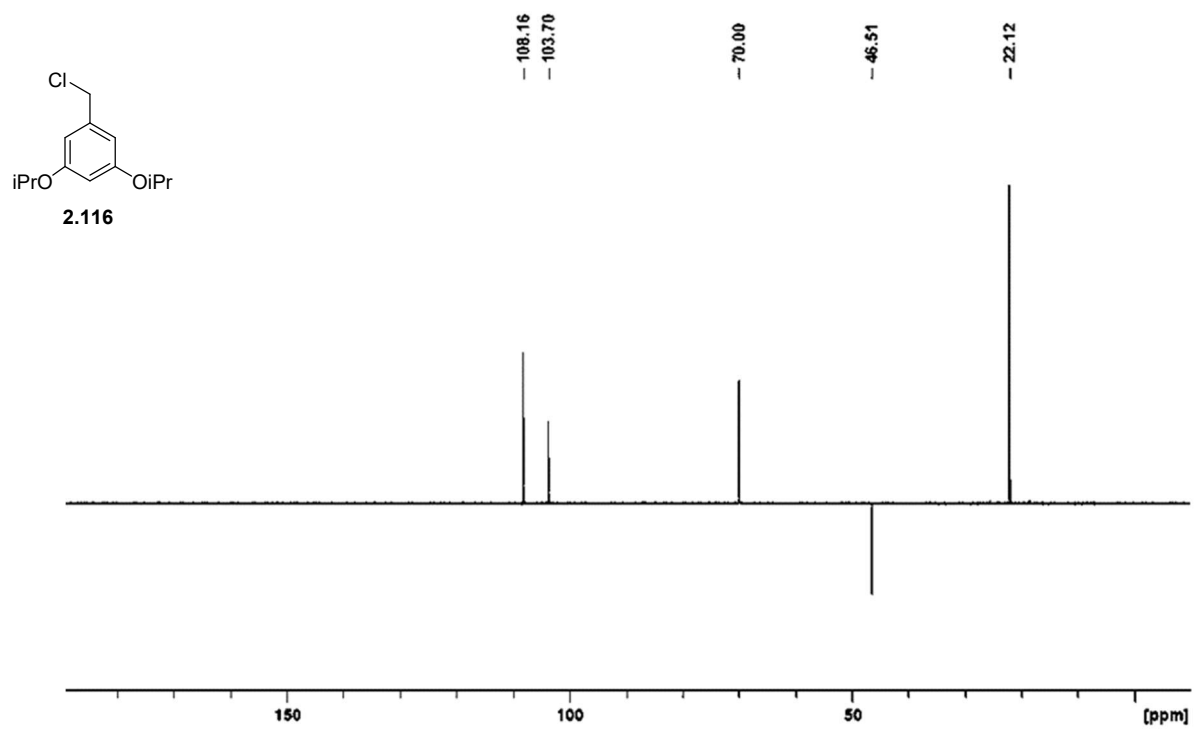
Figure A.40. DEPT-135 (CDCl₃) of **2.116.**
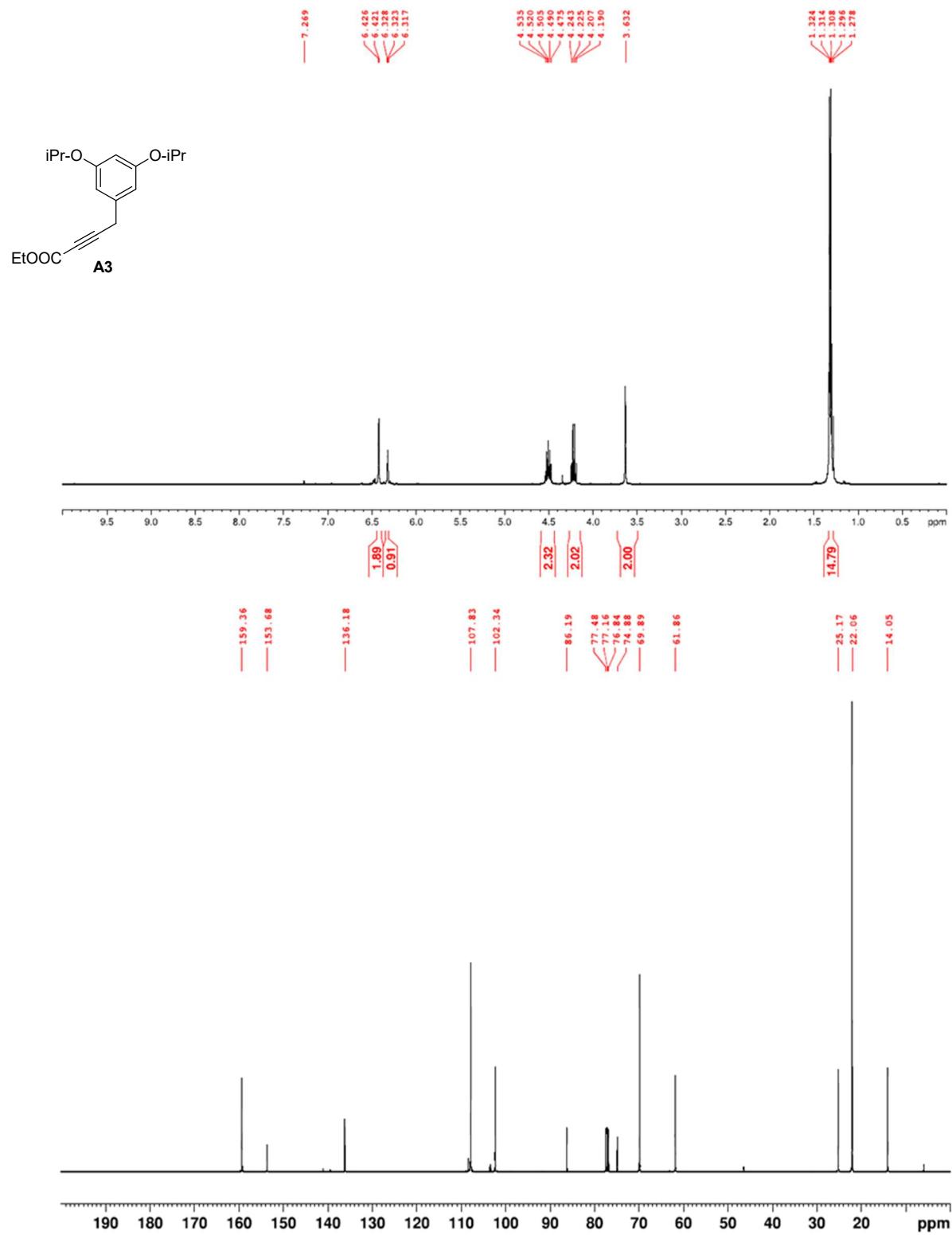
Figure A.41. ^{1}H NMR (400 MHz, CDCl$_3$) and ^{13}C NMR (100 MHz, CDCl$_3$) of **A3.**
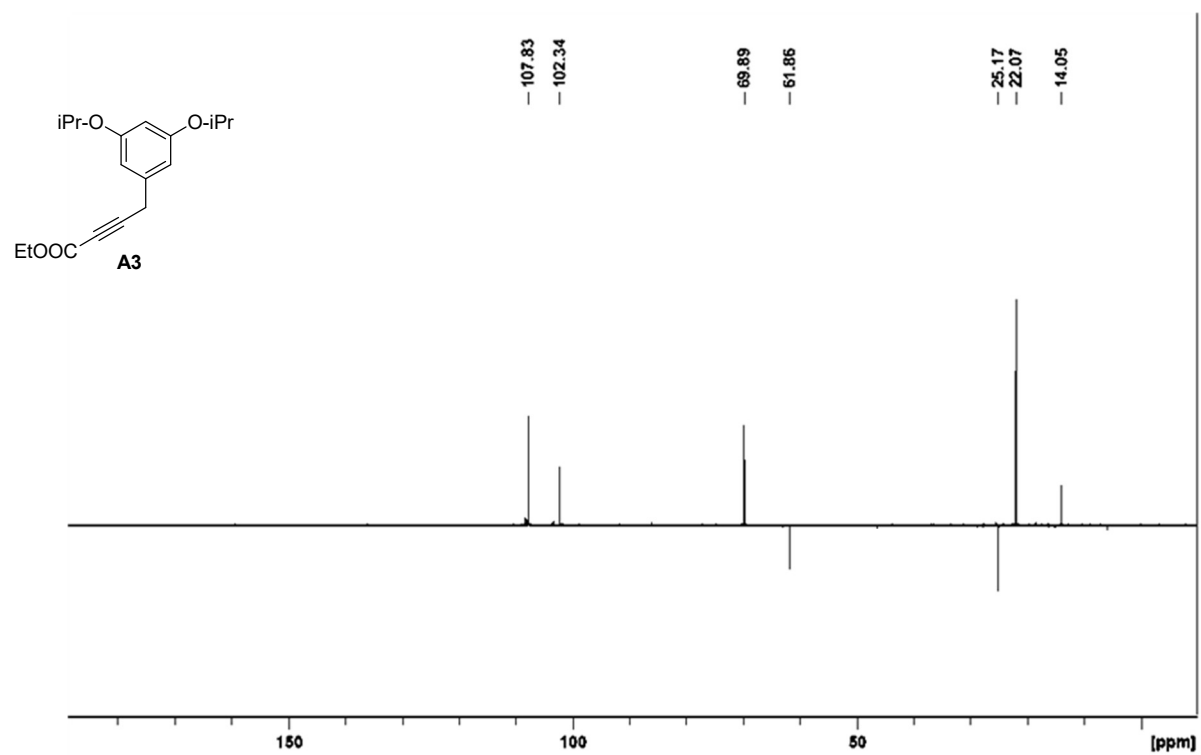
Figure A.42. DEPT-135(CDCl₃) of **A3.**

230
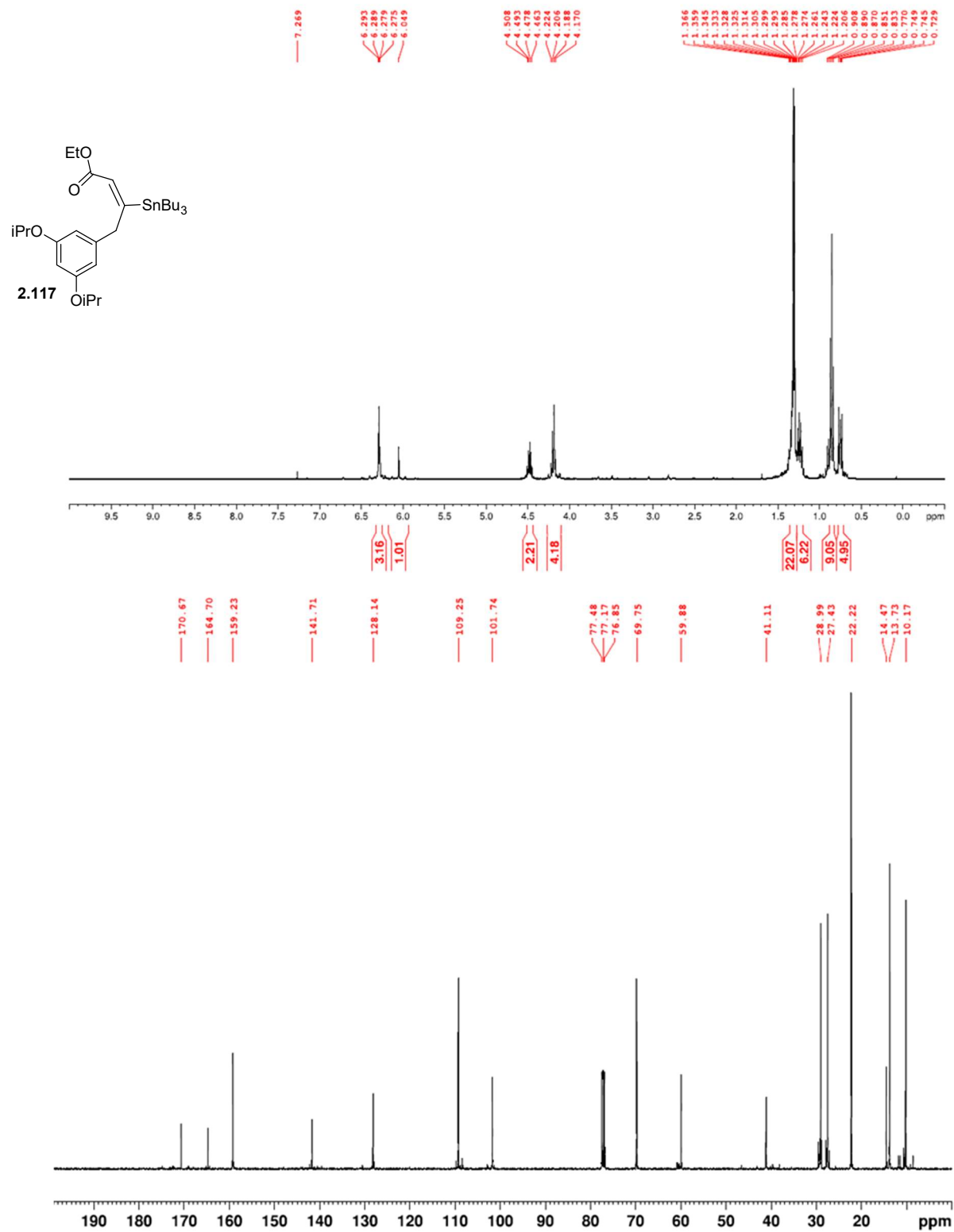
Figure A.43. ^{1}H NMR (400 MHz, CDCl$_3$) and ^{13}C NMR (100 MHz, CDCl$_3$) of **2.117.**
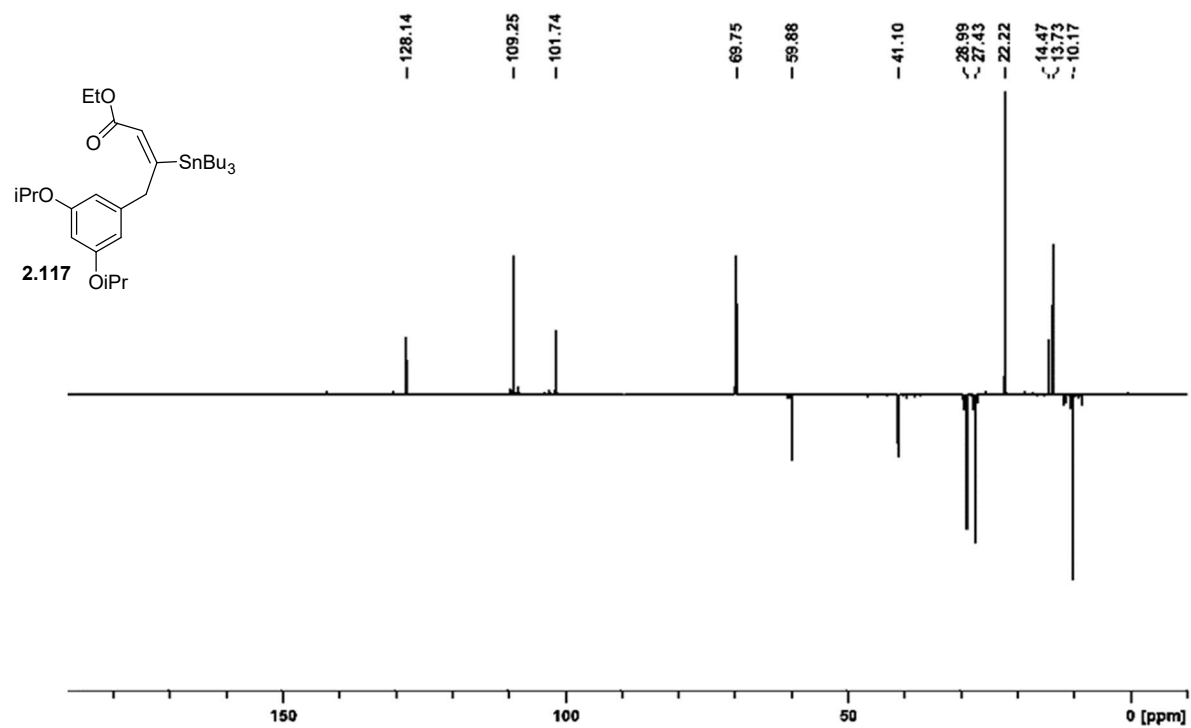
Figure A.44. Figure A.44. DEPT-135(CDCl$_3$) of **2.117.**

Figure A.45. ^{1}H NMR (400 MHz, CDCl$_3$) and ^{13}C NMR (100 MHz, CDCl$_3$) of **A4.**
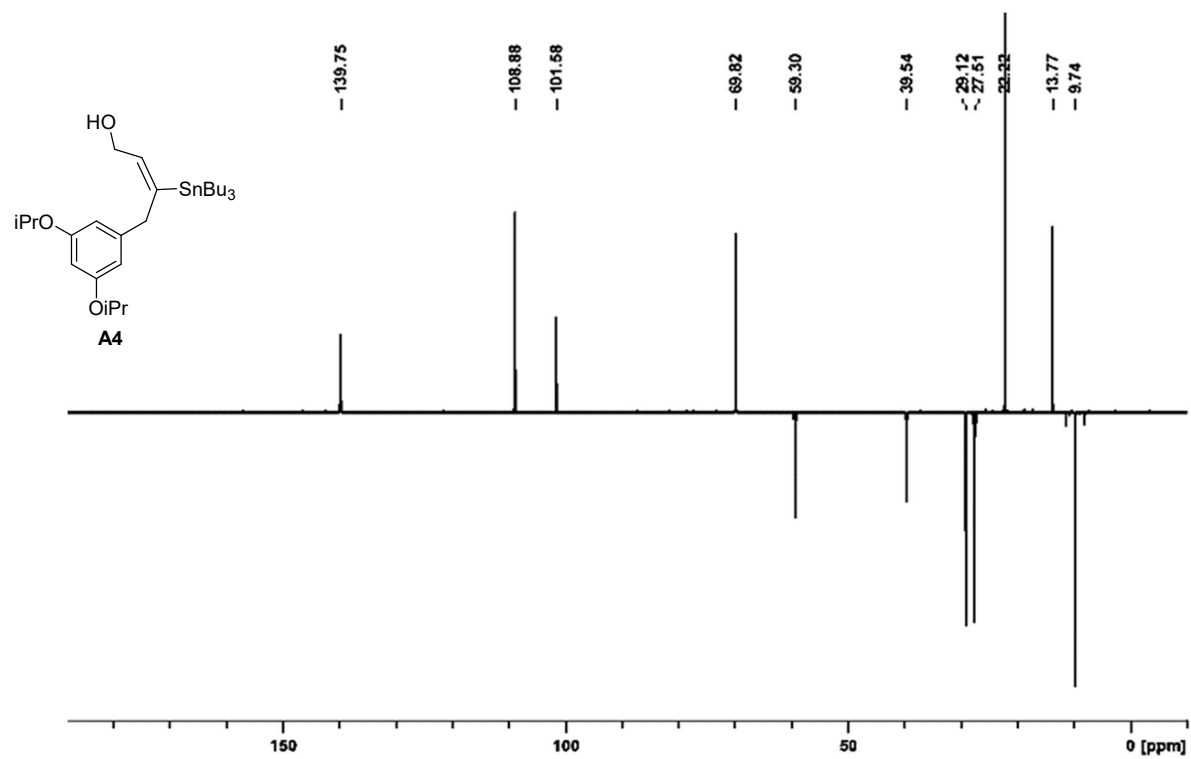
Figure A.46. DEPT-135(CDCl₃) of **A4.**
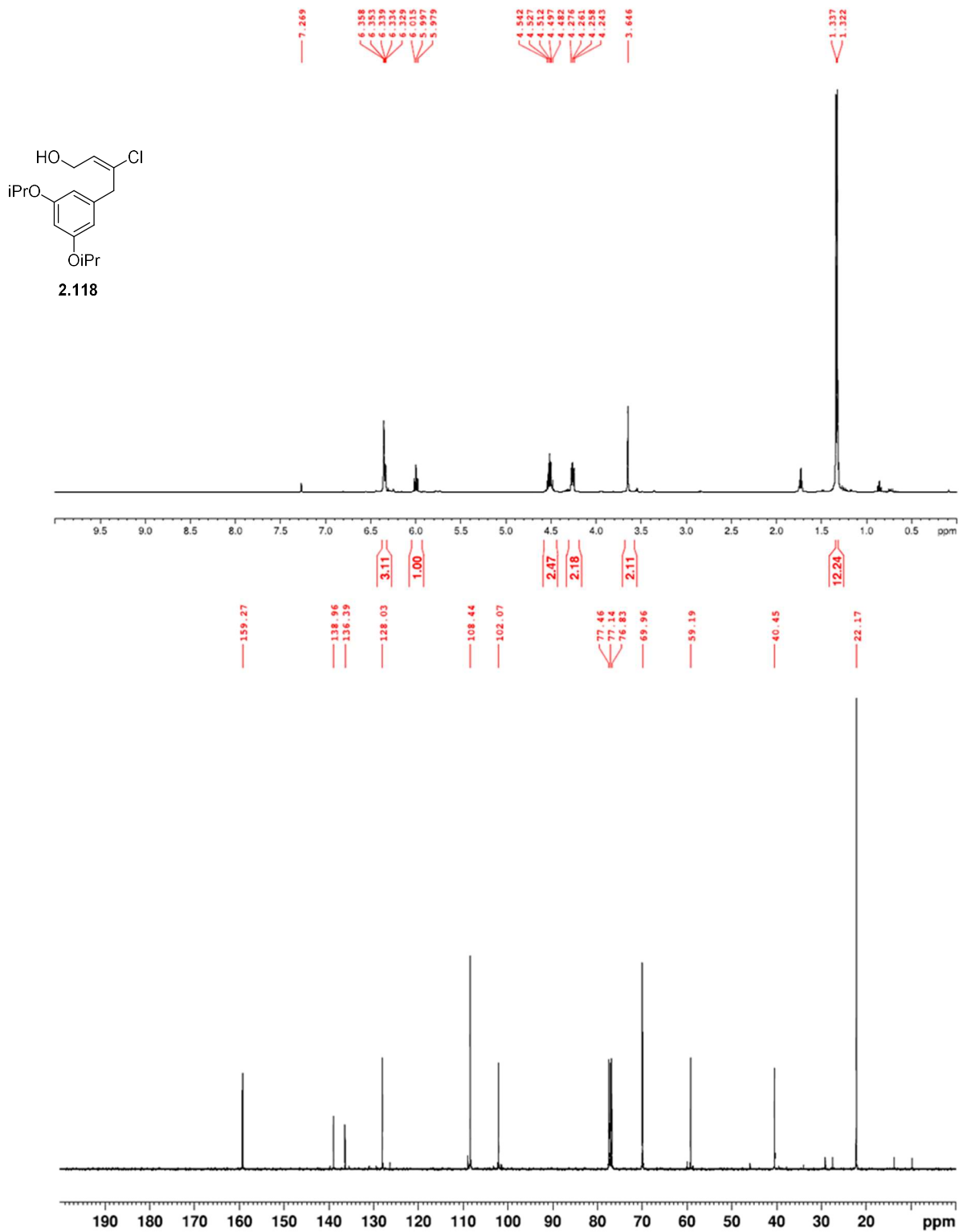
Figure A.47. ^{1}H NMR (400 MHz, CDCl$_3$) and ^{13}C NMR (100 MHz, CDCl$_3$) of **2.118.**
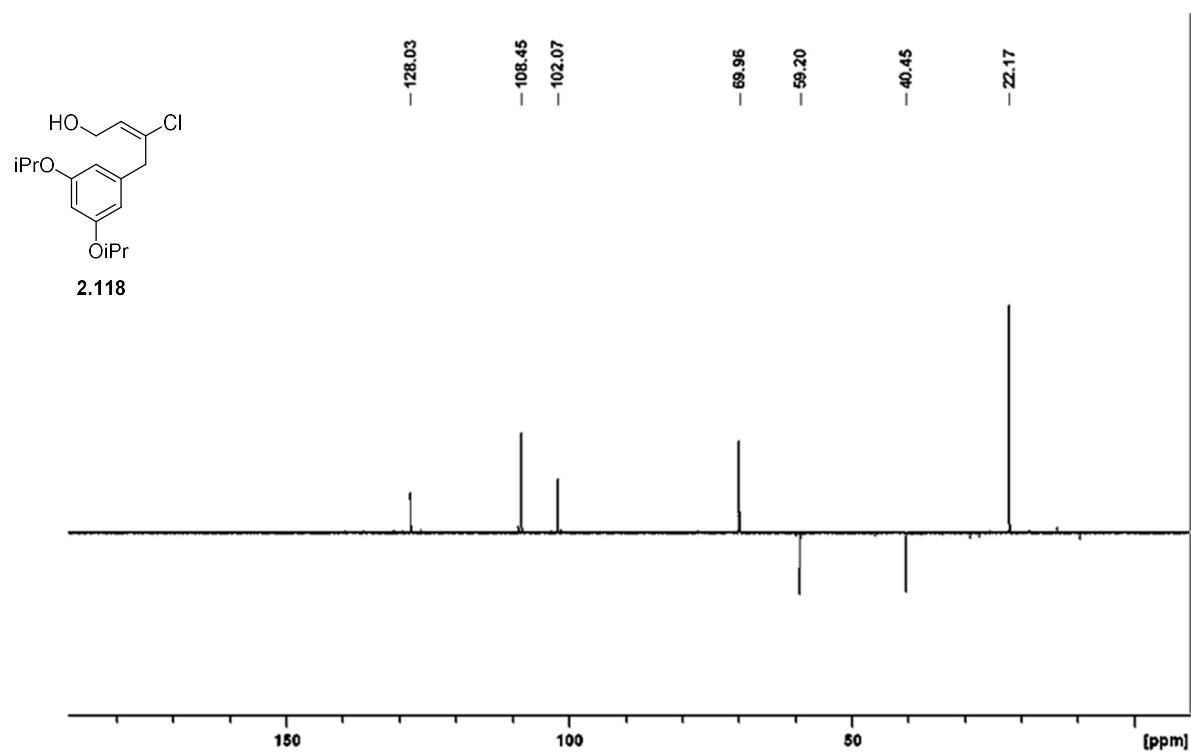
Figure A.48. DEPT-135(CDCl$_3$) of **2.118**.
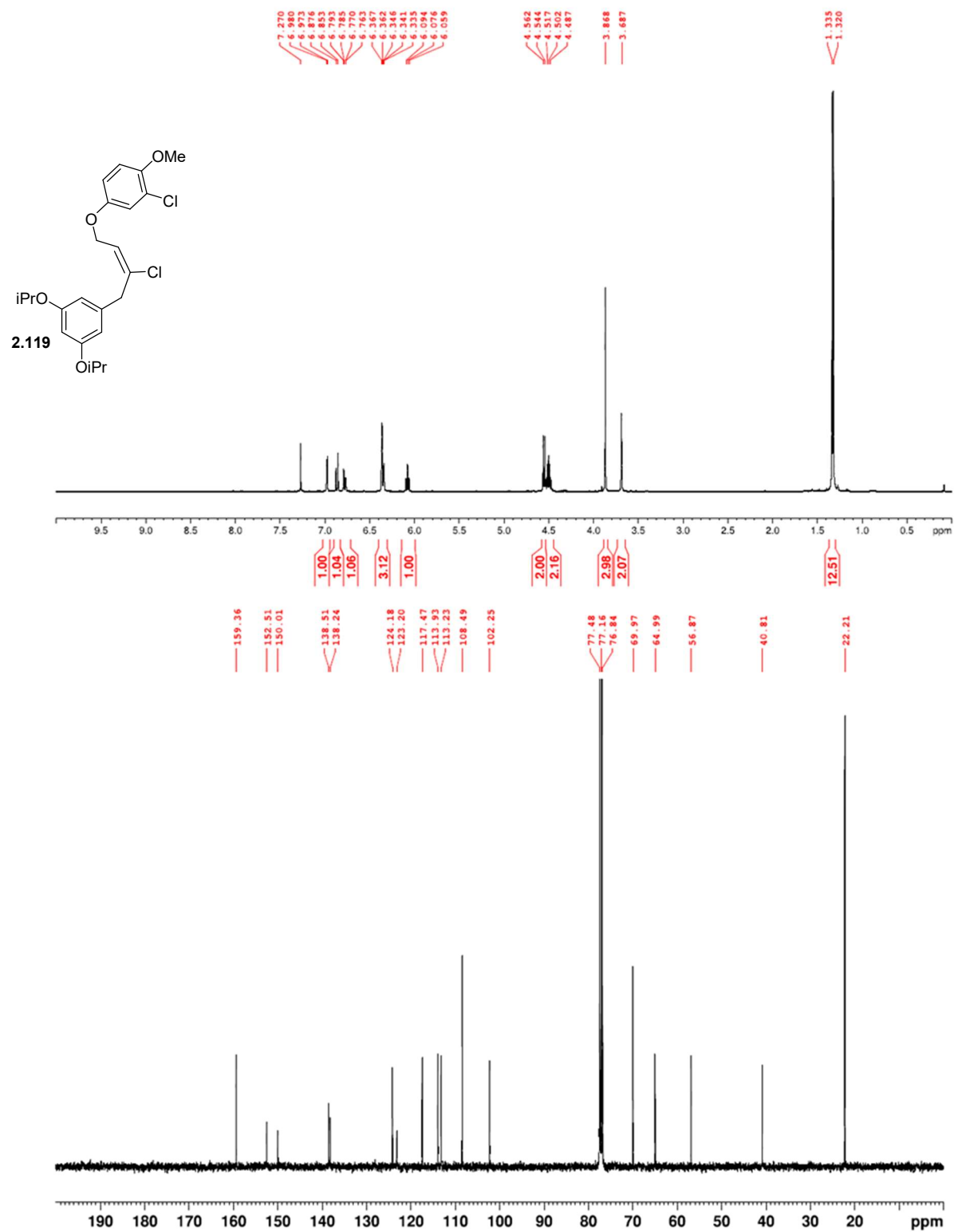
Figure A.49. ^{1}H NMR (400 MHz, CDCl$_3$) and ^{13}C NMR (100 MHz, CDCl$_3$) of **2.119.**
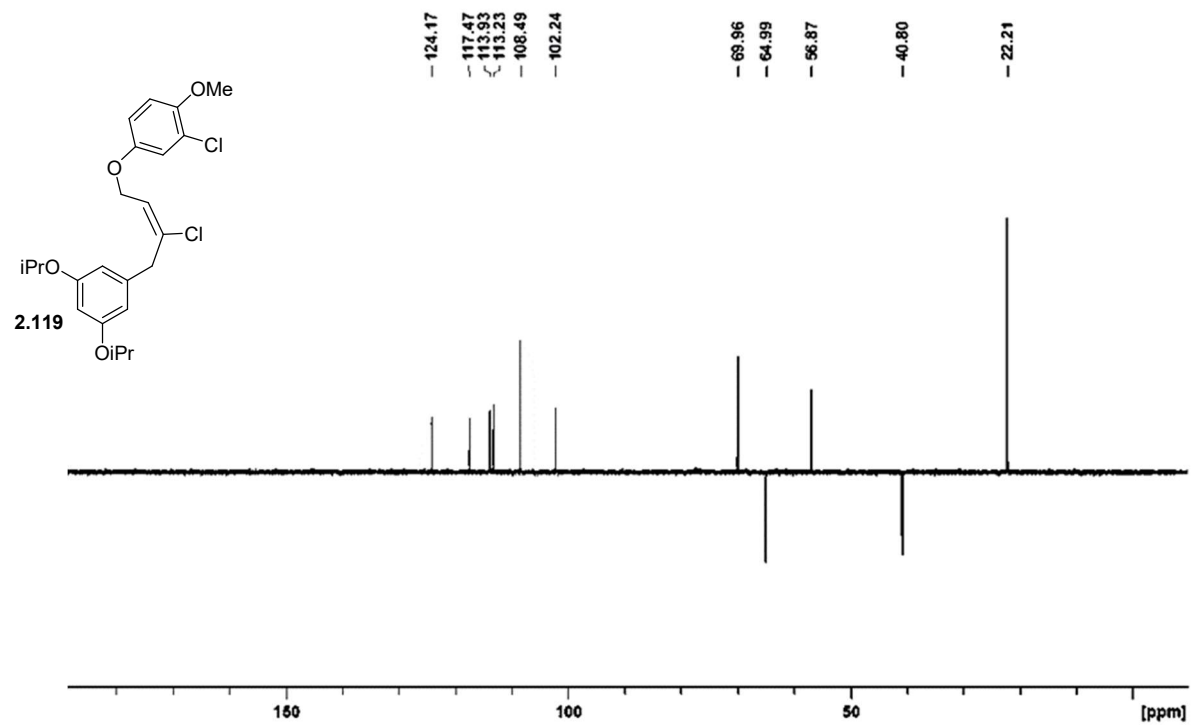
Figure A.50. DEPT-135(CDCl₃) of **2.119.**
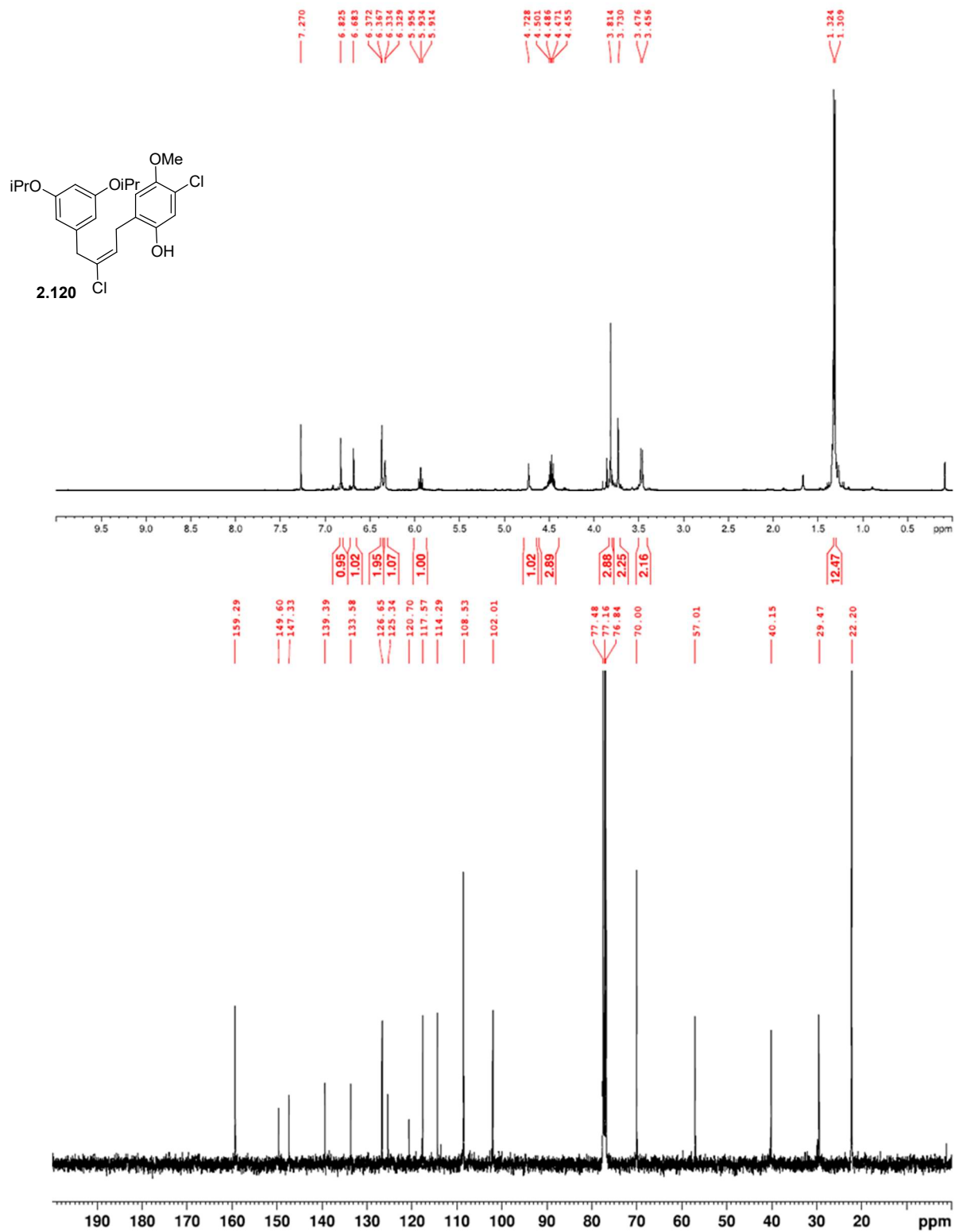
Figure A.51. ^{1}H NMR (400 MHz, (CDCl$_3$) and ^{13}C NMR (100 MHz, CDCl$_3$) of **2.120.**
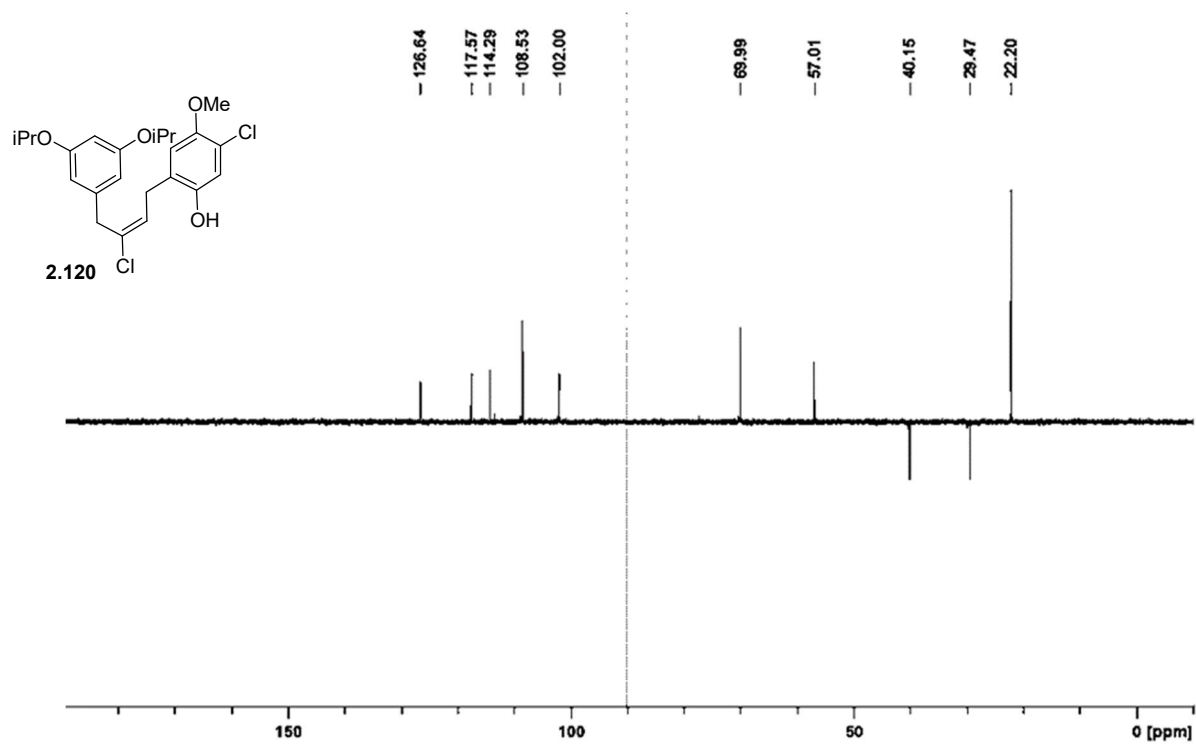
Figure A.52. DEPT-135(CDCl₃) of **2.120.**
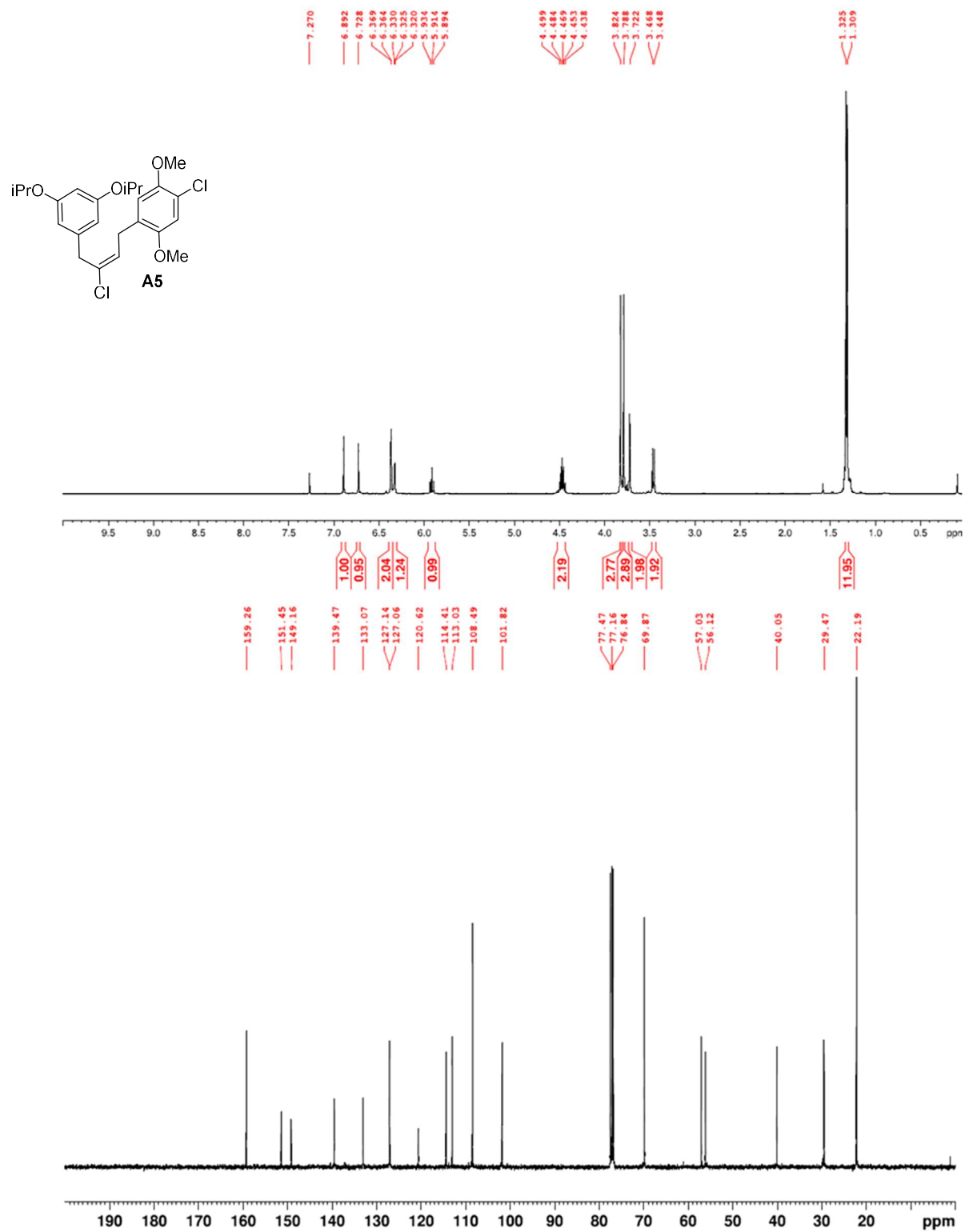
Figure A.53. ^{1}H NMR (400 MHz, (CDCl$_3$) and ^{13}C NMR (100 MHz, CDCl$_3$) of **A5.**
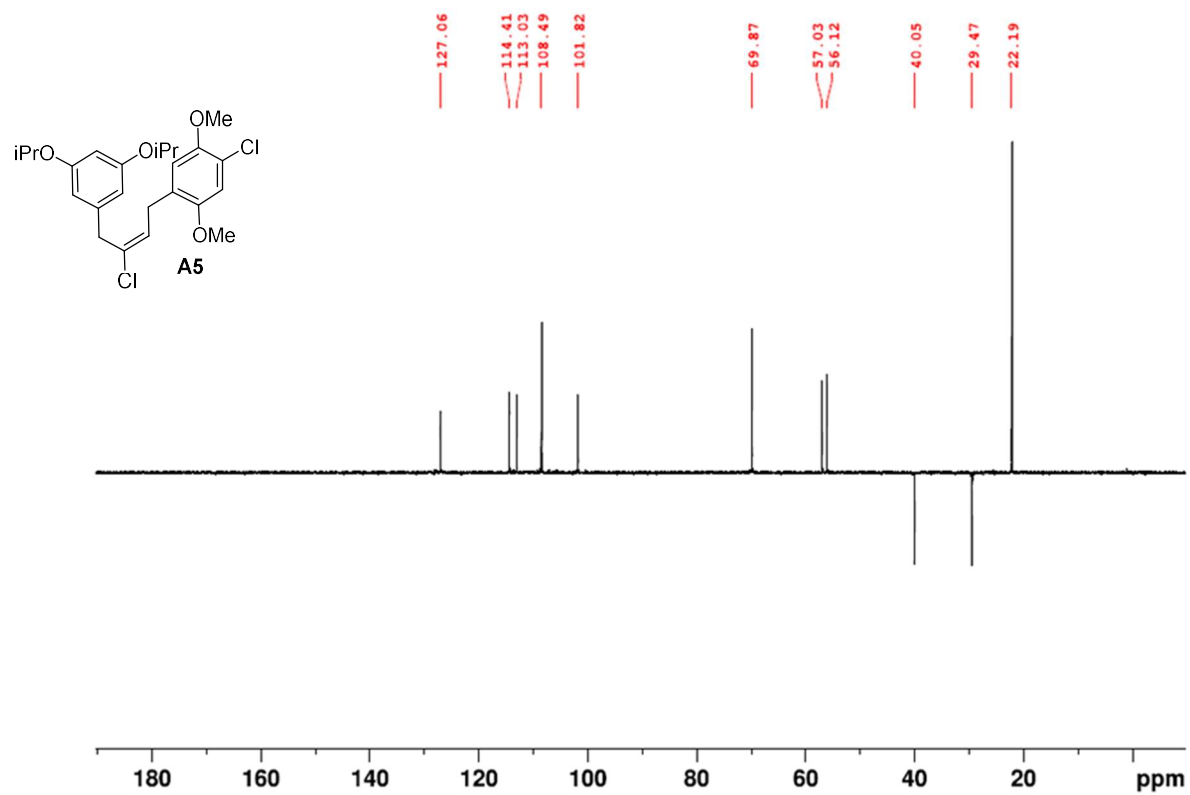
Figure A.54. DEPT-135(CDCl₃) of **A5.**
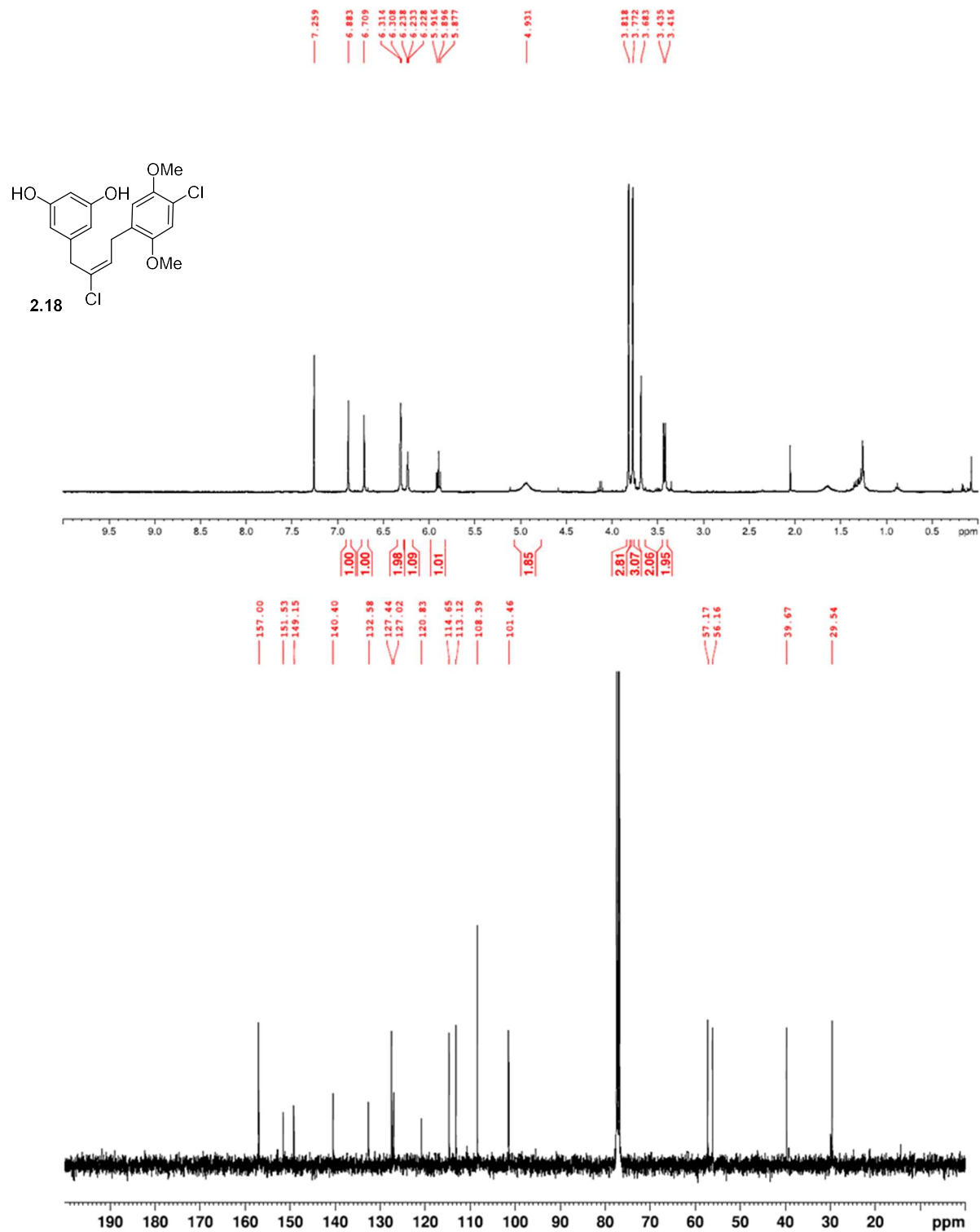
Figure A.55. ^{1}H NMR (400 MHz, (CDCl$_3$) and ^{13}C NMR (100 MHz, CDCl$_3$) of **2.18.**
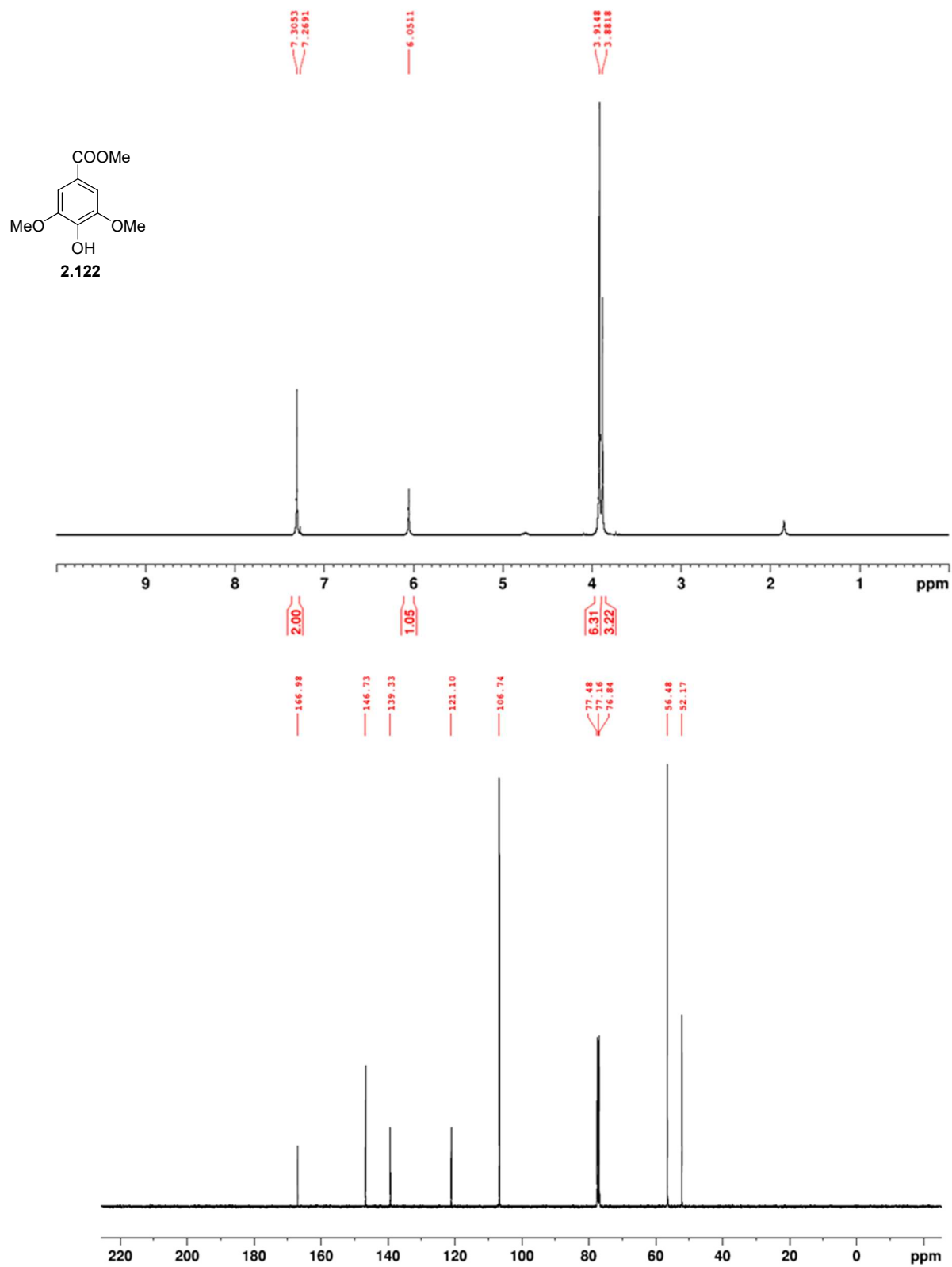
Figure A.56. ^{1}H NMR (400 MHz, (CDCl$_3$) and ^{13}C NMR (100 MHz, CDCl$_3$) of **2.122.**
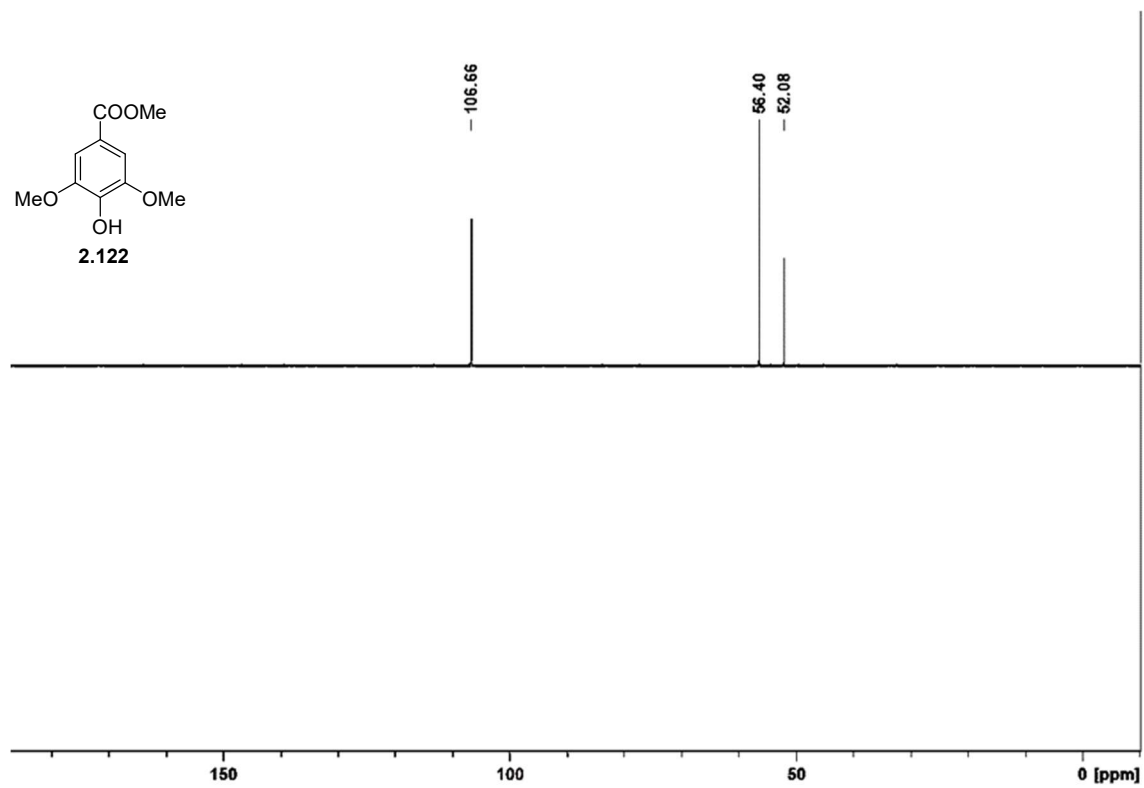
Figure A.57. DEPT-135(CDCl₃) of **2.122.**
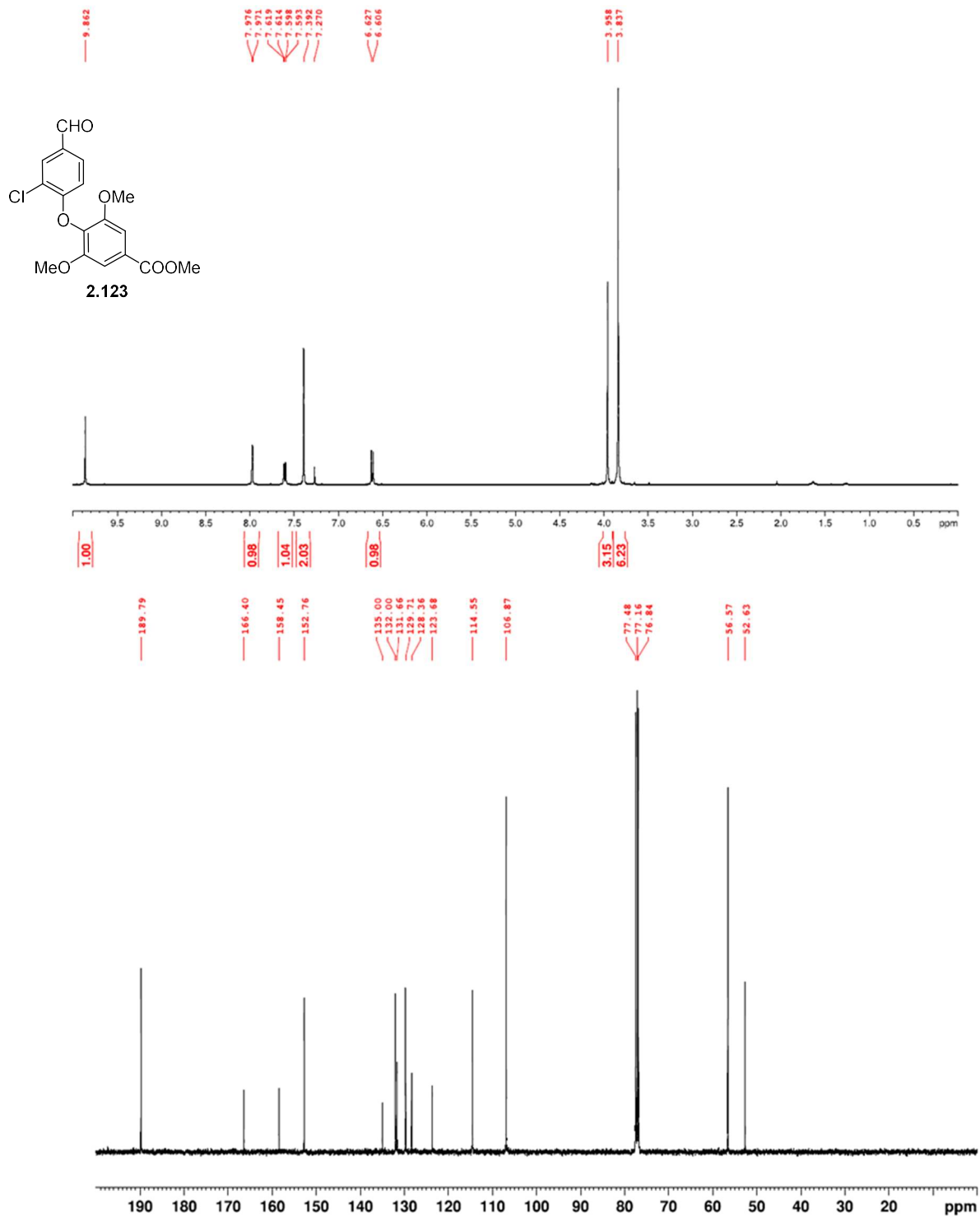
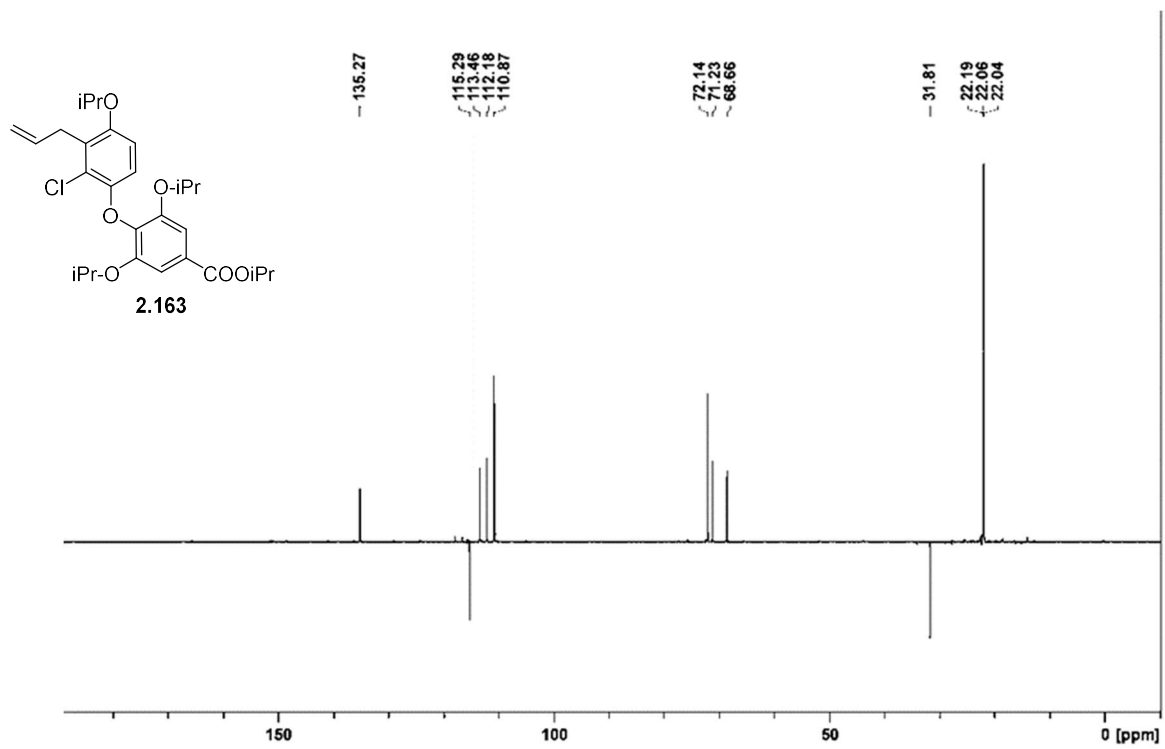**Figure A.58.** ¹H NMR (400 MHz, (CDCl₃) and ¹³C NMR (100 MHz, CDCl₃) of **2.123.**
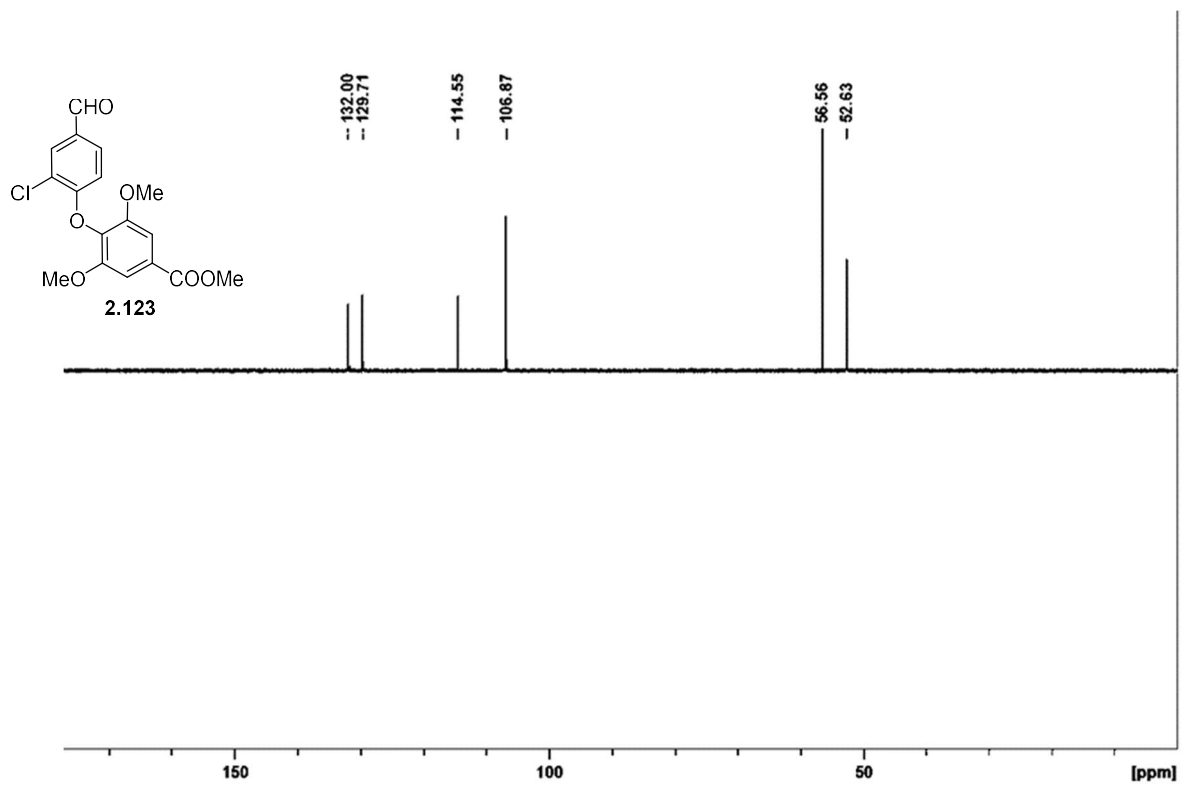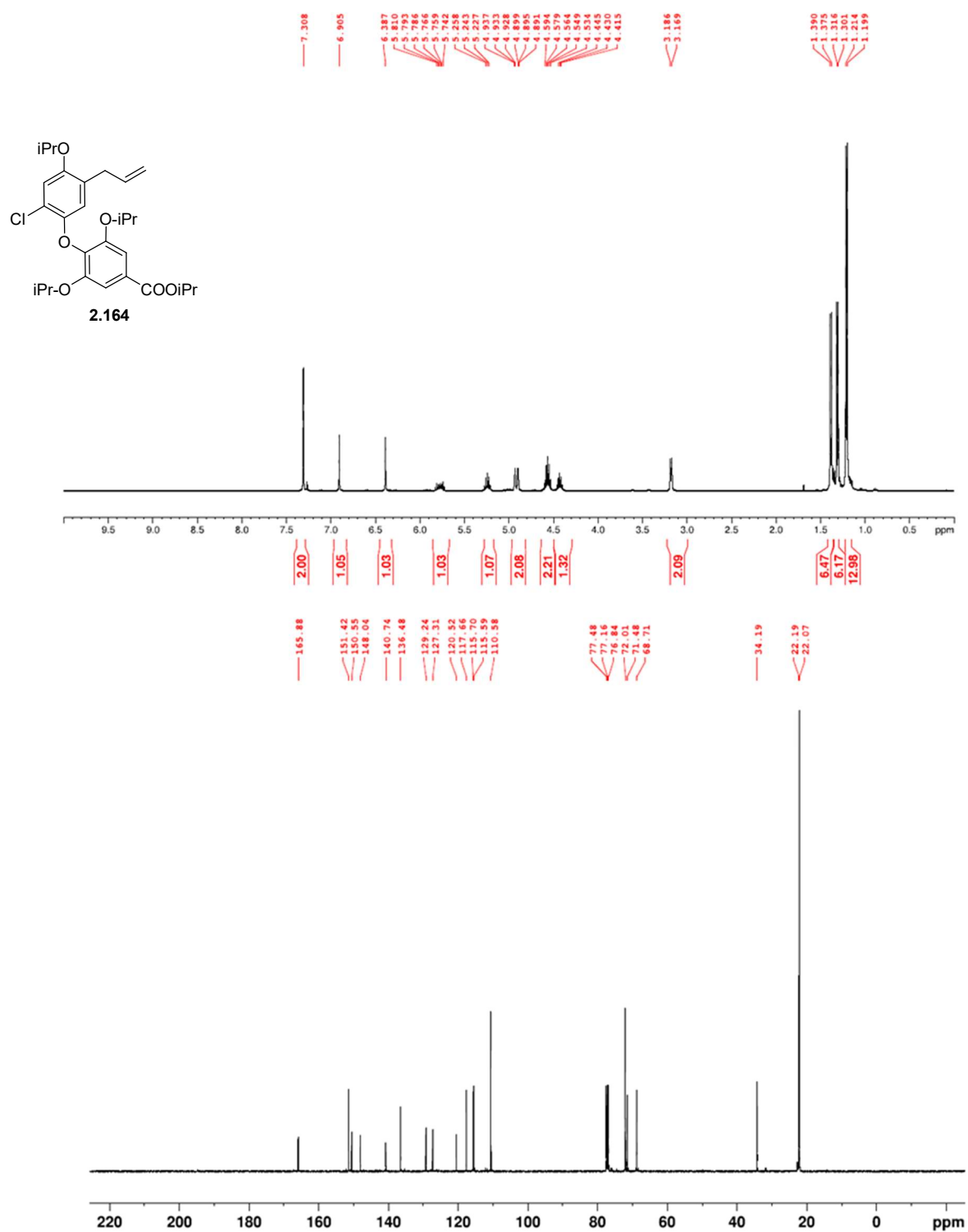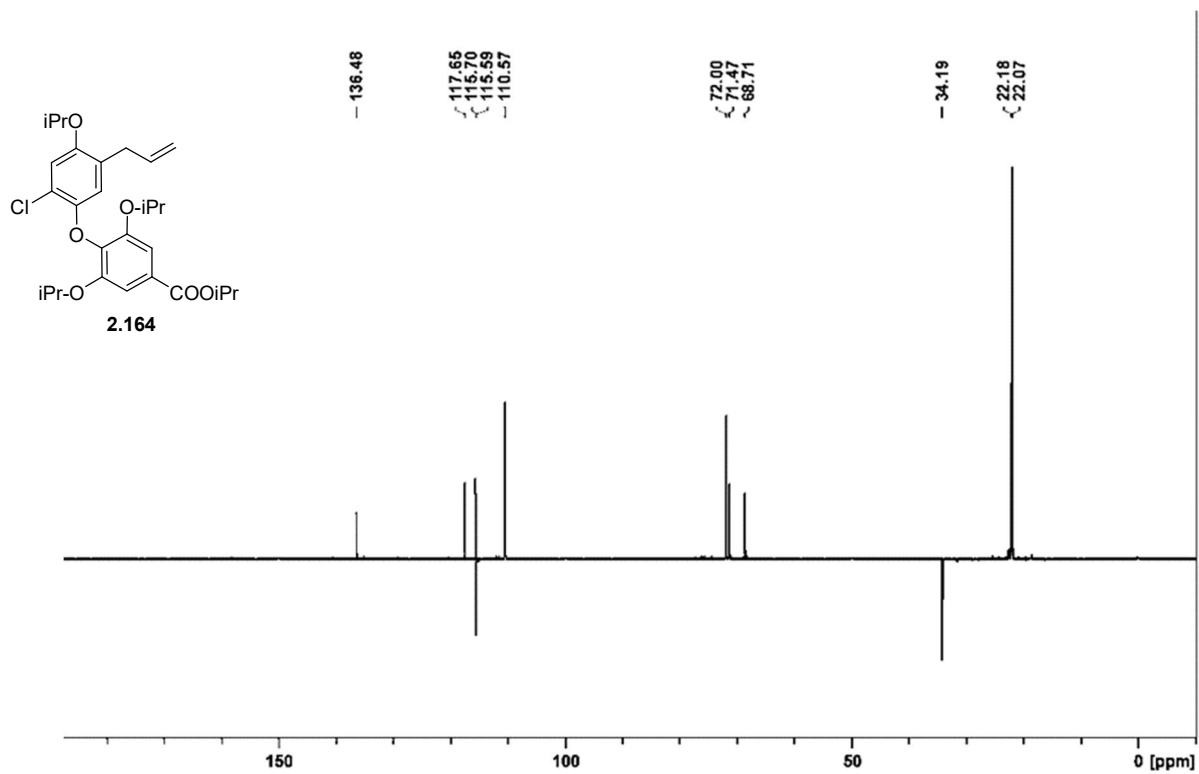
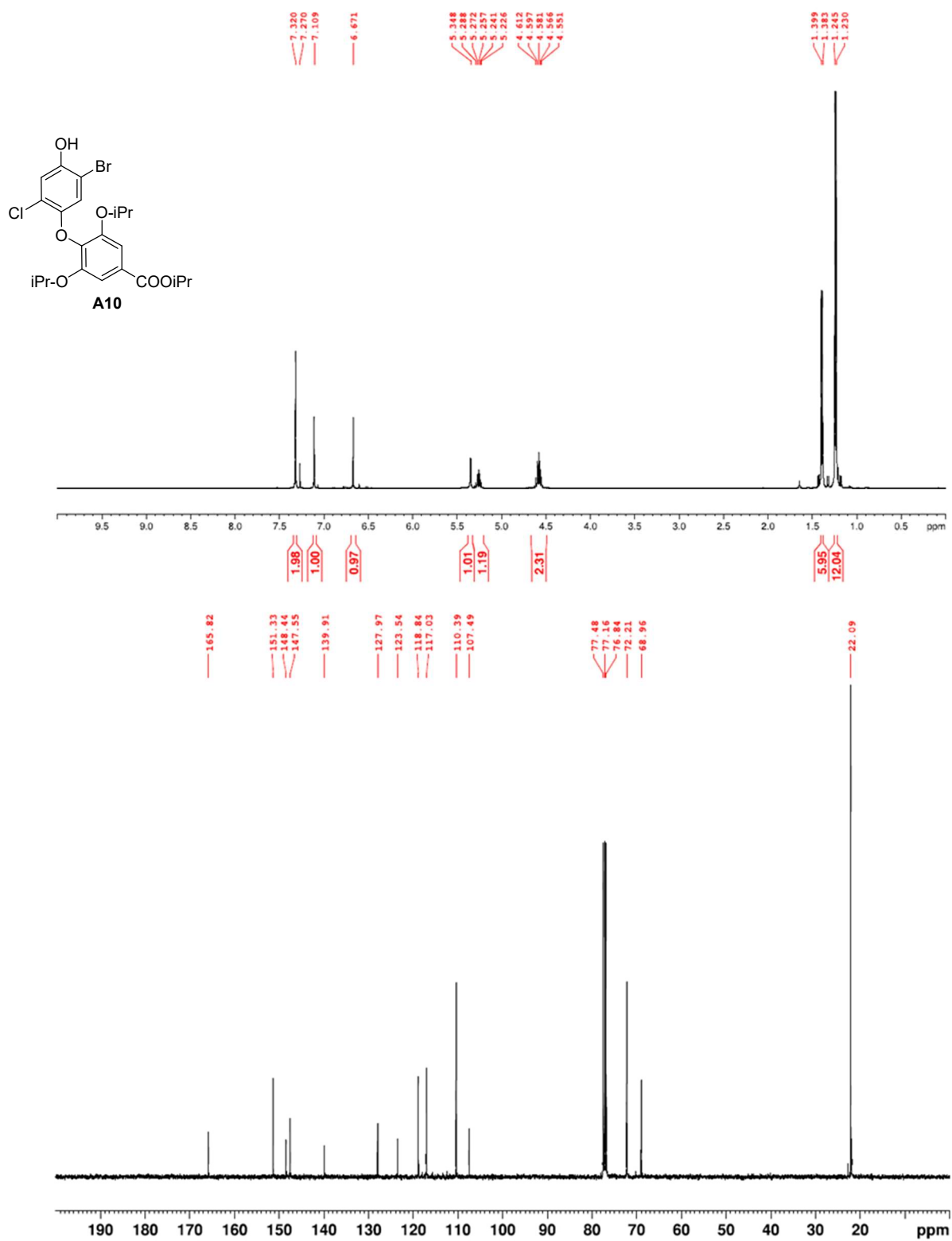**Figure A.59**. DEPT-135(CDCl₃) of **2.123.**
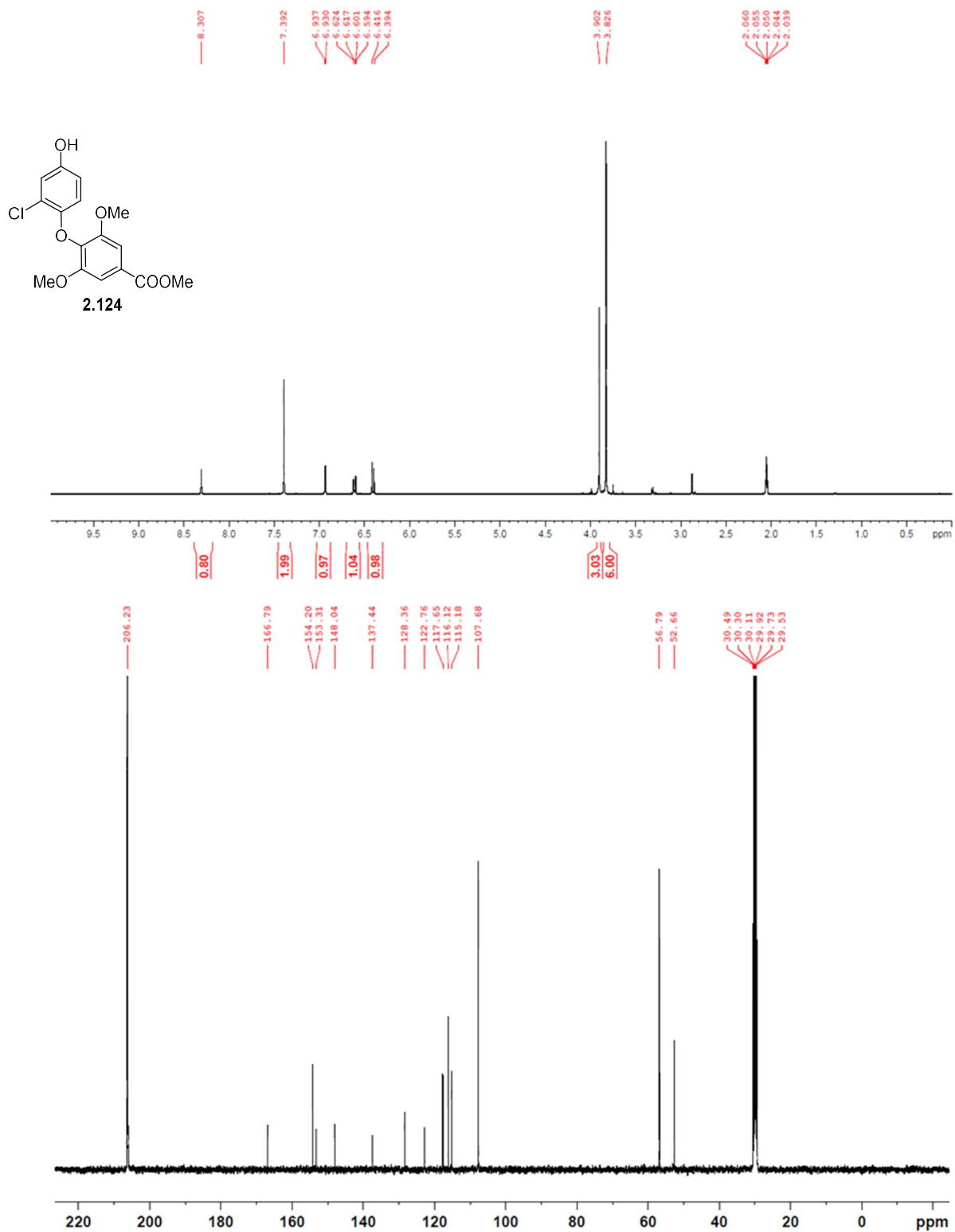
Figure A.60. ^{1}H NMR (400 MHz, CDCl$_3$) and ^{13}C NMR (100 MHz, CDCl$_3$) of **2.124.**
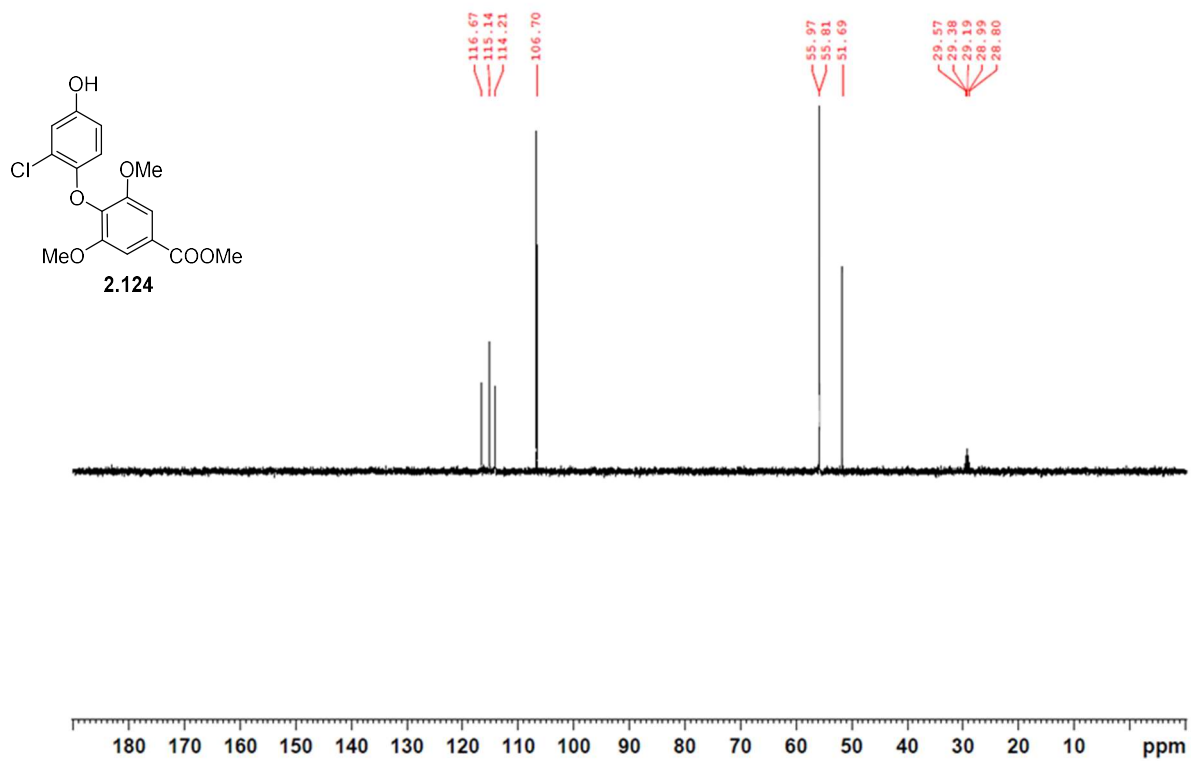
Figure A.61. DEPT-135(CDCl₃) of **2.124.**
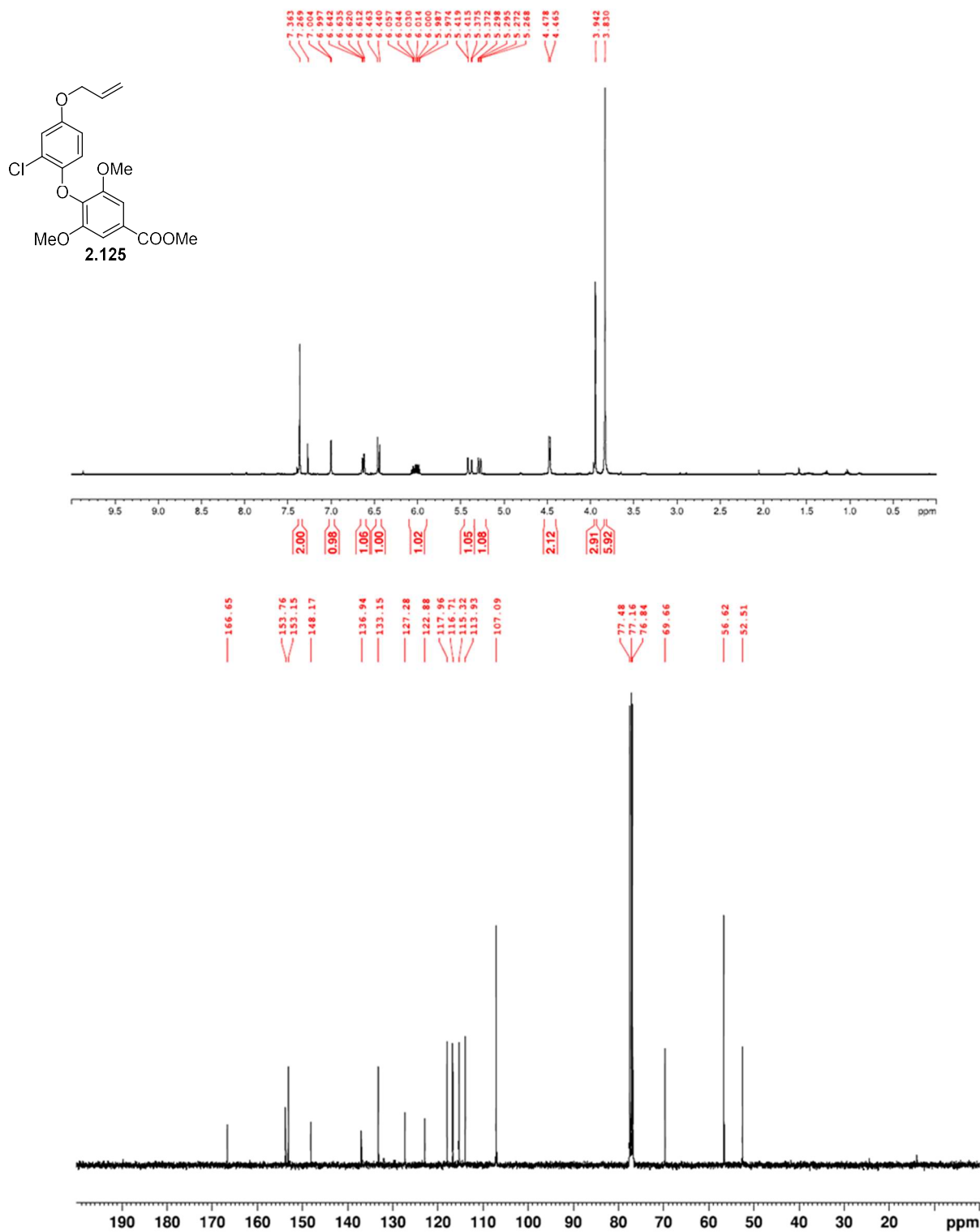
Figure A.62. ^{1}H NMR (400 MHz, CDCl$_3$) and ^{13}C NMR (100 MHz, CDCl$_3$) of **2.125.**
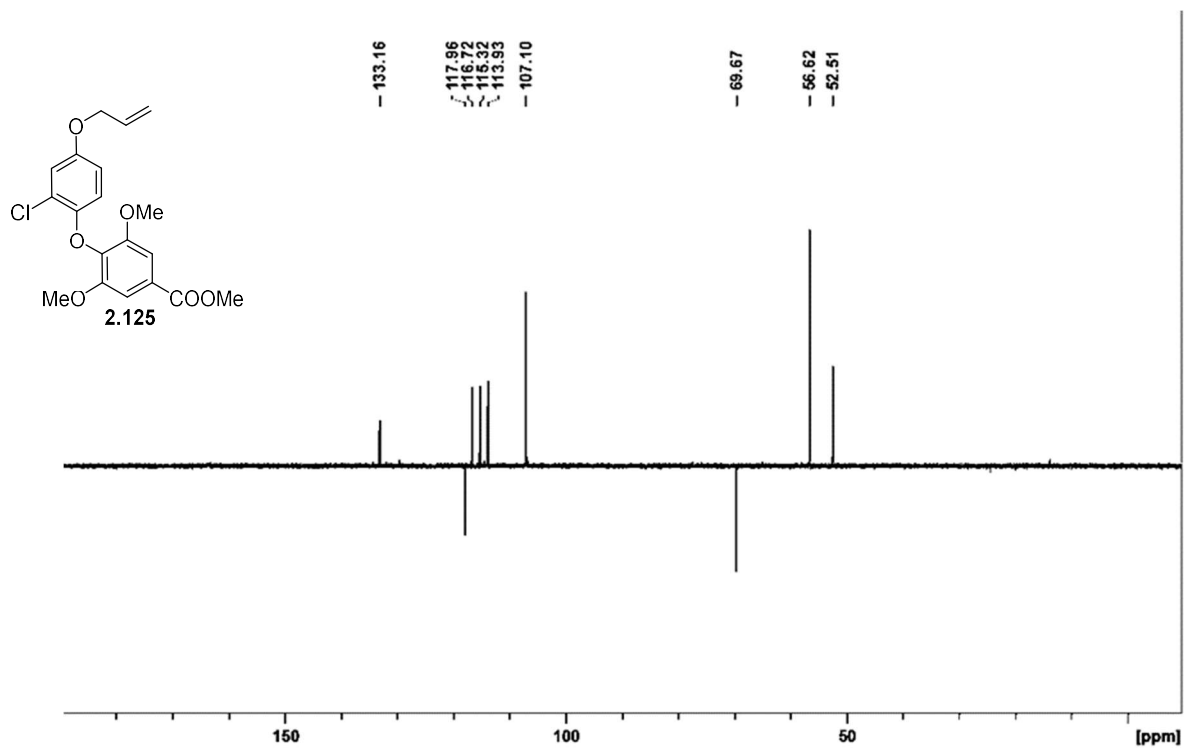
Figure A.63. DEPT-135(CDCl$_3$) of **2.135**.
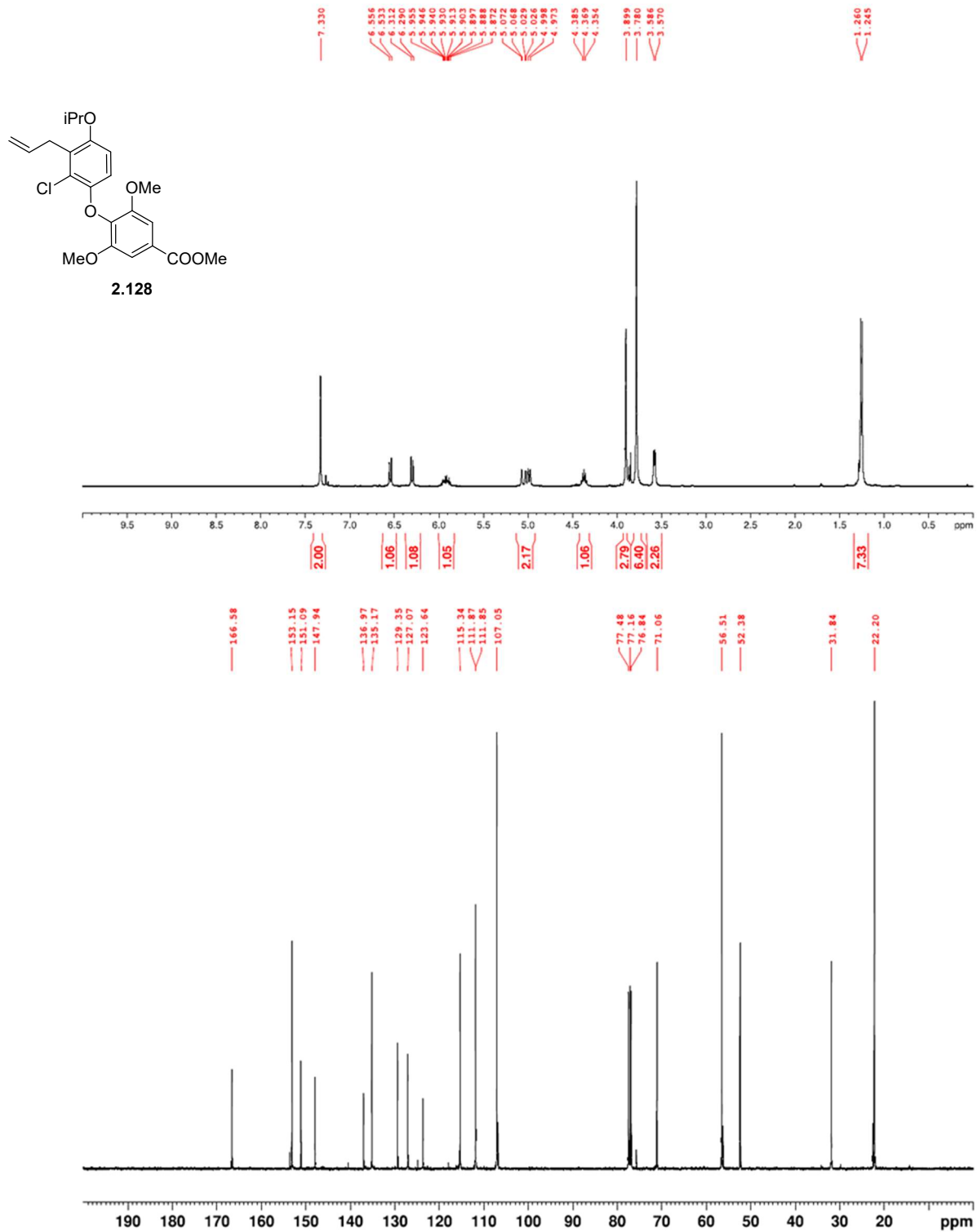
Figure A.64. ^{1}H NMR (400 MHz, CDCl$_3$) and ^{13}C NMR (100 MHz, CDCl$_3$) of **2.128**.
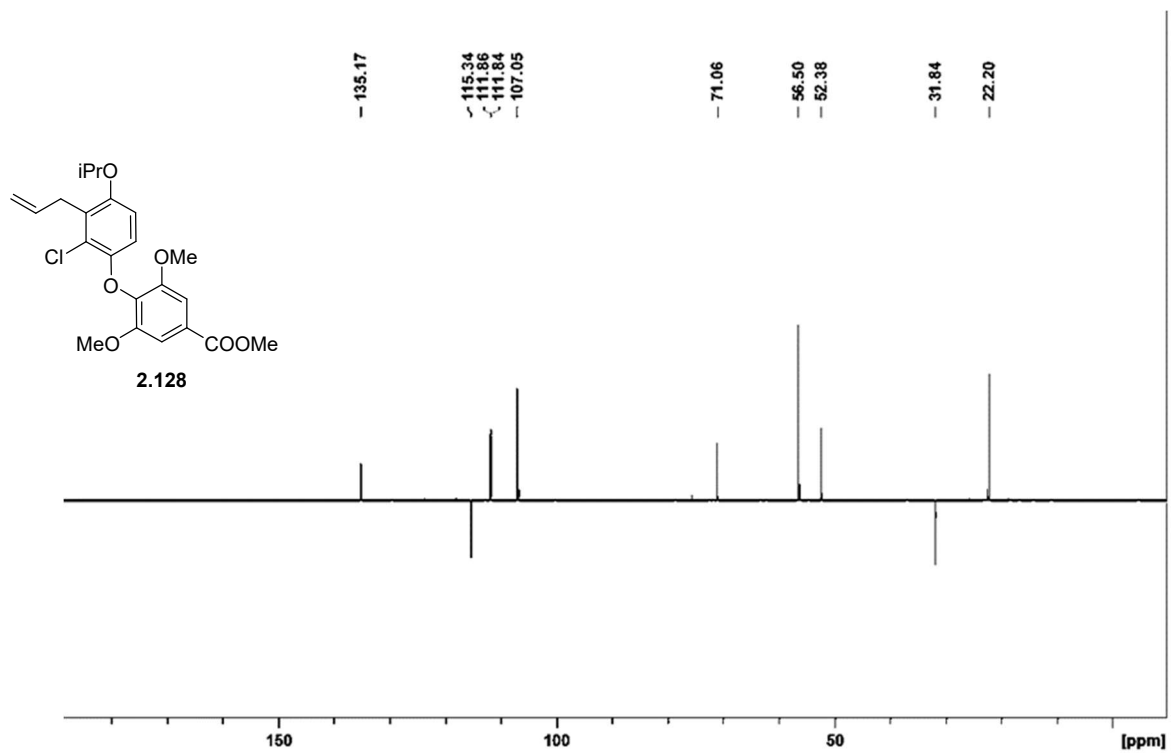
Figure A.65. DEPT-135(CDCl₃) of **2.128**.
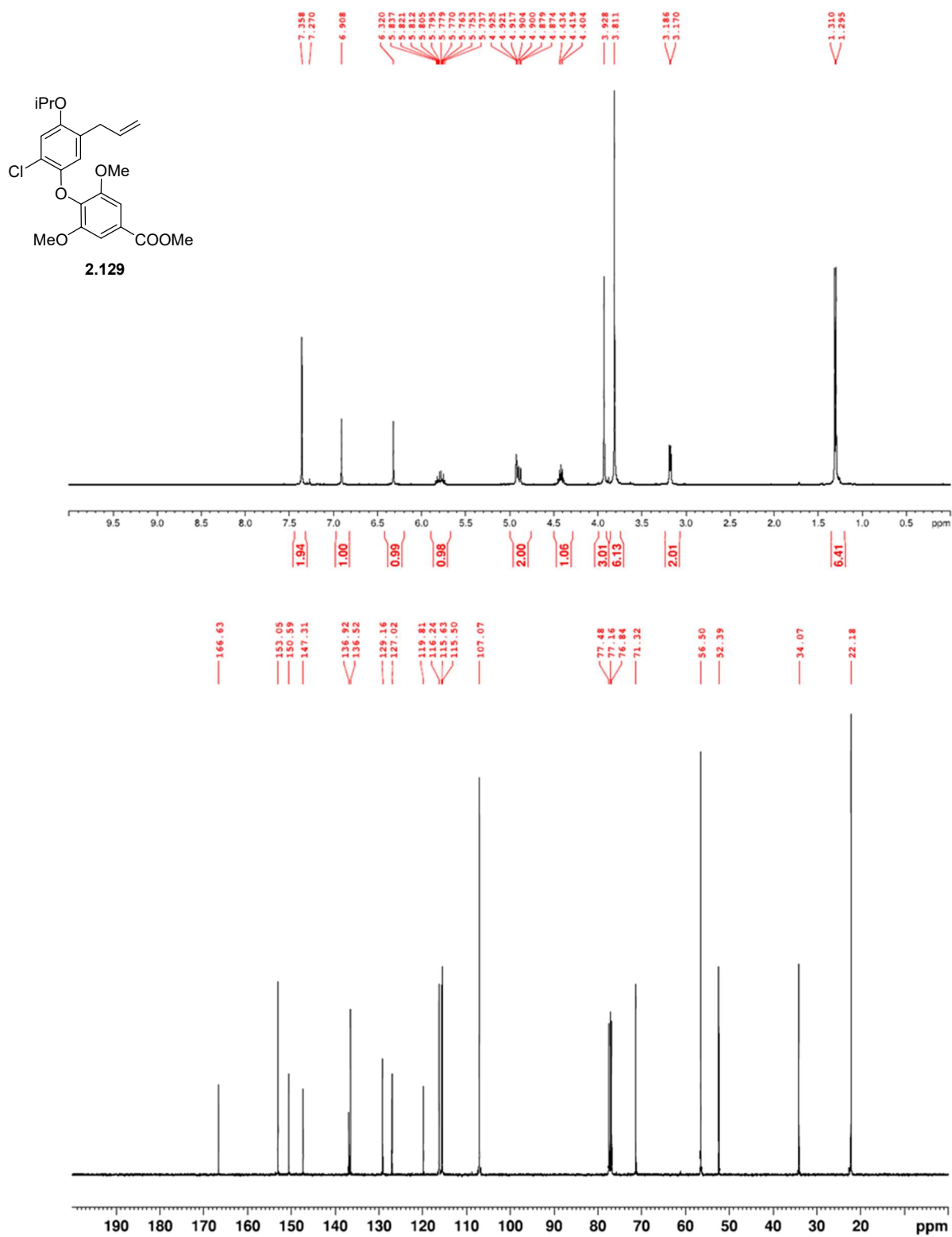
Figure A.66. ^{1}H NMR (400 MHz, CDCl$_3$) and ^{13}C NMR (100 MHz, CDCl$_3$) of **2.129.**
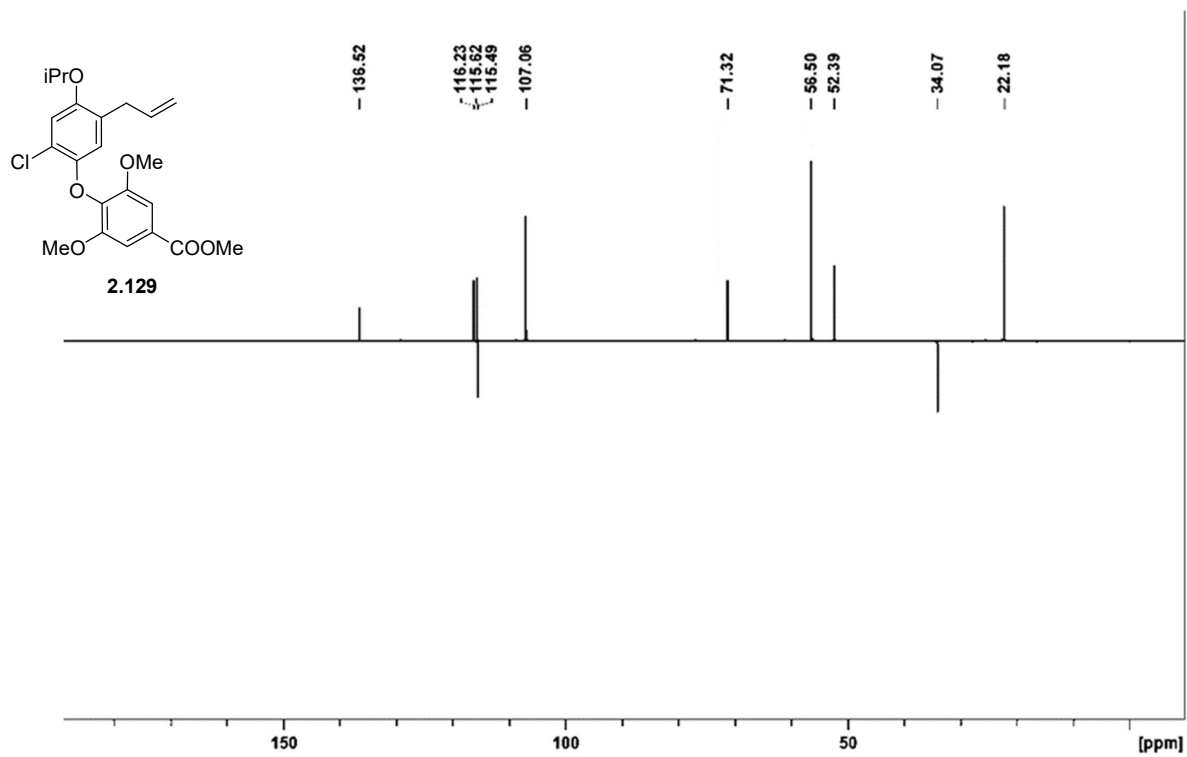
Figure A.67. DEPT-135(CDCl₃) of **2.129.**
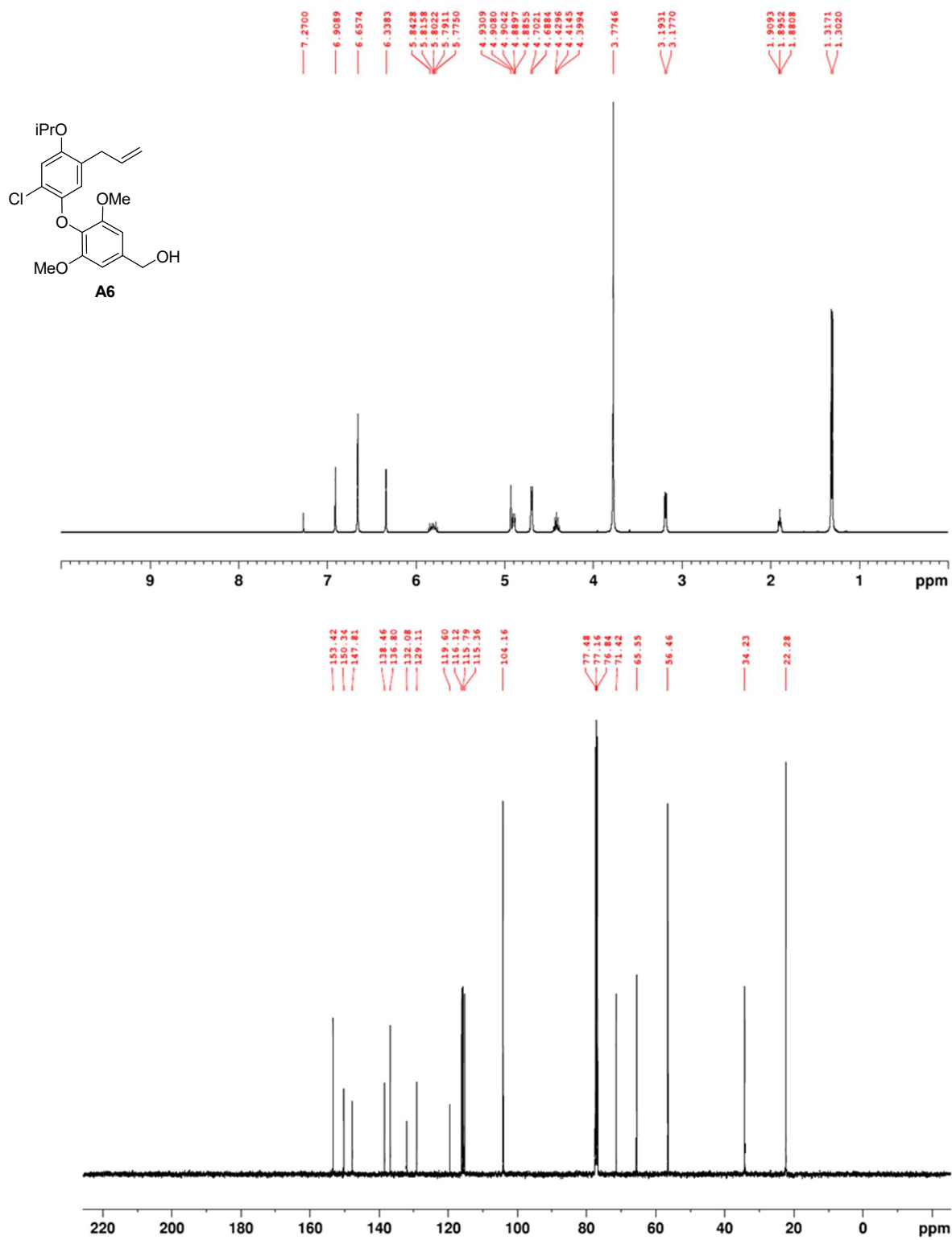
Figure A.68. ^{1}H NMR (400 MHz, CDCl$_3$) and ^{13}C NMR (100 MHz, CDCl$_3$) of **A6.**
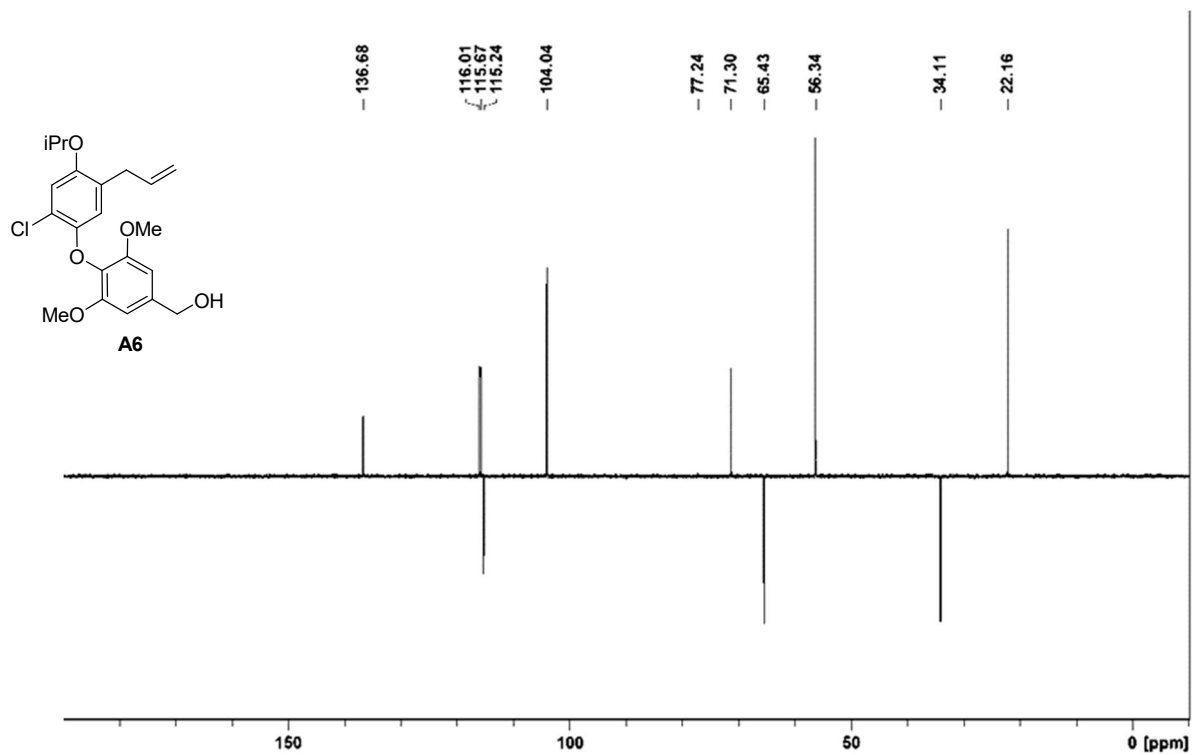
Figure A.69. DEPT-135(CDCl₃) of **A6**.
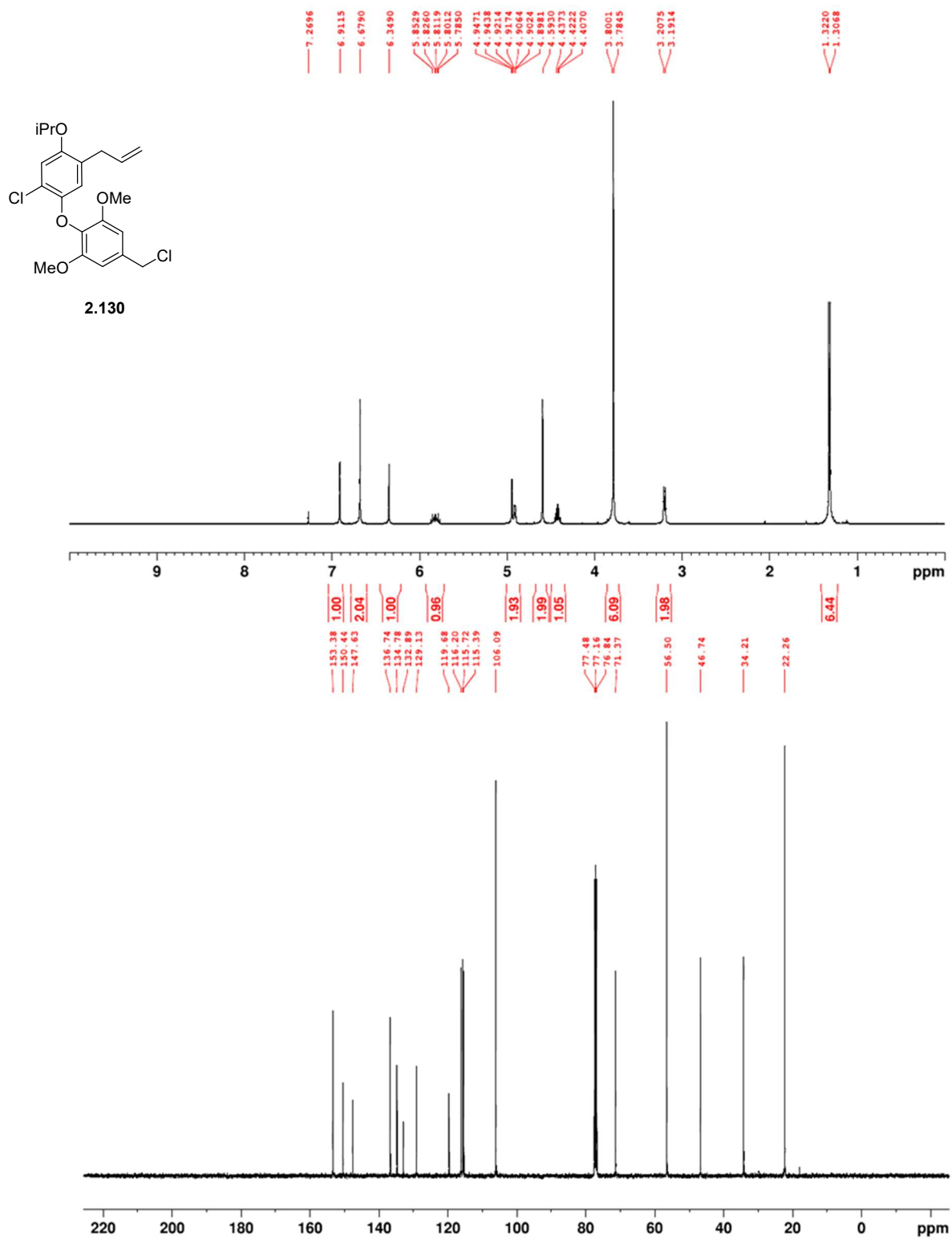
Figure A.70. ^{1}H NMR (400 MHz, CDCl$_3$) and ^{13}C NMR (100 MHz, CDCl$_3$) of **2.130.**
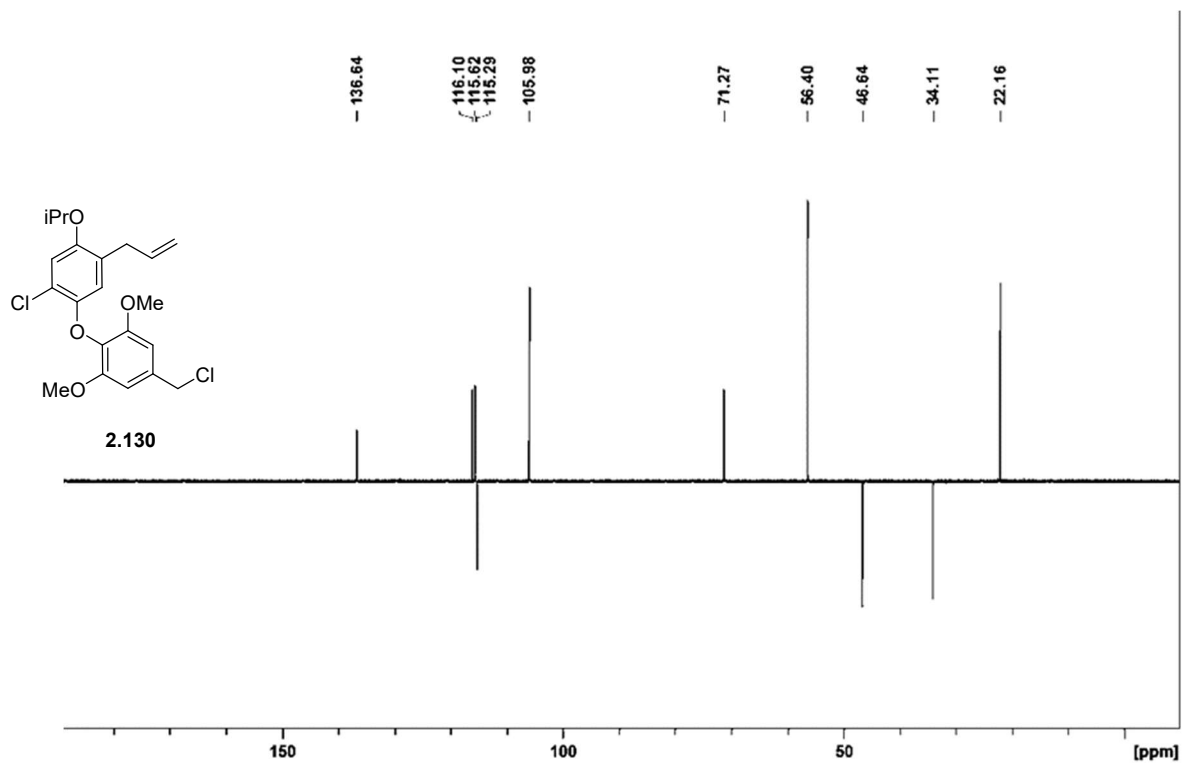
Figure A.71. DEPT-135(CDCl₃) of **2.130.**
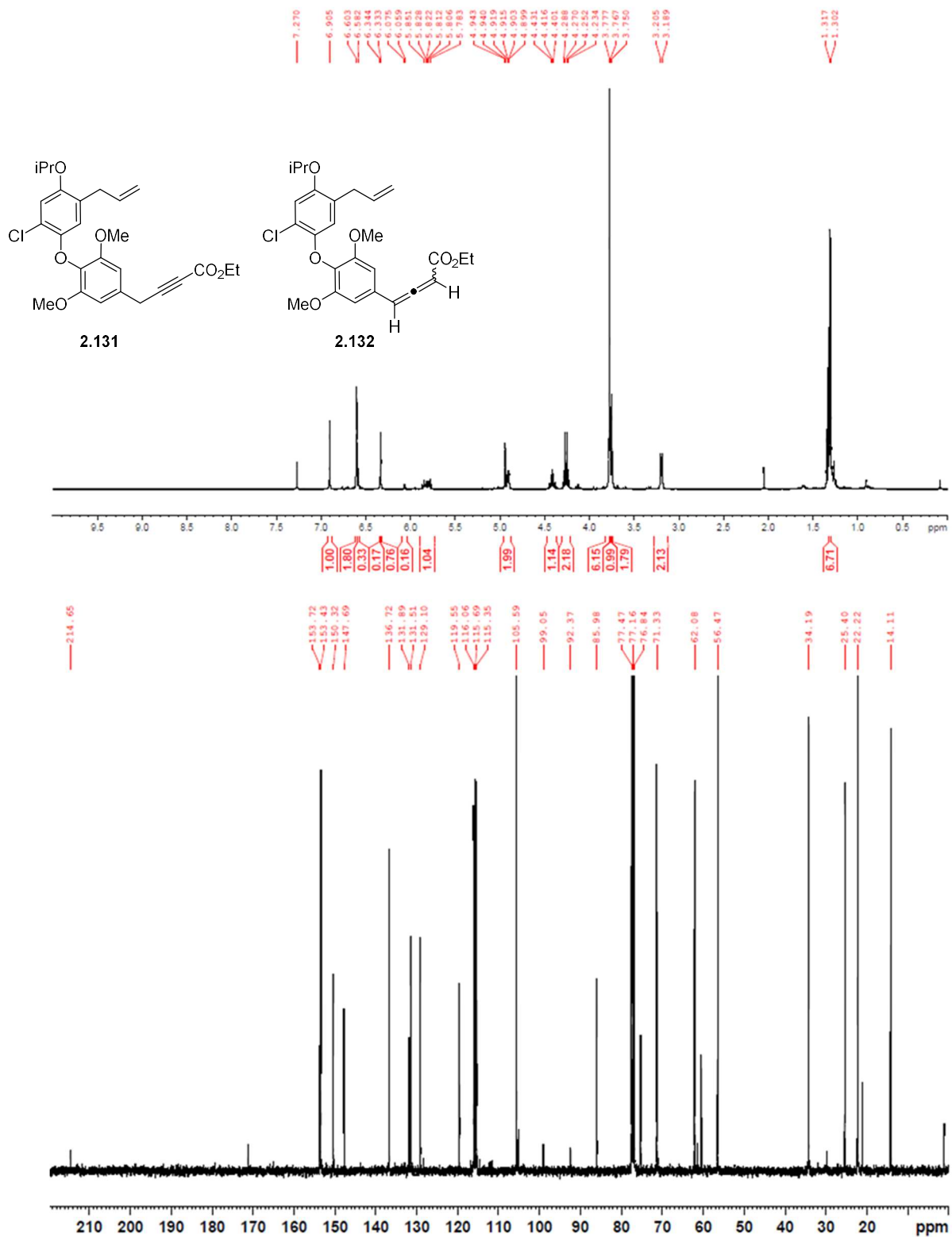
Figure A.72. ^{1}H NMR (400 MHz, (CDCl$_3$) and ^{13}C NMR (100 MHz, CDCl$_3$) of **2.131/2.132.**
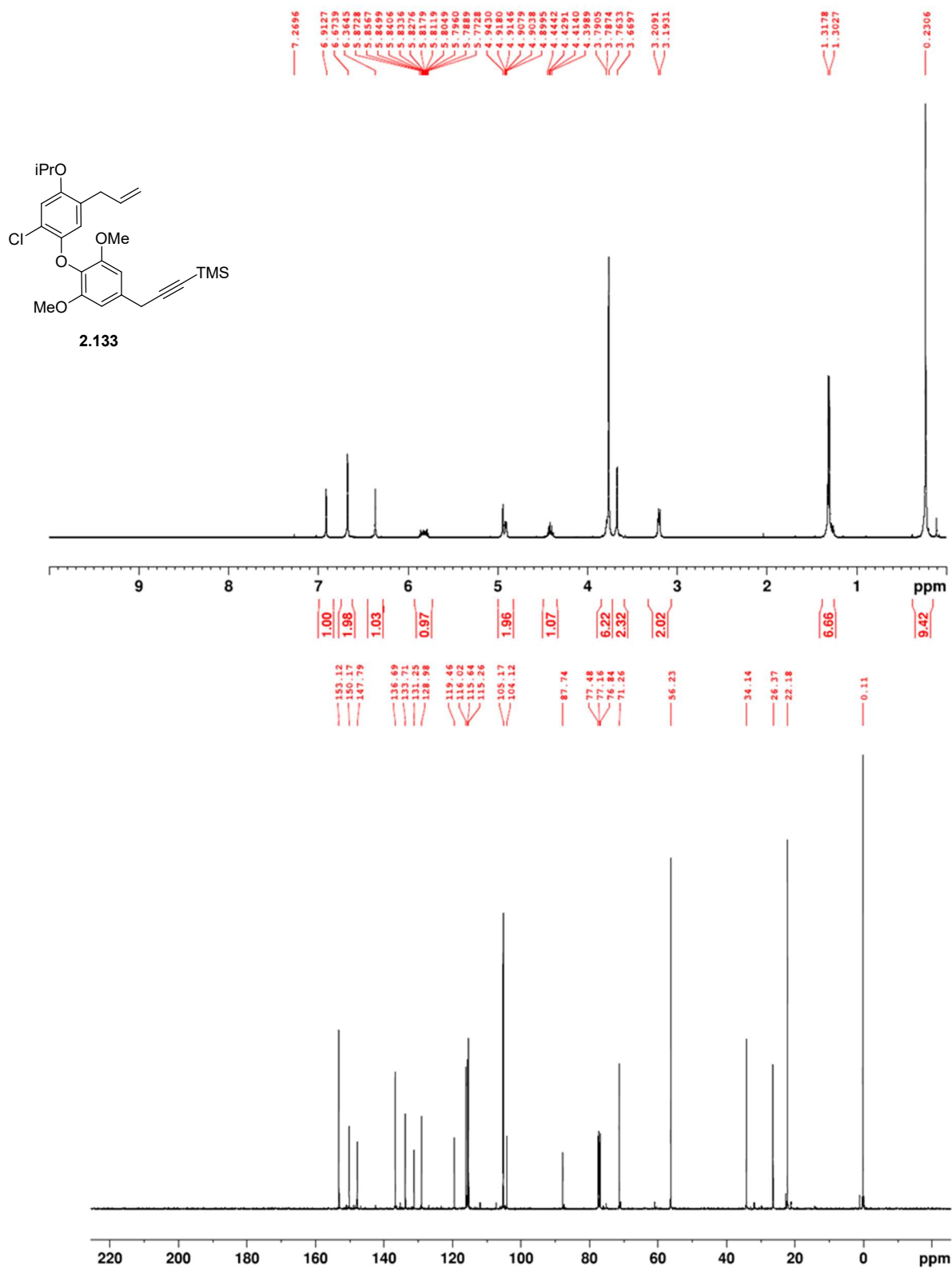
Figure A.73. ^{1}H NMR (400 MHz, CDCl$_3$) and ^{13}C NMR (100 MHz, CDCl$_3$) of **2.133.**
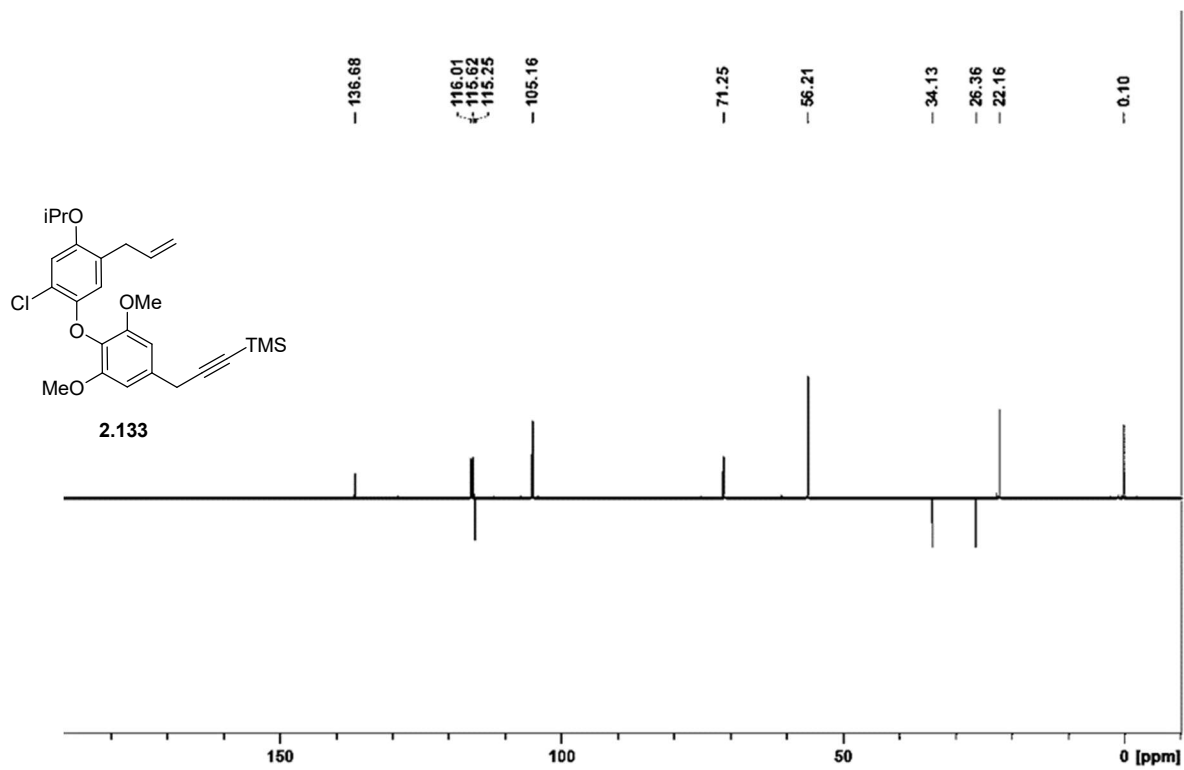
Figure A.74. DEPT-135(CDCl₃) of **2.133.**
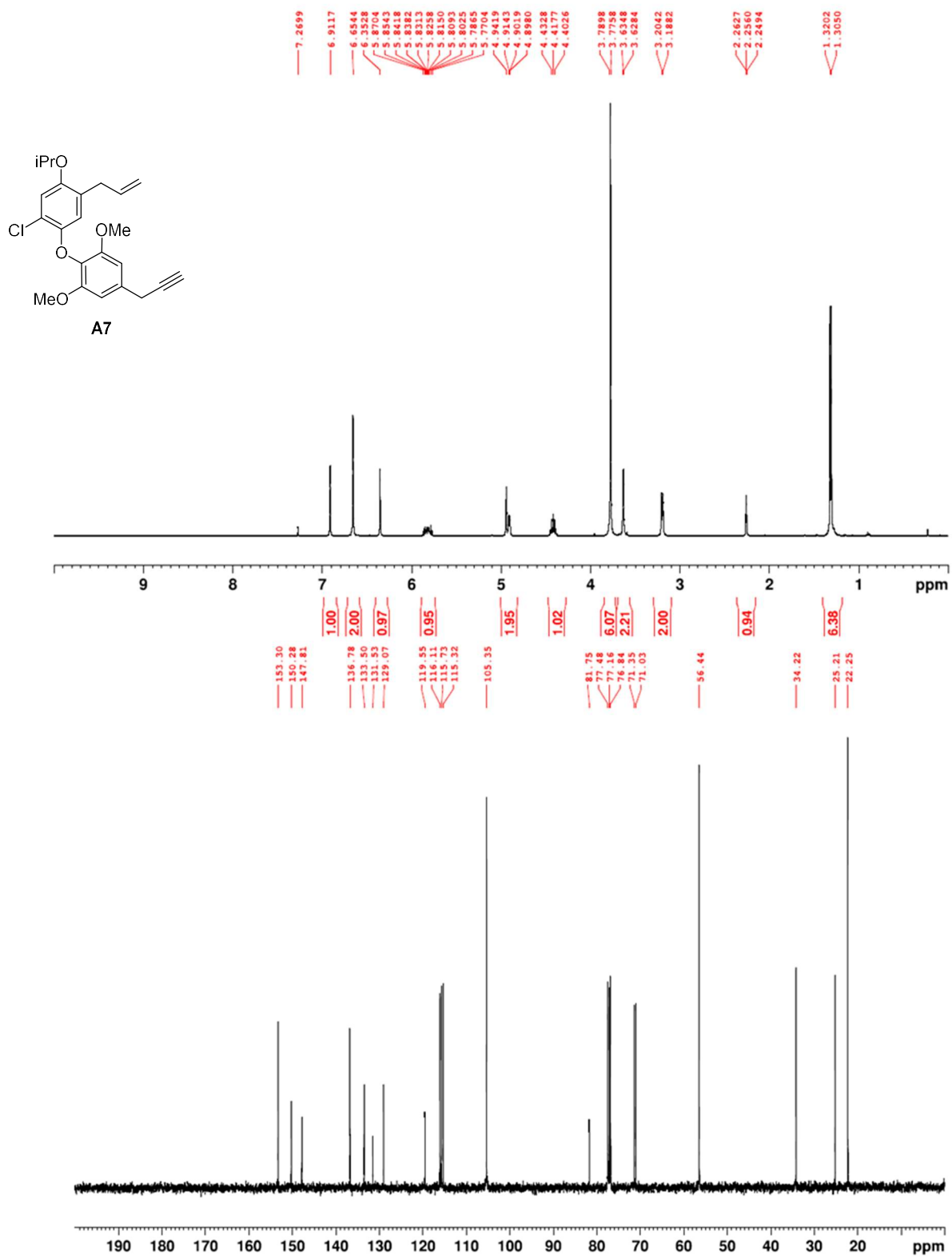
Figure A.75. ^{1}H NMR (400 MHz, CDCl$_3$) and ^{13}C NMR (100 MHz, CDCl$_3$) of **A7.**
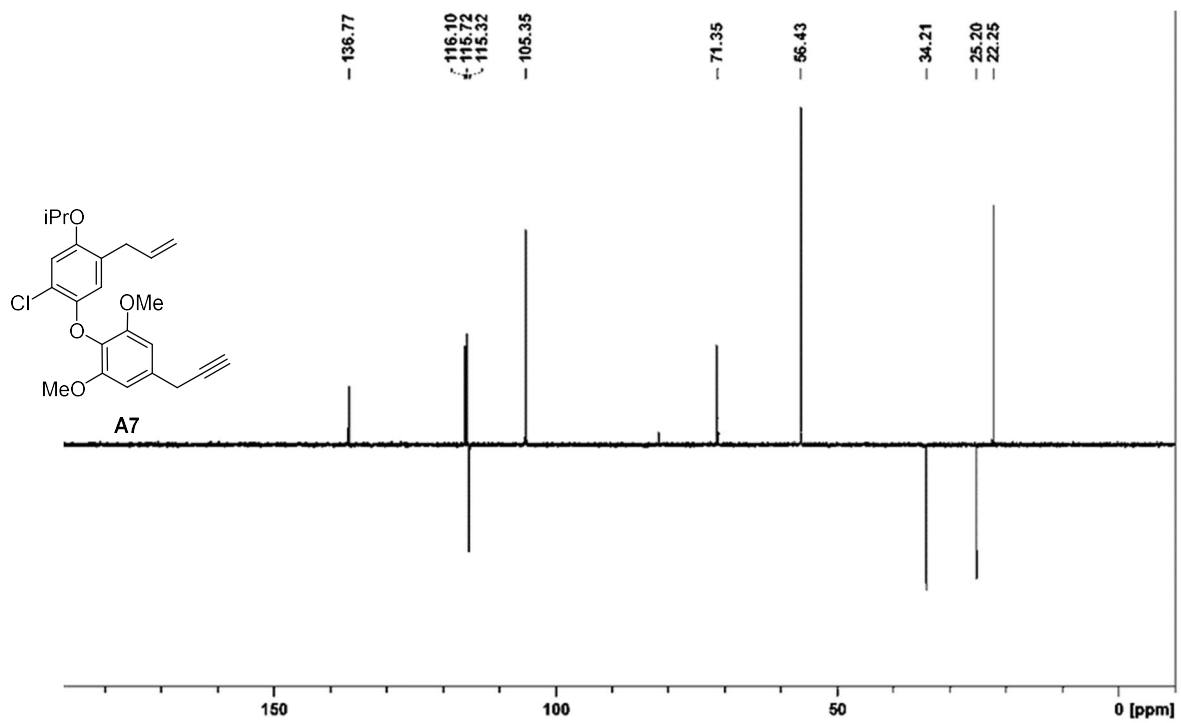
Figure A.76. DEPT-135(CDCl$_3$) of **A7.**
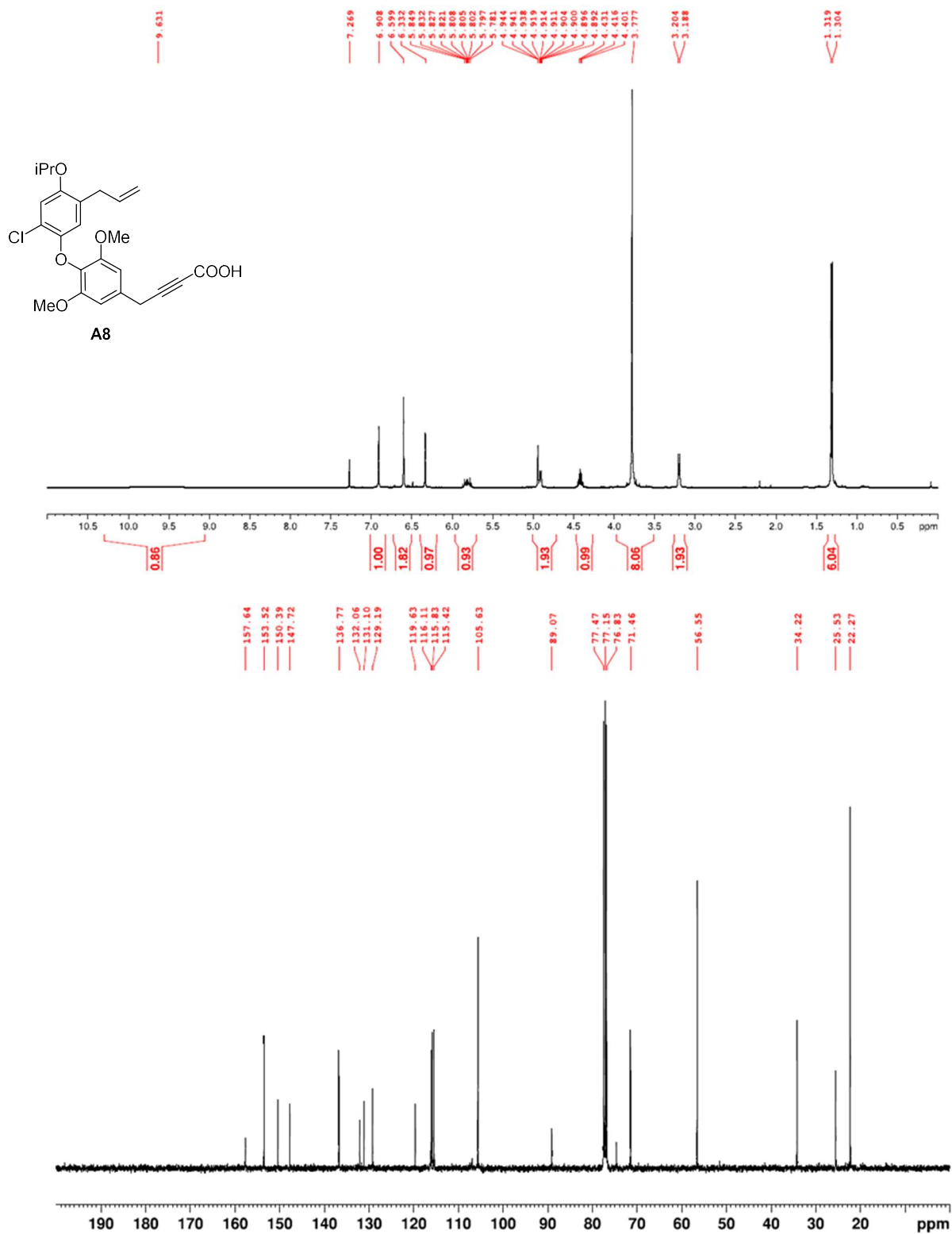
Figure A.77. ^{1}H NMR (400 MHz, (CDCl$_3$) and ^{13}C NMR (100 MHz, CDCl$_3$) of **A8.**
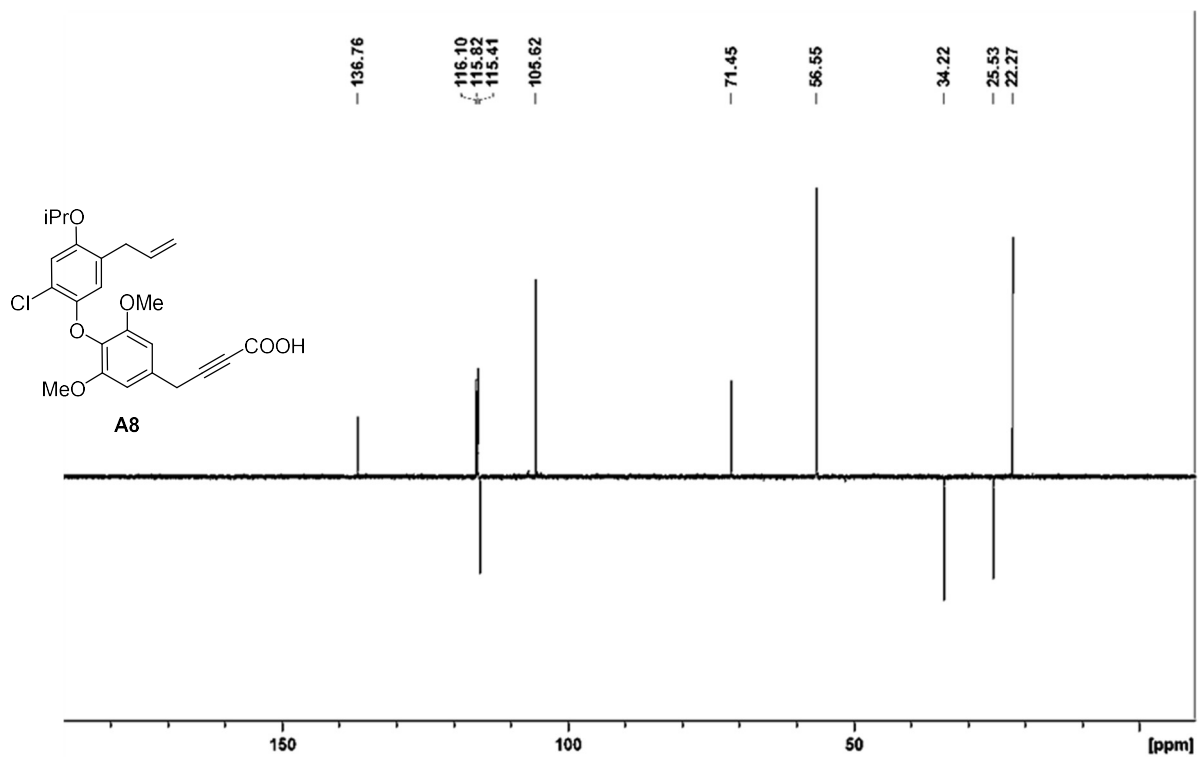
Figure A.78. DEPT-135(CDCl$_3$) of **A8.**
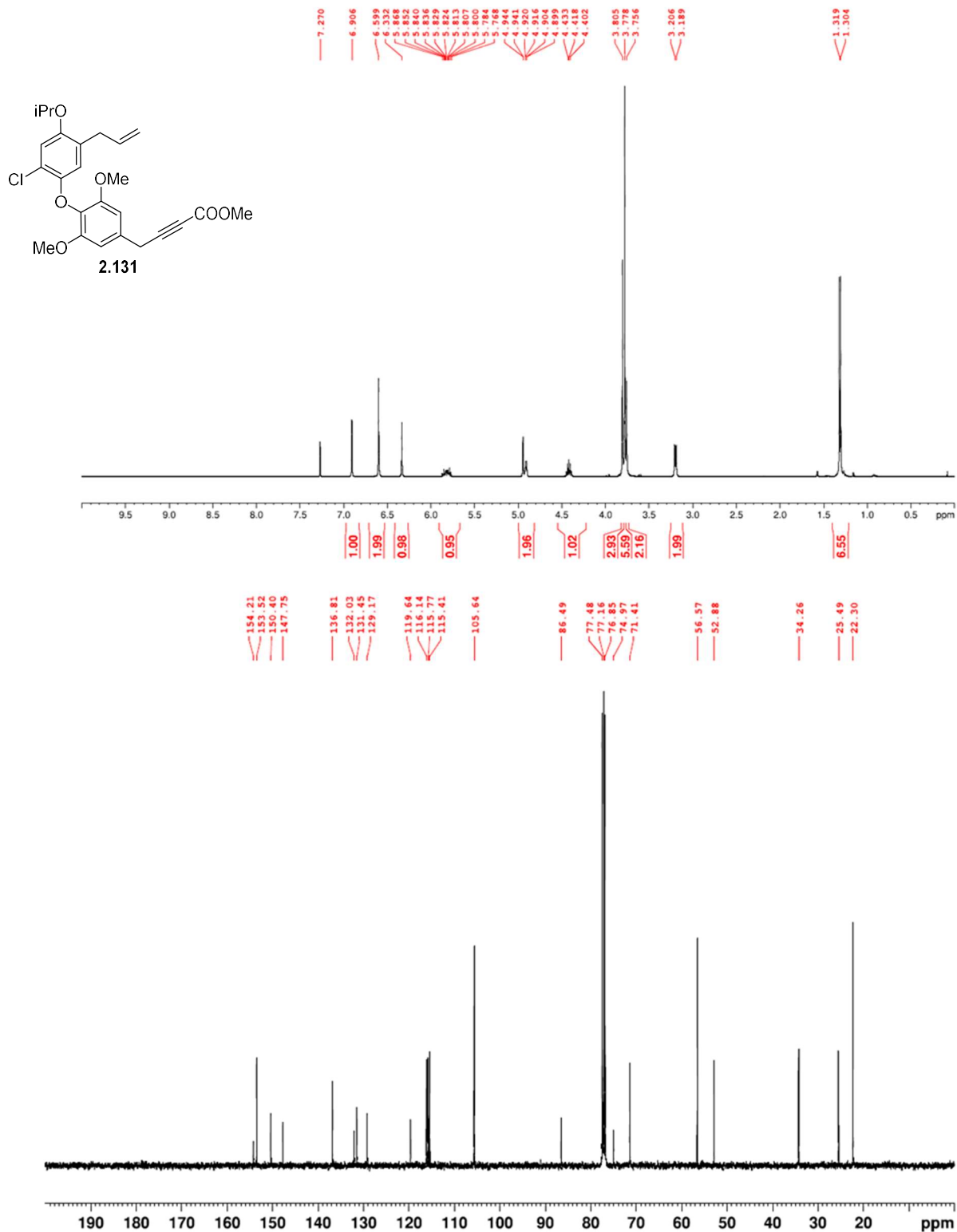
Figure A.79. ^{1}H NMR (400 MHz, (CDCl$_3$) and ^{13}C NMR (100 MHz, CDCl$_3$) of **2.131.**
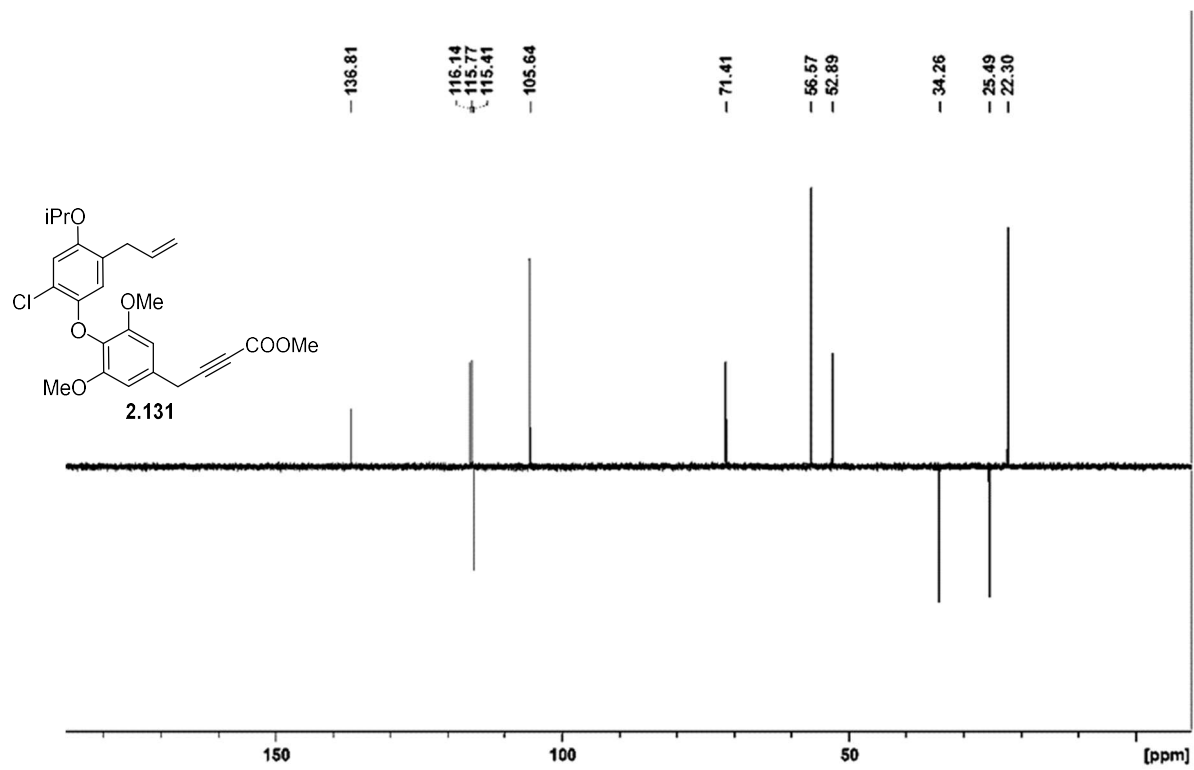
Figure A.80. DEPT-135(CDCl$_3$) of **2.131.**
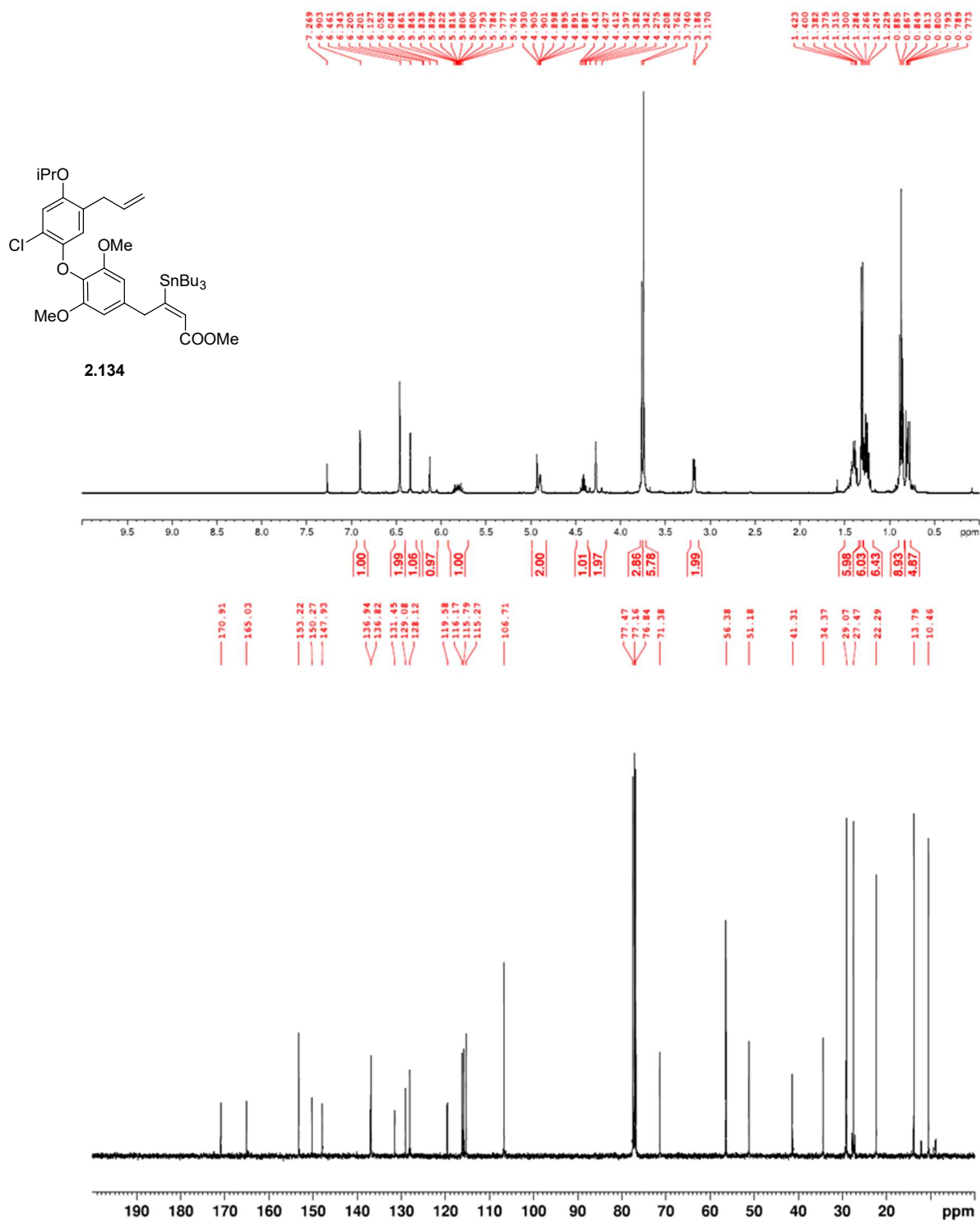
Figure A.81. ^{1}H NMR (400 MHz, CDCl$_3$) and ^{13}C NMR (100 MHz, CDCl$_3$) of **2.134.**
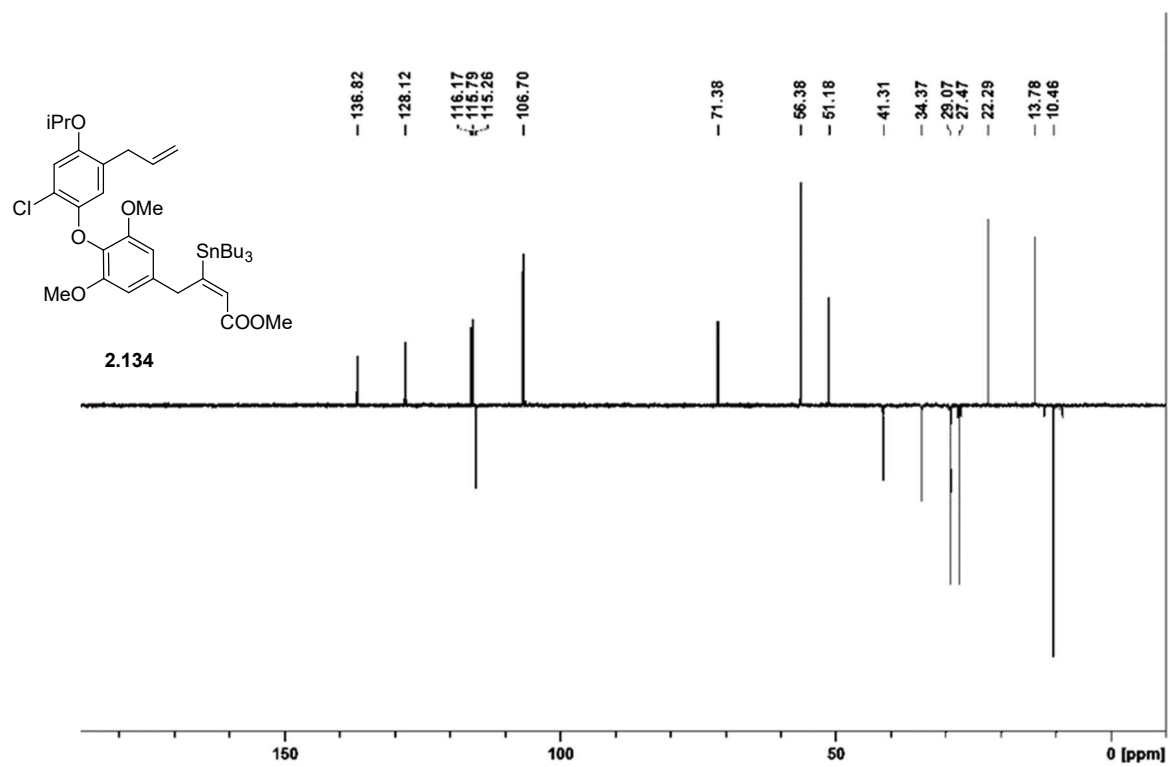
Figure A.82. DEPT-135(CDCl₃) of **2.134.**
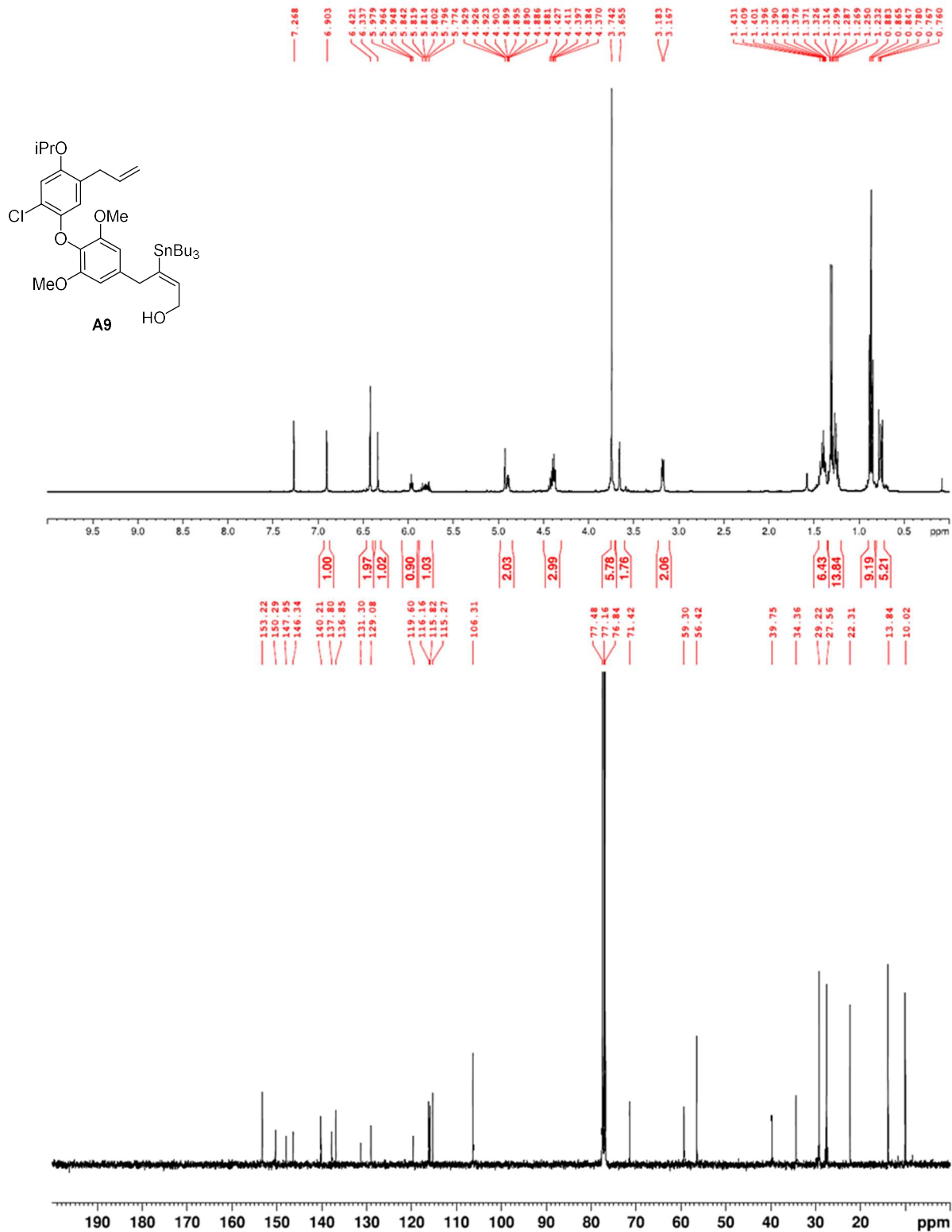
Figure A.83. ^{1}H NMR (400 MHz, CDCl$_3$) and ^{13}C NMR (100 MHz, CDCl$_3$) of **A9.**
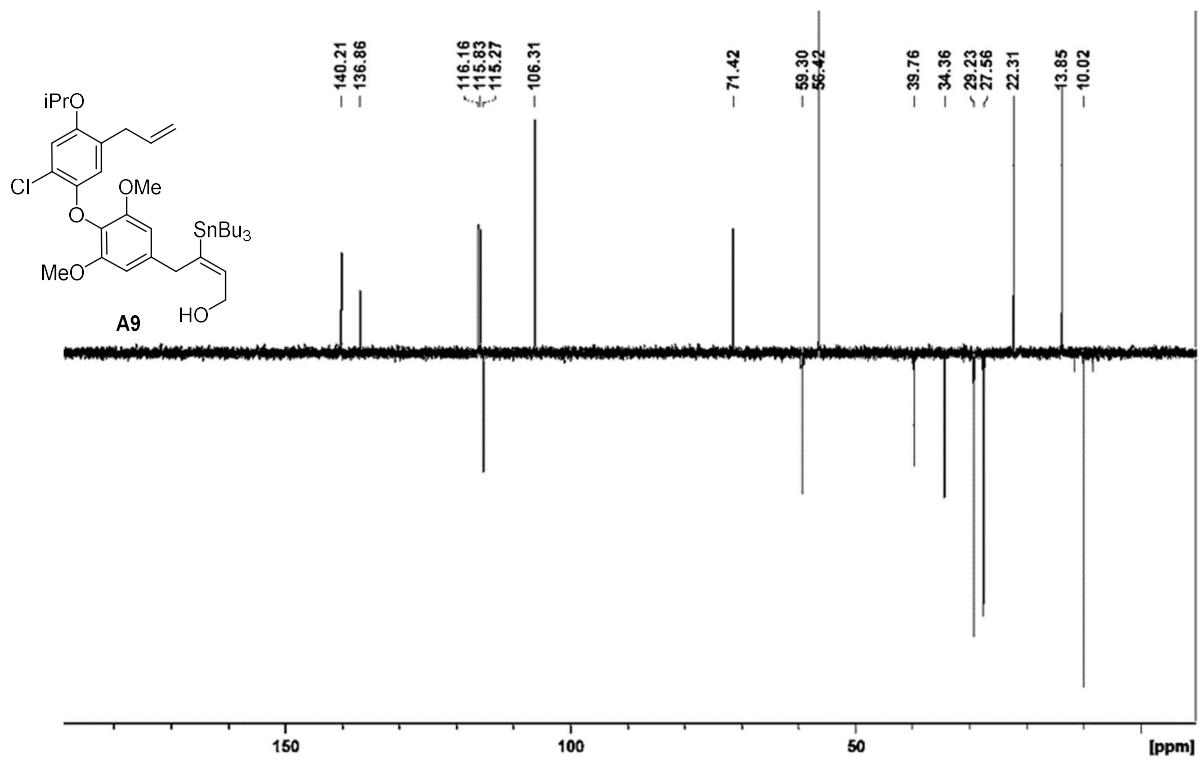
Figure A.84. DEPT-135(CDCl$_3$) of **A9.**
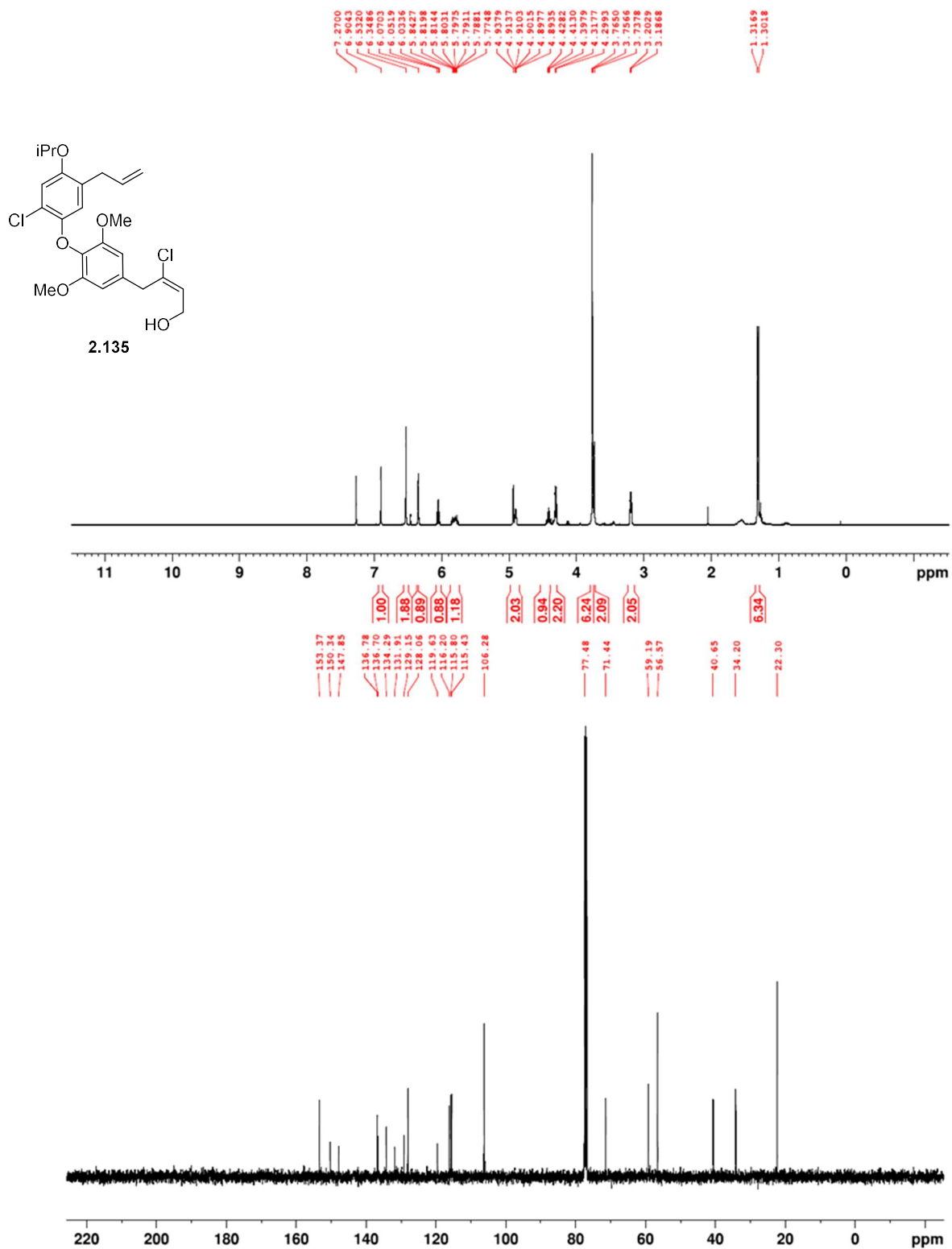
Figure A.85. ^{1}H NMR (400 MHz, CDCl$_3$) and ^{13}C NMR (100 MHz, CDCl$_3$) of **2.135.**

Figure A.86. DEPT-135(CDCl₃) of **2.135.**
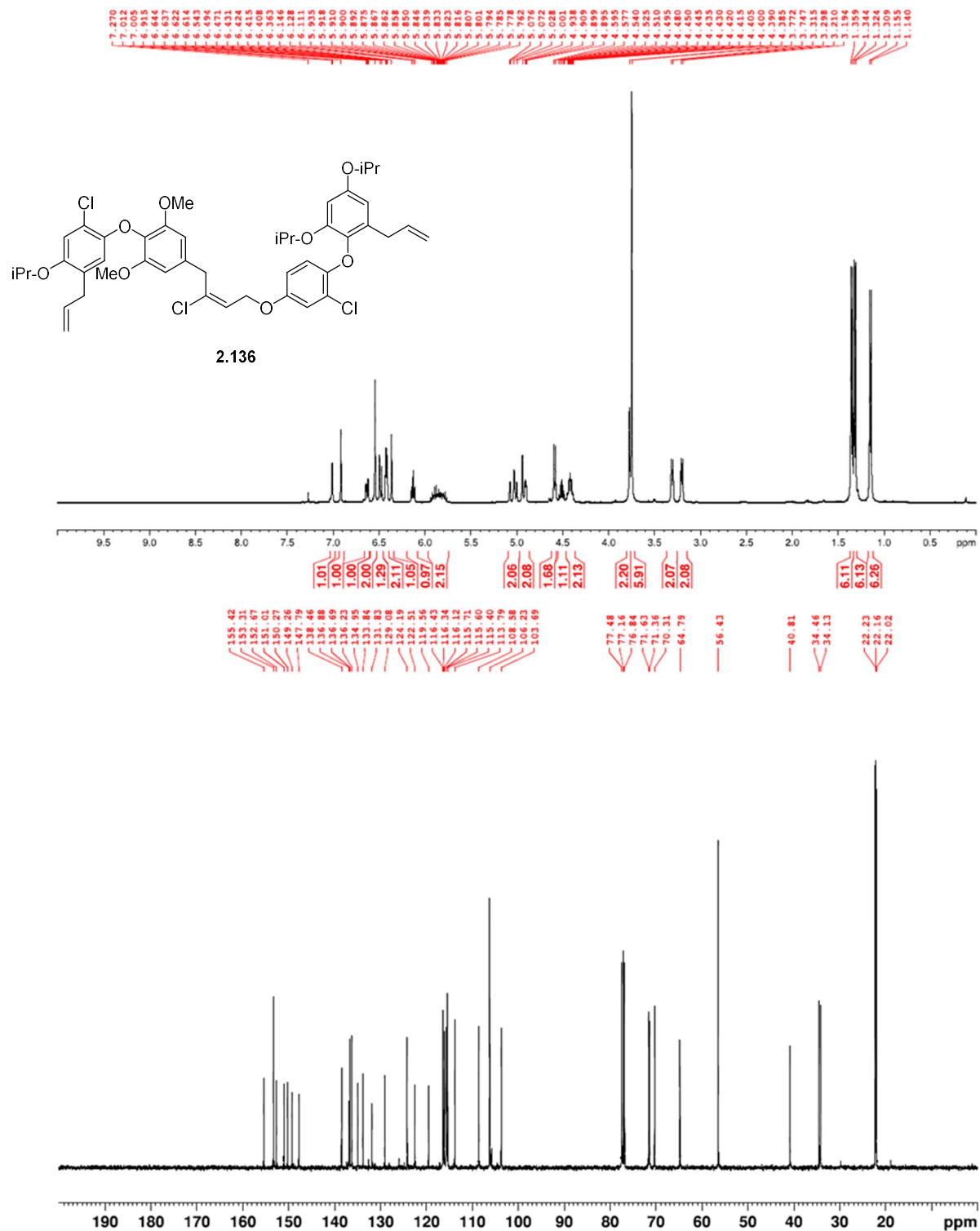
Figure A.87. ^{1}H NMR (400 MHz, CDCl$_3$) and ^{13}C NMR (100 MHz, CDCl$_3$) of **2.136**.
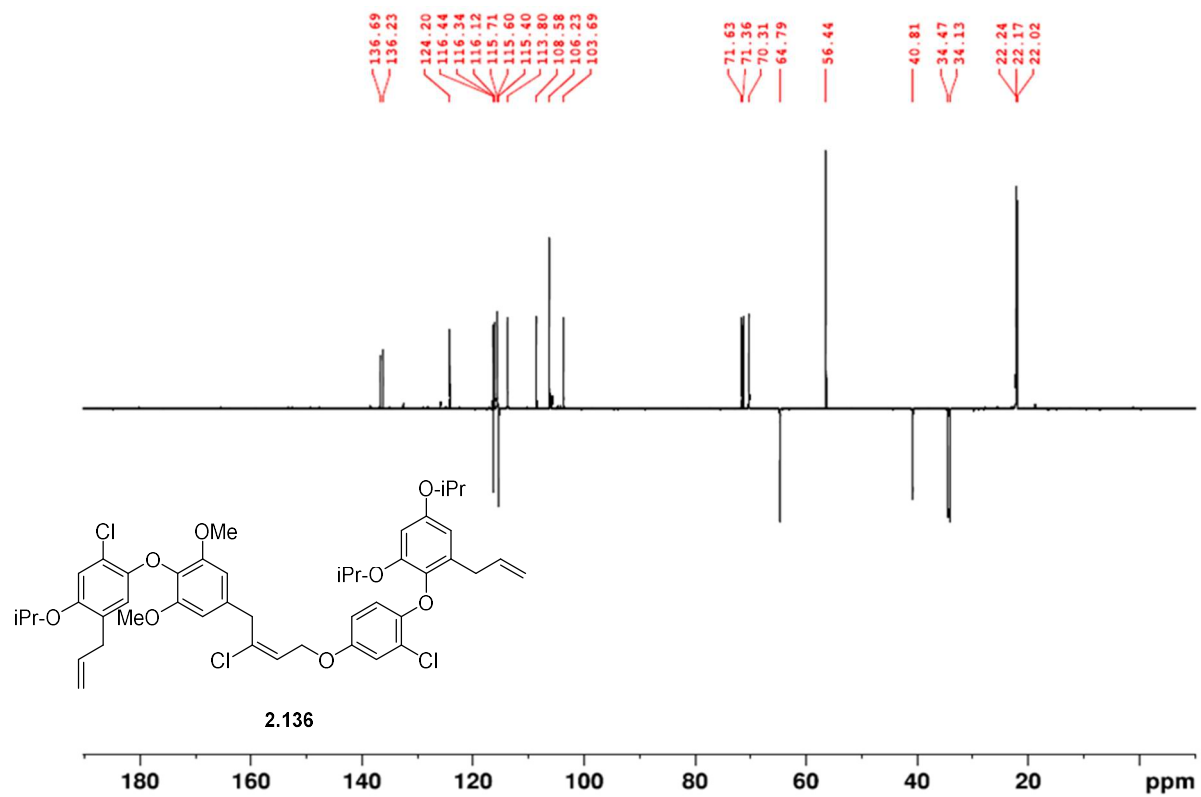
Figure A.88. DEPT-135(CDCl₃) of **2.136.**

Figure A.89. ^{1}H NMR (400 MHz, CDCl$_3$) and ^{13}C NMR (100 MHz, CDCl$_3$) of **2.139.**

Figure A.90. DEPT-135(CDCl₃) of **2.139.**

Figure A.91. ^{1}H NMR (400 MHz, CD$_3$OD) and ^{13}C NMR (100 MHz, CD$_3$OD) of **VU0848355.**
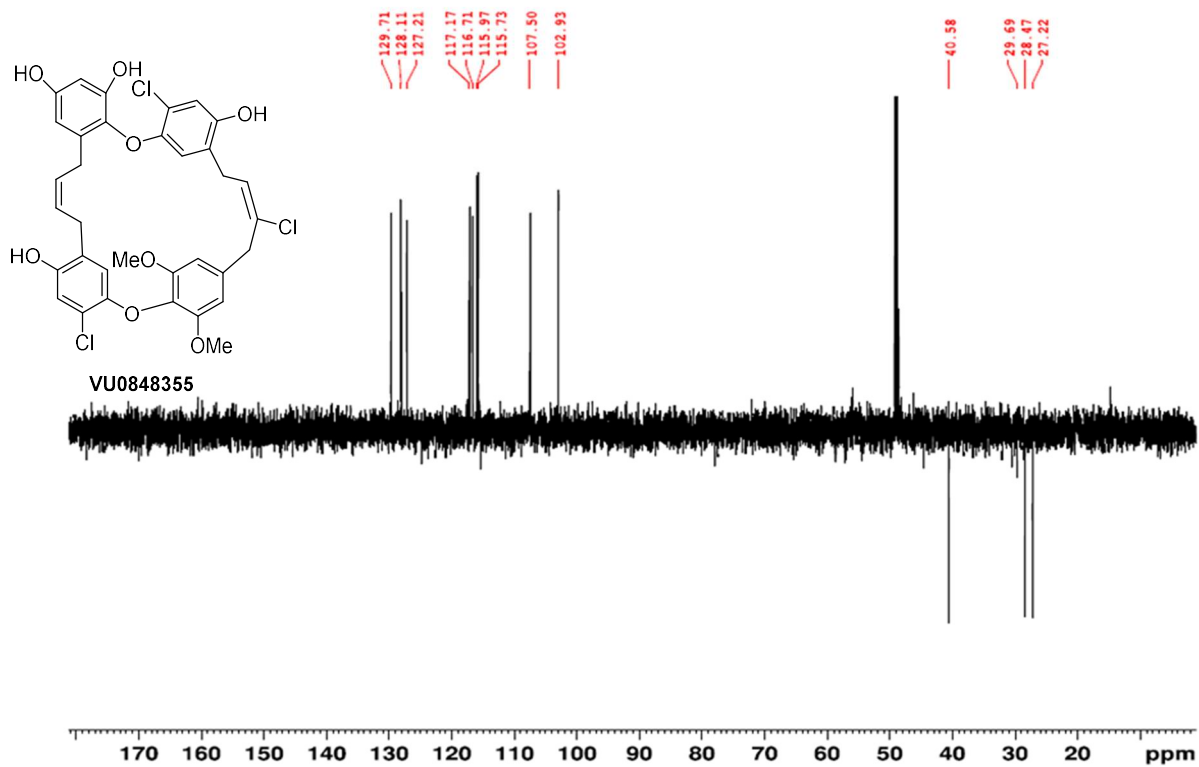
Figure A.92. DEPT-135(CD$_3$OD) of **VU0848355**.
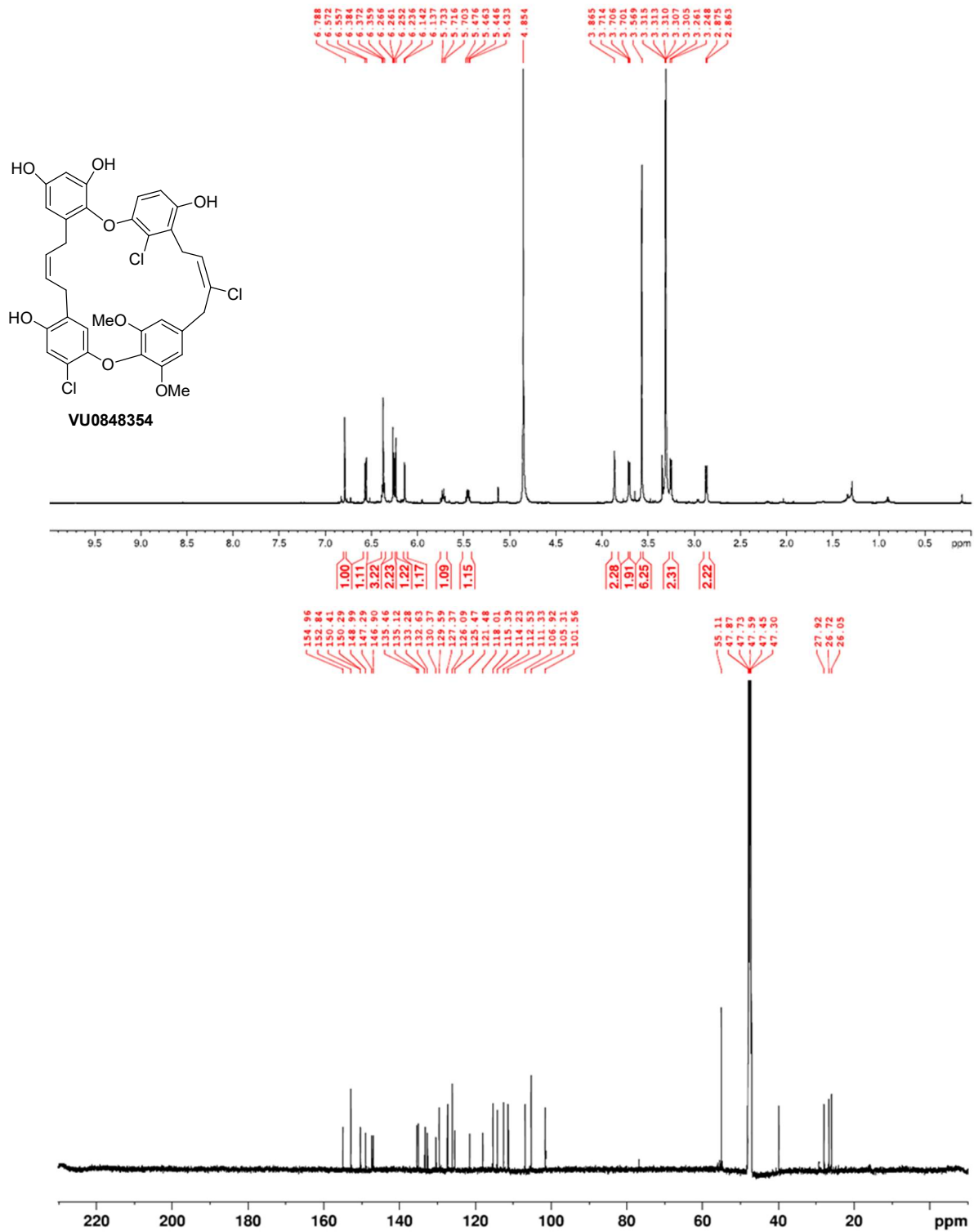
Figure A.93. ^{1}H NMR (400 MHz, CD$_3$OD) and ^{13}C NMR (100 MHz, CD$_3$OD) of **VU0848354.**
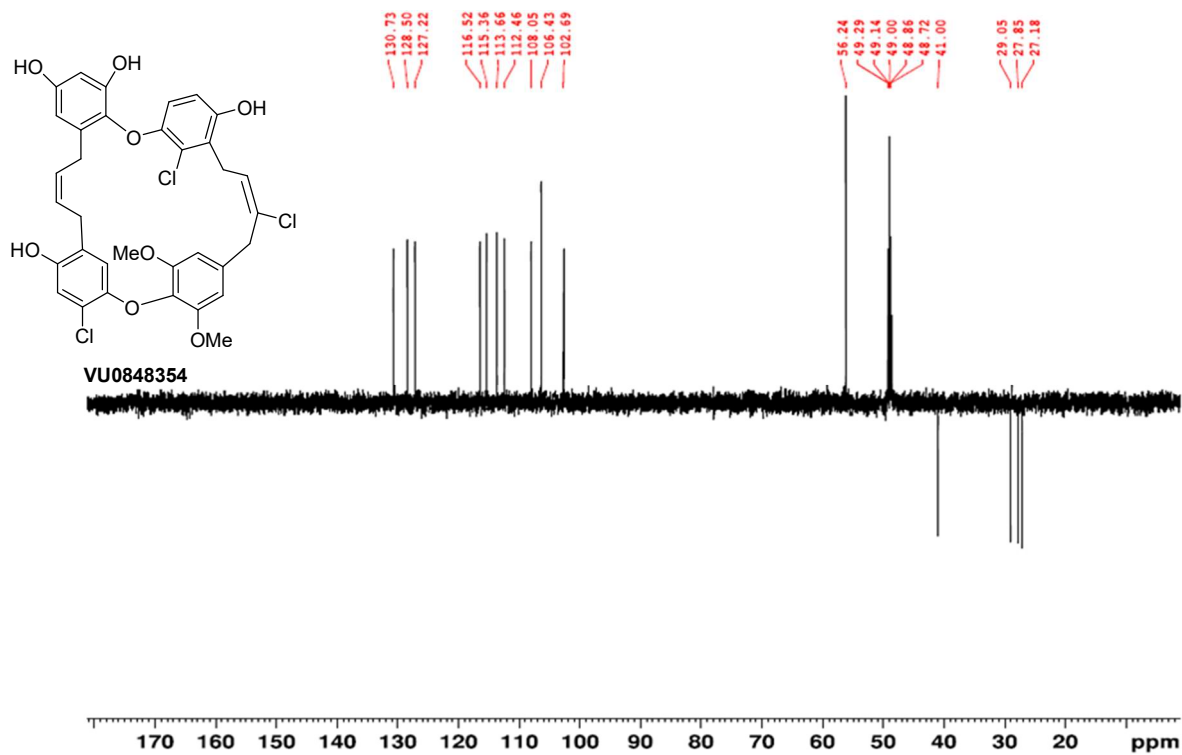
Figure A.94. DEPT-135(CD₃OD) of VU0848354.
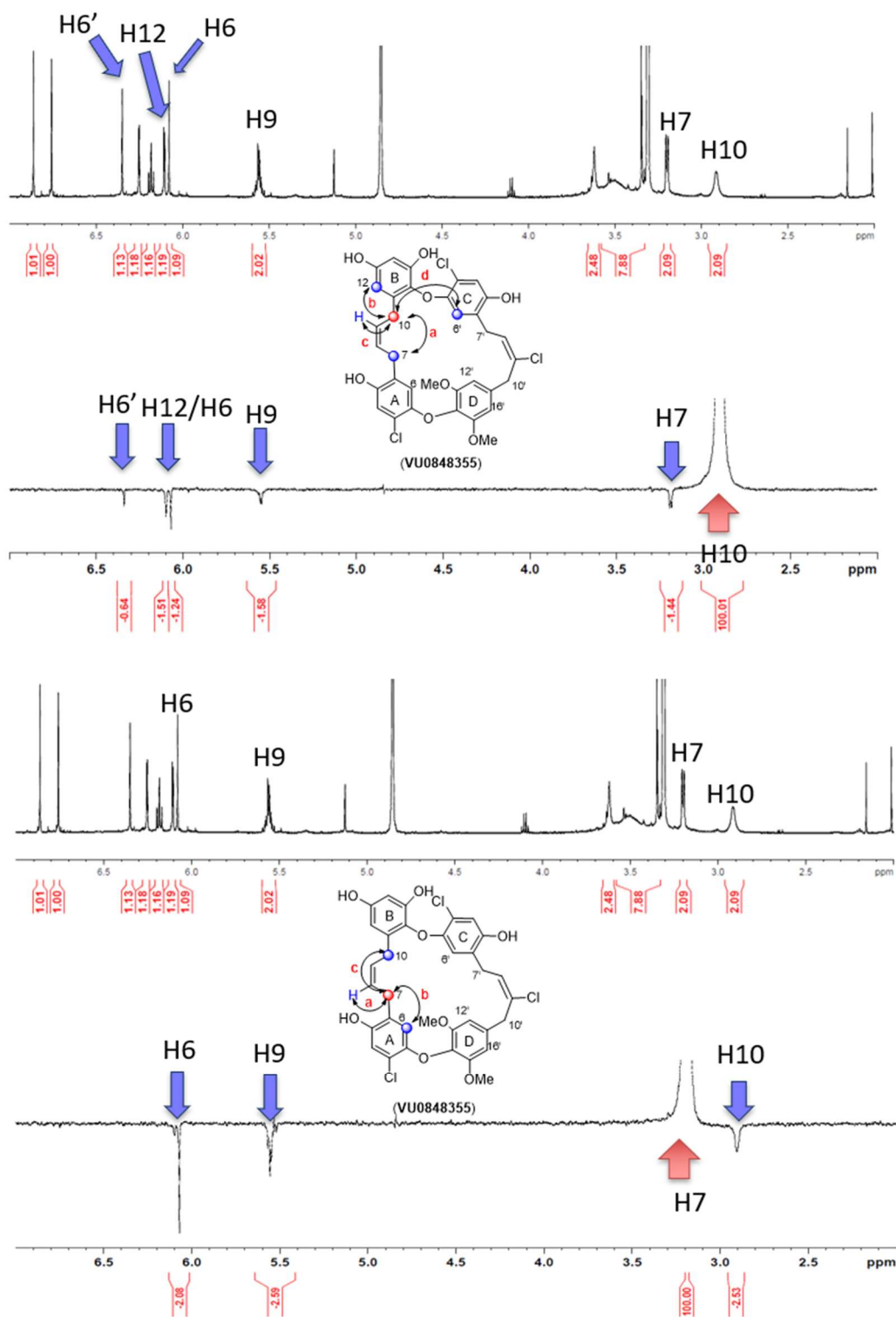
Figure A.95. Assignment of C8-C9 double bond geometry of **VU0848355** (1-D selective NOE, CD$_3$OD).

283
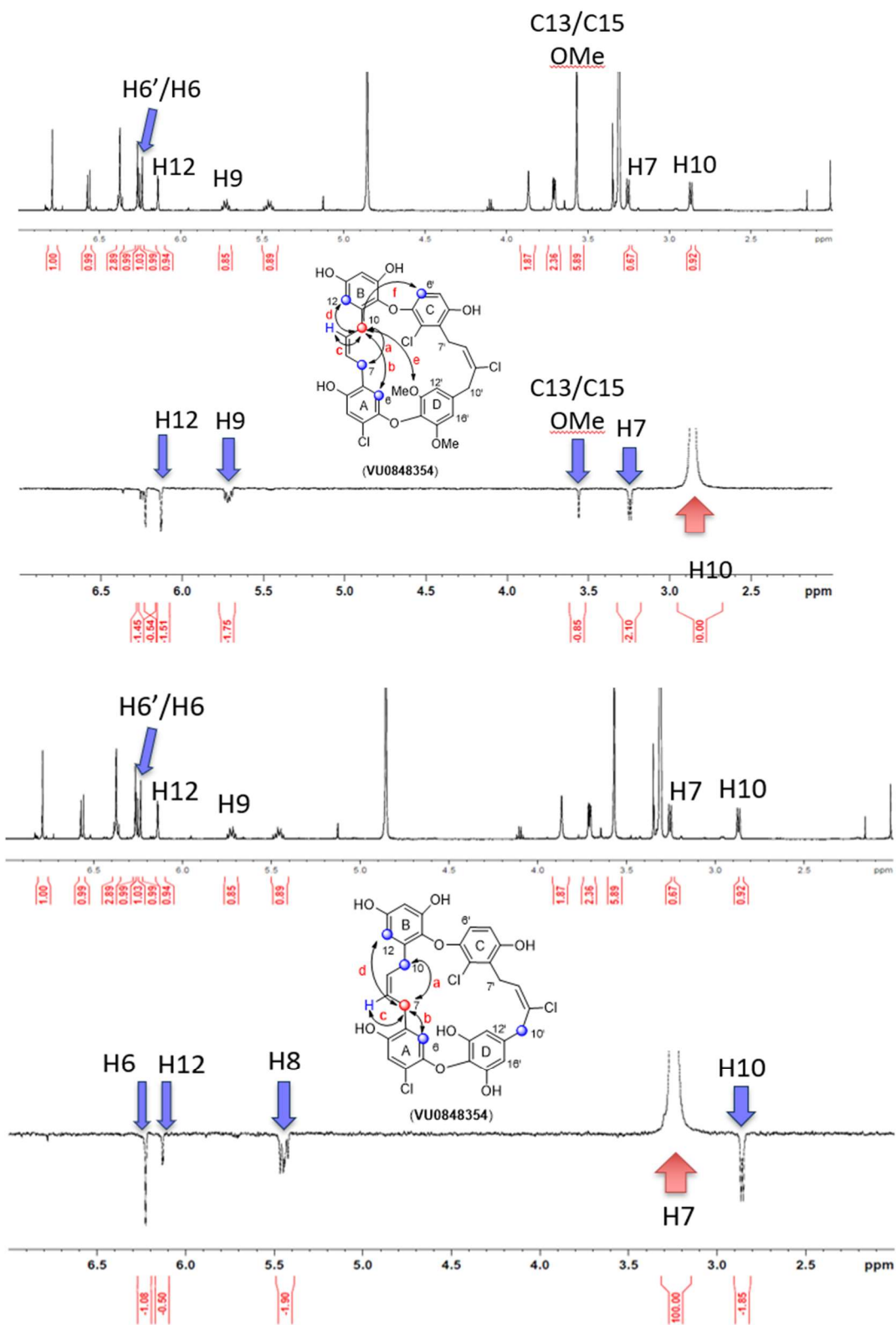
Figure A.96. Assignment of C8-C9 double bond geometry of **VU0848354** (1-D selective NOE, CD₃OD).
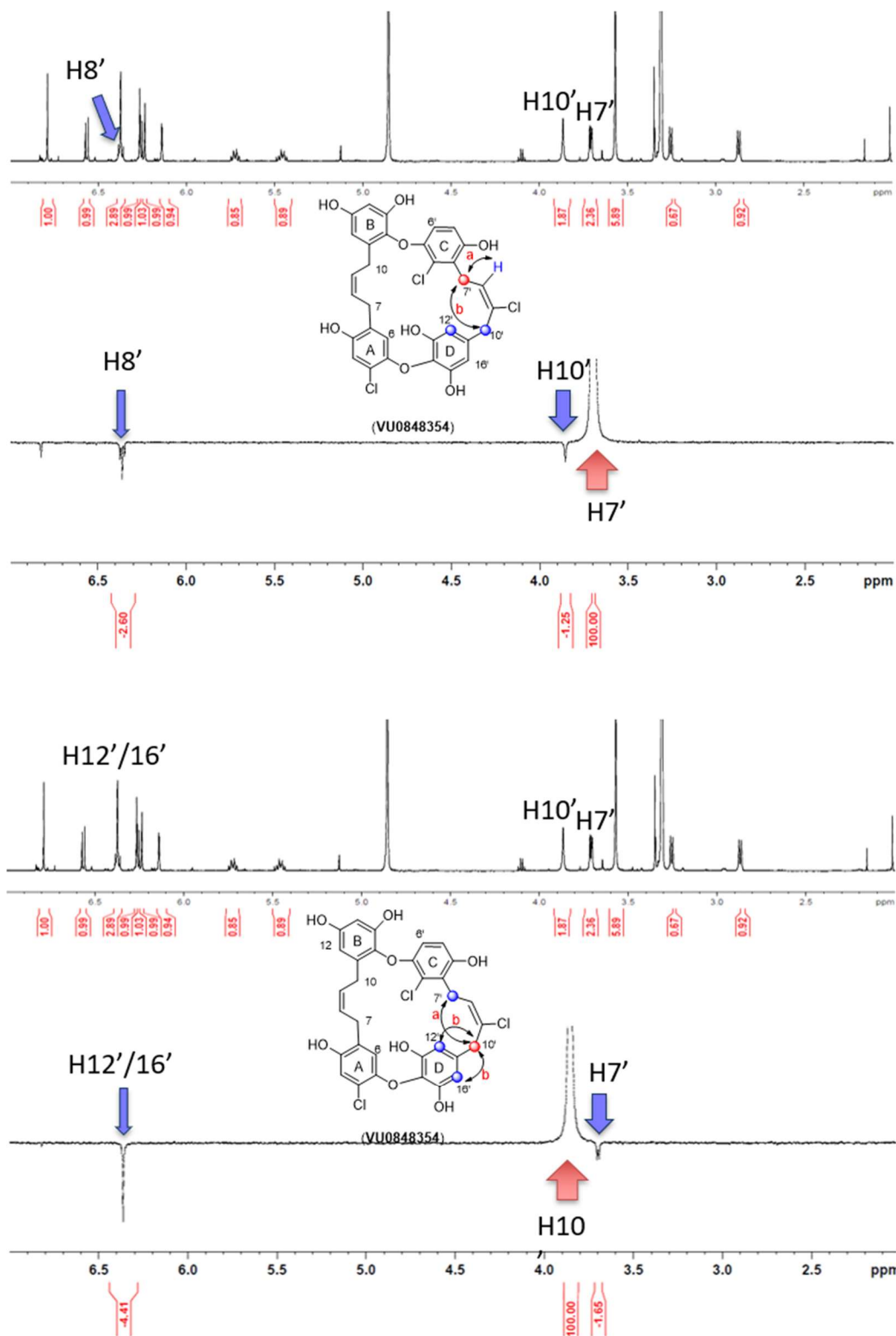
Figure A.97. Assignment of C8'-C9' double bond geometry of **VU0848354** (1-D selective NOE, CD₃OD).
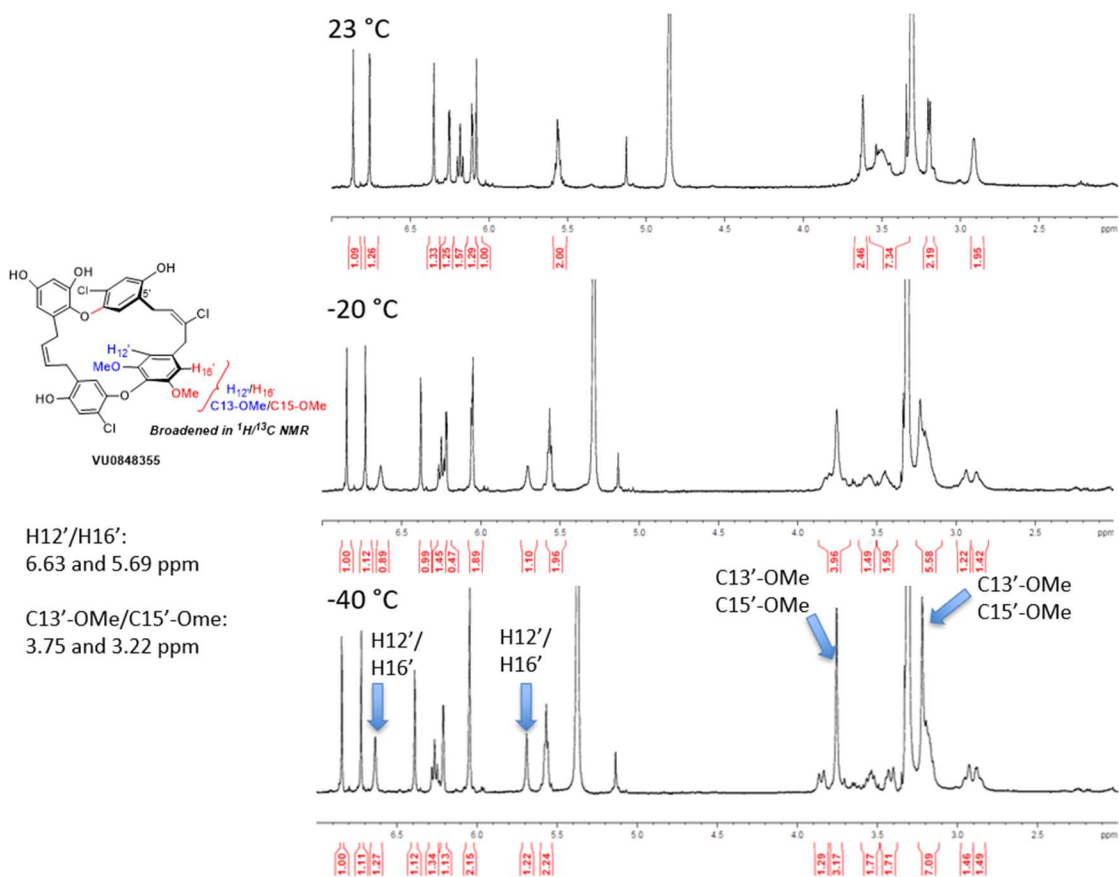
Figure A.98. Low Temperature (23 °C to -40 °C) ^{1}H NMR (600 MHz, CD$_3$OD) assignment of H12', H16' and C13' and C15' methyl ethers of **VU0848355**.
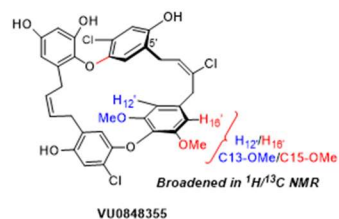
H12'/H16': 6.63 and 5.69 ppm; C12'/C16': 108.1 and 104.4 ppm

^{1}H-OMe (C12')/^{1}H-OMe (C15'): 3.75 and 3.22 ppm; ^{13}C-OMe(C12')/^{13}C-OMe (C15'): 56.3 and 55.4 ppm
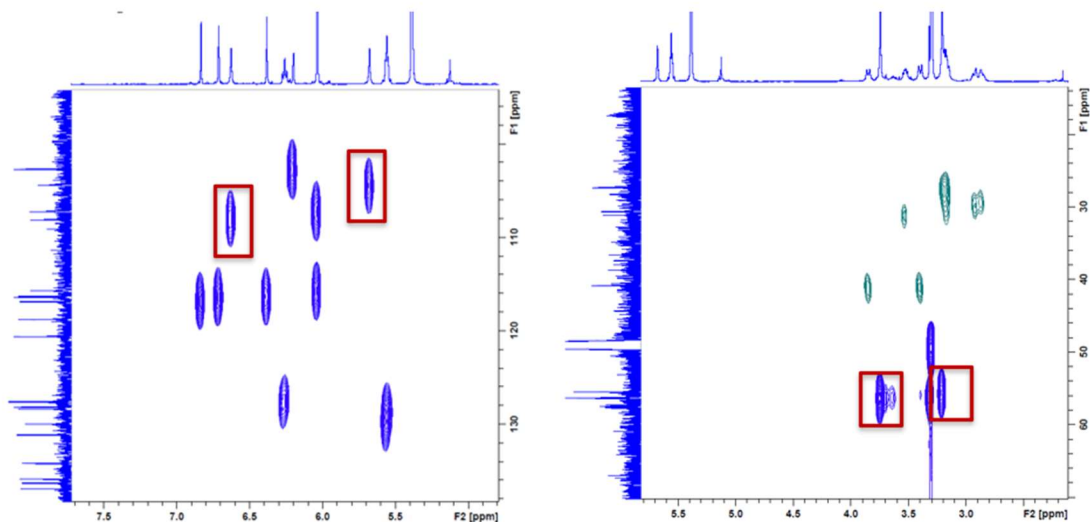
Figure A.99. Low-temperature HSQC (-40 °C, CD$_3$OD) assignment of C12', C16', and C13'-OMe and C15'-OMe of VU0848355.
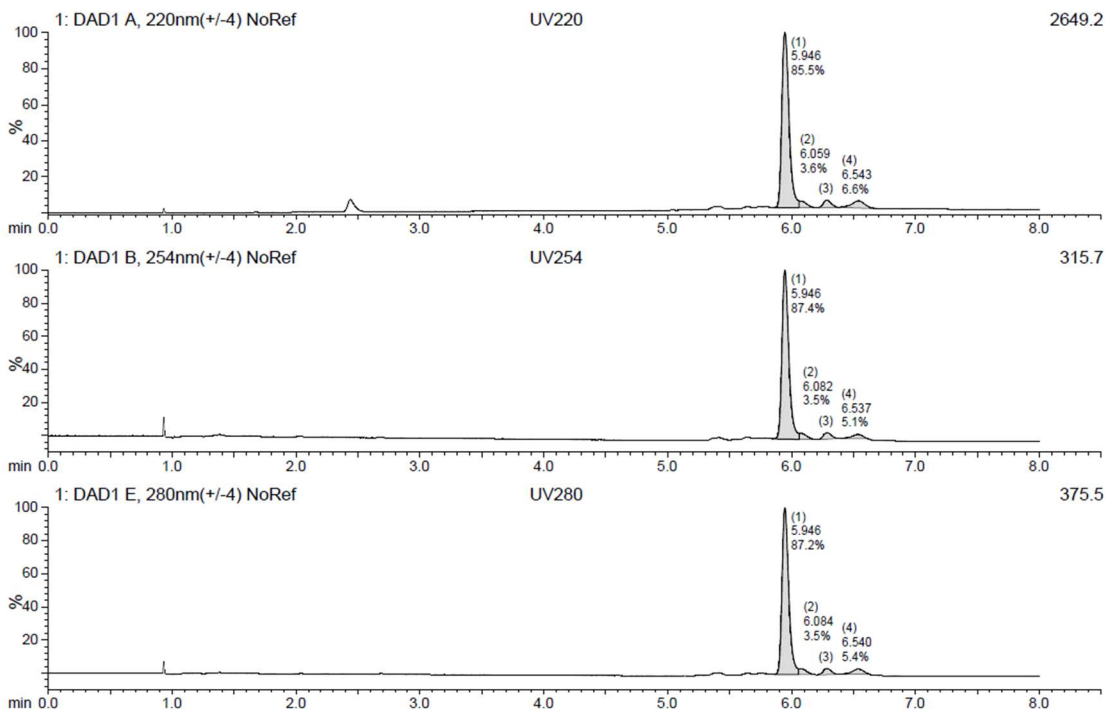
Figure A.100. Chiral HPLC chromatogram of **VU0848355** to determine the presence of potential atropisomers.
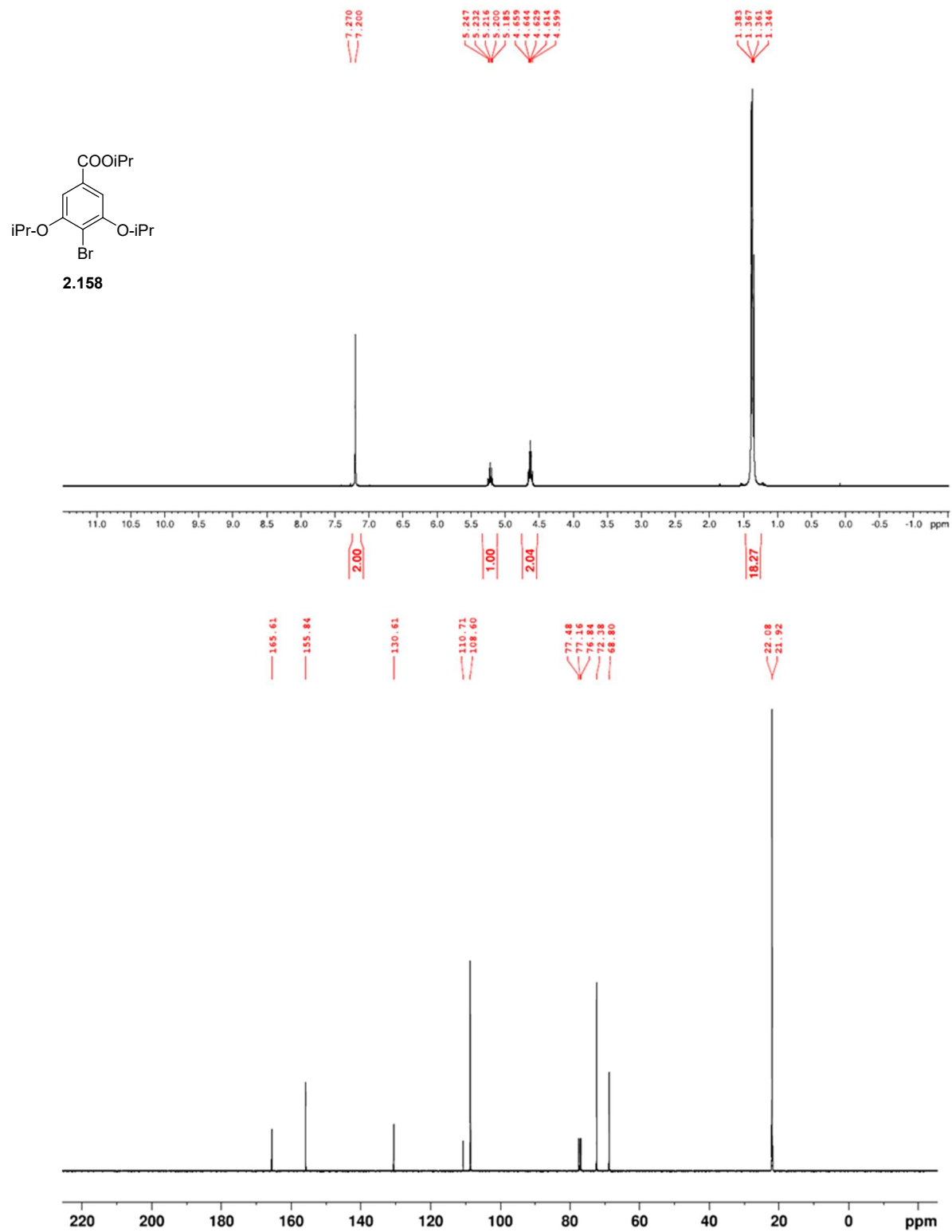
Figure A.101. ^{1}H NMR (400 MHz, CDCl$_3$) and ^{13}C NMR (100 MHz, CDCl$_3$) of **2.158.**
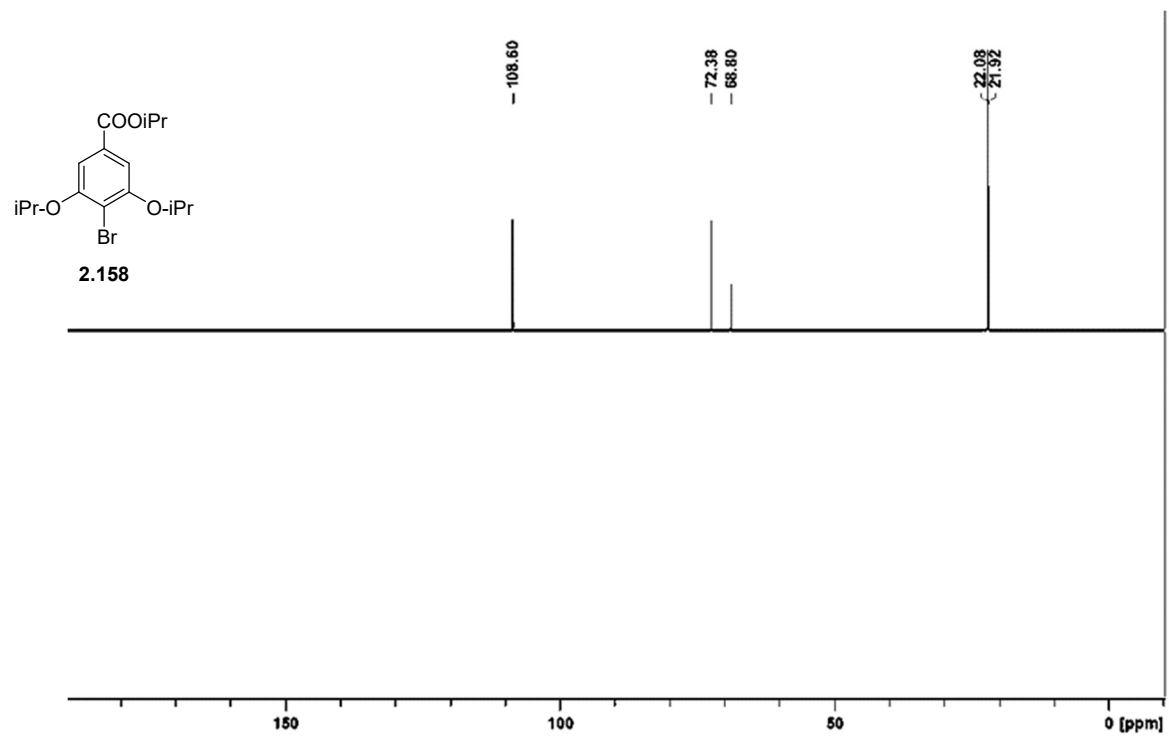
Figure A.102. DEPT-135(CDCl₃) of **2.158.**
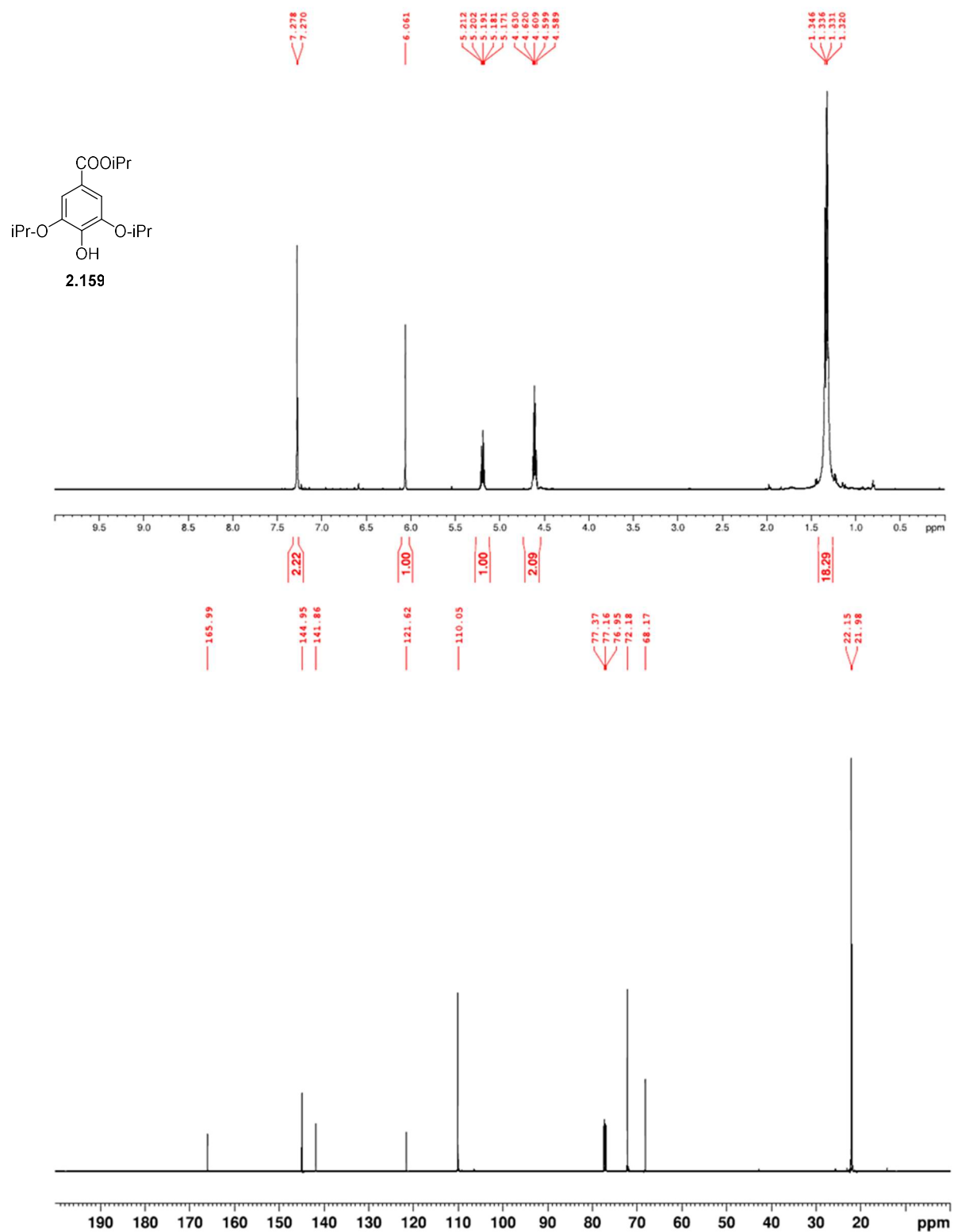
Figure A.103. ^{1}H NMR (400 MHz, CDCl$_3$) and ^{13}C NMR (100 MHz, CDCl$_3$) of **2.159.**
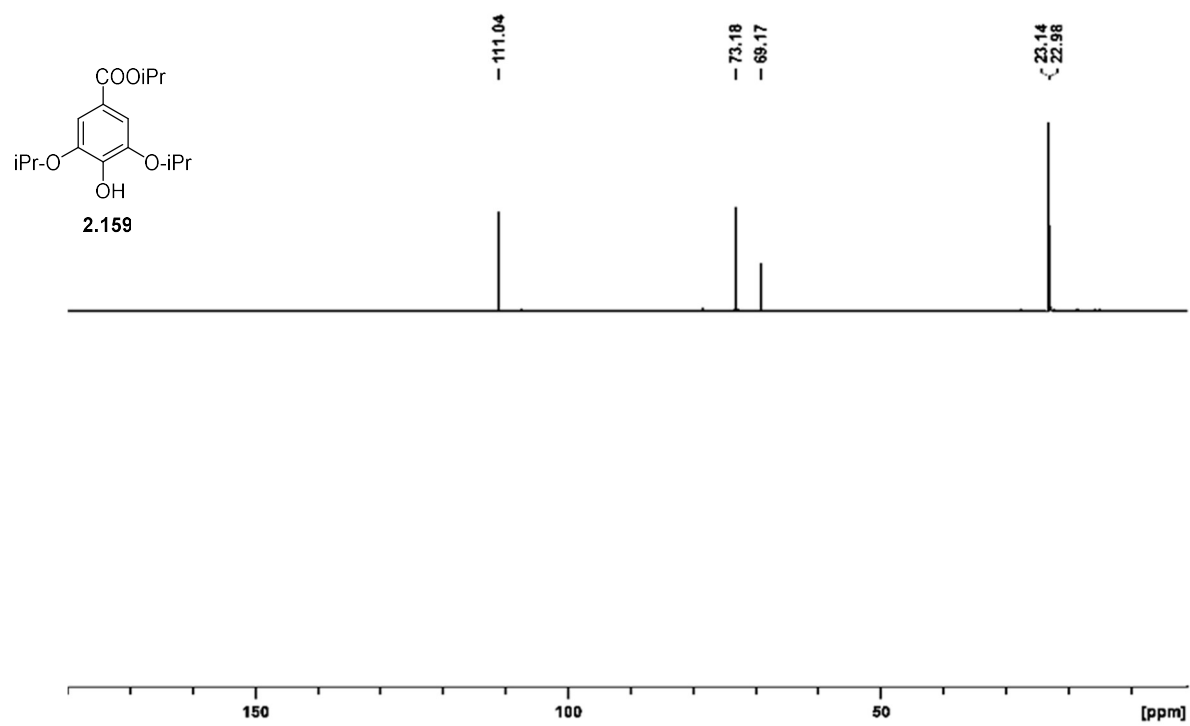
Figure A.104. DEPT-135(CDCl₃) of **2.159.**
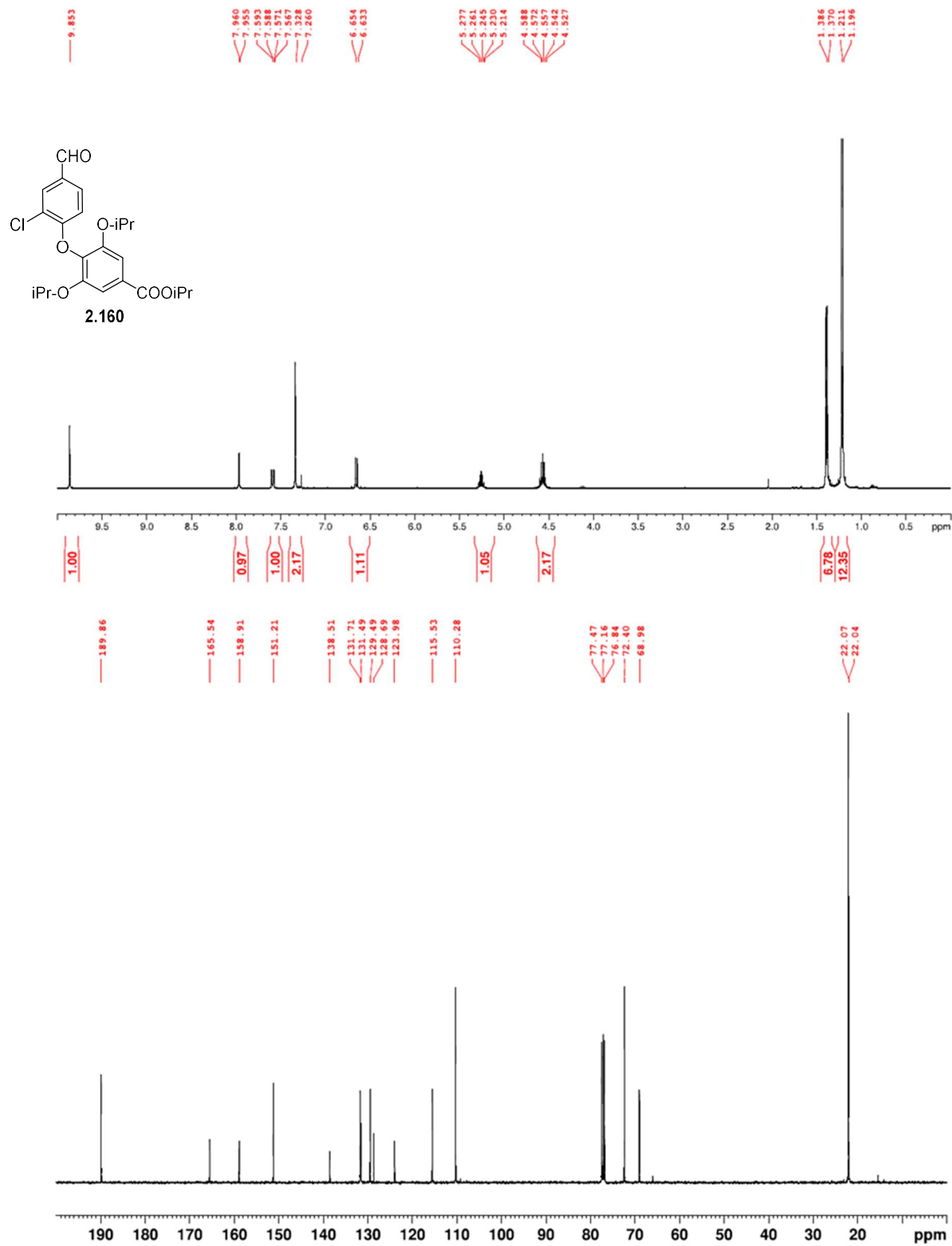
Figure A.105. ^{1}H NMR (400 MHz, CDCl$_3$) and ^{13}C NMR (100 MHz, CDCl$_3$) of **2.160.**
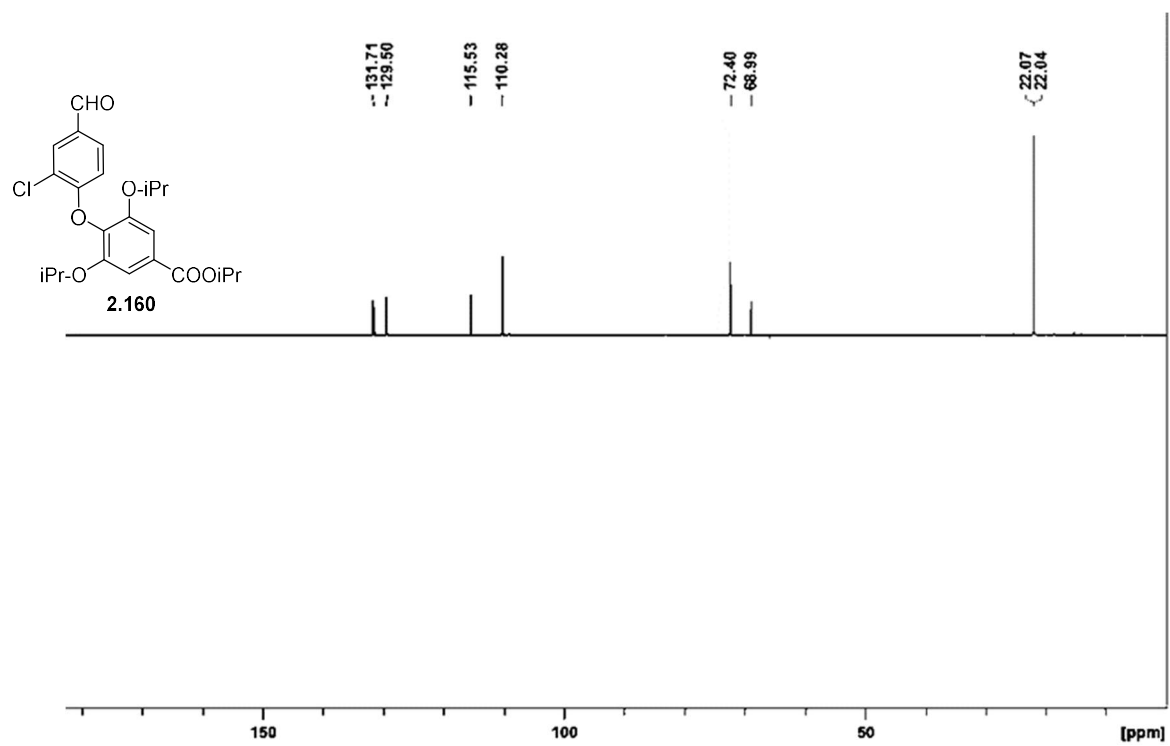
Figure A.106. DEPT-135(CDCl₃) of **2.160.**
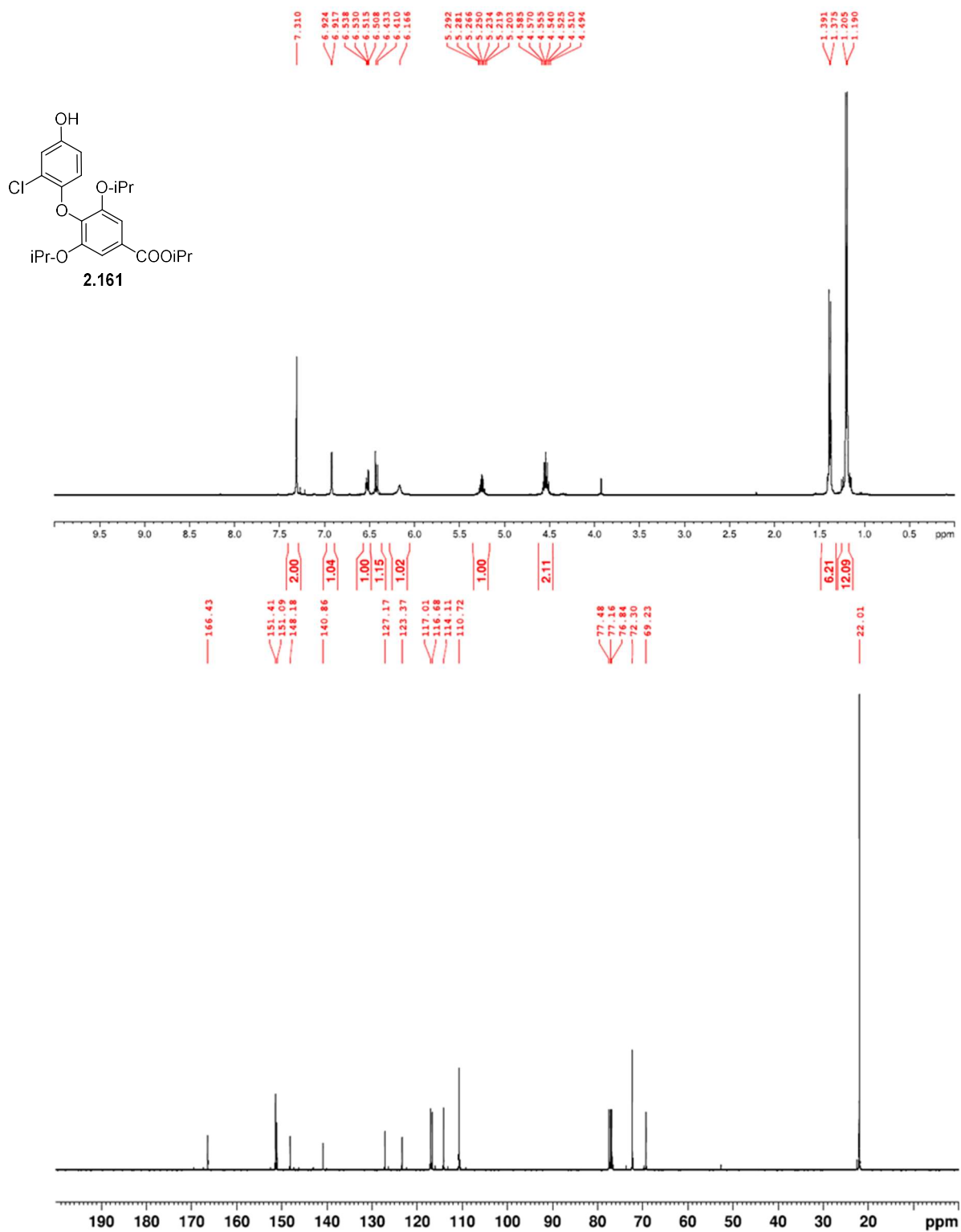
Figure A.107. ^{1}H NMR (400 MHz, CDCl$_3$) and ^{13}C NMR (100 MHz, CDCl$_3$) of **2.161.**
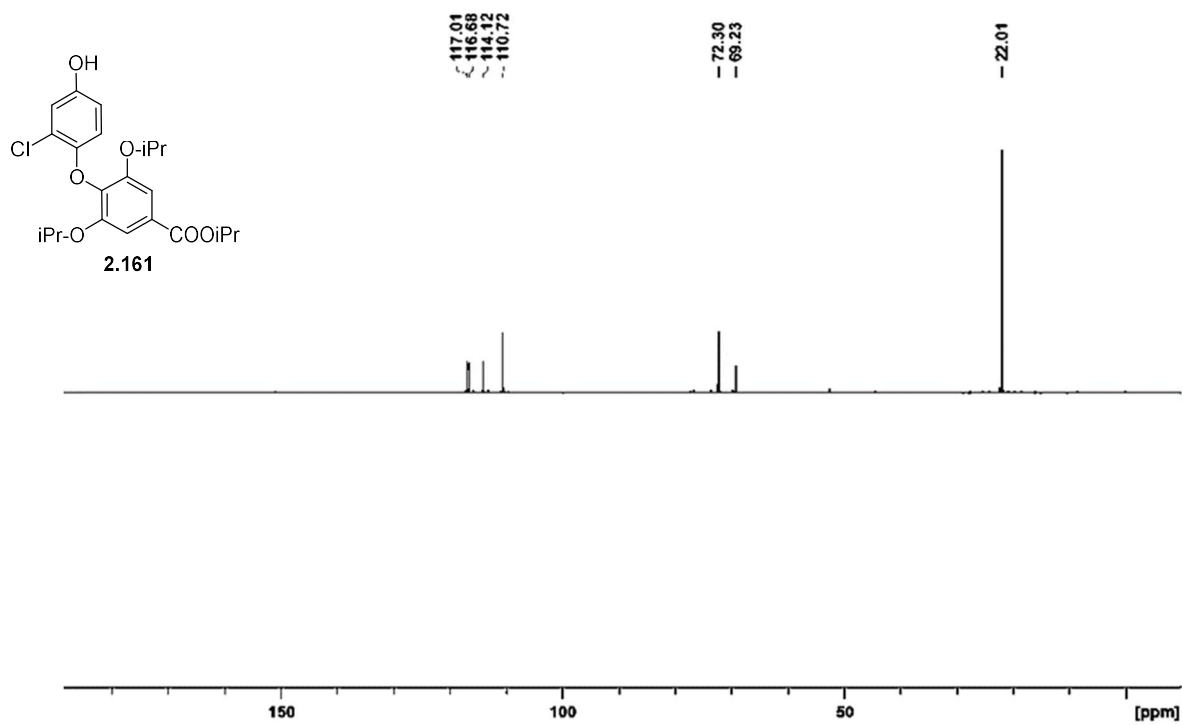
Figure A.108. DEPT-135(CDCl₃) of **2.161.**
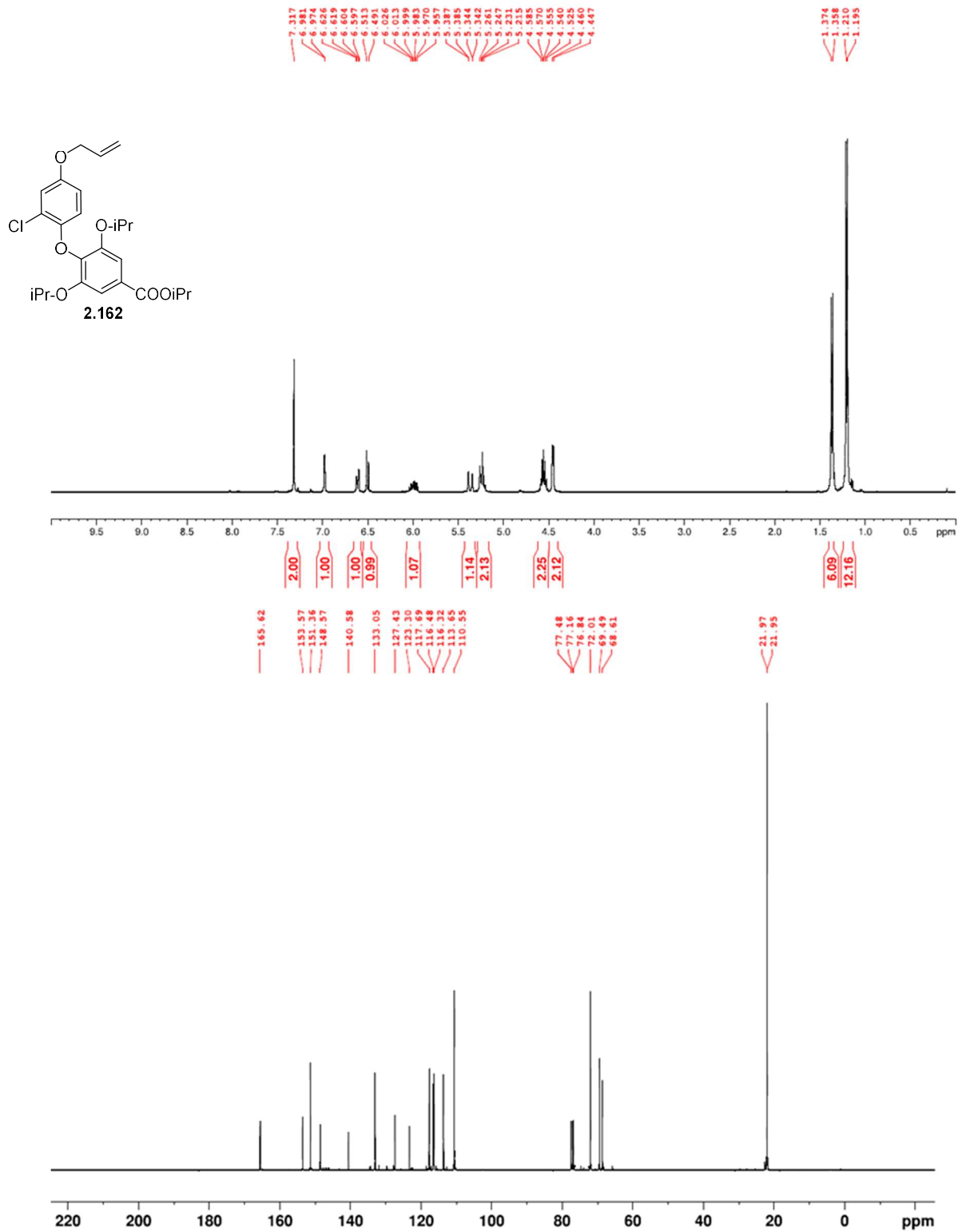
Figure A.109. ¹H NMR (400 MHz, CDCl₃) and ¹³C NMR (100 MHz, CDCl₃) of **2.162.**
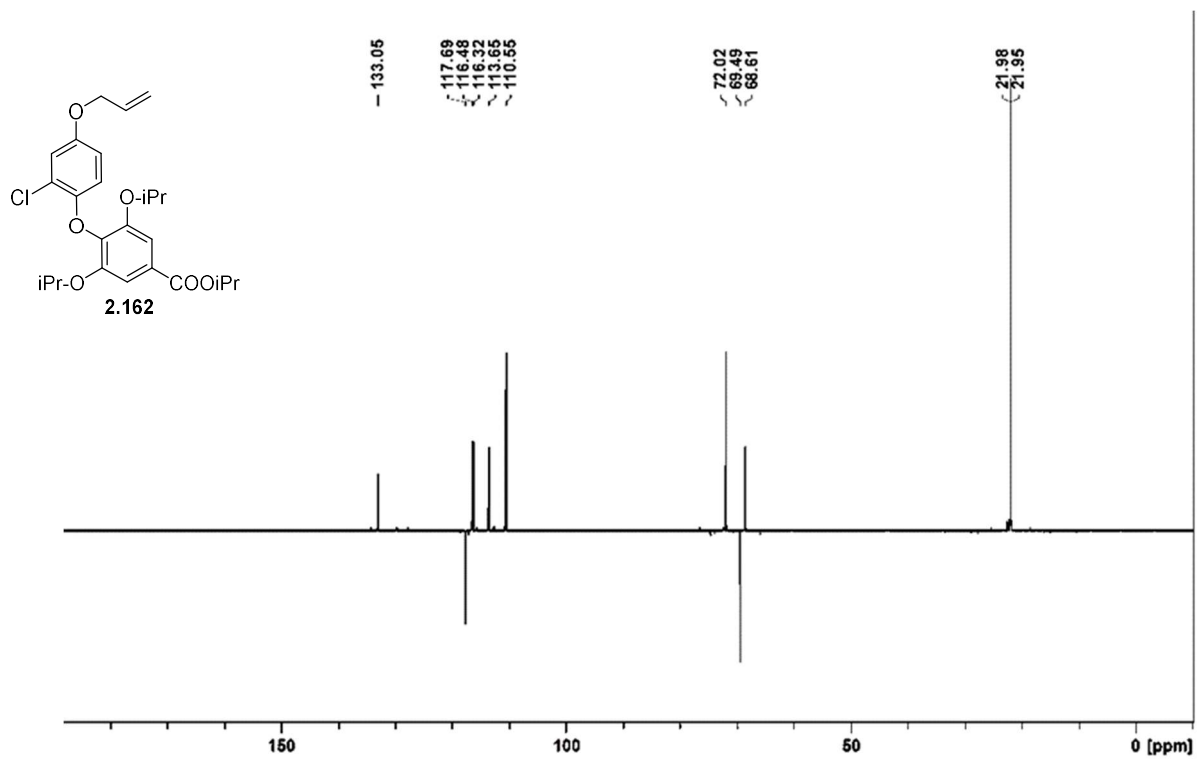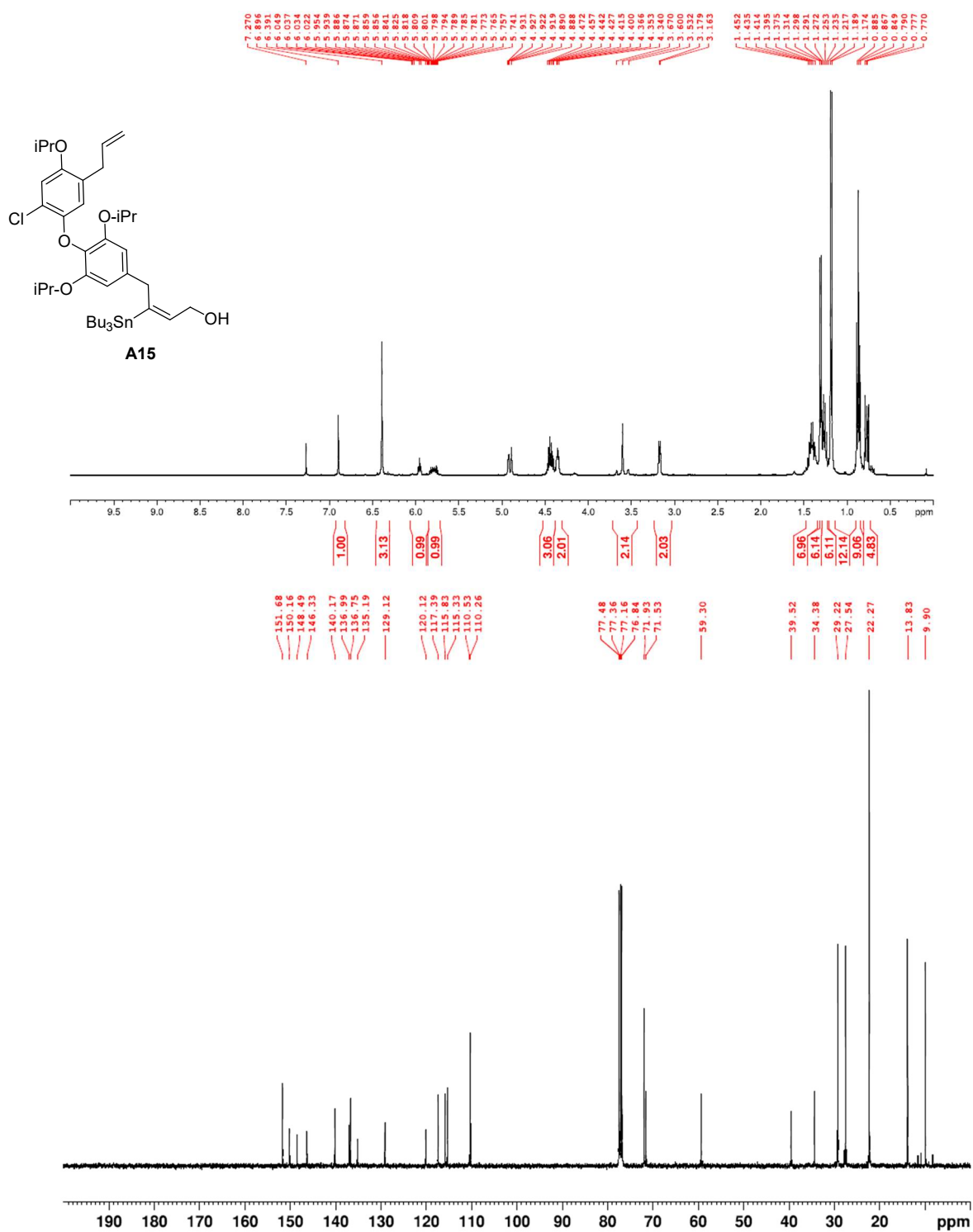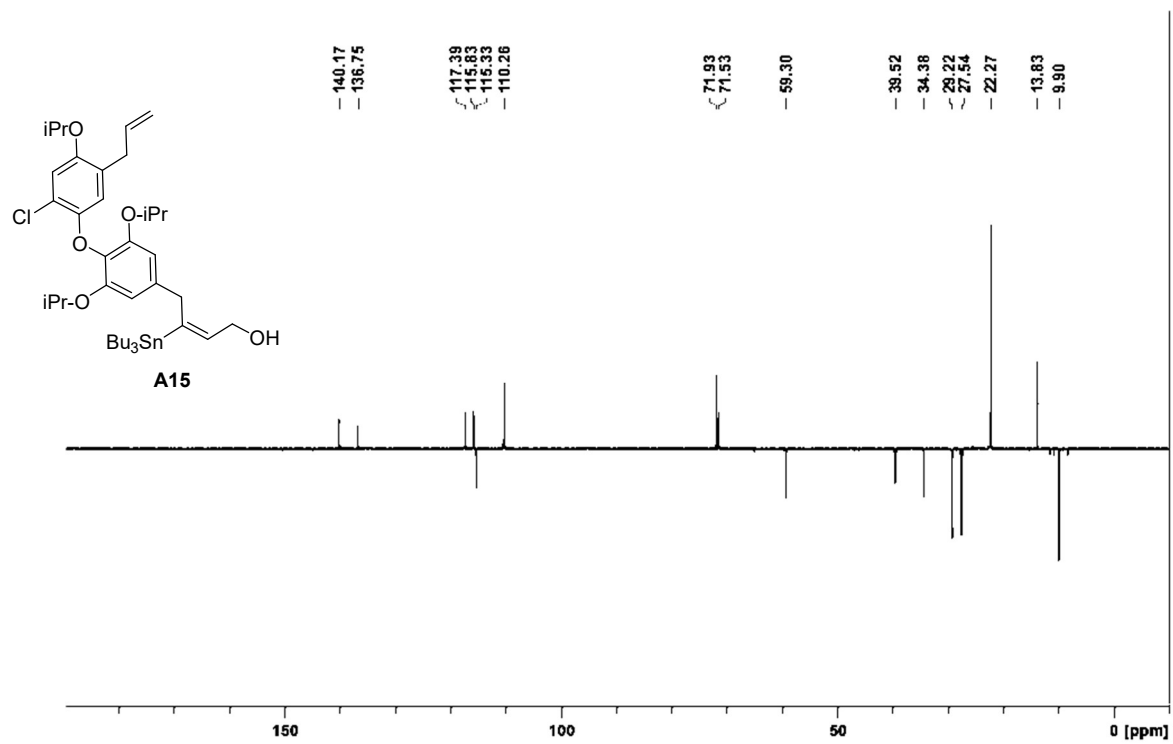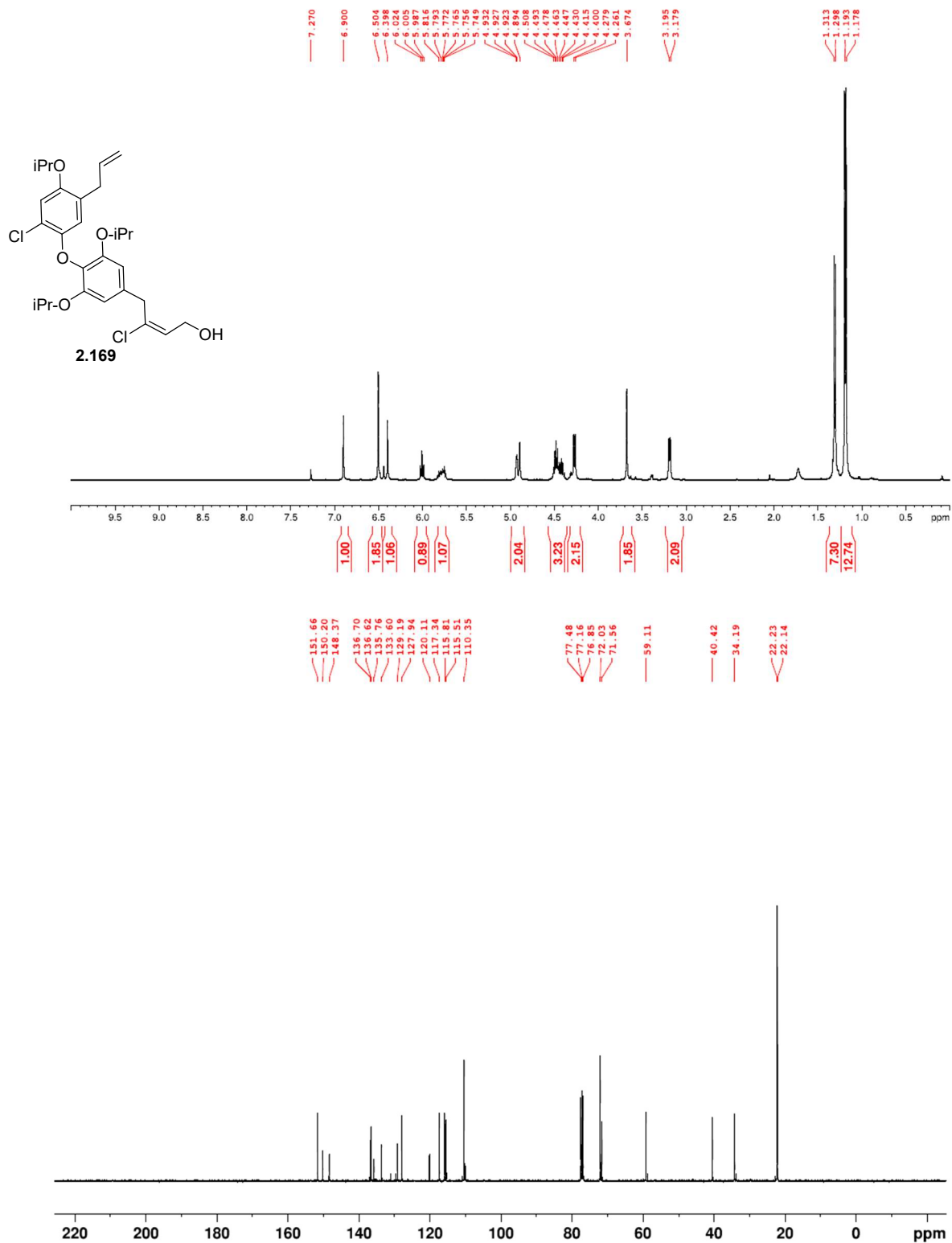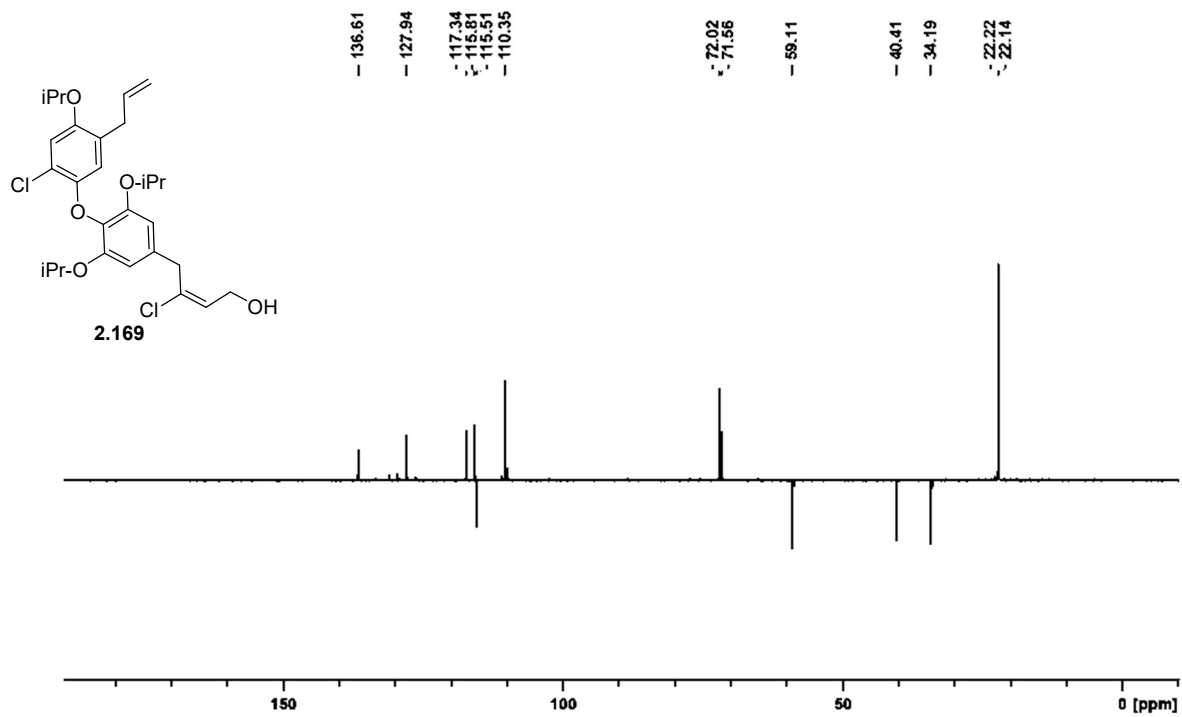
Figure A.110. DEPT-135(CDCl₃) of **2.162.**
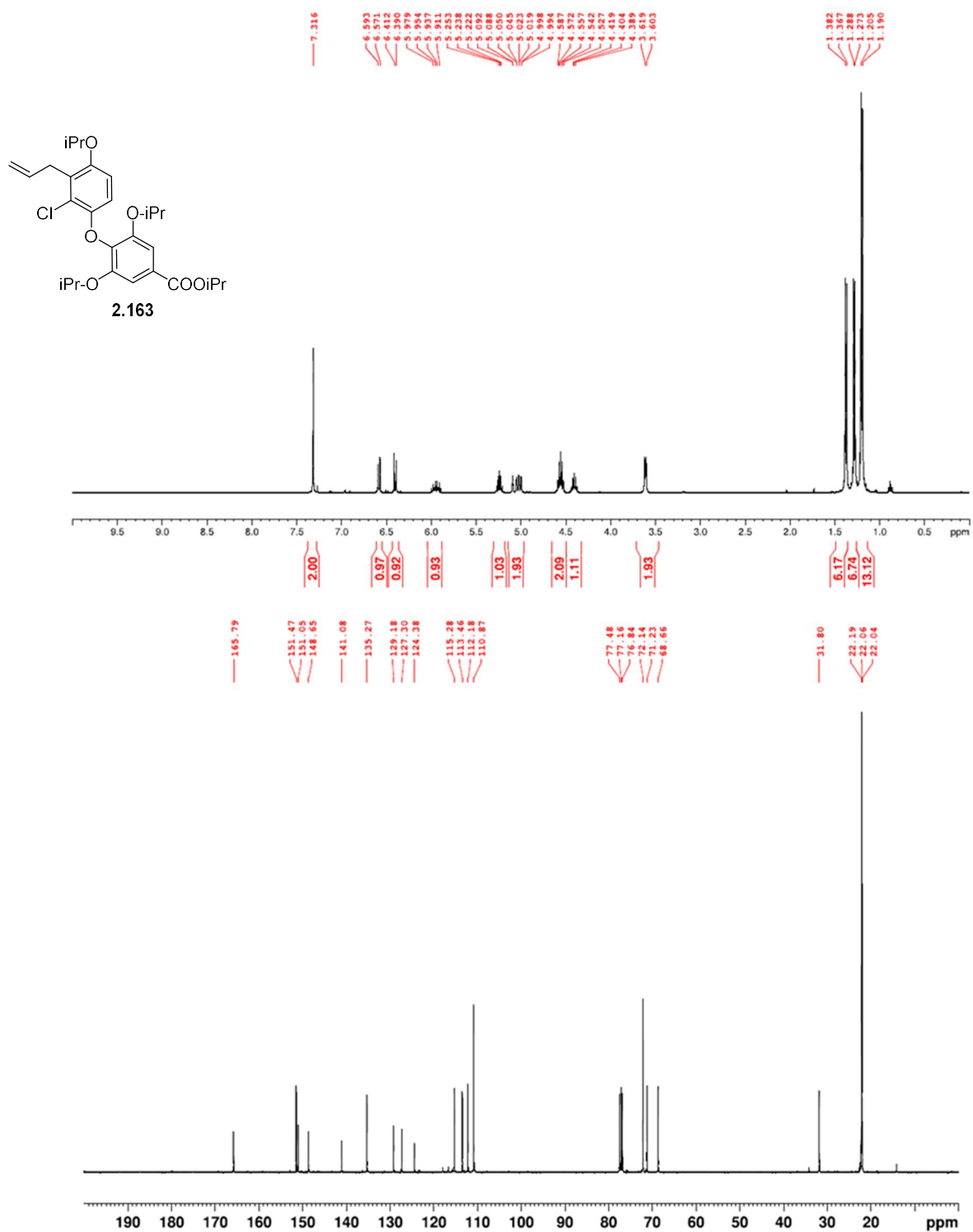
Figure A.111. ^{1}H NMR (400 MHz, CDCl$_3$) and ^{13}C NMR (100 MHz, CDCl$_3$) of **2.163.**

Figure A.112. DEPT-135(CDCl₃) of **2.163.**

Figure A.113. ^{1}H NMR (400 MHz, CDCl$_3$) and ^{13}C NMR (100 MHz, CDCl$_3$) of **2.164.**

Figure A.114. DEPT-135(CDCl₃) of **2.164.**

Figure A.115. ^{1}H NMR (400 MHz, CDCl$_3$) and ^{13}C NMR (100 MHz, CDCl$_3$) of **A10.**
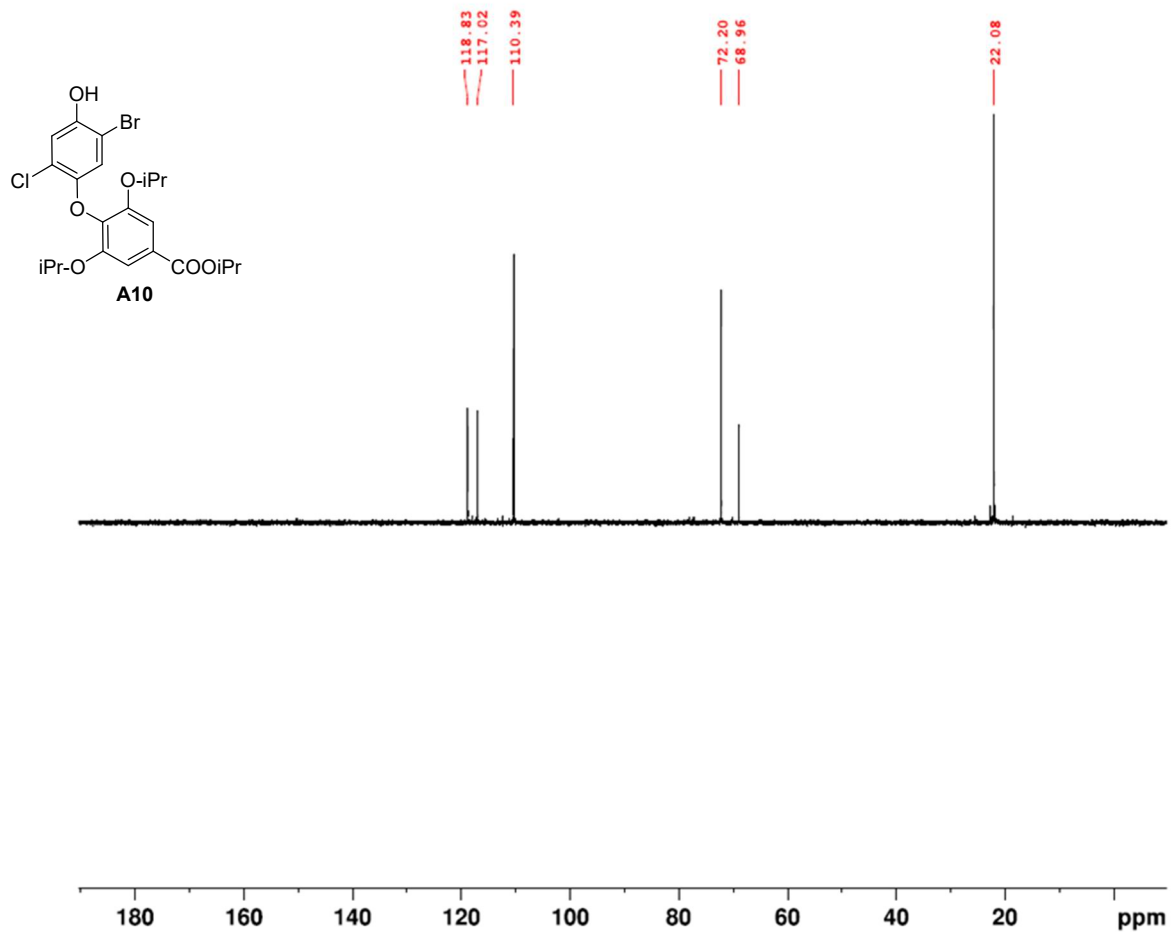
Figure A.116. DEPT-135(CDCl₃) of **A10.**
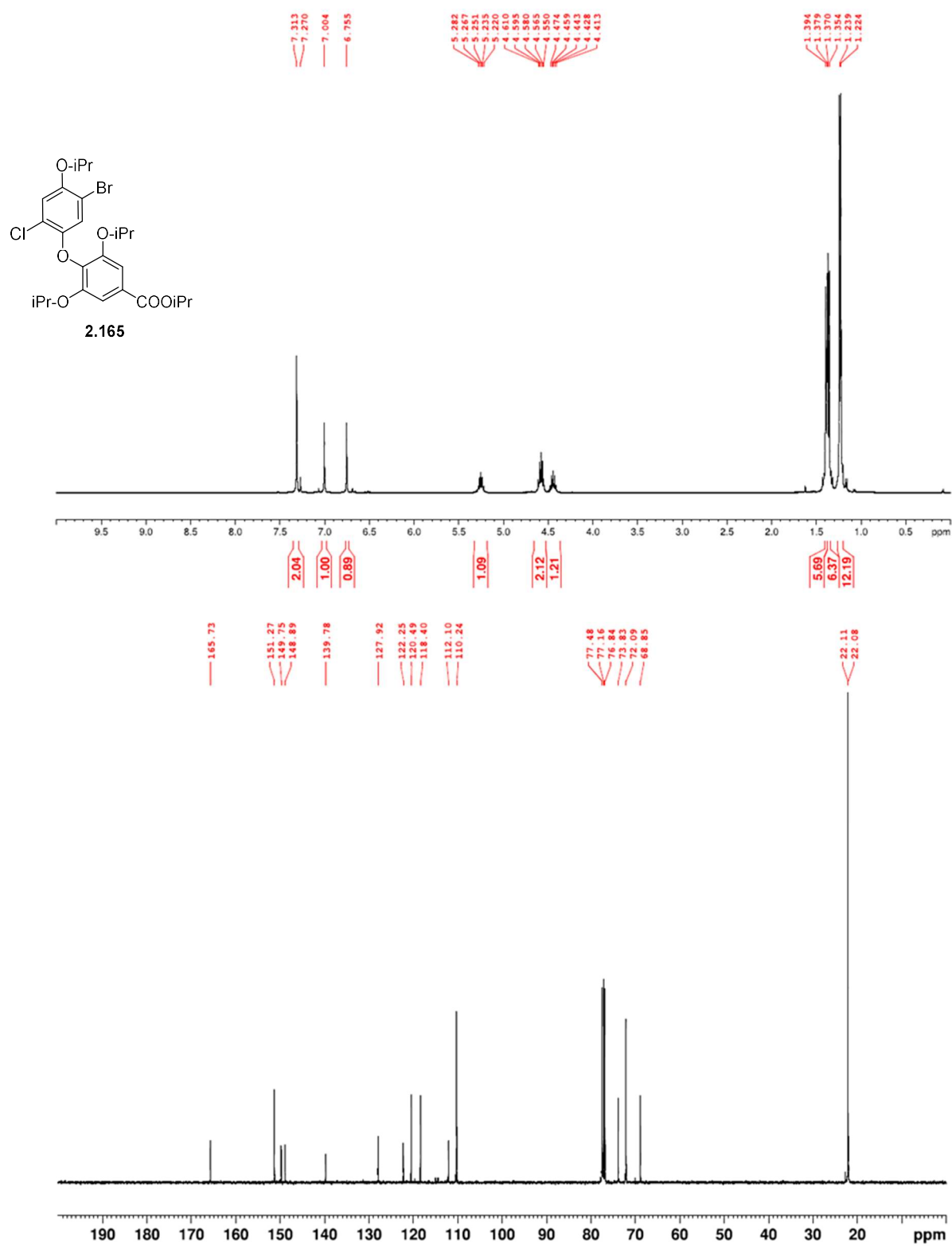
Figure A.117. ^{1}H NMR (400 MHz, CDCl$_3$) and ^{13}C NMR (100 MHz, CDCl$_3$) of **2.165.**
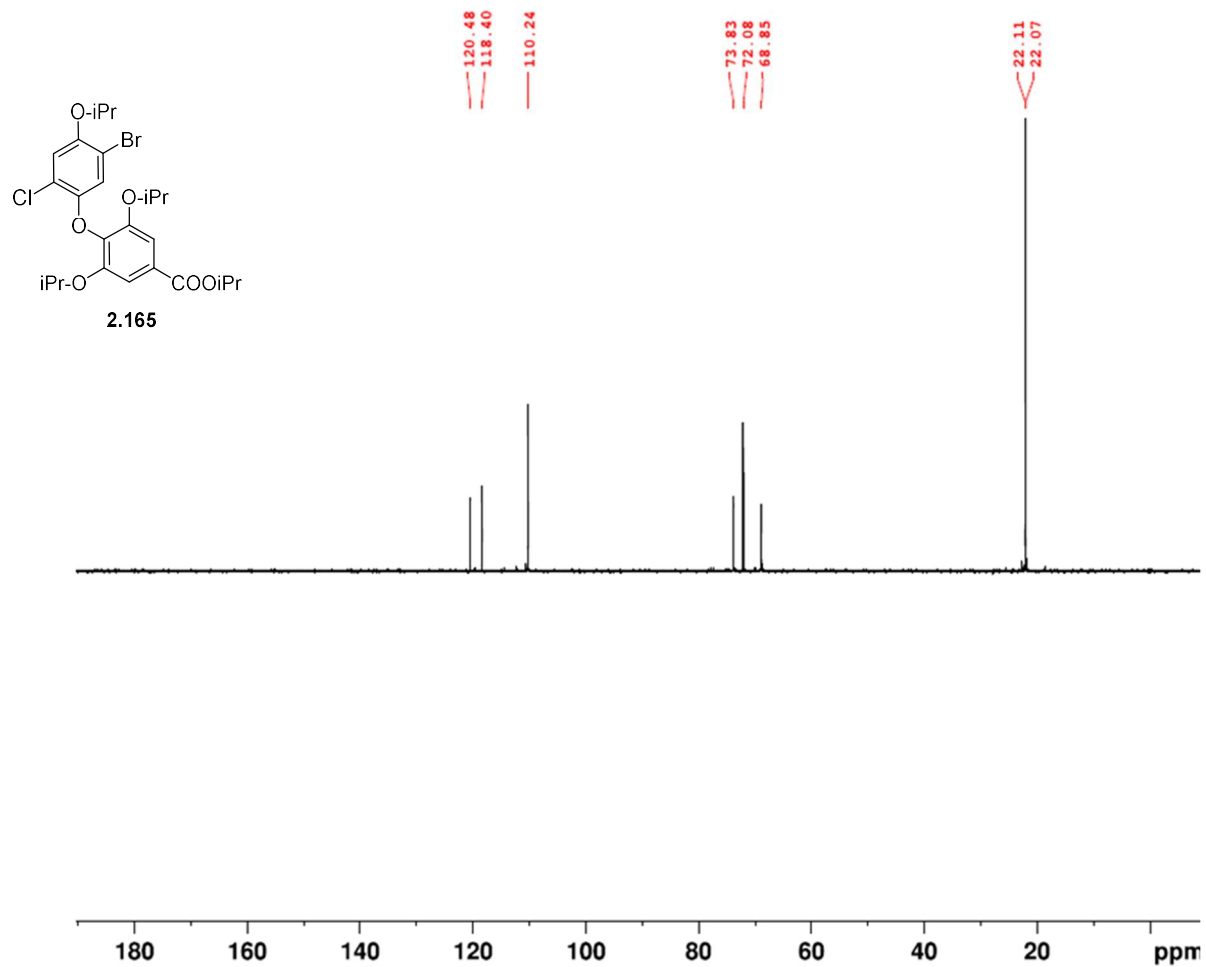
Figure A.118. DEPT-135(CDCl$_3$) of **2.165.**
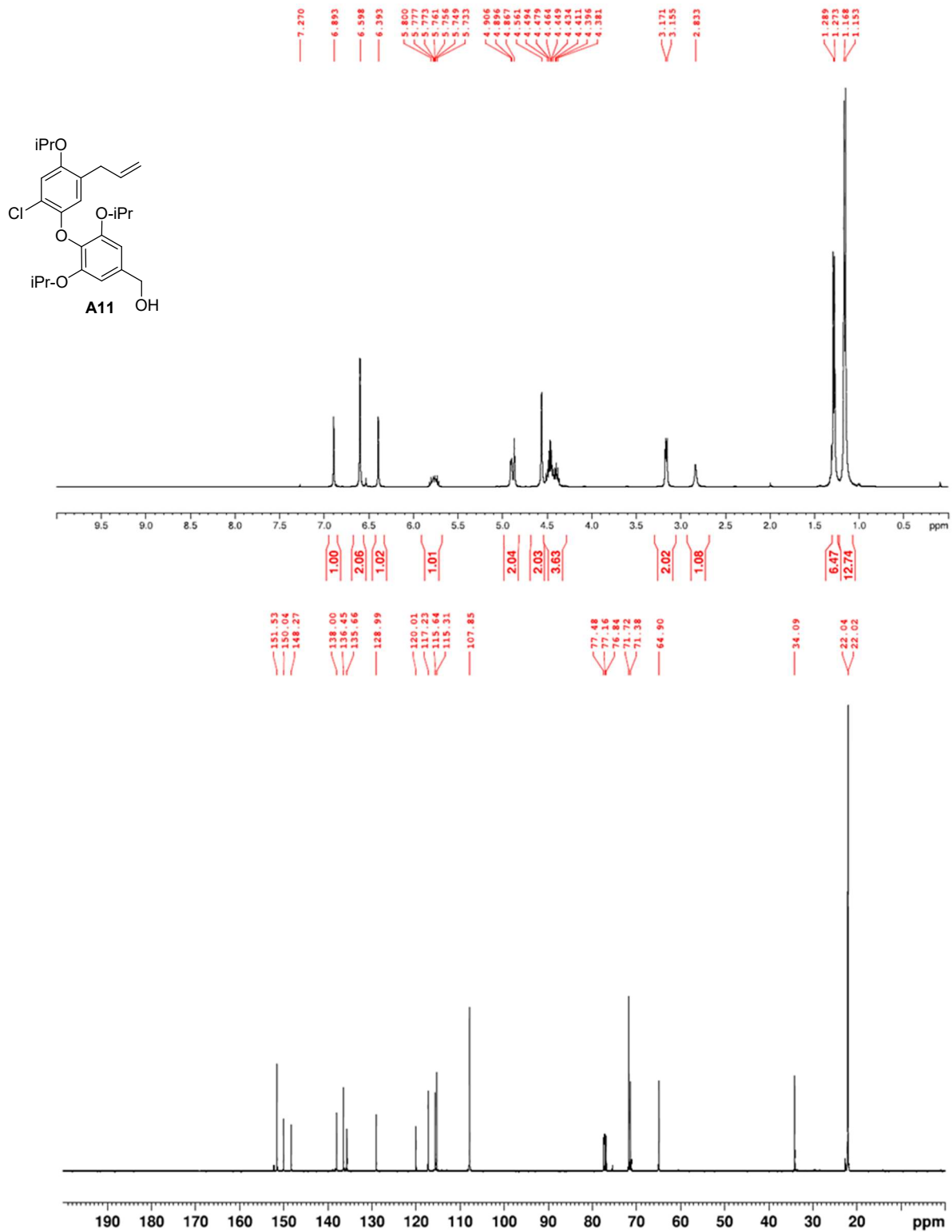
Figure A.119. ^{1}H NMR (400 MHz, CDCl$_3$) and ^{13}C NMR (100 MHz, CDCl$_3$) of **A11.**
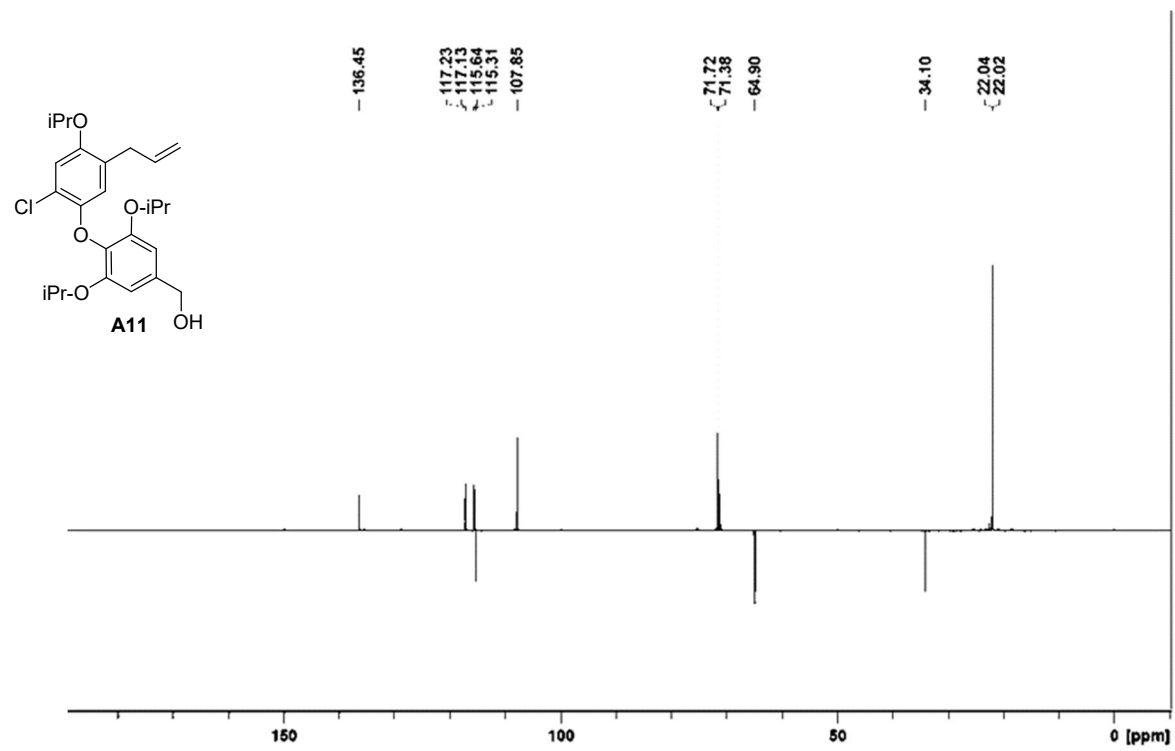
Figure A.120. DEPT-135(CDCl₃) of **A11.**
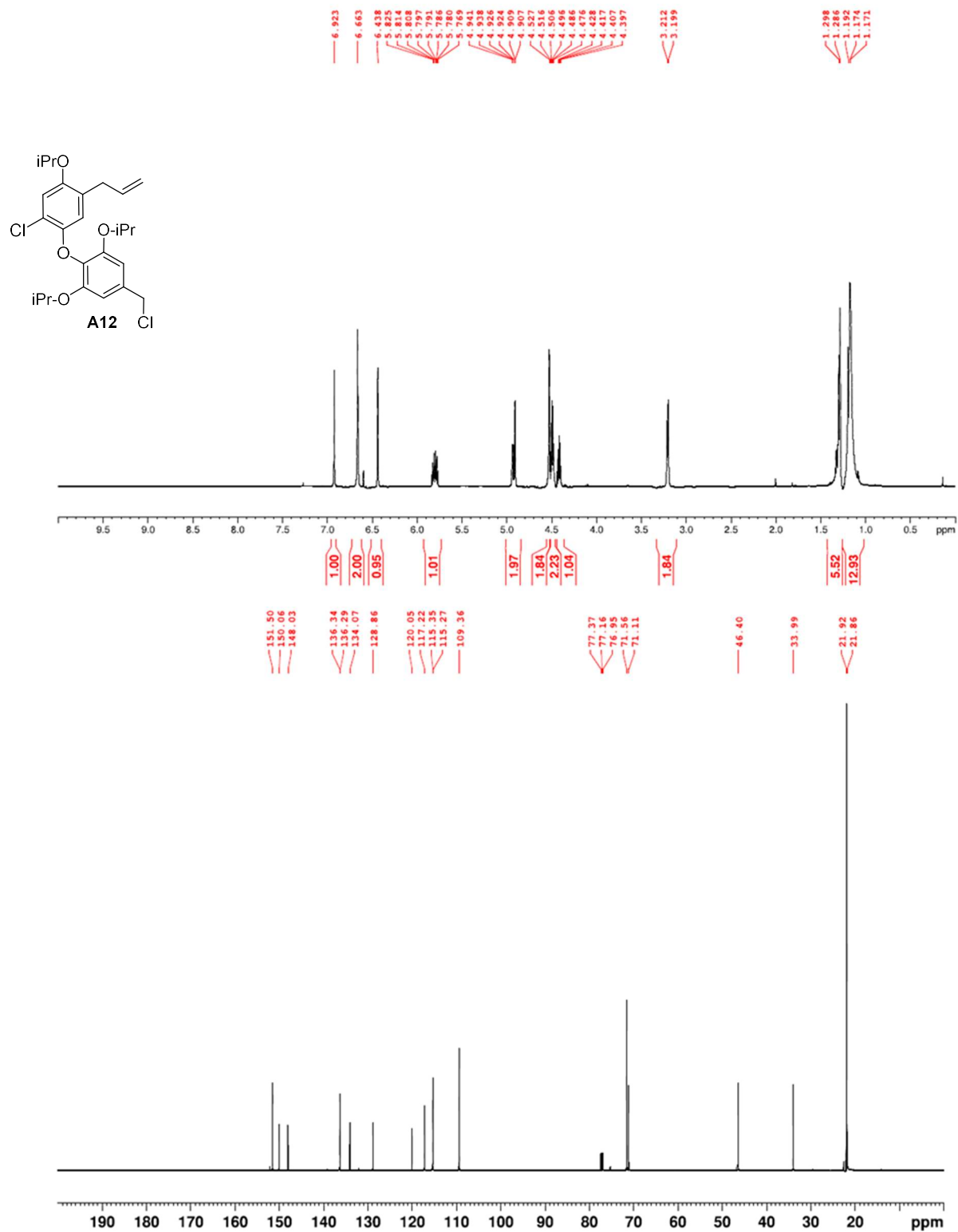
Figure A.121. ^{1}H NMR (400 MHz, CDCl$_3$) and ^{13}C NMR (100 MHz, CDCl$_3$) of **A12.**
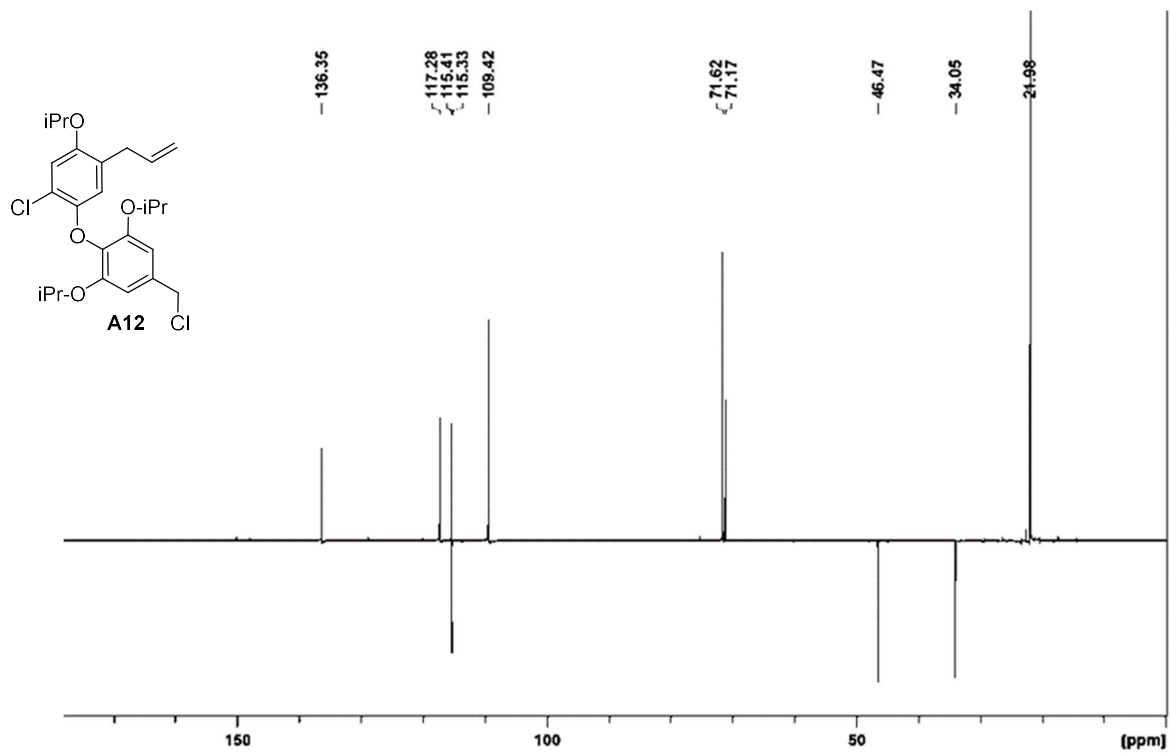
Figure A.122. DEPT-135(CDCl₃) of **A12.**
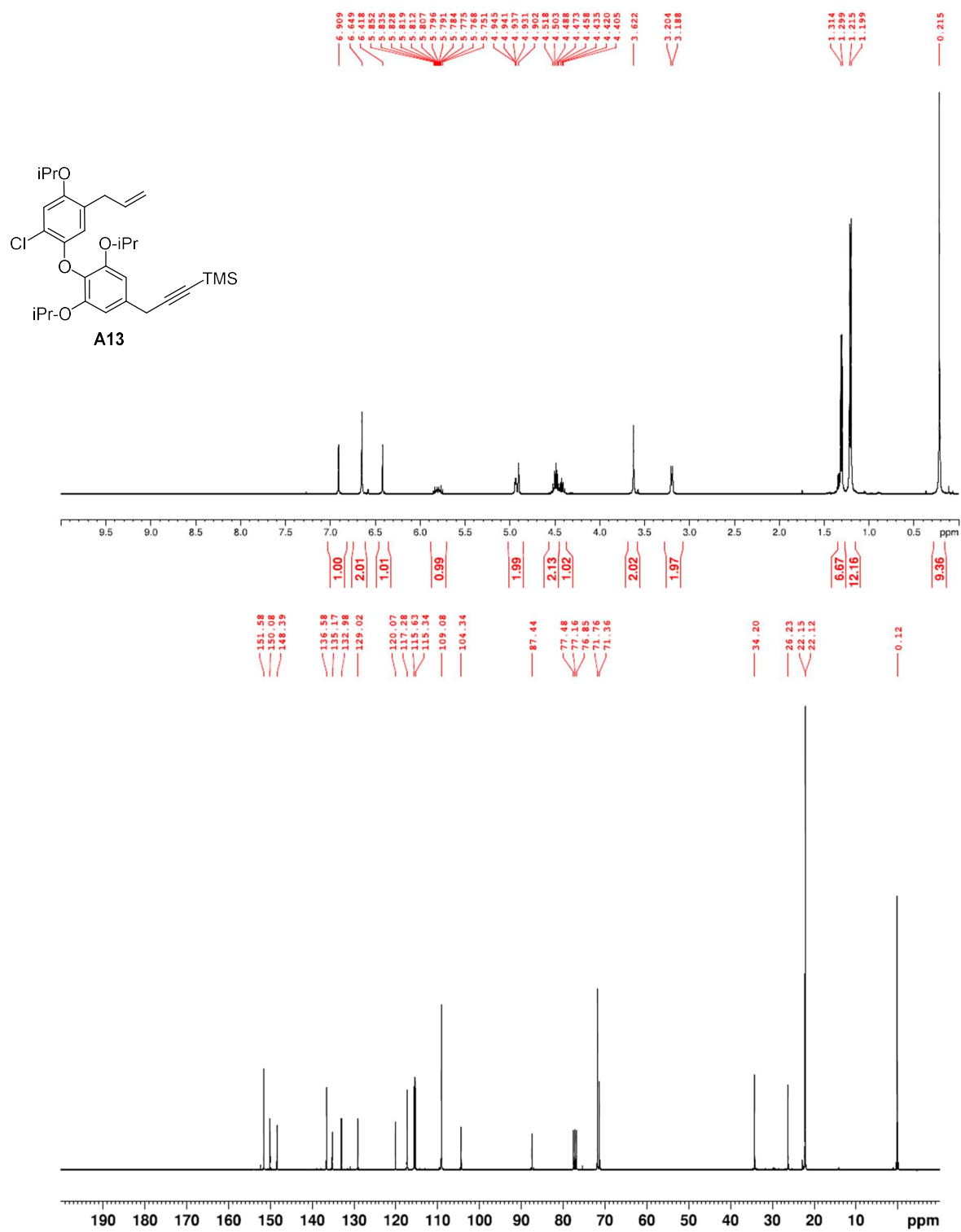
Figure A.123. ^{1}H NMR (400 MHz, CDCl$_3$) and ^{13}C NMR (100 MHz, CDCl$_3$) of **A13.**
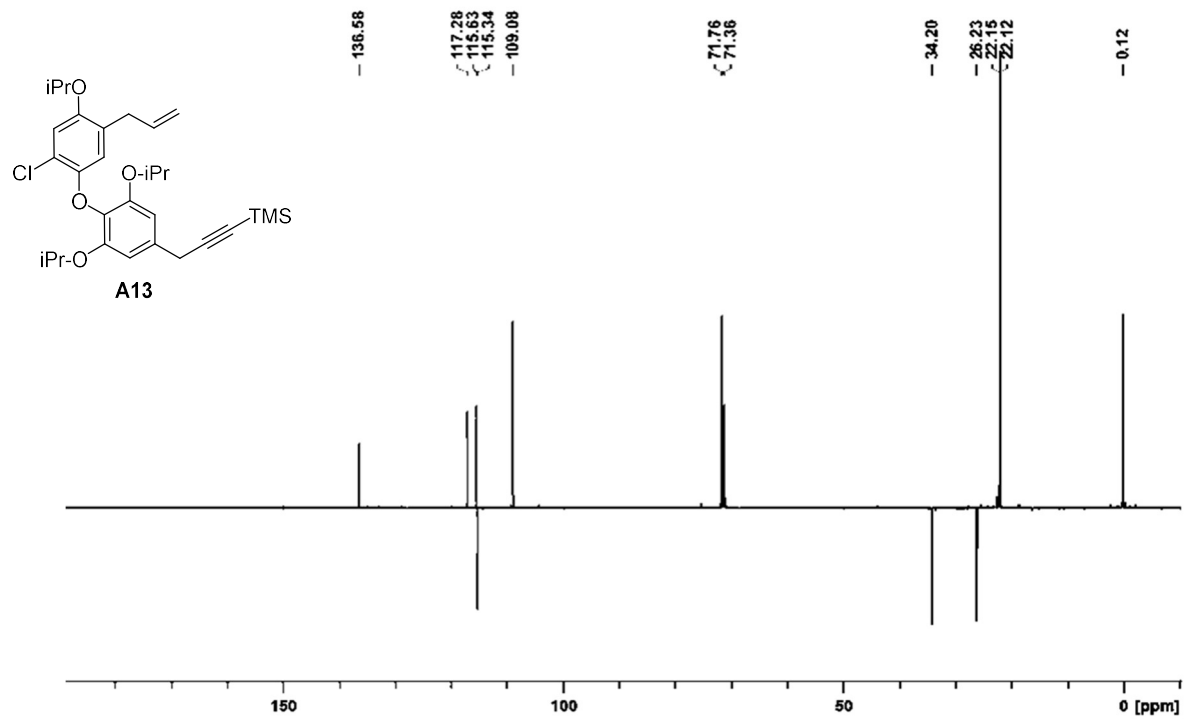
Figure A.124. DEPT-135(CDCl$_3$) of **A13.**
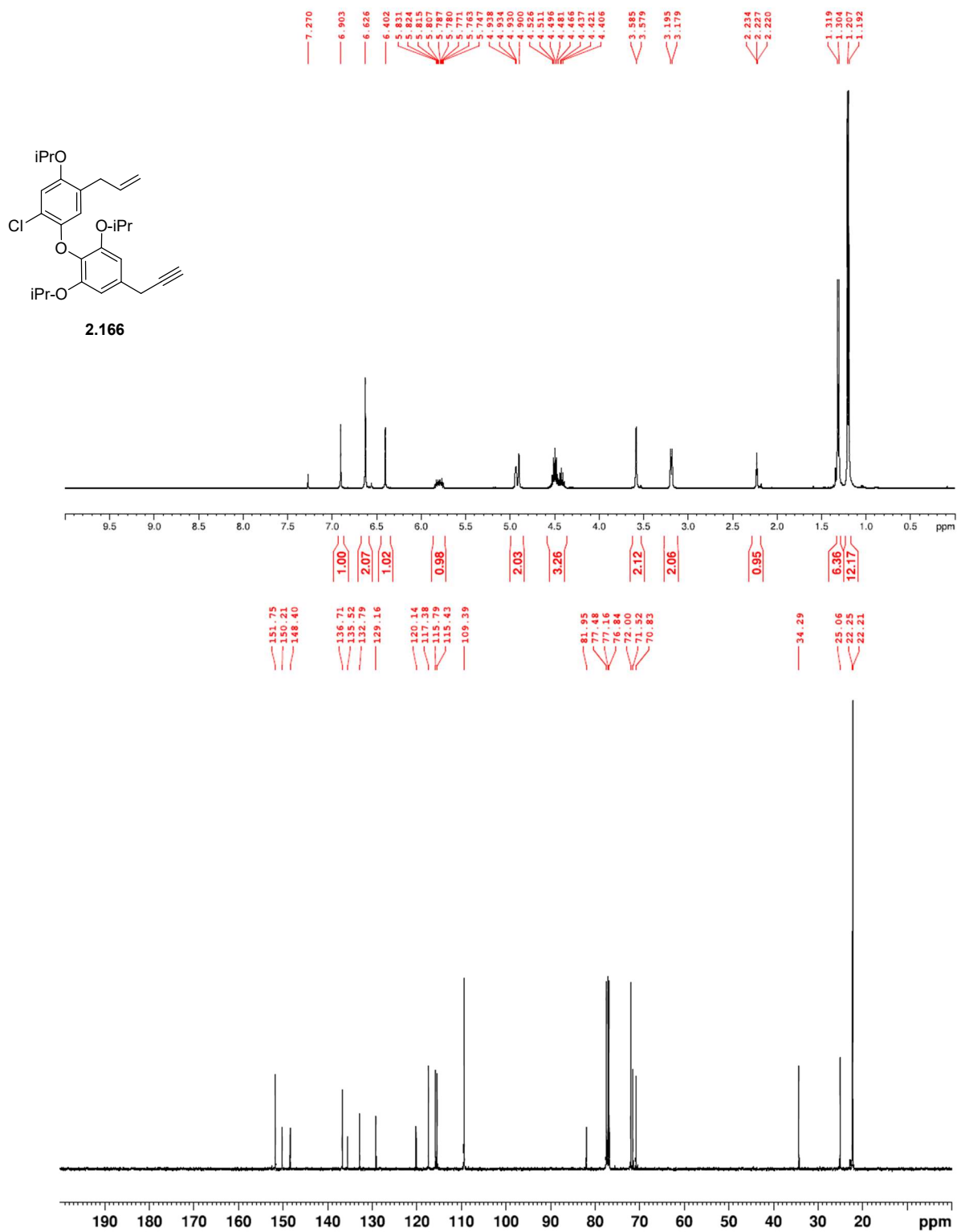
Figure A.125. ^{1}H NMR (400 MHz, CDCl$_3$) and ^{13}C NMR (100 MHz, CDCl$_3$) of **2.166.**
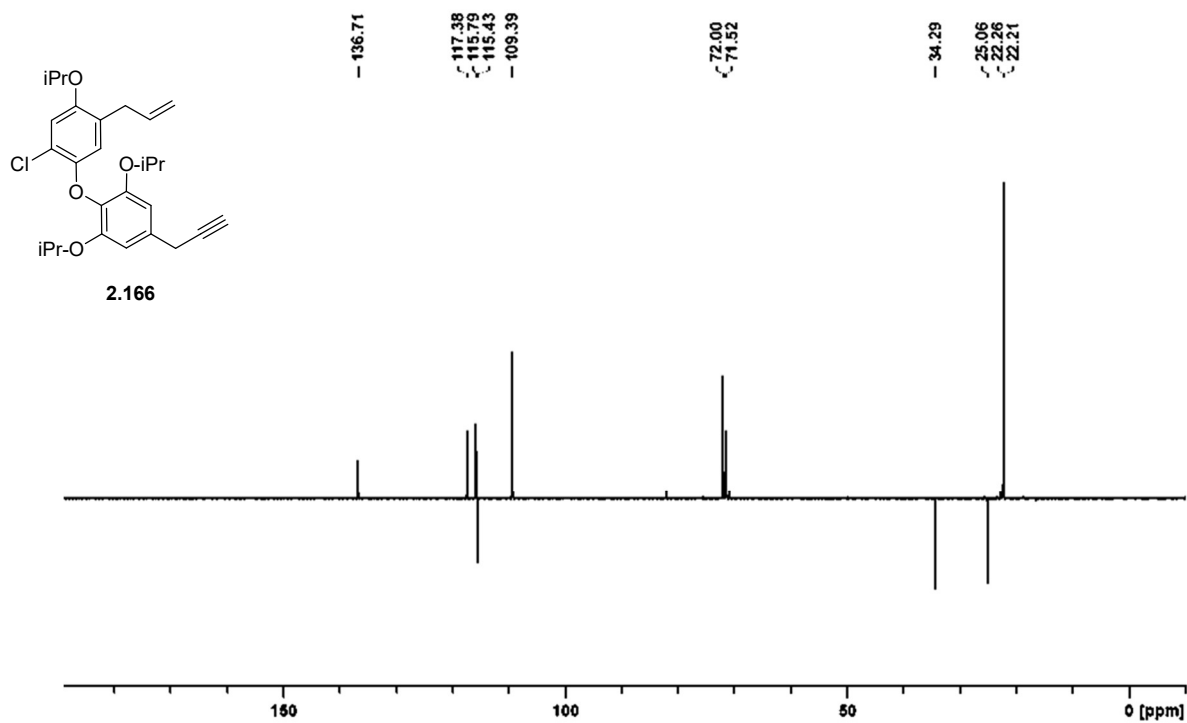
Figure A.126. DEPT-135(CDCl₃) of **2.166.**
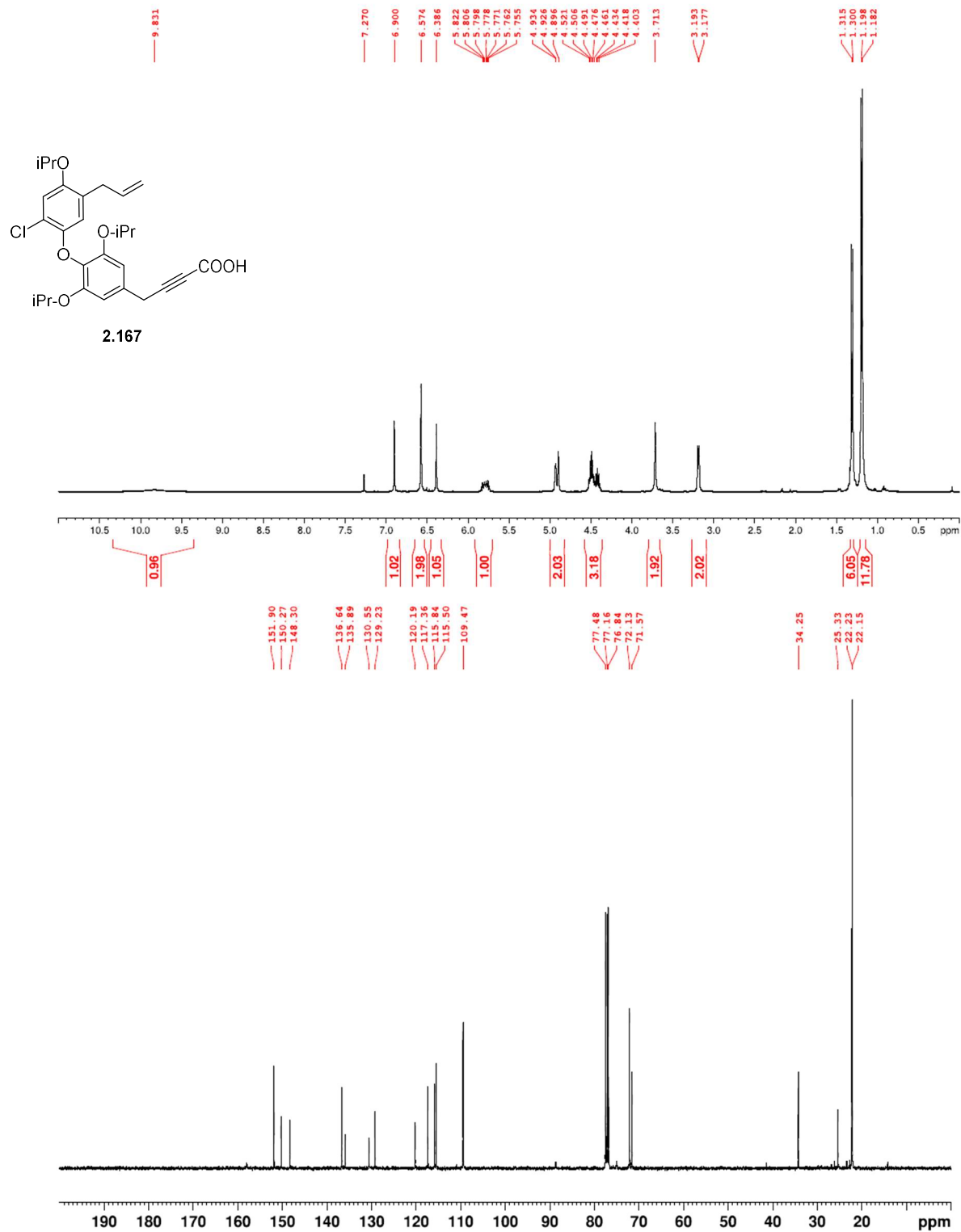
Figure A.127. ^{1}H NMR (400 MHz, CDCl$_3$) and ^{13}C NMR (100 MHz, CDCl$_3$) of **2.167.**
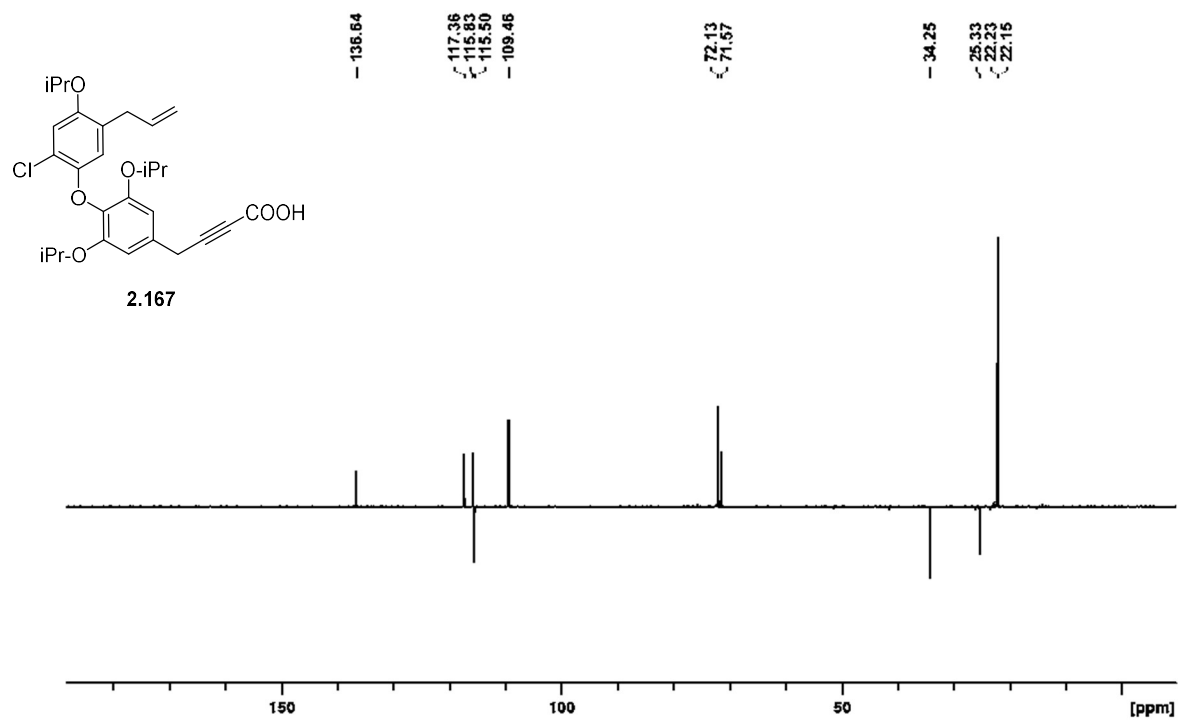
Figure A.128. DEPT-135(CDCl$_3$) of **2.167.**
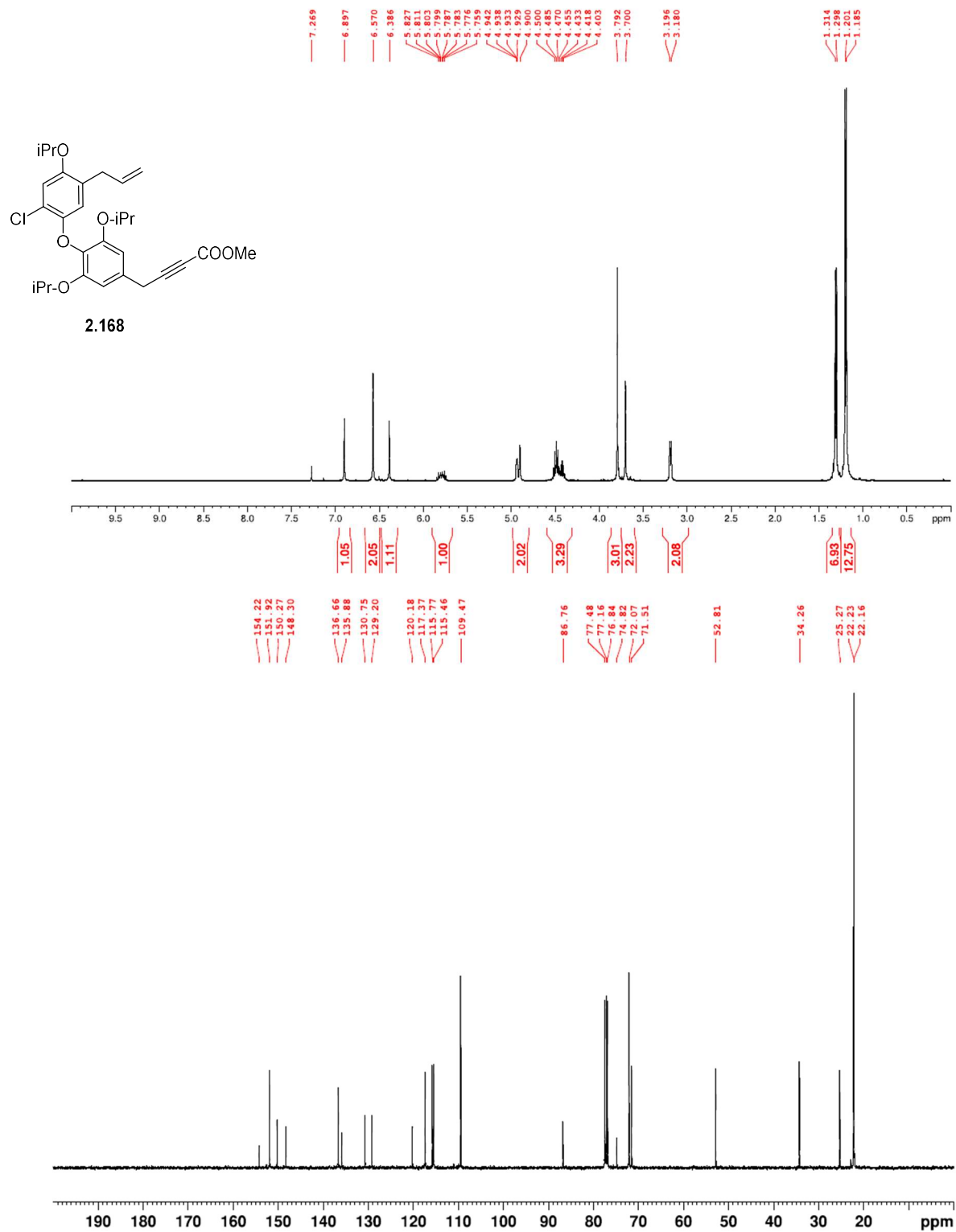
Figure A.129. ^{1}H NMR (400 MHz, CDCl$_3$) and ^{13}C NMR (100 MHz, CDCl$_3$) of **2.168.**
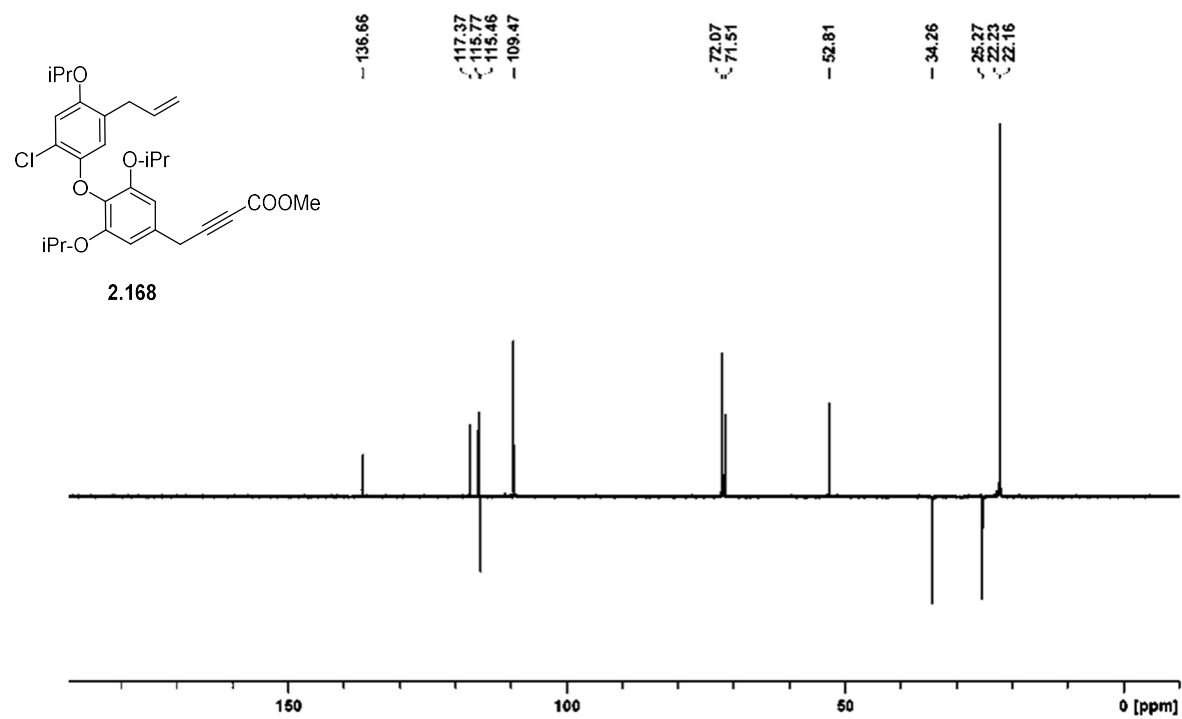
Figure A.130. DEPT-135(CDCl₃) of **2.168.**
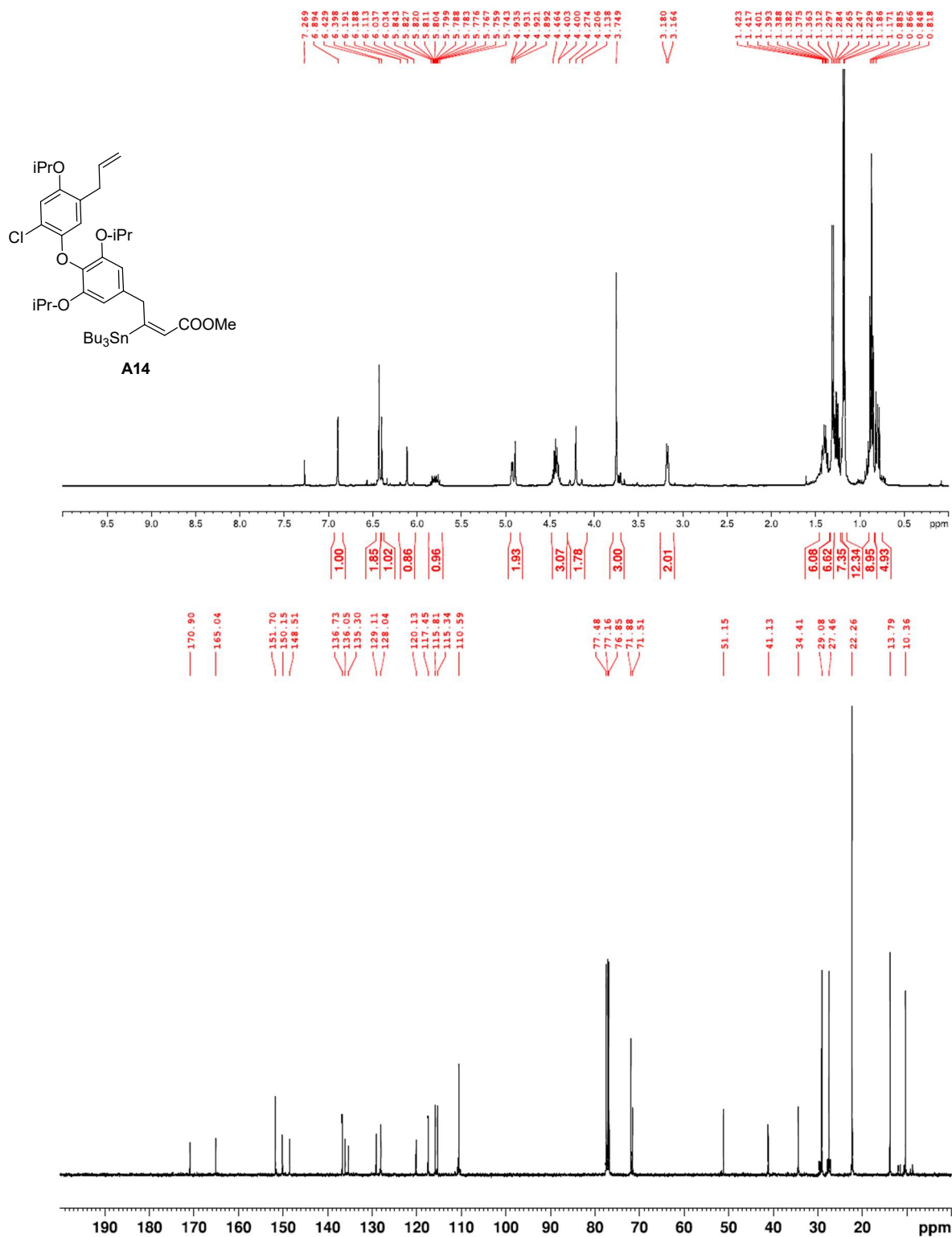
Figure A.131. ^{1}H NMR (400 MHz, CDCl$_3$) and ^{13}C NMR (100 MHz, CDCl$_3$) of **A14.**
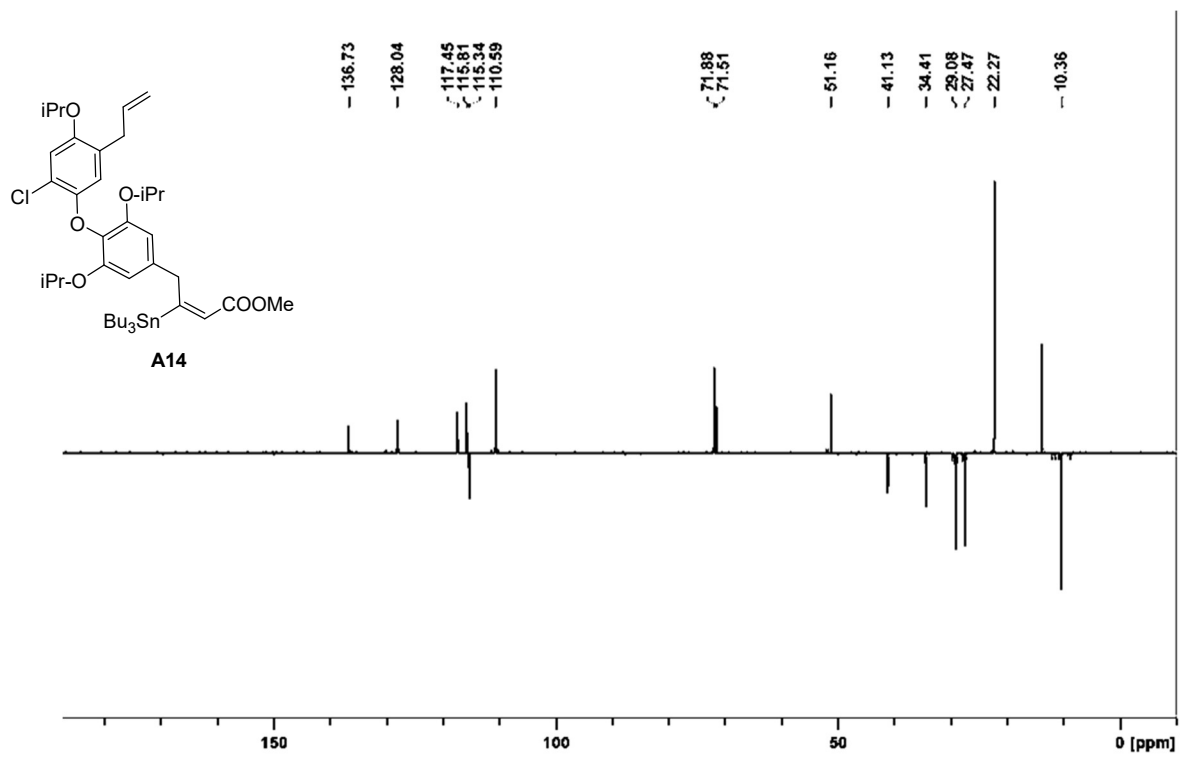
Figure A.132. DEPT-135(CDCl₃) of **A14.**

Figure A.133. ^{1}H NMR (400 MHz, CDCl$_3$) and ^{13}C NMR (100 MHz, CDCl$_3$) of **A15.**

Figure A.134. DEPT-135(CDCl₃) of **A15.**

Figure A.135. ^{1}H NMR (400 MHz, CDCl$_3$) and ^{13}C NMR (100 MHz, CDCl$_3$) of **2.169.**

Figure A.136. DEPT-135(CDCl₃) of **2.169.**
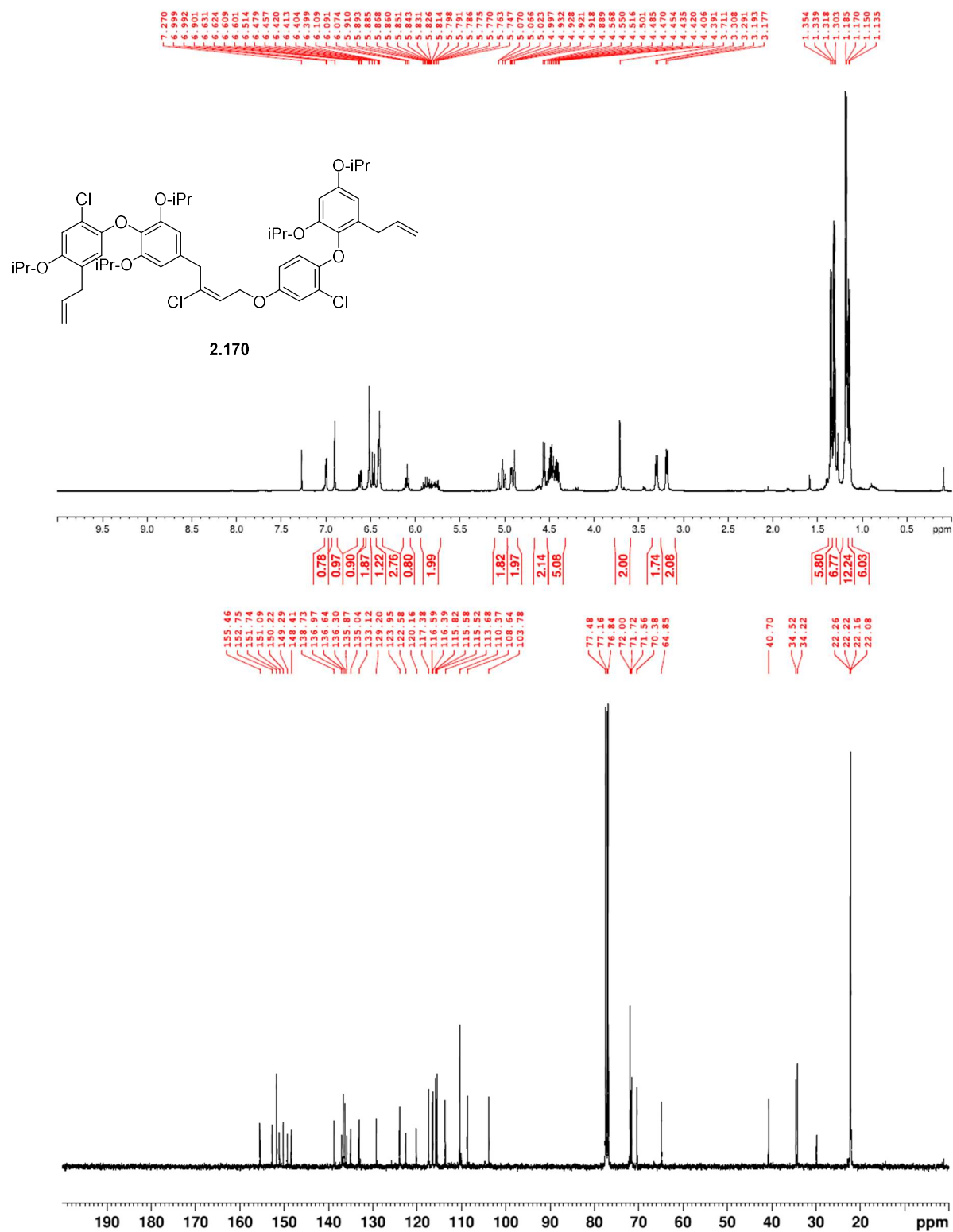
Figure A.137. ^{1}H NMR (400 MHz, CDCl$_3$) and ^{13}C NMR (100 MHz, CDCl$_3$) of **2.170.**
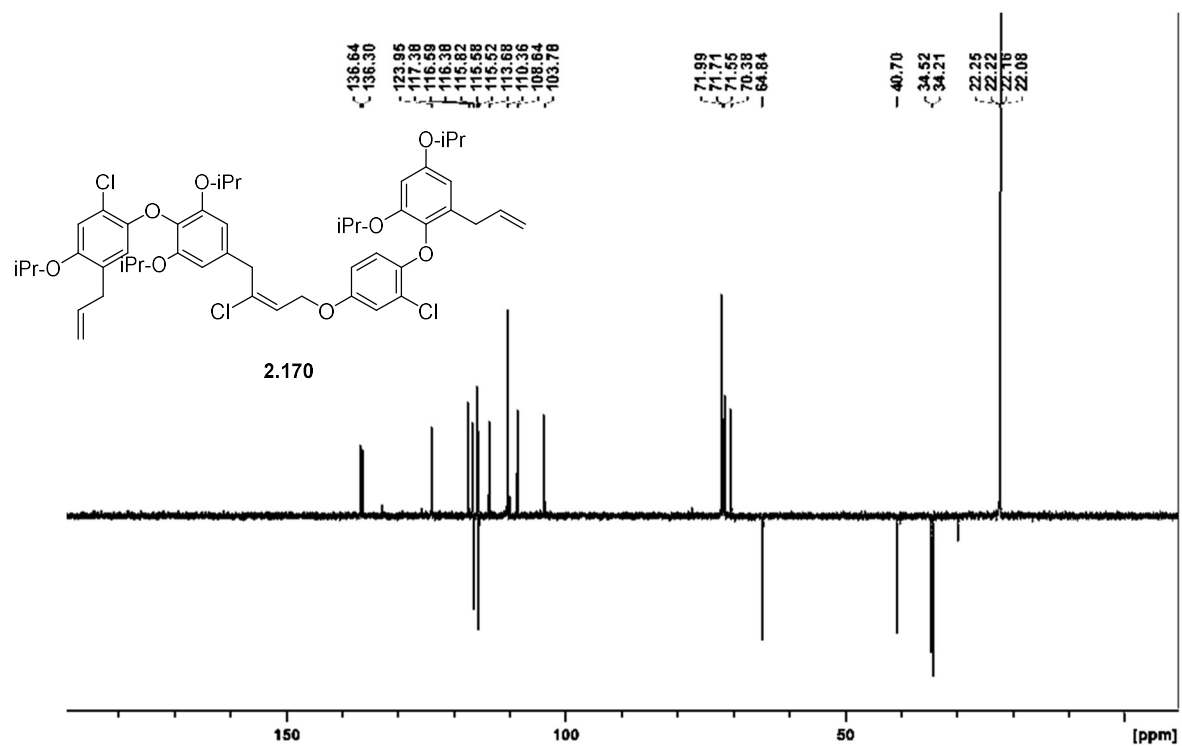
Figure A.138. DEPT-135(CDCl₃) of **2.170.**
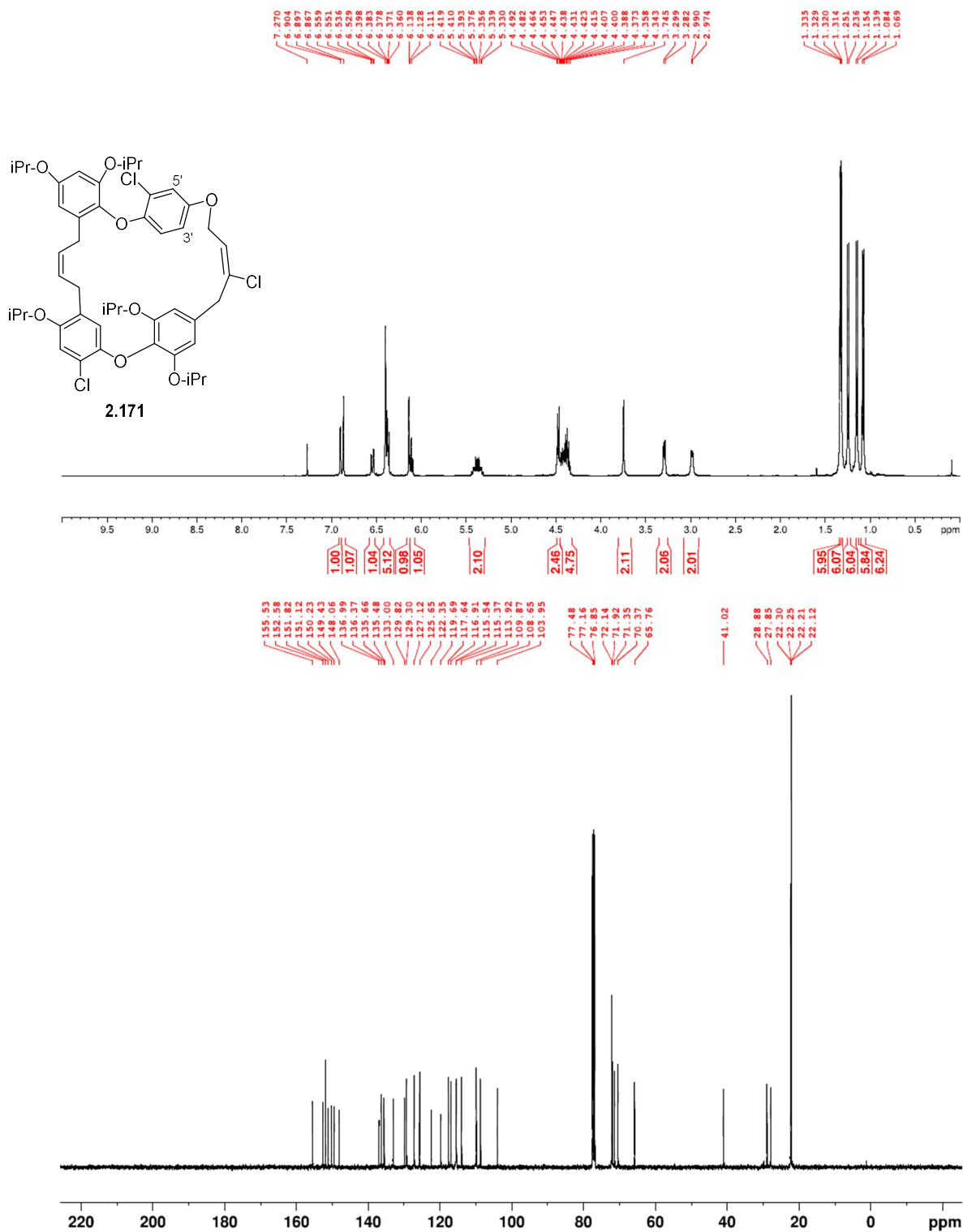
Figure A.139. ^{1}H NMR (400 MHz, CDCl$_3$) and ^{13}C NMR (100 MHz, CDCl$_3$) of **2.171.**
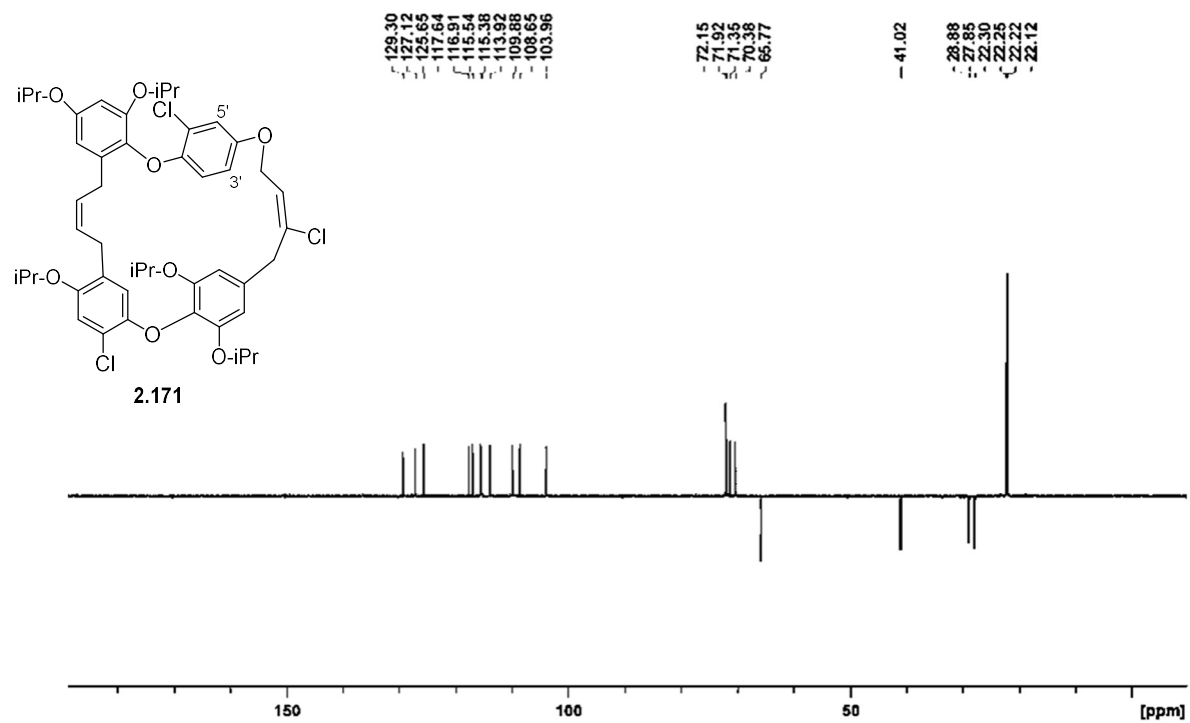
Figure A.140. DEPT-135(CDCl₃) of **2.171.**
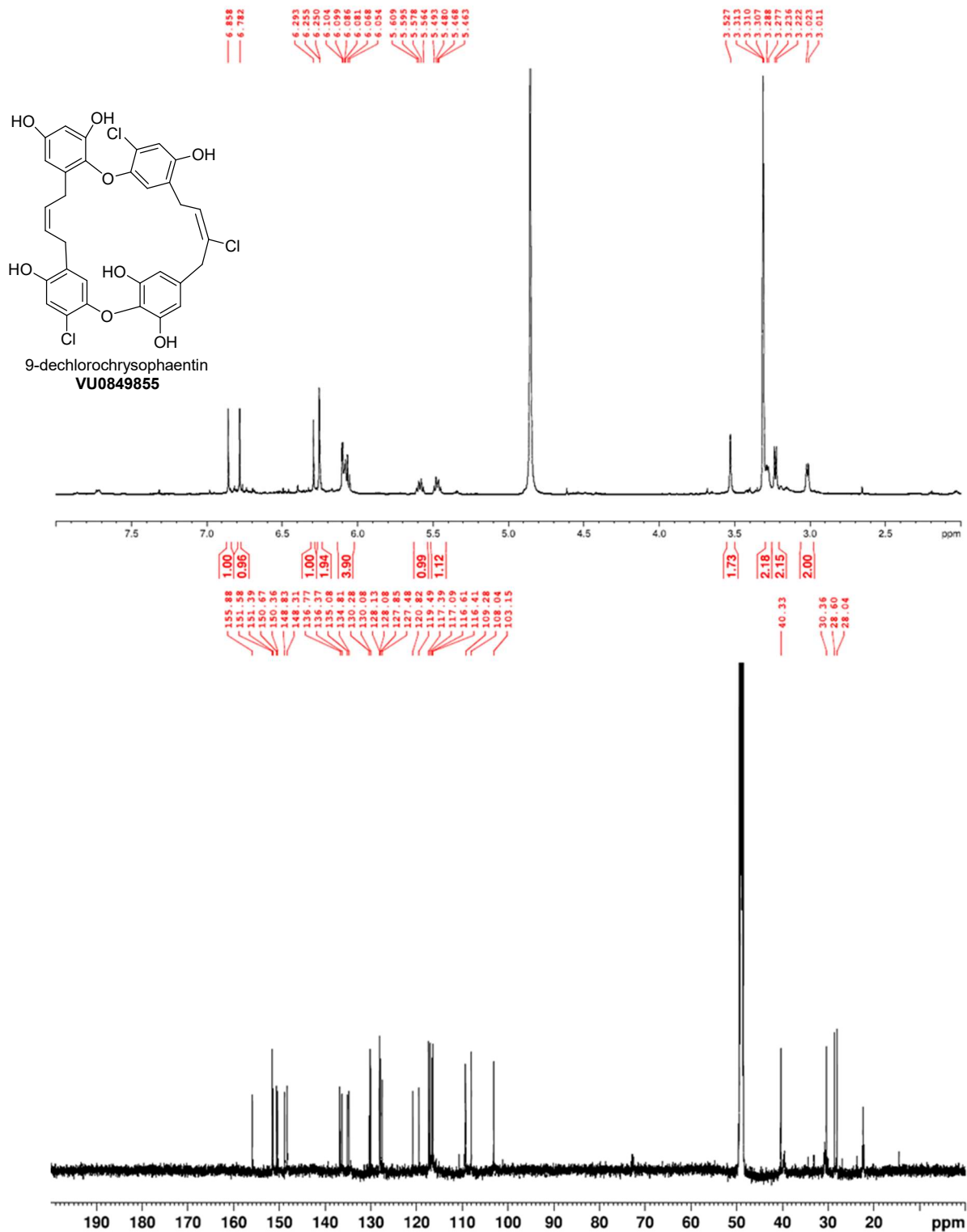
Figure A.141. ^{1}H NMR (400 MHz, CD$_3$OD) and ^{13}C NMR (100 MHz, CD$_3$OD) of **VU0849855.**
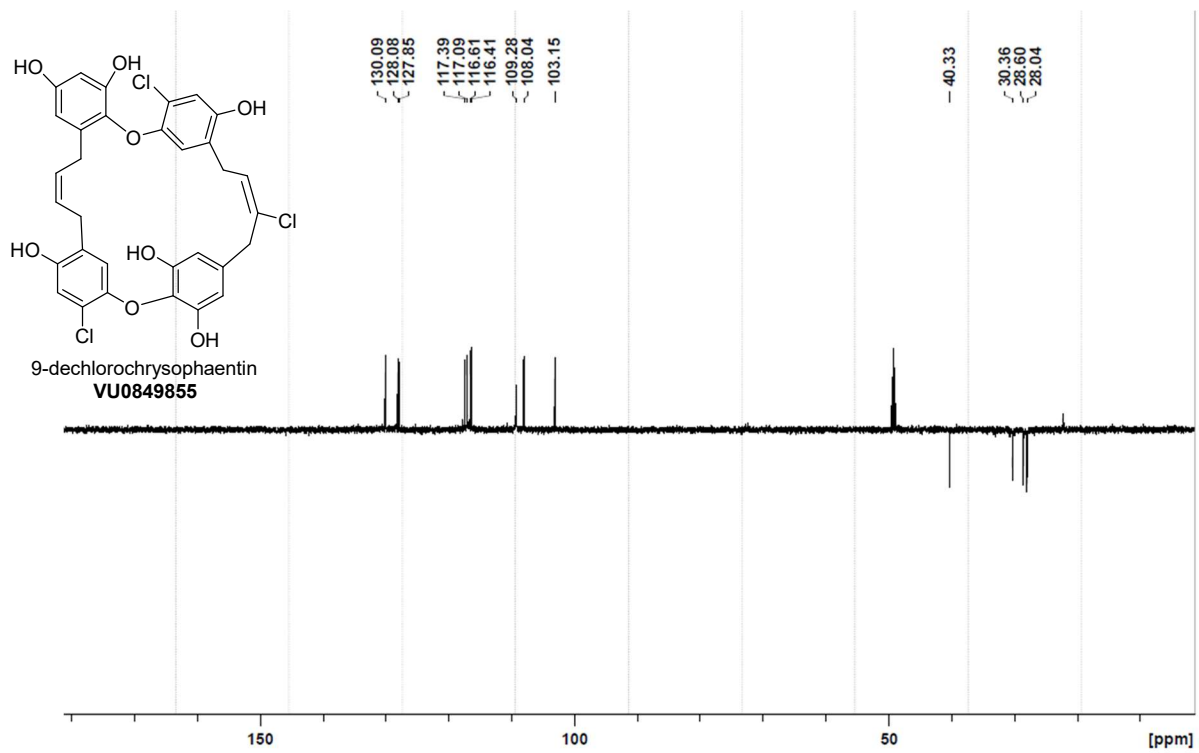
Figure A.142. DEPT-135(CD₃OD) of **VU0849855.**

Figure A.143. ^{1}H NMR (400 MHz, CD$_3$OD) and ^{13}C NMR (100 MHz, CD$_3$OD) of **VU0849838.**
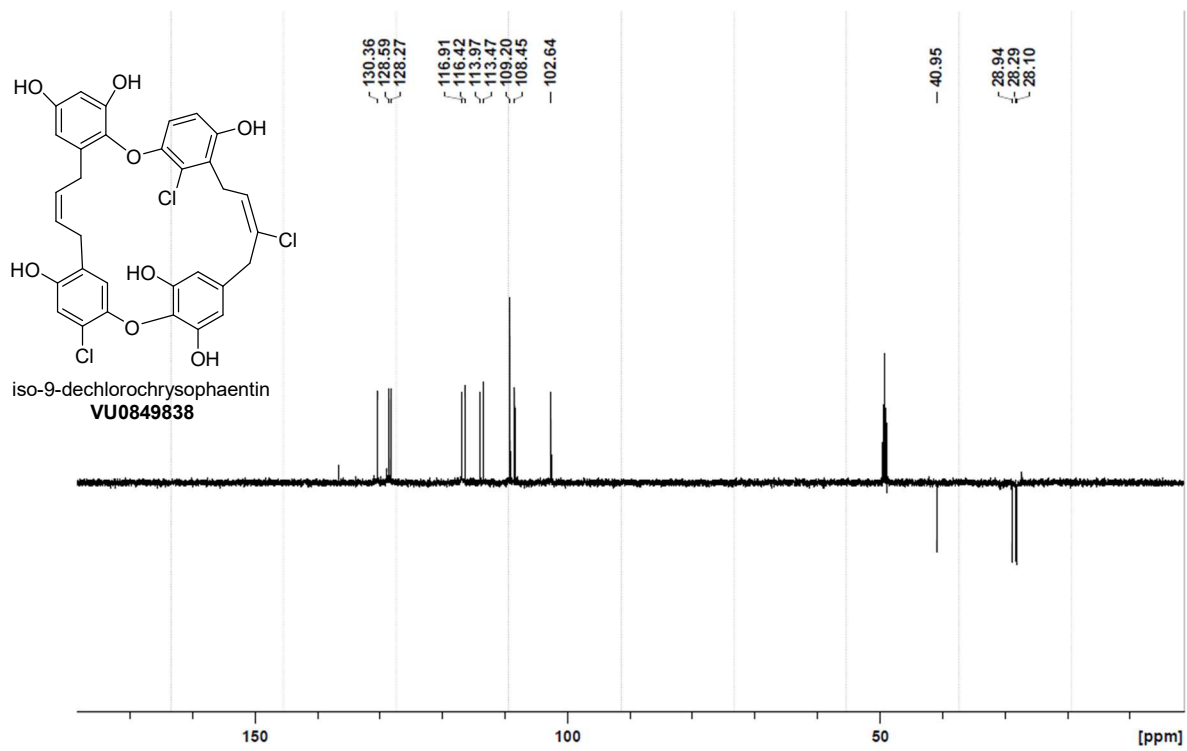
Figure A.144. DEPT-135(CD₃OD) of **VU0849838.**
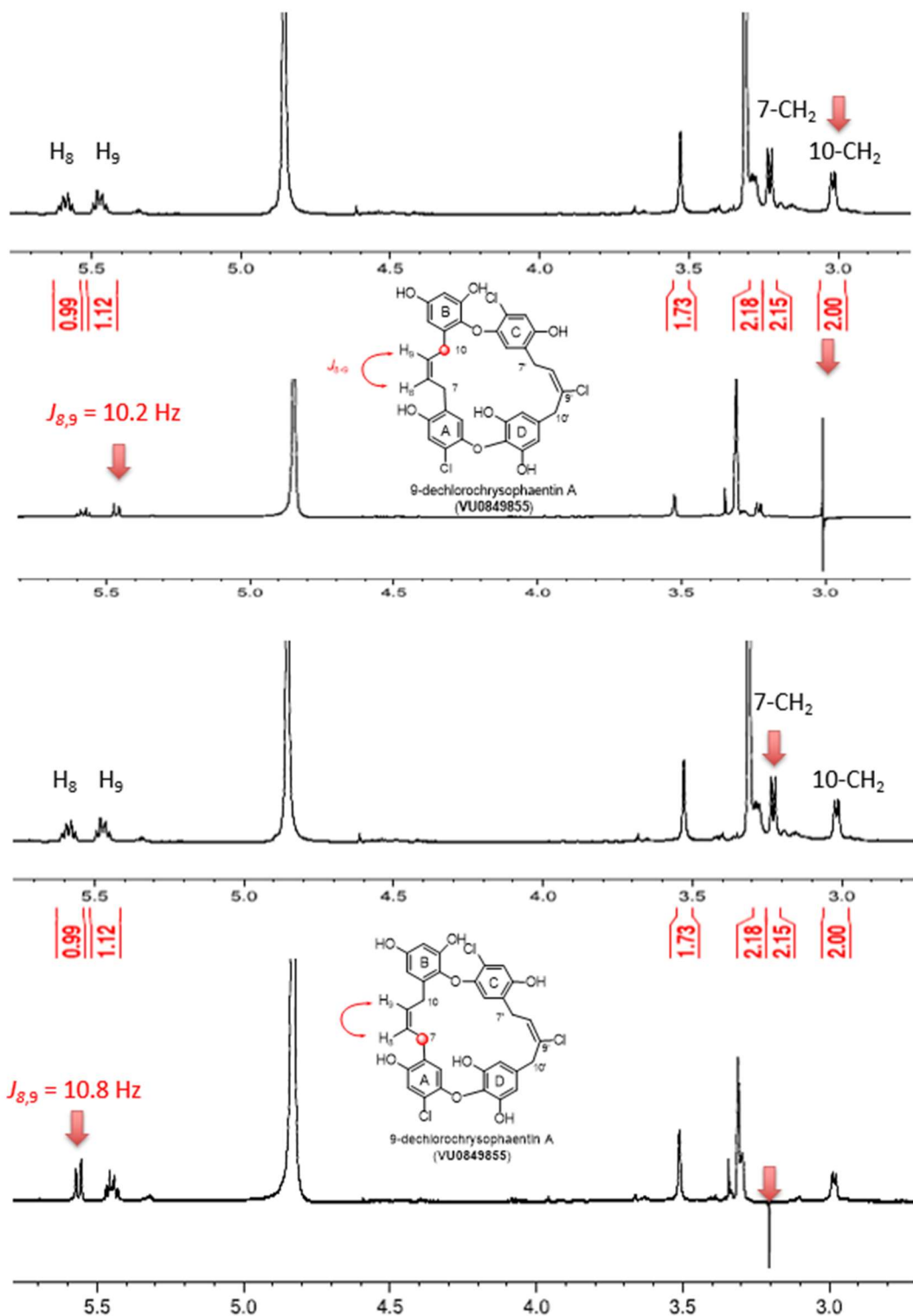
Figure A.145. Assignment of C8-C9 geometry by $J_{8,9}$ of **VU0849855** via homonuclear decoupling NMR.
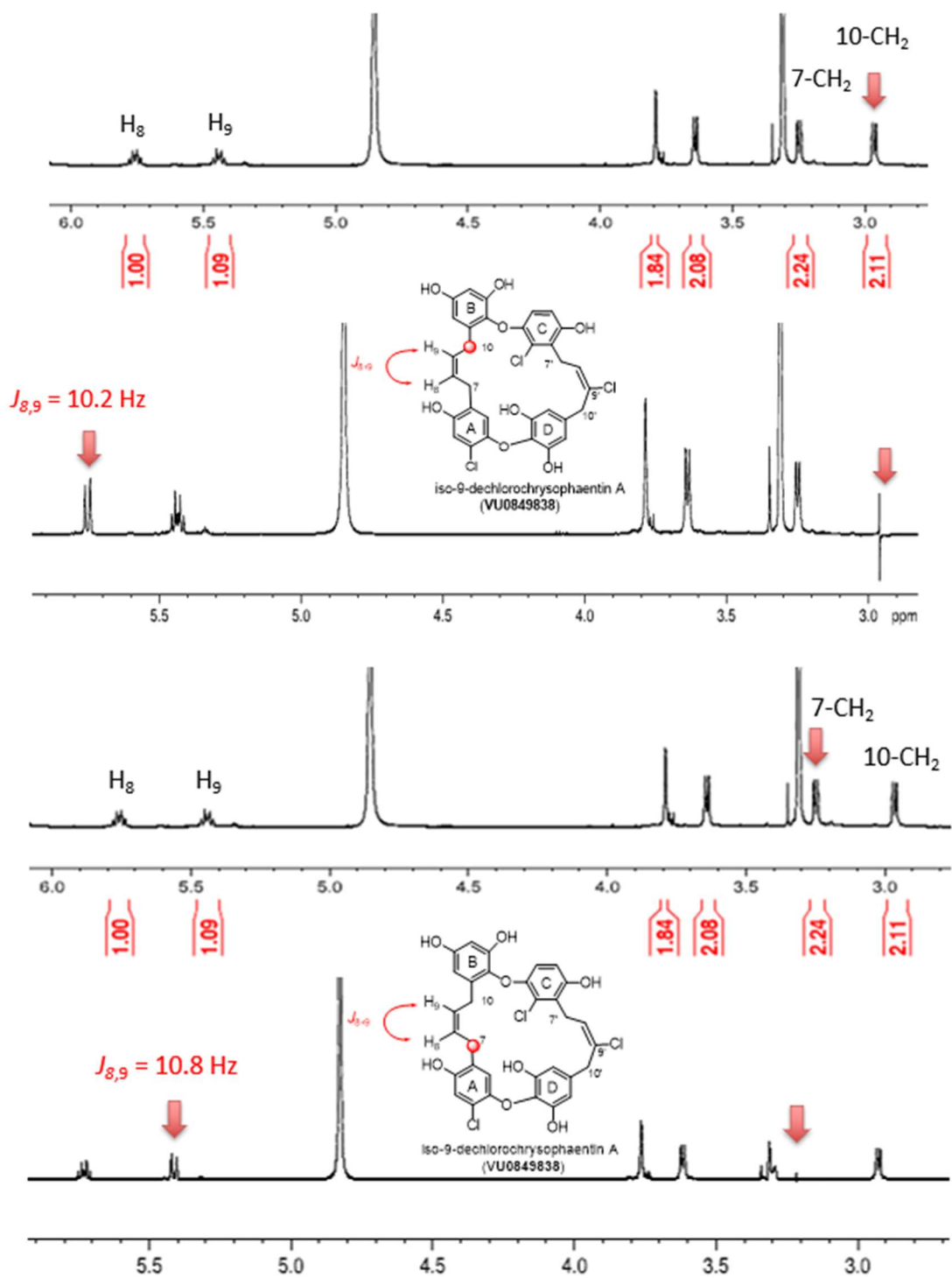
Figure A.146. Assignment of C8-C9 geometry by $J_{8,9}$ of **VU0849838** via homonuclear decoupling NMR.
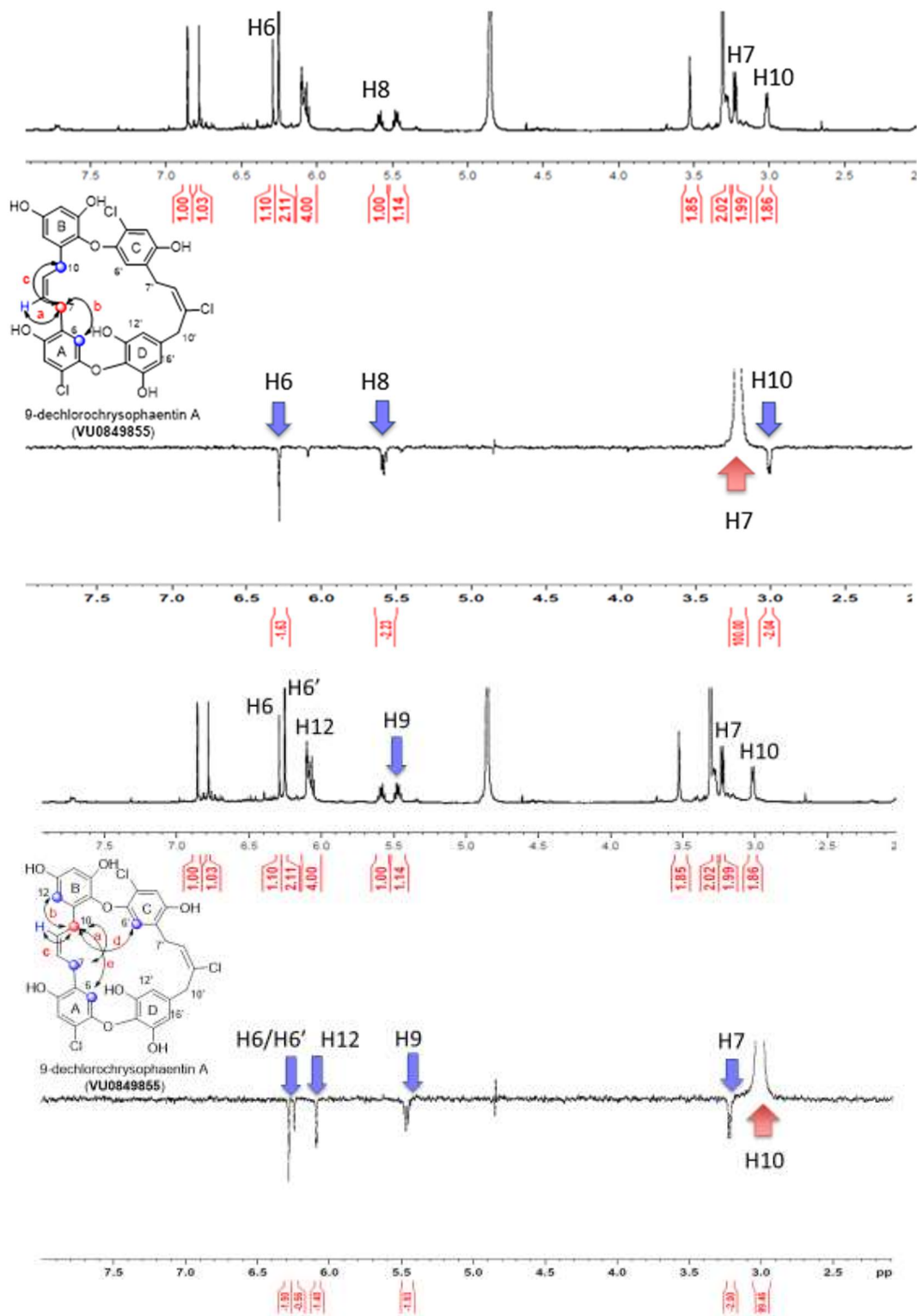
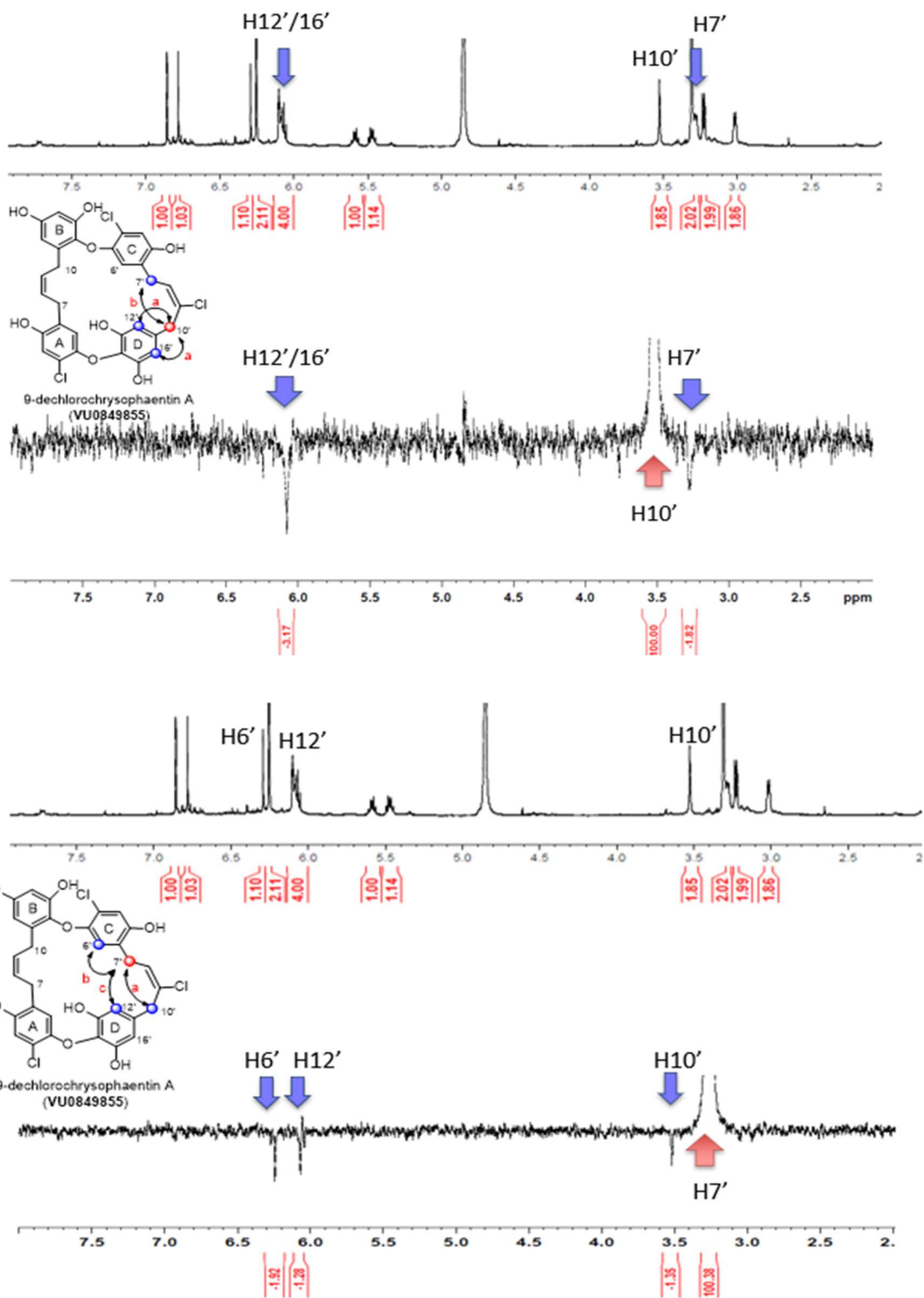**Figure A.147.** Assignment of C8-C9 double bond geometry of **VU0849855** (1D-selective NOE).

Figure A.148. Assignment of C8'-C9' double bond geometry of **VU0849855** (1D-selective NOE).
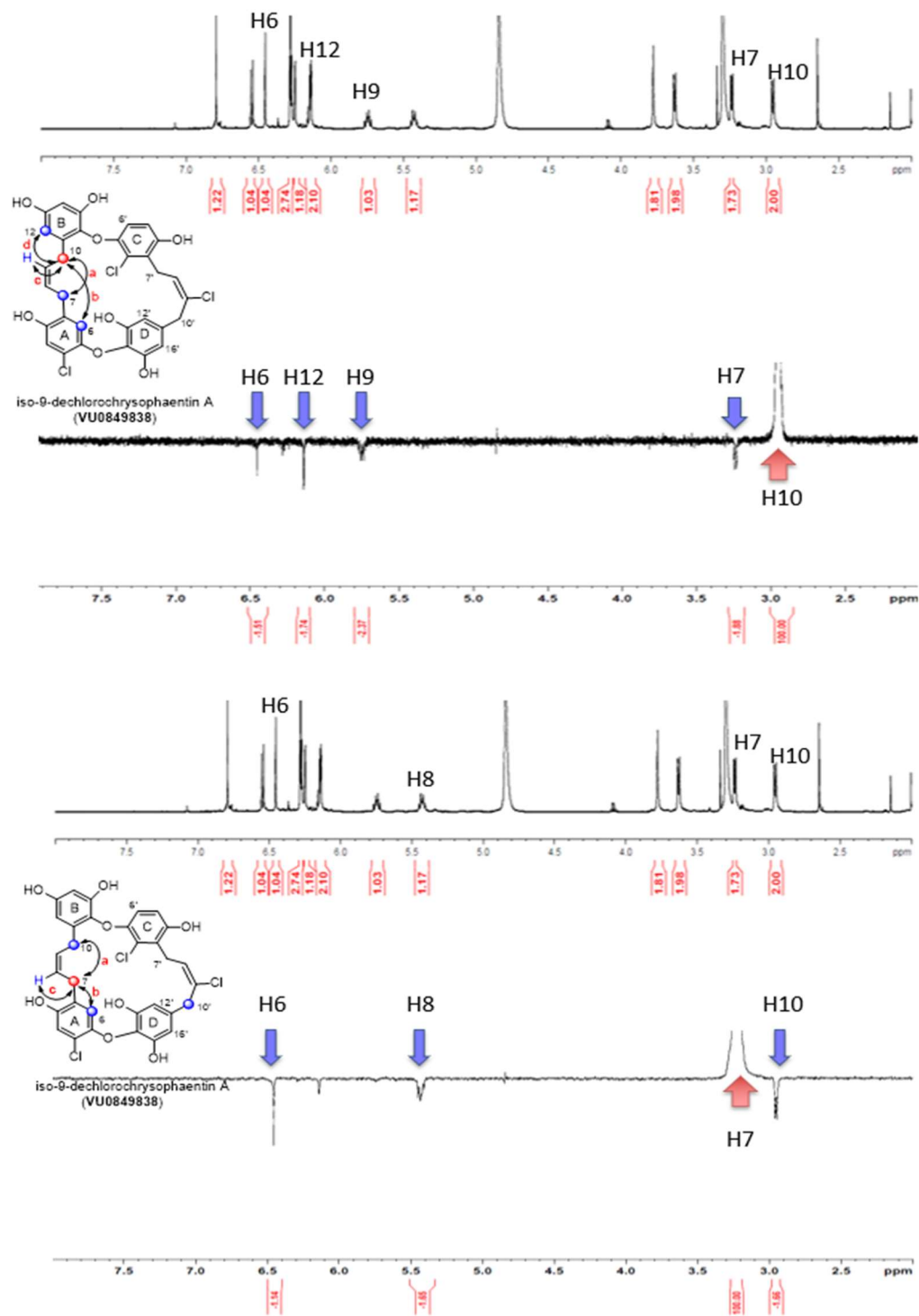
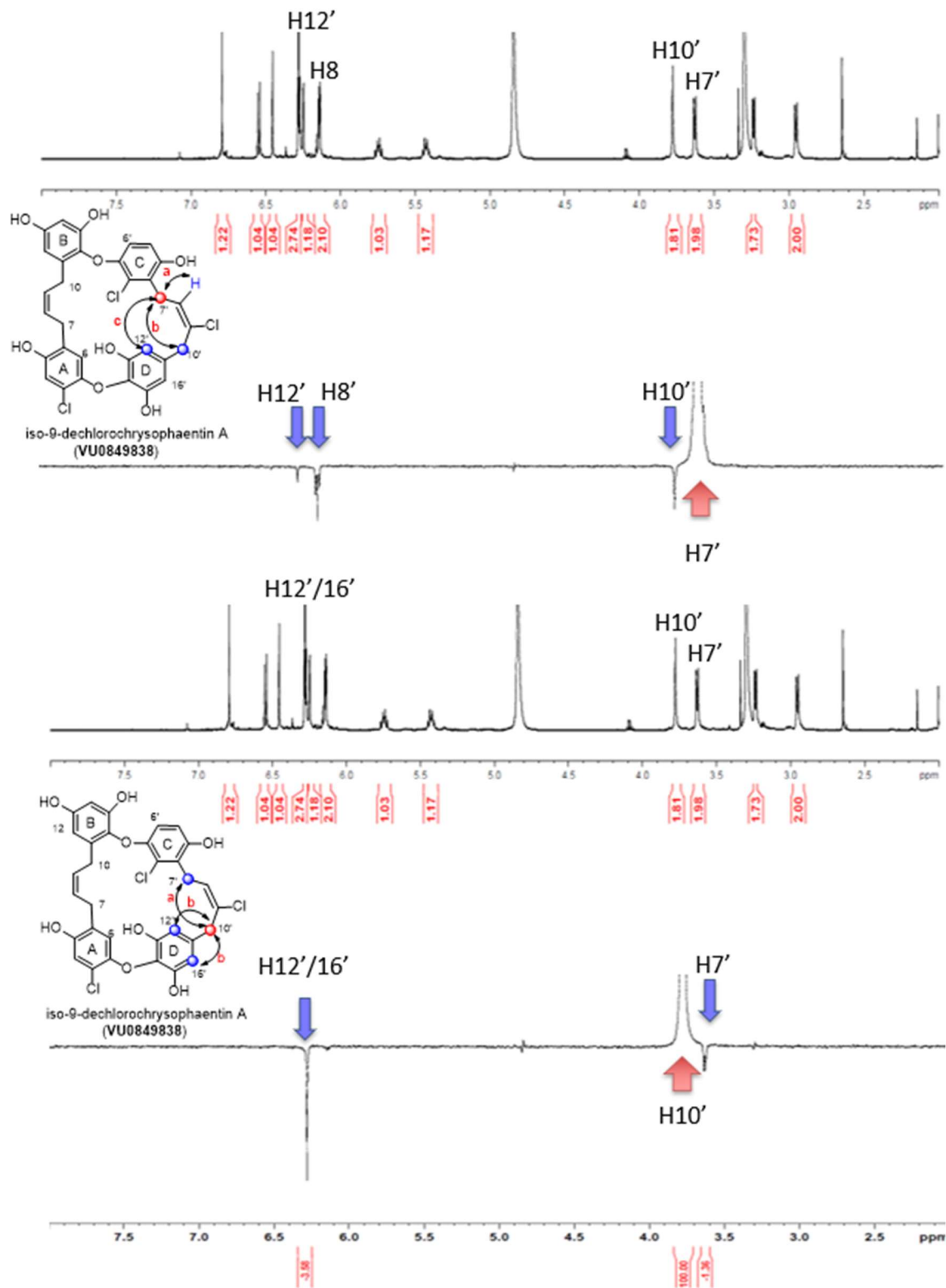**Figure A.149.** Assignment of C8-C9 double bond geometry of **VU0849838** (1D-selective NOE).
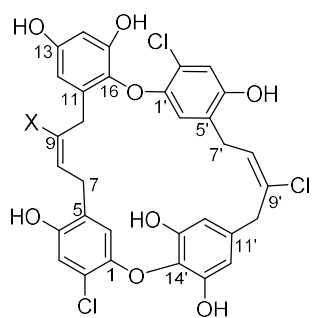
Figure A.150. Assignment of C8'-C9' double bond geometry of **VU0849838** (1D-selective NOE).

Chrysophaentin A (X=Cl)
9-dechlorochrysophaentin A (X=H)

MeOD-D4	Observed Value ^{13}C NMR	Literature Values[1] ^{13}C NMR
C7'	30.4	30.3
C7	30.6	28.0
C10	33.7	28.5
C10'	40.6	40.3
C14	103.8	103.1
C12	107.9	108.0
C12', C16'	109.1	109.2
C6	116.0	117.1
C6'	116.7	117.3
C3	117.1	116.4
C3'	117.3	116.6
C2	120	119.5
C2'	121.1	120.8
C5	126.7	127.5
C5'	127.2	128.1
C8	127.7	127.8
C8'	127.9	128.0
C14'	129.7	130.2
C11	133.0	134.8
C9'	134.4	135.0
C9	134.7	130.0
C16	135.9	136.3
C11'	136.7	136.7
C1	148.1	148.3
C1'	148.9	148.8
C4	150.4	150.3
C4'	150.7	150.6
C15	151.3	151.3
C13', C15'	151.8	151.6
C13	155.6	155.9

Figure A.151. Comparison of ^{13}C shifts between **VU0849855** and Chrysophaentin A.
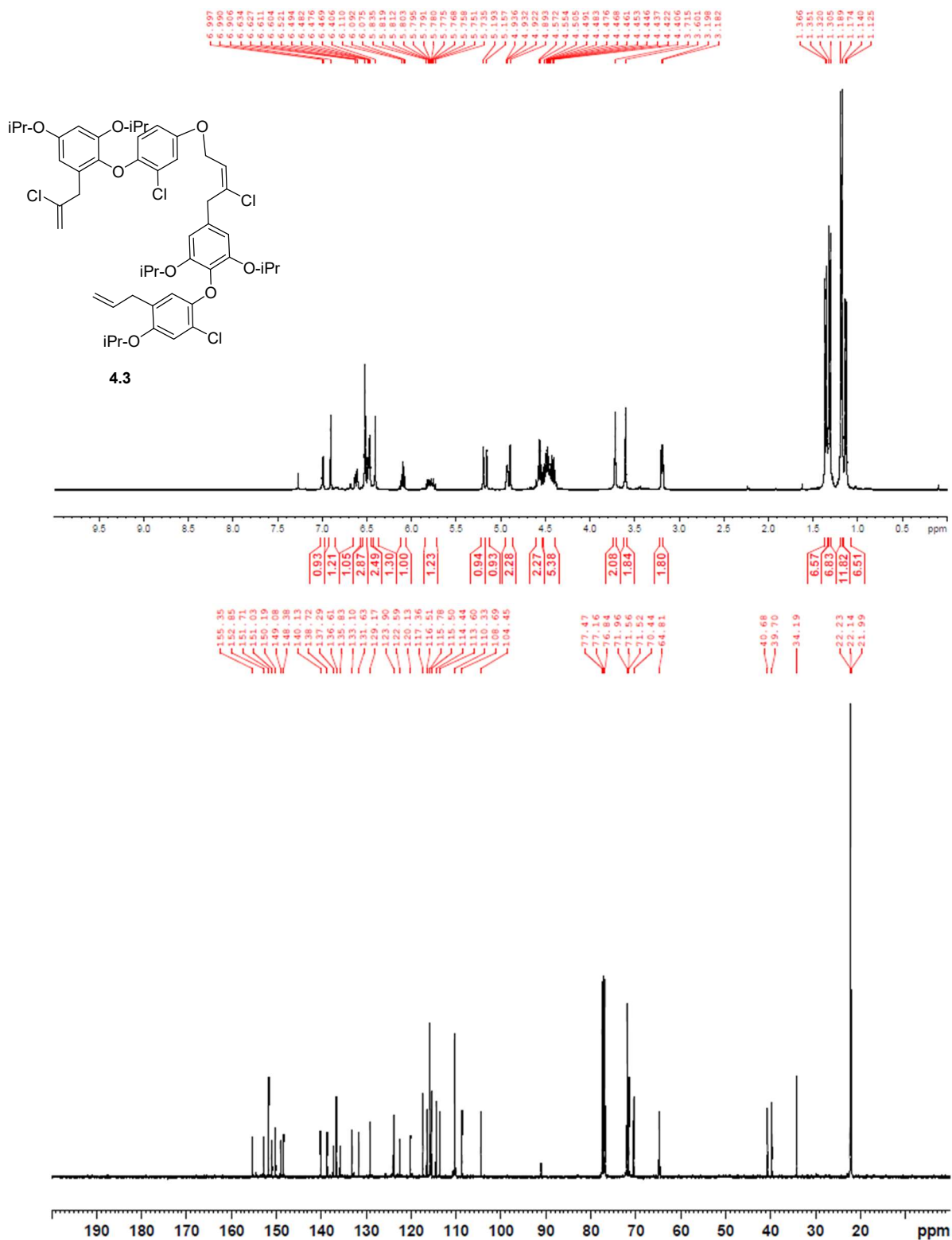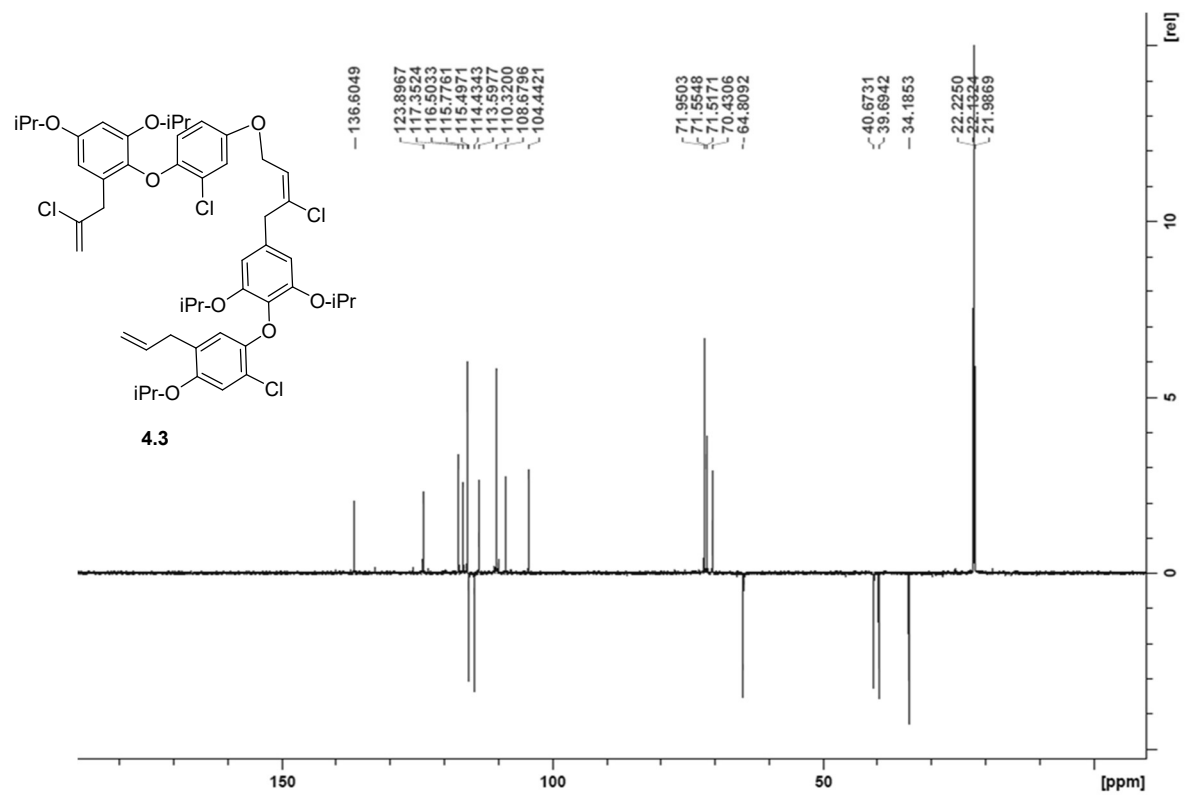
Figure A.152. ^{1}H NMR (400 MHz, CDCl$_3$) and ^{13}C NMR (100 MHz, CDCl$_3$) of **4.3.**

Figure A.153. DEPT-135(CDCl₃) of **4.3.**